ENVIRONMENTAL AND BIOLOGICAL TIN AND LEAD CHEMISTRY

by

Michael Anthony Healy B.Sc., C.Chem., M.R.S.C.

A Thesis submitted to the University of Nottingham for the Degree of Doctor of Philosophy. October 1980.

CONTENTS

PAGE

CHAPTER TWO:

ORGANOTIN STABILIZERS: MECHANISM OF ACTION, SYNTHESIS OF ESTERTINS SPECTROSCOPIC PROPERTIES

PAGE

ABSTRACT

Tin and lead are metals of considerable commercial importance and are used in many forms in the environment. Heat and light stabilization of polyvinylchloride polymer by organotins is now a principle application of that metal. The spectroscopic properties and crystal structures are determined for some estertin precursors of these stabilizers: mono and bis-(β-carbomethoxyethyl) tin chlorides, as well as the bis-(β-carbomethoxyethyl) tin dichloride analogue. The feasibility of using Mössbauer spectroscopy to determine the fate of the organotin species within the PVC is also assessed. The INDOR technique is used to obtain tin-119 n.m.r. data for a series of trimethyl and dimethyltin(IV) compounds and the results interpreted in a manner illustrating the use of this method as a structural probe for the solution chemistry of organotin systems.

In the case of lead, attention is given to the effects of use of that metal in petrol by examining its overall distribution pattern in the dust, soil, grasses, plants and fruit of a roadside environment. Additionally a new aetiology of lead poisoning involving some traditional Asian medicines and cosmetics is also described and a route for gastrointestinal absorption of lead sulphide from this source proposed. The effect of particle size on uptake rate is established.

A chemical model for interaction between body-phosphate systems and lead derived from such sources as those studied is

Abstract (continued)

designed. The reactions found to occur between lead acetate, lead nitrate and dimethylphosphite and trimethylphosphate are interpreted. Preliminary studies show reaction between lead and adenosine di- and triphosphate and the data obtained from the model systems are used to elucidate the reaction pathway with these body-phosphate systems.

ACKNOWLEDGEMENTS

Firstly, my sincere thanks to Dr. Philip G. Harrison whose interest, guidance and friendship over many years has been a source of continual stimulus. Also to Dr. Mohamed Aslam for his cheerful friendship which has extended my scientific and cultural horizons.

Thanks are also due to Professor C.C. Addison who encouraged and enabled my studies to begin, and to his successor, Professor J.J. Turner, who ensured their continuance. I am grateful to Mr. R.A. Fleming for his stimulating company during our studies together and to members of the Technical Staff, in particular Mr. I.R. Marshall, for experimental assistance.

Perhaps most important, my gratitude must go to my wife, Carolyn, who, not only most efficiently prepared this typescript, but has sustained me along the tortuous path to its conclusion; not least with my two sons Graham and Stuart who provided some light on the way. My acknowledgements would not be complete without expressing my appreciation to my parents who started it all.

CHAPTER ONE

INTRODUCTION: THE CHEMISTRY OF TIN AND ITS COMMERCIAL APPLICATIONS

1.1 THE METAL

Tin is a member of Group IVB of the Periodic Table and has an atomic number of 50. Its atomic weight of 118.69 is an aggregate from the contributions of ten naturally occurring isotopes (Table 1.1).

Table 1.1 Natural Isotopes of Tin

ISOTOPE	^{112}Sn	^{114}Sn	^{115}Sn	^{116}Sn	^{117}Sn	^{118}Sn	^{119}Sn	^{120}Sn	^{122}Sn	^{124}Sn
% ABUNDANCE	0.95	0.65	0.34	14.24	7.57	24.01	8.58	32.97	4.71	5.98

It is estimated to form 0.0004 percent of the earths crust and occurs naturally as the tin(IV) oxide, cassiterite (78.6% Sn). The principal sources of the ore are in Malaysia, Indonesia, Bolivia and Nigeria, with a small deposite remaining in Cornwall. Extraction of the metal is achieved by floatation to remove the lighter rocks, such as silica followed by roasting. This oxidises many contaminant metals such as iron, copper and bismuth which can then be washed out by acid. The remaining cassiterite is reduced by carbon in a blast or reverberatory furnace to yield crude tin.

Two allotropic crystalline modifications of the metal exist (Figure 1.1). Below $18^{o}C$ the stable form is α-tin (grey tin) which has four tetrahedral bonds giving a three-dimensional covalent crystal with a structure analogous to the diamond form of carbon.

β-Tin (white tin), which is the stable isotope above 18°C, has a distorted close-packed lattice with four nearest neighbours at 3.01Å and two further neighbours at 3.175Å.

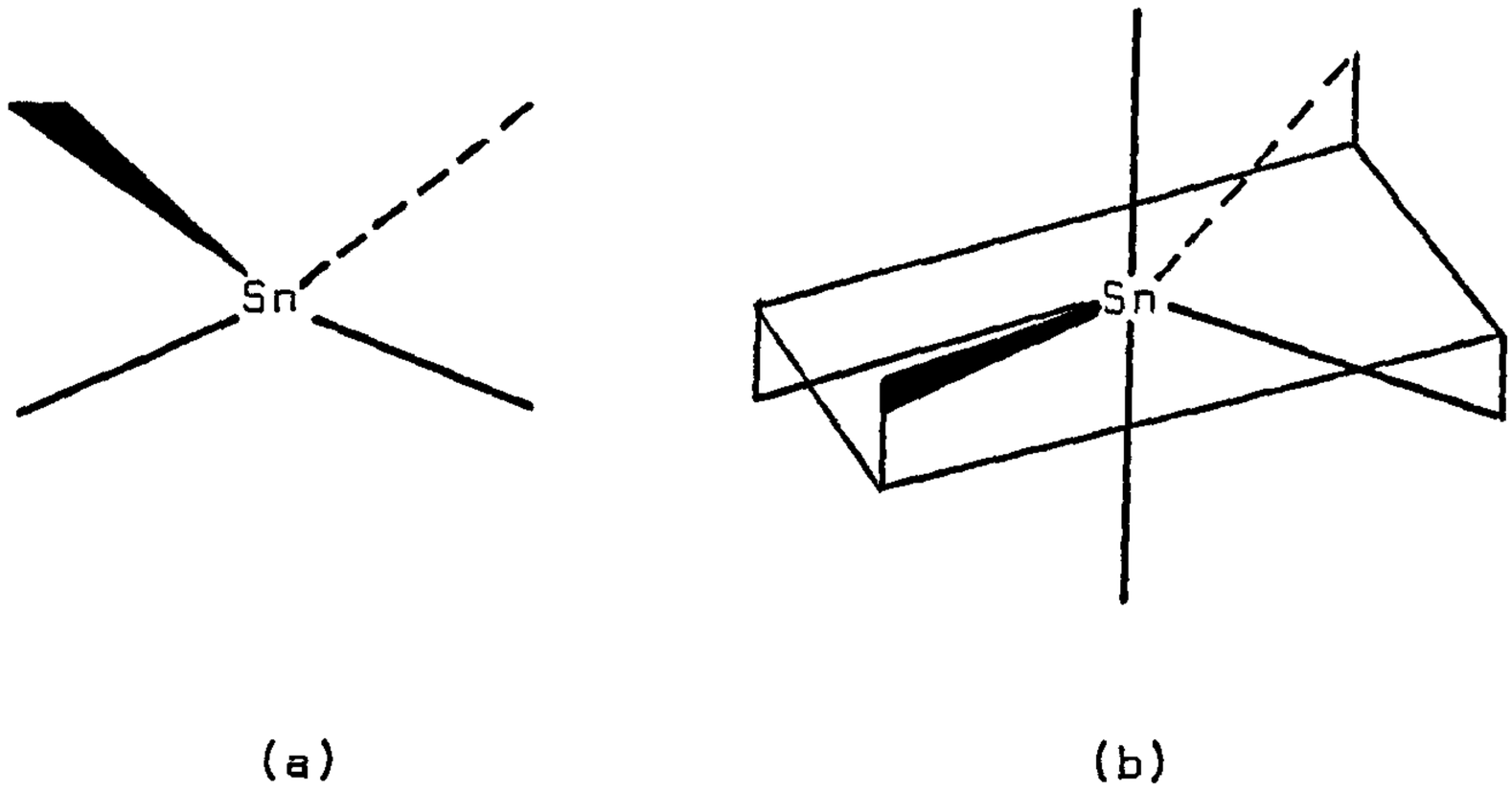

(a) (b)

Figure 1.1 Allotropic Modifications of Tin

a) Tetrahedral environment of α-tin (cubic)

b) Distorted octahedral environment of β-tin (tetragonal)

At normal temperatures tin metal is both moisture and air stable, and is only slowly attacked by dilute acids to yield tin(II) salts and hydrogen. Corrosion of the metal does occur when in contact with a variety of dilute solutions, e.g. potassium hydroxide, silver nitrate, zinc chloride, iron(III) chloride, aluminium chloride, ammonium sulphate and the halogens amongst others. In hot alkali solutions hydrogen is evolved with the formation of a hexahydroxy-stannate(IV):

$$Sn + 4H_2O + 2OH^- \longrightarrow [Sn(OH)_6]^{2-} + 2H_2\uparrow$$

Finely divided, the metal will react with a solution of sodium in liquid ammonia to yield to red, ionic compound Na_4Sn_9[187] which contains the Sn_9^{4-} polyanion which has a novel capped antiprismatic structure with C_{4V} symmetry[188].

Tin is widely used in plating mild steel or iron to resist corrosion (tin plate). In addition, it is one of the most important alloying metals forming, for example, the various bronzes with copper, and fusible alloys with bismuth and lead (Table 1.2). Because of their relatively low melting points (e.g. Woods metal m.p. 70°C), the fusible alloys are often used in fire warning devices.

Table 1.2 Some Tin Alloy Compositions

ALLOY	PERCENT METAL					
	Sn	Cu	Pb	Bi	Sb	Other
Phosphor Bronze	10	79.7			9.5	P0.8
Gun Metal Bronze	10	90				
Medal Bronze	8	90				Zn2
Soft Solder	50		50			
Fusible Alloy	15		32	53		
Woods Metal	12.5		25	50		Cd12.5
Tinfoil	88	3	8		1	
Pewter	85	7		6	2	
White Metal	5	1	75		19	

1.2 BONDING IN TIN COMPOUNDS

Tin has the ground state electronic configuration $[Kr]4d^{10}5s^{2}5p^{2}$.

1.2.1 Tin(II) Compounds

These can be formed in several ways.

i) In the ground state, using the two unpaired p-electrons without the $5s^2$ the covalent bond angle in an SnX_2 molecule would be 90^o. However, hybridisation generally occurs. An ideal sp^2 situation would, of course, result in a 120^o covalent bond with a lone pair of electrons directed along the axis of symmetry, (I).

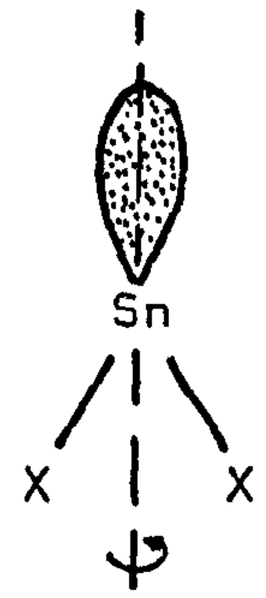

(I)

Structure determination of dicyclopentadienyltin(II) in the gas phase using electron diffraction showed penta-hapto bonding of the C_5 rings to the metal with the angle subtended at tin being ca. 125^o [101]. A consequence of such bonding will be the sterochemical activity of the lone-pair in the sp^2 hybrid orbital, and the facile formation of complexes of the type $(C_5H_5)_2Sn.M^{III}X_3$ ($M^{III}X_3 = BF_3$, BBr_3, $AlCl_3$)[102,103] and $(C_5H_5)_2Sn.M(CO)_5$ (M = Cr, Mo, W)[104] supports this hypothesis. Alternatively compression of the X - Sn - X bond angle can occur. Raman studies on $SnCl_2$ and $SnBr_2$ isolated in Ar or N_2 matrices[105] gave spectra which were consistent with the 'bent' structure deduced by Lister and Sutton[106] for the vapour phase using electron-

diffraction. In this case the valence angle was found to be 95^{o}, although in the condensed phase the structure of the dihalides is more complex[107].

ii) SnX_3^- species can be rationalised by involving $\underline{sp}^3$ hybridisation[108] resulting in a ψ-tetrahedral grouping with atoms at 3 corners of the tetrahedron and a lone pair at the fourth. The SnX_2 bonds and directional lone pair are retained with coordination of the X^- into the vacant $\underline{sp}^3$ orbital. Examination of the X - Sn - X bond angles in a number of $SnCl_3^-$-containing systems (Table 1.3) show values around 90^{o}, indicative of essentially p^3 hybridisation for the metal, in which case the lone pair of electrons is located in the 5s orbital : a proposal which is strengthened by the poor donor qualities to main group Lewis acids of the SnX_3^- system, thus implying considerable s-character in the lone pair.

Table 1.3 X-Sn-X bond angles for complexes containing discrete SnX_3^- anions, (X = Cl, F)

Compound	X - Sn - X valence angles (°)		
$CsSnCl_3$ [a]	86.9	92.3	90.2
$KCl.KSnCl_3.H_2O$ [b]	87.7	87.7	90.8
NH_4SnF_3 [c]	83.1	85.3	85.9
$Co(dpe)_2Cl^+$ $SnCl_3^-$ [d,e]			
red isomer	94.8	93.9	94.6
green isomer	91.4	96.2	93.5

a. ref. 111, b. ref. 112, c. ref 113, d. ref. 114

e. $(dpe)_2$ = bis(diphenylphosphino)ethane

However, with transition metals the donor properties are improved, probably because the tin - metal acceptor bond is strengthened by π-back bonding between the metals[109].

iii) The second ionization potential of tin is only 14.63 eV and hence the loss of the two 5p - electrons to form the dipositive ion of $5s^2$ configuration readily occurs. Orgel[110] has suggested from crystal field arguments that their is evidence for the ability of the stannous ion to adopt its first excited state of $5s^1p^1$ which differ by only 6.64 eV from the $5s^2$ ground state[115]. Clearly, such s - p mixing should lead to extra stability and distortion from the regular octahedral environment expected for the stannous ion. Such distortion is observed in the structures of $SnCl_2$[116,117], SnF_2[118], $SnSO_4$[119], SnS[120], SnSe[121], $NaSn_2F_5$[122] and $KCl.KSnCl_3.H_2O$[112]. In $NaSn_2F_5$ the $Sn_2F_5^-$ ion consists of two SnF_3^- ions sharing a fluorine atom, and in $KCl.KSnCl_3.H_2O$, Ψ-tetrahedral $SnCl_3^-$ and Cl^- ions are observed.

1.2.2 Tin(IV) Compounds

Tin(IV) systems result from three distinct bonding mechanisms

i) loss of the four electrons from $5s^2p^2$ resulting in the stannic ion Sn^{4+} (radius 0.74Å). Whilst $5s^0p^0$ should result in a regular octahedral coordination for tin in the ionic lattice, partial covalent character appears to cause some tendency towards tetrahedral geometry.

ii) Four covalent bonds are formed by hybridisation of available 5s and 5p orbitals resulting in sp^3 tetrahedral symmetry;

R_nSnX_{4-n},(n=1-4) compounds result.

iii) By use of the empty 5d orbitals, which are of similar energy to the 5s and 5p, in complex formation. Thus in $Me_3SnCl.C_5H_5N$, sp^3d hybridisation results in a trigonal bipyramidal environment around the five-coordinate tin. Whilst sp^3d^2 hybrid orbitals are utilized in octahedral molecules or ions of the type L_2SnCl_4 and $SnCl_6^{2-}$.

1.3 THE STEROCHEMISTRY OF TIN COMPOUNDS

Some examples of the wide variety of geometries found in tin compounds are given in Table 1.4.

1.3.1 TIN(II) COMPOUNDS

The structural chemistry of bivalent tin has been reviewed by Harrison[107]. The conformations about the metal atom resulting from various available coordination arrangements are exemplified by the compounds discussed below.

A Ψ-trigonal structure has been found for two-coordinate $Sn(C_5H_5)_2$[101] and $SnCl_{2(g)}$[105]. However, in the condensed phase tin dichloride has a metal atom surrounded in the lattice by nine halogen atoms from three different layers (Figure 1.2).

Addition of water to give the $SnCl_2$-monohydrate results in a three-coordinate tin atom with trigonal pyramidal geometry. In the crystalline dihydrate, alternating layers of $SnCl_2(OH_2)$ units are held together by hydrogen-bonding from interspersed layers of water of crystallization[123].

Table 1.4 The Stereochemistry of Tin Compounds

Valence State	Coordination Number	Geometry	Example
Sn(II)	2	Ψ -trigonal	$SnCl_{2(g)}$ [105]
			$Sn(C_5H_5)_2$ [101]
	3	Ψ -tetrahedral	$SnCl_2.2H_2O$ [123]
		trigonal-pyramidal	$KSn(O_2CH)_3$ [124]
	4	Distorted pyramidal	$SnSO_4$ [125]
	5	Ψ -Octahedral	SnO [126] (blue-black form)
	6	Distorted triangular prism	$Sn(EDTAH)_2$ [127]
	7	Pentagonal bipyramid	$Sn^{II}[Sn(EDTA)H_2O]H_2O$ [128]
Sn(IV)	4	Trigonal bipyramidal	$SnCl_5^-$ [131]
			$Ph_3PCHCO.Me$ Me_3SnCl [132]
	6	Octahedral	$SnCl_6^{2-}$ [133]
			$Sn(S_2CNEt_2)_4$
	7	Pentagonal bipyramid	$(C_7H_5O_2)_3SnCl$ [134]
			$MeSn(NO_3)_3$ [135]
	8	Dodecahedral (Square antiprism at tin)	$Sn(NO_3)_4$ [136]

Figure 1.2 Coordination of tin in the $SnCl_2$ lattice

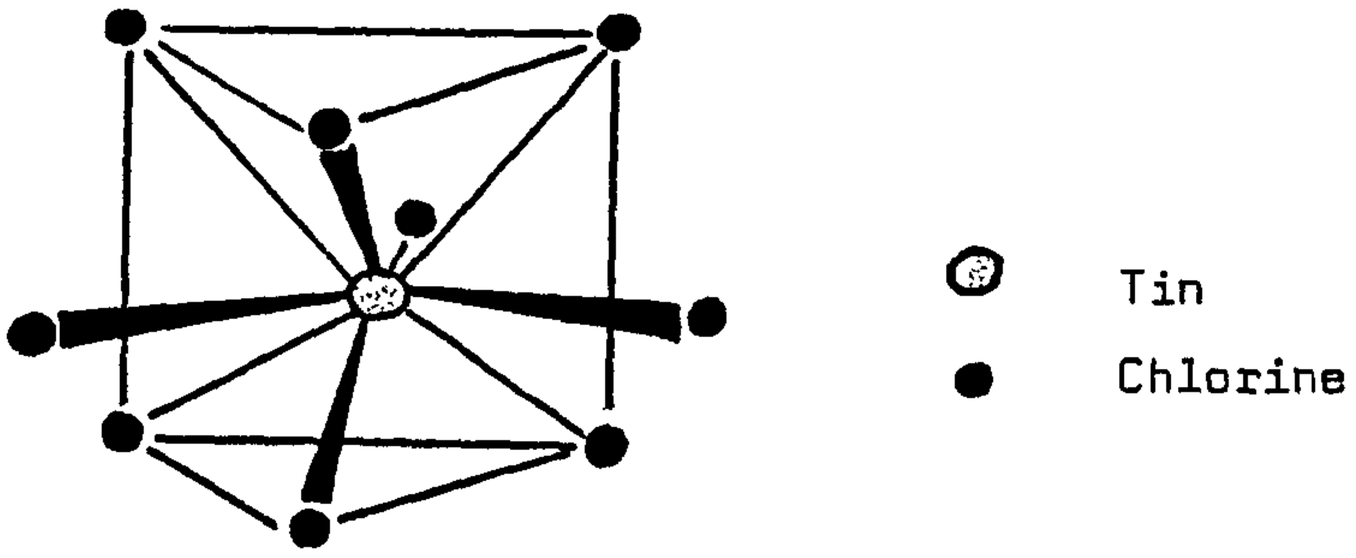

The distorted pyramidal geometry about tin in $SnSO_4$ results from four-coordination to the tin(II)[125]; O-Sn-O bridges link together a framework of sulphate groups. The Sn-O bonding about tin in tin(II) oxide results in a tetragonal lattice with the metal at the apex of a distorted square-pyramid of oxygen atoms. Five-coordination in the blue-black form of tin(II) oxide is achieved by having five oxygens approximately at the verticies of an octahedron. The sixth vertex presumably being occupied by a lone pair[126].

Dihydrogen ethylenediamine tetra-acetatostannate(II) has six-coordination, comprising two nitrogen and four oxygen atoms; the metal atom being centred in the rectangular face of a distorted triangular prism[127]. Distannous ethylene diaminetetraacetate dihydrate has the two tin atoms in different environments. One tin atom experiences pseudo-seven-coordination in a pentagonal bipyramidal arrangement. The tin lone-pair and two nitrogen atoms occupy

equatorial positions whilst the remaining coordination sites are taken up by oxygen atoms from the chelating EDTA molecule; carboxylate bridges connecting this seven-coordinate tin to the other metal atom[128].

1.3.2 TIN(IV) COMPOUNDS

The majority of organotin compounds are tin(IV), four-coordinate species. However, it is only in R_4Sn and SnX_4 compounds in the gas phase that true tetrahedral geometry is approached[129,130]. Generally weak intermolecular forces in the solid phase cause considerable distortions from this ideal. Such distortions from regularity also occur in five-coordinate tin-species. These are based on trigonal-bipyramidal geometry and examples include the pentachlorostannate anion, $SnCl_5^-$ [131], and the triphenylphosphine acetylmethylene complex with Me_3SnCl[132].

There is a significant number of tin(IV) six-coordinate complexes known. Amongst the earliest to have their structure determined were the hexachlorostannate anions in caesium, rubidium, potassium, ammonium and thallous salts[133]. Several of the estertin compounds described in this work also fall into this category. Examples of seven-coordination at tin(IV) are less frequently encountered. The bidentate nitrate groups in crystalline anhydrous methyltin trinitrate result in a pentagonal bipyramid about tin[135]; a similar structure being achieved, again by bidentate chelation, from the tropolonate ion, $C_7H_5O_2^-$ in the tris(tropolonato)monohydroxy- and mono-chlorotin(IV)[134].

Interaction of N_2O_5 with $SnCl_4$ results in $Sn(NO_3)_4$. As in $MeSn(NO_3)_3$ the nitrate groups act as bidentate ligands, here resulting in eight-coordination at tin which thus has a dodecahedral structure[136]. However, few other eight-coordinate tin systems are known.

1.4 BONDS ABOUT TIN

1.4.1 BOND DISSOCIATION ENERGIES AND ELECTRONEGATIVITIES

Bond dissociation energies can provide a guide to reactivity in a series of compounds. The most recently compiled data for Group IVB compounds are those of Jackson[137]. These confirm the general trend first noted by Skinner[138], who found bond dissociation energies (D) fall as the sub-group is descended: the order being D(C-R) > D(Si-R) D(Ge-R) > D(Sn-R) > D(Pb-R). Values for $D(Me_3M—X)$ in compounds of the type Me_3MX (M = C, Si, Ge, Sn, Pb) are given in Table 1.5

Table 1.5 Bond dissociation energies for $(Me_3M—X)$[a, 137]

X	M				
	C	Si	Ge	Sn	Pb
H	440	377	343	310	(260)
CH_3	377	377	318	272	205
MMe_3	377	339	306	234	230
OH	385	527		460	
OEt	343	465	448	352	
Cl	252	465	486	423	
Br	297	394	435	356	

([a], in $KJmol^{-1}$)

However, because the data are derived from homolytic bond fissions of the type

$$Me_3SnX \longrightarrow Me_3Sn^{\bullet} + X^{\bullet}$$

such values do not reflect the ease of heterolysis which is the predominant mode of bond fission. To enable that to be established it is necessary to have a knowledge of the ionicity of the bond. Unfortunately, because their is no satisfactory method of establishing direct electronegativity values, such data for Group IVB elements remain a controversial subject. Indeed, implicit in the Pauling definition of electronegativity[139] "the power of an atom in a molecule to attract electrons to itself", is the fact that the value will be dependent on the molecular environment. The values derived by Allred and Rochow[140] have, so far, the most physical and chemical supportive evidence. The data obtained gave values of C, 2.60; Si, 1.90; Ge, 2.00; Sn, 1.93; Pb, 2.45 and whilst this order has been criticised[141] it emphasizes the polarity of the tin-carbon bond.

1.4.2 BONDING DISTANCES AND NON-BONDING INTERACTIONS

The single-bond covalent radii for a number of elements are listed in Table 1.6. Overall these provide a reasonable guide for internuclear distances in tin compounds.

Table 1.6 Some single bond covalent radii (Å)[108]

Sn	1.40	H	0.28	C	0.77
O	0.66	N	0.70	P	1.10
S	1.04	Cl	0.99	Br	1.14
I	1.33	F	0.64		

However, in order to obtain the limits of bond length which provide the best fit for the majority of organotin compounds much of the available structural data[107,142] has been examined and the results presented in Table 1.7.

Table 1.7 The range of bond lengths involving tin

BOND	BOND LENGTH (Å)
Sn-H	1.7 - 1.8
Sn-C	2.1 - 2.25
Sn-N	2.15 - 2.3
Sn-F	1.9 - 2.2
Sn-Cl	2.3 - 2.55
Sn-Br	2.5 - 2.6
Sn-I	2.6 - 2.85
Sn-O	2.1 - 2.8
Sn-S	2.5 - 2.85

Whilst bonding distances are, clearly, the primary factor in the stereochemistry of a particular compound, non-bonding interactions also produce geometrical constraints when the approach is sufficiently

close. Intermolecular contacts can be considered in terms of van der Waals radii[186] (some examples are given in Table 1.8). Intramolecular forces must also be considered in this context, however.

Table 1.8 Some van der Waals radii (Å)[186]

H	1.1	N	1.46	O	1.42	S	1.80
F	1.40	Cl	1.75	Br	1.87	I	2.05
Ge	1.98	Sn	2.16				

Bartell[143] introduced a set of radii which define the minimum distance of approach of two atoms X and Y in a fragment XMY. The results he obtained have been refined by Glidewell[144-146]. The covalent radius of X in XMY refers to the direction towards M, the van der Waals radius refers to the direction away from M, Bartell's 'one-angle' radius is defined as the radius of atom X in the direction of Y. The intramolecular radii defined in this manner for a number of elements are listed in Table 1.9.

Table 1.9 Intramolecular radii (Å)[146]

C	1.25	N	1.13	O	1.12	F	1.08
P	1.45	S	1.45	Cl	1.44	Br	1.59
I	1.75	Sn	1.82				

1.5. METHODS OF TIN-CARBON BOND SYNTHESIS

Whilst tin metal has many commercial applications as alloys, tinplate etc., in recent years it is the utilization of organotin compounds which has seen the greatest growth. Methods for the formation of tin-carbon bonds are thus of major chemical interest.

Historically organotin compounds were prepared from organomercury or organozinc compounds[147].

$$SnCl_2 + R_2Hg \longrightarrow R_2SnCl_2 + Hg$$

$$SnCl_2 + R_2Zn \longrightarrow [R_2Sn]_n + ZnCl_2$$

$$SnCl_4 + 2R_2Zn \longrightarrow R_4Sn + 2ZnCl_2$$

Currently four different methods are in use for the technical manufacture of organotin compounds, and are similarly applicable on a laboratory scale. In three of these the preparation of R_4Sn compounds from $SnCl_4$ constitutes the first reaction step. These are, namely, the Grignard, the Wurtz and the alkyl aluminium or lithium methods:

$$SnCl_4 + 4RMgCl \longrightarrow R_4Sn + 4MgCl_2$$

$$SnCl_4 + 4RCl + 8Na \longrightarrow R_4Sn + 8NaCl$$

$$3SnCl_4 + 12RM \longrightarrow 3R_4Sn + 12MCl$$

$$(M = Li \text{ or } \tfrac{1}{3} AL)$$

When R = phenyl, the Grignard methods has, so far, proved the most useful and is also widely used commercially in the production of tetrabutyl and tetraoctyltin. Generally, in both the metalalkyl and Grignard reactions the yields for secondary and tertiary aliphatic

groups is poor due to steric hinderance. Formation of organotin halides as byproducts is normally supressed by addition of excess metal reagent. In the case of the Grignard reaction the reagent is usually generated *in situ* by running the organic halide into the tin tetrahalide and magnesium metal mixture, often in a hydrocarbon solvent or the ether, tetrahydrofuran.

The Wurtz synthesis of organotin compounds was originally developed at the Organisch Chemisch Instituut, TNO, Utrecht[148] and is used on a technical scale in both the U.S.A. and East Germany for the manufacture of tetrabutyltin. The reaction is carried out so that equimolar amounts of tetrabutyltin and tributyltin chloride are formed as products. The overall reaction is:

$$2SnCl_4 + 7BuCl + 14Na \longrightarrow Bu_4Sn + Bu_3SnCl + 14NaCl$$

The fourth method of synthesis of tin - carbon bonds which is of particular commmercial interest is, in certain respects, analogous to the Rochow Process for organosilicon halides[149,150]. It involves the direct interaction of alkyl and aryl halides with metallic tin in the absence of a solvent, for example,

$$MeCl + Sn \xrightarrow{175^{o}C} \underset{(6.6\%)}{MeSnCl_3} + \underset{(39\%)}{Me_2SnCl_2} + \underset{(4.6\%)}{Me_3SnCl}$$

The R_2SnX_2 in all cases being the principal product. Catalysts are required : on a laboratory scale, small amounts of iodomethane or triethylamine will suffice[147]. Commercially quaternary ammonium and phosphonium compounds, bifunctional ethers as well as inorganic antimony compounds have been used[148].

The advantage of the direct method over the previous reaction systems described is the elimination of a second step to obtain the more practically important organotins with a lower degree of organic substituents. Thus in the Wurtz, Grignard and metal alkyl syntheses a disproportionation reaction with $SnCl_4$ is required:

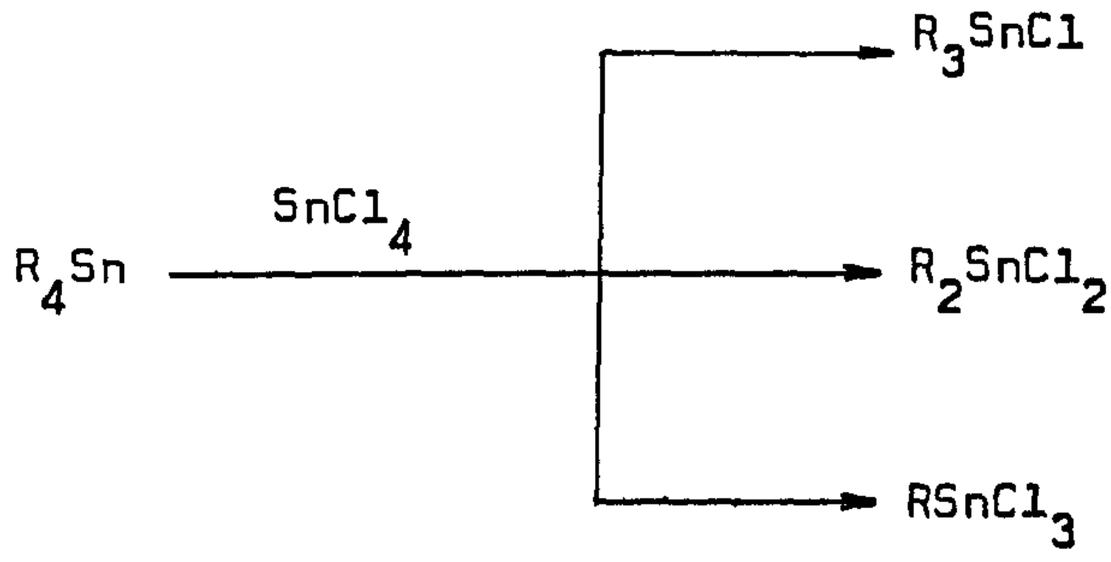

In recent years interest has grown in the use of monoalkyltin compounds as synergists for the dialkyltin PVC stabilizers (*vide infra*). Whilst the monoalkyltins are available from R_4Sn via the redistribution reactions mentioned, a convenient oxidative-addition reaction for their manufacture has been developed which greatly reduces the formation of the di- and trialkyltin byproducts whilst optimizing the monoalkyltin yield[151]. This again uses an antimony species as catalyst.

$$SnCl_2 + RX \xrightarrow[R_3Sb]{\text{catalyst}} RSnCl_2X$$

R = alkyl (C_1 - C_{18})

X = Cl,Br.

The recently developed reaction for the production of estertin intermediates for organotin PVC stabilizers will be discussed

in detail in Chapter 2.

Laboratory scale preparation of tin-carbon bonds has been achieved in a number of ways; several are illustrated below[147].

$$SnCl_4 + 4CH_2N_2 \longrightarrow (CH_2Cl)_4Sn + 4N_2$$

$$SnCl_2 + PhN_2Cl \longrightarrow PhSnCl_3 + N_2$$

$$SnCl_4 + 4PhC{:}CNa \longrightarrow (PhC{:}C)_4Sn + 4NaCl$$

$$SnCl_2 + CH_3Cl \longrightarrow CH_3SnCl_3$$

$$K_2SnO_2 + CH_3I \longrightarrow K\,CH_3SnO_2 + KI.$$

Similarly, metathetical reactions or intermolecular hydride additions have been used in tin-carbon heterocyclic systems.

(a) [152]

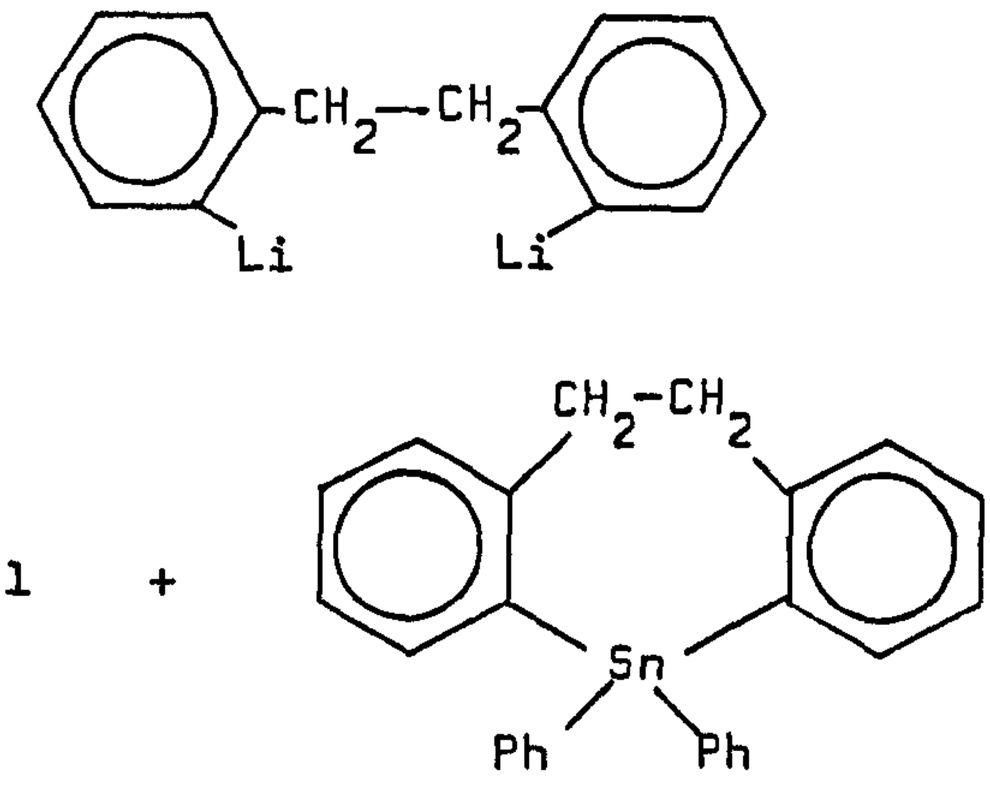

(b) [153]

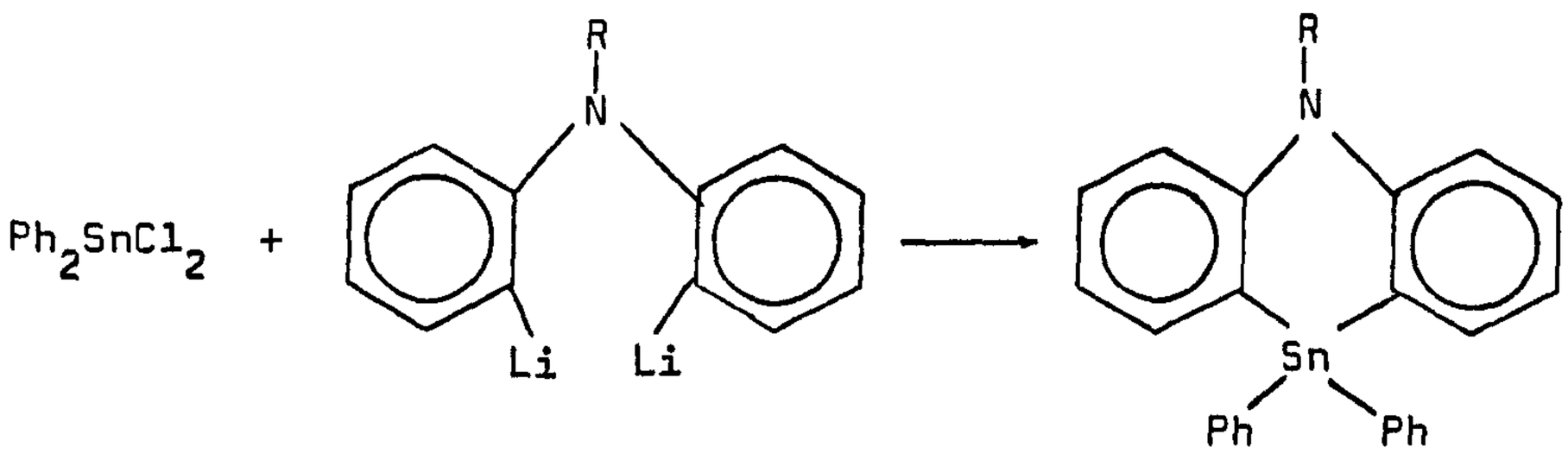

With stannic chloride, spirocyclic systems result:

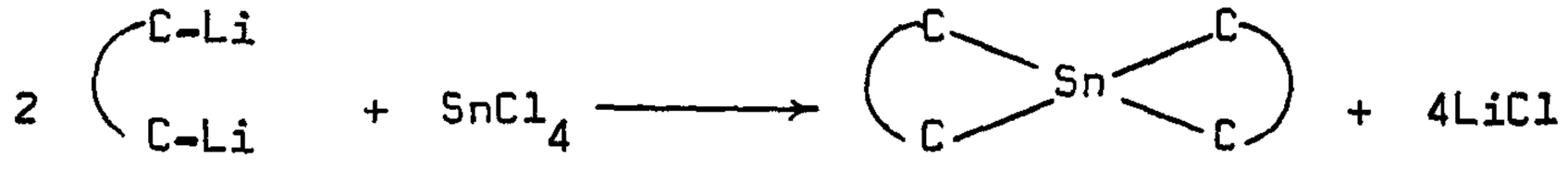

Some measure of the synthetic importance and the extent of products available from simple tin-carbon systems is illustrated by the reaction scheme shown in Figure 1.3.

Unsymmetrical organotins of the type R_3SnR' and R_2SnR_2' can be prepared by modification of a number of the reactions described. For example, the reaction between stannic chloride and a Grignard reagent prepared from an equimolecular mixture of methyl iodide and ethylbromide gives diethyldimethyltin as principal product[154].

Dicyclopentadienyltin(II), $(C_5H_5)_2Sn$, was the first stable divalent monomeric organotin(II) derivative to be prepared[155-156]. It has an angular sandwich structure[101] and the cyclopentadienyl rings are readily removed by protic reagents, enabling many previously inaccessible tin(II) derivatives to be prepared[157] (Table 1.10).

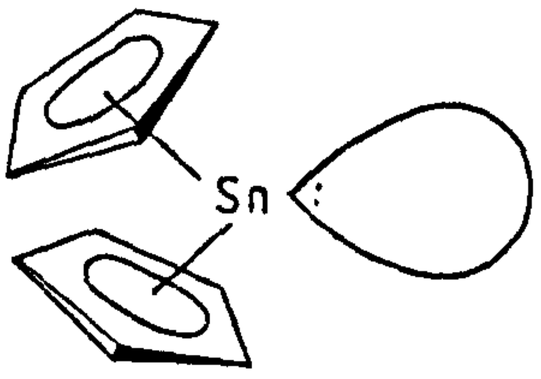

Novel methods of tin-carbon bond synthesis are continually being developed (see, for example, Tin Annual Surveys[158]). However, few of these are of any practical significance to the commcerical production of organotin compounds.

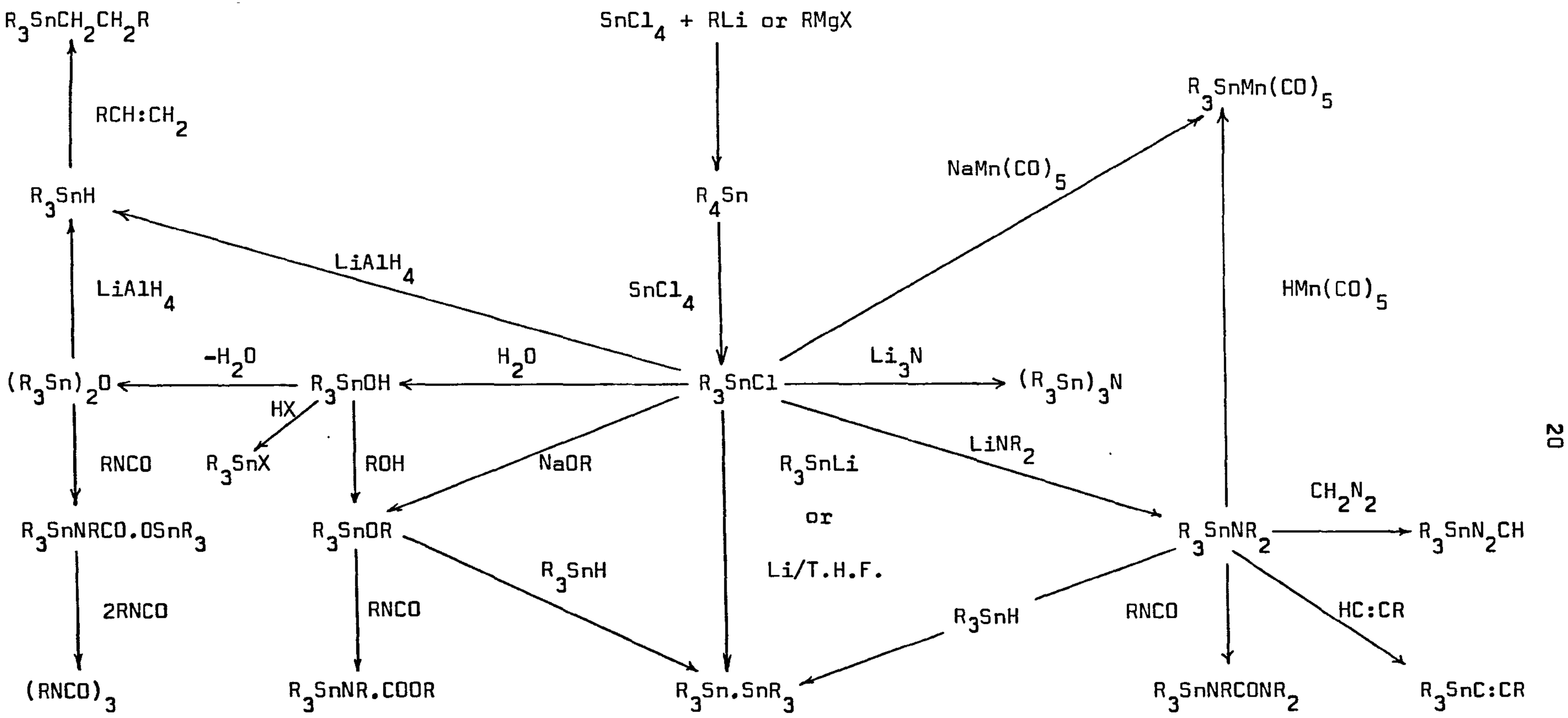

Figure 1.3 Some derivatives available from organotin halides.

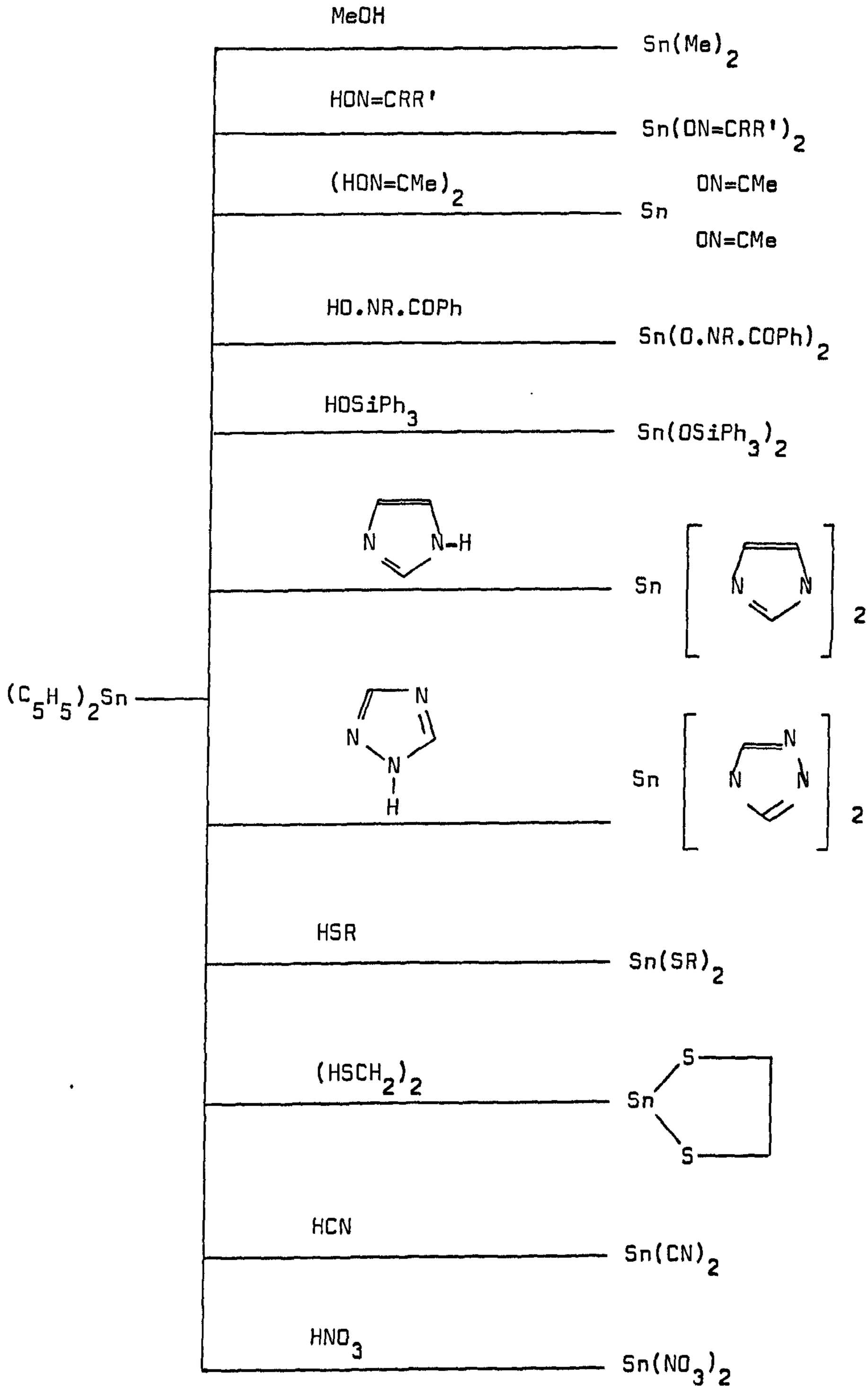

Table 1.10 Preparation of some divalent organotin derivatives.

1.6 PHYSICAL MEASUREMENTS ON ORGANOTIN COMPOUNDS

A wide range of physical techniques is avilable for the investigation of organotin compounds. However, the discussion herein will be restricted to the methods applied and specific aspects of each technique relevent to the systems described in this thesis. The principles of Mössbauer spectroscopy are described in some detail as it is of some considerable importance in tin chemistry and only the results will be discussed later.

1.6.1 VIBRATIONAL SPECTROSCOPY

(i) Tin-Carbon Stretching Frequencies[159]

The aliphatic tin-carbon stretching frequencies have been reported for an extensive range of tin(IV) compounds. The ν_{as} (Sn-C) mode causes absorption in the range 500-600cm^{-1} whilst the symmetric ν_s(Sn-C) vibration is observed between 470-530cm^{-1}.

The number of bands expected in the vibrational spectrum will, naturally, depend on the point group symmetry. Tetrahedral molecules of the type SnR_4 with Td symmetry will ideally give rise to two bands due to Sn-C in the infrared (F_2 + F_2) and four in the Raman spectrum (A_1 + E + F_2 + F_2). If one of the R groups is replaced by X giving R_3SnX compounds, the symmetry of the molecule is lowered to C_{3V}. Further replacement of R to give R_2SnX_2 results in C_{2V} symmetry. This lowering of symmetry splits the degenerate vibrations and activates infrared inactive vibrations as Table 1.11 illustrates. Thus, in principle the number of infrared

Table 1.11 Vibrational Modes for Tetrahedral Molecules and Spectroscopic Activity

Point Group	ν_1	ν_2	ν_3	ν_4
$Td(R_4Sn)$	$A_1(R)$ $\nu_s(R\text{-}Sn)$	$E(R)$ $\delta_d(R\text{-}Sn\text{-}R)$	$F_2(I,R)$ $\nu_d(R\text{-}Sn)$	$F_2(I,R)$ $\delta_d(R\text{-}Sn)R)$
$C_{3V}(R_3SnX)$	$A_1(I,R)$ $\nu(X\text{-}Sn)$	$E(I,R)$ $\delta(RSnR)$	$A_1(I,R) + E(I,R)$ $\nu(RSn)$ $\nu_d(RSn)$	$A_1(I,R) + E(I,R)$ $\delta(R\ SnR)$ $\rho_r(R_3Sn)$
$C_{2V}(R_2SnX_2)$	$A_1(I,R)$ $\nu(X\text{-}Sn)$	$A_1(I,R) + A_2(I,R)$ $\delta(RSnR)$ $\rho_t(R_2Sn)$	$A_1(I,R) + B_1(I,R) + B_2(I,R)$ $\nu(RSn)$ $\nu(RSn)$ $\nu(XSn)$	$A_1(I,R) + B_1(I,R) + B_2(I,R)$ $\delta_r(XSnX)$ $\rho_r(R_2Sn)$ $\rho_w(R_2Sn)$

I, denotes an infrared active mode; R, denotes a Raman active mode.

active vibrations is increased to six in R_3SnX and nine in R_2SnX_2. The R-Sn and X-Sn modes are also indicated in Table 1.11.

Similar band patterns are observed for octahedral complexes, Cis-R_4SnX_2 compounds will have C_{2V} symmetry and exhibit six infrared R-Sn interactions whilst the trans-R_4SnX_2 compounds, which have D_{4h} symmetry, will show three Sn-C infrared active modes. Because of overlap of band contours the assignment of each active mode is not always readily achieved. Further complications may arise due to steric effects in different conformational isomers. For example, the ν(Sn-C) for butyltin trichloride shows two bands resulting from restricted rotation about the Sn-CH_2 — CH_2Et bond in isomers I and II[160].

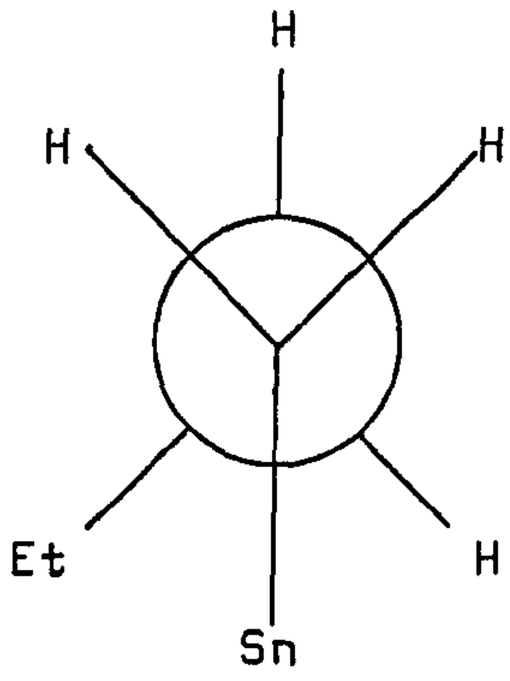

(I)

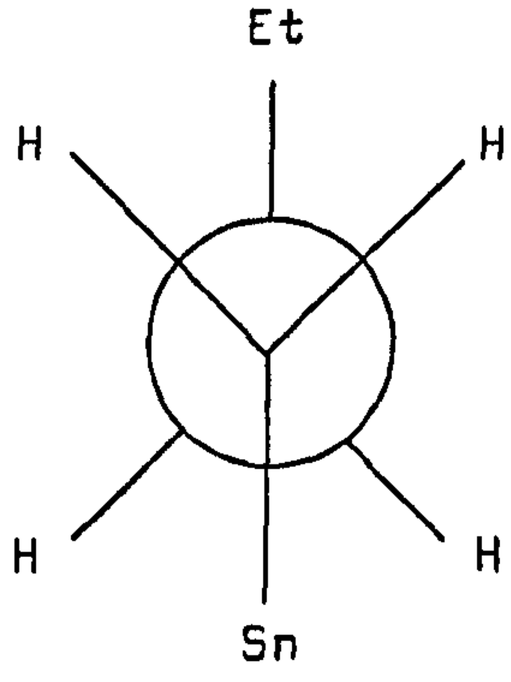

(II)

Generally, however, tin-halogen stretching vibrations are of more use in distinguishing stereochemical isomers.

Studies of methyltin halides[161] have indicated that electronic effects dominate the absorption position of ν(Sn-C). The more

electronegative the halogen and the greater the number of halogen substituents, the greater is the effective nuclear charge on tin and hence the higher the ν(Sn-C) frequencies.

Tin-carbon vibrations are not a particularly sensitive guide to changes in coordination number of the tin atom although it has been shown that in some cases the number of bands may be affected. Tetrahedral $Me_3SnOCOH$ in chloroform solution exhibits both ν_{as}(Sn-C) and ν_s(Sn-C) bands characteristic of a tetrahedral geometry but on addition of pyridine the ν_s(Sn-C) disappears as the 1:1 pyridine complex is formed and the methyltin groups assume a planar configuration[162].

Rocking modes for methyltin compounds have been assigned. They are usually rather strong broad bands in the range 770-791cm^{-1} and for ethyl compounds in the region 685-658cm^{-1} [163].

ii) Tin-Halogen Stretching Frequencies

The ranges observed for alkyl- and phenyltin halide stretching frequencies are ν(Sn-Cl) 385-318cm^{-1}, ν(Sn-Br) 264-222cm^{-1} and ν(Sn-I) 207-170cm^{-1}. This vibrational mode is a particularly sensitive indicator to coordination number changes about the tin. For example conversion of a four-coordinate dichloride to a six-coordinate adduct with a Lewis base causes a reduction in the frequency of the ν(Sn-Cl) bands by some 100cm^{-1} [163]. Wharf and Shriver[164] have also shown that the Sn-X stretching force constants of halogenotin compounds are approximately proportional to the oxidation number of the metal divided by the coordination

number of the complex.

The Sn-X vibrations can provide a useful guide to the point group and hence molecular symmetry of the molecule. For example, cis-R_4SnX_2 type compounds (C_{2V}) exhibiting two Sn-X stretching modes (A_1+B_2) whilst the trans isomer (D_{4h}) should give only one infrared active mode for Sn-X (A_{2u})[165]. Beattie and Rule[166] examined the infrared spectra of cis- and trans- R_2SnCl_4 - type compounds (R = acetone or trimethylamine). They found that the cis- complex is formed with acetone whilst introduction of the more bulky trimethylamine group forces trans geometry on the molecule.

1.6.2 Nuclear Magnetic Resonance

A description of the application of tin-119 magnetic resonance spectroscopy will be omitted from this section as a full treatment of the subject will be given in Chapter 4.

The proton magnetic resonance spectra of methyltin compounds are characterised by high field shifts resulting from the shielding by the metal, and occur in the range $+1 < Me_4Si < -0.5$ ppm. ^{119}Sn and ^{117}Sn satellites are resolvable and enable INDOR spectra to be recorded (Chapter 4). $J(^{119}Sn\text{-}C\text{-}H)$ coupling constants can provide an important probe for investigating the coordination number at tin, being representative of the s-electron density at the metal atom (see Table 4.7)

1.6.3 Mass Spectrometry

The polyisotopic distribution of tin is characteristic in the mass spectrum and considerably simplifies assignment of tin containing peaks. Data have been reported for the behaviour of a variety of organotin compounds[167,168].

1.6.4 Gamma Resonance Spectroscopy - The tin-119 Mössbauer Effect

The Mössbauer effect has been widely reviewed[169-171] and extensive studies made of resulting tin-119 spectra[172-174].

i) The Effect

The phenomenon of nuclear resonance absorption occurs when a gammaray emitted by a nucleus decaying from an excited state to a ground state is captured during excitation of a second nucleus from the ground state to the same excited state. This occurs when there is no dissipation of energy in the form of kinetic motion, i.e. the process is 'recoilless'. Such a condition can be achieved when the nuclei are constrained by embedding in a solid matrix. Thus, the Mössbauer effect is restricted to observations in the solid state.

If the lifetime of the excited state energy level is τ and its energy is E_γ, then the precision in the gamma ray energy, ΔE_γ, is governed solely by the Heisenberg Uncertainty Principle and is given by

$$\tau \Delta E_\gamma \geqslant h$$

h being Plancks constant. For a typical lifetime of 10^{-7}s

and an energy of 10keV the precision of the energy is $E_\gamma / \Delta E_\gamma = 1.5 \times 10^{12}$. In principle, therefore, it would be possible to measure interactions as small as 1 part in 10^{12}. In practice, however, 1 part in 10^6 is the best to which the absolute energy of the gamma ray can be determined. However, because ΔE_γ is of the order of magnitude of a Doppler energy shift from a relative motion with a velocity, V, of only a few mms^{-1}, it is possible to measure relative energies to a high degree of precision.

ii) The Experiment

The experimental procedure involves measuring the transmission rate of a series of different Doppler velocities (i.e. energies). Where resonance occurs their will be a decrease in count rate, typically of a few percent, giving rise to a Lorenzian line shape absorption. In principle, one moves the source with a constant velocity, v, for a fixed period of time and measures the total transmitted radiation. The process is repeated for successive increments of velocity, $v + \delta v$, until the region of interest has been scanned. In practice the entire range of velocities are scanned simultaneously using an electro-mechanical vibration unit in a constant acceleration mode which is driven in sequence with a multi-channel analyzer, each channel of which corresponds to a specific incremental velocity from v to $v + \delta v$. The gamma rays counted at each increment are thus stored in individual channels and together provide a record of the Mössbauer spectrum. Multiple scanning enhances the data by the square-root of the number

of accummulated counts. Hence 4 scans doubles the signal to noise ratio, 16 scans quadruples it, etc.

iii) Chemical Application

The chemical significance of Mössbauer spectroscopy derives from the interdependence of the nucleus on its electronic, and therefore chemical environment, Very weak (hyperfine) interactions between the electrons and the nucleus affect E_γ by quantities of the order of ΔE_γ . Whilst, in principle, any gamma ray transitions to the ground state of a nucleus can give rise to the Mössbauer effect, in many cases the magnitude of the recoil-free fraction, f_s, does not permit experimental measurement. However, tin-119 has proved particularly accessible to study. Fig. 1.4 shows the simplified decay scheme for the ^{119m}Sn source for ^{119}Sn 23.9keV Mössbauer resonances.

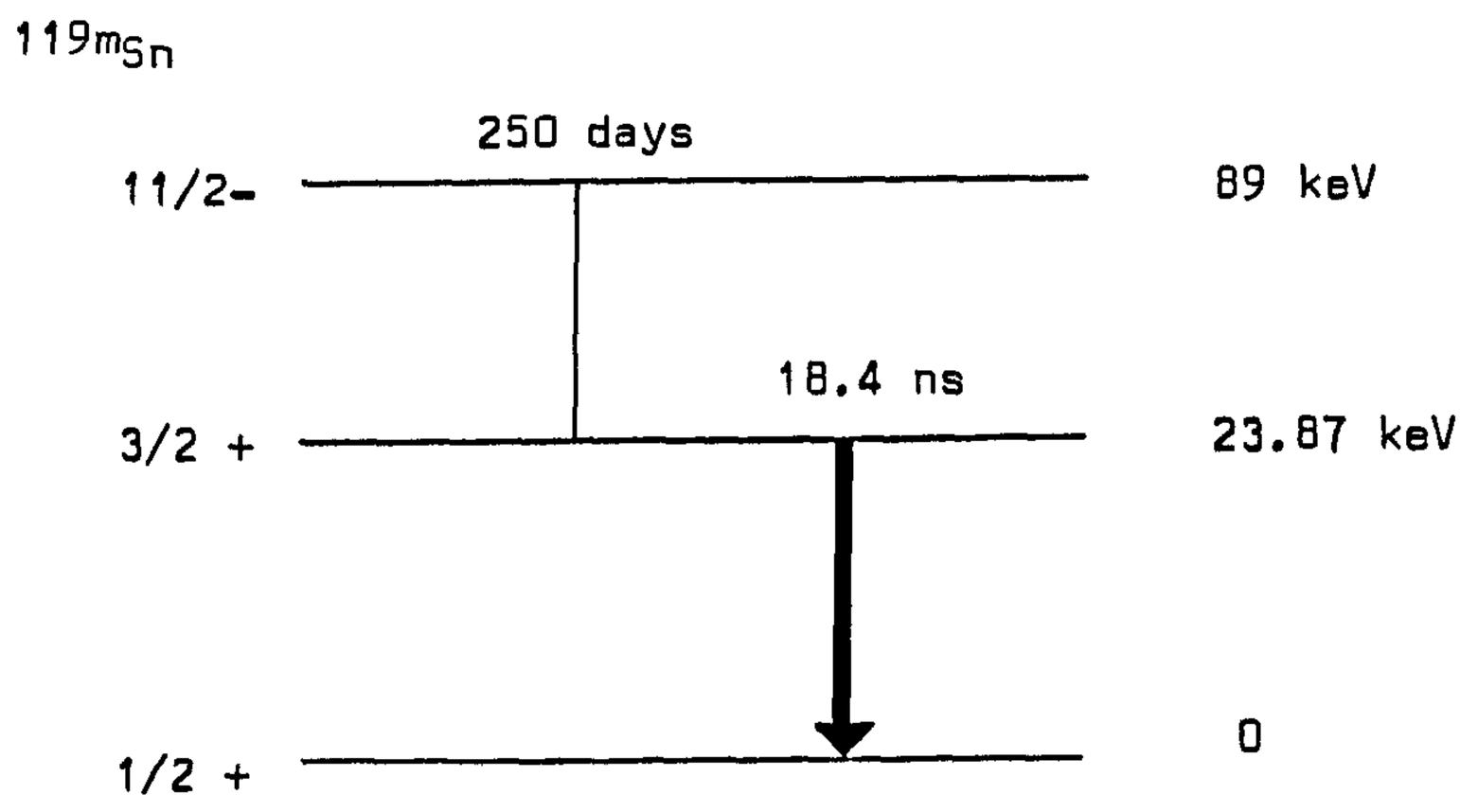

Fig. 1.4 The decay scheme of the ^{119m}Sn source for ^{119}Sn 23.9 keV Mössbauer resonances.

In the absence of a magnetic field two principle parameters are obtained; the isomershift I.S. and the quadrupole splitting, Q.S.

iv) Isomer Shift

Isomer shift is a measure of the 5s-electron density at the tin nucleus. The s-electron density has a finite probability of being found within the nuclear volume. Since during gamma decay there is a change in the radius of the nucleus, r, by a small value, δ r, the fraction of the electron within the nucleus also changes, giving rise to a concomitant alteration in electrostatic energy. Thus, unless the source and absorber (sample) in the Mössbauer experiment are chemically identical, a shift from zero velocity will result. This is called the isomer shift, δ , and is given by:

$$\delta = \frac{4\pi}{5} Z e^2 r^2 \left[|\psi(0)|^2_{absorber} - |\psi(0)|^2_{source} \right] \frac{\delta r}{r}$$

Z is the nuclear charge, e is the electronic charge and the value ψ (0) refers to the s-electron density at the nucleus, As the equation is a product of a chemical term relating to s-electron density, and a nuclear term which is constant for a given isotope, the chemical shift is given by

$$\delta = \text{constant} \frac{\delta r}{r} |\Psi_s(0)|^2$$

r = nuclear radius

δ r = change in nuclear radius from excited to ground state.

This is usually measured relative to a given standard (In this study $CaSnO_3$ = 0 mms^{-1}). For tin δ r/r is positive and hence an increase in δ denotes an increase in 5s-electron density at the tin nucleus.

v) Quadrupole splitting

When the environment of the resonant nucleus has non-cubic symmetry an electric field gradient at the nucleus will result. The gradient is the second differential of the electric potential and is a Cartesian coordinate system which may be defined by nine terms of the form;

$$\frac{\partial^2 V}{\partial x \, \partial y}$$ x, y and z being the axes.

If the z axis is defined as the direction of maximum gradient then two parameters are sufficient to specify the complete field gradient,

$$Vzz = \frac{\partial^2 V}{\partial z^2}$$ and an asymmetry parameter,

$\eta = (V_{xx} - V_{yy}/Vzz)$. Vzz is a vector quantity and therefore,

in principle, can have positive and negative values.

When the nuclear spin state $I > \frac{1}{2}$, it has a quadrupole moment, Q, which can align in the field gradient in several directions. For tin the first excited state has $I = {}^{3}/2$ giving two energy states separated by the quadrupole splitting, Q.S.

$$Q.S. = \frac{e^2qQ}{2}\left[1 + \frac{\eta^2}{3}\right]^{\frac{1}{2}}$$

$$= \text{constant. } q\,Q.$$

Whilst the ground state of ^{119}Sn does not have a quadrupole moment, the first excited state does. The degeneracy is, therefore, removed and two lines result in the spectrum (Fig. 1.5). The separation in the peaks is the difference in energy between the two excited states and is the quadrupole splitting, whilst the centroid of the quadrupole split doublet is the isomer shift.

vi) Spectral data

The decrease from 2 to 0 in the 5s subshell population on going from tin(II) to tin(IV) would be expected to produce a similar decrease in isomer shift. The two allotropes of tin metal, the tetrahedral α -form (I.S. = 2.10mms^{-1}) and the tetragonal β-form (I.S. = 2.65 mms^{-1}) are both formally tin(0) and therefore should provide a dividing line between tin(II) and tin(IV). However, such a generalisation is an over simplification. In covalent compounds where complete electron transfer does not occur, Mössbauer isomer

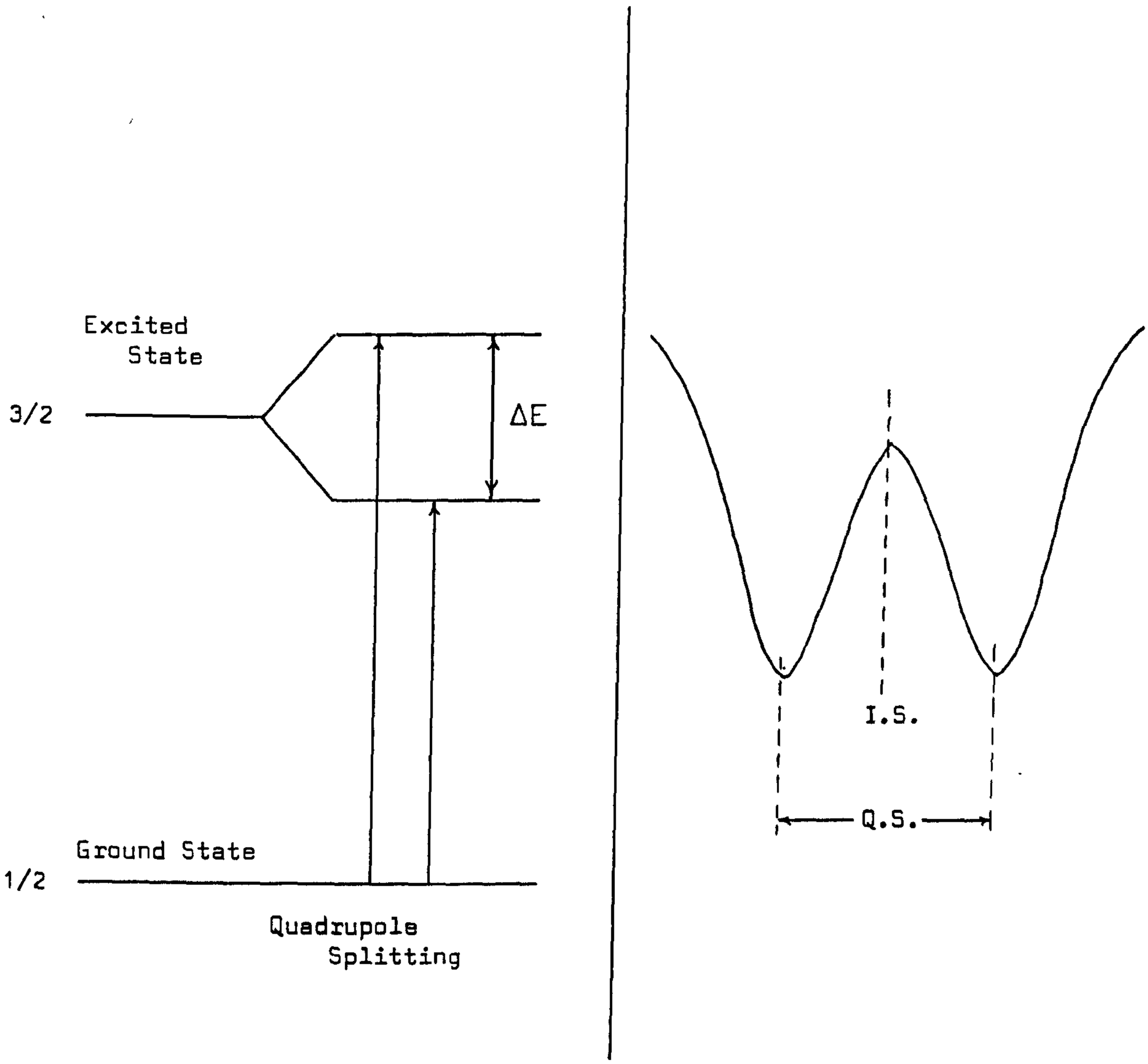

Figure 1.5 The origin of isomer shift and quadrupole splitting.

shifts can not be categorized on oxidation state concepts alone.

Diffraction studies on tin(II) compounds show vacant coordination sites occupied by the lone pair, which is, thus, in a hybrid orbital rather than being localized in the tin $\underline{5s}^2$ atomic orbital. Such compounds do, indeed, have I.S. values greater than tin metal. For example, $(h^5\text{-}C_5H_5)_2Sn$ has a coordination number of two and an isomer shift of $3.74 mms^{-1}$ [175]. However it has been shown by Harrison and Zuckerman[174] that their are four other classes of compounds which also formally contain tin in the +2 oxidation state but whose isomer shift values fall below that of tin metal. These are -

i) adducts of tin(II) compounds with transition metal Lewis acids which have non-bonding electrons available in the valence shells;

ii) complexes of type (i) but with the tin further coordinated;

iii) adducts of tin(II) compounds with subvalent main group Lewis acids which have non-bonding electrons available in the valence shell;

iv) tin(II) compounds with electropositive ligands. Examples of the diamagnetic compounds of (i) are generally of the type $L_2SnM(CO)_n$; $\left[(Me_3Si)_2CH\right]_2SnCr(CO)_5$ [175] being one such example. Coordination of base to (i) giving (ii) appears to confer additional stability, e.g. $(t\text{-}C_4H_9)_2SnCr(CO)_5.C_5H_5N.$[177]. $\left\{\left[(Me_3Si)_2CH_2\right]_2Sn\right\}_2$ [178] and $\left[h^5\text{-}C_5H_5(CO)_3W\right]_2Sn$ are the only known examples of (iii) and (iv) respectively. Two mechanisms are believed to account for the reduction in I.S.; electron withdrawl or shielding of electron density by populating non-$\underline{s}$ atomic orbitals. This may occur either

by adduct formation populating the acceptor orbitals at tin, or by population through the transition metal non-bonding electrons π-interaction along the tin - transition metal axis. In general, however, bonding of tin(II) to electronegative ligands such as oxygen or halogen causes an isomer shift higher than 2.65 mms^{-1}.

As is to be expected, studies on tin(IV) systems are more extensive than those on tin(II). Explanations of the results obtained again generally invoke electronegativities and in a number of cases, for a given series of compounds, the values predicted in this way give a good approximation to the results obtained. However, anomalous results arise for several important series. The methyl- and ethyltin halides have an isomer shift which is substantially smaller than predicted, and for the oxyhalides of tin the trend in the isomer shift is the reverse of that predicted by a simple application of Pauling electronegativities. These effects are related to deviations from the simple $\underline{sp}^3$ configuration; a change in hybridisation resulting in an increase in the $\underline{s}$-electron density at the nucleus and thus a more positive isomer shift[169].

Irrespective of the above considerations, Mössbauer spectroscopy is an extremely useful tool for a preparative tin chemist and its use on an empirical basis should not be decried. For this purpose, one may employ the simple 'rule of thumb' that : divalent tin compounds have isomer shifts from 2.3 to 4.44 mm s^{-1}, tin in a metallic environment has an

isomer shift in the 2.5 mm s^{-1} region and compounds of tetravalent tin range from about 1.9 mm s^{-1} for the essentially covalent compounds to about -0.4 mm s^{-1} for fully ionic compounds.

1.7 COMMERCIAL APPLICATIONS OF ORGANOTIN COMPOUNDS

Three primary commercial applications of organotin compounds can be recognized.

1. The use of tributyltin compounds as industrial biocides in materials protection and as surface disinfectants.
2. Their use as agricultural fungicides and acaricides.
3. Stabilization of polyvinylchloride polymer by dialkyl and monoalkyltin compounds. The latter application being the area of specific interest for the work described herein.

A brief review of the other applications is of value, however.

1.7.1 Trialkyltin Biocides

Trialkyltin compounds, particularly bis(tri-n-butyltin) oxide, TBTO, are now widely used as wood preservatives, antifouling agents and in the disinfection of circulating industrial cooling water.

The biological activity of the tri-n-alkyl species is dependent on the nature of the alkyl group and the species to be controlled (Figure 1.6).

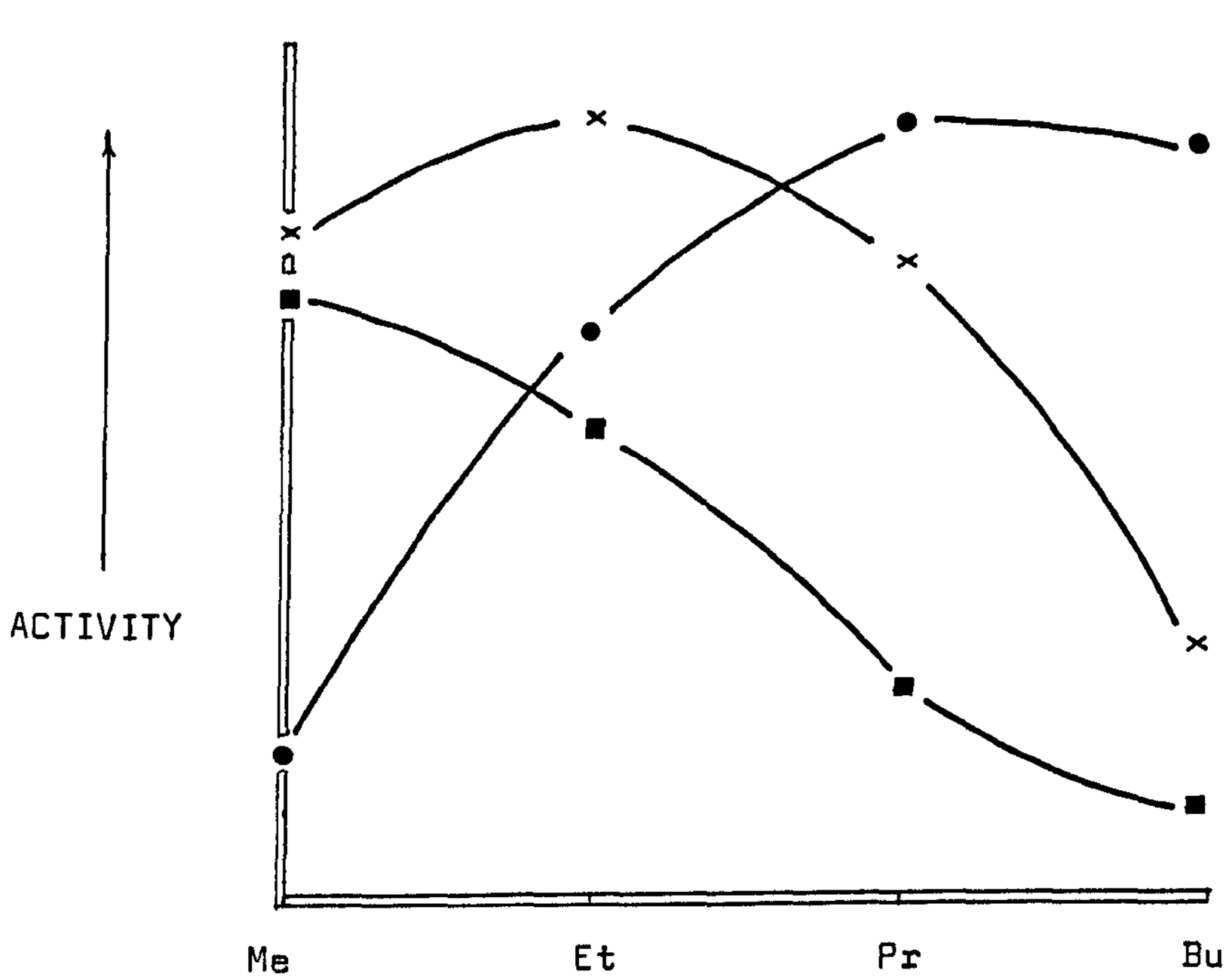

Figure 1.6 Activity variation of tri-n-alkyl acetate with alkyl group and species to be controlled.

As antifungal agents they are highly active and have a broad spectrum of applicability. They are only poorly leached by water and are colourless and non-corrosive. 0.52 kg m^{-3} of TBTO is effective against fungal decay and marine borers such as shipworms (Teredo) and gribble (Limnoria). Higher concentrations in conjunction with insecticides are used against termites and furniture beetles. Hexabutylditin ($Bu_3SnSnBu_3$) has recently been

suggested as a replacement for TBTO, having hydrocarbon properties and therefore a greater penetrating ability into woodwork[151]. Incorporation of TBTO in elastomeric coatings based on nitrile rubber allows a much larger reservoir of biocide and hence increases the fouling free lifetime of marine vessels[179].

Tributyltin formulations are also used as hospital and vetinary disinfectants and potentially they may be effective in combating Bilharzia disease[180]. The compounds have a high activity against the snails which serve as intermediate hosts for the parasitic worms causing the disease.

1.7.2 Agricultural Applications of Organotin Compounds

Triphenyltin acetate was the first organotin agricultural fungicide to be introduced. It was applied, a few ounces per acre, for the control of Phytophthora on potatoes and Cercospora on sugar beet[181]. The mode of action of this and other triphenyltins, such as the hydroxide, appears to be as an antifeedant[182] and fly sterilant[183].

Tricyclohexyltin hydroxide was introduced as a selective acaricide in 1968. It was found to be most effective against phytophagous mites such as spider mites on apples and pears. It is also now used on citrus fruits, hops and stone fruits and appears to have the advantage of low toxicity towards insects such as honeybees[184]. Of similar properties is the Shell company's product, tris(neophyl)tin oxide.

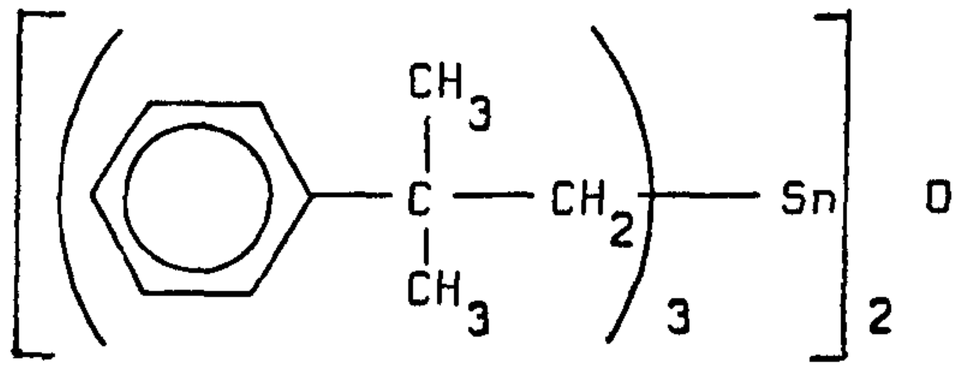

tris(neophyl)tin oxide (Vendex - Shell)

Generally, the lower tri-n-alkyltins from trimethyl to tri-n-phenyl have high biological activity. The trimethyltins are active as insecticides and the tripropyl-, tributyl- and tripentyltins are effective as fungicides and bactericides. Dialkyltin compounds are usually less active than the trialkyl analogues[184]. Table 1.12 lists the relative oral toxicities of a variety of triorganotin compounds and below are given the formulae of several other commercial products.

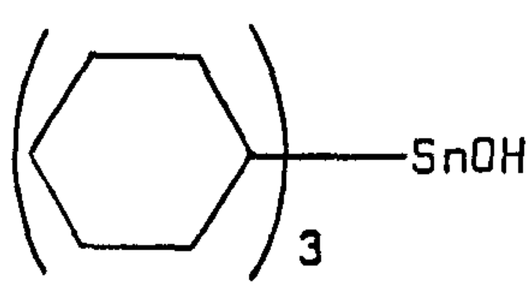

(Plictran - Dow)

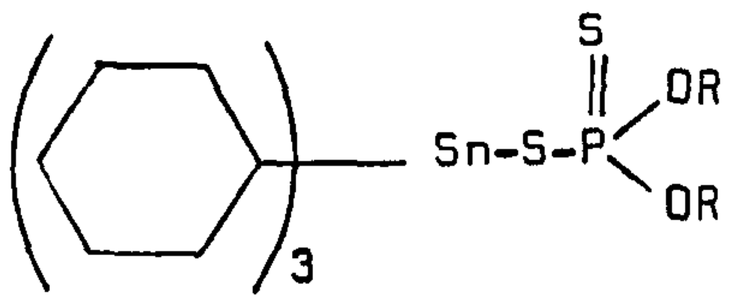

(R-28627 - Stauffer)

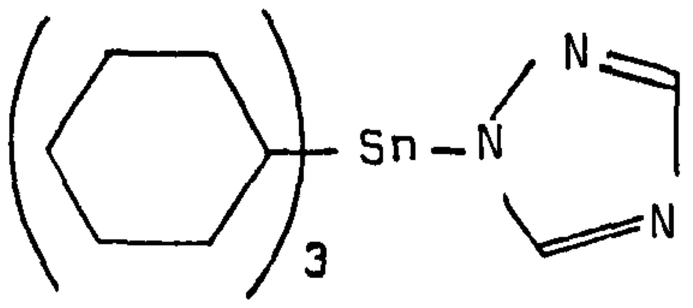

(Tricyclazol - Bayer)

Table 1.12 Oral Toxicity of some Triorganotin Compounds

Compound	LD_{50}^{a} mg/kg	Test animal
Me_3SnOAc	9	rat
Et_3SnOAc	4	rat
Bu_3SnOAc	133	rat
Ph_3SnOAc	380	rat
Cy_3SnOAc[b]	540	rat
$(Neoph)_3Sn_2O$[c]	2630	rat
$(Neoph)_3Sn_2O$	1450	mouse

a) Single dose causing death in 50% of the test animals.

b) Cy = cyclohexyl

c) neoph = neophyl = β, β',-dimethylphenethyl

1.7.3 Organotin PVC Stabilizers

The mechanism of thermal breakdown of PVC is not as yet fully understood. It is believed the process involves a dehydrochlorination reaction at an allylic or tertiary chlorine site with the formation of a double bond. As the degradation continues conjugated unsaturated systems are formed which diminish optical clarity and produce undesirable colour effects in the plastic. As little as 0.1% decomposition can lead to blackening[185]. The dehydrochlorination process is autocatalytic and in the processing of unplasticized PVC resin temperatures well in excess of those required for the initiation of the degradation process ($> 200^{o}C$) are attained. Typical organotin

stabilizers which inhibit this process have the formula R_2SnX_2 where R = Me, Bu, C_8H_{17} and X = SR' or OCOR'. An example would be dibutyltinisooctylthioglycollate, $Bu_2Sn(SCH_2COOC_8H_{17}\text{-}i)_2$ which is known to have good inhibitive properties. However, such a suitable structure was evolved empirically and only recently is any understanding of the chemical mode of action being achieved. This will be discussed more fully in Chapter 2, but in essence exchange of allylic chlorine atoms with the anionic portion of the organotin compound occurs. The absorption of the liberated hydrogen chloride releases compounds which can then add across the unsaturated centres.

Dioctyltins are now also used in place of the dibutyltins with groups such as maleate, laurate and the mercapto derivatives of octyl and isooctyl esters of thioglycolic acid, already mentioned, attached. Addition of small amounts of monoalkyltins has a synergic effect on the inhibition by the dialkyltins.

With the increasing emphasis on rigid PVC products over flexible materials the need for efficient stabilizers has increased, as the former require much higher processing temperatures. Because of the excellent thermal stability of dimethyltins and possible economic advantages in their use, it is possible that these may also find wide applications in this field. In Chapters 2 and 3 the spectroscopic and structural properties of some estertin stabilizers are determined, whilst in Chapter 4 tin-119 magnetic resonance data are used in structural ellucidation of a number of di- and trimethyl-tin compounds.

REFERENCES

101. A. Almenningen, A. Haaland and T. Motzfeldt, J. Organometal. Chem., (1967) 7 97.

102. P.G. Harrison and J.J. Zuckerman, J. Amer. Chem. Soc., (1970) 92 2577.

103. P.G. Harrison and J. A. Richards, J. Organometal. Chem., (1976) 108 35.

104. A.B. Cornwell, P.G. Harrison and J.A. Richards, J. Organometal. Chem., (1976) 108 47.

105. G.A. Ozin and A. Vander Voet, J. Chem. Phys., (1968) 56 1192.

106. M.W. Lister and L.E. Sutton, Trans. Farad. Soc., (1941) 37 406.

107. P.G. Harrison, Coord. Chem. Rev., (1976) 20 1.

108. F. A. Cotton and G. Wilkinson, "Advanced Inorganic Chemistry" Interscience 3rd Edn. 1976. New York and London.

109. J.D. Donaldson, Progress in Inorg. Chem (1967) 8 287.

110. L.E. Orgel, J. Chem. Soc. (1959) 3815.

111. F.R. Poulsen and S.E. Rasmussen, Acta Chem. Scand., (1970) 24 150.

112. K.N. Moller, Mat. Fys. Medd., Dan Vid. Selsk., (1959) 22.

113. G. Bergerhoff and L. Goost, Acta Cryst., Sect B, (1973) 29 632.

114. J.K. Stalick, P.W.R. Corfield and D.W. Meek, Inorg. Chem., (1973) 12 1668.

115. C.E. Moore, 'Rept. on Int. Comm. on Atomic Energy Levels', Nat. Bur. Std. (US) Circ., (1958) 15 913.

116. J.M. vanden Berg, Acta Cryst., (1961) 19 1002.

117. R.E. Rundle and D.H. Olsen, Inorg. Chem., (1964) 3 596.

118. G. Berghoff, Acta Cryst., (1962) 15 509.

119. J.D. Donaldson and W. Moser, J. Chem. Soc., (1960) 4000.

120. W. Hofmann, Z. Krist., (1935) 92 161.

121. A. Okazaki and I. Ueda, J. Phys. Soc. Jpn., (1956) 11 470.

122. R.R. McDonald, A.C. Larson and D.T. Cromer, Acta Cryst., (1964) 17 1104.

123. H. Kiryama, K. Kitahama, O. Nakamura and R. Kiriyama, Bull. Chem. Soc. Jpn., (1973) 46 1389.

124. A. Jelen and O. Lindquist, Acta Chem. Scand., (1969) 23 307.

125. J.D. Donaldson and D.C. Puxley, Acta Cryst., (1972) B28 864.

126. W.J. Moore and L. Pauling, J. Amer. Chem. Soc., (1941) 63 1392.

127. K.G. Shields, R.C. Seccombe and C.H.L. Kennard, J. Chem. Soc., Dalton Trans., (1973) 741.

128. F.P. van Remoortere, J.J. Flynn, F.P. Boer and P.P. North, Inorg. Chem., (1971) 10 1511.

129. H. Fujii and M. Kimura, Bull. Chem. Soc. Jpn., (1971) 44 2643.

130. H.A. Skinner and L.E. Sutton, Trans. Farad. Soc., (1944) 40 164.

131. R.F. Bryan, J. Amer. Chem. Soc., (1964) 86 733.

132. J. Buckle, P.G. Harrison, T.J. King and J.A. Richards. J. Chem. Soc., Chem. Comm., (1972) 1104.

133. G. Engel, Naturwiss, (1933) 21 704.

134 J.J. Park, D.M. Collins and J.L. Hoard, J. Amer. Chem. Soc., (1970) 92 3636.

135. G.S. Brownlee, A. Walker, S.C. Nyburg and J.T. Szymanski, J. Chem. Soc., Chem. Comm., (1971) 1073.

136. C.D. Garner, D. Sutton and S.C. Wallwork, J. Chem. Soc. (A) (1967) 1949.

137. R.A. Jackson, J. Organometal Chem., (1979) 166 17-19.

138. H.A. Skinner, 'Advances in Organometallic Chemistry', Academic Press, New York and London (1964) 2 49.

139. L. Pauling, 'The Nature of the Chemical Bond. 3rd Edn. Cornell Univ. Press (1960) New York.

140. A.L. Allred and E.G. Rochow, J. Inorg. Nucl. Chem., (1958) 5 269.

141. R.S. Drago and N.A. Matwiyoff, J. Organometal Chem., (1965) 3 62.

142. B.Y.K. Ho and J.J. Zuckerman, J. Organometal. Chem. (1973) 49 1.

143. L.S. Bartell, J. Chem. Phys. (1960) 3 827.

144. C. Glidewell, Inorg. Chim. Acta (1975) 12 219.

145. C. Glidewell, Inorg. Chim. Acta (1976) 20 113.

146. C. Glidewell, Inorg. Chim. Acta (1979) 36 135.

147. E. Abel, 'Comprehensive Inorganic Chemistry' Vol. 2. (1973) Pergamon, London.

148. G.J.M. van der Kerk, Chem. and Ind. (1970) 644.

149. H. Tokunaga, Y. Murayama and I. Kijima, Japanese Patent (1964) 24958.

150. Nitto Chemicals, French Patent (1965) 1,393,779.

151. G.J.H. van der Kerk, 'Organotin Compounds: New Chemistry and Applications', Ed. J.J. Zuckerman (1976) 4 Amer. Chem. Soc.

152. H.G. Kuivila and O.F. Beumel, J. Amer. Chem. Soc., (1958) 80 3250.

153. H. Gilman and E.A. Zeuch, J. Amer. Chem., Soc., (1960) 82 2522.

154. F.H. Pollard, G. Nickless and D.N. Nolan, Chem. and Ind., (1965) 1027.

155. E.O. Fischer and H. Gruber, Z. Naturforsch (1956) 116 423.

156. L.D. Dave, D.F. Evans and G. Wilkinson, J. Chem. Soc., (1959) 3684.

157. P.G. Harrison, J. Organometal Chem., (1973) 58 49.

158. P.G. Harrison, J. Organometal Chem. Annual Surveys of Tin 1972-

159. T. Tanaka, Organomet. Chem. Revs., (1970) A5 1.

160. R.A. Cummins, Aust. J. Chem., (1963) 16 985.

161. R.J.H. Clark, A.G. Davies, R.J. Puddephatt, J. Chem. Soc., (C) (1968) 1828.

162. P.B. Simons and W.A.G. Graham, J. Organometal. Chem., (1967) 8 479.

163. R.C. Poller, 'The Chemistry of Organotin Compounds', (1970) Logos Press.

164. I. Wharf and D. Shriver, Inorg. Chem., (1969) 8 914.

165. K. Nakamoto, 'Infrared Spectra of Inorganic and Coordination Compounds', 2nd Edn. (1970), Wiley Interscience, New York.

166. I.R. Beattie and L. Rule, J. Chem. Soc., (1964) 166.

167. A.L. Yergey and F.W. Lampe, J. Amer. Chem. Soc., (1965) 87 4204.

168. M.R. Litzow and T.R. Spalding, 'Mass Spectrometry of Inorganic and Organometallic Compounds', Elsevier (1973) Amsterdam.

169. G.K. Shenoy and F.E. Wagner, 'Mössbauer Isomer Shifts', North Holland Publishing Co. (1978).

170. G.M. Bancroft, 'Mössbauer Spectroscopy: An Introduction for Inorganic Chemists and Geochemists'. McGraw-Hill (1973) LONDON.

171. T.C. Gibb, 'Principles of Mössbauer Spectroscopy', Chapman and Hall (1976) LONDON.

172. R.V. Parish, Prog. Inorg. Chem. (1972) 15 101

173. J.J. Zuckerman, Adv. Organometal. Chem., (1970) 9 21.

174. P.G. Harrison and J.J. Zuckerman, Inorg. Chim. Acta, (1977) 21 L3.

175. P.G. Harrison and M.A. Healy, J. Organometal Chem (1973) 51 153.

176. J.D. Cotton, D.E. Goldberg, M.F. Lappert and K.M. Thomas, J. Chem. Soc., Chem. Comm., (1974) 893.

177. A.B. Cornwell and P.G. Harrison, J. Chem. Soc. Dalton, (1975) 1486.

178. P.J. Davidson and M.F. Lappert, J. Chem. Soc., Chem. Comm., (1973) 317.

179. C.J. Evans and P.J. Smith, J. Oil. Col. Chem. Ass. (1975) 58 160.

180. N.T. Cardarelli, Tin and its Uses (1972) 93 16.

181. K. Hartel, Agr. Vet. Chem. (1962) 3 19.

182. K.R.S. Ascher and S. Nissim, Int. Pest Control (1965) 7 21.

183. E.E. Kenaga, J. Econ. Entomol. (1965) 58 4.

184. M.H. Gitlitz, 'Organotin Compounds'. New Chemistry and Applications', Ed. J.J. Zuckerman (1976) 169. Am. Chem. Soc.

185. J.J. Zuckerman, R.P. Reisdorf, H.V. Ellis and R.R. Wilkinson, 'Organometals and Organometalloids, Occurrence and Fate in the Environment'. (1978) 393, Am. Chem. Soc.

186. J. Bondi, J. Phys. Chem., (1964) 68 441.

187. M. Okada, R.A. Guidotti and J.D. Corbett, Inorg. Chem., (1968) 7 2118.

188. J.D. Corbett and P.A. Edwards, J. Amer. Chem. Soc., (1977) 99 3313.

CHAPTER TWO

ORGANOTIN STABILIZERS: MECHANISM, SYNTHESIS OF ESTERTINS, SPECTROSCOPIC PROPERTIES

2.1 INTRODUCTION

Organotin compounds have been used as heat and light stabilizers for PVC since 1938 when the original patents for dibutyltin compounds were issued to V. Yngve of Carbide and Carbon Chemicals Corporation[216]. Dibutyltin dilaurate and dibutyltin maleate were the initial systems used for this purpose, but other dibutyltin, and more recently, dioctyl- and dimethyltin compounds have been applied. Despite the relatively high cost of these materials they have gained wide acceptance in this market because of their obvious efficiency. However, as mentioned previously, the choice of compound has been largely empirical until more recently when studies have been undertaken which give at least partial ellicidation of the mechanism of stabilization.

2.2 P.V.C. DEGRADATION

Wirth and Andreas[201] have reviewed the stabilization of PVC against heat and light and have listed five routes to the formation of the labile allyl chloride grouping in the PVC (Table 2.1)

Table 2.1 Routes to labile allyl chloride in PVC

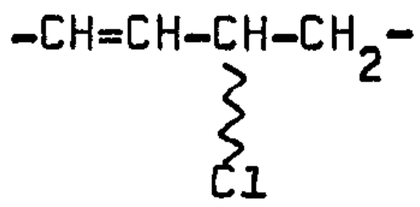

1. Production of Resin	2. Processing
- unsaturations	- thermomechanical effects
- peroxides	- autoxidation reactions
- structure irregularities	

The active group may already be formed during polymerization, as end groups for example. Alternatively, during processing, thermal autoxidation may give rise to hydroperoxides formed from the allylic methyl groups and oxygen. These may act as initial sites for dehydrochlorination. The hydroperoxides change into ketopolyenes, whilst longer polyene sequences add oxygen to form cyclic peroxides which may further degrade to release dehydrochlorinated chains [202]. CO groups are generated by the autocatalytic effect of the eliminated hydrogen chloride on the dehydrochlorination reaction in the presence of oxygen which, in turn, also activate α-chlorine atoms for further elimination. The hydrogen chloride reacts with the ketopolyenes to form deeply coloured carbonium salts[203]. Thus, the mode of action of a PVC stabilizer must consist of deactivation and elimination of the allyl chloride grouping as an initial site.

2.3 P.V.C. STABILIZATION BY ORGANOTINS

Mixtures of di- and monoorganotin compounds are used; the monoalkyltin component having a synergic effect. The heat stabilization mechanism mainly depends on the mercapto substituents, whilst the tin-bonded alkyl groups have a greater significance for the processability, toxicity and volatility of the final material.

2.3.1 The X- Groups

Frye and co-workers[204] have shown, by using radioactive labels on organotin stabilizers, that exchange occurs between the chlorine atoms in the polymer and tin—bound X—groups:

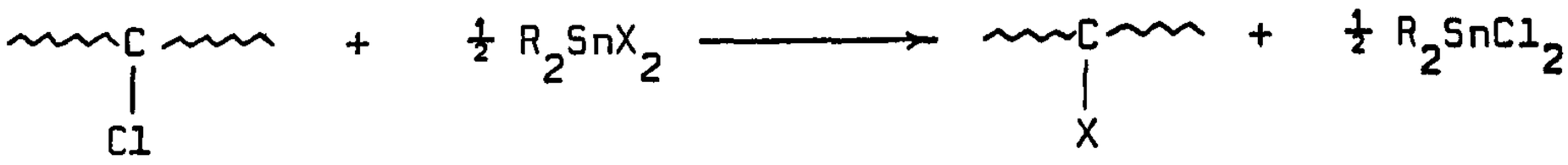

Further work[205] using PVC treated with $Bu_2Sn(^{35}SBu)_2$ revealed that there is a slow uptake during an induction period but with the onset of discolouration the rate of absorption of radioactivity increases.

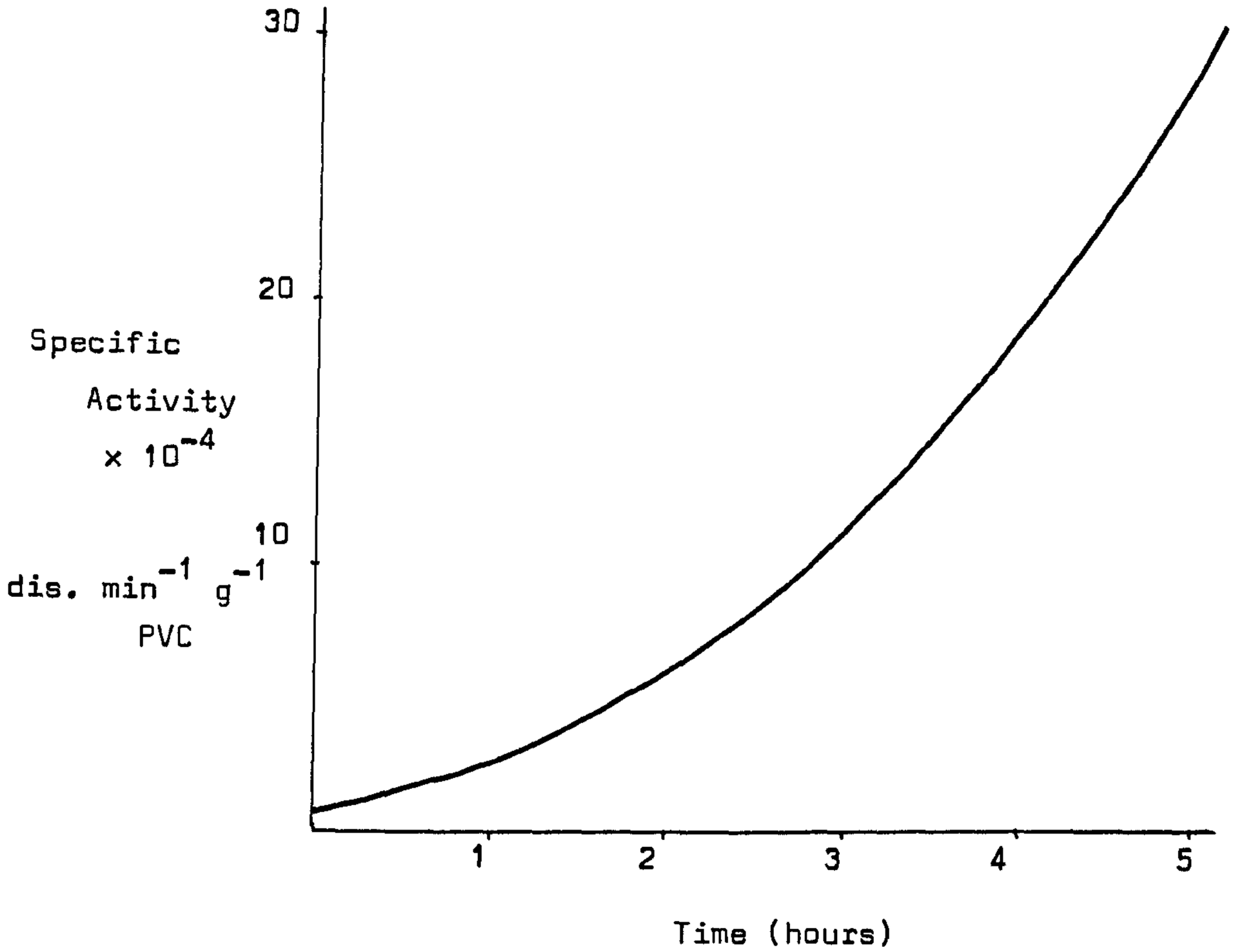

Figure 2.1 PVC and $Bu_2Sn(^{35}SBu)_2$ interaction at 180°C [205].

The induction period represents the action of the preventitive role of the stabilizer. Because the dehydrochlorination process is much faster in the presence of oxygen it is believed that the organotin mercaptide acts as an antioxidant by decomposing the hydroperoxides formed. This action has been demonstrated with t-butyl hydroperoxide[201].

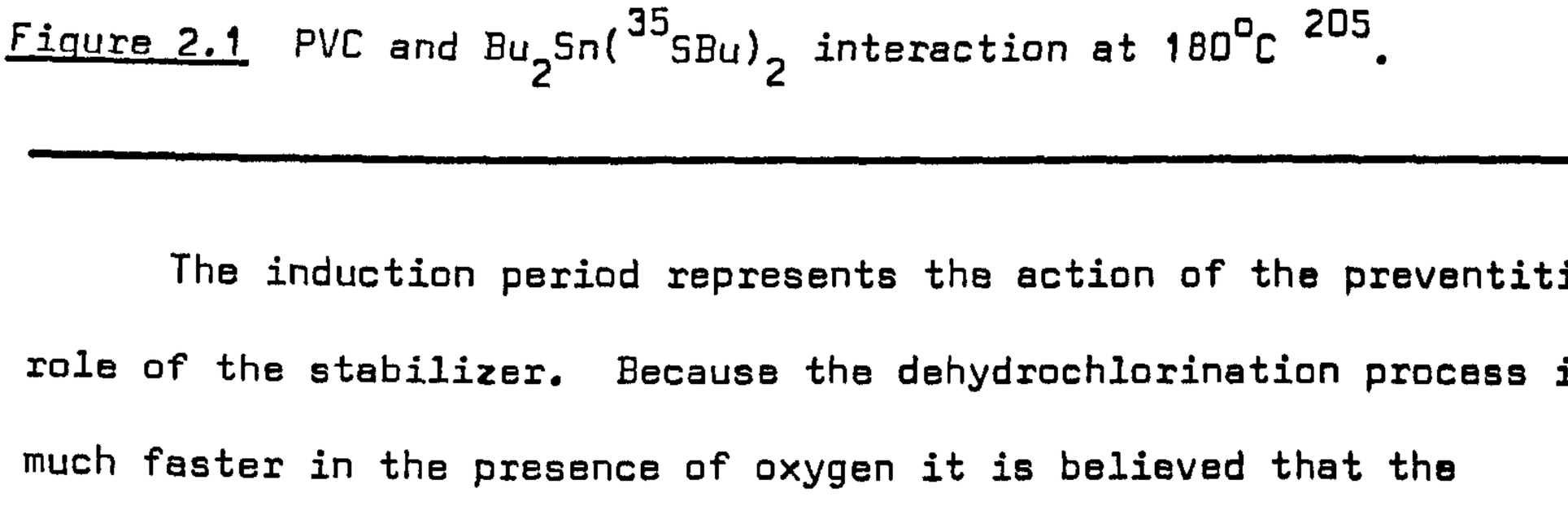

(i Oct = *iso* octyl, C_8H_{17})

This mechanism is in addition to the primary stabilization by exchange with the labile chlorine atoms, acting as initial sites for dehydrochlorination:

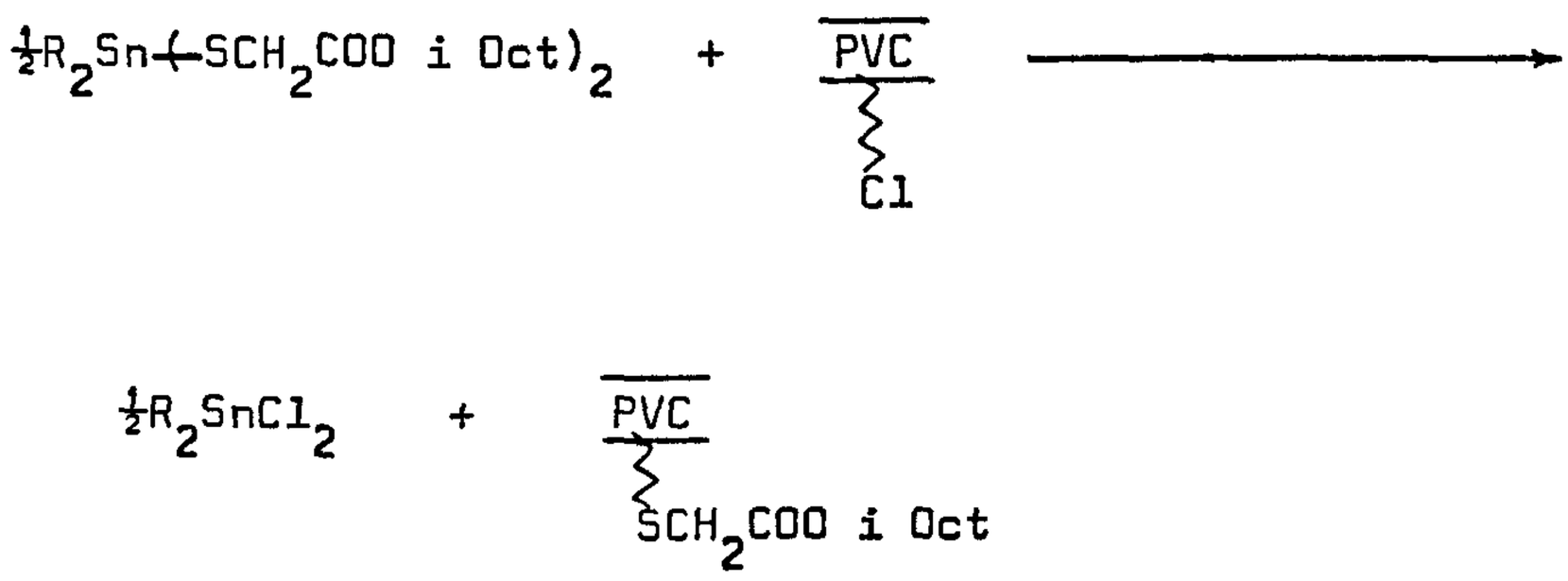

The process has, in essence, an S_N2 mechanism:

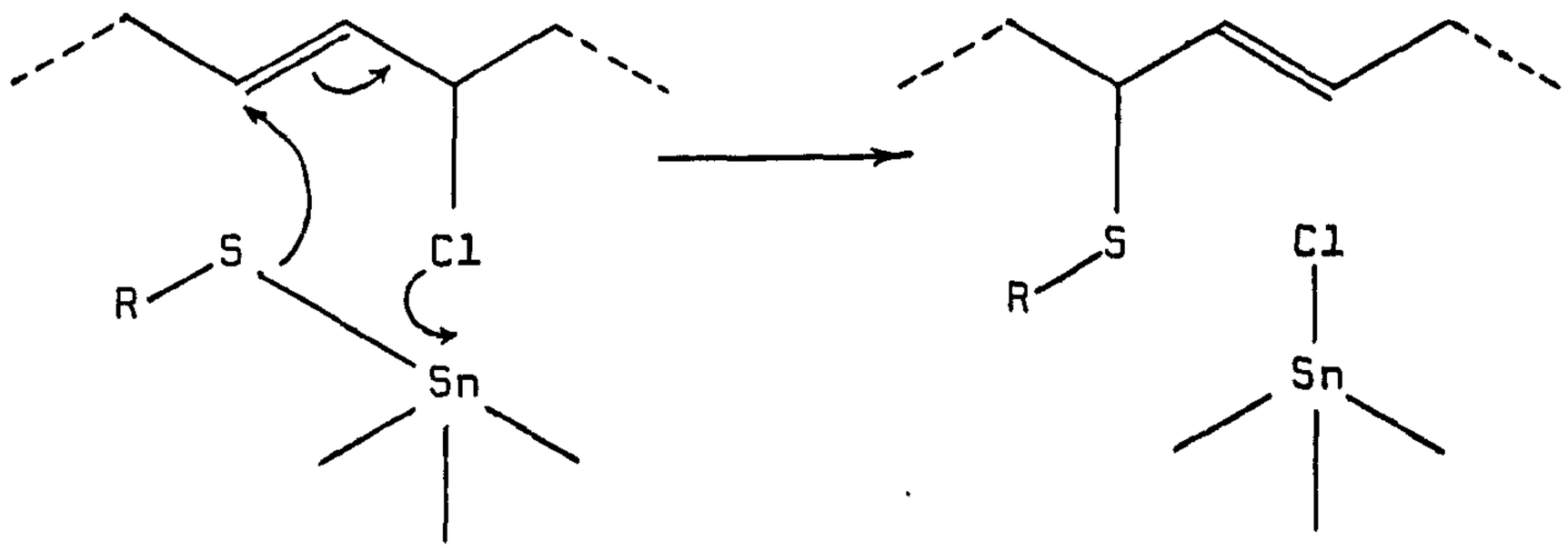

It has been suggested that the resulting organotin chlorides can further inhibit dehydrochlorination by specifically complexing the alkyl chloride groups in the PVC[201]

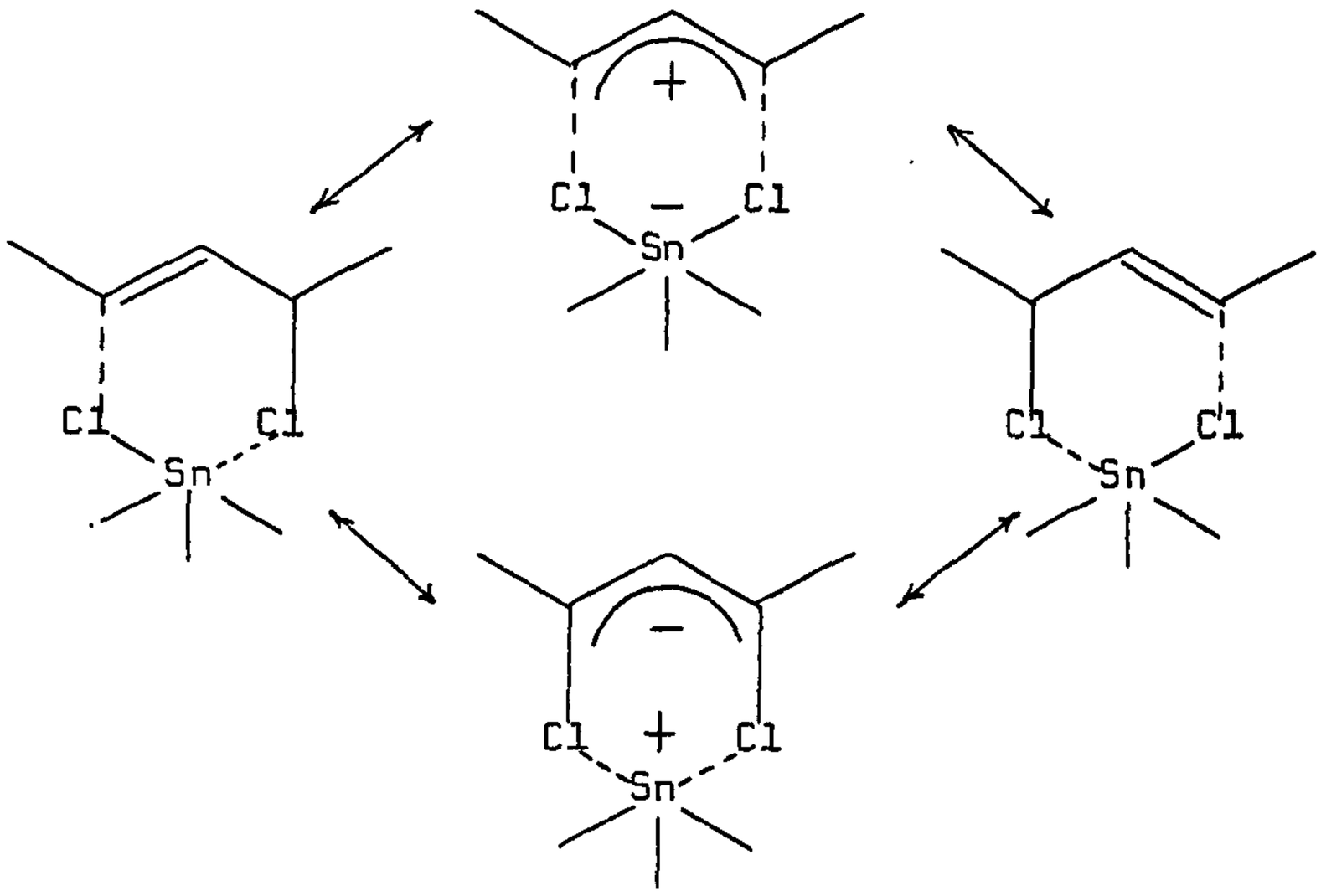

However, this appears unlikely to be an important mechanism as it will be nullified by the deleterious effects of R_nSn-chlorides which, since they are Lewis acids, will promote HCl elimination.

Of greater importance to the preventative role of organotin stabilizers, are their curative properties. These arise from the reaction involving absorption of the generated hydrogen chloride;

$$Bu_2SnX_2 + 2HCl \longrightarrow Bu_2SnCl_2 + 2HX$$

The generation of thiol within the polymer lattice has beneficial effects. Thus, it is the HX which is of importance here (usually this is iso-octylthioglycollate, IOTG), partly because it rapidly leads to the destruction of the coloured carbonium complexes but also because it removes the darkening chromophore due to the longer polyene:

$$HSCH_2COO\ i\text{-}Oct + \underline{\underline{PVC}} \longrightarrow \begin{array}{l}\underline{PVC}\\ |\\ SCH_2COO\ i\text{-}Oct\end{array}$$

Furthermore, it has been found that considerable colour improvement results if thermally discoloured PVC is treated with isooctylthioglycolate[206].

The organotin systems act as light stabilizers, in addition to thermal stabilizers, by preventing the formation of CO -groups and polyene sequences which are responsible for the absorption of UV-light, and thereby light degradation. Thus, all the previous processes are equally applicable to light stabilization mechanisms.

2.3.2 The R-Groups

Poller[205] has reported investigations into the effects on stabilization properties of varying the R group in the organotin stabilizer (Table 2.2). Various organotin bis(isooctylthioglycolate) stabilizer's were milled into PVC samples at 190°C and the resulting films heated at 195°C. The point at which discolouration was complete was noted.

Table 2.2 2% $R_2Sn(SCH_2COOC_8H_{17}\text{-}i)$ stabilizer in PVC heated at 195°C,[205]

R =	Approx. time to complete discolouration (min)
CH_3	90
CH_3CH_2	90
$CH_3CH_2CH_2CH_2$	70
$CH_3(CH_2)_7$	70
$C_6H_5CH_2$	40
$BrCH_2$	0
C_6H_5	60
p - $CH_3OC_6H_4$	10

Lengthening the alkyl chain appears to cause a slight reduction in stabilizer efficiency suggesting that electron release decelerates the rate of reaction. Introduction of the phenyl or bromine electron withdrawing groups into the tin-bonded methyl causes a much greater reduction in stability. However, with a p-methoxy substituent onto the phenyl group the stabilization is again reduced, yet the MeO-group is electron-donating. Poller has rationalized this apparent contradiction by considering the two separate stabilizer reactions with hydrogen chloride. The tin-sulphur bond cleavage is a pro-stabilization reaction, whilst tin-carbon bond cleavage will have a destabilizing effect as the final product will be tin(IV) chloride; a powerful catalyst for dehydrochlorination:

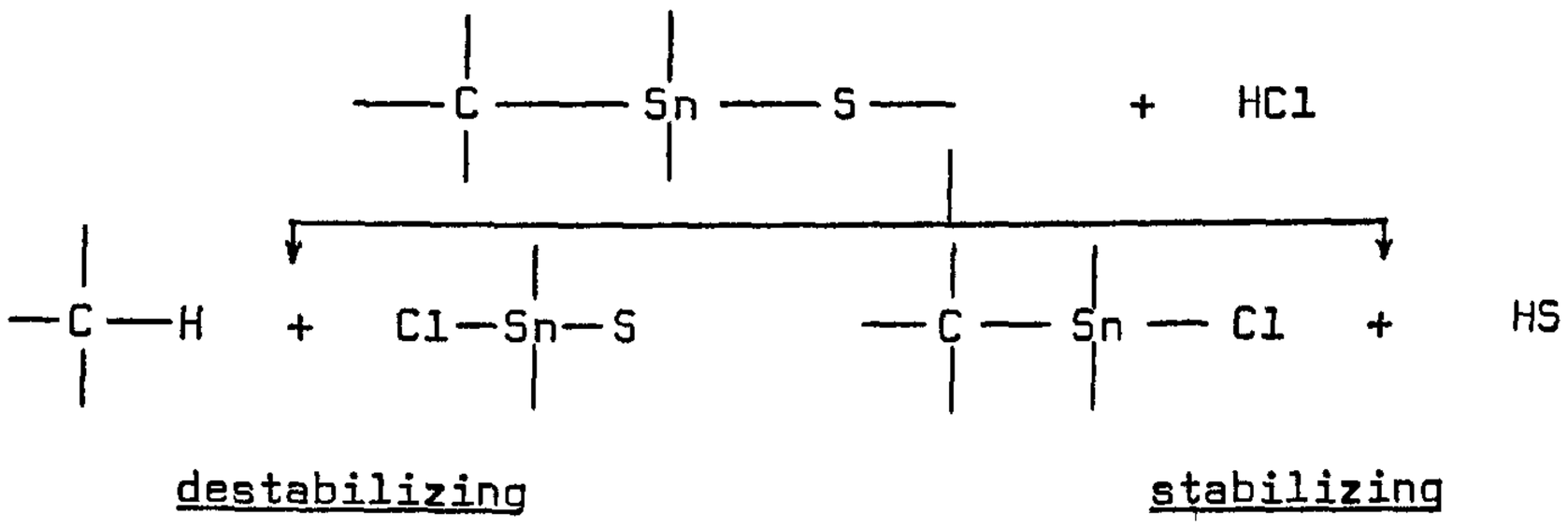

Thus, the simple dialkyltin stabilizers will convert directly to the dialkyltin chlorides in the polymer whereas the benzyl, bromomethyl and phenyl groups will be more readily cleaved from tin than methyl, ethyl, propyl or butyl groups. The p-methoxy substituent will increase the rate of cleavage[207].

2.4 ESTERTINS

Considerable improvements in the effectiveness of alkyltin stabilizers have been made since the original patents were obtained. However, the first major breakthrough in tin chemistry did not occur until 1974 when an entirely new process for organotin intermediates was discovered[208]. This has resulted in the production of a completely new class of organotin stabilizers, known collectively as estertins. The estertins have the general formulae:

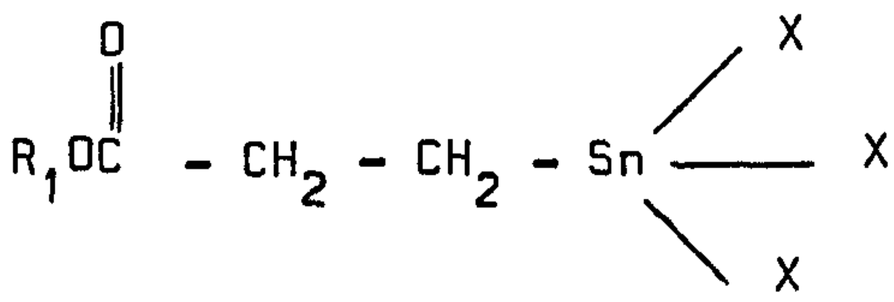

and

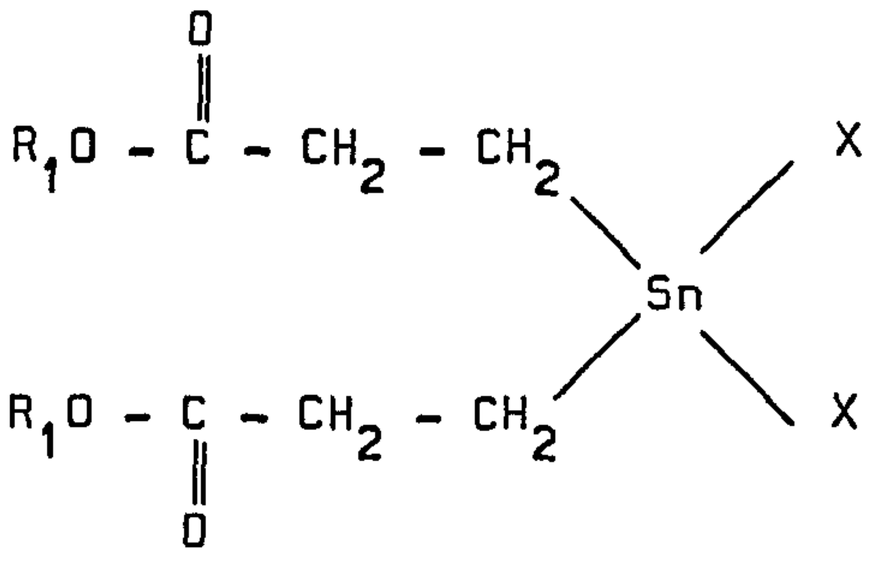

Technical evaluation of the resulting systems has shown them to have similar performance to the existing alkyltins and biological examinations found them to be only mild skin irritants and to cause no eye irritation[209]. Acute oral toxicity values (LD_{50}) in rats showed estertins had a higher value than butyl- or methyltin compounds but lower values than the corresponding octyltin compounds (Table 2.3)

Table 2.3 Comparison of Acute Oral Toxicity (LD_{50}) of Organotin Systems in Rats[209]

R		LD_{50} Values, mg/kg	
		X = Cl	X = IOTG
$RSnX_3$	ester	5500	1230
	methyl	1370	920
	butyl	2300	1063
	octyl	3800	3400
R_2SnX_2	ester	2350	1430
	methyl	75	1210
	butyl	126	510
	octyl	7000	1975

N.B. No R_3SnX systems occur in the estertin process.

The mutagenic effects of the *mono-* and *diestertinisooctylthio-*glycolates have been examined using Salmonella typhimurium and were found to be negative[209]. In addition, long term chronic toxicity tests indicate that the estertins should be suitable for approval as food packaging additives. The rate of migration of estertin stabilizers into food follows closely that of the octyltin stabilizers already used in bottle formulations. TGA experiments show that the estertin stabilizers have volatilities comparable with those of the alkyltins, whilst the chloride compounds are considerably less volatile;

a significant advantage during material processing[209].

Tests carried out by Akzo Chemie (U.K.) Ltd. on a variety of estertin stabilizers have shown that by careful selection of the appropriate stabilizer for a specific application, be it multiple screw extrusion of water pipes, clear extruded sheet or for rigid foams, performances which are equal to, or in many cases, better than the exsiting market leaders in this field can be achieved. However, the real advantage of the estertins is in their synthesis.

As previously discussed (Chapter One), commercially, organotin production is based on either Grignard, Wurtz, aluminium alkyl or direct catalytic methods. Because of the high cost of tin it is essential to obtain high yields and this the first three methods provide. However, they have the disadvantages of using up stoichiometric quantities of another metal and requiring further disproportionation stages with $SnCl_4$ to provide the required R_2SnCl_2 and $RSnCl_3$ industrial intermediates. Whilst, in part, the direct method overcomes these problems, for alkyl groups higher than methyl mixtures of mono- and dialkyltin halides result. The yields also decrease as the alkyl series is ascended thus preventing the synthesis of higher molecular weight products of lower volatility.

In the estertin synthesis of PVC stabilizers the tin is quantitatively converted to the required product, yields being of the order of 98%. The smooth reaction can be achieved in a wide variety of solvents and over a temperature range from around -30 to +120^{o}C. Thus, making this synthetic process very attractive commercially, in terms of chemical and energy conversion.

2.5 SYNTHESIS OF ESTERTINS

2.5.1 The General Method

The basis of formation of the β- substituted alkyl tin systems involves the reaction of tin metal or tin(II) halides with a carbonyl substituted alkene in the presence of hydrogen halide[210-211]. The syntheses, which appear to take place in a wide variety of solvents and over a large temperature range, may be summarised by the equations:

$$Sn + 2HX + 2R_2C{=}CR_2 \longrightarrow X_2Sn(CR_2{-}CR_2H)_2$$

$$SnX_2 + HX + R_2C{=}CR_2 \longrightarrow X_3SnCR_2{-}CR_2H$$

No previous structural data has been available on estertins. It was, therefore, decided to synthesize representative examples of the above systems in order to rectify this omission.

2.5.2 Synthesis of Bis(β-carbomethoxyethyl)tin dichloride, $Cl_2Sn(CH_2CH_2COOMe)_2$

A stirred suspension of tin powder (3.5g, 0.3 mol) in dry tetrahydrofuran (THF) (15 cm^3) was prepared in a three-necked flask fitted with reflux condenser, gas inlet tube and thermometer. To this was added methyl acrylate (5.5 cm^3, 0.06 mol). Anhydrous hydrogen chloride gas was then passed through the mixture for ca. 2h. maintaining the temperature at about 20^oC with a water bath. The white precipitate formed was washed with dry THF (3 x 10 cm^3) to remove any organotin trichloride formed in a side reaction.

The remaining solid was extracted with hot chloroform (30 cm^3) and subsequent slow crystallization (2d) yielded a highly crystalline sample of bis(β-carbomethoxyethyl)tin dichloride.

m.p. 132-133°C (lit.[208] 132°C). Found: C, 26.42; H, 4.14; Cl, 18.62% $C_8H_{14}Cl_2O_4Sn$ requires C, 26.37; H, 3.84; Cl, 19.30%.

2.5.3 Synthesis of β-Carbomethoxyethyltin trichloride,

$Cl_3SnCH_2CH_2COOMe$

$$SnCl_2 + HCl + CH_2{=}CHCOOMe \longrightarrow Cl_3SnCH_2CH_2COOMe$$

A procedure similar to that adopted for the dihalide product above was used for the preparation of this compound. Equimolar quantities of anhydrous tin(II)chloride (4.7g, 0.025 mol) and methyl acrylate (2.25 ml, 0.025 mol) were added to dry toluene (20 cm^3). Anhydrous hydrogen chloride was passed through the solution for 1h when the solvent was then removed under vacuum. The residue was extracted with 15 cm^3 of hot dry toluene and the volatile material distilled off up to 70°C at 3 mm Hg pressure. A white residue crystallised on cooling and after drying was identified by microanalysis as β-carbomethoxyethyltin trichloride.

m.p. 71-72°C (lit.[208] 70°C).

Found: C, 12.54; H, 1.90; Cl, 28.14%. $C_4H_7Cl_3O_2Sn$ requires C, 12.55; H, 1.83; Cl, 27.85%.

Other estertin compounds are prepared in a manner related to one of the appropriate methods above.

2.6 SOME SPECTROSCOPIC PROPERTIES OF ORGANOTIN STABILIZERS

Before crystal structure examinations were made on the above two compounds their spectroscopic properties, together with those of bis(β-amidoethyl)tin dichloride were examined. The results obtained, together with those of a tin-119 Mössbauer study of Bu_2Sn(IOTG); (IOTG = iso octylthioglycollate), BuAcSn(IOTG); (BuAc ≈ $BuOC(:O).CH_2-CH_2-$) and BuAcSn(β-MeOct)$_3$; (β-MeOct = $SCH_2CH_2OCOC_7H_{15}$) are reported herein. The latter samples were supplied by Dr. J. W. Burley of AKZO Chemie (UK) Ltd., and recrystallized where neccessary.

2.6.1 Vibrational Spectroscopy

(i) Experimental

Infrared spectra were obtained using a Perkin Elmer 577 grating infrared spectrophotometer. Raman data were obtained on a Cary 81 using Spectra Physics Model 125 He/Ne and Model 164 Ar^+ laser sources.

(ii) Results

The vibrational spectra of the two β-carbomethoxyethyltin chlorides, $Cl_nSn(CH_2CH_2CO_2Me)_{4-n}$ (n = 2,3), together with that of methyl acrylate are listed in Table 2.4. As expected the ν(C=C) vibration of the alkene at 1637 cm^{-1} is absent in the two tin derivatives. In addition, the ν(C=O) stretching band at 1740 cm^{-1} in methyl acrylate is observed at 1674 cm^{-1} in $Cl_2Sn(CH_2CH_2COOMe)_2$

Table 2.4 Infrared and Raman Data for $Cl_3SnCH_2CH_2CO_2CH_3$ and $Cl_2Sn(CH_2CH_2CO_2CH_3)_2$,(cm^{-1}).

$CH_2=CHCO_2CH_3$	$Cl_3SnCH_2CH_2CO_2CH_3$		
infrared	infrared		Raman
liquid film	KBr disc	Nujol Mull	Solid
3033 (sh)			
3004 m	3010 w		3012 m
2962 s	2962 m		2966 s
2918 w	2930 w		2932 w
2863 w	2872 w		2872 s
1740 s	1650 vvs	1650 vvs	1652 m
1650 (sh)			
1637 m			
1625 (sh)			
1444 s	1448 s	1460 s	1451 m
1408 s	1401 m	1401 m	1404 m
	1370 s	1374 s	1376 w
1280 s	1272 s	1272 s	
1213 s	1250(sh)	1250 (sh)	
1187 (sh)	1188 w	1188 w	
	1134 w	1134 w	1144 m
			1126 m
			1103 m
1073 s	1047 w	1047 w	
992 s			
975 (sh)	956 m	956 m	952 w
859 m	900 w	902 w	900 m
817 s	746 (sh)	730 (sh)	
668 w	700 m	704 m	
	580 vw	578 vw	573 m
		546 vw	548 m
	468 w	470 w	468 m
	422 (sh)	422 vw	
	404 s	404 s	398 m
	365 s	376 s	
	350 s	350 s	345 vs
	322 s	324 s	313 vs
		254 m	267 w
			248 w
			138 vs
			116 m
			105 m
			75 w

$Cl_2Sn(CH_2CH_2CO_2CH_3)_2$

infrared		Raman	Assignment
KBr disc	Nujol Mull	Solid	
3010 w		3010 m	ν(C-H)
2950 m		2963 s	
2930 w		2930 s	
2858 w		2870 w	
1674 vs	1674 vs	1683 m	ν(C=O)
			ν(C=C)
1442 s	1442 s	1464 m	δ(C-H)
1404 m	1404 m	1406 m	
1363 s	1366 s		
1270 s	1270 s		
1228 vs	1228 vs	1235 m	ν(C-O)
1186 m	1186 m		
1155 w	1155 w		
1140 (sh)	1140 (sh)	1140 w	
1132 m	1132 m	1129 m	
1031 m	1031 m		
957 m	957 m	952 w	
922 w	922 w		
892 w	892 w	890 m	
757 m	757 m	750 w	
694 m	694 m		ν(Sn-C)
592 w	592 w	584 m	
553 vw	553 vw		
526 vw	526 vw		
467 vw	467 vw	463 m	
382 m	382 m	373 m	ν(Sn-Cl)
310 s	310 s		
297 vs	297 vs	300 vvs	
288 (sh)	288 s		
		267 w	
240 w	240 w	246 w	skeletal deformation modes
		185 m (br)	
		133 vs	
		117 vs	
		77 w	

and 1650 cm^{-1} in $Cl_3SnCH_2CH_2COOMe$, such a shift in frequency being a clear indication of carbonyl⟶tin coordination. The greater effect on the carbonyl position observed in the trichloride when compared to the dichloride reflects the dissimilarity of the strength of these coordinate interactions (a factor confirmed by the Sn-O bond lengths for the two compounds - see Chapter 3).

Table 2.5 lists the vibrational spectrum of the bis(β -amidoethyl)tin dichloride and the free ligand. Again the loss of the alkene vibration ν(C=C) would be expected as a feature of the spectrum of the tin - methacrylamide product. However, the bands in the free ligand at 1660 cm^{-1} (ascribed to ν(C=O)) and 1605 cm^{-1} (δ(N-H)) are exceptionally broad and, therefore, can reasonably be said to encompass the ν(C=C) although this bands exact position can not be given. It is noteable that on compound formation the infrared spectrum of the peaks in this region becomes sharp and well defined. The change in the δ(N-H) from 1605 cm^{-1} to 1547 cm^{-1} may be representative of changes in the strength of hydrogen bonding with intermolecular factors now being involved.

Alternatively, and probably more likely as the ν(N-H) bands do not show a frequency change, the 1605 cm^{-1} represents a mean position for mixing between ν(C=C) and δ(N-H) in the free ligand. In addition, the ν(C=O) in this organotin is observed as a doublet (Fig. 2.2)at 1651 cm^{-1} and (slightly weaker intensity) at 1625 cm^{-1} instead of the expected singlet found in the other estertins examined. This is readily explained when the crystal structure data is examined,

vide infra, as the carbonyl moiety in each ligand is found to interact with the tin to a markedly different extent (this will be discussed later).

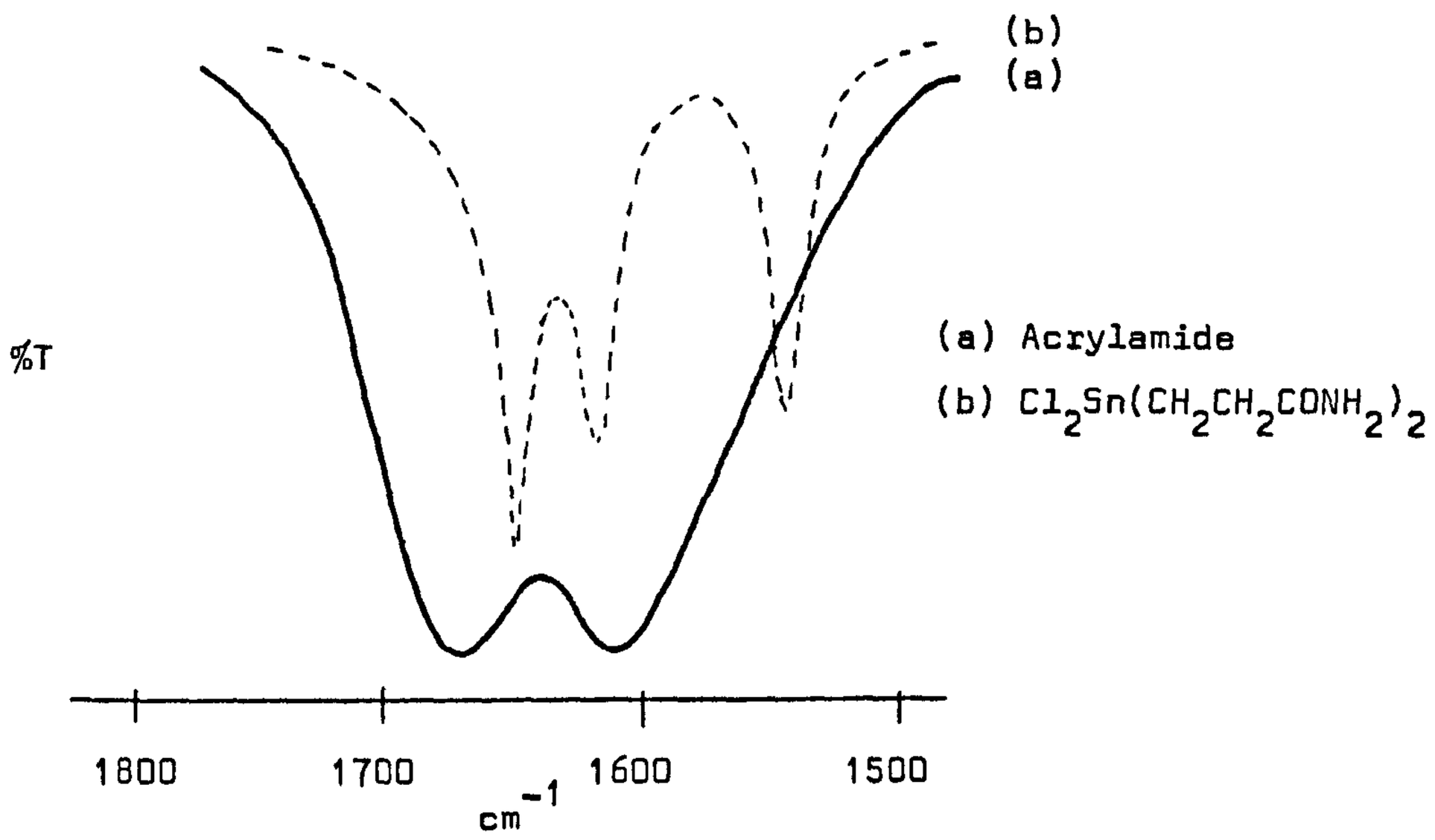

Figure 2.2 The change in the infrared spectrum for ν(C=O), ν(C=C) and δ(N-H) of acrylamide on compound formation with tin.

ν(Sn-C) and ν(Sn-Cl) vibrations occur in the expected frequency ranges in all three compounds and are assigned accordingly.

Clearly, in the bis(β-amidoethyl)tin dichloride there are two possible donor atoms, the carbonyl oxygen and the amido nitrogen. To assist in the assignment of the coordinating species the compound was refluxed in 99.8% D_2O for 1h. The material was then dried and the infrared spectrum recorded using a KBr disc. Whilst complete exchange had not occurred, two additional bands were noted when compared to the untreated material. These were at 2517 cm^{-1} and

Table 2.5

Infrared and Raman Data for $Cl_2Sn(CH_2CH_2CONH_2)_2$ (cm^{-1})

CH_2=CHCONH$_2$	$Cl_2Sn(CH_2CH_2CONH_2)_2$		Assignment
Infrared			
KBr disc	Infrared KBr disc	Raman Solid	
	3420s		
3340vs(br)		3360m (br)	ν(N-H)
3160vs(br)	3280w	3194w (br)	
	2985s	2935	
	2930m (sh)	2958s	ν(C-H)
		2919s	
2800w	2871m		
1660vs(br)	1651vvs	1672w	ν(C=O)
	1625m		
1605vs(br)	1547m		δ(N-H)
		1474w	
1425vs	1450m	1438w	ν(C-N)
		1428w	δ(C-H)
		1409w	
1350s			
1280s	1282m	1297w	
	1266m	1256w	
	1169w		
1137m		1134w	
	1110s	1120s	
1051mw	1067m		
990m	979w		
962m	932w	906vw	
	884w		
841m		852w	
819s	820 (sh)		
	805m		
	775 (sh)		
700m (vbr)	724m	700w (br)	
	683s		
630m (vbr)	650m		
570m	579w	568s	ν(Sn-C)
	537w		
		478s	
	371s	344w	
315m	318vs	312m	ν(Sn-Cl)
		269vvs	
		229w	
		169w (sh)	
		150s	
		112s	
		56vs	
		34s	

2384 cm^{-1} and may readily be assigned to ν(N-D) vibrations when the isotopic shift is considered. A further band at 1613 cm^{-1} can be ascribed to δ(O-H) from incomplete drying and the presence of H_2O after exchange. The bands in the untreated amido compound at 1297 cm^{-1} and 1256 cm^{-1} had coalesced into an ill-defined absorption in the isotopically substituted material. This may have resulted from interference from the δ(N-D) deformation which would be expected in this region.

2.6.2 Mass Spectra

(i) Experimental

Mass spectral data were obtained using an A.E.I. MS902 instrument. The spectrum of the β-carbomethoxyethyltin trichloride was obtained by direct injection at 130°C whilst those of the dichloroestertins were obtained by direct injection at 190°C.

(ii) Results

Mass spectral data for all three compounds are listed in Table 2.6. Both β-carbomethoxyethyltin derivatives exhibit weak parent ions, and in addition $Cl_3SnCH_2CH_2CO_2Me$ exhibited an unidentified low intensity fragment at m/e = $(P + 8)^+$. The fragmentation patterns of both compounds were similar with the major process involving tin-carbon and tin-chlorine bond fission. In addition, loss of the carbomethoxy (CO_2Me) fragment from the organic ligand resulting in $Cl_nSnCH_2CH_2^+$ ions, is observed; particularly for $Cl_3SnCH_2CH_2CO_2Me$.

Table 2.6

Major Fragments[a] In the Mass Spectrum of $Cl_3SnCH_2CH_2CO_2CH_3$, $Cl_2Sn(CH_2CH_2CO_2CH_3)_2$ and $Cl_2(CH_2CH_2CONH_2)_2$.

m/e	Relative Intensity[b]	Assignment
$Cl_3SnCH_2CH_2CO_2CH_3$		
319	4.7	
311	1.4	$Cl_3SnCH_2CH_2CO_2CH_3^+$
276	100.0	$Cl_2SnCH_2CH_2CO_2CH_3^+$
252	29.5	$Cl_3SnCH_2CH_2^+$
224	36.6	Cl_3Sn^+
217	14.0	$Cl_2SnCH_2CH_2^+$
189	26.6	Cl_2Sn^+
154	97.0	$ClSn^+$
147	24.2	$SnCH_2CH_2^+$
119	35.4	Sn^+
$Cl_2Sn(CH_2CH_2CO_2CH_3)_2$		
363	1.5	$Cl_2Sn(CH_2CH_2CO_2CH_3)_2^+$
328	23.3	$ClSn(CH_2CH_2CO_2CH_3)_2^+$
297	1.4	$ClSn(CH_2CH_2CO_2CH_3)CH_2CH_2CO^+$
276	100.0	$Cl_2SnCH_2CH_2CO_2CH_3^+$
241	8.2	$ClSnCH_2CH_2CO_2CH_3^+$
219	4.1	
206	16.4	$SnCH_2CH_2CO_2CH_3^+$
186	8.2	$ClSnCH_2CH_2^+$
154	27.4	$SnCl^+$
119	10.9	Sn^+

Cont./...

Table 2.6 (Continued)

$Cl_2Sn(CH_2CH_2CONH_2)_2$

m/e	Relative intensity[b]	Assignment
333	0.37	$Cl_2Sn(CH_2CH_2CONH_2)_2^+$
299	29.63	$ClSn(CH_2CH_2CONH_2)(CH_2CH_2CONH_3)^+$
280	92.50	$ClSn(CH_2CH_2CONH_2)CH_2CH_2CN^+$
261	48.10	$Cl_2Sn(CH_2CH_2CONH_2)^+$
243	5.53	$Cl_2Sn(CH_2CH_2CN)^+$
226	20.46	$ClSn(CH_2CH_2CONH_2)^+$
208	7.48	$ClSn(CH_2CH_2CN)^+$
191	46.30	$Sn(CH_2CH_2CONH_2)^+$
154	100.00	$ClSn^+$
135	33.34	SnO^+
119	20.37	Sn^+

[a] Based on ^{119}Sn and ^{35}Cl.

[b] Relative to the most intense tin containing fragment.

Loss of a methoxy fragment from one organic group in $Cl_2Sn(CH_2CH_2CO_2Me)_2$ also occurs. In both compounds the most abundant fragment is $Cl_2SnCH_2CH_2COMe^+$.

With the β-amidoethyltin derivative, $Cl_2Sn(CH_2CH_2CONH_2)_2$, tin-carbon and tin-chloride bond fission are again major processes, although dehydration of one of the amidoethyl groups to afford cyanoethyltin ions, $Cl_2Sn(CH_2CH_2CN)^+$ and $ClSn(CH_2CH_2CN)^+$, is also important.

2.6.3 Nuclear Magnetic Resonance Spectra

(i) Experimental

^1H measurements were made on a Varian HA100 c.w. instrument operating at a field strength of 2.345 T. ^{119}Sn data we obtained using an INDOR modification attached to this instrument.

(ii) Results

Table 2.7 combines the n.m.r. data for the three estertin systems studied. The proton chemical shifts for the β-CH_2 and OMe moieties in the two β-carbomethoxyethyltin compounds are the same. An increase in shielding of the α-CH_2 groups in $Cl_2Sn(CH_2CH_2CO_2Me)_2$ is noted, reflecting the change in coordination and hence electron density in the Sn-C system, when compared to the trichloride analogue. The α- and β-CH_2 protons have essentially the same respective chemical shifts in the amidoethyltin derivative as the comparable carbomethoxy system. Two resonances of equal intensity

Table 2.7 Nuclear Magnetic Rescnance Data for Estertin Compounds

COMPOUND	SOLVENT	^{1}H CHEMICAL SHIFT (ppm)[a]				^{119}Sn CHEMICAL SHIFT(ppm)[b,c]	COUPLING CONSTANTS			
		H_α	H_β	OMe	NH_2		$^2J(Sn-H_\alpha)$		$^2J(Sn-H_\beta)$	
							^{119}Sn	^{117}Sn	^{119}Sn	^{117}Sn
$Cl_3SnCH_2CH_2CO_2Me$	$CDCl_3$	2.23t	2.93t	3.97s		-116.0±0.3	108.4	104.3	190.5	186.3
$Cl_2Sn(CH_2CH_2CO_2Me)_2$	$CDCl_3$	1.93t	2.93t	3.97s		- 62.3±0.2	102.2	98.1	153.6	149.7
$Cl_2Sn(CH_2CH_2CONH_2)_2$	DMSO	1.60t	2.89t		8.25s 8.47s	d	113	108	141	137

[a] Relative to Me_4Si

[b] Relative to Me_4Sn

[c] Negative sign denotes low frequency/high field

[d] Tin-119 satellites not sufficiently well defined to enable INDOR spectra to be obtained.

t = triplet, s = singlet

observed for the NH_2 in the amido, assignable to the free N-H and the H—bonded N-H. The expected signal multiplicity is noted for all the methylene groups.

The tin-119 chemical shifts for the $Cl_nSn(CH_2CH_2CO_2Me)_{4-n}$ (n= 2,3) compounds mirrors two competitive effects. The change in coordination around the tin from five, in $Cl_3SnCH_2CH_2CO_2Me$, which is essentially trigonal bipyramidal, to six in the octahedral dichloride compound, because of the resulting increase in electron density at tin, would be expected to produce a higher field shift in the latter. Whereas the increase in the number of electronegative chlorine groups from two to three should produce a shielding effect, and hence a high field shift, in the former compound. Examination of the chemical shift values for four-coordinate R_2SnCl_2 and $RSnCl_3$ systems (Table 2.8) indicates the importance of this latter effect on the relative order of chemical shifts.

Table 2.8 Tin-119 Chemical Shifts data for some $RSnCl_3$ and R_2SnCl_2 systems

R=	$RSnCl_3$ (ppm)	R_2SnCl_2 (ppm)
Me	+21	+137.3
Et	+6.5	+125
Bu	+6.0	+123
Oct	+5.3	+114

Values relative to Me_4Sn = 0

Positive sign denotes high frequency (low field).

As can be seen, in the estertins it would appear that the halogen increase is dominant in affecting the resulting resonance position; $Cl_2Sn(CH_2CH_2CO_2Me)_2$ having a shift of -62.3 p.p.m. whilst the resonance for $Cl_3SnCH_2CH_2CO_2Me$ occurs at -116.0 p.p.m. relative to tetramethyl tin. A result which is in full agreement with trends found for other $R_{4-n}SnX_n$ species. The shielding of the tin being dominated by the paramagnetic term which reflects an electron imbalance in the valence p and d orbitals[212,213]. As n increases in the series $R_{4-n}SnX_n$ the effective electronegativity of the tin atom also increases with a resulting decrease in the p-electron imbalance (due to attached electron-withdrawing groups) and an increase in the shielding of the tin nucleus. This effect has been illustrated for the series $Et_{4-n}SnX_n$ where X = Cl and Br[214]. A more comprehensive review of the factors affecting tin-119 chemical shifts will be given in Chapter four.

2.6.4 Tin-119m Mössbauer Data

(i) Experimental

Tin-119 Mössbauer spectra were collected at 77K using a Harwell spectrometer calibrated with iron and β-tin foil. Data reduction to Lorentzian line shapes was achieved by usual least squares method.

(ii) Results

The tin-119m Mössbauer data for the β-amidoethyl (Fig. 2.3)

and β-carbomethoxyethyltin (Fig. 2.4 and 2.5), as well as several β-carbobutoxytin derivatives, are listed in Table 2.9. In all cases the resulting spectra consisted of a quadrupole split doublet, illustrating non-cubic symmetry. The I.S. and Q.S. for $Cl_3SnCH_2CH_2CO_2Bu$ (I.S. = 1.11, Q.S. 2.06 mm s^{-1}) and $Cl_2Sn(CH_2CH_2CO_2Bu)_2$ (I.S. = 1.45, Q.S. 3.44 mm s^{-1}) are similar to the related $Cl_3SnCH_2CH_2CO_2Me$ (I.S. = 1.00, Q.S. 2.18 mm s^{-1}) and $Cl_2Sn(CH_2CH_2CO_2Me)_2$ (I.S. = 1.50, Q.S. = 3.45 mm s^{-1}) respectively, indicating a general similarity in structure. The amidoethyltin compound, $Cl_2Sn(CH_2CH_2CONH_2)_2$ exhibits a lower I.S. and a higher Q.S. than the equivalent dichlorotin methyl acrylate derivative. This reflects the significantly shorter Sn-O bond distances and lower distortion from linearity of the C-Sn-C unit (see Chapter Three).

Successive replacement of chlorine atoms by sulphur ligands (IOTG and $SCH_2CH_2OCOC_7H_{15}$, (β-MeOct)) results in a progressive increase in the isomer shift (Table 2.9). However, the quadrupole splitting at first increases and then decreases, the final low value of the quadrupole splitting for $BuO_2CCH_2CH_2Sn(IOTG)_3$ (1.64 mms^{-1}) and $BuO_2CCH_2CH_2Sn(\beta\text{-MeOct})_3$ (1.48 mms^{-1}) suggesting a four-coordinate structure for both.

Similar isomer shifts are found for the compounds $(BuO_2CCH_2CH_2)_2SnCl_2$, $(BuO_2CCH_2CH_2)_2Sn(IOTG)_2$ and $Bu_2Sn(IOTG)_2$ but the quadrupole splittings of the two latter compounds are much lower than for the $(BuO_2CH_2CH_2)_2SnCl_2$ (3.44 mms^{-1}). One may deduce, therefore, that the close similarity of the data for the two IOTG derivatives

Table 2.9

Tin-119m Mossbauer Data for Carbonyl-Substituted-Ethyltin Compounds

Compound[a]	I.S.[bc]	Q.S.[c]	Γ_1[cd]	Γ_2[c]	I_1/I_2
$MeAcSnCl_3$	1.00	2.18	1.01	1.01	1.01
$BuAcSnCl_3$	1.11	2.06	1.12	1.07	1.05
$BuAcSnCl_2$(IOTG)	1.26	2.68	0.95	1.02	1.02
$BuAcSnCl(IOTG)_2$	1.33	2.45	1.03	0.98	1.01
$BuAcSn(IOTG)_3$	1.39	1.64	0.89	0.89	1.00
$BuAcSnCl_2$(β MeOct)	1.26	2.32	1.00	1.12	1.01
$BuAcSnCl$(β MeOct)$_2$	1.30	2.15	1.08	1.02	0.99
$BuAcSn$(β MeOct)$_3$	1.38	1.48	0.98	0.87	0.98
$MeAc_2SnCl_2$	1.50	3.45	0.94	0.94	1.00
$BuAc_2SnCl_2$	1.45	3.44	1.06	1.01	1.02
$BuAc_2Sn(IOTG)_2$	1.48	2.16	0.87	0.87	0.99
$Bu_2Sn(IOTG)_2$	1.46	2.31	0.91	0.91	1.01
$AmAc_2SnCl_2$	1.39	3.71	0.90	0.90	0.98

[a] MeAc = $MeO.C(:O).CH_2CH_2$-; BuAc = $BuO.C(:O).CH_2CH_2$-;
AmAc = $H_2N.C(:O).CH_2CH_2$-;
IOTG = iso-octylthioglycollate; β MeOct = $SCH_2CH_2OCOC_7H_{15}$.

[b] Relative to $CaSnO_3$ = 0.

[c] $Mm\ s^{-1}$

[d] The subscripts 1 and 2 refer to the lower and higher velocity lines respectively.

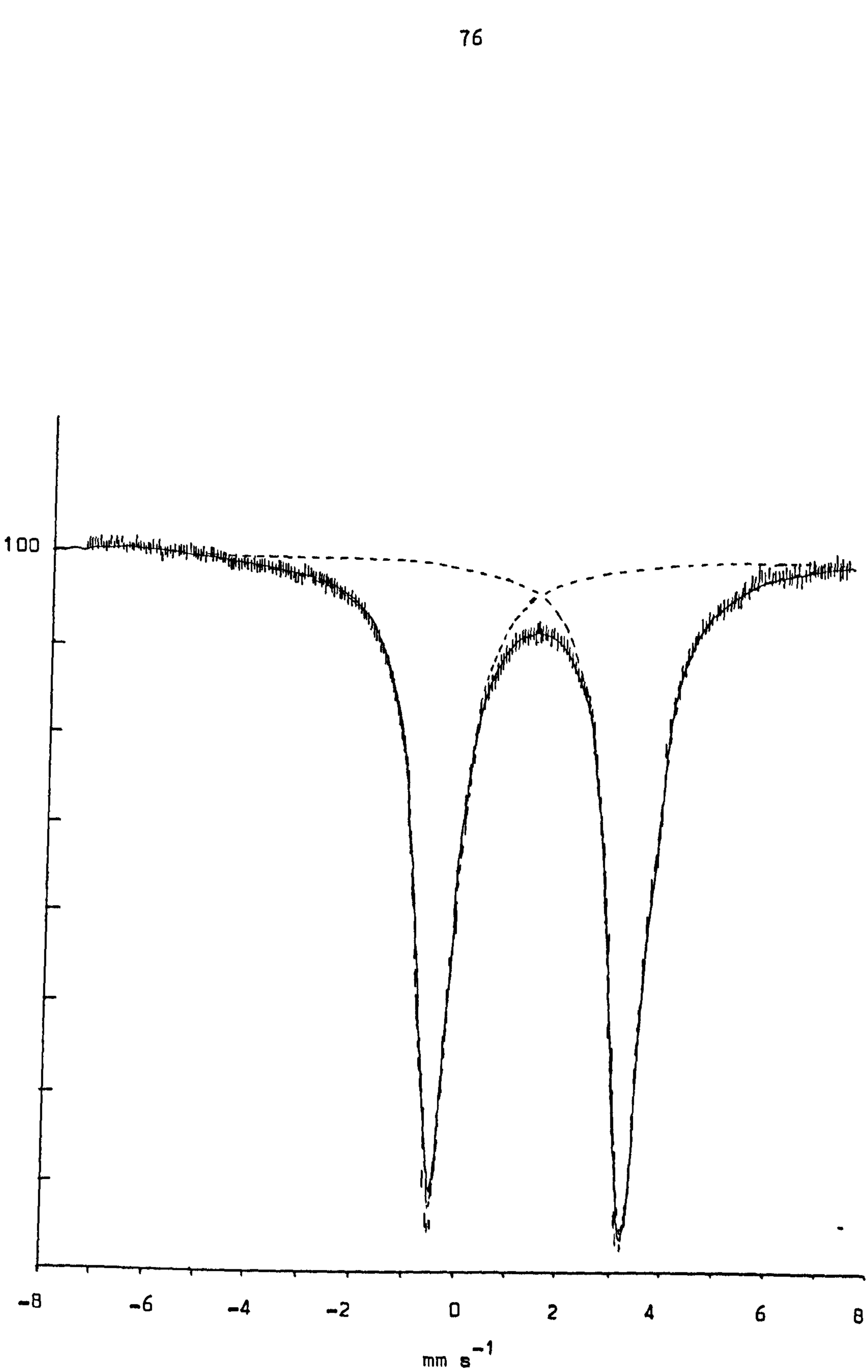

Figure 2.3 Tin-119 Mössbauer spectrum of $Cl_2Sn(CH_2CH_2CONH_2)_2$

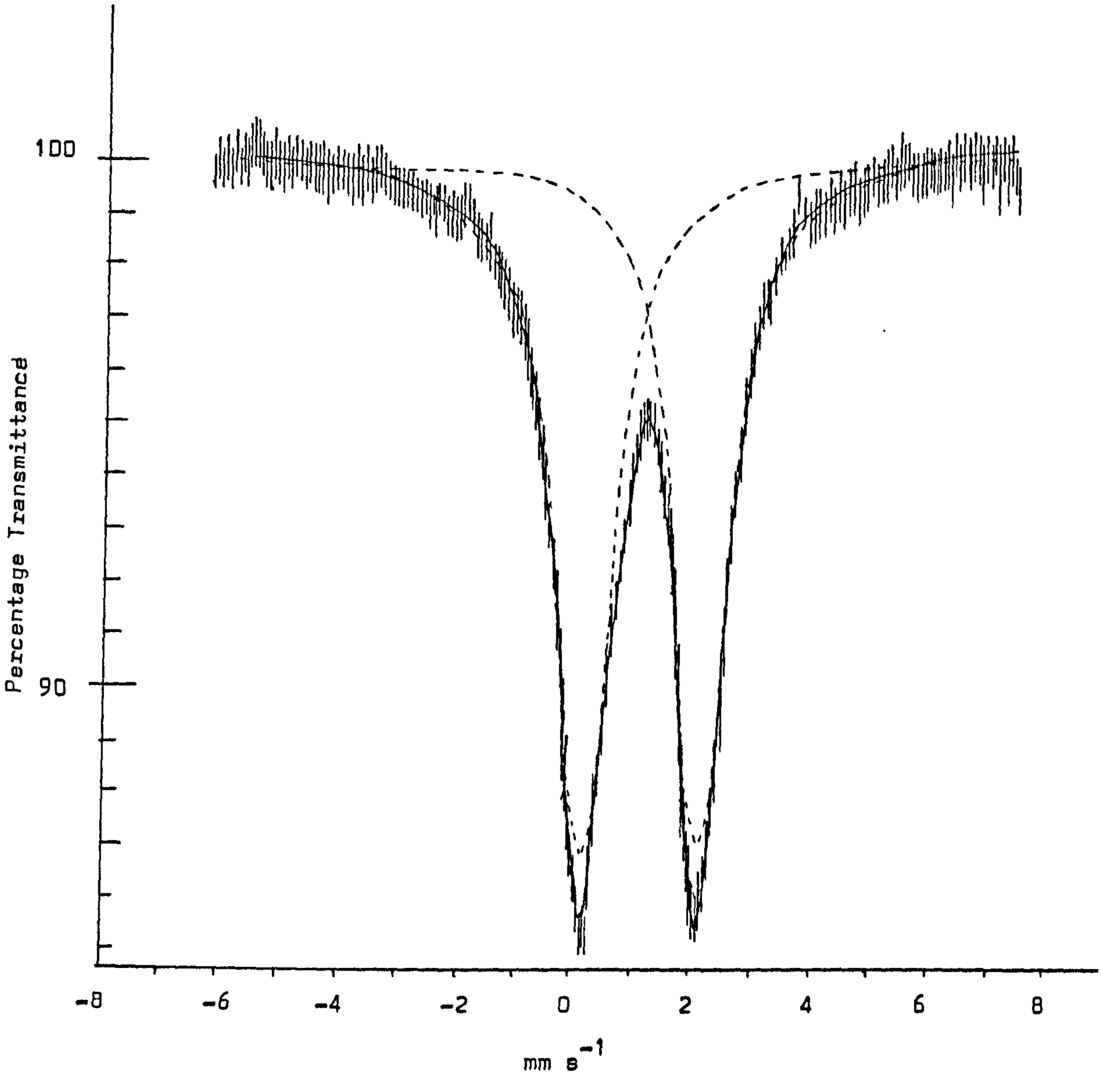

Figure 2.4 Tin-119 Mössbauer spectrum of $Cl_3SnCH_2CH_2CO_2CH_3$

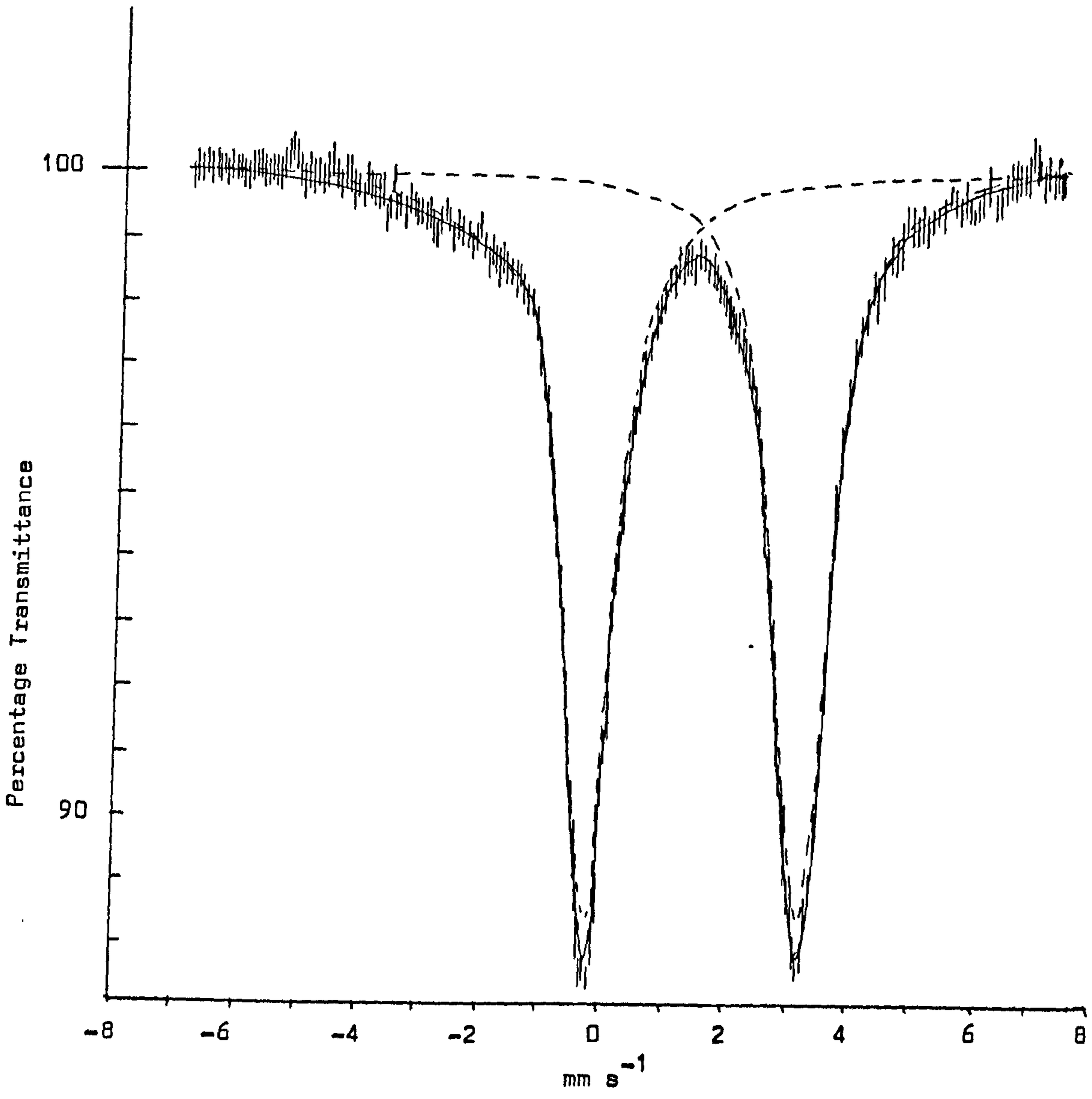

Figure 2.5 Tin-119 Mössbauer spectrum of $Cl_2Sn(CH_2CH_2CO_2CH_3)_2$

strongly suggest that both possess similar structures, most probably a tetrahedral conformation.

2.7 THE IDENTIFICATION OF ORGANOTINS IN PVC BY MOSSBAUER SPECTROSCOPY

To be able to identify the organotin species within PVC by a non-destructive method would clearly be of considerable help in monitoring the stabilization processess and their efficiency. As is illustrated in Table 2.9, the I.S. and Q.S. values obtained from the Mössbauer spectra of the compounds examined show significant differences and each should be identifiable when present in a PVC matrix. To test this hypothesis an attempt was made to record spectra from PVC samples containing 1-2 percent of various thiolatotin additives as stabilisers. Three different organotin compounds in PVC were investigated: $Bu_2Sn(IOTG)_2$, $BuO_2CCH_2CH_2Sn(IOTG)_3$, and $BuO_2CCH_2CH_2Sn(\beta\text{-MeOct})_3$. Thermally degraded as well as freshly milled samples were studied. Doublet spectra were observed in all cases. However, because of the weakness of the Mössbauer source several of the spectra could not be quantified. Nevertheless, several of the samples did yield useful results and a typical spectrum is shown in Figure 2.6. Although the signal-to-noise ratio in this spectrum is not entirely satisfactory it does demonstrate that useful spectra can be obtained from PVC samples and the structure of the tin species present investigated. Thus, an insight into the mechanism of stabilization can be gained through

Mössbauer spectroscopy. The useful data obtained are listed in Table 2.10, together with comparative data.

The isomer shift of freshly-milled $Bu_2Sn(IOTG)_2$-PVC was unchanged from that of neat $Bu_2Sn(IOTG)_2$ although a slight increase in quadrupole splitting is observed (from 2.31 to 2.48 mms^{-1}). This suggests that in the freshly-milled PVC sample only part of the available IOTG groups have been exchanged for chlorine and the organotin species present is most probably $Bu_2SnCl(IOTG)$. On thermal degradation there is a substantial increase in both the I.S. and Q.S. to values which are close to those of Bu_2SnCl_2, complete IOTG-for-chlorine exchange has, therefore, taken place at this stage. Both the freshly milled samples of $BuO_2CCH_2CH_2Sn(IOTG)_3$-PVC and $BuO_2CCH_2CH_2Sn(\beta\text{-MeOct})_3$-PVC exhibited spectra identical to that of $BuO_2CCH_2CH_2SnCl_3$. In these cases, therefore, complete sulphur-for-chlorine ligand exchange has taken place in the milling process. The spectra from the thermally degraded samples were generally of lower quality but it was noteable that the Q.S. values were much lower ($\sim$ 1.0 mms^{-1}) than those for the freshly-milled materials, suggesting further degradation, possibly to monoalkyltin oxides or sulphides.

Table 2.10

Tin-119m Mossbauer Data for Organotin-Stabilised PVC Samples Together with Comparative Data

Sample	I.S.[a,b]	Q.S.[a]
PVC - $Bu_2Sn(IOTG)_2$		
- Freshly milled	1.48	2.48
- Thermally degraded	1.58	3.14
PVC - $BuAcSn(IOTG)_3$		
- Freshly milled	1.1	2.0
PVC - $BuAcSn(\beta MeOct)_3$		
- Freshly milled	1.09	1.98
- Thermally degraded	1.0	1.0
Bu_2SnCl_2	1.60	3.25

[a] mm s^{-1}. [b] Relative to $CaSnO_3$ = 0

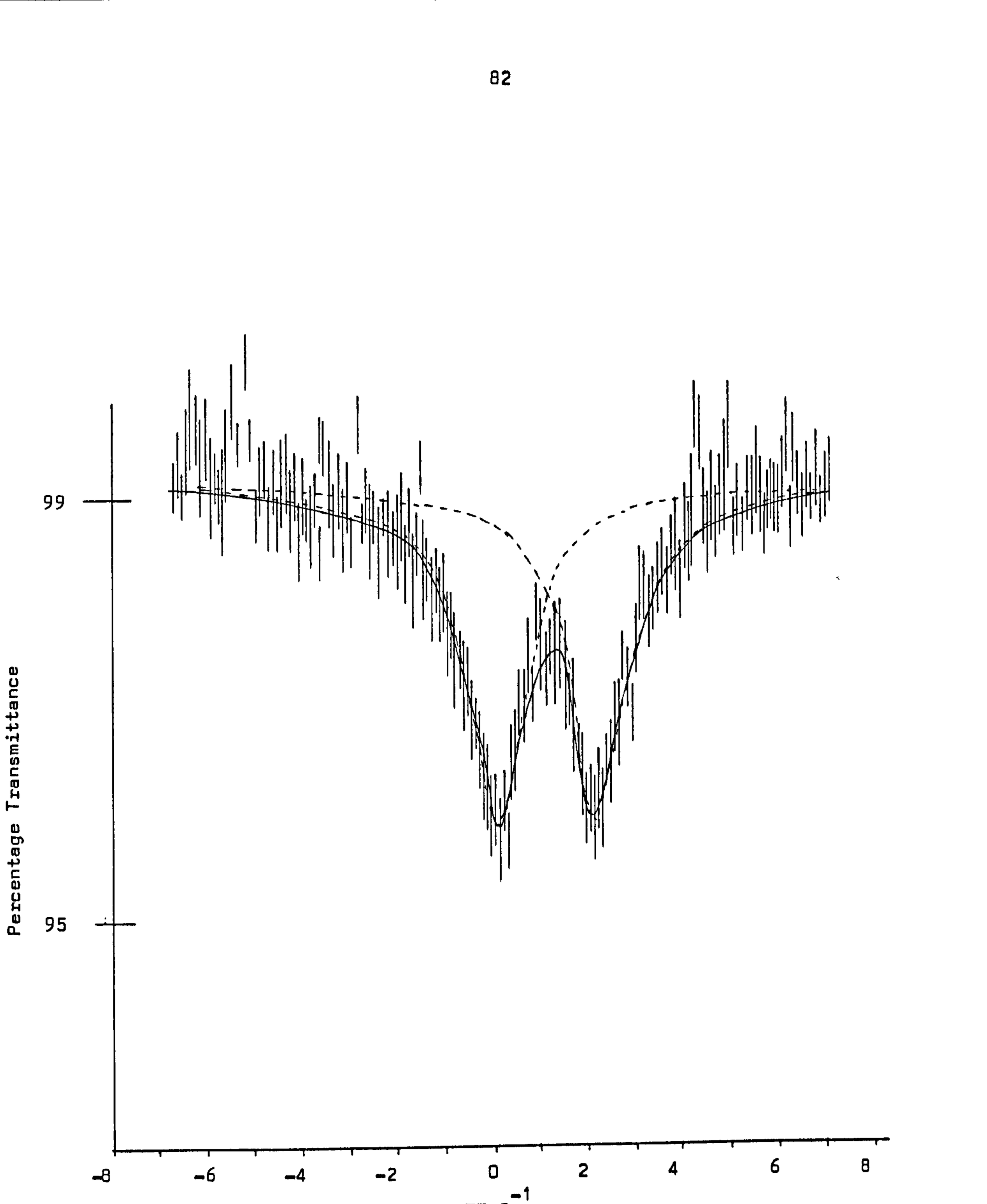

Figure 2.6 Tin-119 Mössbauer spectrum of $Bu_2Sn(IOTG)_2$ in PVC.

REFERENCES

201. H.O. Wirth and H. Andreas. Pure and Appl. Chem. (1977) 49 627-648.

202. R.M. Aseeva, J.G. Aseev, A.A. Berlin and A.A. Kasatockin. Zurn Strukturnoy Chim., (1965) 6 47.

203. R. Schlimper, Plaste u. Kautschuk, (1967) 14 657.

204. A.H. Frye, R.W. Horst and M.A. Paliobagis, J. Polym. Sci. (1964) 42 1765, 1785, 1801.

205. R.C. Poller. Organotin Cpds. New Chemistry and Applications. Ed. J.J. Zuckerman (1976)p Am. Chem. Soc. Washington D.C.

206. Manual of PVC-additives, CIBA-GEIGY Marienberg GMbH (1971) 33.

207. C. Eaborn, J. Organometal. Chem. (1975) 100 43.

208. J.W. Burley, R.E. Hutton and V. Oakes, J.C.S. Chem. Comm. (1976) 803.

209. D. Lanigan and E.L. Weissberg. Organotin Compounds, New Chemistry and Applications., Ed. J.J. Zuckerman (1976) Am. Chem. Soc. Washington D.C.

210. R.E. Hutton and V. Oakes, Organotin Compounds New Chemistry and Applications (1976) p. 123, Ed. J.J. Zuckerman, Am. Chem. Soc. Washington D.C.

211. R.E. Hutton, J.W. Burley and V. Oakes, J. Organometal. Chem., (1978) 156 369.

212. A. Saika and C.P. Slichter, J. Chem. Phys., (1954) 22 26.

213. H.S. Gutowsky and C. Juan, J. Chem. Phys., (1962) 37 2198.

214. W. McFarlane, J.C. Maire and M. Delmas, J. Chem. Soc., Dalton Trans. (1972) 1862.

215. A. Yu. Aleksandrov, Ya. G. Dofman, O.L. Lependina, K.P. Mitofanov, M.V. Plotnikov, L.S. Polak, A.Y. Jemkin and V.S. Shpinel, Russ. J. Phys. Chem. (1964) 38 1185.

216. V. Yngve, British patent 497, 879, Dec. 1938. Chem. Abs. (1939) 40 3923.

CHAPTER THREE

THE CRYSTAL AND MOLECULAR STRUCTURES OF SOME ESTERTINS AND THE REACTION MECHANISM FOR THEIR PRODUCTION

3.1 X-RAY DIFFRACTION STUDIES

3.1.1 Bis-(β-Carbomethoxyethyl)tin dichloride

A crystal of the title compound, prepared as described previously, and of approximate dimensions 0.3 x 0.3 x 0.4 mm, was loaded into a Lindemann capillary. This was used for the initial photography and subsequent intensity data collection.

(i) Crystal Data

$C_8H_{14}Cl_2O_4Sn$, M = 363.81. Monoclinic, $\underline{a}$ = 8.0107, $\underline{b}$ = 15.9104, $\underline{c}$ = 13.4109 Å, β = 131.0044°, V = 1289.13 Å^3, Z = 4, F(000) = 712, μ (Mo - K_α) = 23.96 cm^{-1}. Space group $P_{2_1/C}$ by systematic absences ($0\underline{k}0$ for $\underline{k}$ = 2n + 1 and $\underline{h}0\underline{l}$ for $\underline{l}$ = 2n + 1).

(ii) Cell Measurements and Data Collection

The space group and initial cell parameters were determined from oscillation and zero- and first-layer Weissenberg photographs obtained using a Nonius-Weissenberg camera. Relative intensities up to θ = 25° were collected by use of Mo - K_α radiation (λ = 0.71069 Å) on a Hilger and Watts Y290 four-circle automatic

diffractometer. Cell parameters were further refined by least-squares methods using ca. 10 reflections. All reflections were brought to the same relative intensity by taking reference reflections every 100 reflections recorded, the diffractometer being referenced every 200 reflections recorded. Background counts were low and were included. All reflections with intensities less than three times the standard deviation were considered non-observed, thus reducing the total number of reflections from 3109 to 2388. The intensities were corrected for Lorentz and polarization effects but because the μ value was low, no absorption corrections were made.

(iii) Structure Determination and Refinement

A three-dimensional Patterson synthesis was used to obtain the positional parameters of the tin atom in the asymmetric unit. These were then employed to phase the initial structure factor calculation. Two cycles of full matrix isotropic least-squares refinement of these positions followed by a Fourier synthesis yielded the positions of the remaining (non-hydrogen) light atoms in the asymmetric unit. The positional parameters of all atoms were further refined by two cycles of full matrix least-squares refinement before the tin atom was allowed to vary anisotropically. After two further cycles of full matrix least-squares refinement all atoms were allowed to vary anisotropically. Six further cycles of full matrix least-squares refinement brought convergence in the value of 'R' at 0.048. At this point each reflection was weighted using a scheme based on the

Chebychev series in T(n)(X) to five terms:

$$\omega = \frac{1}{A(0)T(0)X + A(1)T(1)X + ... + A(n-1)T(n-1)X}$$

where A(n) is the coefficient of the n^{th} term and $X = F_o/F_{o(max)}$. The coefficients A(0) to A(4), calculated by least squares methods to minimise $\sum (F_o - F_C)^4$ over all reflections are 162.91, 246.44, 118.66, 42.08 and 14.33. A final 'R' value of 0.046 was obtained after a further three cycles of full matrix, anisotropic, least-squares refinement. Calculations were performed using the CRYSTALS suite of programmes[301] and the scattering factors used were those for neutral atoms[302].

Final fractional atomic coordinates and corresponding anisotropic thermal parameters are listed in Tables 3.1 and 3.2 respectively. Intramolecular bond lengths and angles are given in Table 3.3 and least-square planes data are collected in Table 3.4. Figure 3.1 shows the molecular geometry and atomic labelling, and a projection of the unit cell onto the bc plane is illustrated in Figure 3.2.

3.1.2 β-Carbomethoxyethyltin trichloride

A procedure similar to that employed for the dichloride analogue was used. A crystal of $Cl_3SnCH_2CH_2CO_2Me$ of approximate dimensions 0.3 x 0.3 x 0.5 mm was used, mounted in a Lindemann tube, to obtain the cell parameters and intensity data acquisition.

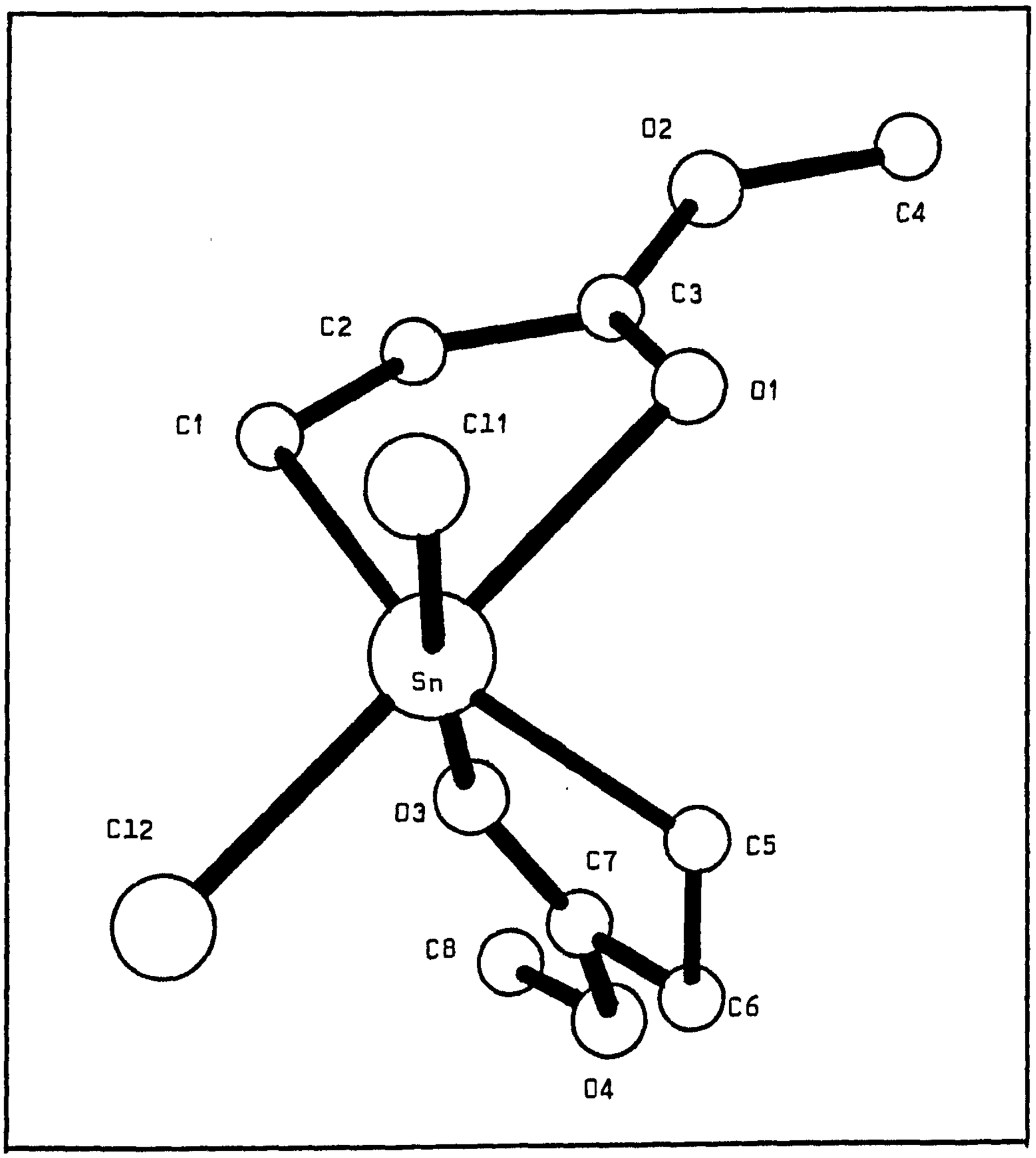

Figure 3.1 The molecular structure and atomic labelling in $Cl_2Sn(CH_2CH_2CO_2CH_3)_2$.

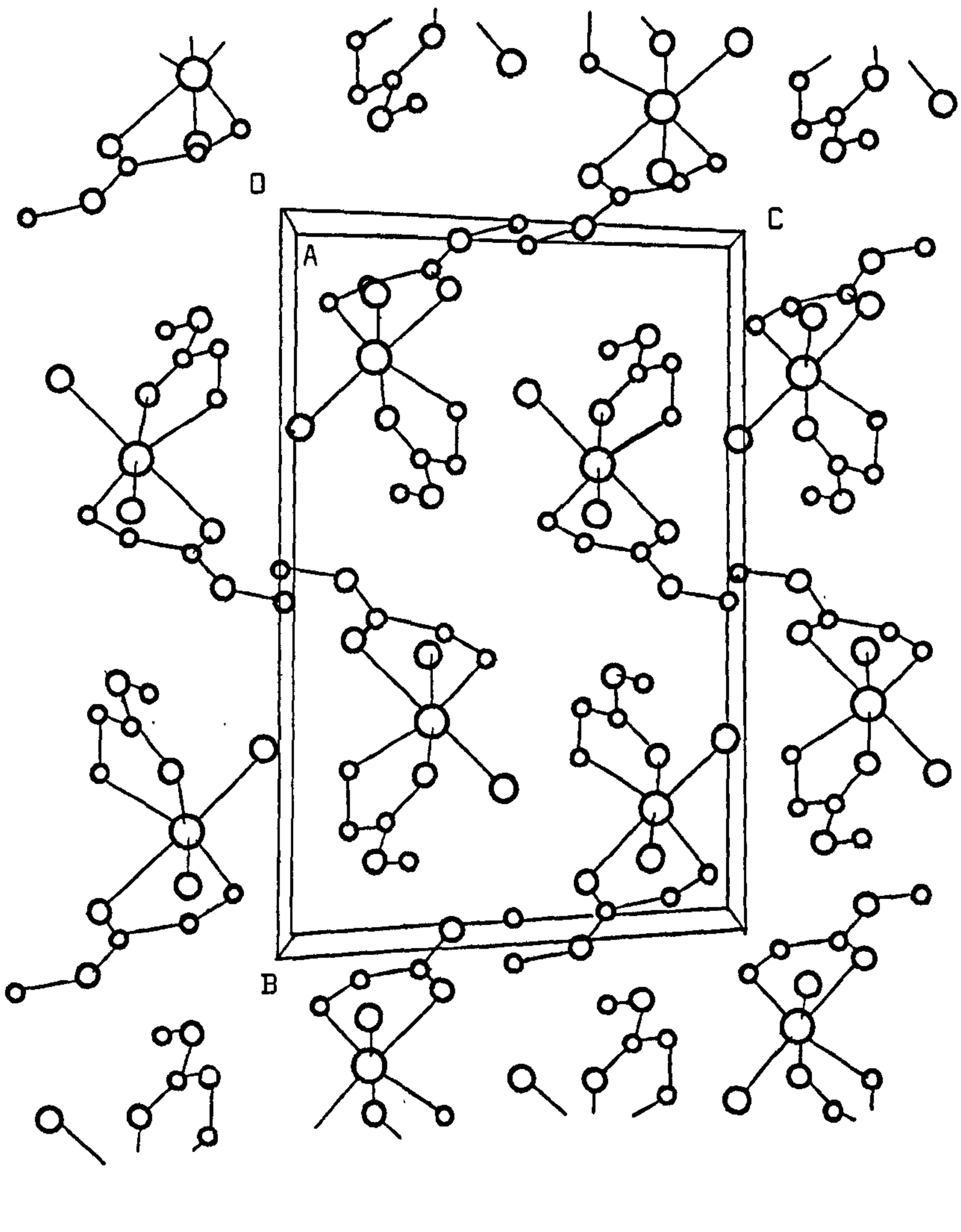

Figure 3.2 $Cl_2Sn(CH_2CH_2CO_2CH_3)_2$; Projection of the unit cell onto the b c plane.

Table 3.1

Final Fractional Atomic Coordinates in Bis-(β-Carbomethoxyethyl)Tin(IV) Dichloride, $Cl_2Sn(CH_2CH_2CO_2CH_3)_2$.

Atom	x/a	y/b	z/c
Sn(1)	0.17179(6)	0.17907(2)	0.18179(3)
Cl(1)	0.4307(3)	0.0989(1)	0.1864(2)
Cl(2)	0.0891(4)	0.2811(1)	0.0220(2)
O(1)	-0.0814(8)	0.2608(3)	0.1960(5)
O(2)	-0.0664(7)	0.3725(3)	0.2935(4)
O(3)	0.229(10)	0.0744(4)	0.3432(7)
O(4)	0.0147(9)	-0.0033(3)	0.3579(6)
C(1)	0.3810(7)	0.2525(3)	0.3566(4)
C(2)	0.2633(7)	0.3302(3)	0.3502(4)
C(3)	0.024(1)	0.3162(4)	0.2760(6)
C(4)	-0.303(10)	0.3636(4)	0.2259(7)
C(5)	-0.108(10)	0.0978(5)	0.0714(7)
C(6)	-0.158(10)	0.0651(4)	0.1567(7)
C(7)	0.0478(9)	0.0462(3)	0.2945(6)
C(8)	0.208(10)	-0.0240(5)	0.4937(8)

Estimated standard deviations in parentheses.

Table 3.2

Final Anisotropic Thermal Parameters for Bis-(β-Carbomethoxyethyl)tin(IV) Dichloride

Atom	U(11)	U(22)	U(33)	U(23)	U(13)	U(12)
Sn(1)	4.90(20)	4.60(20)	4.85(20)	0.14(20)	3.45(20)	0.23(20)
Cl(1)	6.85(9)	8.30(1)	7.80(1)	1.56(9)	5.78(9)	2.42(8)
Cl(2)	10.10(1)	5.12(8)	7.20(1)	1.48(7)	6.30(1)	0.87(8)
O(1)	5.80(2)	6.00(2)	5.90(3)	-1.50(2)	3.90(2)	-0.60(2)
O(2)	7.70(2)	5.60(2)	7.00(2)	-1.20(2)	5.50(2)	-0.50(2)
C(3)	4.90(3)	6.70(4)	5.80(4)	0.70(3)	3.40(3)	-0.60(3)
O(4)	6.10(3)	6.20(3)	6.40(3)	0.60(2)	4.60(3)	-0.40(2)
C(1)	5.70(2)	6.10(2)	5.60(2)	-1.20(2)	2.80(2)	-0.30(2)
C(2)	5.70(2)	6.20(2)	6.60(2)	-2.00(2)	3.90(2)	-1.10(2)
C(3)	6.40(3)	4.80(3)	5.00(3)	-0.10(2)	4.10(3)	0.10(3)
C(4)	6.20(3)	8.80(3)	7.40(4)	-0.20(3)	4.90(3)	0.90(2)
C(5)	5.10(4)	4.50(4)	5.60(4)	-0.30(3)	3.30(3)	-0.30(3)
C(6)	5.20(3)	5.20(4)	7.20(3)	1.00(3)	4.20(3)	0.40(3)
C(7)	5.70(3)	4.00(3)	6.30(3)	0.10(2)	4.50(3)	0.40(3)
C(8)	6.40(4)	7.80(5)	6.30(4)	1.70(4)	4.20(3)	0.70(4)

U(ij) are of the form: $10^2 \exp[-2\pi^2(h^2U(11)a^{*2} + k^2U(22)b^{*2} + l^2U(33)c^{*2} + 2hkU(12)a^*b^* + 2klU(23)b^*c^* + "hlU(13)a^*b^*)]$. Estimated standard deviations in parentheses.

Table 3.3

Intramolecular Bond Lengths (A) and Angles (°) of Bis-(β-Carbomethoxy-ethyl)tin(IV) Dichloride

Distances			
Sn(1)-Cl(1)	2.401(2)		
Sn(1)-Cl(2)	2.409(2)		
Sn(1)-C(1)	2.124(6)		
Sn(1)-C(5)	2.127(5)		
Sn(1)-O(1)	2.520(4)		
Sn(1)-O(3)	2.524(4)		
Cl(1)-C(2)	1.523(9)	C(5)-C(6)	1.531(8)
C(2)-C(3)	1.487(9)	C(6)-C(7)	1.491(9)
C(3)-O(1)	1.205(7)	C(7)-O(3)	1.220(7)
C(3)-O(2)	1.306(7)	C(7)-O(4)	1.307(7)
C(4)-O(2)	1.463(8)	C(8)-O(4)	1.457(8)
Angles			
Cl(1)-Sn(1)-O(1)	175.5(1)		
Cl(1)-Sn(1)-Cl(2)	96.3(1)		
Cl(1)-Sn(1)-C(5)	101.0(2)		
Cl(1)-Sn(1)-O(3)	87.7(1)		
Cl(1)-Sn(1)-C(1)	102.8(2)		
Cl(2)-Sn(1)-C(1)	99.7(2)		
Cl(2)-Sn(1)-C(5)	103.9(2)		
Cl(2)-Sn(1)-O(3)	175.5(1)		
Cl(2)-Sn(1)-O(1)	87.4(1)		
O(1)-Sn(1)-C(1)	74.0(2)		
O(1)-Sn(1)-C(5)	80.5(2)		
O(1)-Sn(1)-O(3)	88.7(2)		
O(3)-Sn(1)-C(1)	81.3(2)		
O(3)-Sn(1)-C(5)	73.3(2)		
C(1)-S(1)-C(5)	144.1(3)		
Sn(1)-C(1)-C(2)	111.9(4)		
C(1)-C(2)-C(3)	113.3(5)		

Cont./..

Table 3.3 continued

Angles	
C(2)-C(3)-O(1)	123.2(5)
C(2)-C(3)-O(2)	114.2(5)
O(1)-C(3)-O(2)	122.5(6)
C(3)-O(2)-C(4)	116.9(5)
Sn(1)-O(1)-C(3)	108.4(4)
Sn(1)-C(5)-C(6)	111.0(4)
C(5)-C(6)-C(7)	112.2(5)
C(6)-C(7)-O(3)	123.2(6)
C(6)-C(7)-O(4)	113.4(4)
O(3)-C(7)-O(4)	123.4(6)
C(7)-O(4)-C(8)	116.5(5)
Sn(1)-O(3)-C(7)	107.5(4)

Estimated Standard deviations in parentheses.

Table 3.4

Equations of the Mean Planes through Groups of Atoms in Bis-(β-Carbomethoxyethyl)tin(IV) dichloride and Deviation of Atoms from the Planes (Å)

PLANE 1 Sn(1),Cl(1),C(1),O(3),C(5)

equation of the plane:

$-1.12287x' + 11.87909y' - 5.34819z' = 0.203$

Sn(1), 0.759; Cl(1), - 0.508; C(1), 0.461; O(3), -1.411; C(5), 0.698

PLANE 2 Sn(1),Cl(1),Cl(2),O(3),O(1)

equation of the plane:

$2.87599x' + 8.83637y' + 4.43250z' = 2.887$

Sn(1), -0.005; Cl(1), 0.051; Cl(2), 0.049; O(3), -0.050; O(1), 0.052

PLANE 3 Sn(1),Cl(2?,O(5),O(1),C(1)

equation of the plane:

$4.95338x' - 11.04934y' - 1.71743x' = -2.203$

Sn(1), 0.763; Cl(2), -0.500; C(5), 0.467; O(1), -1.419; C(1), 0.689

Angle between plane 1 and plane 2 = 97.09^{o}

Angle between plane 1 and plane 3 = 147.61^{o}

Angle between plane 2 and plane 3 = 83.55^{o}

Equations are of the form $px' + qy' + rz' = s$ where x', y' and z' are orthogonal coordinates related to the monoclinic coordinates by:

$x' = x + z \cos$, $y' = y$ and $z' = z \sin$ (7).

(i) Crystal Data

$C_4H_7O_2Cl_3Sn$, M = 312.29, orthorhombic, $\underline{a}$ = 9.2981, $\underline{b}$ = 10.5389, $\underline{c}$ = 10.0885 Å, V = 988.59 Å^3, Z = 4, F(000) = 592, μ (Mo - K_α) = 33.45 cm^{-1}. Space group $P_{2_12_12_1}$ by systematic absences ($\underline{h}$00 for $\underline{h}$ = 2n + 1, 0k0 for $\underline{k}$ = 2n + 1 and 00$\underline{l}$ for $\underline{l}$ = 2n + 1).

(ii) Cell Measurements and Data Collection

Again, from oscillation and zero- and first-layer Weissenberg photographs the space group and initial cell parameters were determined. Relative intensities up to θ = 27.5° were collected using the same (Mo - K_α) radiation at λ = 0.71069 Å on the Hilger and Watts Y290 four-circle automatic diffractometer. Cell parameters and data were obtained as before. Systematically absent reflections and those with $I < 3\sigma(I)$ were discarded, reducing the total number of reflections from 1365 to 1198. Background counts were low and were included. Intensity corrections were made to allow for Lorentz and polarization effects but none were made for absorption as the value of μ was low.

(iii) Structure Determination and Refinements

The positional parameters of the tin atom in the asymmetric unit were determined using a three-dimensional Patterson synthesis. These enabled phasing of the initial structure factor calculation. Two cycles of full-matrix isotropic least-squares refinement followed

by a Fourier synthesis yielded the positions of three chlorine atoms and produced an 'R' value of 0.265. Two further cycles of full matrix isotropic refinement followed by a Fourier synthesis enabled the positions of the remaining carbon and oxygen atoms attached to tin to be determined in the asymmetric unit. Two further cycles of refinement of these positional parameters produced an 'R' value of 0.093, after which all atoms were allowed to vary anisotropically during the course of six further cycles of full matrix least-squares refinement. At this stage the 'R' value had settled to 0.042 and a weighting scheme based on the Chebychev series, described, to five terms was inserted to minimise $\Sigma (F_o - F_c)^4$ over all reflections. The coefficients employed being 791.49, 1350.07, 854.89, 379.59 and 94.37. After four further cycles of full matrix anisotropic least-squares refinement a final 'R' value of 0.0332 was obtained.

As for the dichloride, the CRYSTALS suite of programmes[301] was used for all calculations and the scattering factors were those for neutral atoms[302].

The final fractional atomic coordinates and corresponding anisotropic thermal parameters are listed in Tables 3.5 and 3.6 respectively. Intramolecular bond distances and angles are given in Table 3.7. The molecular geometry and atomic numbering is shown in Figure 3.3 and a projection of the unit cell onto the bc plane is illustrated in Figure 3.4 Planes data are given in Table 3.8.

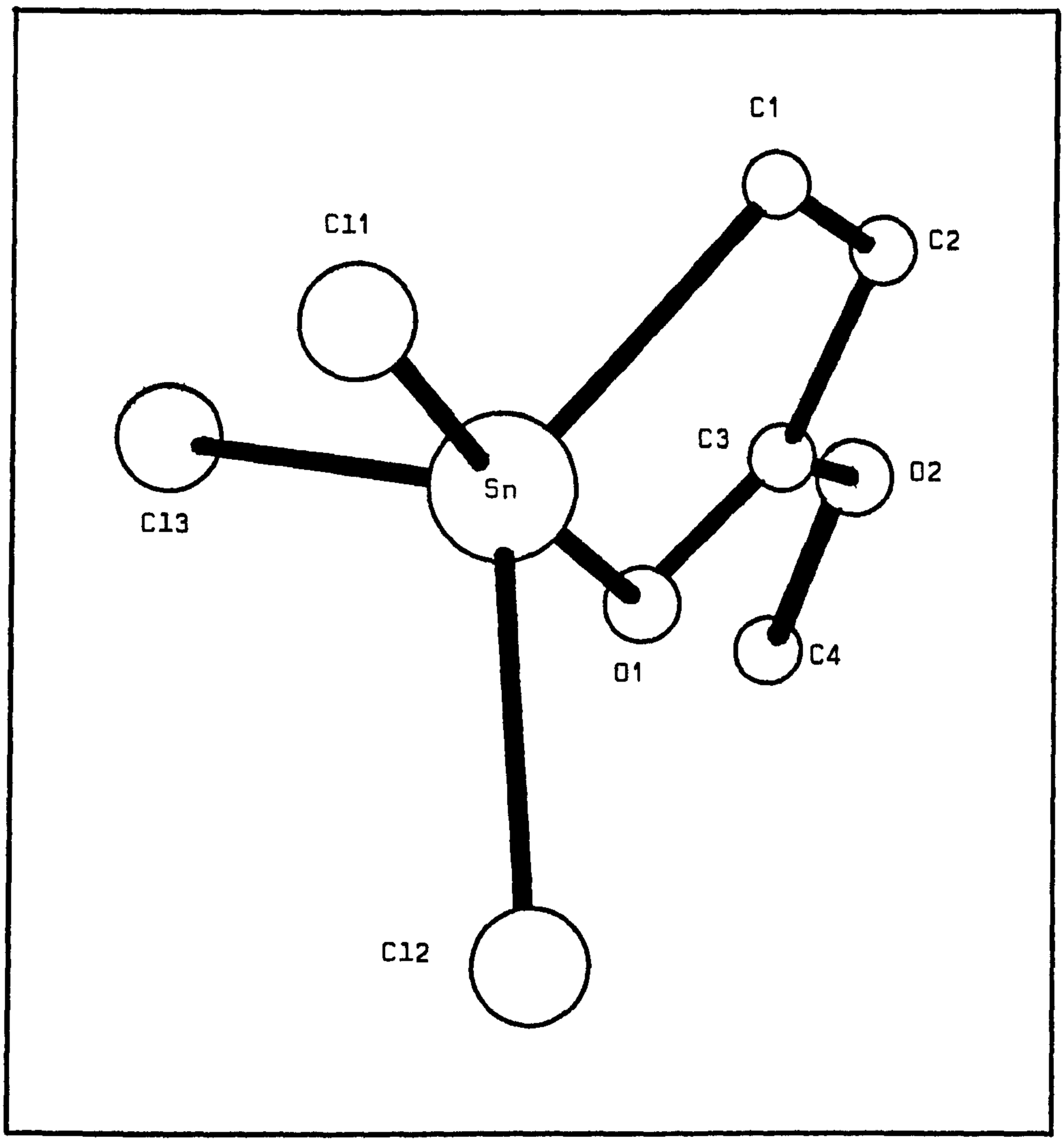

Figure 3.3 The molecular structure and atomic labelling in $Cl_3SnCH_2CH_2CO_2CH_3$.

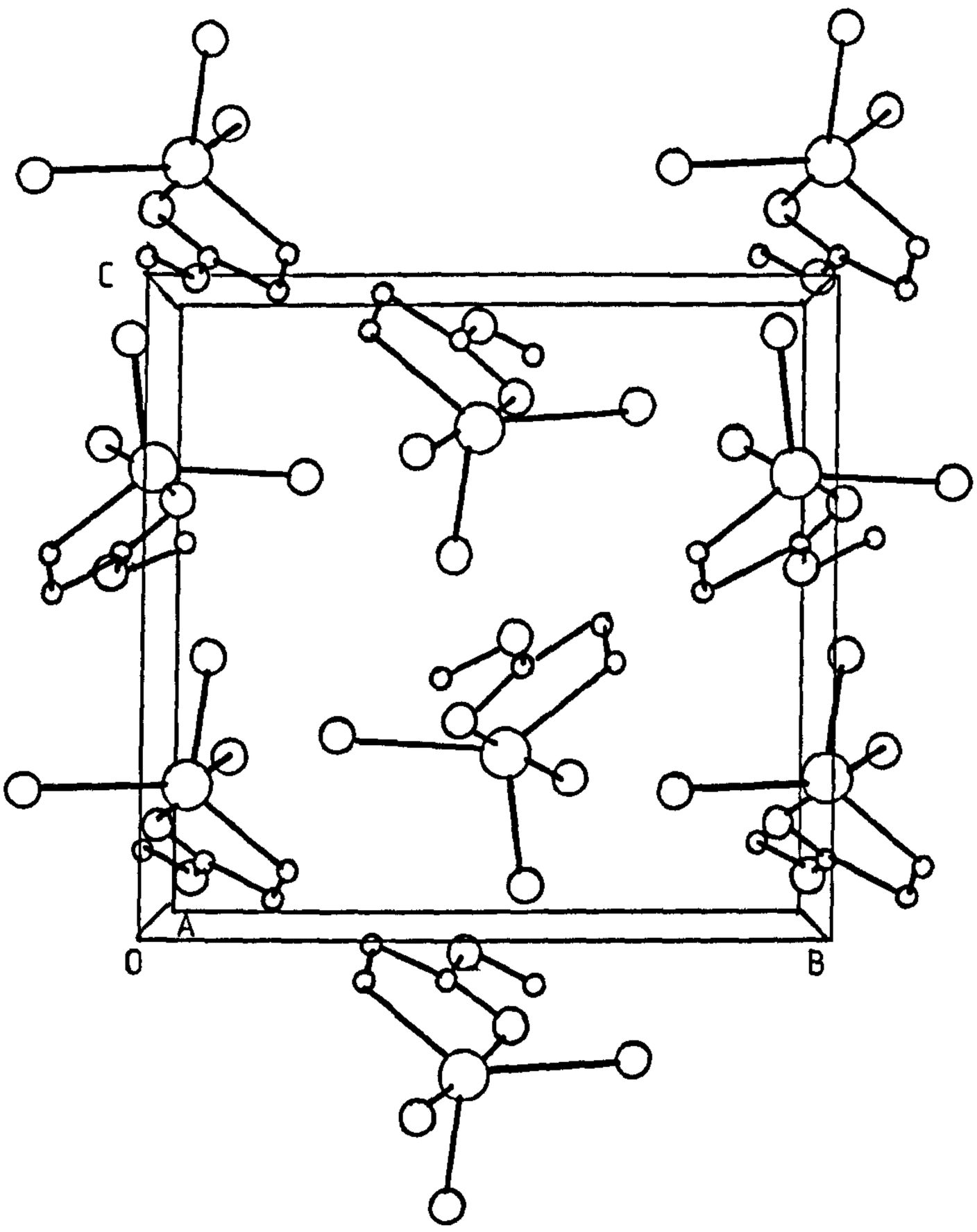

Figure 3.4 $Cl_3SnCH_2CH_2CO_2CH_3$: Projection of the unit cell onto the b c plane

Table 3.5

Final Fractional Atomic Coordinates in β-Carbomethoxyethyltin(IV) Trichloride $Cl_3SnCH_2CH_2CO_2CH_3$

Atom	x/a	y/b	z/c
Sn(1)	0.18463(3)	0.02702(5)	0.22049(4)
Cl(1)	0.4036(2)	0.1007(3)	0.2639(3)
Cl(2)	0.2227(3)	-0.2165(2)	0.2038(3)
Cl(3)	0.1036(2)	0.0558(3)	0.4246(2)
O(1)	-0.0351(5)	-0.0340(6)	0.1707(5)
O(2)	-0.1966(6)	0.03346(7)	0.0435(6)
C(1)	0.1335(7)	0.1821(8)	0.0788(7)
C(2)	0.0038(9)	0.1560(1)	0.0202(8)
C(3)	-0.768(9)	0.0440(1)	0.0855(9)
C(4)	-0.2840(9)	-0.0660(1)	0.1060(1)

Estimated standard deviations in parentheses

Table 3.6

Final Anisotropic Thermal Parameters for β-Carbomethoxyethyltin(IV) trichloride

Atom	U(11)	U(22)	U(33)	U(23)	U(13)	U(12)
Sn(1)	5.150(20)	5.580(20)	5.730(20)	1.350(20)	0.090(20)	0.00(20)
Cl(1)	5.120(9)	9.90(2)	10.20(2)	0.90(1)	-0.40(1)	-0.50(1)
Cl(2)	9.50(1)	5.80(1)	8.70(1)	1.10(1)	1.30(1)	1.40(1)
Cl(3)	7.10(1)	9.30(1)	5.90(1)	-0.30(1)	8.60(9)	-0.50(1)
O(1)	5.70(2)	6.10(3)	7.60(3)	1.90(3)	-1.60(2)	-0.40(3)
O(2)	6.90(3)	7.50(3)	9.60(4)	-0.60(3)	-3.20(3)	1.70(3)
C(1)	6.70(4)	7.10(4)	8.10(4)	3.20(3)	0.20(3)	0.00(3)
C(2)	8.20(5)	7.30(5)	6.50(4)	1.90(4)	-0.30(4)	1.10(5)
C(3)	5.90(4)	5.60(5)	6.10(5)	-1.10(4)	-0.80(4)	1.40(5)
C(4)	5.70(4)	8.20(6)	14.00(1)	0.40(6)	2.10(5)	0.50(4)

U_{ij} are of the form $10^2 \exp\left[-2\pi^2(\underline{h}^2 U_{11}\underline{a}^{*2} + \underline{k}^2 U_{22}\underline{b}^{*2} + \underline{l}^2 U_{33}\underline{c}^{*2} + 2\underline{hk}U_{12}\underline{a}^*\underline{b}^* + 2\underline{kl}I_{23}\underline{b}^*\underline{c}^* + 2\underline{hl}U_{13}\underline{a}^*\underline{c}^*)\right]$

Table 3.7

Intramolecular Bond Lengths (Å) and Angles (b) of

β-Carbomethoxyethyltin(IV) Trichloride

Bond lengths	
Sn(1)-Cl(1)	2.357(2)
Sn(1)-Cl(2)	2.303(2)
Sn(1)-Cl(3)	2.317(2)
Sn(1)-O(1)	2.347(5)
Sn(1)-C(1)	2.139(8)
Cl(1)-C(2)	1.47(1)
C(2)-C(3)	1.50(1)
C(3)-O(1)	1.23(1)
C(3)-O(2)	1.29(1)
C(4)-O(2)	1.45(2)
Angles	
Cl(1)-Sn(1)-Cl(2)	98.3(1)
Cl(1)-Sn(1)-Cl(3)	96.7(1)
Cl(2)-Sn(1)-Cl(3)	104.1(1)
Cl(1)-Sn(1)-O(1)	176.7(2)
Cl(1)-Sn(1)-C(1)	99.5(2)
Cl(2)-Sn(1)-O(1)	84.4(2)
Cl(2)-Sn(1)-C(1)	130.5(2)

Cont./..

Table 3.7 continued

Angles	
Cl(3)-Sn(1)-O(1)	84.4(2)
Cl(3)-Sn(1)-C(1)	119.0(2)
O(1)-Sn(1)-C(1)	77.2(3)
Sn(1)-C(1)-C(2)	113.6(6)
C(1)-C(2)-C(3)	113.9(7)
C(2)-C(3)-O(1)	124.3(8)
C(2)-C(3)-O(2)	113.4(7)
O(1)-C(3)-O(2)	122.3(8)
Sn(1)-O(1)-C(3)	110.2(5)
C(3)-O(2)-C(4)	117.1(7)

Table 3.8

Equations of the Mean Planes through Groups of Atoms in β-Carbomethoxyethyltin(IV) Trichloride and Deviations of Atoms from the Planes (Å)

PLANE 1. Sn(1), Cl(1), C(2), C(3), O(1), O(2), C(4)

Equation of the plane:

3.22384x -6.20558y - 7.0889z = -1.167

Sn(1), 0.032; Cl(1), -0.27; C(1), -0.091; C(1), 0.066; C(3), 0.043; O(1), 0.055; O(2), 0.010; C(4), -0.086.

PLANE 2. Sn(1), Cl(2), Cl(3), C(1)

Equation of the plane:

9.49338x + 2.67305y + 1.88094z = 1.998

Sn(1), 0.242; Cl(2), -0.079; Cl(3), -0.067; C(1), -0.096

Angle between plane 1 and plane 2 = 90.64°

3.1.3 Bis(β-amidoethyl)tin dichloride

The sample of bis(β-amidoethyl)tin dichloride supplied by Dr. J.W. Burley was analysed as follows: Found C, 21.49; H, 4.16; N, 8.36; Cl 21.11% $C_6H_{12}Cl_2N_2O_2Sn$ calcd.: C, 21.56; H, 3.59; Cl, 21.26%; N, 8.38. Although the material was air stable (decomp. $> 260^{o}C$), for convenience a Lindeman capillary was again used to mount a suitable crystal (approximate dimensions 0.3 x 0.3 x 0.2mm).

(i) Crystal Data

$C_6H_{12}Cl_2O_2N_2Sn$, M = 333.89, Monoclinic, $\underline{a}$ = 9.1314, $\underline{b}$ = 12.8672, $\underline{c}$ = 13.0317 Å, β = 126.6032°, V = 1229.196 $Å^3$, Z = 4, F(000) = 648, μ ($Mo - K_\alpha$) = 24.94 cm^{-1}. Space group C_C by systematic absences ($\underline{hkl}$ for $\underline{h}$ = 2n + 1, $\underline{h0l}$ for $\underline{l}$ = 2n + 1 ($\underline{h}$ = 2n + 1), $0\underline{k}0$ for $\underline{k}$ = 2n + 1).

(ii) Cell Measurements and Data Collection

From oscillation and zero- and first-layer Weissenberg photographs the initial cell parameters were determined and the space group assigned as C_C.

Relative intensities up to $\theta = 25^{o}$ were collected in the manner employed for the crystal measurements described above. Accurate cell parameters were obtained by least-squares refinement using 22 reflections and subsequently the intensities of 1472 independent reflections were measured in the range $0 < \theta < 25^{o}$. The techniques employed were as described before. Reflections with

a corrected count of less than three times the estimated standard deviations were considered non-observed and excluded. This reduced the total number of reflections used to 1024. Because of the low value absorption corrections were not made, although corrections for Lorentz and polarization effects were applied.

(iii) Determination and Refinement of the Structure

After determining the positional parameters of the tin atom from a three-dimensional Patterson synthesis, use of these coordinates was made in phasing the initial structure factor calculations. A Fourier synthesis following two cycles of full matrix isotropic least-squares refinement yielded the positions of the two chlorine atoms and two further cycles of refinment and a Fourier synthesis gave the positions of two of the oxygen and three of the carbon atoms. However, because of the unsatisfactory nature of the thermal parameters of one of the chlorine atoms this was discarded. Two further cycles of isotropic full matrix least-squares refinement gave the parameters of a new chlorine atom. At this stage the 'R' value was 0.149. Again, because of unsatisfactory thermal parameters it was found necessary to delete one of the nitrogen and two of the carbon atoms. However, a further cycle of refinement and a Fourier synthesis provided the parameters for all the atoms of the molecule; these were to prove satisfactory. The 'R' value was now 0.141 and for the next four cycles of refinement the tin atom was allowed to vary anisotropically. This was followed by two further cycles of

full matrix least squares refinement in which the chlorine atoms were also varied anisotropically. Four cycles of refinement with all atoms varying anisotropically produced an 'R' value of 0.029.

Although it was now clear that in one ligand the bond distances showed coordination by the carbonyl oxygen to the tin, in the other ligand the distances from the carbonyl carbon to the oxygen and nitrogen were at variance with expected values. It was, therefore, decided to exchange the assignments of the oxygen and nitrogen atoms in this ligand and observe any resulting changes in their thermal parameters and the 'R' value. However, it was found that the original ordering had been correct as the 'R' value rose to 0.031 and reduced to 0.029 on returning to the original assignment.

A weighting scheme based on the Chebychev series was now introduced with five terms being inserted to minimise $\Sigma\ (F_o - F_c)^4$ over all reflections; these coefficients being 144.84, 219.39, 99.79, 22.75 and 1.86. Six further cycles of full matrix least-squares anisotropic refinement resulted in convergence of 'R' to a terminal value of 0.0268.

Programmes[301] and scattering factors[302] were as used in the crystal data collections previously described. The final fractional atomic coordinates and corresponding thermal parameters are collected in Table 3.9 and 3.10 respectively. Table 3.11 lists the intramolecular bond lengths and angles and the least-squares planes data are listed in Table 3.12. The molecular geometry and atomic labelling is given in Figure 3.5 and a projection of the unit cell onto the ac plane illustrated in Figure 3.6.

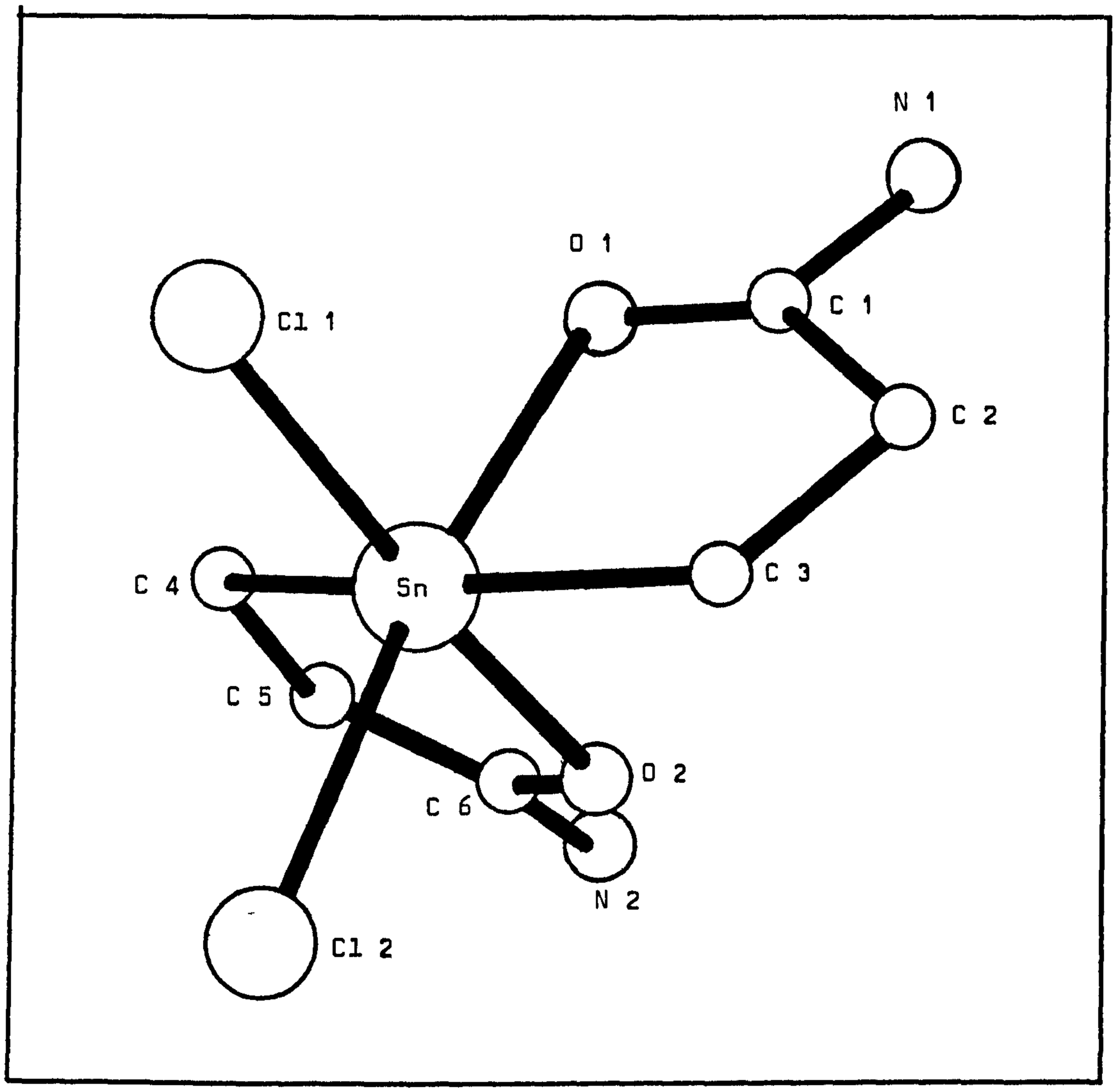

Figure 3.5 Molecular structure and atomic labelling in $Cl_2Sn(CH_2CH_2CONH_2)_2$.

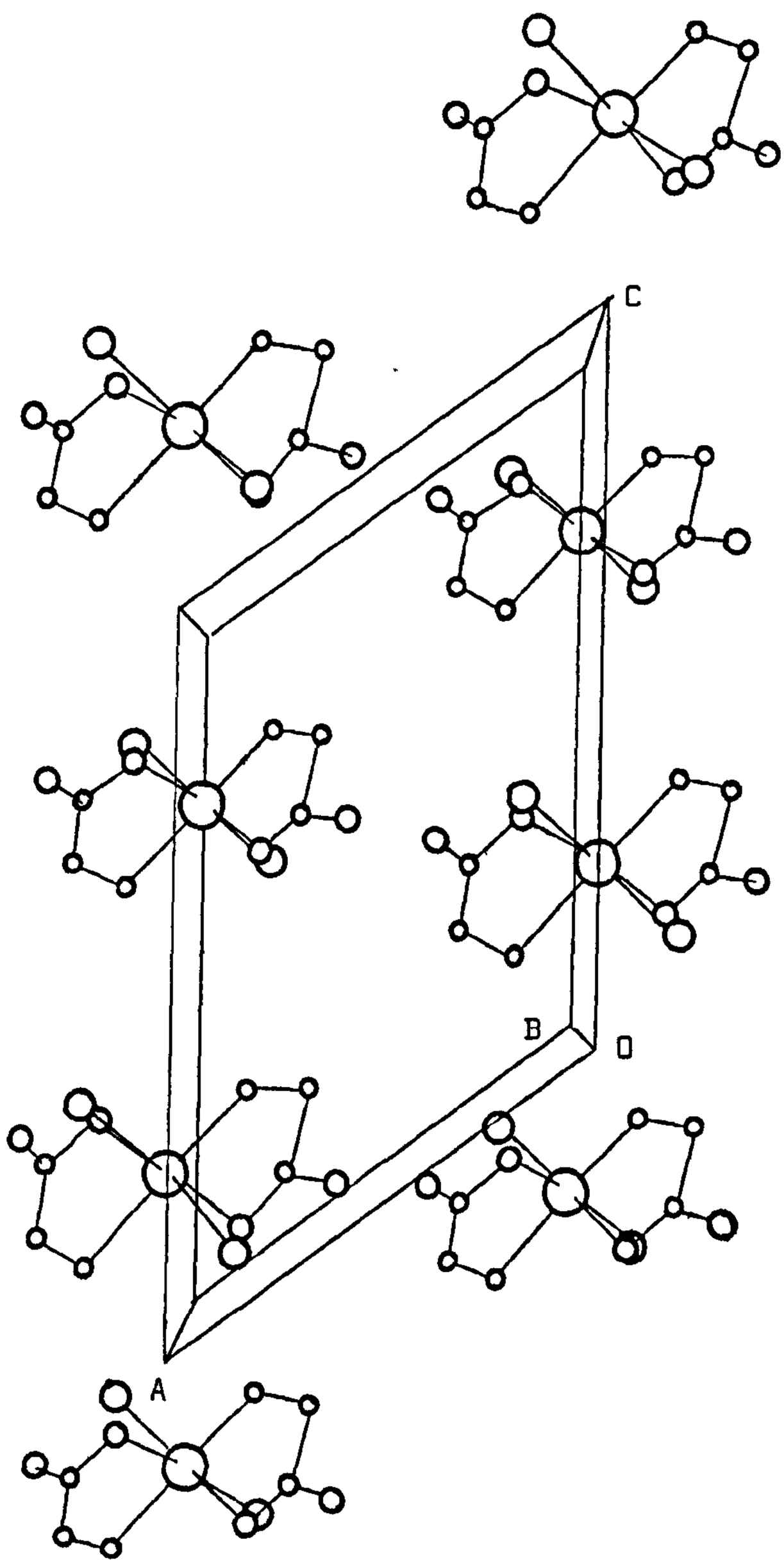

Figure 3.6 $Cl_2Sn(CH_2CH_2CONH_2)_2$: Projection of the unit cell onto the a c plane.

Table 3.9

Final Fractional Atomic Coordinates in Bis-(β-Amidoethyl)tin(IV) Dichloride.

$Cl_2Sn(CH_2CH_2CONH_2)_2$

Atom	x/a	y/b	z/c
Sn(1)	0.0000	0.00672(3)	0.2500
Cl(1)	0.1844(8)	-0.1254(6)	0.4156(7)
Cl(2)	-0.1908(9)	-0.1184(6)	0.0756(8)
N(1)	0.397(2)	0.253(1)	0.436(1)
N(2)	-0.373(3)	0.265(1)	0.065(2)
O(1)	0.171(2)	0.141(1)	0.392(1)
O(2)	-0.170(2)	0.146(2)	0.117(2)
C(1)	0.279(2)	0.1732(9)	0.375(1)
C(2)	0.324(3)	0.123(2)	0.281(2)
C(3)	0.187(2)	0.036(1)	0.214(2)
C(4)	-0.191(3)	0.032(2)	0.297(2)
C(5)	-0.315(3)	0.122(2)	0.212(2)
C(6)	-0.297(3)	0.181(2)	0.127(2)

Standard deviations in parentheses.

Table 3.10

Final AnisotropicThermal Parameters for Bis-(β-Amidoethyl)tin(IV) Dichloride

Atom	U(11)	U(22)	U(33)	U(23)	U(13)	U(12)
Sn(1)	4.60(30)	4.09(30)	5.34(30)	-0.13(90)	3.34(20)	-0.16(80)
Cl(1)	5.7(3)	6.2(3)	9.4(4)	3.7(3)	4.8(3)	2.2(2)
Cl(2)	5.5(3)	8.1(4)	7.1(3)	-2.6(3)	3.2(2)	-0.1(2)
N(1)	5.6(7)	7.7(9)	7.9(8)	-3.8(7)	4.3(7)	-2.0(7)
N(2)	7.0(1)	5.6(8)	1.1(1)	1.0(8)	6.0(1)	2.7(7)
O(1)	4.5(6)	5.3(8)	6.5(7)	-1.5(6)	4.1(6)	-1.5(5)
O(2)	9.0(1)	6.3(9)	9.0(10)	2.1(7)	7.1(9)	2.9(8)
C(1)	5.4(8)	3.1(5)	5.1(7)	-2.0(5)	3.9(7)	-1.9(5)
C(2)	14.0(2)	10.0(1)	9.0(1)	-3.0(1)	8.0(1)	-2.0(1)
C(3)	4.8(7)	5.3(7)	4.5(7)	0.3(5)	2.9(6)	1.9(6)
C(4)	8.0(1)	5.8(9)	10.0(1)	2.5(7)	8.0(1)	3.1(7)
C(6)	3.9(7)	10.0(2)	8.0(1)	-4.0(1)	3.9(8)	-0.3(8)

U_{ij} are of the form $10^2 \exp[-2\pi^2(h^2U(11)a^{*2} + k^2U(22)b^{*2} + 2hkU(12)a^*b^* + 2klU(23)b^*c^* + 2hlU(13)a^*c^*)]$.

Standard deviations in parentheses.

Table 3.11

Intramolecular Bond Distances (Å) and Angles (°) of

Bis-(β-Amidoethyl)tin(IV) Dichloride

Bond lengths			
Sn(1)-Cl(1)	2.460(7)	N(1)-O(2') = 3.04(3)	
Sn(1)-Cl(2)	2.464(7)		
Sn(1)-O(1)	2.327(16)		
Sn(1)-O(2)	2.321(18)	N(2')-O(1) = 2.83(3)	
Sn(1)-C(3)	2.059(17)		
Sn(1)-C(4)	2.190(16)		
C(3)-C(2)	1.52(3)	C(4)-C(5)	1.52(3)
C(2)-C(1)	1.64(3)	C(5)-C(6)	1.43(3)
C(1)-N(1)	1.36(2)	C(6)-N(2)	1.28(3)
C(1)-O(1)	1.21(2)	C(6)-O(2)	1.32(3)
Bond Angles			
Cl(1)-Sn(1)-Cl(2)	95.5(1)		
Cl(1)-Sn(1)-C(3)	95.6(5)	Cl(2)-Sn(1)-C(3)	97.7(6)
Cl(1)-Sn(1)-O(1)	91.8(5)	Cl(2)-Sn(1)-O(1)	171.9(5)
Cl(1)-Sn(1)-O(2)	171.6(5)	Cl(2)-Sn(1)-O(2)	91.4(5)
Cl(1)-Sn(1)-C(4)	95.7(5)	Cl(2)Sn(1)-C(4)	96.4(6)
Cl(3)-Sn(1)-O(1)	78.0(6)	Cl(4)-Sn(1)-O(2)	78.7(6)
C(3)-Sn(1)-O(2)	88.2(6)	C(4)-Sn(1)-O(1)	86.3(6)

Cont./..

Table 3.11 continued

Bond Angles			
Sn(1)-C(3)-C(2)	121(1)	Sn(1)-C(4)-C(5)	106(11)
C(3)-C(2)-C(1)	103(1)	C(4)-C(5)-C(6)	126(1)
C(2)-C(1)-N(1)	106(1)	C(5)-C(6)-N(2)	132(2)
C(2)-C(1)-O(1)	127(1)	C(5)-C(6)-O(2)	114(2)
N(1)-C(1)-O(1)	128(1)	N(2)-C(6)-O(2)	114(2)
C(1)-O(1)-Sn(1)	110(1)	C(6)-O(2)-Sn(1)	115(2)
C(4)-Sn(1)-O(1)	75.6(6)	O(1)-Sn(1)-O(2)	79.8(6)
C(4)-Sn(1)-C(3)	191(1)		

Standard deviations in parentheses

Table 3.12

Equations of the Mean Planes through Groups of Atoms in Bis-(β-Amidoethyl)tin(IV) Dichloride and Deviations of Atoms from the Planes (Å)

PLANE 1. Sn(1), Cl(1), O(2), C(6), N(2), C(5), C(4), C(3).

Equation of the plane:

-1.59410x - 8.25039y - 6.46102z = 1.859

Sn(1), 0.188; Cl(1), -0.085; O(2), 0.171; C(6), 0.022; N(2), -0.155; C(5), -0.013; C(4), -0.018; C(3), -0.114.

PLANE 2. Sn(1), Cl(1), Cl(2), O(1), O(2)

Equation of the plane:

8.81727x + 0.22689y - 10.21725z = 2.563

Sn(1), 0.010; Cl(1), -0.086; Cl(2), 0.081; O(1), 0.098; O(2), -0.103.

PLANE 3. Sn(1), Cl(2), O(1), C(1), N(1), C(2), C(3), C(4)

Equation of the plane:

-1.83290x + 8.66639y - 5.38257z = 1.230

Sn(1), -0.182; Cl(2), 0.108; O(1), -0.170; C(1), 0.015; N(1), 0.133; C(2), 0.051; C(3), -0.063; C(4), 0.108.

Angle between Plane 1 and Plane 2 = 89.20°

Angle between Plane 1 and Plane 3 = 82.25°

Angle between Plane 2 and Plane 3 = 89.85°

3.2 RESULTS AND DISCUSSION

No crystal structure of an organotin trichloride has previously been reported. β-carbomethoxyethyltin trichloride is a somewhat less hygroscopic compound than an unsubstituted alkyl or aryltin analogue, and the structure determination has shown that the tin is five-coordinated via intramolecular coordination of the carbonyl group (Figure 3.3). The geometry at tin is, thus, distorted trigonal bipyramidal with the carbonyl oxygen and one chlorine atom occupying axial sites. The organic residue and the two remaining chlorine atoms are bonded at equatorial sites. Not unexpectedly, due to slight d-orbital contribution in this direction the $Sn-Cl_{ax}$ bond distance (2.357(2)Å) is longer than the $Sn-Cl_{eq}$ distances (2.303(2) and 2.317(2)Å). The Sn-C bond length (2.129(8)Å) falls well within the normal range (Table 1.7) whilst the Sn-O coordinate bond distance (2.347(5)Å) is quite short when compared with values of 2.332(6)Å for $Me_3SnCl.(Ph_3PCHCOMe)$[303] and 2.308(4)Å for $Ph_3Sn.ONPh.CO.Ph$[304]. The slight difference in the two $Sn-Cl_{eq}$ distances may be of significance and can be rationalized when intermolecular interactions are considered. The contact distance between Cl(3) (Figure 3.3) and the tin atom of an adjacent molecule is 3.857Å which is of the same order as the sum of the relevant van der Waals radii (3.91Å)[305]. The effect of these secondary bonds on the molecules of the crystal can be seen in an expansion of the Cl(2)-Sn-C(1) bond angle to 130.5° and a consequent compression of the angle about Cl(2)-Sn-Cl(3) to 104.09°. Although these secondary bonds are weak and the description of the molecular

structure as pseudooctahedral would confer undue significance, they appear to hold sufficient influence to produce ordering of the crystal lattice into zig-zag chains of molecules, as can be seen from the projection of the unit cell onto the bc plane in Figure 3.4.

Bis(β-carbomethoxyethyl)tin dichloride and bis(β-amidoethyl)-tin dichloride possess distorted octahedral geometries with both substituted ethyl groups functioning as chelating ligands. In both compounds the two chlorine atoms occupy cis positions whilst the two carbon atoms are mutually trans. The oxygen atoms are therefore in cis positions. Although very similar within each compound, the Sn-Cl bond distances of the amido-ethyl derivative are longer (2.462(7)Å) than those in the carbomethoxyethyl derivative (2.405(2)Å). Both are shorter than those of Ph_2SnCl_2.bipyridyl (2.520(2)Å)[306] but longer than in Et_2SnCl_2(2.385(3)Å)[307]. In $Cl_2Sn(CH_2CH_2CONH_2)_2$, the Sn-O bond lengths (2.324(18)Å) are similar to that in $Cl_3SnCH_2CH_2CO_2Me$ and $Me_2Sn(ONMeCOMe)_2$ (2.377(5)Å)[308], but longer than in $Me_2Sn(ONHCOMe)_2$ (2.228(4)Å), in which intermolecular hydrogen-bonding occurs[309]. However, in $Cl_2Sn(CH_2CH_2CO_2Me)_2$ the Sn-O bond distances are significantly longer (2.522(4)Å) reflecting a considerably weaker coordinate bond. A fact supported by the smaller change in the ν(C=O) frequency from that of the free ligand when compared with the infrared spectrum from the trichlorotin analogue. The Sn-C distances in $Cl_2Sn(CH_2CH_2CO_2Me)_2$, (2.126(6)Å), are slightly shorter than in Et_2SnCl_2 (2.132(13), 2.167(15)Å)[307], whilst those in the amidoethyl compound are quite dissimilar (2.059(17) and 2.190(16)Å).

The angles subtended by the methyl acrylate residues at the

tin (81.26°, 73.99°) in the dichloro compound illustrates the steric demands of these ligands leading to the distortion from regular octahedral geometry. The angle of inclination between the planes containing the organic moieties is 97.09° and a similar distortion is noted for the Cl-Sn-Cl (96.30°). Similar steric strain is imposed by the ligand in $Cl_3SnCH_2CH_2CO_2Me$ which subtends an angle at the tin of 77.24°, intermediate with those of the dichloride. The bond distances within the carbomethoxy residues of the two compounds, $Cl_2Sn(CH_2CH_2CO_2Me)_2$ and $Cl_3SnCH_2CH_2CO_2Me$, are similar, with the C=O distances falling in the range 1.205(7) - 1.227(10)Å. The Me-O distances are much longer (1.448(15) - 1.463(8)Å) than the C(3) - O distances (1.290(10) - 1.307(7)Å).

A marked dissimilarity is found in the distances within the two amidoethyl residues in $Cl_2Sn(CH_2CH_2CONH_2)_2$. In one, the carbonyl distances is short (1.205(20)Å) and the C-N and C(:O)—C distances relatively long (1.355(20) and 1.638(26)Å, respectively). In the other ligand the carbonyl distance is very long (1.321(25)Å), whereas the corresponding C-N and C(:O)—C distances are short (1.277(29)Å and 1.427(30)Å respectively). Examination of the nearest intermolecular approaches between atoms (Table 3.13) affords some explanation in terms of hydrogen-bonding, involving the amide and carbonyl groups. The longer carbonyl and C-N distances being associated with a short (2.827Å) C:O.....H-N hydrogen-bond, and the shorter carbonyl and C-N distances with the longer (3.043Å) C:O....H-N hydrogen-bond.

Table 3.13 Nearest Intermolecular Approaches between atoms in bis(β-amidoethyl)tin dichloride

N(1) - O(2')	=	3.043 Å
N(2') - O(1)	=	2.827 Å
Cl(1) - O(1')	=	3.470 Å
Cl(2) - O(2')	=	3.410 Å

Atoms in different molecules denoted by a primed assigned number.

3.3 THE MECHANISM OF ESTERTIN FORMATION

The reaction mechanism initially proposed by Hutton, Burley and Oakes[310] for estertin formation involved the intermediate $HSnCl_3.2Et_2O$, which was believed to hydrostannate the alkene;

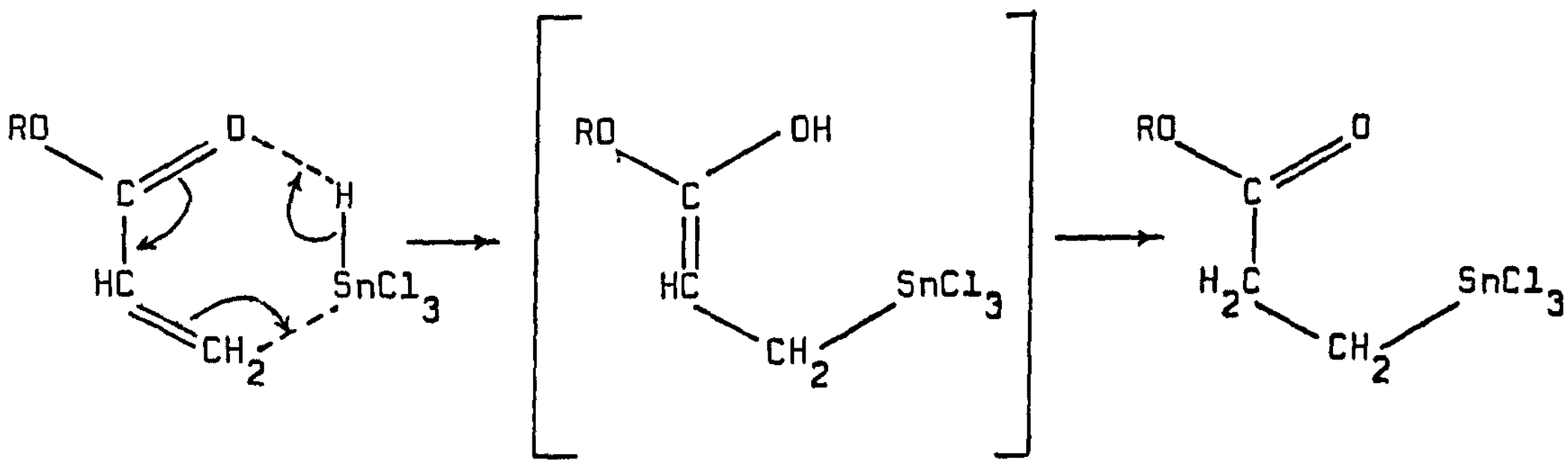

The monohalogenostannanes have been characterised by Jolly[311]

who found them to be solids which were unstable at temperatures above $-40^{o}C$ and thus their involvement in the above reaction might appear unlikely. Nefedov[312] examined the addition of excess dry gaseous hydrogen chloride to a slurry of anhydrous tin(II) chloride in ether and observed the formation of a pale yellow oily phase which he considered to be 'solvated trichlorostannane' $HSnCl_3.2Et_2O$. However, more recently Bulten and vanden Hurk[313] reexamined this system and from n.m.r. data concluded that the yellow phase was principally solvated, strongly ionized, dihydrogen tetrachlorostannate(II) $2H^{+}.SnCl_4^{2-}.2Et_2O$, with only small quantities of trichlorostannate(IV), $HSnCl_3$.

Preparation of the β-carbonyl-substituted ethyltin compounds can be achieved in a wide variety of solvents and at temperatures ranging from -30 to $+120^{o}C$. Whilst ethereal solutions are frequently employed they are not essential. Homogeneous solutions are produced from the reaction of HCl and $SnCl_2$ in THF, ethylacetate and methanol and by dissolution of $SnCl_2$ in concentrated hydrochloric acid; although the exact constituents of these solutions has not been investigated. The protons in such systems are highly acidic having an ^{1}H n.m.r. shift in the region of 10.9 to 12.8 . Therefore, the most likely mechanism for estertin formation may involve a 1,4 addition with initial protonation of the carbonyl oxygen of the β-carbonyl activated alkene.

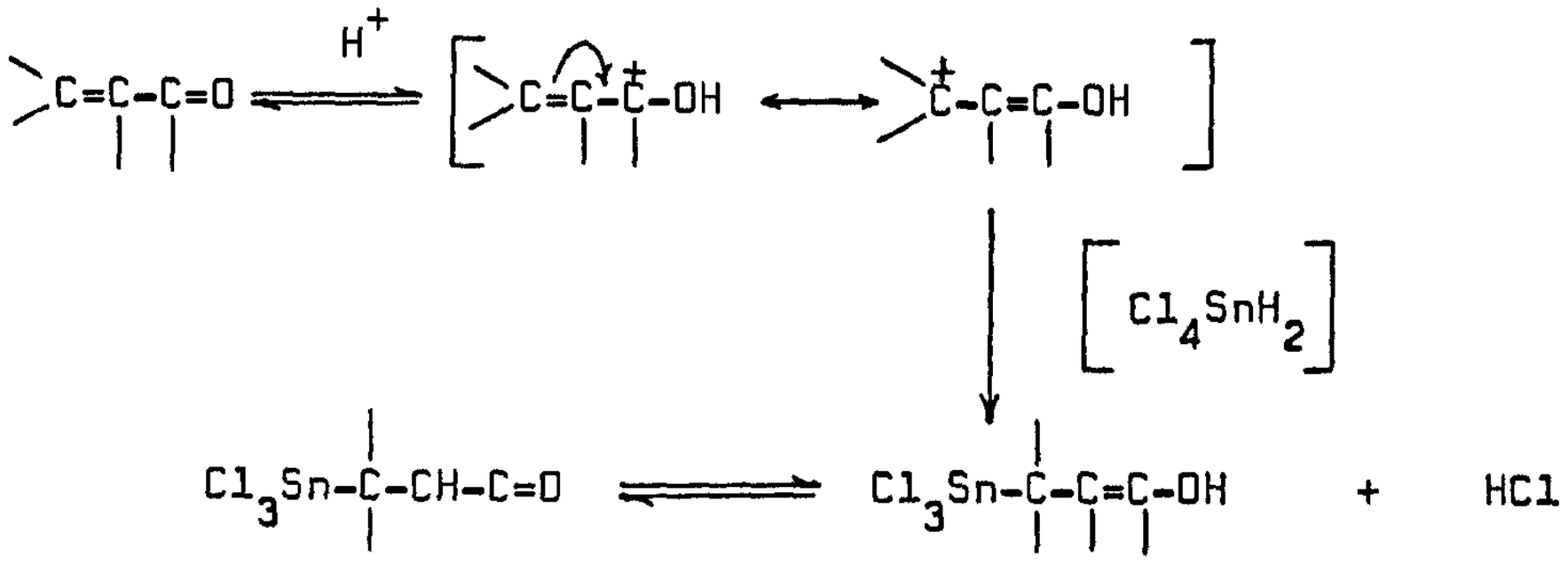

The mechanism proposed for the formation of the β-substituted dialkyltin dihalides[314] involves initial formation of the monoalkyltin trichloride ($Cl_3SnCH_2CH_2CO_2Me$) followed by conversion to the dialkyltin dichloride via the halogenostannane intermediate $Cl_2SnHCH_2CH_2CO_2Me$. $[HSnCl]$ is proposed as effecting the reduction, viz:

$$HCl + Sn \longrightarrow [HSnCl] \xrightarrow{HCl} H_2 + SnCl_2$$

$$CH_2{=}CHCO_2Me : HCl + SnCl_2 \longrightarrow [CH_2{=}CHCO_2Me : HSnCl_3] \downarrow RSnCl_3$$

$$RSnCl_3 + [HSnCl] \longrightarrow [RHSnCl_2] + SnCl_2$$

$$[RHSnCl_2] + CH_2{=}CHCO_2Me \longrightarrow R_2SnCl_2$$

($R = CH_2CH_2CO_2Me$)

However, similar arguments to those used against the involvement of $HSnCl_3$ in the trialkyltin synthesis can be made in

this case. An identical $H_2SnCl_4.2Et_2O$ phase to that produced with tin(II) chloride is obtained when hydrogen chloride is passed into a suspension of tin metal under similar conditions. Addition of tin metal to a monoalkyltin trihalide induces disproportionation.

$$2Cl_3SnCH_2CH_2CO_2Me + Sn \longrightarrow Cl_2Sn(CH_2CH_2CO_2Me)_2 + SnCl_2$$

Trace quantities of the trialkyltin monohalide also occur, as is the case with $MeSnCl_3$[313].

$$2MeSnCl_3 + Sn \xrightarrow{Et_2O} Me_2SnCl_2 + 2SnCl_2$$

Whilst the first reaction proceeds rapidly and quantitatively at room temperature, the latter gives 100% conversion over 24h at 20^oC into a 17:1 Me_2SnCl_2/Me_3SnCl mixture with the $SnCl_2$. Thus, the most likely route for the dialkyltin dihalide formation from tin metal is the initial hydrostannation of the alkene by the $H_2SnCl_4.2Et_2O$ intermediate, as before, followed by a subsequent disproportionation of the trihalide into the dihalide product under the action of the tin metal[313]. Examinations we have made of the n.m.r. spectra of the resulting products did not reveal the presence of any monohalotrialkyltin product, but because of the obvious ease of reaction the ratio of monohalo to dihalo product may be much greater in favour of the latter product than in the 1:17 observed for the slow $MeSnCl_3$ conversion.

It may be that consideration of the active tin intermediate in terms of simple solution species is ignoring a possible initial

step in the reaction process: that of a heterogeneous metal/solution interaction between the tin metal and the solvated hydrogen chloride. Thus, the '[HSnCl]' may be a chemisorbed surface species:

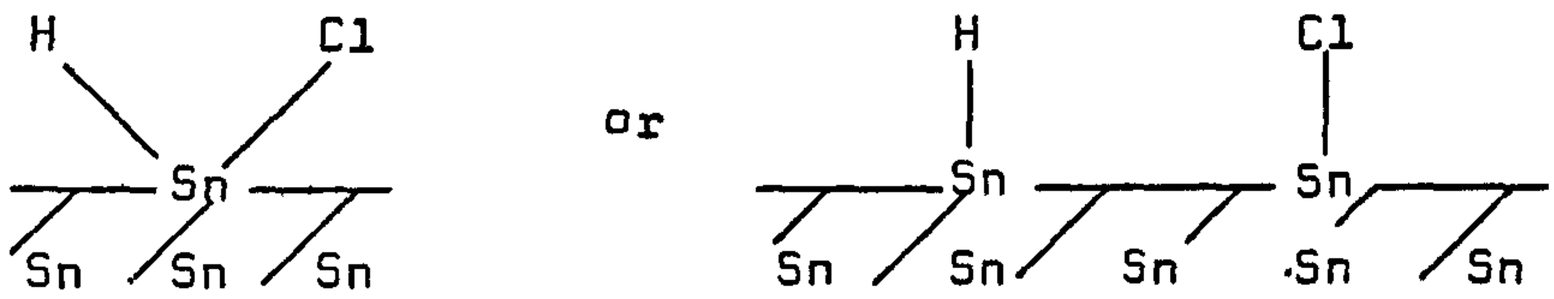

which then desorbed releasing $SnCl_2$, viz:

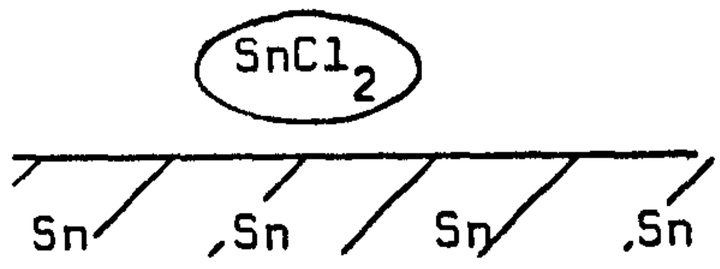

Measurements with lead and HCl[316,317] have shown the strong affinity for such a process with that metal, the extension of this mechanism to tin is, therefore, not unreasonable.

The structure of β-carbomethoxyethyltin trichloride may be represented as:

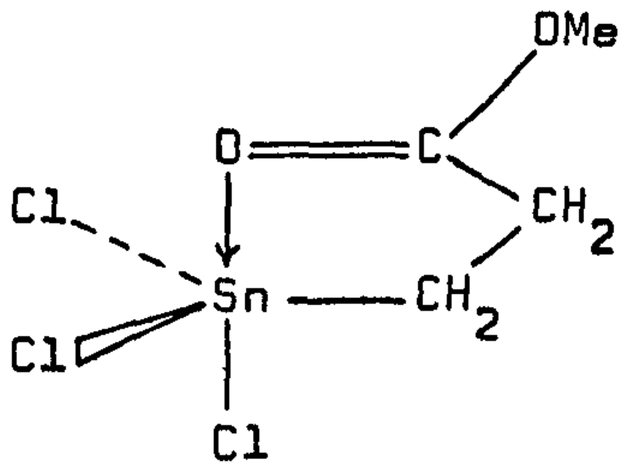

However, the Sn-O distance of 2.347(5) Å is within the limits of more formal Sn-O bond formation. Whereas the Sn-O distance of 2.52 Å for the bis-alkyl analogue is at the limit for such interactions. The suggestion has been made that the methoxy oxygen lone-pair electrons are involved in the delocalisation of the ester carbonyl electron density on to tin[310] resulting in the intramolecular co-ordination represented by:

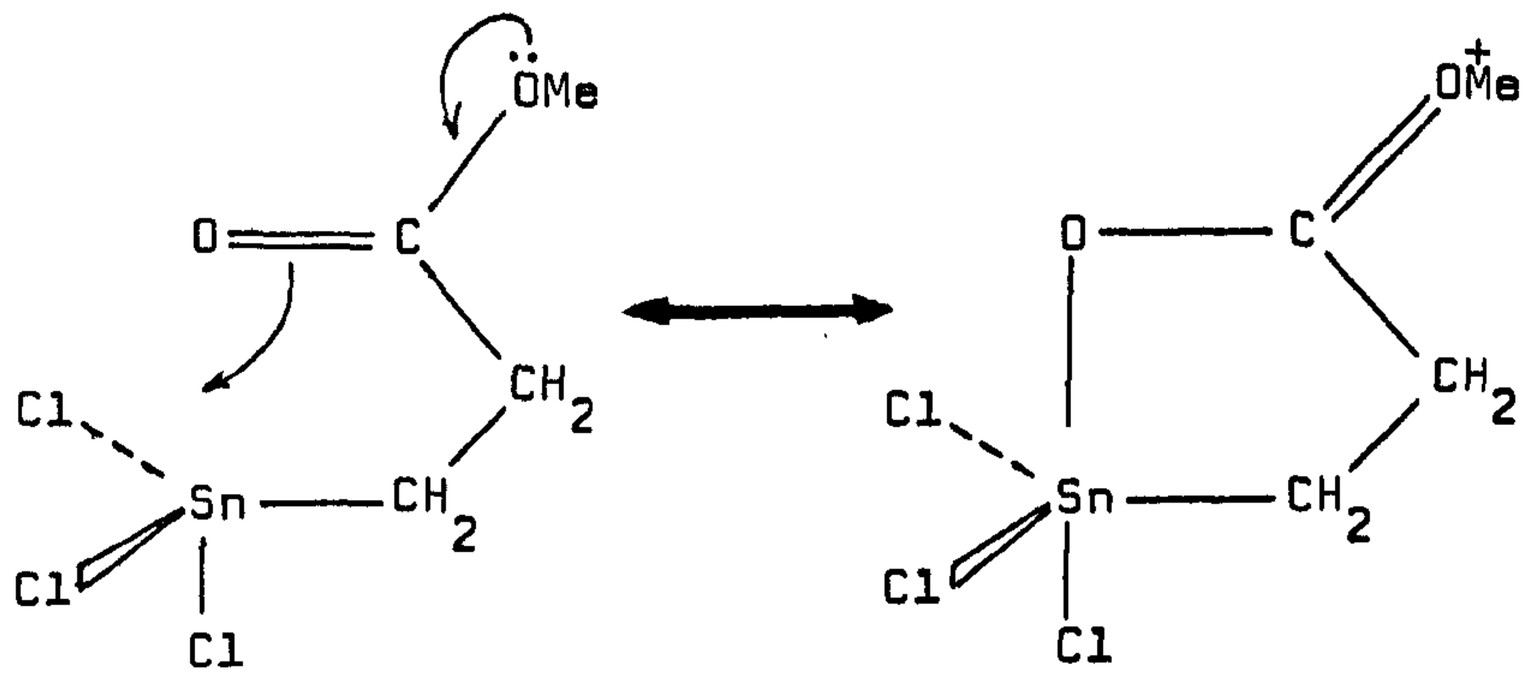

The shift in the ν(C-O) frequency to 1272 cm^{-1} in the infrared spectrum of $Cl_3SnCH_2CH_2CO_2Me$ from 1213 cm^{-1} in the free ligand

CH_2=$CHCO_2Me$ may be supportive of this proposal. However, a similar shift is observed with the bis(β-carbomethoxyethyl)tin dichloride compound (1270 cm^{-1}) where the Sn-O bond distance is unlikely to indicate any such formal tin-ligand electron interaction. E.S.R. measurements on these systems have recently been made by Davies et al[135]. Di-t-butyl peroxide was photolysed in the presence of the β-carbonylalkyltin di- and trichlorides, the radicals which formed were monitored by e.s.r. β-carbomethoxyethyltin trichloride gave a strong alkyl radical spectrum indicating cleavage of the ligand with simultaneous alkoxyl radical substitution at the tin centre in a bimolecular homolytic substitution mechanism.

$$Me_3CO^{\bullet} + (MeO_2CCH_2CH_2)_2SnCl_2 \longrightarrow Me_3COSn(CH_2CH_2CO_2Me)Cl_2 + \dot{C}H_2CH_2CO_2Me$$

However, the dichloride analogue did not give any spectrum under the same conditions. This result could be interpreted as indicative of stronger coordination in the latter compound. Such a conclusion is, however, not tenable when the crystallographic evidence is taken into account. More likely, the two chelating carbonyl groups sterically inhibit peroxyl radical approach and thus prevent a rapid S_H2 reaction.

Finally, it appears from experimental data that only unsaturated carbonyl compounds with a cis conformation can undergo reaction with the tin intermediate. Thus, for example, phorone is active whilst isophorone is not.

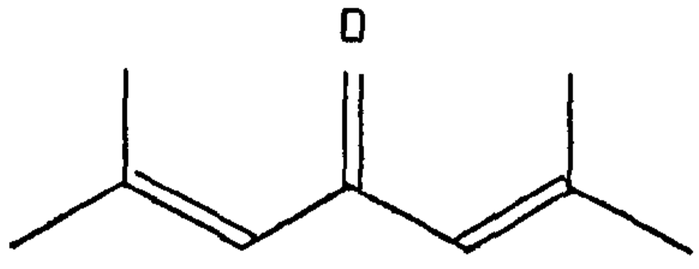

phorone - active

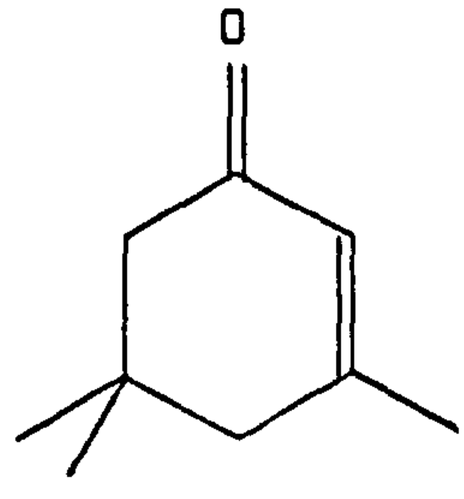

isophorone - inactive

Whilst this observation would support the Hutton and Oakes proposal of a concerted mechanism:

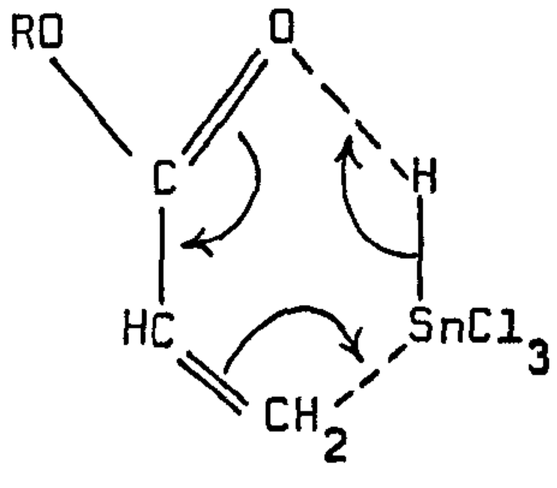

it is difficult to rationalise such a conformational requirement with the stepwise 1,4-addition. The ability to perform these reactions in non-polar solvents such as hexane indicates that solvation of the tin intermediate by the carbonyl compound may be a feature of the mechanism. However, this probability would not affect the reaction route, although it has been employed to explain the fact that only one of the C=C bonds in phorone is active towards the tin intermediate[310]. This appears an unnecessary complication as, surely, once the product

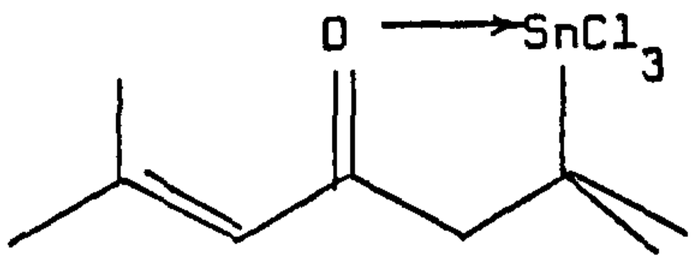

has formed the strong carbonyl coordination to the tin centre effectively deactivates the remaining C=C double bond. Clearly, further work will be required to arrive at a completely satisfactory explanation of the mechanism of formation of the estertin compounds. It is probably unlikely that one single, simple mechanism is involved.

REFERENCES

301. CRYSTALS suite of programmes. Oxford University.

302. International Tables for X-ray Crystallography, Vol. III. Kynoch Press, Birmingham (1963).

303. J. Buckle, P.G. Harrison, T.J. King and J.A. Richards, J. Chem. Soc. Dalton (1975) 1552.

304. P.G. Harrison and T.J. King, J. Chem. Soc., Dalton, (1974) 1723.

305. J. Bondi, J. Phys. Chem., (1964) 68 441.

306. P.G. Harrison, T.J. King and J.A. Richards, J. Chem. Soc., Dalton, (1974) 1723.

307. N.W. Alcock and J.F. Sawyer, J. Chem. Soc. Dalton, (1977) 1090.

308. P.G. Harrison, T.J. King and J.A. Richards, J. Chem. Soc., Dalton, (1975) 826.

309. P.G. Harrison, T.J. King and R.C. Phillips, J. Chem. Soc., Dalton, (1976) 2317.

310. R.E. Hutton, J.W. Burley and V. Oakes, J. Organometal. Chem., (1978) 156 369.

311. J.R. Webster, M.M. Millard and W.L. Jolly, Inorg. Chem., (1971) 10 879.

312. O.M. Nefedov and S.P. Kolesnikov, Izv. Akad. Nauk SSSR, Ser. Khim., (1966) 2 201.

313. E.J. Bulten and J.W.G. vanden Hurk, J. Organometal. Chem., (1978) 162 161.

314. J.W. Burley, P. Hope and R.E. Hutton, J. Organometal. Chem., (1979) 170 21.

315. R.M. Haigh, A.G. Davies and Mau-Wing Tse, J. Organometal. Chem., (1979) 174 163.

316. Y.M. Dadiza and J.M. Saleh, J. Chem. Soc., Faraday I, (1972) 68 269.

317. P.G. Harrison and R. Smith, J. Chem. Soc., Faraday I, (1980) 76 442.

CHAPTER FOUR

THE USE OF TIN-119 N.M.R. AS A STRUCTURAL PROBE FOR METHYLTIN COMPOUNDS IN SOLUTION

4.1 INTRODUCTION

4.1.1 Tin Magnetic Resonance

Of the ten naturally occurring isotopes of tin, three possess a magnetic moment : tin-115, tin-117 and tin-119, each of which have a spin quantum number I = $\frac{1}{2}$. Tin-119 has the greatest abundance of these nuclei (8.58%) and is slightly more sensitive to the n.m.r. experiment (5.2×10^{-2} of ^{1}H at constant field). It also has the advantage of a parent radioactive isotope (^{119m}Sn, $t_{\frac{1}{2}}$ = 245d) which enables analogous solid state data to be obtained by Mössbauer spectroscopy, c.f.

Burke and Lauterbur[401] reported the first n.m.r. measurements for tin in which they examined eighteen inorganic and organometallic compounds by direct observation at a frequency of 8.5 MHz. However, until the advent of convenient, commercial Fourier transform spectrometers, the low sensitivity, low natural abundance and long relaxation times limited the use of direct techniques and INDOR has been the method of choice for obtaining organotin n.m.r. data.

4.1.2 INDOR n.m.r.

INDOR (InterNuclear DOuble Resonance) is an acronym first proposed by Baker in 1962[402] for a double resonance experiment he performed on ^{13}C, ^{14}N and ^{29}Si magnetic nuclei; obtaining by indirect methods spectra equivalent to those from direct observations but at enhanced sensitivity.

In a single resonance experiment the sample is placed in a main magnetic field, B_o, where it is irradiated with an 'observing' r.f. field of frequency ν_1 and amplitude B_1. At some appropriate frequency given by

$$\nu_n = \gamma B_n / 2\pi$$

where γ = magnetogyric ratio of the nucleus undergoing the transition and

B_n = field experienced at that nucleus,

the nuclei absorb energy which can be detected. In double resonance experiments the sample is simultaneously irradiated with a second r.f. field offrequency ν_2 and amplitude B_2. This is termed the 'irradiating' or 'decoupling' field. In the INDOR experiment the frequency ν_1, of the observing field B_1 is set exactly on a resonance line in the spectrum of a certain nucleus. The frequency ν_2 of the irradiating field is swept through the resonance region of another nucleus which is directly coupled to the first. When ν_2 exactly coincides with the resonance position of the second nucleus the

coupling between the two nuclei is perturbed. This results in a change in intensity of the resonance line at frequency ν_1. An INDOR spectrum is thus obtained by plotting this variation in intensity of the observed line on the ordinate axis against the frequency of the decoupling field. The ^1H spectrum and the resulting tin-119 INDOR spectrum of dimethyltin dichloride are shown in Figure 4.1.

A useful notation, due to Baldeschwieler and Randall[403], for describing this type of decoupling is; $A-\{X\}$. A is the observed nucleus which resonates at a frequency ν_1 and X is the irradiated nucleus at ν_2.

A number of advantages result from this indirect method of obtaining the n.m.r. spectrum, the most important being that it enables nuclei of low abundance and inherently poor sensitivity towards the n.m.r. experiment to be studied at a sensitivity equivalent to that of the observing nucleus, which is most often ^1H or ^{19}F. In this way long relaxation times which give rise to saturation problems with direct observation techniques can be disregarded and the precision of the measurements is greatly increased. Provided the lines of the irradiated nucleus are well separated so that only one line at a time is affected by the irradiating field, the resulting spectrum will be an accurate representation of that for the decoupled nucleus. If however B_2 is of the same order of magnitude as the line separation then several lines will be perturbed simultaneously with a resulting

Figure 4.1 ^{1}H spectrum of $(CH_3)_2SnCl_2$ and associated INDOR spectrum

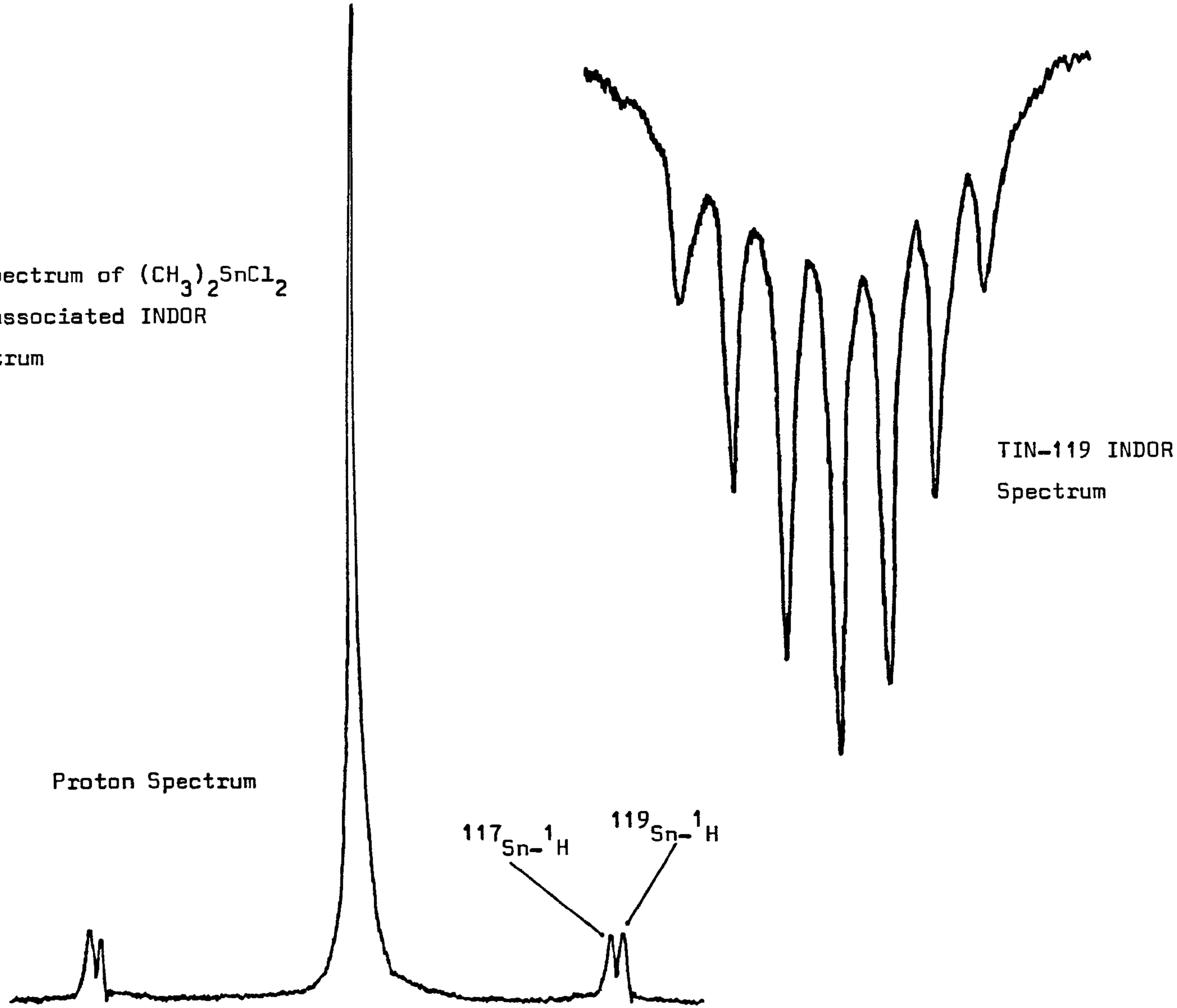

loss in the definition of the spectrum obtained. This effect is well illustrated by the spectrum of tetramethyltin, Me_4Sn, (Figure 4.2), obtained by monitoring the high-field tin-119 satellite in the proton spectrum due to $(CH_3)_4{}^{119}Sn$ present in natural abundance.

The condition for decoupling in an A - $\{X\}$ system is:

$$\gamma_X B_2 / 2\pi \gg J_{AX}$$

For $(CH_3)_4{}^{119}Sn$, $^2J(^{119}Sn \ldots {}^1H) = 52.6$ Hz. So that Figure 4.2a illustrates the case where $\gamma_{(^{119}Sn)}B_2/2\pi \gg 52.6$ Hz; Figure 4.2b has $\gamma_{(^{119}Sn)}B_2/2\pi \simeq 52.6$ Hz and in Figure 4.2c $\gamma_{(^{119}Sn)}B_2/2\pi < 52.6$Hz. It can be seen from this example that the INDOR technique is essentially a 'tickling' experiment rather than a true decoupling and the use of the correct B_2 level is, therefore, of considerable importance to the spectrum obtained.

According to Freeman and Anderson[404] the INDOR effect arises because the passage of the irradiating r.f., ν_2, through a transition line with an energy level in common with that of the observed transition at ν_1 causes a shift off-resonance of parts of the observed signal due to a splitting effect and hence a reduction in its intensity. Other fluctuations in the monitored signals' intensity arise due to the generalised nuclear Overhauser effect[405]. This latter effect can provide a method for determining the character of the connection between the irradiated and observed

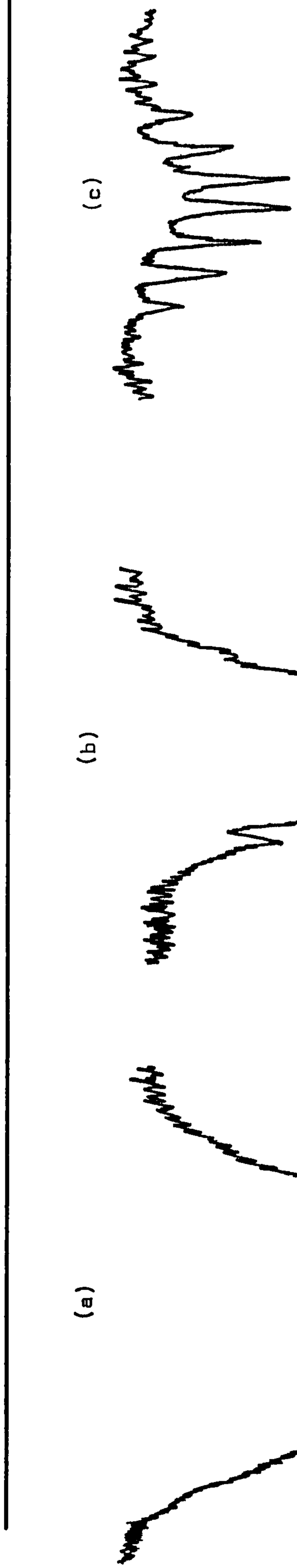

(a) $\gamma_{^{119}Sn} B_2 / 2\pi >> 52.6$ Hz

(b) $\gamma_{^{119}Sn} B_2 / 2\pi \simeq 52.6$ Hz

(c) $\gamma_{^{119}Sn} B_2 / 2\pi < 52.6$ Hz

Sample: Me_4Sn.

Figure 4.2 The effect on the signal of variation in the power level of the irradiating oscillator.

transitions and hence the associated energy level diagram.

Consider the energy level diagram for a simple AX system giving rise to a four line spectrum (Figure 4.3).

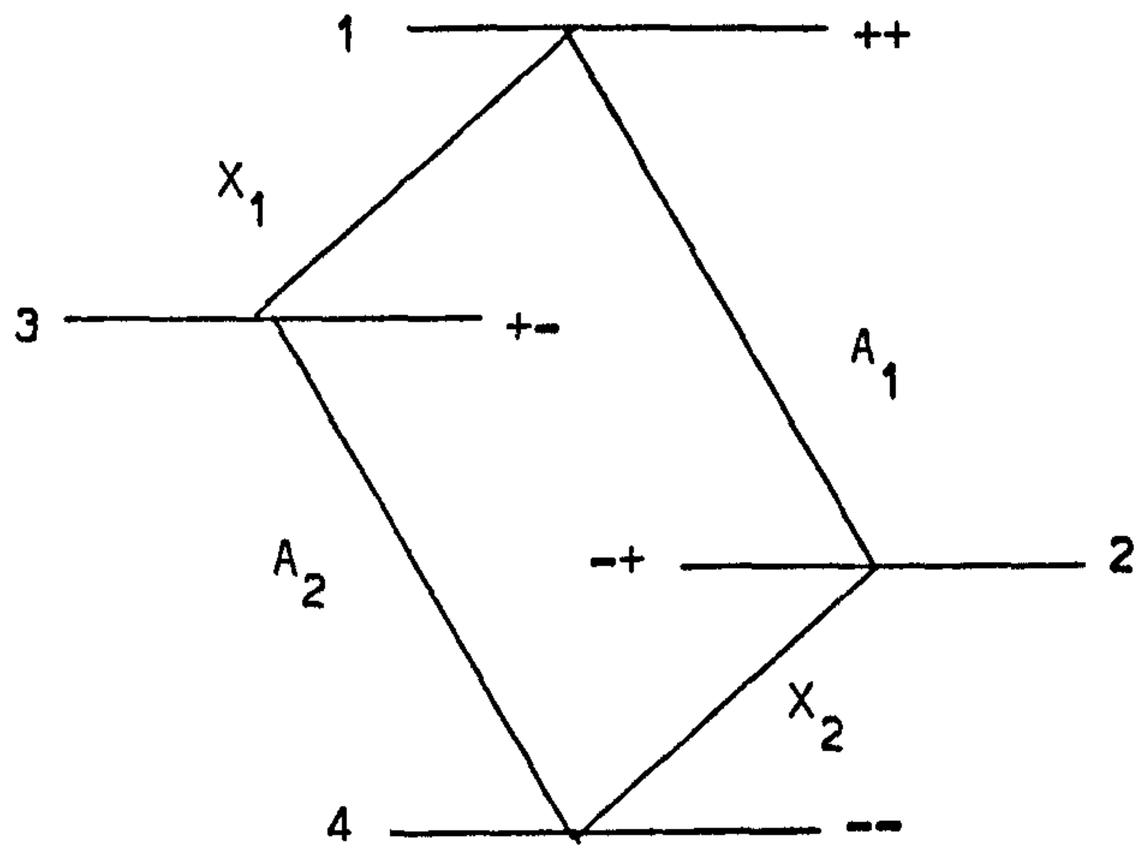

Figure 4.3 Energy level diagram for an AX system.

The amplitude of the A_1 signal is a function of the population distribution between states 1 and 2. If A_1 is monitored and X_1 irradiated, an increase in the population of state 1 will result. The population difference between states 1 and 2 is therefore reduced and the amplitude of A_1 decreases. At the same time the population of state 3 is decreased causing an increased differential in the population level between states 3 and 4, so that an increase in the intensity of A_2 will result if this line is monitored. Similar effects are found when X_2 is irradiated. When an increase in signal intensity occurs the observed and irradiated transition

are said to have a 'progressive' relationship. If the signal amplitude falls the relationship is described as 'regressive'.

From the above discussion it would appear that only certain sections of the spectrum of the irradiated nucleus can be observed at any one time, and yet the spectrum of Me_2SnCl_2 (Figure 4.1) clearly shows all seven lines. This apparent anomaly can be reconciled.

It is found that when dealing with a non-symmetrical system where all the transitions are non-degenerate (as in the AX case) only the partial spectrum is obtained. However, in the case of degenerate transitions the whole spectrum is obtained. Thus for an A_3X system the orientations at the X nucleus arising from spin-spin coupling with the three A nuclei are:

- - -	X_1
+ - - - + - - - +	X_2
+ + - + - + - + +	X_3
+ + +	X_4

whilst two possible orientations result at the A nucleus due to the X nucleus, viz.

-	A_1
+	A_2

Thus each of the X spin states is split by A_1 and A_2 into two. This gives rise to the energy level diagram and associated

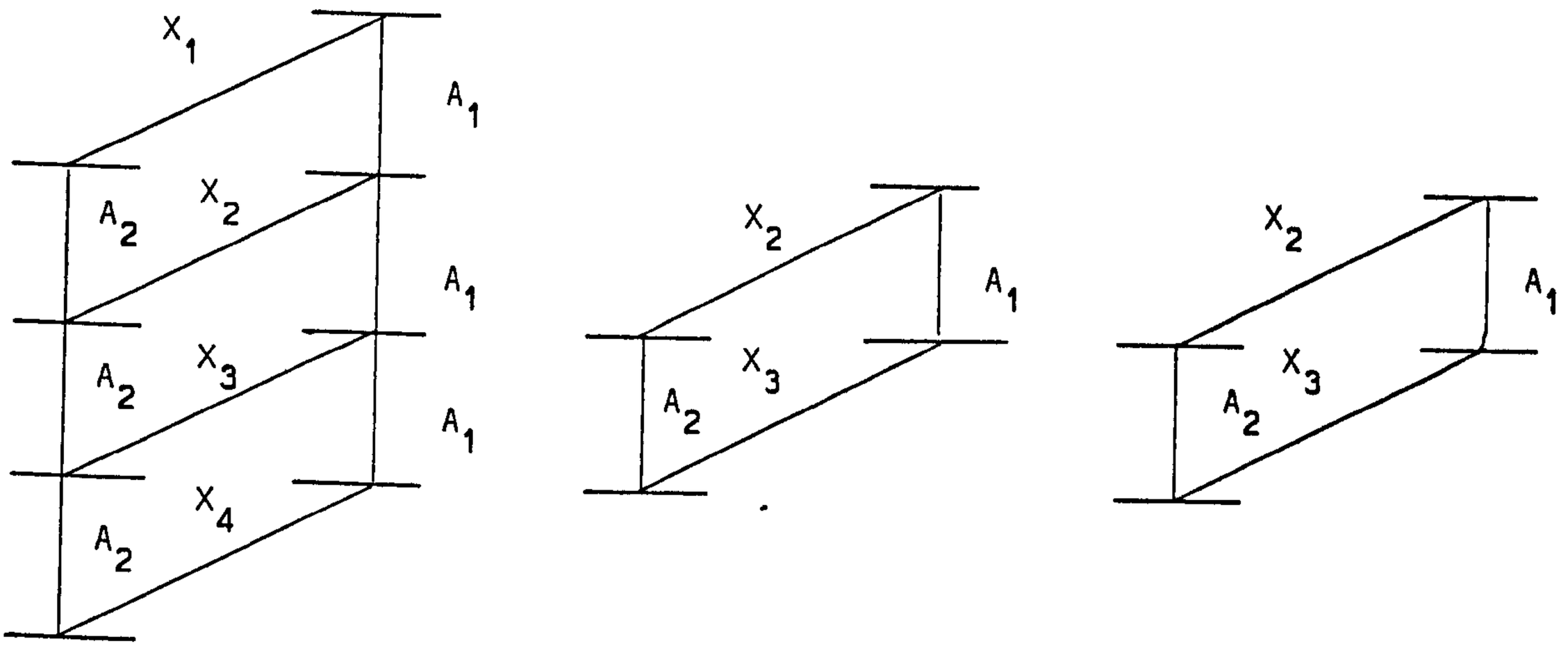

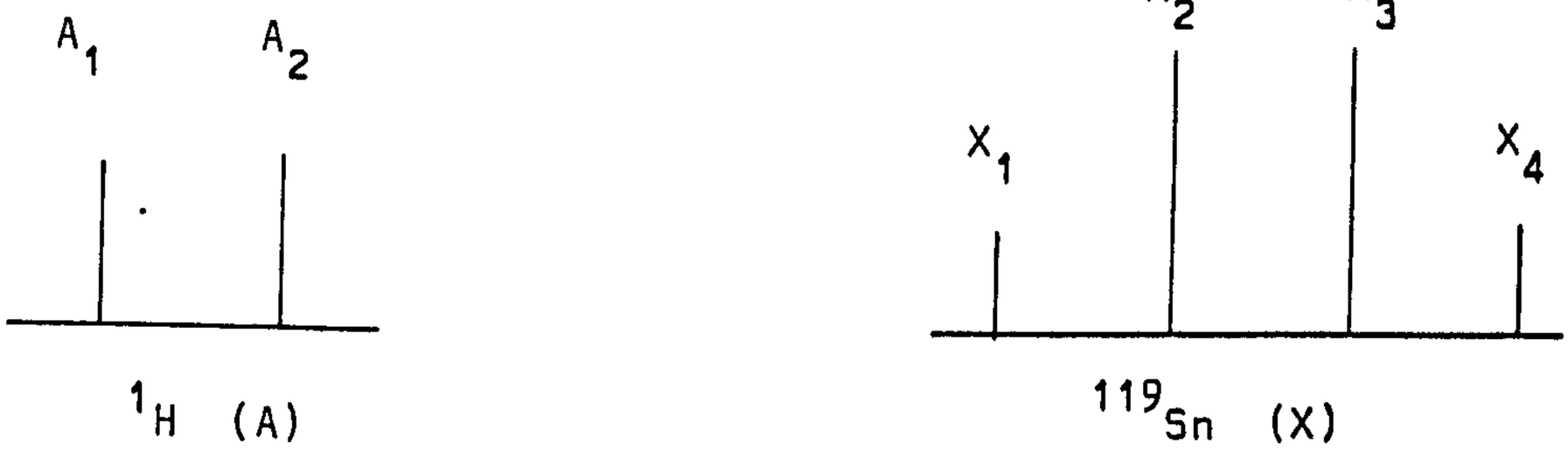

Figure 4.4 Energy level diagram and associated spectra for an A_3X system.

spectra shown in Figure 4.4. Thus, if the monitoring frequency ν_1 is set on the ^{119}Sn satellite lines, either A_1, or A_2, each of which is composed of five coincident transitions, sweeping the X (^{119}Sn) spectrum will cause at least one component of this transition to be perturbed and hence the full spectrum will be obtained.

A general discussion of the INDOR effect has been included in a number of papers on magnetic double resonance[406,407], and specifically reviewed by Kowalewski[408].

4.2 EXPERIMENTAL

The range of tin chemical shifts so far established, relative to Me_4Sn, is from -1712 ppm for SnI_4 in a 1 : 1 mixture with $SnCl_4$ [401] to +199 ppm for diethyltin thioglycollate[409], overall about 2000 ppm. Organotin derivatives extend over a range of 861 ppm, to -662 ppm for $CH_3SnBr_5^{2-}$ in water[410].

However, some contradiction is found in the literature with sign conventions used for tin-119 chemical shifts. Until 1972, all papers listed high-field shifts from the standard as positive. However, tin n.m.r. has now adopted the convention used in proton magnetic resonance, where shifts to high-field of the standard are negative; a procedure which will be used throughout this thesis. The situation with choice of reference compound is not as confused. Tetramethyltin, $(CH_3)_4Sn$, has been almost universally accepted as 0 ppm since the early work of Hunter et al[411]. A standard solution

of 50% tetramethyltin in methylene chloride is found to have a tin-119 frequency of 37, 290, 662 $\pm$ 2 Hz [412] at a field of 23.487 K. Gauss. All shift values quoted in this present work will be relative to this standard. The absolute frequency, Ξ, for the spectra measured in this work, is derived using the convention proposed by Allen and other[413], whereby the resonance frequency of the nucleus is that frequency in a field strength for a tetramethylsilane (T.M.S.) proton resonance to be exactly at 100 MHz. Using 100 MHz spectrometer with an internal lock, the correction formula[414] is

$$\Xi = \chi_{obs.}\ 1 - (f + g - 100\,\delta) / 10^{8}$$

where Ξ is the absolute frequency required in hertz, $\chi_{obs.}$ is the experimental frequency in hertz, f is the high-field sideband frequency in hertz used for locking the resonance, g is the amount by which the spectrometer r.f. oscillator centreband exceeds 10^{8} hertz and δ is the chemical shift in ppm relative to T.M.S. of the compound actually used to provide the locking resonance. This formula must be modified if used for field-sweep, the above form only applying to frequency-sweep operation.

Measurements were made using a Varian HA100 C.W. n.m.r. spectrometer operating at a field strength of 2.3487 T. The INDOR modification was based on that described by Charles[415], and employed a Schlumberger Solatron 4601 180 MHz frequency synthesizer which was

driven from a digital frequency sweeper. Synchronisation with the proton frequency was obtained by replacing the generating crystals in the latter with a stabilised frequency of 16.649 MHz fed to the oscillator doubler and tripler stages from a Schlumberger FS 100 X, which was linked, in turn, to the frequency synthesizer. Spectra were recorded in the frequency sweep mode, and the INDOR spectrum obtained from the high field satellite of tin-119 in the proton spectrum. Calibration of the proton spectra was achieved by taking the difference of the manual and swept oscillator frequencies, whilst the tin spectra were calibrated directly from the frequency synthesizer.

Although, as stated, tetramethyltin has been universally adopted as the standard for ^{119}Sn chemical shift data, no study has previously examined its suitability as such. In Tables 4.1 and 4.2 are listed the chemical shifts of tetramethyltin in two different solvents, acetone and chloroform, at various concentrations and temperatures. The data are also plotted graphically in Figure 4.5 from which it can be seen the chemical shift is zero at concentrations of 40 vol. % in both solvents at temperatures around 30^{o}. The maximum variation of chemical shift with concentration is ca. $\pm$ 0.5 ppm, whilst decrease in temperature causes an increase in chemical shift in both solvents of ca. 0.014 ppm/degree in acetone and ca. 0.019 ppm/degree in chloroform. Accurate calibrations should therefore be performed with about 40 vol. % solutions at temperatures around 30^{o}.

Table 4.1 Concentration Dependence of the ^{119}Sn Chemical Shifts of $(CH_3)_4Sn$ in Acetone and Chloroform (at 31.4°)

A. Acetone

Concentration Volume Per Cent	Resonance Position (Hz)	Shift
10	37,290,682	+0.54
20	37,290,673	+0.29
40	37,290,663	0
60	37,290,650	-0.32
80	37,290,644	-0.48

B. Chloroform

Concentration Volume Per Cent	Resonance Position (Hz)	Shift
5	37,290,685	+0.59
10	37,290,684	+0.59
20	37,290,675	+0.34
40	37,290,662	0
60	37,290,649	-0.37
80	37,290,642	-0.53

Table 4.2

Temperature Dependence of the ^{119}Sn Chemical Shift of $(CH_3)_4Sn$ in Acetone and Chloroform

A. Acetone

Temperature ^oC	Absolute Frequency (Hz)	Shift (ppm)
+31.4	37,290,663	0
+25.0	37,290,662	0
0.0	37,290,674	+0.32
-10.0	37,290,679	+0.45
-20.0	37,290,684	+0.58
-30.0	37,290,690	+0.75
-40.0	37,290,694	+0.84
-50.0	37,290,699	+0.99
-60.0	37,290,705	+1.15
-70.0	37,290,711	+1.31

B. Chloroform

Temperature ^oC	Absolute Frequency (Hz)	Shift (ppm)
+31.4	37,290,662	0
+25.0	37,290,662	0
+10.0	37,290,671	+0.24
0.0	37,290,674	+0.32
-10.0	37,290,681	+0.50
-20.0	37,290,688	+0.69
-30.0	37,290,694	+0.86
-40.0	37,290,705	+1.15
-50.0	37,290,714	+1.39

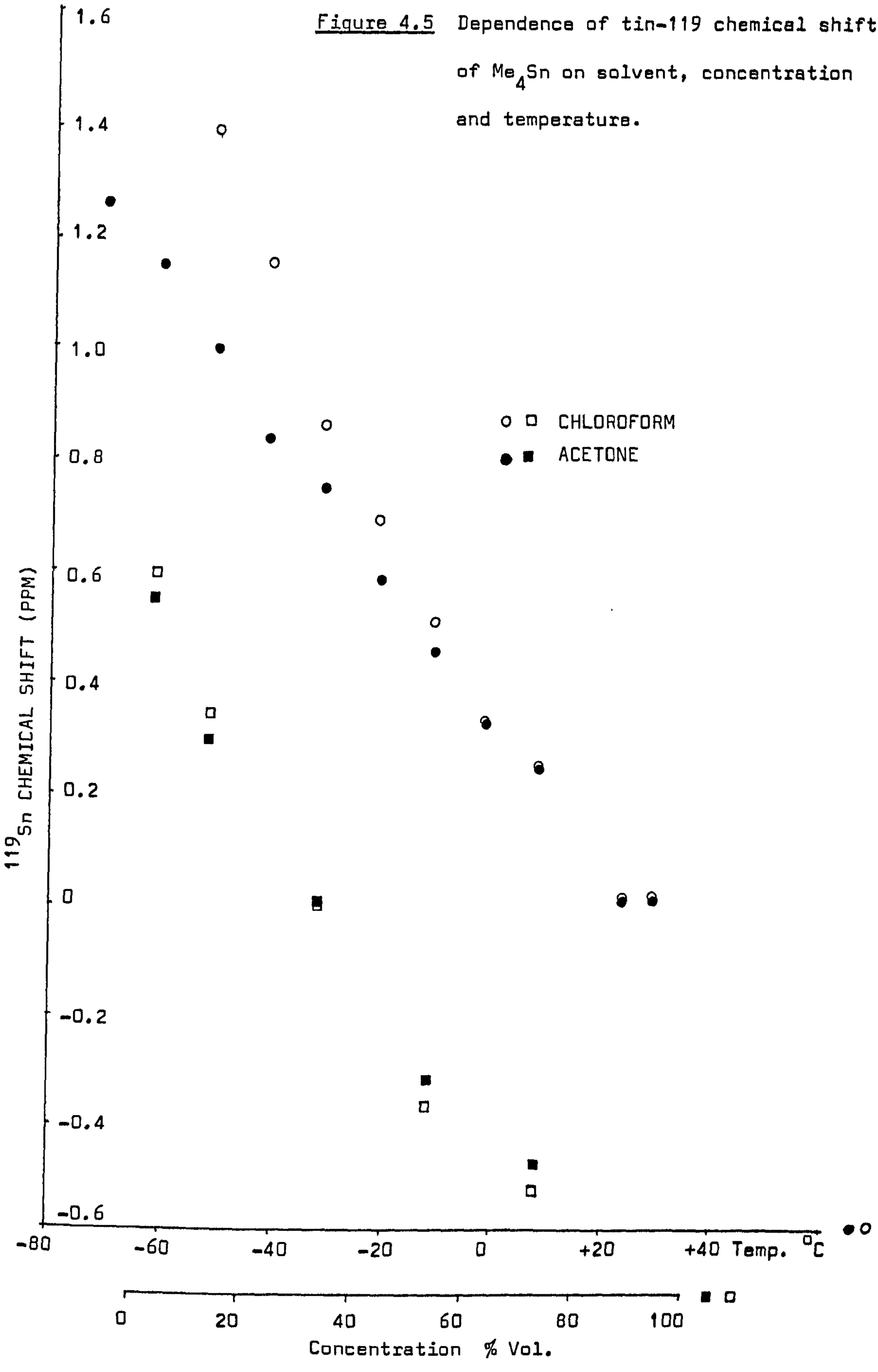

Figure 4.5 Dependence of tin-119 chemical shift of Me_4Sn on solvent, concentration and temperature.

With the exception of $Me_2Sn(OMe)_2$, all compounds were air-stable and required no special precautions. For concentration studies on $Me_2Sn(OMe)_2$ a specially designed sealing valve was used to facilitate the addition of solvent. The valve is in three main sections, the filling port and tap, the valve body, and the sample tube clamp and spinner turbine (Figure 4.6).

The tap is surmounted by a B 10 size cone to enable connection to a vacuum system. Below the cone is a knurled ring which assists tightening of the "V" cross-sectioned base onto an "O" ring in the valve body. A double "O" ring seal is used around the sides of the tap to prevent escape of liquid through the threaded section. The tap is hollow with two holes drilled immediately above the base to meet the orifice so formed.

The internal construction of the valve body has a thread to accept the tap, a narrow section which acts as a guide to the sample tube, and a further threaded section for the tube clamp. A good seal onto the sample tube is obtained by sloping the seat of the sealing ring which is thus forced in toward the tube on tightening the clamp.

The tube clamp is shaped to form the spinner turbine and, with careful manufacture, the resulting assembly gives perfect spinning.

Material is introduced to the sample tube by connection of the B 10 cone to a vacuum system. The tap is raised off the "O" ring seat in the valve body and the sample distilled into the sample

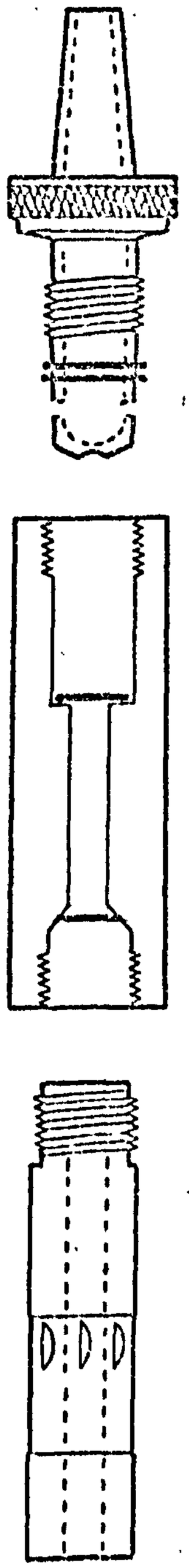

(a)

(b)

(c)

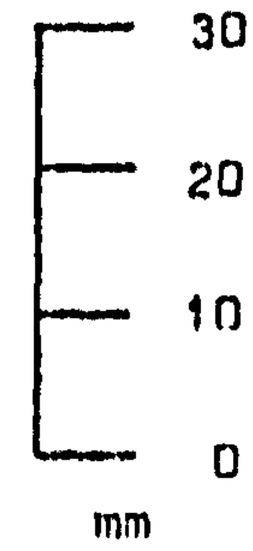

Figure 4.6 Internal construction of sealing valve showing (a) tap, (b) valve body, and (c) tube clamp with spinner turbine.

tube via the small holes in the base of the tap.

Involatile solids may be loaded into the sample tube in a dry-box before the tube is connected to the sealing valve. Solvent can then be distilled onto the solute using the above procedure. On completion of sample preparation the tap is tightened onto the "O" ring seat and the system is ready for use.

P.T.F.E. was used in the valves construction and the "O" ring seals were Edwards High Vacuum Limited Viton type VIT 2A for the tap base and tube and two type VIT 0009 on the side seal of the tap.

4.3 RESULTS AND DISCUSSION

4.3.1 Chemical Shifts and Magnetic Shielding

Tin-119 chemical shift data for eight trimethyltin and fourteen diorganotin compounds are listed in Table 4.3. The magnitude of magnetic shielding of a tin nucleus is the result of the sum of a number of contributions:

$$\sigma_A = \sigma^d_{AA} + \sigma^p_{AA} + \sum_{B \neq A} \sigma^d_{AB} + \sigma^1_A + \sigma_E + \sigma_M$$

where σ_A = shielding constant for nucleus A

and A = tin-119.

$\sum_{B \neq A} \sigma^d_{AB}$, σ^1_A, σ_E and σ_M are of small importance to the

overall value of σ_A for heavy atoms. σ^d_{AB} arises from electronic circulation from other atoms within the molecule and is, therefore, inversely proportional to the separation of A and B. σ^1_A is the contribution from electrons not associated with a given atom, e.g. aromatic ring currents. σ_E considers the permanent or induced electric dipole in the molecule and σ_m accounts for, inter alia, magnetic and electric anisotropies in the molecular environment.

The Lamb term, σ^d_{AA}, accounts for the shielding of the nucleus by an induced diamagnetic current from a spherical electron distribution. The major contribution to this being, therefore, the inner core electrons and so, whilst this term is important for lighter elements such as ^{13}C and ^{14}N, for heavier elements changes in the valence shell will have little effect on its value. The dominant contribution for tin-119 shielding, therefore, arises from the magnetic fields set up by the orbital motion of the valence electrons; the paramagnetic term, σ^p_{AA}. Generally, these fields, whilst at any one time having a value of several thousand gauss, average to zero. However, in the presence of a static magnetic field slight polarization can occur which, in orbital fields of such magnitude, may generate appreciable magnetic shielding. Thus, a mixing of ground and excited states results and hence σ^p_{AA} may, to an approximation, be considered as due to opposition by substituents on the tin to diamagnetic circulation. It is, therefore, of opposite sign to σ^d_{AA} and is defined by the equation:

$$\sigma^p_{AA} = (2e^2h^2/3m^2c^2\Delta E)(\langle r^{-3}\rangle_p Q_p + \langle r^{-3}\rangle_d Q_d)$$

ΔE is the average electronic excitation energy which determines the degree of interaction between the ground and excited states of the magnetic field. However, there is no a priori method for selecting a value for ΔE and, particularly in the case of tin, little information is available as to the effect of substituents on its value. However, for a given series of compounds it is probably reasonable to consider ΔE as constant as the resultant chemical shifts are, essentially, invariant with temperature, as the measured values for $Me_3SnONPhC(O)Ph$ illustrate in Table 4.4. A total shift of only 6.4 ppm over a temperature range of 110^{o} is observed.

Table 4.4 Variation of Chemical Shift of $Me_3SnONPhC(O)Ph$ with Temperature

Temperature (^{o}C)	Chemical Shift (ppm)[a]
+60	+94.5
+25	+95.6
0	+96.7
-30	+99.4
-50	+100.9

[a] relative to Me_4Sn.

$\langle r^{-3} \rangle_p$ and $\langle r^{-3} \rangle_d$ are the mean inverse cube of the valence p- and d-electron-nuclear distances respectively. Q_p and

Table 4.3 Chemical Shifts of some Trimethyltin and Dimethyltin Compounds

Compound	Solvent/Concentration	Absolute Frequency (Hz)	Chemical Shift (ppm)
Me_3SnCl	C_6H_6 / 25% w/v	37,296,642 ± 5	+160.4
$Ph_3PCHCOMe.Me_3SnCl$	$CHCl_3$ / 20% w/v	37,289,899 ± 5	- 20.46
$Me_3SnONPhC(O)Ph$	$CDCl_3$ / 29.65% w/v	37,294,283 ± 5	+ 97.1
$Me_3Snoxin$	C_6H_6 / 4 Molar	37,292,431 ± 6	+ 47.4
Me_3SnSpy-2	$CHCl_3$ / 30.15% w/v	37,292,822 ± 2	+ 57.9
$Me_3SnO_3SC_6H_5$	$CDCl_3$ / satd. soln. (0.148g/ml)	37,293,859 ± 40	+ 85.7
"	MeOH / 30% w/v	37,292,836 ± 15	+ 58.3
$Me_3SnO_3SC_6H_4Me$-4	MeOH / 29.04% w/v	37,292,497 ± 15	+ 49.2
Me_3SnOpy-2	CH_2Cl_2 / 10.2% w/v	37,294,289 ± 15	+ 97.2
Me_3SnOpy-3	MeOH / 29.6% w/v	37,291,859 ± 5	+ 32.1
Me_3SnO_2Cpy-2	CD_3OD / 30.08% w/v	38.291,565 ± 5	+ 24.2
Me_2SnCl_2	$CDCl_3$ / 20% w/v	37,295,783 ± 1	+137.3
"	CH_3CN / 28.5% w/v	37,292,319 ± 0.5	+ 44.4
"	$(CH_3)_2CO$ / 30.6% w/v	37,291,841 ± 5	+ 29.7
$MeSnCl_2.Ph_3PO$	C_6H_6 / 16% w/v	37,289,533 ± 5	- 30.3

cont./..

Table 4.3 continued

Compound	Solvent/Concentration	Absolute Frequency (Hz)	Chemical Shift (ppm)
$Me_2SnCl_2.2Ph_3PO$	C_6H_6 / 23.3% w/v	37,287,538 ± 5	- 83.8
$Me_2Sn(OMe)_2$	C_6H_6 / 38.3% w/v	37,285,685 ± 20	- 132.5
$Me_2ClSnONPhC(O)Ph$	$CDCl_3$ / 30.09% w/v	37,288,509 ± 5	- 57.7
"	DMSO / 29.6% w/v	37,284,219 ± 40	-172.7
$Me_2BrSnONPhC(O)Ph$	$CDCl_3$ / 29.29% w/v	37,287,824 ± 5	- 76.1
$Me_2ISnONPhC(O)Ph$	$CDCl_3$ / 30.64 % w/v	37,285,998 ± 5	-125.1
$Me_2Sn(ONMeCOMe)_2$	$CDCl_3$ / 16.4% w/v	37,283,016 ± 5	-205.0
$Me_2Sn(acac)_2$	$CDCl_3$ / 29.4% w/v	37,277,045 ± 10	-365.1
$Me_2Sn(tfac)_2$	$CDCl_3$ / 28.9% w/v	37,278,154 ± 5	-335.4
$Me_2Sn(O_3SC_6H_5)_2$	MeOH / 30.3% w/v	37,278,323 ± 3	-330.9
$Me_2Sn(S_2CNEt_2)_2$	$CDCl_3$ / 30.0% w/v	37,278,182 ± 5	-344.6
$Me_2Sn(oxin)_2$	$CDCl_3$ / 31.2% w/v	37,281,845 ± 5	-236.5
$Me_2Sn(ONPhC(O)Ph)_2$	$CDCl_3$ / 29.24% w/v	37,283,692 ± 4	-186.9
$Me_2Sn(Spy\text{-}2)_2$	$CDCl_3$ / 29.2% w/v	37,286,103 ± 2	-122.2

acac = Acetylacetone, tfac = trifluoroacetylacetone, py = pyridyl, oxin = 8-hydroxyquinolate.

Q_d are measures of the electron imbalance in the ground state p- and d-orbitals. In four-coordinate organotin(IV) compounds with approximately sp^3 hybridised tin, changes in shielding will largely arise from electronegativity differences in the ligands bonded to tin. In such compounds there will be no contribution from the Q_d term, but contributions will occur for coordination numbers higher than four. Examination of the available data for four-coordinated compounds shows that the magnitude of the downfield shifts (decreased shielding) is approximately proportional to the degree of electronic imbalance in the σ-framework, but population of 5d orbitals in five- and six-coordinated compounds results in much larger (usually dominant) upfield shifts. As would be expected, the presence of electron-rich and highly polarizable ligands such as alkynyl and iodide also result in large upfield shifts. Thus, this susceptibility of the tin-119 chemical shift to changes in coordination number should enable the n.m.r. technique to be used as a structural probe for the solution chemistry of organotin species. The data reported here can, therefore, be interpreted in this way.

4.3.2 Six-coordinate Structures

Three possible conformations may be assumed by six-coordinate tin compounds: cis (I), trans (II) and an intermediate configuration (III).

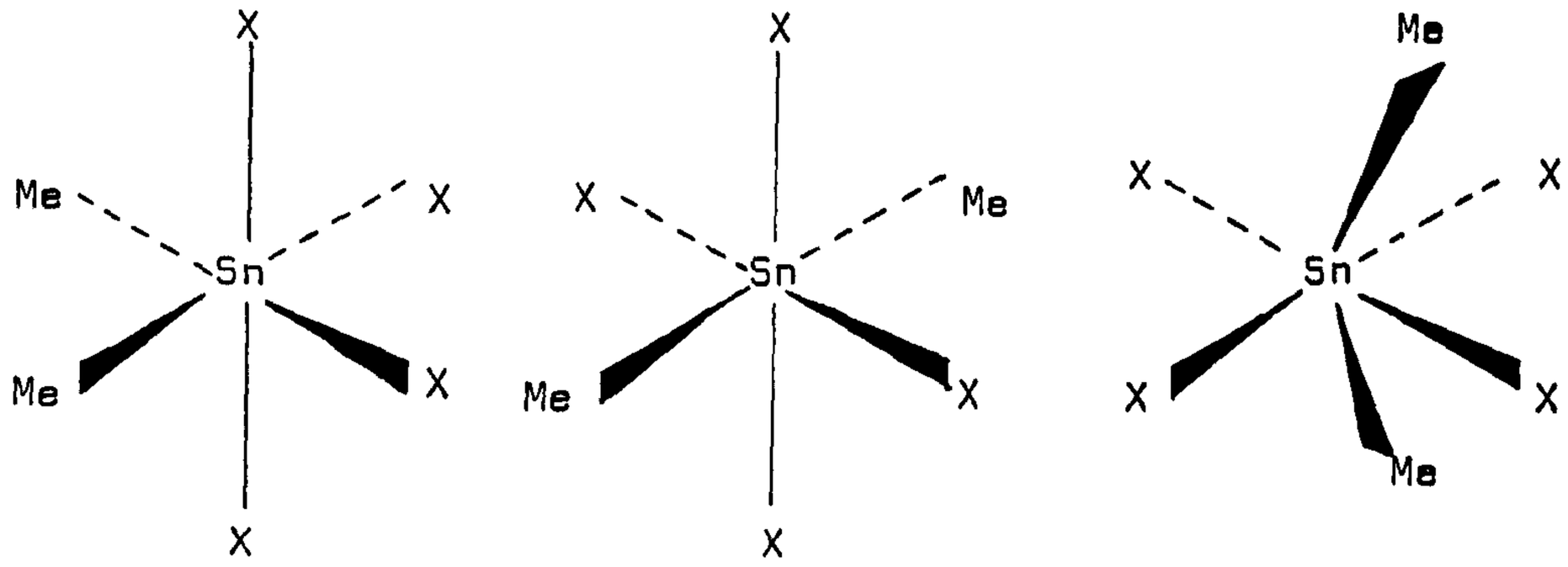

(I) Cis- (II) Trans- (III) Intermediate

For these the C-Sn-C bond angle is 90^{o}, 180^{o} and in the range 90^{o} - 180^{o}. respectively.

Crystallographic data for dimethyltin(IV) bis(acetylacetonate)[416], $Me_2Sn(acac)_2$, shows a linear C-Sn-C bond angle, and, therefore, the measured chemical shift of -365.1 ppm, may be considered representative of a trans-configuration in solution. The analogous bis(trifluoroacetylacetonate) also has a shift in this region, at -335.4 ppm, and thus may also be ascribed a trans-geometry. Presumably the slight deshielding reflects the influence of the fluorine electrons on the environment of the system. By analogy to these two compounds, $Me_2Sn(O_3SC_6H_5)_2$ with a shift of -330.9 ppm should also have a trans-structure, although crystal structure studies on dimethyltin(IV) dithiocarbamate, $Me_2Sn(SCSNEt_2)_2$, has shown a bond angle of only 136^{o} [416], and yet the chemical shift is

-344.6 ppm. This may reflect a solution effect with relaxation from the limiting structure, although changes in the electronegativity of the substituents, i.e. the changed shielding at tin from oxygen to sulphur, vide infra, could account for the shift.

For dimethyltin(IV) bis(8-hydroxyquinolate), crystal structure data shows the methyl groups assume a cis-structure with a C-Sn-C angle of 110.7° [417]. The chemical shift value of -236.5 ppm for this compound may, therefore, be taken as indicative of the area of resonance for this geometry in dimethyltin(IV) systems. Replacement of methyl by ethyl groups in $Et_2Sn(oxin)_2$ does not markedly alter this position. The reported shift for this latter compound being -264 ppm [418]. Further distortion from ideal cis-geometry and a weakening in chelation of the bidentate ligand is reflected in the lower field shift of -120 ppm for the related thiopyridine compound, $Me_2Sn(S\text{-}py\text{-}2)_2$. Whilst a similar structure, and effects, are expected for $Me_2Sn(ONPhC(O)Ph)_2$, the increased shielding of the oxygen on the tin when compared with sulphur, as observed for $Me_2Sn(O_3SC_6H_5)_2$ and $Me_2Sn(SCSNEt_2)_2$, is reflected in a chemical shift of -186.9 ppm. Structures of this type are generally not tightly packed within the unit cell and in the solid slight changes in chemical environment can lead to marked alterations in stereochemistry. Bis(N-acetylhydroxylamino)dimethyltin(IV)[432], for example, has cis-methyl groups in the solid with a bond angle to tin of 109.1°. Insertion of a water molecule to give the monohydrate results in a distorted trans-configuration to the crystal with a C-Sn-C angle of 156.8°. In solution, therefore, such modifications are equally

probable.

4.3.3 Five-coordination at tin

As expected, lowering the coordination leads to a deshielding of the tin nucleus and a concomitant downfield chemical shift. Comparison of the resonance position when one (ONPhC(O)Ph) ligand is replaced by halogen or methyl well illustrates this, and other effects (Table 4.5).

Table 4.5 Chemical shifts for some tin(IV) hydroxamic acid derivatives.

COMPOUND	COORDINATION	CHEMICAL SHIFT (ppm)
$Me_2Sn(ONPhC(O)Ph)_2$	6	-186.9
$Me_2SnCl(ONPhC(O)Ph).DMSO$	6	-172.7
$Me_2SnCl(ONPhC(O)Ph)$	5	- 57.7
$Me_2SnBr(ONPhC(O)Ph)$	5	- 76.1
$Me_2SnI(ONPhC(O)Ph)$	5	-125.1
$Me_3Sn(ONPhC(O)Ph)$	5	+ 97.1

Replacement with a chlorine atom causes a shift to -57.7 ppm, although addition of DMSO forces a return to six-coordination, via this solvents strong attachment, vide infra, and the shift increases to

a value close to that of the $Me_2Sn(ONPhC(O)Ph)_2$. The changing electronegativities between the halogens is reflected in a general increase in shielding, I > Br > Cl. The change from a -I to a +I inductive effect on going to $Me_3Sn(ONPhC(O)Ph)$ contributes to the large downfield shift of +97.1 ppm in this latter compound. However, it is more likely that this arises predominantly from a change to cis-geometry in the oxygen atoms of the coordinating ligand, and an associated alteration in the Q_d term of σ^p_{AA}, which has been shown crystallographically to be the preferred orientation for the related methyl compound, $Me_2Sn(ONMeC(O)Me)$[433], and in the N-benzyl-N-phenyl-O-(triphenylstannyl) hydroxylamine analogue[419]. Infrared data[420] confirms Sn-O coordination for $Me_3Sn(ONPhC(O)Ph)$ by a lowering of the $\nu(C{=}O)$ to 1547 cm^{-1}. Thus, trans-geometry of the electronegative groups in five-coordinate tin produces upfield shifts from the cis-X-group configuration.

Triphenylphosphine-acetylmethylene complexed with trimethyltin chloride, $Ph_3PCH.CO.CH_3.(CH_3)_3SnCl$, has a chemical shift of -20.46 ppm and in the solid has been shown to possess cis-methyl groups with an almost planar Me_3Sn moiety and the ylide residue bonded through the oxygen rather than the methylene carbon[421]. Complexation of triphenylphosphine oxide with dimethyltin dichloride in a 1 : 1 ratio gives a tin-119 resonance at -30.3 ppm, indicative of cis-methyl configuration. In a 2 : 1 ratio with Me_2SnCl_2, however, where 6-coordination might be expected, the shift moves to only -83.8 ppm. It is likely that this value represents a mean position for an equilibrium of the type $A + B \rightleftharpoons AB \rightleftharpoons AB_2$,

between the 1 : 1 and 2 : 1 Ph_3PO : Me_2SnCl_2 ratio with exchange occurring in solution.

The effect of donor strength on the tin stereochemistry in solution is well reflected in the chemical shift values (Table 4.6). Whilst the magnitude of the effect is concentration dependent, the order DMSO > pyridine > methanol >> acetone ~ acetonitrile > dioxan is observed, reflecting the relative importance of the intermediate structure (V) between the limiting tetrahedral (IV) and trigonal bipyramidal (VI).

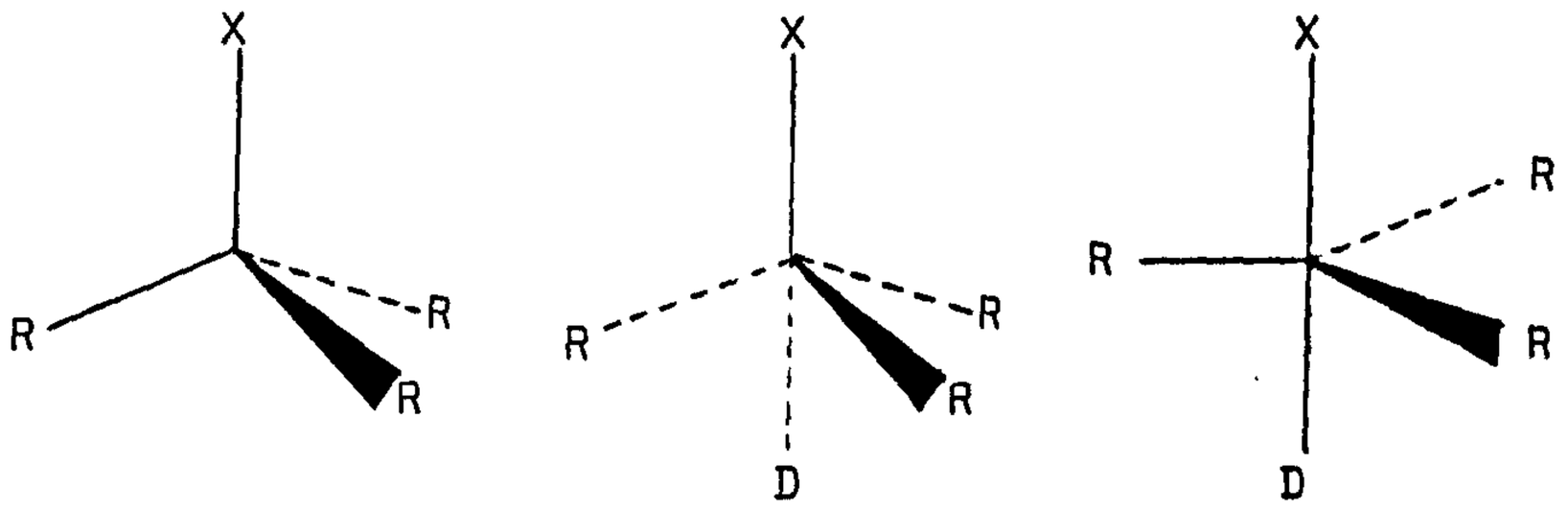

(IV) (V) (VI)

In the solid both trimethyltin(IV)-8-hydroxyquinolate and trimethyltin(IV)-2-thiopyridone have been ascribed five-coordinate <u>cis</u>-methyl geometry[424] but the tin-119 n.m.r. values of +47.4 and +57.9 ppm respectively indicates an intermediate structure between <u>cis</u> and <u>trans</u>. Similarly for trimethyltin(IV) phenylsulphonate, $Me_3SnO_3SC_6H_5$. This might be expected to possess a structure

Table 4.6 Trimethyl and dimethyltin(IV) chlorides with various donor systems.

Compound	Chemical Shift (ppm)	Reference
Me_2SnCl_2	+137.3	a
$Me_2SnCl_2.Ph_3PO$	- 30.3	a
$Me_2SnCl_2.2Ph_3PO$	- 83.8	a
$Me_2SnCl_2.2DMSO$	-246	422
$Me_2SnCl_2.CH_3CN$	+ 44.4	a
$Me_2SnCl_2.(CH_3)_2CO$	+ 29.7	a
Me_3SnCl	+160.4	a
$Me_3SnCl.Ph_3PCHCOCH_3$	- 20.46	a
$Me_3SnCl.DMSO$	- 3	422
$Me_3SnCl.CH_3CN$	-113	423
$Me_3SnCl.(CH_3)_2CO$	+113.2	423
$Me_3SnCl.$pyridine	+ 25.4	411
$Me_3SnCl.$dioxan	+124	423
$Me_3SnCl.MeOH$	+ 45	423

[a] This work

similar to that of $Me_3SnONPhC(O)Ph$ with the sulphonate moiety acting as chelating ligands. However a value of +85.7 ppm in $CDCl_3$, which moves to +58.3 ppm in MeOH, is observed. The latter effect presumably due to additional shielding at the tin nucleus from weak coordination by the solvent. A similar shift (+49.4 ppm) is observed for the toluene-4-sulphonate analogue, $Me_3SnO_3SC_6H_4$-Me-4. Thus, for weakly coordinating five-coordinate systems <u>trans</u>-geometry of the electronegative groups appears to give rise to a chemical shift in a similar region to that for the strongly coordinating <u>cis</u>-compounds. This is supported by the known <u>trans</u>-X-group configuration of the 3-pyridonyl compound, Me_3SnO-py-3, which has a shift of +32.1 ppm; similar to that for trimethyltin-2-pyridyl-carboxylate, Me_3SnO_2Cpy-2 at +24.2 ppm in methanol.

4.3.4 <u>Four-coordinate Structures</u>

In compounds with true four-coordination, such as Me_2SnCl_2 and Me_3SnCl, the chemical shifts are below +100 ppm. Values of +137.3 and +160.4 ppm, respectively, were obtained for the above two compounds. However, diethyltin(IV) dimethoxide, $Et_2Sn(OMe)_2$ has a resonance at -181 ppm, which is clearly not that of a four coordinate system. This high field shift has been attributed to a dimer structure (VII)[425].

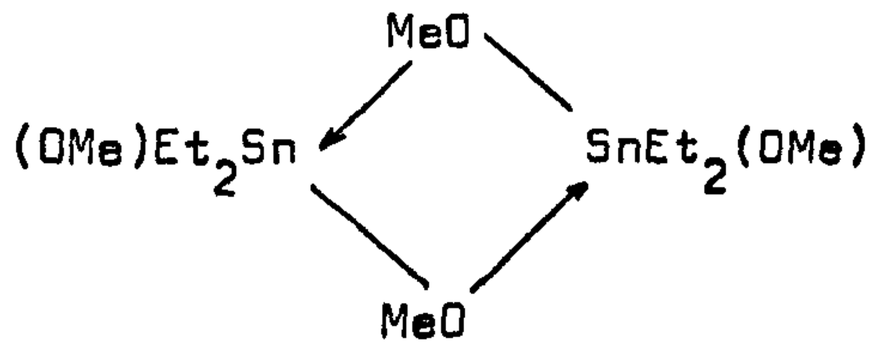

(VII)

The measured shift for the analogous $Me_2Sn(OMe)_2$ was again in this region at -133.4 ppm and, therefore, presumably also exists in dimeric form in solution. $Me_2Sn(OMe)Cl$ has been found to exhibit two resonances at +126 ppm and -90 ppm[425] which were explained, respectively, in terms of a tetrahedral monomer (VIII) and an alkoxy-bridged dimer structure (IX) with five-coordinate trigonal-bipyramidal cis-R_2SnX_2 units,

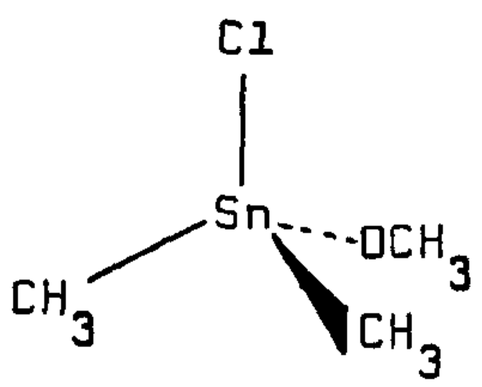

(VIII)

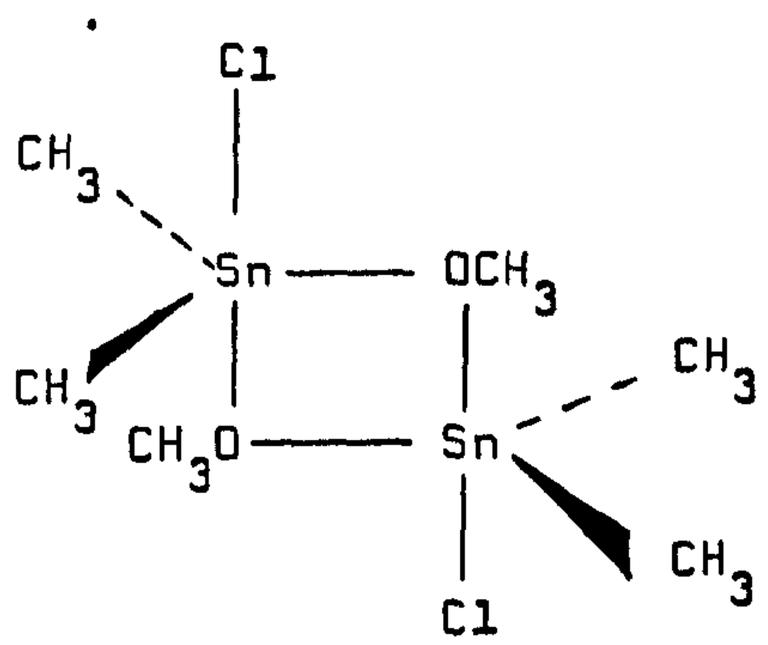

(IX)

However, as for the ethyl analogue, no low field resonance was observed for $Me_2Sn(OMe)_2$. Interestingly the sulphur, $Me_2Sn(SMe)_2$, and selenium, $Me_2Sn(SeMe)_2$, analogues have shifts of +144[427], and +57.1 ppm[426] respectively, illustrating absence of dimerisation and showing a shielding trend of O > S > Se. Thus as the atomic number of the chalcogen increases there is a decrease in electronegativity and a reduction in electron imbalance about the tin, i.e. the Q_p term. A contribution from the σ^{d}_{AB} term might also be expected

as this will depend on the atomic number of the substituent atom. However, its value is inversely proportional to the internuclear distance and, therefore, will decrease inversely with increasing atomic radius of the shielding atom.

4.3.5 Coupling Constants

It has been proposed that a linear relationship exists between $^{2}J(^{119}Sn...^{1}H)$ and the percentage s-character in the Sn-C bond[428]. For methyltin systems the relationship is

$$^{2}J(^{119}Sn...^{1}H) = 2.16\rho$$

The constant 2.16 was evaluated from the measured coupling constant for Me_4Sn and by assuming the percentage s-character, ρ, in the Sn-C bond to be 25% for this compound[429]. Clearly, such a relationship does not consider, *inter alia*, changes in effective nuclear charge on the tin with different ligands. However, values obtained in this way appear to support predicted values and have been used satisfactorily in calculation of enthalpies of formation for such complexes[430].

For trimethyltin systems with five-coordination where the three methyl carbons are coplanar, all the tin s-orbitals bond to carbon and anupper limit for ρ of 33% is achieved, whilst with tetrahedral sp^3 the Sn-C bond will have 25% s-character at the limit. Table 4.7 lists the $^{2}J(^{119}Sn...^{1}H)$ data and derived ρ-values for the

Table 4.7 Coupling Constants and Calculated Percentage s-character (ρ) of some Dimethyl- and Trimethyltin Compounds

Compound	Solvent	$^2J(^{117}Sn...^1H)$ (Hz)	$^2J(^{119}Sn...^1H)$ (Hz)	(%)
Me_3SnCl	C_6H_6	55.8	58.1	26.9
Me_3SnO_2Cpy-2	CD_3OD	65.7	69.3	32.0
$Me_3SnO_3SC_6H_4Me$-4	MeOH	66.0	69.0	31.9
Me_3SnOpy-3	MeOH	63.6	66.6	30.8
Me_3SnSpy-2	$CHCl_3$	54.7	57.2	26.5
$Me_3SnONPhC(O)Ph$	$CDCl_3$	53.3	56.0	25.9
$Me_3Snoxin$	C_6H_6	53.4	55.7	25.7
$Me_3SnO_3SC_6H_5$	$CDCl_3$	62.0	67.9	31.4
$Me_3SnO_3SC_6H_5$	MeOH	65.5	68.3	31.6
Me_2SnCl_2	$CDCl_3$	66.2	69.4	32.1
Me_2SnCl_2	CH_3CN	79.2	83.0	38.4
Me_2SnCl_2	$(CH_3)_2CO$	81.0	84.2	38.9
$Me_2Sn(tfac)_2$	$CDCl_3$	97.1	101.9	47.2

cont./..

Table 4.7 continued

Compound	Solvent	$^2J(^{117}Sn...^1H)$ (Hz)	$^2J(^{119}Sn...^1H)$ (Hz)	(%)
$Me_2Sn(acac)_2$	$CDCl_3$	96.4	100.4	46.5
$Me_2Sn(O_3SC_6H_5)_2$	MeOH	105.8	109.2	50.5
$Me_2Sn(Spy\text{-}2)_2$	$CDCl_3$	74.7	77.7	36.2
$Me_2Sn(ONPhC(O)Ph)_2$	$CDCl_3$	74.9	78.2	36.2
$Me_2Sn(S_2CNEt_2)_2$	$CDCl_3$	81.8	85.2	39.4
$Me_2Sn(oxin)_2$	$CDCl_3$	66.7	69.8	32.3
$Me_2Sn(OMe)_2$	C_6H_6	73.0	75.6	35.0
$Me_2ClSnONPhC(O)Ph$	$CDCl_3$	74.2	77.3	35.7
$Me_2ClSnONPhC(O)Ph$	DMSO	80.7	83.6	38.7
$Me_2ISnONPhC(O)Ph$	$CDCl_3$	72.9	76.1	35.2
$Me_2BrSnONPhC(O)Ph$	$CDCl_3$	71.3	74.3	34.4

systems studied.

Me_3SnCl which has sp^3-bonding has a value approaching the Me_4Sn limit, whilst Me_3SnS-py-2, $Me_3SnONPhC(O)Ph$ and Me_3Sn oxin are also similar and presumably indicate little change in the s-electron distribution around the tin on attachment of these ligands. With Me_3SnO_2Cpy-2, $Me_3SnO_3SC_6H_5$ and $Me_3SnO_3SC_6H_4Me$-4 there is a general increase in ρ-values which would support the previous assignments from chemical shift data towards more planar Me_3Sn units and <u>trans</u>-X-group configuration.

For the dimethyltin compounds a marked increase in percentage s-character is observed, Me_2SnCl_2, which is tetrahedral might be expected to have a value close to the 25% of Me_4Sn. However, literature values range from 25%[431] to between 33 and 48% depending on solvent[428]. Replacement of a methyl by chlorine might well force additional s-character into the Sn-C bond of the remaining tin-methyls. X-ray diffraction studies have shown a decrease in Sn-C bond length and an increase in Sn-Cl bond distance, with, therefore, a corresponding increase in the s-character of the Sn-C bond, as the series Me_4Sn to $SnCl_4$ is traversed. $^2J(^{119}Sn...^1H)$ values obtained in this study ranged from 69.4 Hz in $CDCl_3$ to 83.0 Hz in acetonitrile and 84.2 Hz in acetone. These correspond to ρ-values of 32.1, 38.4 and 38.9% respectively and are therefore in complete agreement with the latter literature values cited[428].

Trends observed in the other dimethyltin compounds measured shows those systems ascribed <u>trans</u> geometry have a higher ρ-value

than those considered to have a cis-structure. $Me_2Sn(S_2CNEt_2)_2$ does not fit this pattern, but as discussed, is expected to have a C-Sn-C bond angle of 136° and so the ρ-value would support this deviation from ideal trans-configuration.

4.4 STRUCTURE PREDICTIONS FROM COMBINED CHEMICAL SHIFT AND COUPLING CONSTANT DATA

From the point of view of use of tin-119 n.m.r. data as a simple structural probe for methyltin compounds, a useful approach to the data is to consider the chemical shifts and coupling constants simultaneously. As the foregoing discussion shows, to an approximation one may group the compounds examined in this study with respect to hybridization in order of the listing given in Table 4.8. The effect of change in percentage s-character (calculated from $^2J(^{119}Sn...^1H)$ values) must, perforce, reflect the C-Sn-C bond angle. If the organic moieties are considered in isolation in this way then the chemical shift will, primarily, be a function of the electronegativity of the remaining attachments to tin. Figure 4.7 is a plot of percentage s-character against chemical shift. From this, some interesting results are observed.

For compounds 1-4 (Table 4.8) where the C-Sn-C angle is essentially constrained to a tetrahedral geometry, the percentage s-character, and hence the bond angle, shows little change. The chemical shift, however, well reflects the decreased shielding about tin with electronegativity changes from chlorine to the

Table 4.8 Grouping of compounds according to C-Sn-C geometry

Compound Reference	Compound	Hybridization
1	Me_3SnCl	
2	$Me_3SnONPhCOPh$	sp^3
3	Me_3Sn oxin	
4	Me_3SnSpy-2	
5	Me_3SnO_3SPh ($CDCl_3$)	
6	Me_3SnO_3SPh (MeOH)	
7	$Me_3SnO_3SC_6H_4$-Me (MeOH)	
8	Me_3SnOpy-3 (MeOH)	sp^2
9	Me_3SnO_2Cpy-2	
10	Me_2SnCl_2 ($CDCl_3$)	
11	Me_2Sn $(oxin)_2$	
12	Me_2SnCl_2 (MeCN)	
13	Me_2SnCl_2 (Me_2CO)	
14	$Me_2Sn(OMe)$	
15	$Me_2SnCl(ONPhCOPh)$	
16	$Me_2SnCl(ONPhCOPh)$ (DMSO)	$sp^2 > x > 1$
17	$Me_2BrSn(ONPhCOPh)$	
18	$Me_2ISn(ONPhCOPh)$	
19	$Me_2Sn(S_2CNEt_2)_2$	
20	$Me_2Sn(ONPhCOPh)_2$	
21	$Me_2Sn(Spy$-2$)_2$	

cont./..

Table 4.8 continued

Compound Reference	Compound	Hybridization
22	$Me_2Sn(acac)_2$	
23	$Me_2Sn(tfac)_2$	sp
24	$Me_2Sn(O_3SPh)_2$ (MeOH)	

Figure 4.7 Percentage s-character against chemical shift

(Numbers against points indicate compound designation in Table 4.8)

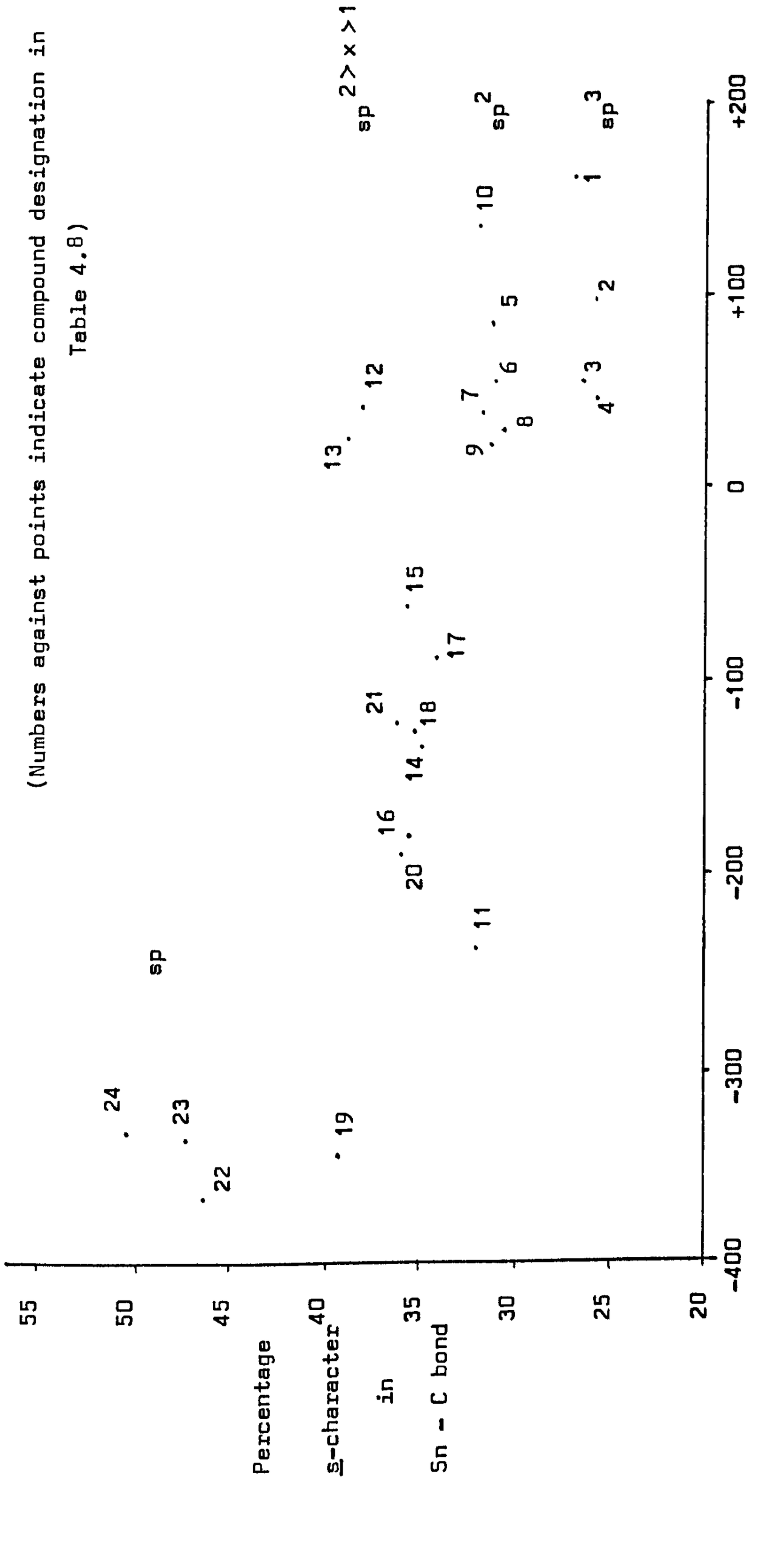

thiopyridyl complex and the effect of changing the attached chalcogen from oxygen to sulphur.

Compounds 5-11 all fall in the range with the C-Sn-C bond angle, x, of $120^{o} > x > 109^{o}$ and this is observed in their Sn...H coupling constants and, hence, ρ-values. The chemical shift for Me_3SnO_3SPh in $CDCl_3$ and MeOH illustrates the weak donor action of the latter solvent whilst the ρ-value shows the C-Sn-C angle is essentially unaffected. The electronegativity of the halogens in Me_2SnCl_2 cause an upfield shift whilst a marked downfield resonance position characterises the bidentate nature of the 8-hydroxyquinolate attachment in $Me_2Sn(oxin)_2$. Interaction of more strongly coordinating solvents with Me_2SnCl_2 forces distortion about tin and MeCN and Me_2CO show this shift away from $\underline{sp}^2$ hybridization. Similar effects are exhibited by the other compounds in the list 12-21, whilst the essentially <u>trans</u>-geometry of the methyl groups in the compounds 22-24 is reflected in a grouping of the ρ-values for the <u>sp</u>-hybridized C-Sn-C bonds of these materials.

4.5 CONCLUSION

The results reported here support our original proposal that tin-119 n.m.r. can be used as a structural probe for the stereochemistry of tin(IV) systems in solution. Insertion of the measured values for coupling constant and chemical shift for a particular compound into Figure 4.7, together with consideration of the general comments made about the effect of coordination number

on the chemical shift position, should enable a good prediction of the stereochemistry of the system in solution. It is perhaps surprising that the $^{2}J(^{119}Sn...^{1}H)$ coupling constants appear to mirror so well the bond angle changes in the C-Sn-C moiety almost to the exclusion of any contribution from the electronegative groups attached to tin. Conversely, the domination of the chemical shift by the attached ligands to the methyltin unit is also notable.

The treatment of the coupling constant data is an approach which is infrequently used. However, we believe the results, which agree well with the chemical shift interpretation, justify this approach and again provide a useful 'rule-of-thumb' in the initial analysis of a compound.

4.6 REPRESENTATIVE SPECTRA

The following traces are typical of the tin-119 INDOR spectra obtained in this study. In each case, the lower trace is the methyl-tin section of the ^{1}H spectrum and the upper trace is the associated tin-119 resonance obtained by decoupling the highfield proton tin-119 satellite.

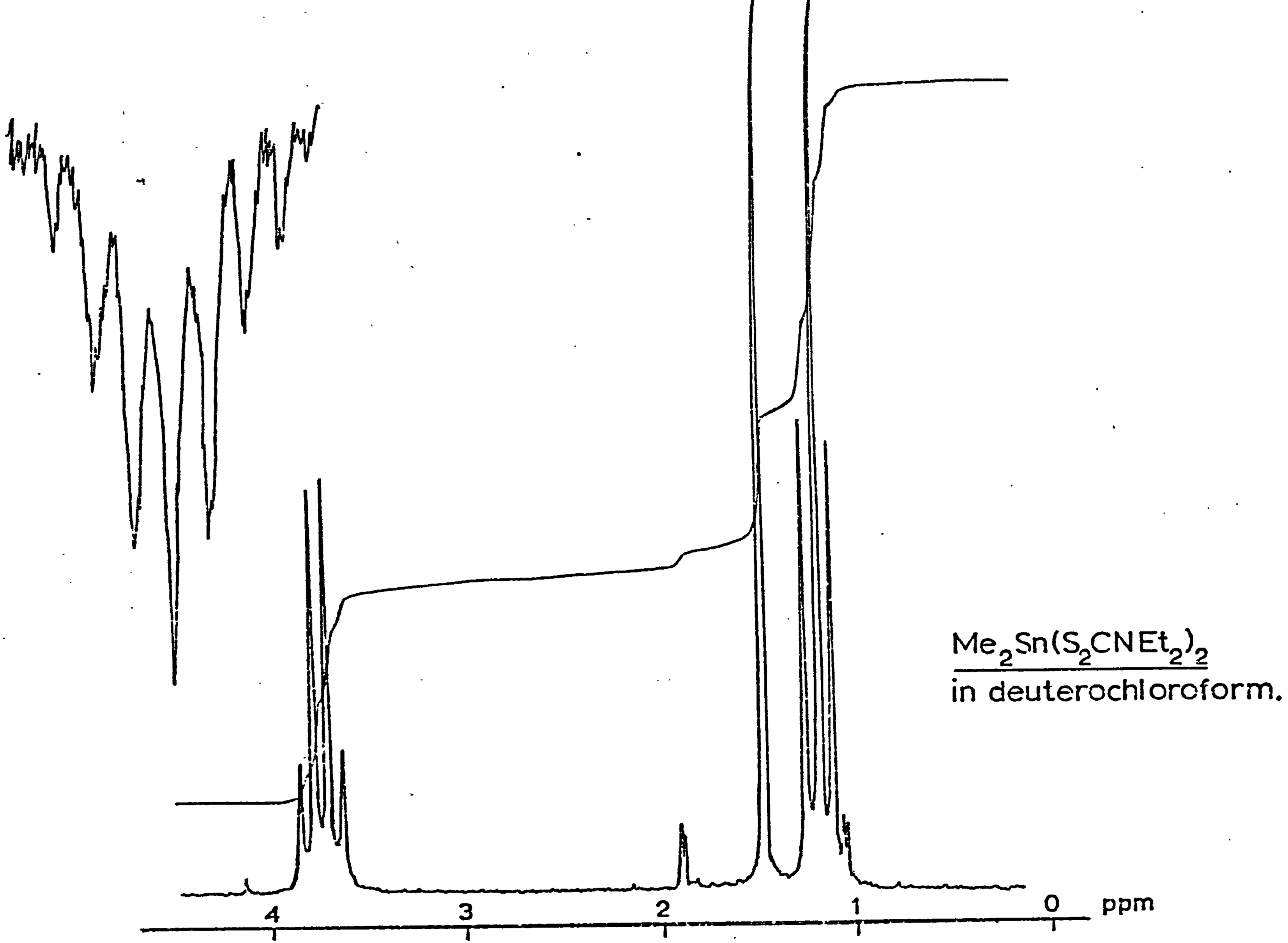

$\underline{Me_2Sn(S_2CNEt_2)_2}$
in deuterochloroform.

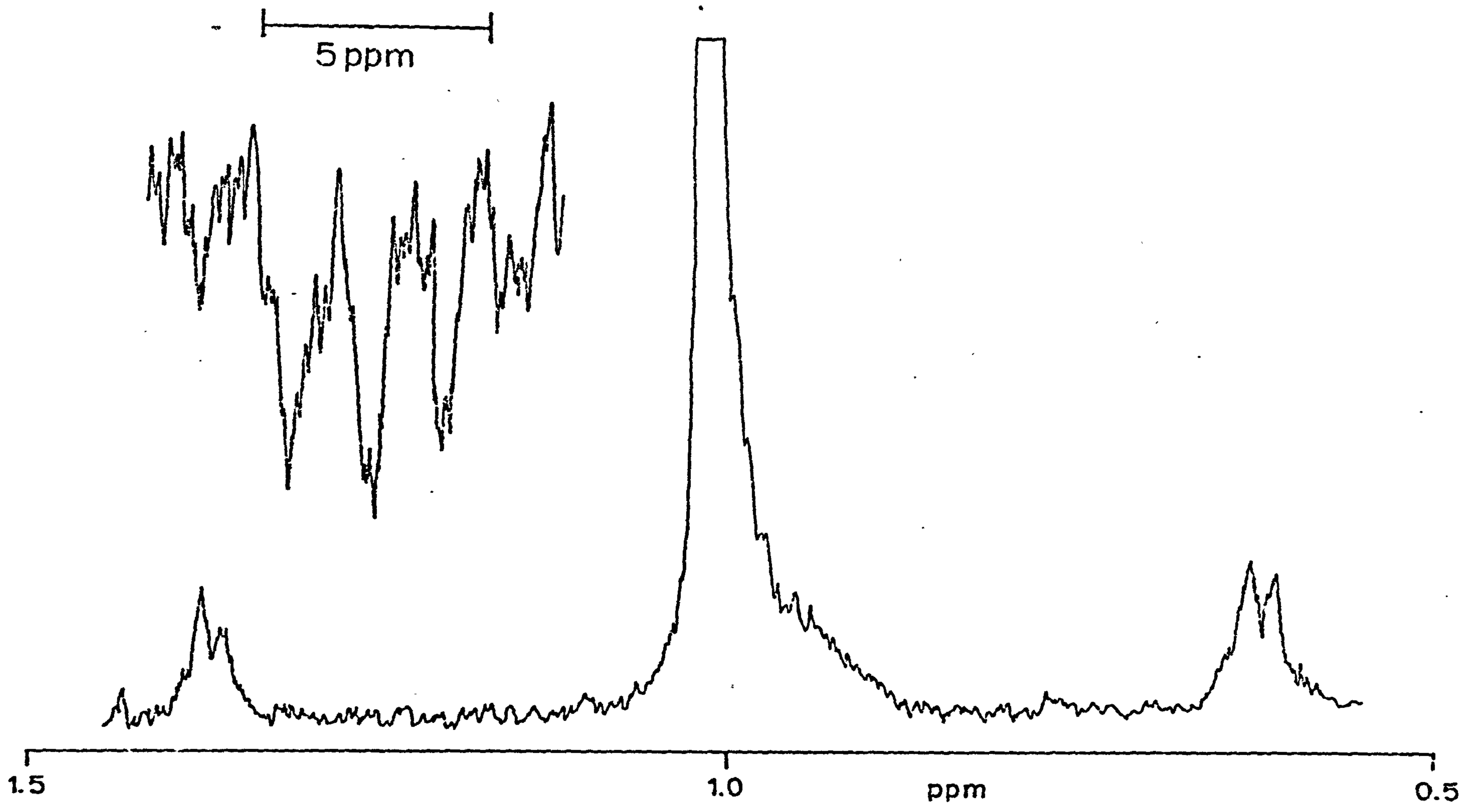

$ClMe_2SnONPhC(O)Ph$ in deuterochloroform.

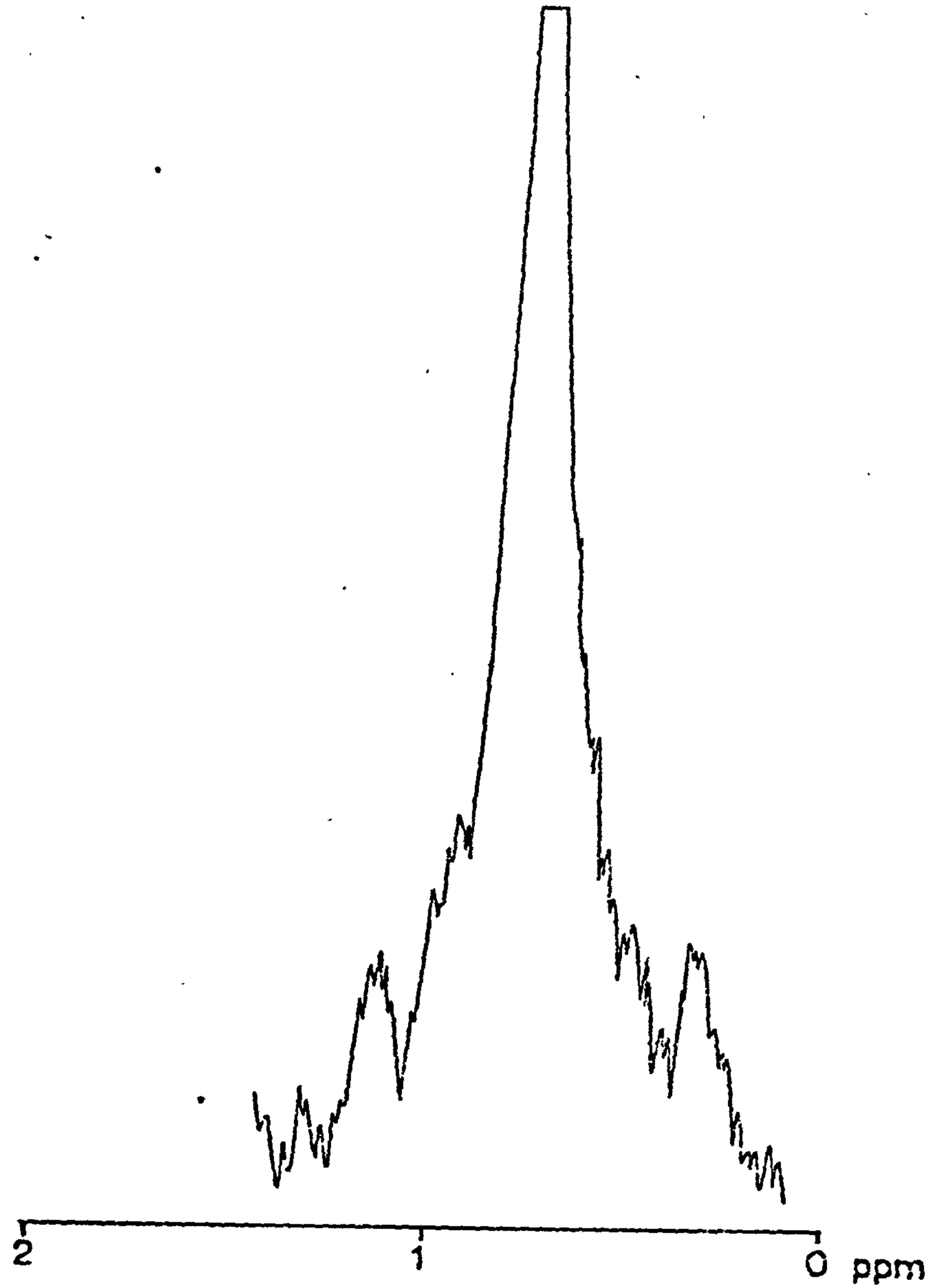

$ClMe_2SnONPhC(O)Ph$ in D.M.S.O.

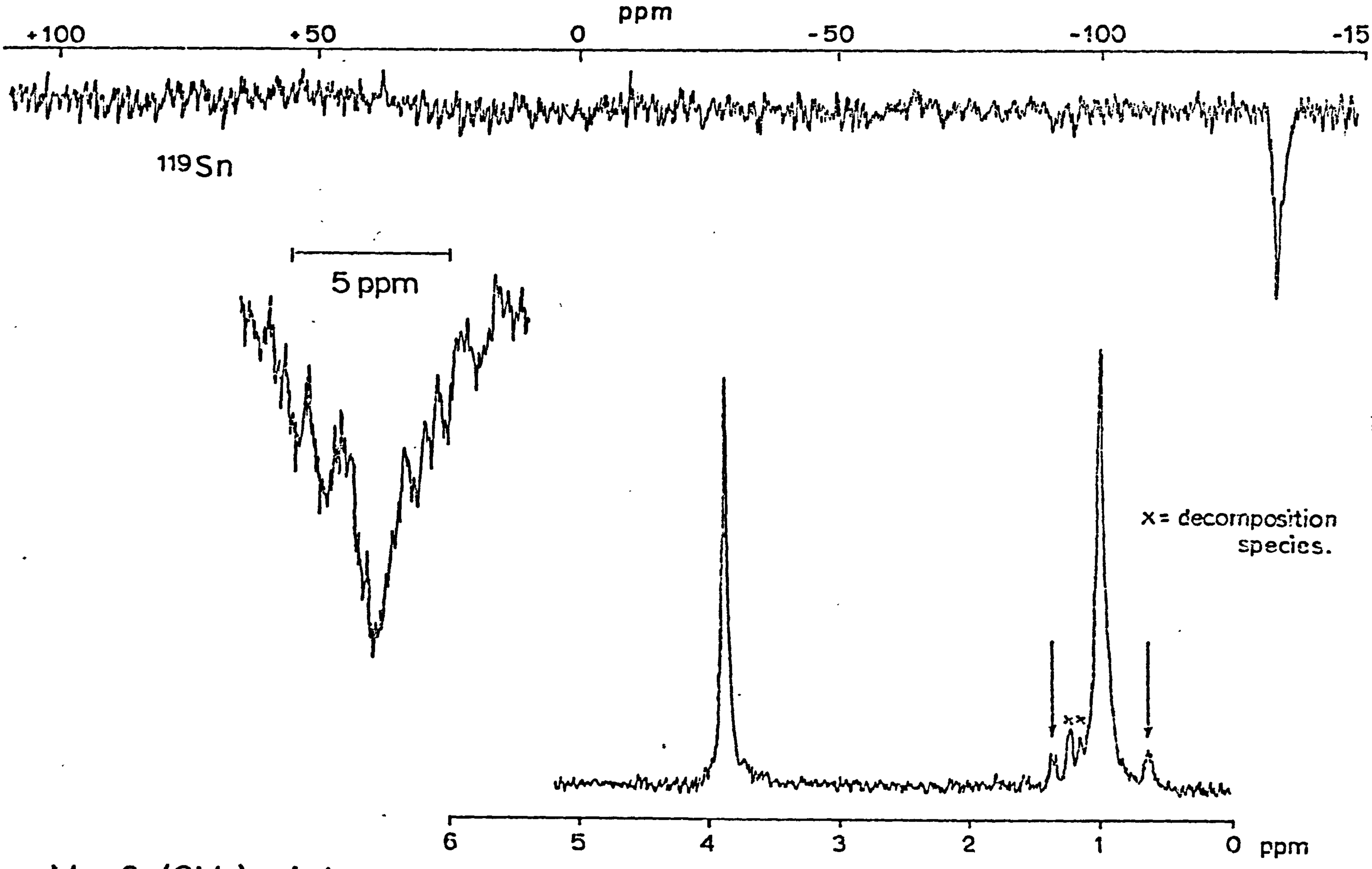

$\underline{Me_2Sn(OMe)_2}$ in benzene.

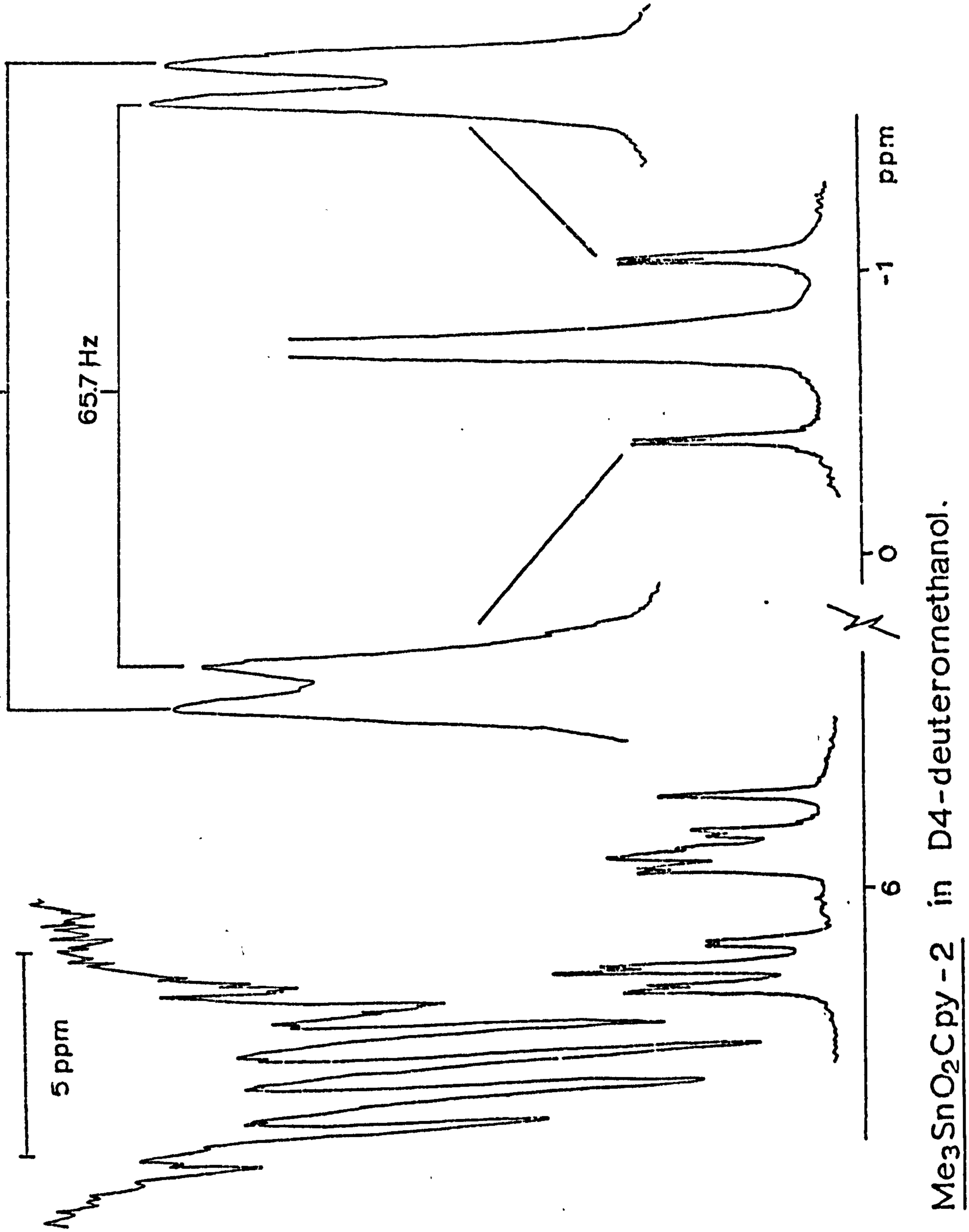

Me_3SnO_2Cpy-2 in D4-deuteromethanol.

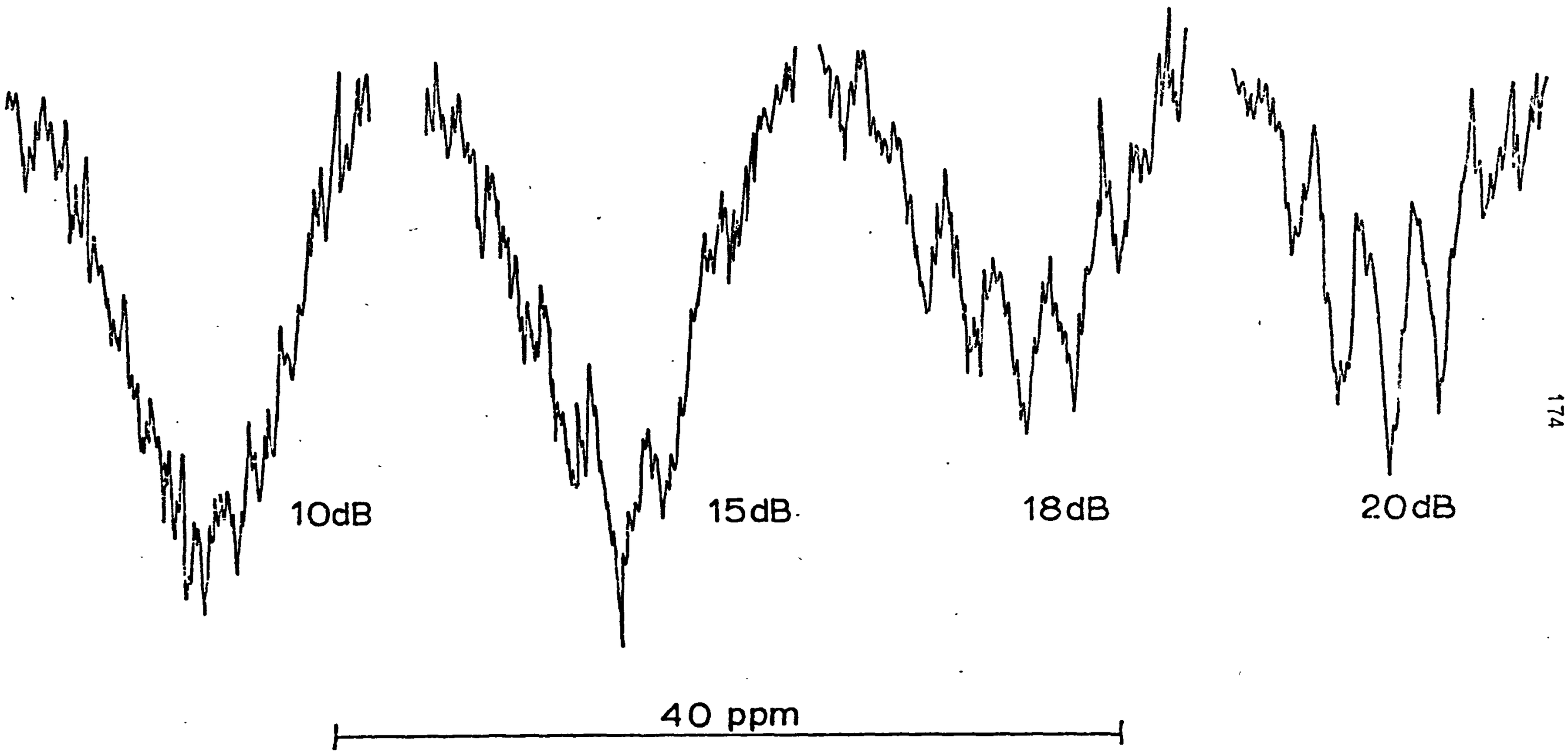

$\underline{Me_2Sn(O_3SC_6H_5)_2}$: In methanol (at various power levels).

REFERENCES

401. J.J. Burke and P.C. Lauterbur, J. Amer. Chem. Soc., (1961) 83 326.

402. E.B. Baker, J. Chem. Phys. (1962) 37 911.

403. J.D. Baldeschwieler and E.W. Randall, Chem. Rev., (1963) 63 81.

404. R. Freeman and W.A. Anderson, J. Chem. Phys., (1962) 39 806.

405. A.V. Overhauser, Phys. Rev., (1953) 91 476.

406. W. McFarlane, Ann. Rev. N.M.R. Spec. (1968) 1 135.

407. W. McFarlane, Ann. Rev., N.M.R. Spec. (1972) 5A 353.

408. V.J. Kowalewski, Prog. N.M.R. Spec. (1969) 5 1.

409. W. McFarlane, J.C. Maire and M. Delmas, J. Chem. Soc., Dalton Trans., (1972) 1862.

410. A.G. Davies, P.G. Harrison, J.D. Kennedy, T.N. Mitchell, R.J. Puddephatt and W. McFarlane, J. Chem. Soc., C, (1969) 1136.

411. B.K. Hunter and L.W. Reeves, Can. J. Chem., (1968) 46 1399.

412. P.G. Harrison, S.E. Ulrich, and J.J. Zuckerman, Inorg. Nucl. Chem. Letters, (1971) 7 865.

413. J.H. Allen, J.K. Beconsall and D.W. Turner, J. Sci. Instrym. (1964) 41 673.

414. W. McFarlane, J. Chem. Soc. A, (1967) 1660.

415. A. Charles, J. Sci. Instrument (1968) 1 64.

416. B.Y.K. Ho and J.J. Zuckerman, J. Organometal. Chem., (1973) 49 1.

417. E.O. Schlemper, Inorg. Chem., (1967) 6 2012.

418. W. McFarlane, J.C. Maire and M. Delmas, J. Chem. Soc., Dalton (1972) 1862.

419. P.G. Harrison and T.J. King, J. Chem. Soc., Dalton, (1974) 2298.

420. P.G. Harrison, Inorg. Chem., (1973) 12 1545.

421. J. Buckle, P.G. Harrison, T.J. King and J.A. Richards, J. Chem. Soc., Chem. Comm., (1972) 1104.

422. J.D. Kennedy and W. McFarlane, J. Chem. Soc., Perkin II, (1974) 146.

423. V.N. Torocheshnikov, A.P. Tupciauskas, N.M. Sergeyev and Yu. A. Ustynyuk, J. Organometal Chem., (1972) 35 C25.

424. P.G. Harrison and R.C. Phillips, J. Organometal. Chem., (1975) 99 79.

425. A.C. Chapman, A.G. Davies, P.G. Harrison and W. McFarlane, J. Chem. Soc. C., (1970) 821.

426. E.V. van. den. Berghe and G.P. van der Kelen, J. Organometal. Chem., (1971) 26 207.

427. J.D. Kennedy and W. McFarlane, J. Chem. Soc. Dalton, (1973) 2134.

428. J.R. Holmes and H.D. Kaesz, J. Amer. Chem. Soc., (1961) 83 3903.

429. N. Flitcroft and H.D. Kaesz, J. Amer. Chem. Soc., (1963) 85 1377.

430. T.F. Bolles and R.S. Drago, J. Amer. Chem. Soc., (1966) 88 5730.

431. P.J. Smith and L. Smith, Inorg. Chim. Acta Rev., (1973) I 11.

432. P.G. Harrison, T.J. King and R.C. Phillips, J. Chem. Soc., Dalton, (1976) 2317.

433. P.G. Harrison, T.J. King and K.C. Molloy, J. Organometal. Chem., (1980) 185 199.

CHAPTER FIVE

THE CHEMICAL AND PHYSIOLOGICAL PROPERTIES OF LEAD

5.1 INTRODUCTION

In many respects the chemistry of tin and lead have parallels and the commercial importance of these metals is well established. In biological systems, however, there is a marked disparity in their toxicological effects. The remaining discussion in this thesis will centre, initially, on the environmental distribution and occurrence of lead, with data relating to a new aetiology of lead poisoning. Subsequently a model for physiological absorption and a mechanism of action of ingested lead will be proposed. The chemistry of the metal and compounds relevent to this discussion is now briefly reviewed, the biological consequences of its absorption examined and some environmental sources described.

5.2 THE METAL

Whilst native lead does occur in nature it is rare and the metal is obtained, primarily, from the ore galena (PbS). The principal sources being in Australia, Canada, Mexico, Russia and the U.S.A. Extraction involves concentration by floatation, to remove lighter impurities such as zinc sulphide, followed by roasting with quartz in air to produce the oxide.

$$2PbS + 3O_2 \longrightarrow 2PbO + 2SO_2$$

Any sulphate generated is converted to lead silicate by reaction with the quartz. Smelting in a blast furnace with limestone and coke yields crude lead. The reactions involved being:

$$PbO + C \longrightarrow Pb + CO$$

$$PbO + CO \longrightarrow Pb + CO_2$$

$$PbSiO_3 + CaO + CO \longrightarrow Pb + CaSiO_3 + CO_2$$

The last equation explaining the function of the limestone. The crude lead is subsequently melted at a temperature below the melting point of copper, which can then be removed in crystalline form. Further purification by controlled remelting removes the principal impurities, gold, silver, arsenic, antimony and bismuth, to yield 99.9% pure lead. Electrolysis using the lead as the anode in an electrolytic bath consisting of a solution of lead in fluorsilicic acid (SiF_6^{2-}) followed by zone refining produces the metal with a purity of 99.9999%[501]. Gelatin is added to the electrolytic bath to ensure a smooth coherent deposit of the metal; the impurities forming a sludge and are not deposited at the cathode. Other naturally occurring lead ores include the sulphate, anglesite ($PbSO_4$); carbonate, cerrusite ($PbCO_3$); and mixed chloride-phosphates and -arsenates, pyromorphite $PbCl_2.3Pb_3(PO_4)_2$ and $PbCl_2.3Pb_3(AsO_4)_2$ minietesite[502].

The metal is bluish-white with a bright lustre and crystallises with a face-centred cubic structure having a lattice constant $a = 4.9408$ Å [503]. The unique combination of physical properties: low melting point (327.502°C, b.p. 1740°C), low solubility in water

(0.311 mg/l at 24°C), high density (11.348 at 25°C), high malleability and ductility, corrosion resistance and poor electrical conductivity, have enabled its use in a wide variety of applications.

Twenty-five isotopes have been recognised but only four stable isotopes occur in natural lead: ^{204}Pb (1.48%), ^{206}Pb (23.6%), ^{207}Pb (22.6%) and ^{208}Pb (52.3%). Lead isotopes are the end products of each of the three series of naturally-occurring radioactive elements: the uranium series decays to ^{206}Pb, whilst ^{207}Pb and ^{208}Pb are the final products from decay of the actinium series and thorium series, respectively. No allotropes of lead occur.

Chemically, lead forms lead(II) hydroxide and an oxycarbonate on exposure to the atmosphere. This has the effect of removing the bright lustre and protecting the underlying surface. In oxygenated water polyhydroxyl species result which, with soft water, can give rise to toxic levels of the metal when lead piping is used in domestic water supplies. Generally, however, in hard water this effect is markedly reduced by conversion of the lead(II) hydroxides to lead carbonate or silicate which provide a protective lining to the pipe in contact with water. With sulphuric acid, formation of an insoluble sulphate coating prevents rapid reaction, whilst the more soluble chloride, nitrate and acetate compounds allow a progressive increase in dissolution and hence reaction rate in the respective mineral acid. With nitric acid oxides of nitrogen are also produced.

Finely divided lead will dissolve in solutions of sodium in liquid ammonia to produce a green solution of Na_4Pb_9 analogous to the Na_4Sn_9 system previously described. Heating finely divided

lead in air produces litharge PbO which with further oxidation yields 'red lead', Pb_3O_4. Careful heating of lead tartrate produces very finely divided lead which is pyrophoric.

As with tin many alloys of lead are known. Indeed, tin is frequently a major component of lead alloys, for example solder (50% Sn), Pewter (85% Sn) and type metal (10% Sn), the latter also containing antimony (18%) and copper (2%). Within the history of the uses of lead its application as radioactive screening is, perforce, a most recent development. As well as lead bricks and sheets, glass impregnated with a high percentage of lead oxide is also used in this field. The more traditional uses of lead, as piping, for roofing, in containers, etc. are all well known. However, with the increased awareness of the potential hazard presented by the metal if ingested, as well as rising costs, many such applications have been replaced by other materials. Primary applications remain in the field of alloys and by conversion to organolead compounds for use as anti-knock agents in petrol.

5.3 COMPARATIVE PROPERTIES OF SOME INORGANIC TIN AND LEAD COMPOUNDS

5.3.1 General Comments on Group IV B

Group IV B of the Periodic Table provides an excellent example of the changes which can occur within a group. The tendency away from electronegativity towards electropositive character with increasing atomic number is one example. Carbon is a non-metal; the chemical properties of silicon are essentially non-metallic;

germanium is a metalloid whilst tin and lead are true metals. The predominant oxidation state for the group is four. However, with germanium and tin the divalent state becomes increasingly stable and predominates for lead. An explanation may be found in terms of bond strengths for covalent compounds or lattice energies in the case of ionic systems. Generally, bond energies decrease in the order Si - X > Ge - X > Sn - X > Pb - X. The result is that for reactions of the type $MX_2 + X_2 \longrightarrow MX_4$ the situation may arise where the M-X bond energy is insufficient to compensate for the $M(II) \longrightarrow M(IV)$ promotion energy and hence the MX_2 species is the more stable. Thus:

$$GeCl_2 + Cl_2 \longrightarrow GeCl_4 \quad \text{(rapid, } 25^{o}C\text{)}$$

$$SnCl_2 + Cl_2 \longrightarrow SnCl_4 \quad \text{(slow, } 25^{o}C\text{)}$$

$$PbCl_2 + Cl_2 \longrightarrow PbCl_4 \quad \text{(forcing conditions only)}$$

$PbCl_4$ rapidly decomposes at ambient temperatures.

For ionic compounds it is probable that the increasing size of the (real or hypothetical) M^{4+} ion down the group will make the lattice energy difference involved in the $M^{2+} \longrightarrow M^{4+} + 2e$ process energetically unfavourable, hence enabling the M^{2+} compound to predominate.

5.3.2 Chemical Compounds

The examples discussed below are not intended as a comprehensive survey of the inorganic compounds of tin and lead, but are chosen on

the basis of their relevance to the chemical model for physiological absorption of lead proposed in this work. As such, whilst the list is highly selective with emphasis given to the inorganic chemistry of lead it is presented in a form enabling comparisons to be drawn between the chemical properties of the two metals. Comprehensive reviews have been prepared by Abel[502].

(i) Oxides

Hydrolysis and subsequent dehydration of tin(II) salts yields the black, orthorhombic modification SnO. Indeed, this preparation was first used by Berzelius in 1812 when he added excess potassium carbonate to an aqueous tin(II) salt solution. The crystal structure is layered with oxygen atoms forming the base of a square pyramid with a tin atom at the apex. Oxidation at 300°C yields tin(IV) oxide whilst at lower temperatures under less oxidising conditions disproportionation into tin(IV) oxide and the metal results. The nature of cassiterite (SnO_2), the primary ore of tin has already been discussed (Chapter One).

Mixed valence oxides of both tin and lead are known being formulated as Sn_2O_3 and Pb_2O_3. However, whilst they are of definite composition their crystal structures have not been determined.

Lead(II) oxide, at normal temperatures, crystallises in a tetragonal form with the metal atom at the apex of a distorted square pyramid of oxygen atoms. This results in the well-known red, litharge. However, the system is dimorphic and above 480°C a yellow orthorhombic modification known as massicot results[504].

This is also obtained at room temperature by precipitation from a lead acetate solution using ammonium hydroxide. Inclusion of only trace impurities markedly reduces the rate of transition to the red form[505]. The presence of a thin surface film of elemental lead on either the red or yellow forms of the oxide results in 'black' lead(II) oxide. Lead monoxide is amphoteric dissolving readily in acids to give the corresponding lead(II) salts and, more slowly, in alkali to form hydroxyplumbites, e.g. $Na_2Pb(OH)_4$. It is only sparingly soluble in water.

Oxidation of lead(II) acetate with hypochlorite yields lead(IV) oxide which has a rutile structure[506]. Alternatively, electrolysis of lead nitrate or acetate causes anodic deposition of an orthorhombic form of PbO_2[507]. Although rare, native PbO_2 is found in the mineral plattnerite which is isomorphous with SnO_2. Anhydrous PbO_2 is difficult to obtain as the necessary heating causes decomposition to Pb and Pb_3O_4, (Minium),which has a chain system of $Pb^{IV}O_6$ octahedra linked via pyramidally coordinated oxygen atoms to Pb(II) ions (Figure 5.1) at distances of 2.13 and 2.23 Å. Its properties are those of 'plumbous plumbate' i.e. $Pb_2^{II}Pb^{IV}O_4$, hence in dilute nitric acid the plumbous moiety dissolves to give lead(II) nitrate, whilst the plumbic part precipitates as lead(IV) oxide:

$$Pb_2^{II}Pb^{IV}O_4 + 4HNO_3 \longrightarrow 2Pb(NO_3)_2 + PbO_2 + 2H_2O$$

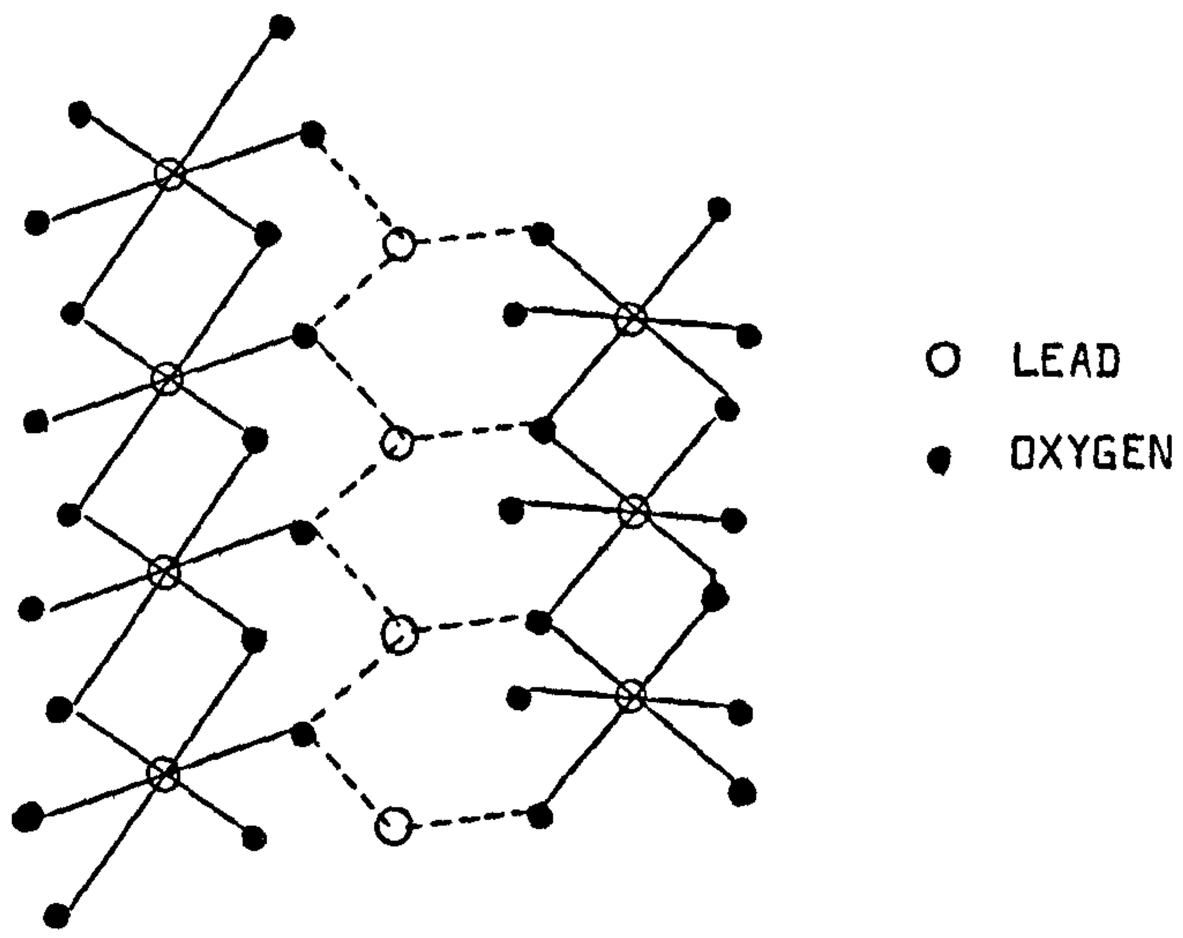

Figure 5.1 Structure of Pb_3O_4 [502]

The use of Pb_3O_4 in paint has been known for many years and has given rise to cases of lead poisoning (vide infra). Commercially, it is usually prepared by the action of heat on Pb or $PbCO_3$ in air[502]. Lead oxides also provide the basis for the accumulator. The battery plates consist of a lead-antimony grid infilled under pressure with red lead (Pb_3O_4). During initial charging oxygen released at the anode converts the Pb_3O_4 to PbO_2 i.e. $Pb_3O_4 + O_2 \longrightarrow 3PbO_2$, whilst at the cathode the liberated hydrogen reduces the red lead to the metal in a fine spongy condition. Dilute sulphuric acid acts

as electrolyte. When the cell is fully charged the specific gravity of the acid is 1.25. On discharging, however, reversal of the above chemical processes occurs and water is released lowering this value. The electrode reactions are

(i) $PbO_2 + SO_4^{2-} + 4H^+ + 2e^- \longrightarrow PbSO_4 + 2H_2O$

(ii) $PbSO_4 + 2e^- \longrightarrow Pb + SO_4^{2-}$

giving 1.685V and -0.356V respectively. Ideally, therefore, an overall potential of 2.041V is developed.

Interestingly a mixed metal $SnPb_2O_4$ system has been made which is isomorphous with Pb_3O_4 and, thus, has tetragonal symmetry.

In addition to the systems described a wide variety of non-stoichiometric lead-oxygen compositions have been reported between PbO and PbO_2 [502].

(ii) Hydroxides

Until recently, neither tin(II) nor tin (IV) hydroxides were known. Hydrolysis of tin(II) salt solutions had indicated the presence of such ions as $SnOH^+$, $Sn_2(OH)_2^{2+}$ and $Sn_3(OH)_4^{2+}$ [508]. The hydroxy-stannate(II) ion, $Sn(OH)_3^-$ is well characterised and many of its salts have been isolated. The structure (I) is pyramidal

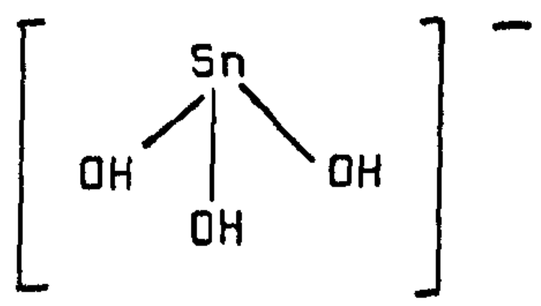

(I)

and on partial dehydration yields oxotetrahydroxyditin anions $\left[Sn(OH)_2\right]_2O^{2-}$ (II).

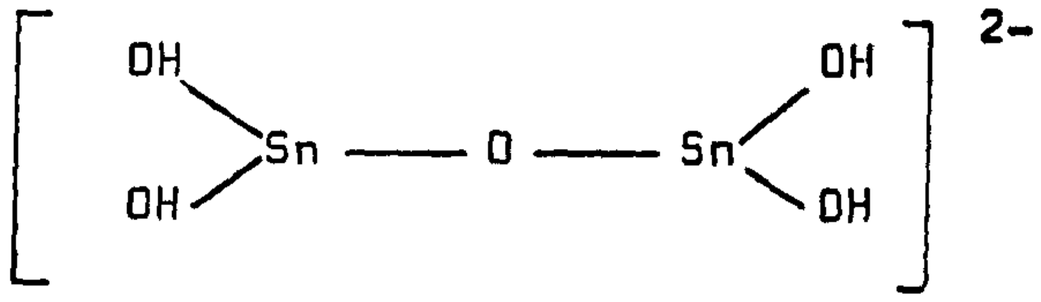

(II)

However, whilst many attempts have been made to prepare $Sn(OH)_2$ by aqueous routes it has finally been synthesized by an anhydrous, organometallic route[573]. An exchange reaction between tin(II) chloride and trimethyltin hydroxide results in a white, infusible, amorphous solid.

$$2Me_3SnOH + SnCl_2 \longrightarrow Sn(OH)_2 + 2Me_3SnCl$$

The material is soluble in acid and alkali and has an infrared spectrum containing ν(Sn-O) at 575 cm^{-1} and 340 cm^{-1}, and ν(SnO-H) at 3390 cm^{-1}.

For tin(IV), hydrolysis of salt solutions produces an amorphous precipitate probably containing bonded water in a tin oxide gel[502]. However, the octahedral $Sn(OH)_6^{2-}$ anion and many of its salts are well characterised[509].

Both the tin(II) and lead(II) oxide-hydroxide compounds $Sn_6O_8H_4$[510] and $Pb_6O_8H_4$[511] have been characterised. Octahedral

M_6 clusters are contained within a cube of hydrogen-bonded oxygen atoms(III).

<u>M_6O_8 units in $Sn_6O_8H_4$ and $Pb_6O_8H_4$</u>

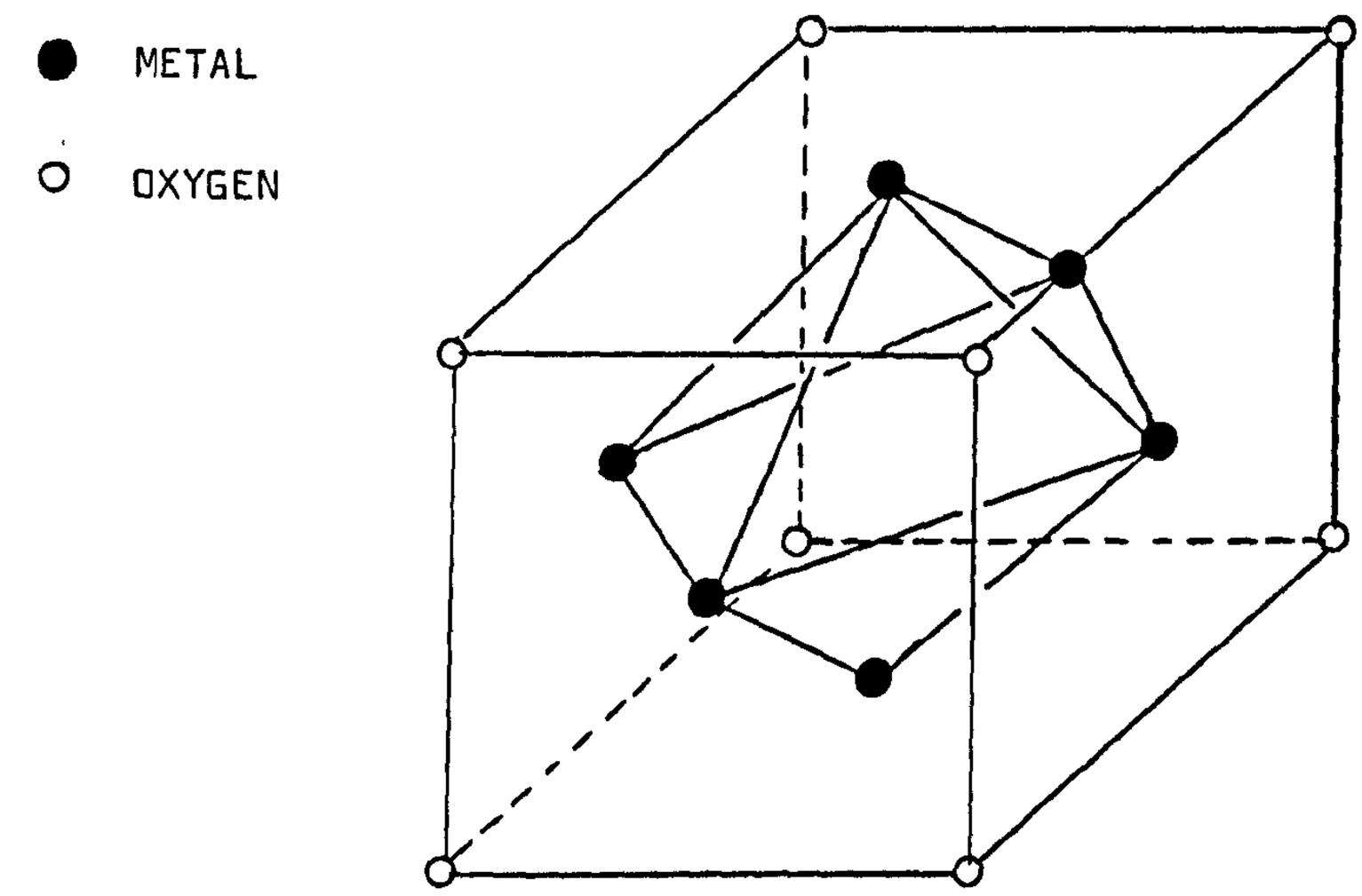

Partial hydrolysis of lead(II) salts is believed to produce the ions $Pb_3(OH)_4^{2+}$ and $Pb_6(OH)_8^{4+}$, which, like tin, may exist in metal clusters. Conversely, reaction with alkali yields various crystalline basic salts such as the carbonate $2PbCO_3.Pb(OH)_2$ (formed by boiling lead chloride or sulphate with Na_2CO_3 solution),

and nitrate, for which the stoichiometries $Pb(NO_3)_2.Pb(OH)_2$ and $Pb(NO_3)_2.5Pb(OH)_2$ are known[512]. $2PbCO_3.Pb(OH)_2$ was, at one time, used as a white pigment in paint but was susceptible to discolouration by sulphide formation.

Studies of Pb^{2+} and OH^- in perchlorate solutions[513] have enabled hydroxyl species such as $PbOH^+$, $Pb(OH)_3^-$, Pb_2OH^{3+}, $Pb_3(OH)_4^{2+}$, $Pb_4(OH)_4^{4+}$ and $Pb_6(OH)_8^{4+}$ to be identified. $Pb_4(OH)_4^{4+}$ predominates and has a cyclic, bridged structure similar to $Sn_4(OH)_4^{4+}$ [513].

The first equilibrium is probably

$$Pb^{2+} + H_2O \rightleftharpoons PbOH^+ + H^+ \quad \log k = -7.9$$

but clearly species of the type $Pb(OH_2)_n^{2+}$ are most likely also to be involved in the first coordination sphere of lead. Exchange equilibria such as

$$Pb(OH_2)^{2+} \underset{-OH^-}{\overset{+OH^-}{\rightleftharpoons}} Pb(OH_2)OH^+ \underset{-OH^-}{\overset{+OH^-}{\rightleftharpoons}} Pb(OH)_2$$

can be drawn which may well contribute to the overall reaction system.

(iii) Halides

The chemical and structural properties of the halide and mixed halogen compounds of tin(II) and tin(IV) have been extensively studied. Previous mention has been made of the structure of

$SnCl_2.2H_2O$ [514] and of the angular geometry of the analogous anhydrous halogen systems. The tin(IV) halides are volatile covalent species and are readily hydrolysed by aqueous alkali. The chloride forms a number of hydrates with the pentahydrate being stable at normal temperatures. The iodide, bromide and chloride can be prepared directly from the halogen and metallic tin, whilst the fluoride results from the action of anhydrous HF on tin(IV) chloride[515].

Lead(IV) fluoride is obtained as white, needle-like crystals from lead(II) fluoride by direct fluorination at 300°C[516], whilst lead(IV) chloride results from the action of concentrated sulphuric acid on pyridinium hexachloroplumbate[517]. Alternatively, the action of cold (0°C) concentrated hydrochloric acid on PbO_2 yield $PbCl_4$ in small quantities

$$PbO_2 + 4HCl \longrightarrow PbCl_4 + 2H_2O$$

However, chlorine readily evolves by the reversible reaction,

$$PbCl_4 \rightleftharpoons PbCl_2 + Cl_2$$

Addition of ammonium chloride to the above cold suspension results in precipitation of the yellow ammonium hexachloroplumbate(IV)

$$2NH_4Cl + PbCl_4 \longrightarrow (NH_4)_2\, Pb^{IV}\, Cl_6$$

Filtration and addition of cold, concentrated H_2SO_4 allows separation of the oily yellow liquid, $PbCl_4$

$$(NH_4)_2PbCl_6 + H_2SO_4 \longrightarrow (NH_4)_2SO_4 + PbCl_4 + 2HCl$$

The lead(IV) fluoride and chloride are both unstable; the chloride requiring storage in the dark under pure, concentrated sulphuric acid at $-80^{o}C$. The analogous bromide and chloride compounds are not known, probably because of the inability of those halides to oxidise lead(II)[502].

Lead(II) halides are stable and the chloride,bromide and iodide are readily formed by the addition of the appropriate halide to a solution of lead(II) ions. The fluoride results from rapid decomposition of the hydrofluoride formed by dissolving lead(II) carbonate in hydrofluoric acid. In solution with other halide ions, PbX_3^- ions occur which probably have the pyramidal geometry of SnX_3^-.

Studies on the $PbCl_2$-Cl^- solution system have not confirmed the existence of species such as $PbCl_3^-$ or $PbCl_4^{2-}$, although $PbCl_6^{4-}$ has been postulated[518]. In the solid, octahedral PbX_6^{4-} anions have been identified in the salts K_4PbF_6, K_4PbCl_6 and K_4PbBr_6 [519]. In solution in the absence of additional halide ions some PbX^+ cations result from combination of the principal ions, i.e.

$$Pb^{2+} + X^- \longrightarrow PbX^+$$

Studies on the mixed halides PbBrCl and PbICl has shown them to be isomorphous with $PbCl_2$.

(iv) Acetates

Tin(II) acetate is stable and can be obtained in pure form by sublimation at 150°C. It is prepared by dissolving tin(II) oxide in acetic acid[520]. In acetate solutions a variety of more complex tin(II) systems such as CH_3COOSn^+, $(CH_3COO)_2Sn$, $(CH_3COO)_7Sn_3^-$, $(CH_3COO)_5Sn_2^-$ and $(CH_3COO)_3Sn^-$ are formed[521] whilst in glacial acetic acid tin(II) acetate forms the stable adduct $(CH_3COO)_2Sn.2CH_3COOH$.

The preparation of lead(II) acetate is analogous to the tin compound involving lead(II) oxide and acetic acid. The resulting 'sugar of lead', $(CH_3COO)_2Pb.3H_2O$ is very soluble in water (44.3g/100 cm^3 at 20°C) and is only partially ionized in solution[522].

$$Pb^{2+} + CH_3COO^- \rightleftharpoons CH_3COOPb^+ \qquad K_1 = 145$$

$$Pb^{2+} + 2CH_3COO^- \rightleftharpoons (CH_3COO)_2Pb \qquad K_2 = 810$$

$$Pb^{2+} + 3CH_3COO^- \rightleftharpoons (CH_3COO)_3Pb^- \qquad K_3 = 2950$$

Lead(IV) acetate is produced from Pb_3O_4 and glacial acetic acid. The resulting crystals are hygroscopic, decomposing to PbO_2 and acetic acid[523].

(v) Phosphates and Phosphites

Many phosphate systems of tin(II) and tin(IV) are known. The stoichiometry is dependent on the particular phosphate ion complexing to the tin. For example, in sulphuric acid tin(II)

sulphate reacts with sodium hydrogen phosphate to yield the ortho-phosphate $Sn_3(PO_4)_2$. Other phosphates, such as $SnHPO_4$, $Sn(H_2PO_4)_2$, $Sn_2P_2O_7$ and $Sn(PO_3)_2$, are also known[524].

The structure of $SnHPO_4$ has been determined and is found to be formed from pairs of hydrogen bonded HPO_4^{2-} ions, which lie in sheets parallel to the (1 0 0) plane with the tin(II) ions lying mid-way between the phosphate sheets. The metal is surrounded by a total of eight oxygen atoms from six different phosphate ions.

Tin(IV) phosphates are similarly numerous, examples being, $Sn_2O(PO_4)_2.10H_2O$, $Sn_2O(PO_4)_2$ and SnP_4O_7 as well as complex phosphates of the form $Na_2Sn(PO_4)_2$ and $KSn(PO_4)_3$ [502]. In his review, Abel[502] notes the surprising stability of the hypophosphite, $Sn(H_2PO_2)_4$, considering it contains tin(IV) and a strong reducing anion:

$$Sn^{4+} + 2e \longrightarrow Sn^{2+} \qquad E = 0.15V$$

$$H_3PO_3 + 2H^+ \longrightarrow H_3PO_2 + H_2O \qquad E = -0.50V$$

As would be expected no corresponding lead(IV) hypophosphite has been isolated although mono- and diacid lead(IV) phosphates have been synthesized, $Pb(HPO_4)_2$ results from lead(IV) acetate and phosphoric acid[525];

$$Pb(OCOCH_3)_4 + 2H_3PO_4 \longrightarrow Pb(HPO_4)_2 + 4CH_3COOH$$

whilst the diacid, $Pb(H_2PO_4)_4$ is precipitated as white crystals from

an electrochemical reaction involving strong phosphoric acid and lead electrodes[526]. The analogous lead(II) compounds are also known. $PbHPO_4$ can be prepared from lead nitrate and phosphoric acid[527] and is converted to $Pb(H_2PO_4)_2$ by dissolution in phosphoric acid[527]. The product is stable in air but decomposes in water.

Ortho- and metaphosphates of lead(II) have been characterized. The orthophosphate $Pb_3(PO_4)_2$ has been prepared in a variety of ways; for example, from lead(II) chloride and Na_2HPO_4 [528]. This reaction:

$$3PbCl_2 + 2Na_2HPO_4 \longrightarrow Pb_3(PO_4)_2 + 4NaCl + 2HCl$$

has also been proposed to occur <u>in vivo</u> on the red cell membrane[529]. A low temperature monoclinic (α) phase of $Pb_3(PO_4)$ is known which transforms reversible at 185°C to a rhombohedral (β) phase. In both forms the tetrahedral $(PO_4)^{3-}$ anions coordinate to two inequivalent lead cations. $Pb_3(PO_4)$ also results from neutralization of $PbHPO_4$ with ammonia[530]. This latter compound occurs in nature as the mineral monetite. For the metaphosphates the di-, $Pb(PO_3)_2$; tri, $\frac{1}{2}\ Pb_3(PO_3)_6.3H_2O$; tetra, $Pb(PO_3)_4$ and hexa, $Pb(PO_3)_6$ have been reported, but products vary widely depending on reaction conditions.

The acid phosphites $PbHPO_3$ and $Pb(H_2PO_3)_2$ have been prepared[531] and a variety of basic lead(II) phosphites with formulations such as $2PbHPO_3.PbO.H_2O$ and $PbHPO_3.PbO.\frac{1}{2}H_2O$ claimed. Lead(II) hypophosphite results from a metathetical reaction between calcium hypophosphite and lead(II) nitrate.

In a detailed study of the infrared spectra of phosphates,

Corbridge and Lowe[532] have measured the absorption bands and intensities of the orthophosphate, $Pb_3(PO_4)_2$, pyrophosphate, $Pb_2P_2O_7$ as well as $Pb_2P_4O_{12}.4H_2O$, $PbHPO_3$ and $Pb(H_2PO_2)_2$. In a similar manner they have also characterized $Pb_2P_2O_6$ [533]. The correlation tables resulting from this work have been employed in elucidating the infrared data obtained from the lead-phosphorus-oxygen systems prepared as models for the mechanism of lead absorption proposed in this work and described in Chapter Eight. The wider effects of inorganic lead are now reviewed.

5.4 LEAD IN PERSPECTIVE

In recent years the terms 'lead', 'pollution' and 'environment' have become part of the general vocabulary. They frequently form the basis of often emotive and sometimes ill-informed comment in the popular press. Combination into the phrase 'environmental lead pollution' is a ready headline eagerly siezed by lobby groups occassionally assisted by scientist who, not always, present a totally unbiased view. The effect is counter-productive and serves only to reduce the credibility of any data presented. The right to hold an individual opinion is not in doubt, but the duty of a professional chemist, when speaking in that role, should be to at all times attempt to present all relevent facts from which balanced conclusions can be drawn. An attempt has been made to present the work detailed herein on that basis alone. Any conclusions drawn are, hopefully, based only on good scientific reasoning.

Unlike inorganic tin, the absorption of which has no known deleterious effects, without question lead can present a serious risk to health. Several potential areas of exposure, other than those experienced occupationally can be identified (see Section 5.6). The question of how general is the risk is, however, still open to debate. Evidence for the use of lead extends back about 6000 years and symptoms of plumbism were recognised by Egyptian, Greek and Roman physicians. Hippocrates in 370 BC described a severe attack of colic in a man extracting metals, and Pliny reported cases of lead poisoning between AD23 and 79. In more recent times Thackrah in 1831[534] first drew a direct association between lead poisoning and the 'miners sickness' described by Paracelsus in the sixteenth century : a conclusion supported by a contemporary study of the health of the lead miners in Derbyshire in 1857[535]. The effects of the metal on the body were by this time becoming better understood. In 1774 Thomas Percival had reviewed the current knowledge in his 'Observations and Experiments on the Poison of Lead'[536]. However, little was done for the protection of its workers. Not until the publication of the definitive text 'Lead Poisoning and Lead Absorption' in 1912 by Legge and Goadby[537] did the whole problem of industrial exposure in mining, the potteries, the paint industry and other areas of lead use in Great Britain receive serious, comprehensive attention. More than any other contribution, it was this work which formed the basis for the statutory legislation and preventitive measures which have produced the marked reduction in the incidence of serious occupational lead poisoning.

In 1900, 1058 cases of lead poisoning were listed in the 'Annual Report of the Chief Inspector of Factories'; 38 of these cases proved fatal. In 1958 the number of cases had fallen to 55, none of which was fatal. By 1966 the disease ceased to be classified as a separate cause of death (Figure 5.2). These figures contrast sharply with the growth in world consumption of the metal (Table 5.1) which must reflect the degree of improvement in safety standards when handling the metal.

Table 5.1 World Consumption of Refined Lead[538,539]

(Metric Tons x 10^3)

	U.K.	Europe	U.S.A.	World Total
1940	348	747	563	1653
1945	240	374	704	1325
1950	236	640	803	1856
1955	285	880	735	2262
1960	286	1061	647	2633
1965	312	1197	753	3179
1970	262	1358	826	3805
1975	238	1169	811	3878
1977	241	1380	988	4436

The uses to which refined and remelted scrap lead are put within the United Kingdom are detailed in Table 5.2.

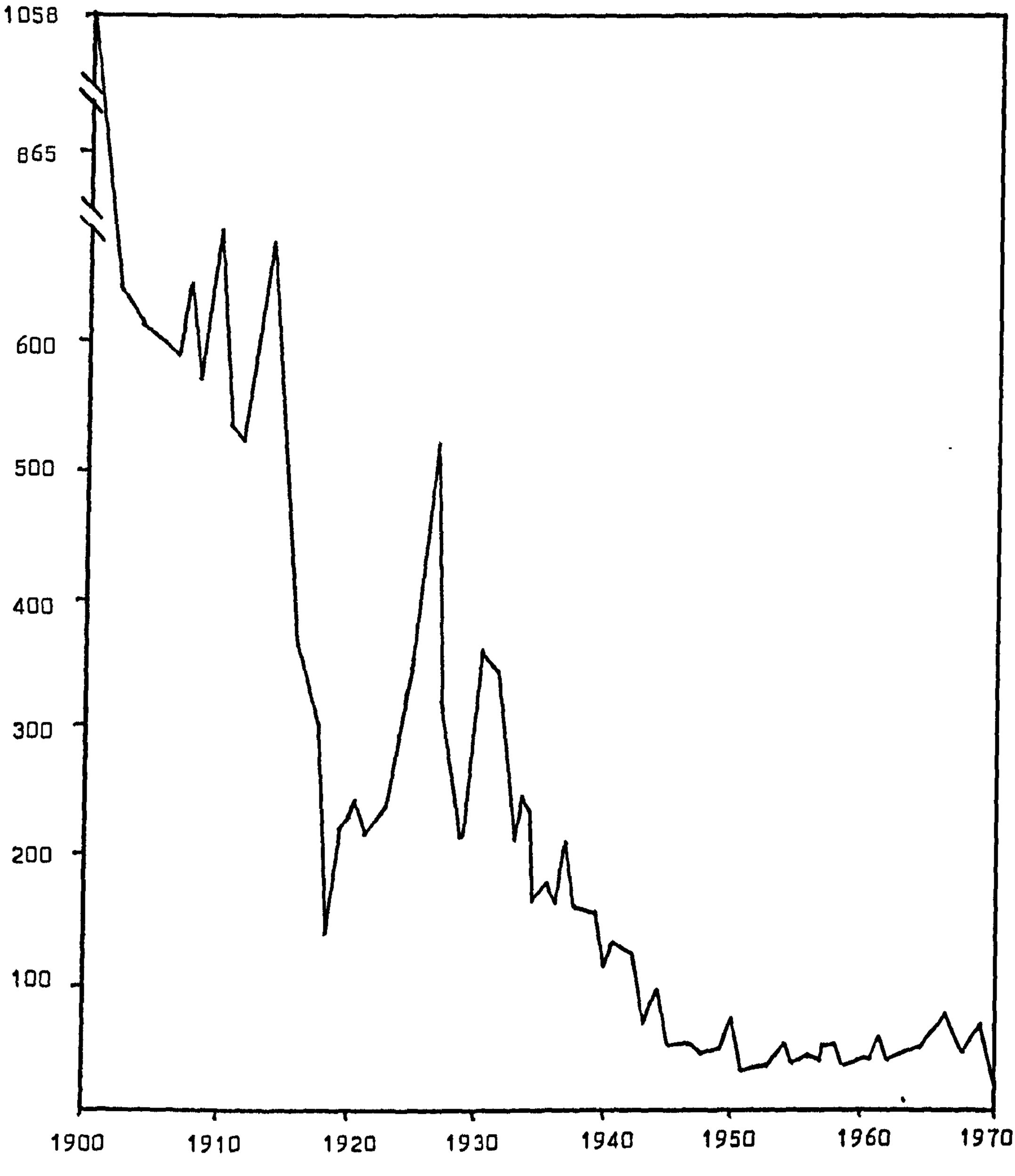

Figure 5.2 Annual notification of industrial lead poisoning to the Factory Inspectorate.

Table 5.2 Uses of Lead Within the United Kingdom in 1977[539]

	Metric Tons $\times 10^3$	Percent
Batteries	68	23.4
Lead Alkyls	55	18.9
Sheet and Pipe	47	16.2
Cables	31	10.7
Oxides	31	10.7
Alloys	13	4.5
Solder	14	4.8
Shot	8	2.7
White Lead	2	0.7
Collapsible tube	1	0.3
Rolled and Extruded Products	1	0.3
Miscellaneous	19	6.5

From this it can be seen that the battery industry remains the main user of metallic lead. However, this use of the metal is now almost parallelled by the production of lead alkyls; tetramethyl, tetraethyl and mixed alkyl lead compounds for use as petroleum additives. In Britain in 1951, 62,000 tons (metric) of lead were used for batteries compared with 68,000 in 1977; very little change. Within the same period the use of the metal for lead alkyl production has increased by in excess of an order of magnitude from 5,000 tons

in 1951 to 55,000 tons in 1977. However, only approximately 16,000 tons of this production are used in Britain, the remainder being exported[539].

Thus, on the data so far presented it would not be unreasonable to ask 'why all the concern?" For surely more has been written in recent years about the hazards presented by lead than any other metal. To understand this concern one must first define the stages in lead poisoning; three of which can be recognised:[540]

(i) Metabolic poisoning; occurs when it is possible to detect alterations in metabolism which are the result of lead poisoning.

(ii) Clinical poisoning; is diagnosed when the signs or symptoms of lead absorption are manifest to the patient or his doctor.

(iii) Sub-clinical poisoning; results from lead absorption producing morbidity or mortality without the appearance of the recognised symptoms of clinical lead poisoning.

It is this latter catagory which has given rise to the recent concern. The possibility being that lead absorption may have latent sequelae at levels which have only recently become routinely detectable as developments in analytical techniques enabled low concentrations of the metal from within the body to be measured.

Table 5.3 details some of the reported effects on health associated with various levels of lead in blood[541].

Table 5.3 Levels of lead in blood associated with changes in body processes[541].

Blood lead level (μg/100ml)	
10	delta - ALA-d inhibited
15-20	Elevation of erythrocyte protoporphyrin
40	Anaemia, increased coproporphyrin and delta - ALA in urine
50-60	Disturbance of mental processes (CNS) peripheral nephropathy
80	Encephalopathy

ALA-d = aminolaevulinic acid dehydratase

Such levels of lead in whole blood are used as a monitor of lead exposure. Whilst the currently accepted level of lead in blood for British workers occupationally exposed to the metal is 80μg/100 cm^3 the E.E.C. directive[542] used in the 1979 U.K. Blood Lead Survey[543] of a group of non-occupationally exposed individuals recommended:

a maximum of 20μg/100 cm^3 for 50% of the group

a maximum of 30μg/100 cm^3 for 90% of the group

a maximum of 35μg/100 cm^3 for 98% of the group

It is likely that these values will provide the basis for future legislation.

In summary, levels of the metal in the body giving overt symptoms of clinical poisoning have now largely been removed by legislative control. The scientific debate currently centres on the consequences or otherwise of absorption of the metal at levels giving sub-clinical poisoning. As the results reported herein (Chapter Six) demonstrate, such levels of lead are readily available within the environment to which the general public is exposed. In addition, data presented in Chapter Eight indicate a reaction between lead and certain essential biochemical units of the body which, even at low concentrations will cause fundamental alterations in the metabolic processes of the body.

5.5 LEAD METABOLISM AND PATHOLOGY

5.5.1 Symptoms of Poisoning

Unfortunately there are no symptoms specific to lead poisoning and diagnosis is often assisted by prior knowledge of exposure. Table 5.4 lists the common presenting symptoms and illustrates the marked differences between inorganic and organic lead poisoning.

Table 5.4 Common Presenting Symptoms of Inorganic and Organic Lead Poisoning[54]

INORGANIC		ORGANIC
Adults	Children	
Abdominal pain	Drowsiness	Sleep pattern disturbance
Constipation	Irritability	Nausea
Vomiting	Vomiting	Vomiting
General pain	Gastrointestinal	Vertigo and headaches
Asthenia	symptoms	Muscular weakness
Paraesthesia	Ataxia	Anorexia
Psychological	Stupor	Weight loss
symptoms	Fatigue	Tremor
Diarrhoea		Diarrhoea
Headaches		Abdominal pain
Metallic taste in		Hyperexcitability
mouth		Mania

Neurological and psychological symptoms often including behavioural and personality changes as well as hallucinations are an early sign of organic lead poisoning, whereas such effects are late presenting in inorganic poisoning. Differences are observed between the effects of inorganic lead on children and adults. In the former colic and constipation are not usually early signs whereas progressive anorexia and clumsiness or frank ataxia are.

General stomach disorders and headaches as well as occassionally a metallic taste in the mouth are associated with adult plumbism. Clinical anaemia can be an important guide to inorganic lead poisoning but not in organic poisoning whilst hypotension occurs in the latter. Progressive poisoning can lead to a blue line on the gums due to lead sulphide formation in the gingival margin. If the disease remains undiagnosed, particularly in children, peripheral neuropathy and encephalopathy leading to permanent injury or death may result.

5,5.2 Uptake of Lead in the Body

Three routes of uptake of lead by the body can be recognised : ingestion, inhalation and skin absorption.

Ingested lead is absorbed in the gastrointestinal system. In adults about seven percent of the total lead ingested is absorbed[544]. In children, however, the figure is believed to be between 25 and 50%[545]. A more detailed account of lead absorption through the gastrointestinal system will be presented later.

As will be demonstrated for ingestion (Chapter Seven), the quantity of lead absorbed after inhalation into the lungs is dependent on particle size (Table 5.5)

Table 5.5 ^{212}Pb retention in lungs in relation to particle size [546]

Subject	% of inhaled lead retained	Particle Size (μ)
A	38	0.2
B	27	0.23
C	50	0.025
D	62	0.02

Generally sub-micron particles entrapped in the lungs are absorbed completely within 24 hours, although some modification to this rate is observed dependent on solubility of the lead species involved. Knelson et al[547] have calculated the potential increase in body burden of lead due to inhalation using the formula

$$B_{inhal} = L.V.R.D. \times 10^{-3} \ \mu g/day$$

where L = air lead concentration $\mu g/m^3$

V = pulmonary ventilation m^3/day

R = fraction of inhaled lead retained

D = duration of exposure in days

Skin absorption is of importance only for organolead compounds. Lead alkyls are rapidly absorbed, and a three- to four-fold increase in renal lead concentration has been observed when the skin is

traumatized before application[548]. The absorption rate of tetraethyl-lead (TEL) through the skin when contained in petrol is inhibited[549] although lung absorption is unaffected[550]. The breakdown of the TEL in the body may involve diethyl intermediates[551]:

$$(CH_3CH_2)_4Pb \longrightarrow (CH_3CH_2)_3Pb^+ \longrightarrow (CH_3CH_2)_2Pb^{2+} \longrightarrow Pb^{2+}$$

This proposal is supported by laboratory data but has been contested and <u>in vivo</u> a coincident metabolism to triethyl lead and inorganic lead suggested[552]:

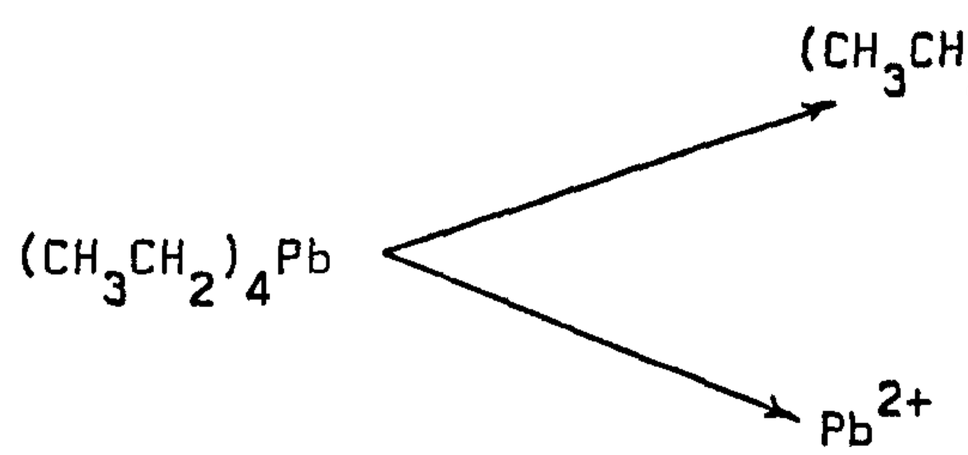

However, it would appear unlikely that simultaneous removal of four ethyl groups will occur.

The various routes involved in lead uptake result in an increase in the total body burden. This may be expressed as

$$B = \Sigma (A - E)$$

where B is the body burden

A is the amount of lead absorbed

and E is the quantity of lead excreted.

It was proposed in 1838[553] that lead is naturally present in normal persons due to the native occurrence of lead in the soils of the earth. Although this original suggestion was controversial it has been confirmed by modern analytical techniques. Measurements on blood lead show a range of typical values from 10 - 40 μ g/100 cm^3. Levels greater than this indicate more than general environmental exposure. Total body burdens vary with geographical location, age, sex and overall body weight so that representative values are not readily obtained. However, Table 5.6, gives a guide to variation with age and sex.

Table 5.6 Variation in lead body burden with age and sex[554] (mg Pb)

Age Group	Male	Female
0 - 9	1.4	1.7
10 - 19	56.5	
20 - 29	85.5	30.6
30 - 39	178.6	
40 - 49	166.7	99.5
50 - 59	184.7	111.4
60 - 69	260.3	122.4
70 - 79		118.5
80 +	265.7	172.8

5.5.3 Excretion of lead

The principal routes for removal of lead from the body are via faeces and urine. The former route is the most important for inorganic lead; the ratio of faecal removal to urinary excretion of the metal being about 100 : 1 [555]. Radio-lead studies have demonstrated that the faecal lead derives primarily from the bile[556] although a large contribution is from lead passing directly through the body without absorption. Renal excretion can be measured by the amount of lead removed from the plasma in unit time, i.e. the clearance rate :

$$C = \frac{UV}{P}$$

where C = clearance ml/min

U = urine concentration mg%

V = urine volume per min.

P = plasma concentration mg%

Difficulties are experienced, however, in accurate plasma measurements.

Other routes for excretion are sweat, where the concentration of the metal is of the same order as in the urine. Mammalian milk is another potentially important route because of the high absorption rates found in neonates. However, the levels of lead found are small[557].

5.5.4 Pathological effects of Lead

(i) Haem synthesis

The biosynthetic pathway for haem synthesis is well established. The primary steps involve formation of porphobilinogen (PBG) via δ-aminolaevulinic acid (ALA) from glycylpyridoxal phosphate and succinyl coenzyme A by the enzymic action of aminolaevulinic acid synthase (ALA-S) and aminolaevulinic acid dehydratase (ALA-D) as illustrated in Figure 5.3. PBG is then converted through a series of pyrrole and porphyrin intermediates to protoporphyrin which reacts with iron(II) under the catalytic action of ferrochelatase to form haem, Figure 5.4. Lead has the ability to inhibit this total synthesis in at least five of the stages, although the mechanism of inhibition is understood with varying degrees of certainty. However, as diagnostic tests for plumbism these modifications offer a number of possibilities.

An increase in plasma ALA is one of the earliest signs of metabolic lead poisoning, closely followed by a markedly raised urinary ALA excretion level. Correspondence between PBG excretion and lead poisoning is, however, still a matter for debate[540]. Coproporphyrin excretion in the urine was the earliest biochemical abnormality discovered in lead poisoning and has been used as a screening method for industrial exposure. Its correspondence to levels of ALA in blood and urine in such cases has recently been examined[558]. However, lead in whole blood was found to give the

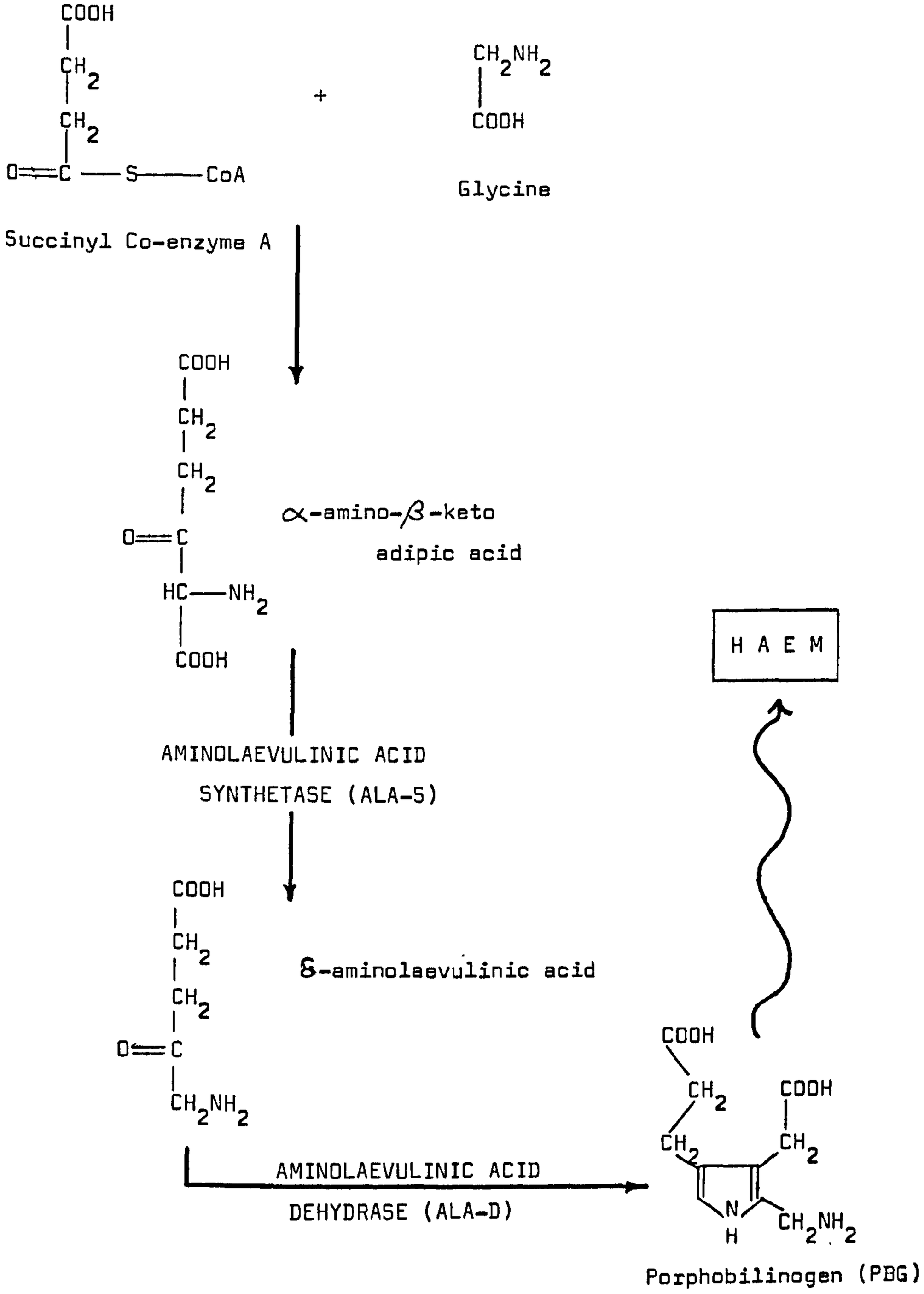

Figure 5.3 Initial steps in haem synthesis

Figure 5.4 Major stages in haem biosynthesis.

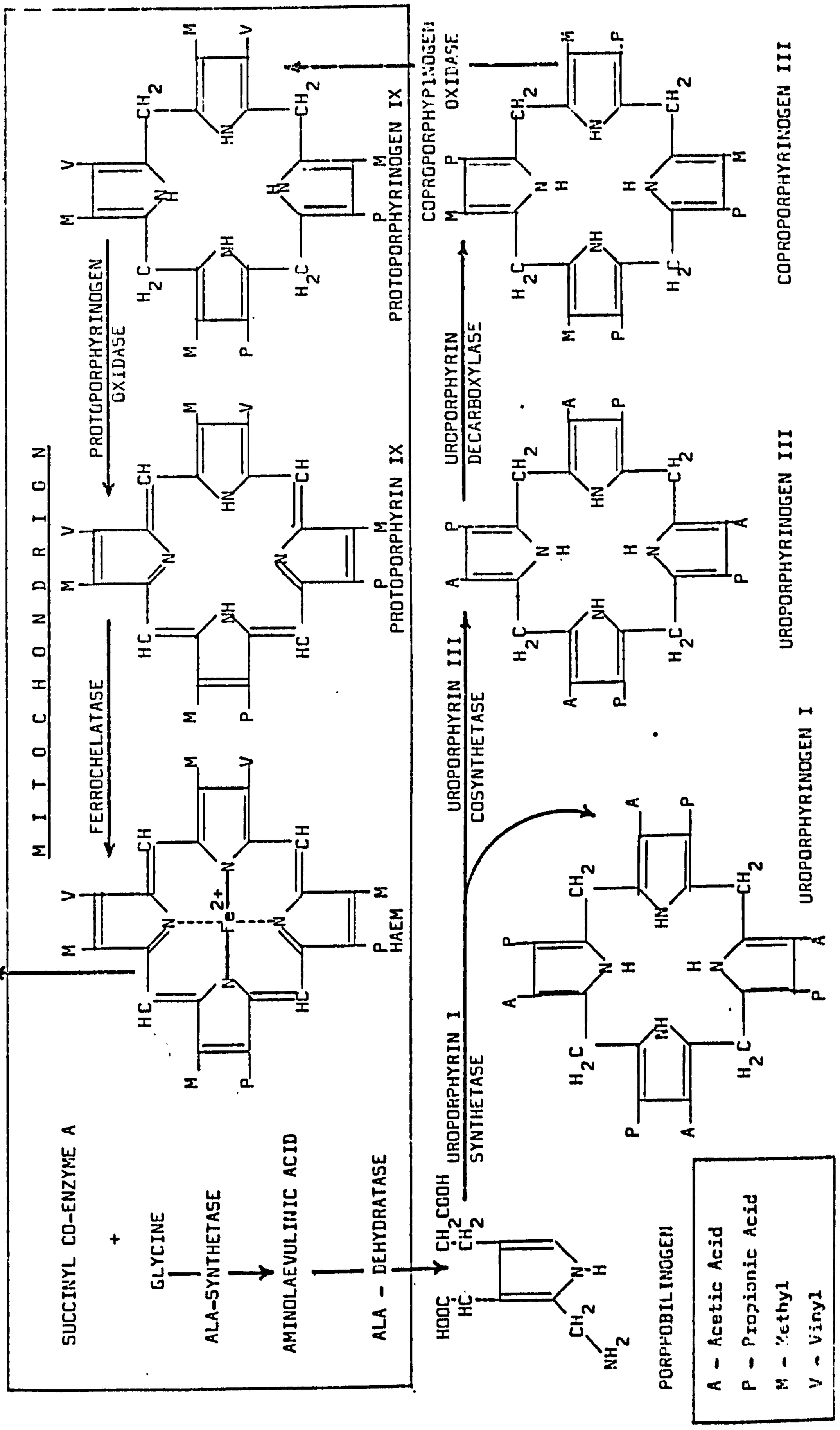

best index of environmental exposure.

Higher coproporphyrin levels may occur in blood, but in this medium the increased erythrocyte protoporphyrin concentration is the most notable feature. This has also been used as a screening monitor[559] and a simple fluorimetric method has been developed for its assay[560].

Enzyme inhibition is, of course, the primary reason for the appearance of excess concentrations of the above species in the blood and urine. Measurement of ALA - D activity in red blood cells is a sensitive index of intoxication. Ferrochelatase is almost totally inhibited at a concentration of about 10^{-4} M of lead but ALA-S is less supressed. The combination of reduction in haem synthesis together with a lowering in total iron binding capacity in lead poisoning contribute to the anaemia associated with the disease.

(ii) Neurological effects

The biochemical aspects of lead neurotoxicity have recently been reviewed[561]. Peripheral neuropathy caused by demyelination is a characteristic symptom of lead poisoning. The central nervous system may also be affected along with other neurological changes. Work carried out on mice has shown a marked effect on the development of the optic nerve[562] and association between lead poisoning and mental retardation in children has been examined[563]. Lead encephalopathy was common amongst early workers with the metal

and appears to be associated with interferences in the blood-brain barrier which may be associated with some energy regulating system[540]. Signs of neurological impairment are typical symptoms of clinical lead poisoning : tingling sensation in the fingers, wrist drop, etc.

(iii) Other effects

The kidneys are damaged in acute lead poisoning principally because the epithelial cells in the proximal tubules atrophy and then regenerate causing thickening. Inclusion bodies are a characteristic sign and analysis has shown these to contain lead, with detectable amounts of iron, calcium and glycogen as well as a protein with a high content of -SH groups which may well provide a binding site for the lead. Similar -SH binding may be involved in the depression of thyroid function noted with lead. Iodine uptake is inhibited possibly due to its displacement by lead in a protein sulphonyl iodine carrier[564]. Disruption of the heart functions has also been associated with lead poisoning[540]. Other secondary effects which have been associated with lead intoxication are effects on chromosome distribution[565], mobilization of bone mineral, particularly calcium and phosphorus[566] and, recently, inhibition of bacterial clearance of the lungs[567]. An increased susceptibility to infection has also been reported[568].

5.6 ENVIRONMENTAL SOURCES OF LEAD

Lead is present in the soils of the earth; the estimated average content being 16 ppm. As a consequence it enters the food chain and thus becomes a component of the human body. Its presence in the atmosphere arises from volcanic activity, forest fire smoke, silicate dust from natural soils etc. Again this may enter the body through inhalation. However, natural mobilization does not give rise to toxic levels of the metal, these arise from man-made mobilization. As described in Section 5.4 this has been occurring since ancient times, but it was only with the coming of the Industrial Revolution that people additional to those working the metal became widely affected. With the increased scale of working the area surrounding a lead smelter became contaminated. An effect which can still occur[569]. A recent survey of 18 children living within 250 metres of a smelter in Chester, which has worked since the mid-eighteenth century, showed that four had levels of lead in blood higher than the E.E.C. maximum and one had double this value (Sunday Times, Feb. 10, 1980). A more modern means of lead distribution and the source of considerable debate is the tetraalkyllead petroleum additives, anti-knock agents. Many instances of high levels of lead associated with this source have been reported, although the recent Government Commission chaired by Professor Lawther[543] is unclear as to any direct connection between this source and individual cases of poisoning. Significant levels of deposited lead originating from traffic fumes have

recently been found in a number of schools in South Wales, and blood tests are being made by the Mid-Glamorgan County Council on 1064 children involved.

The report of the Lawther Commission is the most recent official study on the problem of lead and health, and highlights the need for awareness of such possible sources as contaminated drinking water from leaded pipes[570,571] and the dangers to children, particularly in cases of pica, of eating leaded paint flakes[572]. For example, in collaboration with a local general practitioner, I was recently requested to examine paint flakes from a piano constructed in 1905. This was found to contain 3000 ppm of lead. The patient was a 9 month old child who was at the crawling stage and used to suck the bottom rail of the piano from which the paint assayed originated. Fortunately, tests on the child showed that the time period involved was insufficient for any serious build-up of the metal within the body to have occurred.

A third main scurce of serious lead poisoning noted by the Government report is the use of cosmetics and medicines originating in the Indian sub-continent. Chapter Seven of this thesis reports our involvement, with Professor S.S. Davis and Dr. Mohamed Aslam of the Pharmacy Department at Nottingham University in the original discovery of this source.

REFERENCES

501. W.A. Tiller and J.W. Rutter, Can. J. Chem., (1949) 34 96.

502. E.W. Abel, Comprehensive Inorg. Chem., Vol. 2. Pergamon, LONDON 1972.

503. H.P. Khig, J. Amer. Chem. Soc.,(1946) 68 1493.

504. W. Kwestroo and A. Huizing, J. Inorg. Nucl. Chem., (1965) 27 1951.

505. W. Kwestroo, J. de Tonge and P.H.G.M. Vromans, J. Inorg. Nucl. Chem., (1967) 29 39.

506. A. Bystrom, Arkiv. Kemi., Min. Geol., (1965) 20A 11

507. A.I. Zaslavsky, Yu. D. Kondrashev and S.S. Tolkachev, Dokl. Akad. Nauk S.S.S.R, (1950) 75 559.

508. R.S. Tobias, Acta Chem. Scand., (1958) 12 198.

509. R.W.G. Wyckoff, Amer. J. Sci., (1928) 15 297.

510. R.A. Howie and W. Moser, Nature,(1968) 219 372.

511. G. Todd and E. Parry, Nature, (1964) 202 386.

512. J.L. Pauley and M.K. Testerman, J. Amer. Chem. Soc., (1954) 76 4220.

513. B. Carrell and A. Olin, Acta Chem. Scand., (1960) 14 1999.

514. H. Kiryama, K. Kitahama, O. Nakamura and R. Kiriyama, Bull. Chem. Soc. Jpn., (1973) 46 1389.

515. O. Ruff and W. Plato, Chem. Ber., (1904) 37 673.

516. H. von Wartemburg, Z. anorg. Chem., (1940) 244 337.

517. W. Blitz and E. Meinecke, Z. anorg. Chem., (1923) 131 1.

518. G.P. Haight and J.R. Peterson, Inorg. Chem., (1965) 4 1073.

519. G. Bergerhoff and O. Schmitz-Dumont, Z. anorg. Chem., (1956) 284 10.

520. J.D. Donaldson, W. Moser and W.B. Simpson J. Chem. Soc., (1964) 5942.

521. J.D. Donaldson and J.F. Knifton J. Chem. Soc. (A), (1966) 332.

522. E.A. Burns and D.N. Hume, J. Amer. Chem. Soc. (1956) 78 3958.

523. H. Mendel, Rec. Trav. Chim., (1940) 59 720.

524. P.J. Shapiro and E.I. Becker, J. Org. Chem., (1962) 27 4668.

525. A. Hutchinson and W. Pollard, J. Chem. Soc., (1896) 69 212.

526. K. Elbs and R. Nubling, Z. Electrochem., (1903) 9 776.

527. H. Alders and A. Stahler, Chem. Ber., (1909) 42 2261.

528. L.T. Fairhall, J. Amer. Chem. Soc., (1924) 46 1593.

529. J.C. Aub and P. Reznikoff, J. Expt. Med., (1924) 40 189.

530. J.J. Berzelius, Ann. Chim. Phys., (1816) 2 258.

531. L. Amat, Ann. Chim. Phys. (1891) 24 315.

532. D.E.C. Corbridge and E.J. Lowe, J. Chem. Soc., (1954) 493.

533. D.E.C. Corbridge and E.J. Lowe, J. Chem. Soc., (1954) 4555.

534. C.T. Thackrah, 'The Effects of Arts, Trades, Professions and of Civic States and Habits of Living on Health and Longevity' (1831) Longmans, LONDON.

535. W. Webb, Brit. Med. J. (1857) 687.

536. T. Percival, 'Observations and Experiments On the Poison of Lead' (1774) J. Johnson, LONDON.

537. T.M. Legge and K.W. Goadby, 'Lead Poisoning and Lead Absorption' (1912) Longmans, Green and Co. LONDON AND NEW YORK.

538. M.E. Hilburn, Chem. Soc. Rev., (1979) 8 63.

539. (a) Metallgeiellschaft, 1938-1959.

(b) World Bureau of Metal Statistics, 1942-1961.

(c) World Metal Statistics, 1961-1978.

540. H.A. Waldron and D. Stöfen , 'Sub-Clinical Lead Poisoning', (1974) Academic Press, LONDON and NEW YORK.

541. 'Air Quality Criteria for Lead' Environmental Protection Agency, 1977, U.S.A.

542. E.E.C. Directive 77/312/EEC. Official Journal L 105/10, 28 April 1977.

543. 'Lead and Health' D.H.S.S. (1980) H.M.S.O. LONDON.

544. R.A. Kehoe, J. Cholak, D.M. Hubbard, K. Bambach and R.R. McNary, J. Ind. Hyg. (1943) 25 71.

545. F.A. Alexander and H.T. Delves, Arch. Disease Childhood, (1972) 47 446.

546. J.B. Hursh and T.T. Mercer, J. Appl. Physiol., (1970) 28 268.

547. J.H. Knelson, R.J. Johnson, F. Coulston, L. Goldberg and T. Griffin, Int. Symp. Envir. Hlth. Aspects of Lead. (1972) AMSTERDAM paper 36.

548. E.P. Lang and F.M. Kunze, J. Ind. Hyg., (1948) 30 256.

549. R.A. Kehoe and F. Thamann, Am. J. Hyg., (1931) 13 478.

550. R.A. Mortensen, J. Ind. Hyg., (1942) 24 285.

551. S.R. Henderson and L.J. Snyder, Anal. Chem., (1961) 33 1172.

552. W. Bolanowska, Brit. J. Ind. Med., (1968) 25 203.

553. A. Devergie and O. Hervy, Annales d'Hygiene (1838) 20 463.

554. P.S.I. Barry and D.B. Mossman, Brit. J. Ind. Med., (1970) 27 339.

555. R.A. Kehoe, Arch. Envir. Health, (1964) 8 235.

556. M. Cikrt, Brit. J. Ind. Med., (1972) 29 74.

557. R.A. Kehoe, F. Thamann and J. Cholak, J. Ind. Hyg., (1933) 15 301.

558. M.R. Moore and P.A. Meredith, Biochem. Soc. Trans., (1979) 7 37.

559. R. Schiele, H.M. Wagner and C. Kranse, B.G.A. Ber. (1978) 1 138.

560. (a) S. Piomelli, J. Lab. Clin. Med. (1973) 6 939.

(b) S. Piomelli, Clin. Chem., (1977) 23 265.

561. M.M. Cohen, Handb. Clin. Neurol., (1979) 36 65.

562. G. Tennekoon, C.S. Aitchison, J. Fangia, D.L. Price and A.M. Goldberg, Ann. Neurol., (1979) 5 558.

563. H.L. Needleman, C. Gunnoe, A. Leviton, R. Reed, H. Peresie, C. Maher and P. Barrett, New Eng. J. Med., (1979) 300 689.

564. H.H. Sanstead and R. Galloway, Proc. Soc. Expmt. Biol. Med., (1967) 124 18.

565. L. Verschaeve, M. Driesen, M. Kirsch-Volder, L. Hens and C. Susanne, Hum. Genet., (1979) 49 147.

566. Y. Kato, Y. Sugita and S. Takimoto, Shika Kiso Igakkai Zasshi, (1977) 19 458.

Chem. Abs. (1978) 91 84527.

567. H.W. Schlipkoeter and L. Frieler, Zentralbl. Bakteriol. Parasiteuka, Infestionskr, Hyg. Abt. 1: Orig., Reshe B, (1979) 168 256.

Chem. Abs. (1980) 91 103101.

568. W. Zimmermann, U. Kuhnen, M. Lehnen, K. Schubert and R.D. Rurainski, Zentralbl. Gakteriol., Parasiteukd., Infektionskr. Hyg., Abt. 1 : Orig., Reihe B (1979) 168 387. Chem. Abs. (1980) 91 134909.

569. S. Rehnlund, P.G. Bergors, K.H. Gustavson and H. Kollberg, Ambia (1979) 8 118.

570. D.L. Morse, W.N. Watson, J. Housworth, L.E. Witherell and P.J. Landrigan, Am. J. Pub. Hlth., (1979) 69 711.

571. M.R. Moore, A. Goldberg, P.A. Meredith, R. Lees, R.A. Low and S.J. Pocock, Clin. Chim. Acta., (1979) 95 129.

572. C. Gilbert, R.W. Tuthill, E.J. Calabrese and H.A. Peters, J. Environ. Sci. Health, Part A (1979) A14 145.

573. W.D. Honnick and J.J. Zuckerman, Inorg. Chem., (1976) 15 3034.

CHAPTER SIX

DISTRIBUTION OF DEPOSITED LEAD IN A ROADSIDE ENVIRONMENT

6.1 INTRODUCTION

"There is no indication from the surveys that . . . . relatively raised blood concentrations are due to lead from petrol ..." So concludes the Report of the DHSS Working Party on lead in the environment[601]; and the debate continues.

Tetraethyllead (TEL) was first introduced into petrol in Dayton, Ohio in February 1923, and was distributed widely throughout the United States. However, in May 1925 its sale was stopped and an investigation commenced by the U.S. Public Health Service. Regulations governing the handling and manufacture of TEL were introduced in 1926 and its sale in petrol recommenced in the summer of that year. Although introduced in petrol in this country during the 1930's TEL manufacture in Britain did not ccmmence until 1940. Tetramethyllead (TML) was introduced as an anti-knock agent in 1960 and currently a variety of compositions are used ranging from TEL to triethylmethyl-, diethyl—dimethyl-, ethyltrimethyl-lead and TML. Within the United Kingdom there has been a phased reduction in the lead content of petrol from the 1971 limit of 0.84 g l^{-1} to the current figure of 0.46 g l^{-1}. However, this reduction has coincided with an increase in traffic density so that overall lead emissions have not decreased[602].

Added to the anti-knock fluids are 1,2-dihaloethanes which act as scavengers of the decomposition products from the lead alkyls. The oxides resulting from combustion of the lead alkyls are thus able to react to form mixed halides. The principal chemical forms of the metal found after emission from car exhausts are, therefore, lead bromochloride (PbBr.Cl) and the alpha- and beta-forms of ammonium chloride lead bromochloride ($NH_4Cl.2PbBr.Cl$ and $2NH_4Cl.PbBr.Cl$), together with trace amounts of mixed oxide ($PbO.PbBr.Cl.H_2O$) and sulphate ($PbSO_4$)[603]. The presence of the ammonium compounds has been explained as follows. The SO_2, common in polluted atmospheres, is slowly oxidised to form H_2SO_4 which, in turn, is progressively neutralised by atmospheric ammonia to yield NH_4HSO_4 and $(NH_4)_2SO_4$. Reaction then occurs with the lead bromochloride from the exhaust emissions[604]:

$$6\ PbBrCl + 2NH_4HSO_4 \longrightarrow 2PbSO_4 + 2PbBrCl.NH_4Br$$

$$+ \alpha\text{-}2PbBrCl.NH_4Cl + HCl + HBr$$

Further degradation of these particles leading to halogen loss and conversion to oxide and/or carbonate produces a reduction in particle size with a concomitant increase in solubility[605].

Dissipation and precipitation of the emitted aerosol lead is dependent on particle size and meteorological factors, but about half the lead containing particulate matter is removed from the air by gravity within a few hundred feet of a roadway[606]. Incorporation in rainwater

can substantially increase the lead ccncentration, but generally causes more rapid deposition[607].

A number of studies have been made of lead levels in the soils and vegetation[608-610] and tree leaves and grasses[611] adjacent to major road systems as well as in roadside fruit and berries[612]. However, no previous work has enabled the overall distribution pattern of deposited roadside lead to be established. Because of the disparity in site locations, geological and meteorological variations and sampling patterns, correlation between previous studies of the various sections of the roadside environment have not been meaningful. To rectify this omission and in order to establish the magnitude of the problem within the Nottinghamshire area the overall distribution pattern of deposited and absorbed lead at the boundaries of a typical trunk road system has been determined.

6.2 LOCATION OF STUDY

Sites along a dual carriageway section of the A52 trunk road between the M1 Motorway, Junction 25, at Sandiacre, Derbyshire (ordinance survey ref. 472 356) and the five-road intersecting island at Bramcote, Nottinghamshire (ordnance survey ref. 505 378) were chosen for this study(Figure 6.1). The road runs in an east/west direction at this section with a prevailing westerly wind. As well as providing the main link between Nottingham and Derby, the road acts as a feed road from both cities to the M1 motorway. The traffic density is of the order of 24,000 vehicles in a 24 hour period[613].

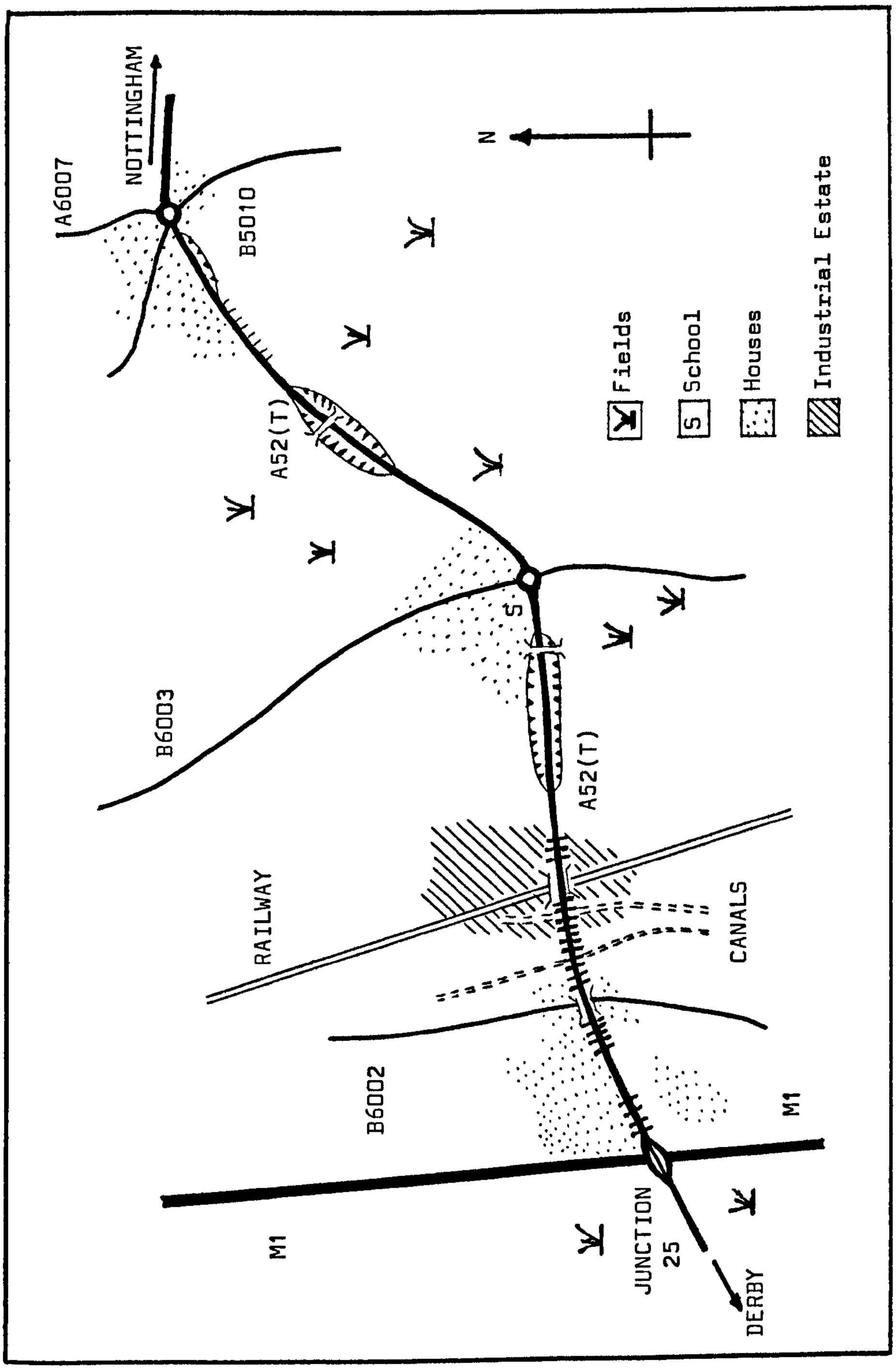

Figure 6.1 Location of Study.

The selected section of this road is bordered by various areas of fields and rose gardens, a school with playingfields, an industrial estate and houses with gardens in places extending to within 4 metres of the roadway. The terrain is undulating with several sections of the A52 elevated in turn, over a road, a railway system and canals. There is thus a complete cross section of the population from babies in prams in gardens to school children, and adults at home and at work represented within the confines selected. Where possible, sites on both sides of the carriageway adjacent to each of the areas described were chosen for the collection of samples of road dust, soil, grasses, blackberry plants and fruits for examination of lead content.

6.3 EXPERIMENTAL PROCEDURE

(i) Dust

Dust deposits were collected at sites from each direction along the roadway. Sampling was first made during a period of dry weather (no rainfall over a period in excess of 7 days) and again from the same locations after a day of heavy rainfall (0.78 ins). Material was collected randomly and no attempt was made to select particle size which was found to vary between approximately 0.2mm and about 3mm for the samples taken. This material was weighed and the lead extracted by digestion in hot 5M A.R. nitric acid. The resulting solutions were filtered under reduced pressure and the filtrate made up to known volumes using triply-distilled, deionized

water.

(ii) Soil

Samples of soil were collected at various intervals between 1 and 9m from the roadway. They were obtained by making borings (with an agricultural soil sampler) 2.5 cm in diameter to a depth of 60 cm. Sections at known depths were removed from each drill, dried, weighed and the lead extracted into solutions as the nitrate.

(iii) Grasses

The grasses removed from each site were carefully trimmed to remove any root system. The samples were then divided. One portion was dried to constant weight at 110^{o}C in an oven. 20g amounts were then digested by simmering in A.R. nitric acid for 15 minutes. After filtering, 100ml aqueous solutions were prepared for analysis. The second portion of the grasses collected was thoroughly washed by immersion and agitation for one hour in a pneumatic trough fed by continuously running (lead-free) cold water. Samples were then dried to constant weight and treated in a similar manner to the unwashed grasses.

(iv) Blackberry Plant Canes

Blackberry plant canes, each approximately 2m in length were selected. All fruit was removed but the leaves were retained. The shoots were then sectioned to lengths of about 5 cm and thoroughly washed for one hour in a manner similar to that used for the grass samples. Because of the greater difficulty of digestion of the

plant stems it was necessary to simmer known weights of the blackberry plants for about 35 minutes in nitric acid. After which, solutions for analysis were prepared as previously described.

(v) Blackberry Fruit

Samples of blackberry fruit were collected during mid-September and mid-October. Care was taken to achieve a uniformity of development of fruit chosen so that samples did not contain very young undeveloped fruit or old overripe berries, but were representative of the type most likely to be picked for use. The fruit from each site was divided. One portion was subjected for one hour to the washing procedure described. The fruit was then allowed to drain on absorbent tissue under a stream of warm air. Samples from both portions were then weighed as undried fruit and treated with nitric acid to extract the lead content. Resulting solutions were filtered under reduced pressure and made up to known volumes with the triply-distilled, deionized water used throughout these measurements.

In all cases during the extraction process the vessel containing the material was partially covered to prevent loss of any material by evaporation.

The lead content of the samples of materials obtained was determined by atomic absorption spectrophotometry using a Perkin-Elmer Model 603. Because of a possibility of molecular interferences, background correction from a deuterium arc was used for all measurements and final results were obtained as an average

of at least five readings over a ten second integration time. Because of the stability of the particular instrument system used, results were found to be reproducible to ± 0.01 p.p.m. Standard solutions were prepared from B.D.H. atomic absorption reagents and results obtained, via the microprocessor of the instrument, in direct concentration units.

6.4 RESULTS AND DISCUSSION

6.4.1 Qualitative Data

Using X-ray powder diffraction techniques attempts were made to speciate the deposited lead in the roadside dust and in the sub-surface levels of soil. Unfortunately only limited success was achieved. The low solubility of the lead compounds did not enable clean crystalline material to be obtained. Finely grinding and washing allowed some concentration, but analysis of this fine particulate residue from dust and soil gave only poor quality data. $PbSO_4$ could be identified in the roadside dust. A result which concurrs with the findings of other workers[614,615]. However, $PbCl_2$ also appeared to be present. This has not previously been reported but perhaps may be explained in terms of a redistribution of ions in solution:

$$2PbBr.Cl \longrightarrow 2Pb^{2+} + 2Cl^{-} + 2Br^{-} \longrightarrow PbCl_2 + PbBr_2$$

Or during reaction in the midly acidic carbonic acid present in

rainwater:

$$2PbBr.Cl + H_2CO_3 \longrightarrow PbCl_2 + PbCO_3 + 2HBr$$

However, such systems are speculative and because of the inconclusive nature of the data obtained, require confirmation. The lead sulphate, in addition to the mechanism of reaction with the NH_4HSO_4 previously described, is probably more likely formed directly from the H_2SO_4, also present in rainwater from oxidised SO_2:

$$PbBrCl + H_2SO_4 \longrightarrow PbSO_4 + HBr + HCl$$

No data was obtained from the lead systems in the soil samples measured. Attempts at speciation of the lead contained in and on the blackberry fruits was made by collecting the expressed juices and determining the low frequency Raman spectrum. Again the results were inconclusive; any metal systems present probably being at concentrations below the detection limit of the technique. It is probable that any pre-concentration will modify the lead systems involved. Other workers[615] have experienced similar difficulties and concluded that only a small proportion of lead in street dust is in a crystalline form susceptible to X-ray diffraction analysis. The postulate being that the crystalline forms of lead compounds progressively dissolve in water and re-deposit in the chemical forms typical of the soils forming the major component of the roadside dust[616].

6.4.2 Quantitative Data

(i) Roadside Dust

The results obtained showed significant concentrations of lead in the dust collected, the highest value being 210 p.p.m. However, the range of values (Table 6.1) is wide, reflecting the variability in sample composition. No distinct pattern emerges as to distribution of the lead between east and west traffic directions although, in general, a higher level was found in the offside section of roadway. This is probably due to lead deposition occurring from traffic travelling in both directions. The central reservation being approximately 3 m in width.

The overall lead content is lower than might have been expected from earlier data. For example, Giubileo[617] found between 1360 - 2360 p.p.m. in the street dust of central Milan with a decrease to 800 p.p.m. in peripheral street. Högger[618] found a maximum level of 2040 p.p.m. in Zurich. However, in both these locations wind distribution of the aerosol lead is confined by the surrounding buildings, whereas in the sites of this present study the area is open and in places elevated which would enable a much wider spread of the material to be achieved.

The effect of rainwater is interesting. Whilst at a number of sites, there was a reduction in lead content of between 20 and 30% after rainfall, it is notable that in others an increase was observed. The efficiency of rainwater in fractionating the lead, is clearly, dependent on a number of factors. Rameau[619] has shown a

TABLE 6.1 Lead content of dust collected from a section of the A52 trunk road

Sample	Location on road and gradient	Traffic direction	Lead content (ppm) Before Rain	After Rain
G1	Nearside/inclined	East	180	160
G2	Offside/inclined	East	210	156
G3	Nearside/level	West	132	147
G4	Offside/level	West	146	132
G5	Nearside/inclined	East	117	112
G6	Offside/inclined	East	92	76
G7	Nearside/level	West	121	118
G8	Offside/level	West	137	142
G9	Lay-By/level	East	180	191
G10	Lay-By/inclined	West	142	107

correlation between increasing lead content and decreasing particle size of street dust. Clearly, the increased surface area assisting the solubility. However, in the case of roadside dust the results reported here indicate that particle size is of minor importance, the most significant factor in lead distribution after rainfall appears to be the mobility and direction of flow of the resulting surface water. Thus, the primary process will then be one of simple transport of dust and lead combined rather than dependent on lead solubility and hence particle size. It is this factor which Table 6.1 illustrates. Where samples were collected at sites on inclined sections of roadway where the surface water is free-flowing a reduction of overall lead content was observed after rainfall. At sites on level sections of roadway where pools of water could collect the lead level had decreased by a smaller amount or, infact, increased after rainfall.

A minor health hazard which one may associate with the roadside dust arises because the lead coated particles are of a size which readily adheres to clothing and thereby can be transported. Analysis of the dust deposited on the shoes of the author during collection of samples showed the presence of lead. Thus, the dust provides a vehicle for distribution of the lead to areas which would normally be relatively uncontaminated.

(ii) Soil

Table 6.2 and Figures 6.2 and 6.3 show the distribution of lead in the soil bordering the A52 roadway.

TABLE 6.2 Lead distribution with depth of soil and distance from roadway

Distance from road (m)	Depth (cm)	Lead content (ppm)	
		East	West
1	5	134	126
1	15	61	67
1	30	43	45
1	60	36	29
3	5	114	102
3	15	67	69
3	30	45	39
3	60	27	34
6	5	87	95
6	15	73	68
6	30	42	31
6	60	31	32
9	5	82	89
9	15	56	52
9	30	34	34
9	60	23	30

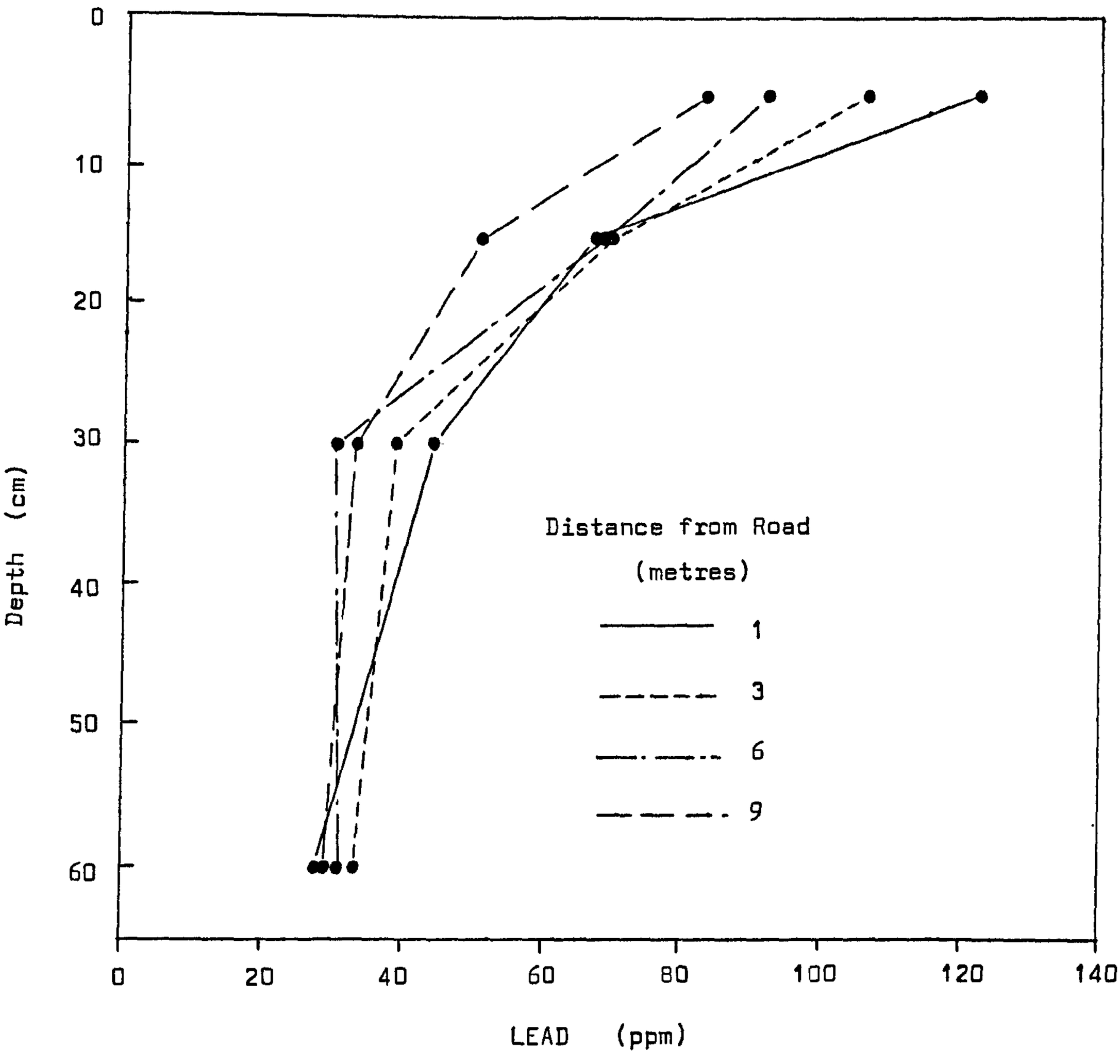

Figure 6.2 Distribution of lead in soil with depth and distance from roadway - traffic direction west.

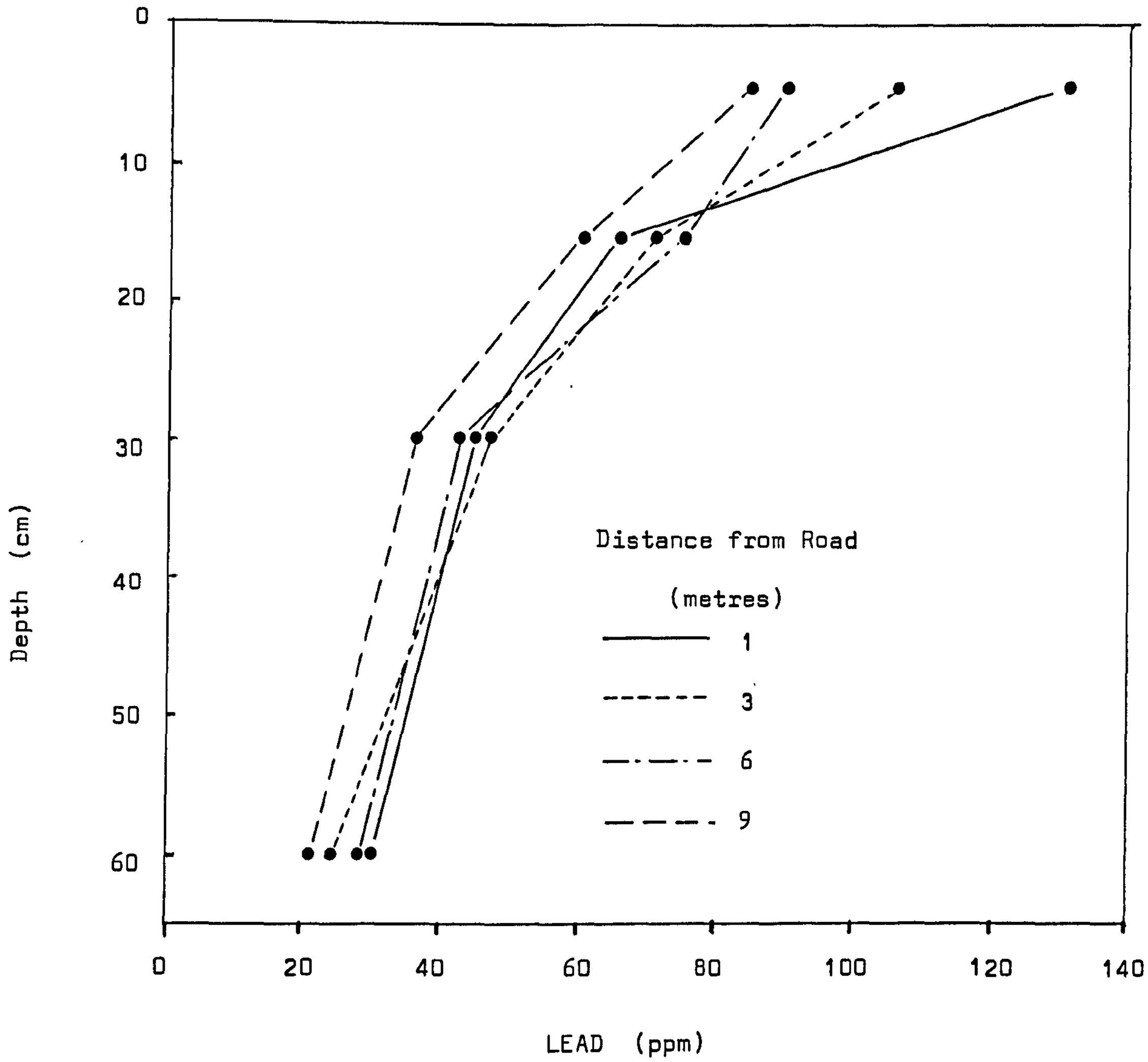

Figure 6.3 Distribution of lead in soil with depth and distance from roadway - traffic direction east

A significant concentration is built up in the top few centimetres of soil, the amount showing a clear relationship to proximity to the roadway. The quantities of metal in the top levels of soil are similar to those found adjacent to certain sections of the A491 and A456 road systems in Birmingham[611]. Interestingly the traffic density of these roads (19,267 and 17,497 vehicles per day, respectively) is comparable to the A52, although a much wider variation in lead levels was found in the Birmingham study.

At greater depths the lead concentrations do not vary as widely with distance from traffic, indicating some retention in the upper levels, possibly associated with cycling of the lead between the soil and plant root system.

Ward et al[620] measured the lead in the soil along a New Zealand State Highway and related its distribution to an empirical function of the form

$$Y_S = Bkg_s + A_s e^{-k_s (D)^{\frac{1}{2}}}$$

where Y_S = soil lead concentration (ppm)

Bkg_s = background lead level (ppm)

A_S = concentration at pavement edge (ppm)

D = distance from road edge (m)

k = constant (1/m)

Analysis of the data obtained in this present study was made

in terms of the above equation to see if it adequately represented the distribution along the A52. A value for background lead was obtained by taking the average concentration of lead from three samples taken from a field approximately 150m from the roadway and well removed from any other traffic. This gave a result of 18 ppm. Plots were made (Figure 6.4) of $\ln(Y - Bkg_s)$ against the square root of distance, D, (Table 6.3) for the lead concentrations in an east and west direction at a soil depth of 5cm.

TABLE 6.3 Analysis Data for Figure 6.4

Soil depth = 5 cm

D(m)	$\sqrt{D}$	Y(ppm)	ln(Y -Bkg)	Y(ppm)	ln(Y - Bkg)
1	1.0	134	4.753	126	4.682
3	1.732	114	4.564	102	4.430
6	2.449	87	4.234	95	4.343
9	3.0	82	4.150	89	4.262

As Figure 6.4 illustrates the fit is not good. For comparison the data from the Birmingham study[611] was taken and fitted to the above equation; again satisfactory correspondence was not achieved. If one considers the variables involved in the distribution of the lead, meteorological, traffic density and type, particle size of emitted lead, etc., it would seem surprising that the simple single exponent equation can adequately describe the lead distribution. One of the most important factors must be particle size which will, clearly,

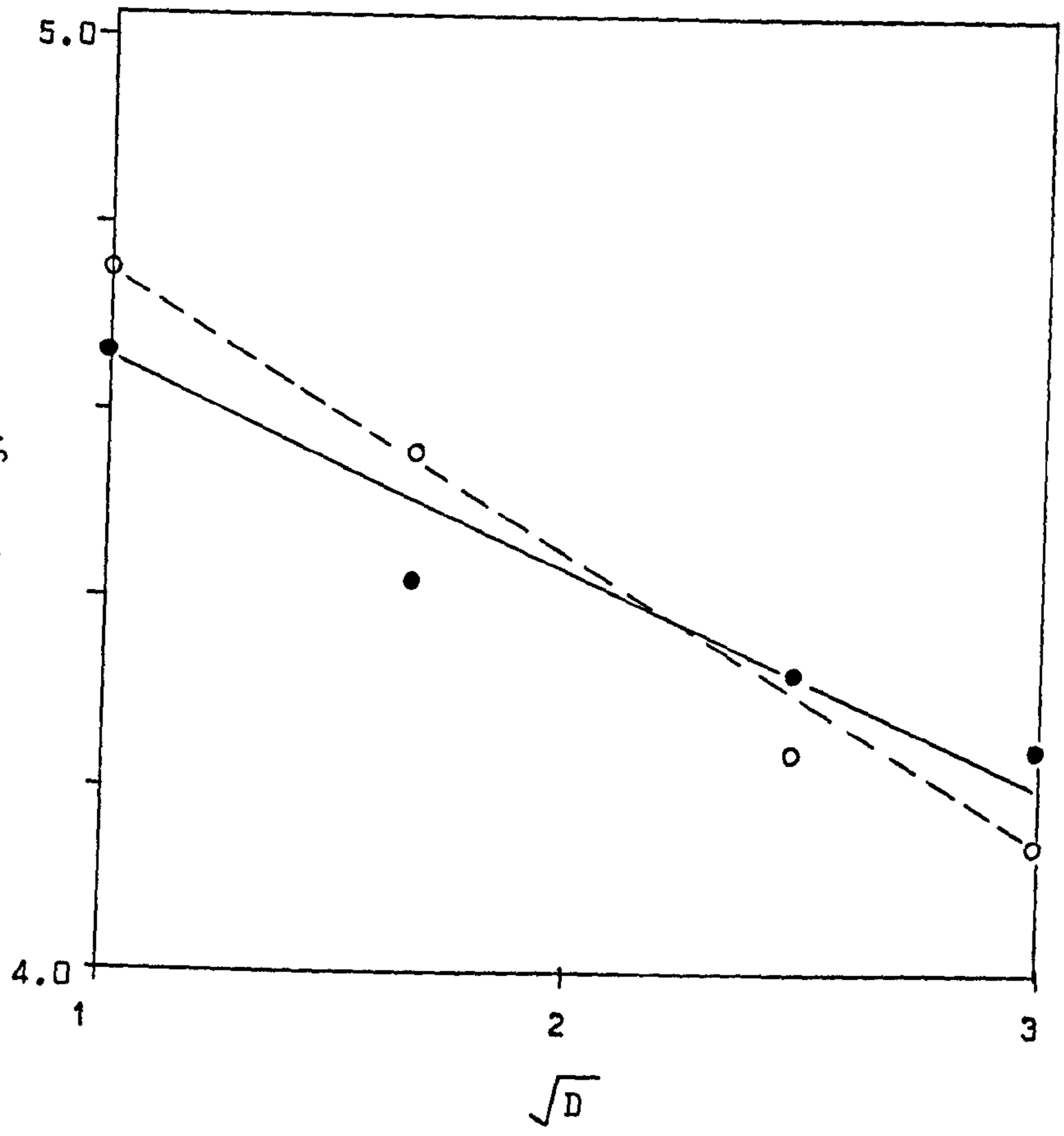

Figure 6.4 Analysis of pattern of lead distribution in soil.

affect settlement. Daines et al[606] found a marked change in the mean particle size of lead deposited as one moves away from the road system. This factor is excluded from the analysis using the New Zealand data. Since the work reported herein was completed other workers[610] have published a modification of the above formula. This is of a double exponential form taking into account particle size; their conclusions supporting the results of our study. In this equation the lead concentration is expressed by the relationship

$$Y_S = Bkg + A_1 e^{-K_1 D} + A_2 e^{-K_2 D}$$

A_1 represents the large particles which are deposited adjacent to the roadside and A_2 corresponds to the smaller particles which settle more slowly. A good fit is obtained with their own data. However, one may still question the value of the expression when translocated to other sites because of the many variable involved in the lead distribution.

The concentrations of lead in the soil measured in our study at the lower depths can not be considered as significantly raised when taken in relation to the measured background value of 18 ppm. No significant variations were observed between the lead content of soil from the verges of the east bound carriageway to those from the west.

(iii) Grasses

The lead content on the blades of grasses again showed a

decrease with distance from the roadway (Figure 6.5). The highest concentrations (Table 6.4) were much lower than those found in the sub-surface soils, indicating that the lead levels in the soil reflect an accumulation of the metal. The grasses must thus provide a physical trap for the collection and retention of lead in a given site.

TABLE 6.4 Lead content of grasses

Distance from roadway (m)	Mean lead content (ppm)	
	Unwashed	washed
1	45	32
3	38	31
6	34	26
9	28	23

Washing the grasses did not produce a marked change in the lead level, the overall reduction being about 23%. Because of the smooth surface of the grass blades it was anticipated that the surface deposited lead would be only weakly adsorbed and therefore readily removed. This did not prove to be the case. Whilst the work of Motto *et al*[608] showed an increased lead content in plants growing adjacent to a highway, it would be unwise to draw the conclusion that the high lead yield obtained in the present work with the washed grasses reflects absorbed lead within the plant

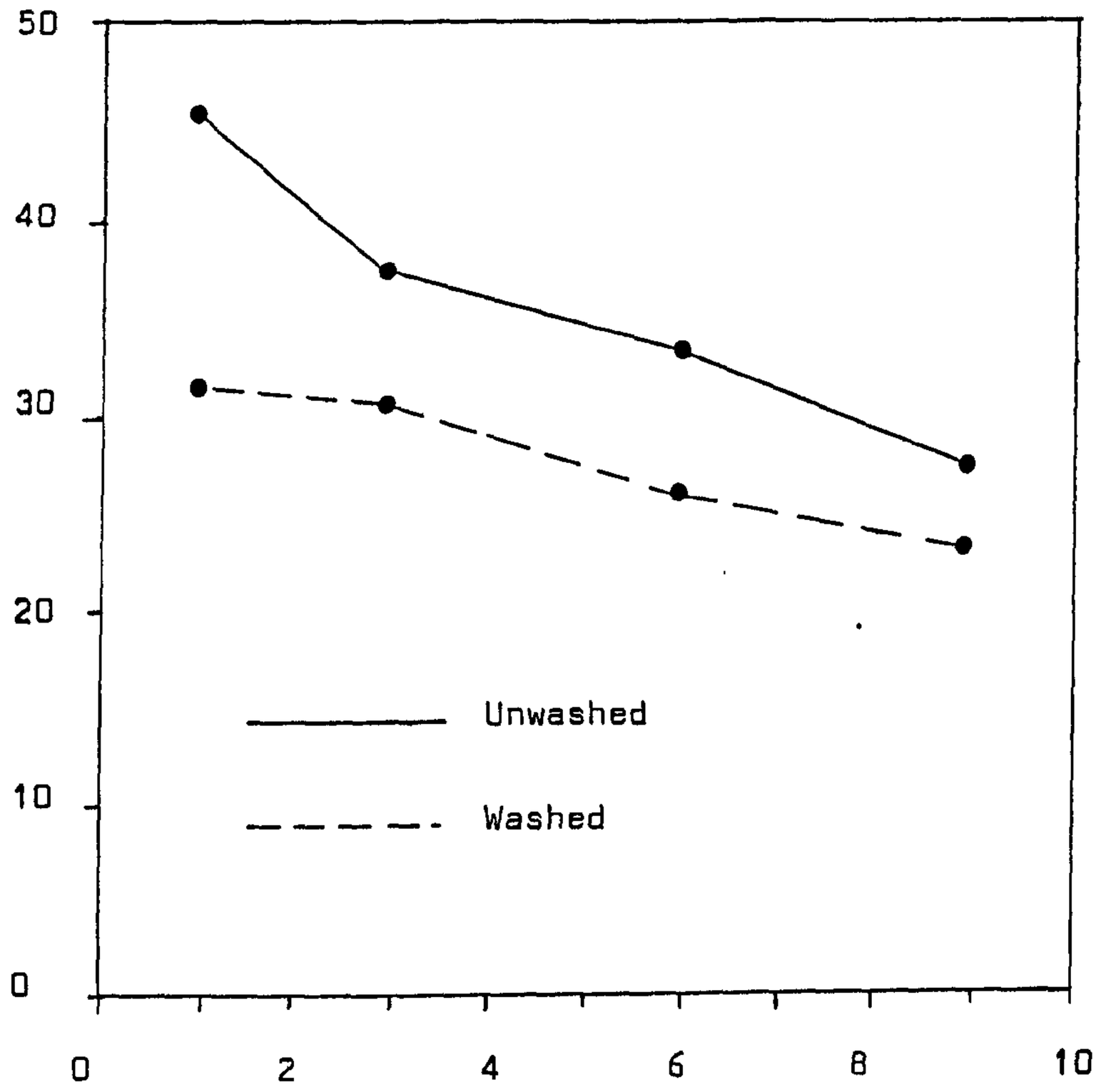

Figure 6.5 Distribution of lead in grasses with distance from roadway

structure. It is possible that the use of a surfactant may have improved the efficiency of the washing process. However, the results obtained are in good agreement with the values recently published in an American study[610]. Unfortunately, they can not be compared with the Birmingham data[611] as their results related to plant ash. A point which illustrates the raison d'etre of this work in order to obtain compatible data for a complete roadside environment.

(iv) Blackberry plants

Care was taken to ensure that as much of the surface deposited lead as possible was removed from the canes used in the experiment by thoroughly washing and wiping with absorbent tissue. The results obtained gave a mean lead content within the shoots of 1.6 ppm. This did not vary outside experimental error for any of the samples analysed. The inference being, that at a certain level the amount of lead absorbed by the plant is largely independent of the concentration of the element in the surrounding soil. The significance of the lead content in the blackberry plant arises from the annual habit of the growth of the fruit bearing shoots. This yearly replacement process enables a convenient measure of the ability of the plant to absorb lead in a single growth cycle to be established. In addition, the level of 1.6 ppm in the canes gives an indication of the maximum probable lead content within the fruit. Because of the relatively short period of development and growth of the fruit, it is unlikely to concentrate the lead to a higher value.

(v) Blackberry fruit

The hedgerows of the particular section of the A52 employed in this study is particularly well endowed with blackberry plants and paths to the fruit are well trodden during the season. Because of the obvious direct route for ingestion of lead which this opportunity present, it is, clearly, of some interest to ascertain the metal concentrations within the fruit.

The duplet structure of the fruit renders it almost impossible to ensure complete removal of surface deposited material, and hence obtain an accurate measure of the lead contained within. For the reasons given, vide supra, the extrapolated value from the plant canes, as measured, should give an acceptable fit to the maximum absolute value of lead contained within the fruit. Table 6.5 gives the levels of lead found in wild blackberry fruit.

The correspondence between values obtained in the mid-September collection to those in mid-October was found surprising; a) because the values correspond so closely and b) because it had been anticipated that a much higher level would be seen in the later collection samples. However, both effects appear to be corroborated by the work of Fowles[612]. Elderberries he collected from a roadside location over a period of time gave values of 4.77, 4.74 and 4.63 ppm. A very similar small variation to that observed in this study.

Examination of the lead values in relation to the site of collection shows some interesting trends. Site references A1 and A2 were to the rear of an embankment and show the lowest levels of

TABLE 6.5 Lead contamination of wild blackberry fruit

Site reference	Mean distance from roadway (m)	Lead content (ppm) - undried fruit			
		Mid-September		Mid-October	
		Unwashed	Washed	Unwashed	Washed
A1	7	0.46	0.31	0.45	0.33
A2	7	0.44	0.28	0.49	0.37
A3	6	0.87	0.71	0.87	0.64
A4	7	0.86	0.67	0.91	0.68
B5	3	2.74	2.05	2.66	1.89
B6	3	2.77	1.89	2.83	1.74
B7	2.5	2.81	1.97	3.12	2.22
B8	3	2.76	2.07	2.67	1.89
C9	3.5	2.62	1.73	2.65	1.94
C10	3.5	2.73	2.10	2.83	1.93
C11	2.5	2.71	1.82	2.59	1.77
C12	3	2.68	1.86	2.76	1.93
D13	1	3.96	2.56	4.07	2.87
D14	1	3.59	2.31	3.32	2.56
D15	1	5.77	4.60	5.98	4.77
D16	1	6.12	4.97	6.36	5.04

lead on the blackberry fruit. Fruit taken from plants at the same distance but facing the roadway show almost twice the level of lead (A3, A4). The bank, therefore, appears to act as an efficient partial barrier to the lead.

The highest lead contents were found in fruit from plants directly adjacent to lay-bys (D15 and D16). These had levels of lead much higher than from plants at the same distance but adjacent to moving traffic (D13 and D14). Presumably this illustrates the build up which can occur from stationary traffic leaving the engine running. Sites B5 and C9 were elevated 4-5 metres above road level. Fruit collected in these locations did show a slightly lower lead content than fruit from plants at sites similar distances but not elevated (B6 and C10) from the roadway. It was not possible to compare particle sizes between these locations, but it is probable that the lead deposited at the elevated site was predominantly of a smaller particle size. Fruit samples from B7 and B8, and C11 and C12 were to the front and rear, respectively, of the same plants. Over such small distances no meaningful variation in the lead content of the fruit was observed. The sharp increase in lead content which occurs between 7m and 3m from the roadside was unexpected. This may relate to the efficient design of the blackberry fruit for entrapment of airborne dust particles which will be carried in the following vortices of passing traffic. These will have sufficient energy to effect the distribution of additional lead laden dust to the shorter distances from the roadway.

Washing the fruit reduced the lead content by between 20-35%.

However, it is reasonable to assume that the overwhelming contribution to the lead contamination arises from surface deposited lead and not absorbed lead.

The values show a slight increase in most cases between fruit collected in mid-September and that gathered in mid-October. This probably arises because the mean age of the fruit in the latter case was probably higher, and therefore the samples had experienced a longer exposure to the leaded atmosphere. However, as stated, the difference is only slight and is of no great significance.

The overall lead contamination of the fruit observed in this study is higher than that reported by Fowles[612] for blackberry fruit. However, his highest values were obtained from samples collected from sites which probably had a lower traffic density. Taking this into account, the value he obtained of 0.57 ppm at a distance of 6m from the roadside is in good agreement with our value of 0.87 ppm at site A3. The highest value of 6.36 ppm is less than the highest values reported for elderberries (6.77ppm) and hawthorn berries (23.8 ppm) collected from similar roadsystems[612].

Whilst atmospheric lead has been estimated to contribute about 13 μg a day to the body burden in urban areas of Britain[621], it is the diet, especially plants, which provides the major source of the metal in man. Table 6.6 shows the average estimated daily intake of lead in food[622].

TABLE 6.6 The estimated average daily intake of lead from food

Food type	Mean lead Content (mg/kg)	Weight of food eaten (kg)	Lead intake per person (µg/day)
Cereals	0.12	0.27	32
Meat and Fish	0.16	0.18	29
Fruits and Preserves	0.11	0.25	28
Green Vegetables	0.19	0.11	21
Root Vegetables	0.09	0.21	19
Milk	0.02	0.40	8
Fats	0.08	0.08	6
TOTALS	0.09*	1.50	143

*Weighted according to proportion of food type eaten.

From this it can be seen that fruits and preserves make a significant contribution. In 1961 the Lead in Food Regulations set a maximum content for lead in undried fruit and vegetables of 2 ppm. On this basis the levels of lead detected in wild blackberries are unacceptable and give rise to particular concern in the case of children where the absorption of lead is considerably more facile than in adults.

All the sites chosen for this study showed clear signs of regular use and in many instances actual gathering of fruit was observed before and after our sampling. The fruit growing on plants adjacent to lay-bys is particularly accessible for collection, yet it is in

precisely these locations that the fruit is most contaminated. The simple action of gathering the fruits ensures that lead is transferred to the hands as one clambers up a bank holding to the grass for support or brushing against the dust covered plants. In children this lead could readily be transferred to the mouth and hence to the digestive tract.

Whilst eating the fruit directly presents an unnecessary health hazard, because of the relatively short season for the crop the risk is limited. Of perhaps greater concern is the use of the blackberries gathered from such locations in preserves. From the results obtained, it would be quite possible, using fruit collected at sites similar to those of this study, to prepare jams containing between 2 and 4ppm of lead. These are then available for consumption over a much longer period than the fresh fruit and hence, particularly if fed to young children and babies, could present a distinct accumulative hazard.

6.4.3 Conclusions

This study has enabled, for the first time, the overall distribution of deposited lead in a roadside environment to be measured. Correlations between quantities of lead in dust, soil, grasses and plants can now be made. The overall picture of lead deposition is shown diagramatically in Figure 6.6. The results indicate that the only real threat to health arises from collection of roadside fruit and this should be discouraged. However, the distribution of deposited lead appears to fall off quite rapidly with distance from

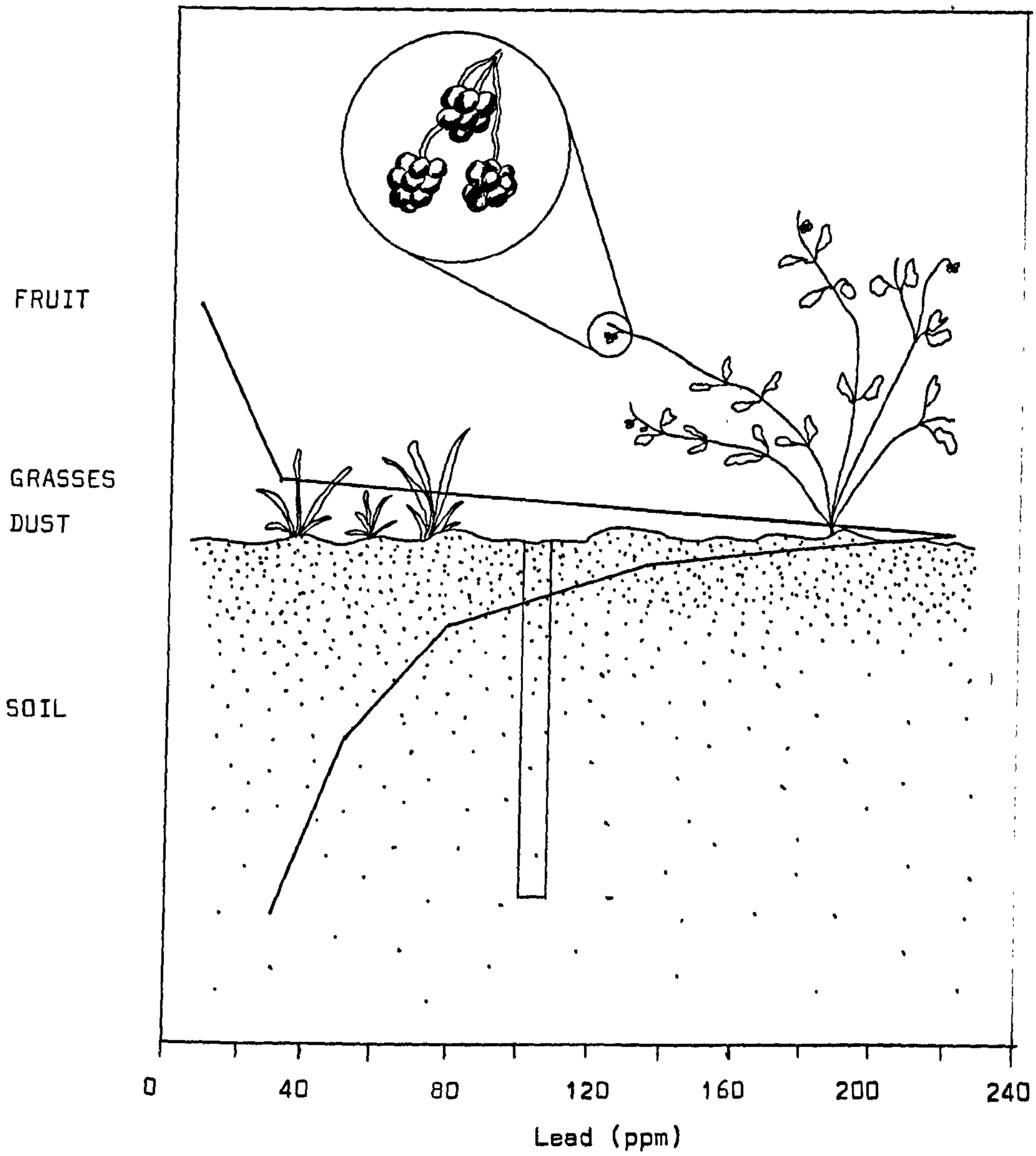

Figure 6.6 Diagrammatic representation of the distribution of deposited lead in the roadside environment of the A52(T).

the roadway; a result in agreement with other studies[610,611].

Of concern in this particular survey was that fact that many houses have been built with gardens extending well into the 'high risk' area bordering the A52. The closest approach of some gardens is 4 m from the highway. Here the possibility of contamination of home-grown produce arises, and over a long period this must, clearly give rise to the possibility of sub-clinical lead poisoning. The results would suggest that new houses should not be built with gardens which extend closer than about 15 m of such a road system. With existing houses in such locations, where home-grown produce is used the risk can be significantly reduced by using cloches. The evidence being that absorption of lead is of minor importance relative to adsorbed surface lead deposited from the air.

This study would appear to support the findings of the recent Government Commission[601] in that, other than specific instances and certain 'hot spots', in environments similar to those used in this study, generally lead in petrol may not be the major contributor to lead in blood. However, it would be foolish to consider any one study as the definitive case and work must surely continue in this area to remove lead emissions into the atmosphere. In this way the debate loses any significance.

REFERENCES

601 'Lead and Health' DHSS (1980) H.M.S.O. LONDON.

602 M.E. Hilburn, Chem. Soc. Rev., (1979) 8 63.

603 D.A. Hirschler, L.F. Gilber, F.W. Lamb and L.M. Niebylski, Ind. Eng. Chem., (1957) 49 1131.

604 P.D.E. Biggins and R.M. Harrison, Envir. Sci. Technol., (1979) 13 838.

605 G. Ter Haar and M. Bayard, Nature, (1971) 232 553.

606 R. Daines, H. Motto and D. Chilko, Envir. Sci. Technol., (1970) 4 318.

607 R.M. Harrison, R. Perry and R.A. Wellings, J. Air Pollut. Cont. Assoc., (1975) 25 627.

608 H.L. Motto, R.H. Daines, D.M. Chilko and C.K. Motto, Envir. Sci. Technol., (1970) 4 231.

609 W.J. Vandenabeele and O.L. Wood, Chemosphere (1972) 5 221.

610 G.L. Wheeler and G.L. Rolfe, Envir. Pollut., (1979) 18 265.

611 B.E. Davies and P.L. Holmes, Agric. Sci., Camb., (1972) 79 479.

612 G.W.A. Fowles, Food Chem., (1976) 1 33.

613 Personal Communication, (1979) Data Collection Dept. Nottinghamshire County Council.

614 K.W. Olson and R.K. Skogerboe, Envir. Sci. Technol., (1975) 9 227.

615 P.D.E. Biggins and R.M. Harrison, Envir. Sci. Technol., (1980) 14 336.

616 R.M. Harrison and D.P.H. Laxen, Chem. in Britain (1980) 16 316.

617 M. Giubileo, Med.del Lavoro (1957) 48 165.

618 D. Högger, Bull. Eidenössichen Gesundheitsamtes (1971) B3.

619 J. Th.L.B. Rameau, Int. Symp. Envir. Hlth. Aspects Lead (1972) Amsterdam.

620 N.I. Ward, R.D. Reeves and R.R. Brooks, Envir. Pollut., (1975) 9 243.

621 'Lead in the Environment and its Significance to man'. Dept. Envir. (1974) H.M.S.O. LONDON.

622 'Survey of Lead in Food'. Min. Ag. Food Fish. (1970) H.M.S.O. LONDON.

CHAPTER SEVEN

ADVENTITIOUS LEAD IN SOME ASIAN MEDICINES AND COSMETICS

In this Chapter a new aetiology of lead poisoning associated with the use of some Asian medicines and cosmetics is discussed. This work was undertaken in collaboration with Dr. Mohamed Aslam who, under the direction of Professor S.S. Davis of the Pharmacy Department at Nottingham University, and with the financial support of the Department of Health and Social Security, was engaged on a major study of Asian medical practices within the United Kingdom[701]. Credit for discovering these new sources of lead poisoning must, therefore, largely reside with the initiators of that particular study.

7.1 INTRODUCTION

Since 1950 there has been a marked increase in the number of Asian immigrants to the United Kingdom, a high proportion coming from the Indo-Pakistan sub-continent. With this influx has come not only the religions and dietary practices of these Peoples but also their own systems of medicine. These traditional systems, known as Auyervedic and Unani, differ in many respects from the Western Allopathic medical practices. One specific aspect is the materials used in treatment. These are usually herbal in origin, and, unlike Western medicines which, generally, rely on a single active

ingredient, are designed to act on a holistic basis : one herb assisting the efficacy of another; with often ten or more 'active' ingredients. One example of such a medicine is the traditional baby tonic known as Bal Jivan Chamcho.

7.2 BAL JIVAN CHAMCHO

In October 1976 a child was admitted to hospital in Luton with clinical lead poisoning. Just prior to this time Dr. Aslam had been at Aston University in Birmingham undertaking a study of patient compliance to medical instructions amongst the Asian community. Because this child was Asian in origin Dr. Aslam became involved in the case, and it was at this point that our collaborative work commenced.

At the time of the childs admission to hospital the source of the poisoning was unknown. After our discussions, investigations were made into known possible causes of lead poisoning such as contaminated drinking water from dcmestic lead piping, or pica, the habit sometimes found amongst young children of eating materials other than food such as leaded paint flakes. However, these sources proved fruitless in this case.

Being of Asian ethnic origin the childs diet varied in certain respects from that of a Western child. However, there was no evidence that this was a contributory factor. What did come to our attention was the fact that the child was regularly being dosed with the traditional Asian baby tonic, Bal Jivan Chamcho. Medicines,

such as Bal Jivan Chamcho, have been available on the Indian market for many years and, in principle, appear innocuous. They are compounded preparations from a variety of botanical substances; the extracts and remainders of which are made into a paste, spread on a spatula shaped spoon and allowed to dry. The dried preparation, with the spoon as carrier, is then packaged into a small carton for sale (Figure 7.1). The label on the carton is printed in English, Gujerati and Hindi with the directions:

> "Children Diseases viz Varadha Capillary, Bronchitis, Greenish Diarrhoea, Rickets, Croup, Convulsions etc. Rubbing the medicine with water or milk until it gets colour. To be taken twice a day."

The herbal preparation is thus activated by allowing the material to soak, on the spoon provided, in about 5 cm^3 of milk or water, for several minutes until the liquid becomes coloured. The liquid alone is then administered to the child and the preparation, still on the spoon, is allowed to dry in readiness for re-use. In this way the same preparation may be used for a period of several months.

When the sample of the herbal compound, used to dose the child suffering from lead poisoning, was removed from the carrier spoon it was observed that the plating of the spoon in this area showed considerable corrosion, revealing a dark grey metal beneath. Small pieces of metal were then cut from the spoon and digested in hot nitric acid. The resulting solution was analysed by atomic absorption spectroscopy on a Perkin-Elmer Model 603 system (see Chapter Six).

Figure 7.1 Bal Jivan Chamcho. Lower photograph shows herbal preparation on spoon and package used for sale. Upper plate shows the preparation removed from the spoon revealing the extent of corrosion in this area.

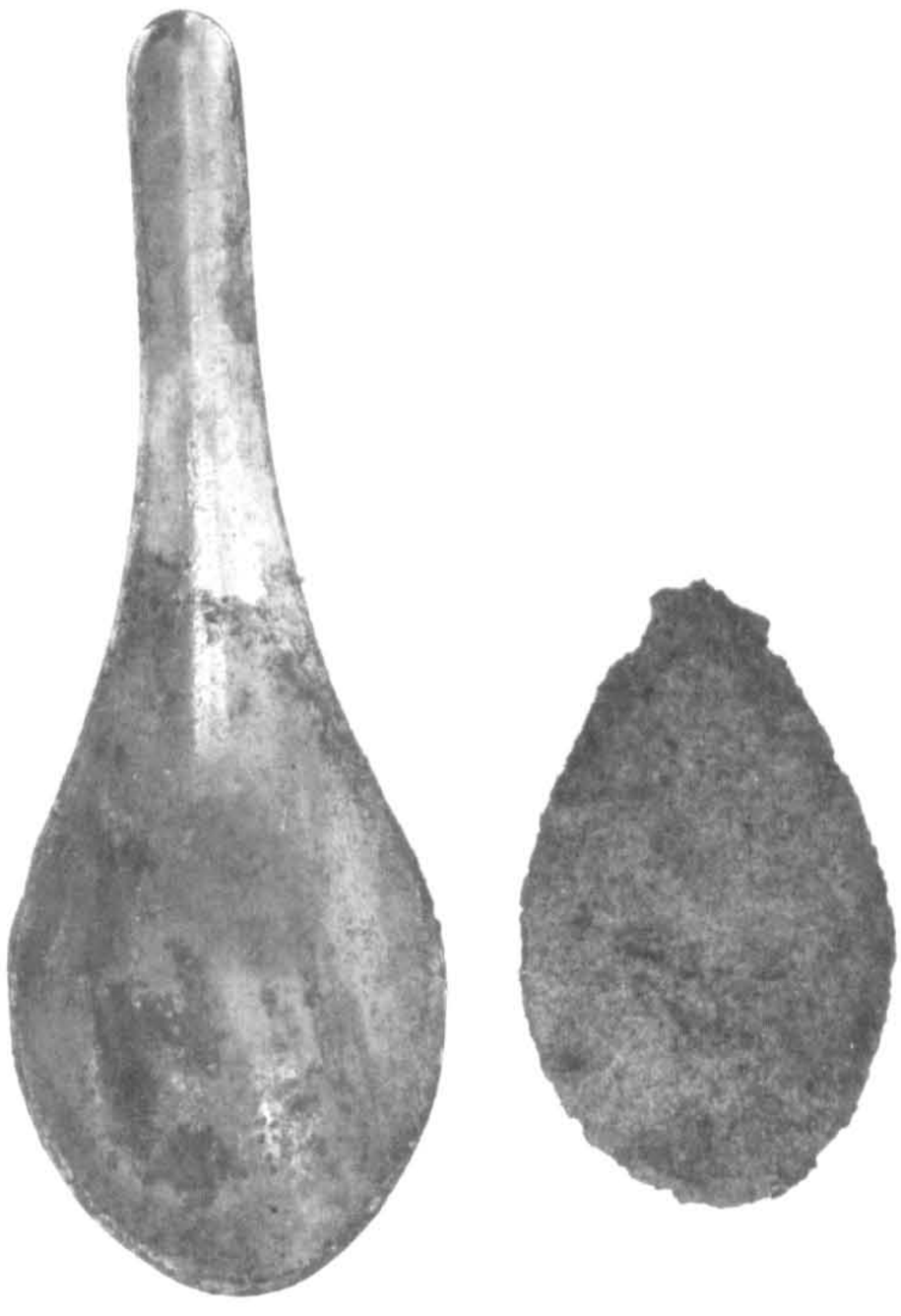


प्रल्हादना बालवैरा
चीमनलालजी बी पडीतना
बालजीवन
चमचो
छोटे बच्चोंकी
महानशक्तिवर्धक
कीमत १ रुपया
बालजीवन
चमचा ऑफीस
बडोदा १

The analyses revealed that lead contributed 83.3% of the total weight of the spoon. Similar measurements were made on the herbal compound which was found to contain 1,040 ppm of lead. By following the recommended procedure for administering the medicine it was found that 12 ppm of lead was inadvertently given each time the material was used. Clearly the process appeared to be a simple leaching action. The repeated moistening and drying caused further corrosion of the plating, which, in turn, increased the available lead dose in the preparation. Even with new samples of the material it was found possible to obtain a dose of 6 ppm of lead. If the material remained moistened, a progressive increase in lead concentration in the resulting solution was observed (Table 7.1), thus confirming the leaching action.

TABLE 7.1 Increasing lead concentration with time of solutions derived from Bal Jivan Chamcho

Time Period after moistening compound (hours)	Lead concentration in resulting solutions (ppm)
0.1	6
12	12
24	18
36	21
48	21

In all the samples of Bal Jivan Chamcho examined the carrier spoons showed signs of corrosion and were badly plated. Although the herbal compound was itself quite harmless, indeed may even have been beneficial, and the obvious remedy was to change the spoon, because the product was imported no such change could be enforced. In these circumstances the high lead content of the Bal Jivan Chamcho presented a distinct health hazard, particularly to young children for whom it was recommended. It was, therefore, proposed that the import, sale and supply of this material should be proscribed. A temporary order to this effect was introduced by the Government in February 1977 and made permanent in May of that year. Following these findings, analyses were made of a number of other Asian medicines and cosmetics.

The distinction between cosmetic and medicinal use of a preparation is sometimes difficult to make, particularly where traditional religious beliefs play a major role in their use. However, where heavy metals were found in this study, we were able to classify the substances into those which had the metals there as contaminants, such as Bal Jivan Chamcho, or those in which the metals were present by deliberate addition. Into this latter catagory comes the eye cosmetic known as Surma.

7.3 SURMA

Surma is a fine black powder applied to the conjunctival margins of the eyes of young Asian children and women. Its use

can be traced back many centuries and the belief is held that it strengthens and protects the eyes against disease as well as improving the appearance. In texture it is similar to a mascara and ranges in colour from black through the various shades of grey to white. The name is derived from the Urdu word for antimony as this was the metal from which they were originally prepared.

X-ray powder diffraction studies were made on an initial batch of 13 samples of Surmas obtained in this country, using the Philips PW 1010 X-ray generator with a Cu - K_{α} source run at 40 KV and 26 mA, and the Philips Debye-Scherrer camera type PW 1024 equipment employed in the roadside lead studies previously described. From this, eleven of the thirteen samples were found to contain lead as lead sulphide. Portions of these eleven samples were treated with nitric acid and analysed quantitatively by atomic absorption spectroscopy. The results obtained (Table 7.2) for these proprietary Surmas showed a mean lead concentration of 59.8% (w/w), with the highest value being 82.9% (w/w).
Trace quantities of iron, copper, zinc and antimony were also found and additional analyses made by the Pharmacists revealed the presence of a number of herbs used in the preparations.

The Surmas are often supplied in decorative containers together with an applicator (Figure 7.2). The applicator is dipped into the Surma powder and then applied to the conjunctivae. A number of the Surmas analysed also contained the terpene, menthol. This induces profuse lachrymation which, in turn, causes the child to rub his eyes. Invariably he then sucks his fingers as a palliative.

Figure 7.2(a) A range of Surma materials obtained within Britain.


هانيمن
سرمه
جواهر


جوهر
النورة


Ringer

Figure 7.2(b) A typical decorative Surma container with the applicator removed.

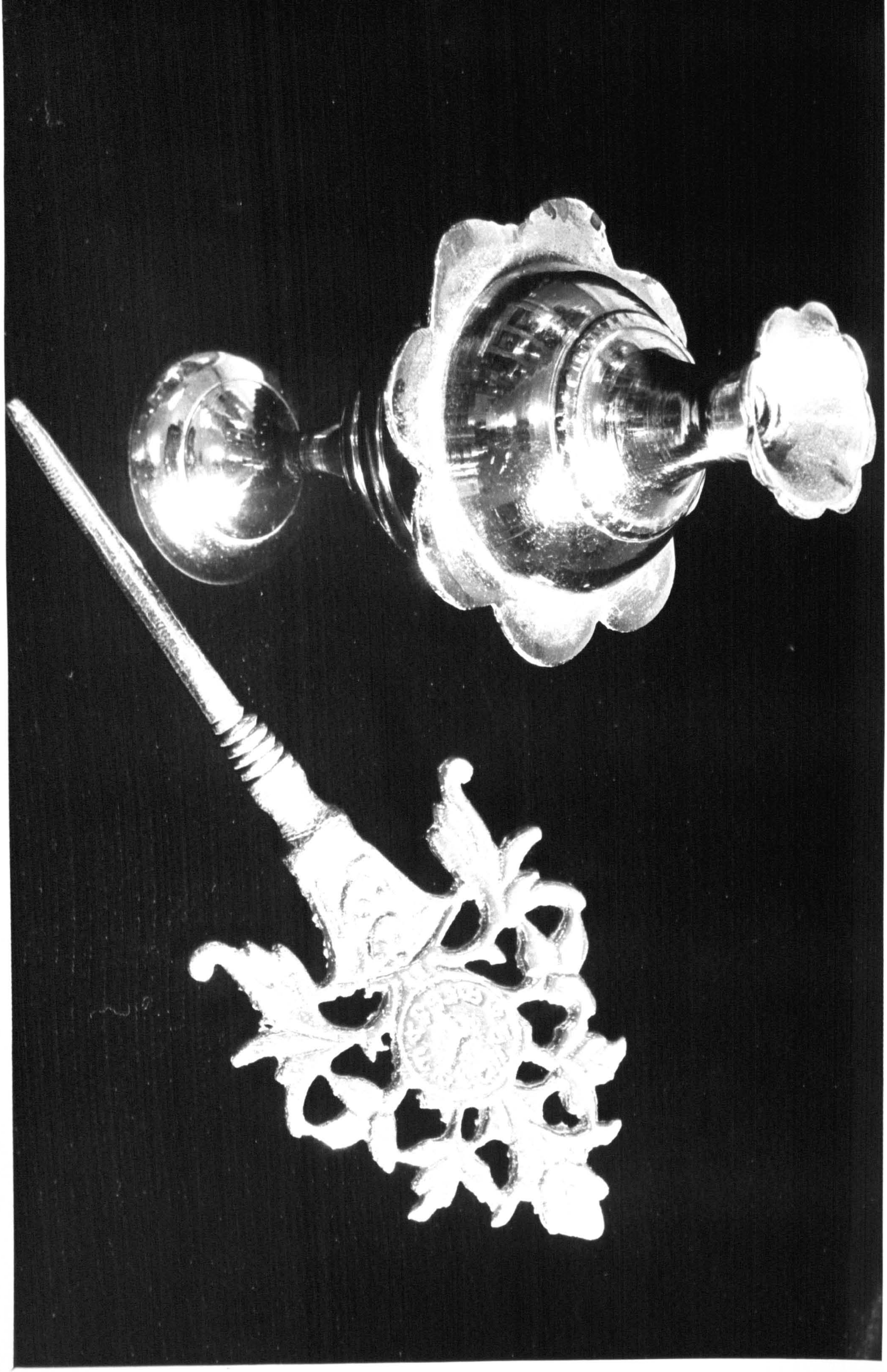

TABLE 7.2 Chemical analysis of proprietary Surmas sold or brought into the United Kingdom but manufactured in India or Pakistan

Description	Powder colour	Percentage lead
Hashmi Surma Jowahar Chaharam, Karachi	Grey	80.2
Surma Moqawi,Basar Taj Company, Lahore	Grey	53.7
Multani, Ayurvedic,36-H Connaught Circus, Delhi	Grey	Trace
Nag Jyoti, Murrari Brothers, Delhi	White	Trace (Zinc 4.5% + Menthol)
MD Hashim Surma, Bunder Road, Karachi	Grey	82.9
Bal Jyoti, Murrari Brothers, Delhi	Grey-Black	38.4
Indian Surma	Cream	Trace
Bhimsaini Kajal With Aela, Murrari Brothers, Delhi	Black Paste	Trace
Nargasi Surma, Hamdard, Pakistan	Grey	77.3
Binger Surma, Hamdard, Pakistan	Black	26.3
*(Bhimsaini Kajal With Aela)	Black Paste	(Trace)

Trace = 0.5%

*Carbon in soft paraffin base

The lead is thus transferred via the fingers to the mouth and hence to the alimentary canal. This appears to be the primary route for poisoning, as experiments which were made on rabbits showed no evidence for transcorneal transport[701]. Although, clearly, on lachrymation the tear formation from the lachrymal gland has the effect of washing some of the lead sulphide into the naso-lachrymal duct where, again, it passes into the mouth and on to the gut (Figure 7.3). Experiments I have made indicate that some 20 mg of surma is deposited on the conjunctivae at each application. One can estimate from the amount transferred to the fingers on wiping the eyes and then sucking the fingers that about 0.2% of the applied surma is being ingested. If a Surma with an average lead content of say 60% (w/w) was applied once daily this could produce a weekly ingestion of lead of 168 μ g. In children 25-50% of ingested lead may be absorbed in the gut[702] so that Surma could contribute between, approximately, 40-80 μ g of lead per week to the total body burden of the metal in the child. It would seem reasonable, therefore, that differences in the blood lead levels of Surma users, when compared to non-Surma controls, should be detectable. Such measurements have now been made by other workers and the results showed that of 62 Asian children in Nottingham[703] the Surma users had a mean blood lead level of 34.2 μ g/100 ml (1.65 μ mol/l) whilst the non-Surma users had 20.3 μ g/100 ml of lead in blood (0.98 μ mol/l). (Blood lead : 1 μ mol/l ≡ 20.7 μ g/100 ml). A similar study in Bradford confirmed these results[704]. The recent death of a child in Oldham from lead encephalopathy was attributed

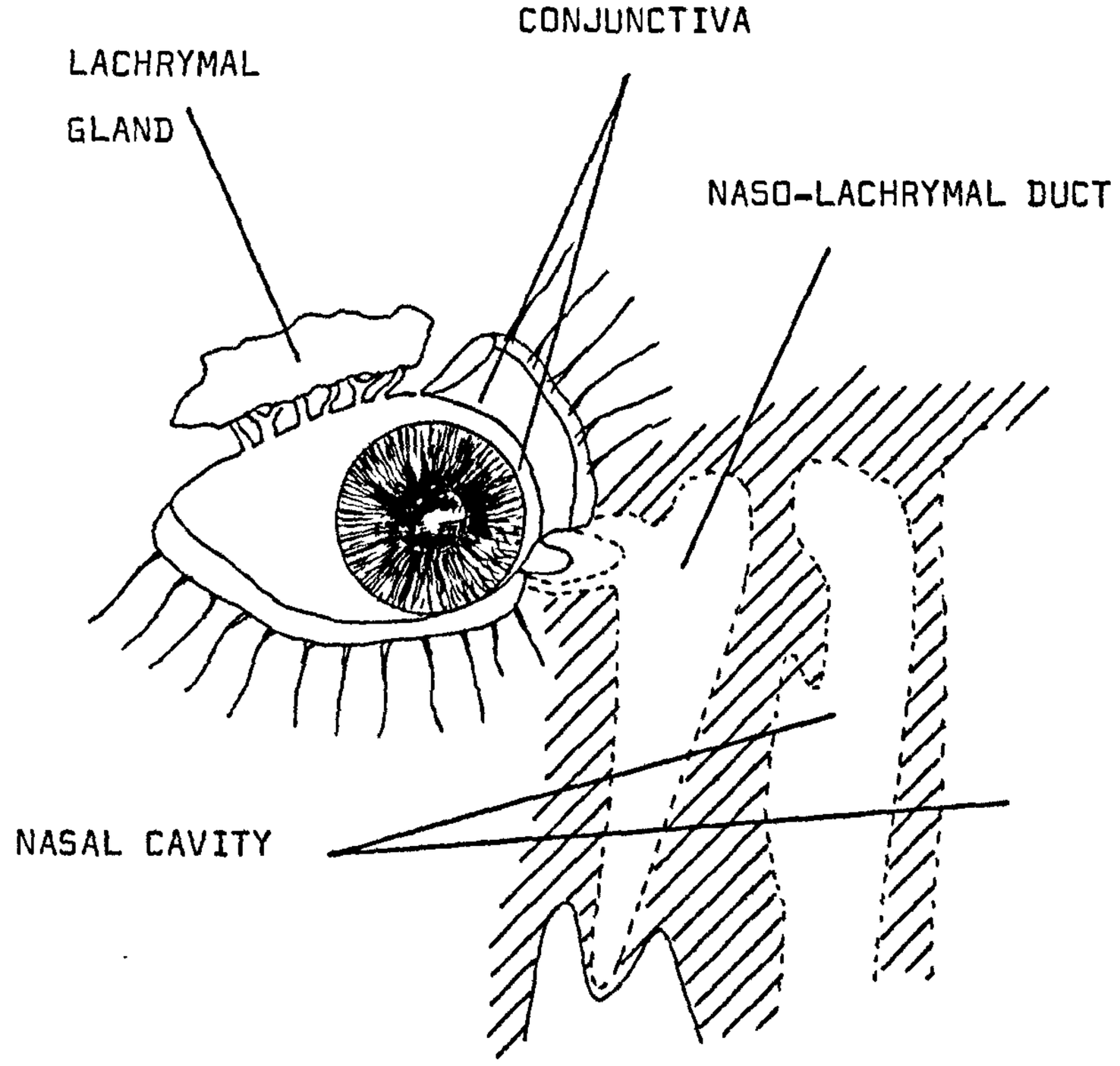

Figure 7.3 Diagram of the lachrymal apparatus.

to the regular use of Surma. Post-mortem investigations showed abnormal levels of lead in the body (Table 7.3)[701].

TABLE 7.3 Post-mortem tissue lead levels of Oldham child[701] compared with normal values for children aged 16 years and under[705].

Tissue	Lead Concentration (ppm wet weight)	
	Oldham Child	Normal Child
Bone: Petrous Temporal	14.3	4.85
Calvarium	19.4	4.17
Tibia	9.3	2.27
Liver	1.34	0.62
Kidney	2.3	0.40

The high concentrations of lead in the bone confirmed that exposure had been prolonged.

Despite the attendent publicity which has followed these reports the use of these materials is continuing in many Asian homes. Nor is the problem specific to the Indian sub-continent and immigrant communities within the United Kingdom. Recent analyses I have made on Surmas from Kuwait and Saudi Arabia, supplied by Dr. Aslam, showed concentrations of lead as lead sulphide similar to those found in materials already measured.

Following our contribution to this original study of the pharmaceutical aspects of Asian medicines and cosmetics, we proposed to examine the chemical mechanisms involved in an attempt to construct a model of the physiological absorption processes of lead from these materials.

7.4 A MODEL FOR ABSORPTION OF LEAD SULPHIDE IN RELATION TO THE EYE COSMETIC SURMA

7.4.1 Solubility Studies

As stated, the principal chemical form of the metal in the lead containing Surmas is the sulphide, as they are generally produced by direct crushing of the ore galena (PbS). The work of Allcroft[706], who fed a series of different lead compounds to calves, indicated that lead sulphide was only poorly absorbed. Whilst, clearly, differences do occur between metabolism of the metal in animals and in man, as illustrated by the generally much lower rate of absorption of the metal found to occur in the gut of the former, the results of Allcroft would appear at variance with the established relationship between the use of Surma and lead poisoning in man. It is, therefore, of some interest to investigate the fate of ingested lead sulphide.

The estimations made of the possible contribution of Surmas to the total body burden of lead of a child employed a generalized absorption quotient for lead of between 0.25 and 0.5[702]. Whilst these are the only values available in the literature, the rate of

uptake of ingested lead by the body must, perforce, depend on a number of factors, _inter alia_, the solubility of the particular lead system within the gastrointestinal tract. In order to study solubility effects three Surmas were selected. These were

(i) a home-made Surma from Bradford.

(ii) a commercial Surma obtained in Saudi Arabia.

(iii) a commercial Surma from Kuwait.

A sample of pure lead sulphide was used as a control.

Prior to study the materials were qualitatively examined by X-ray powder diffraction techniques. Apart from the Bradford Surma the materials gave a pattern identical to the pure PbS. In the former material a single extraneous line was observed which could not be ascribed to any particular system with certainty. However, the intensity of this was minimal (Figure 7.4).

The solubilities were measured in turn in water (deionized and triply distilled), saliva and simulated gastric juice[707]. The latter consists of NaCl (2g), concentrated hydrochloric acid (7 ml) and distilled water (to make up 1 litre). The resulting solution, prepared according to the reference given, has a pH = 2.0. Saturated solutions were prepared in each of the three media. These were allowed to equilibrate for 4 hours at 36^{o} in a water bath. Aliquots were removed, centrifuged and filtered (to avoided suspended material) and the lead content, determined as the metal, measured by atomic absorption spectroscopy. For the saliva and simulated gastric fluid the standard solutions were 'spiked' with the equivalent volumes

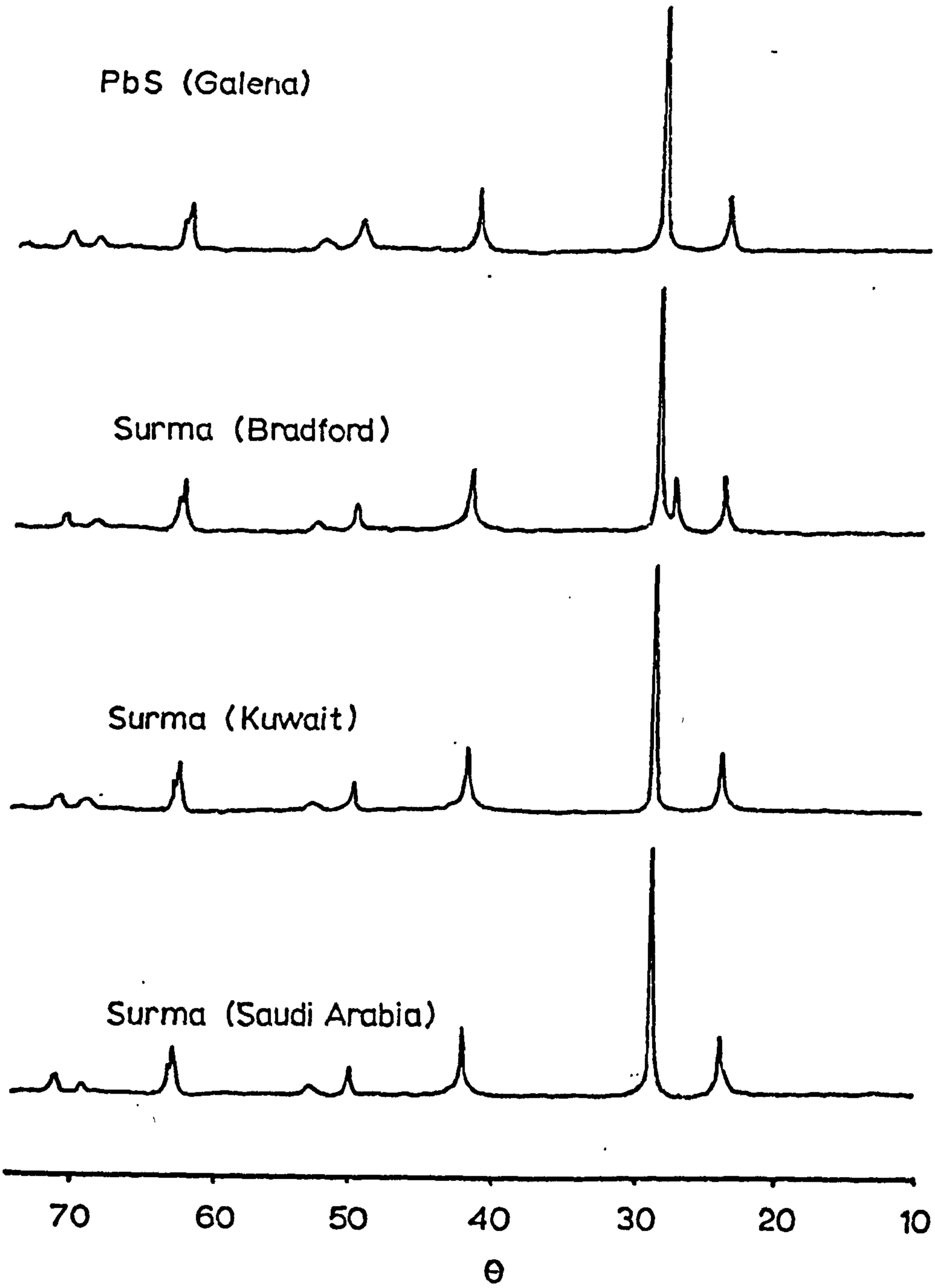

Figure 7.4 X-ray powder diffraction traces from Surma samples used in solubility measurements.

of the particular medium. The overall metal content of the solids was determined in a similar manner after digestion in nitric acid. The results obtained are presented in Table 7.4

TABLE 7.4 Lead solubility (g/1000 cm^3 at 36^o) and lead content of Surma samples

Material	Water	Saliva	Simulated Gastric Juice	% Pb (w/w)
PbS (Galena)	0.0011	0.0016	0.892	86.6
Bradford Surma	0.0012	0.0017	0.870	76.5
Kuwait Surma	0.0011	0.0017	0.805	71.6
Saudi Surma	0.0011	0.0016	0.835	67.0

The degree of dissolution of the materials in pure water is low for all the Surmas, as is known for lead sulphide. In saliva a slight increase in solubility is noted. This follows the trend exhibited by other lead compounds, for example, titanate, chromate and carbonate in other body fluids such as human pleural fluid and blood serum[708]. However, examination of the solubilities of the lead sulphide and Surmas in simulated gastric juice reveals an, approximately, five-hundred-fold increase. It would seem reasonable to take such a magnitude of increase as indicative of a reaction process. Karhausen[709] has postulated that, contrary to Allcroft's findings,

galena is readily absorbed from the gut in the presence of gastric acid secretions because it is converted to lead chloride.

$$PbS + 2HCl \longrightarrow PbCl_2 + H_2S$$

Reconversion to the sulphide of any chloride not absorbed occurring in the colon. To test the validity of this proposal saturated solutions of the Surmas in the simulated gastric fluid were prepared and allowed to slowly reduce in volume by evaporation. After approximately two weeks the formation of several white, needle-shaped crystals was observed. These were collected from the solutions and analysed by X-ray diffraction techniques which confirmed the material as crystals of lead chloride.

Whilst, clearly, no suggestion is made that crystallization would occur in the body, from this evidence it is not unreasonable to propose that lead chloride is indeed generated from lead sulphide in vivo in gastric juice.

Although at this stage there is no evidence to the contrary, it is probably unlikely that lead chloride is the only species formed in the medium. One could postulate the formation of a sulphochloride as a side reaction:

$$2\ PbCl_2 + H_2S \longrightarrow Pb_2SCl_2 + 2HCl$$

and it is well known that species such as $PbCl^+$ exist in lead(II) chloride solutions (Chapter Five).

In the discussion which follows a model for the processes involved in absorption of lead sulphide from the Surmas is described.

In Chapter Eight an *in vitro* chemical analogue is examined which lends support to this proposed system.

7.4.2 A Postulated Mechanism for lead Absorption after Ingestion of Surmas

The processes involved in the passage of ingested lead from the gut lumen to incorpoation in the body structure, i.e. from ingestion to absorption, are not well understood. The effects of other metals has been studied with respect to the rates of absorption. For example, measurements have shown that retention of lead varies inversely with dietary calcium content[710], although a residual degree of lead absorption remains unaffected by calcium concentration[711]. However, the actual mechanism of this interaction has been less well investigated. The above data would indicate that two separate routes are involved in the absorption process. Figure 7.5 illustrates the model which has been constructed to represent the proposed absorption routes for lead sulphide.

A more detailed description of the intestinal membrane will be presented in Chapter Eight, at this stage it is sufficient to mention that the protein covering the two sides of the lipoidal sheet of this membrane is orientated perpendicularly to the cell surface, and has frequent water-filled pores approximately 4 Å in radius. The increased solubility of the lead sulphide from the Surmas resulting from conversion to the chloride, as shown above, will release lead into solution in the area of the intestinal epithelium

Figure 7.5 Proposed model for gastrointestinal absorption of lead sulphide

INGESTION OF LEAD SULPHIDE FROM SURMA

REACTION WITH GASTRIC JUICE TO FORM LEAD CHLORIDE

IONIZED Pb^{2+}

PORE-DIFFUSION

ABSORPTION

UNIONIZED $PbCl_2$ DUE TO COMMON ION EFFECT

INCREASE IN SURFACE AREA OF UNREACTED LEAD SULPHIDE BY LOSS OF LEAD(II) IONS

PASSIVE DIFFUSION

in the form of Pb^{2+} ions. Generation of $Pb(OH_2)^{2+}$ type species involving the first coordination sphere of lead is most probable and as the ionic radius of Pb^{2+} is about 1.21 Å it is reasonable to assume that such ions may be carried through the membrane as hydrated species by the solvent drag of the water, which is continually passing through the membrane pores. It is unlikely that such pore-diffusion will be affected by the Ca^{2+} concentration to any marked extent. The formation of species such as $Pb_6(OH)_8^{4+}$ and $Pb_3(OH)_4^{2+}$, believed to form on partial hydrolysis of lead(II) salts, are unlikely to be present in any significant quantity in the acid medium of the stomach and the physical bulk of any such metal cluster-type systems which did result would effectively prevent their pore-diffusion. Species such as $PbCl^+$ may, however, make a contribution.

Because of the common-ion effect of Cl^- which will occur between the HCl of gastric juice and the $PbCl_2$ of its reaction product with the lead sulphide, the extent of ionization will be limited. The equilibrium will, therefore, move in favour of the undissociated $PbCl_2$ i.e.

$$PbCl_2 \rightleftharpoons Pb^{2+} + 2Cl^-$$

In such circumstances agglomeration of the $PbCl_2$ may occur and, together with the original PbS, an appreciable amount of the lead is likely to remain in unionized form and, therefore, not pore-diffusible. However, whilst the neutral PbS and $PbCl_2$ will be of lower permeability than the ionic Pb^{2+}, they can undergo a partition process from the

aqueous gastrointestinal fluids into the oleaginous membrane. Thus allowing diffusion followed by reverse partition from the lipoidal material into the aqueous blood and tissue fluids. We believe that the passage of the various lead species through the membrane probably involves a contribution from a transitional state with the metal attached to suitable protein and phospholipid binding sites on the mucosal cells. Evidence to support this proposal is given in the next Chapter.

Clearly, in the $PbCl_2 \rightleftharpoons Pb^{2+} + Cl^-$ equilibrium and the $PbS + 2HCl \longrightarrow PbCl_2 + H_2S$ reaction, the species absorbed and the site of gastrointestinal absorption will be pH dependent. Thus, in the stomach where the pH varies between 1 and 3.5 the common-ion effect will favour neutral $PbCl_2$ production and, hence, passive diffusion. In the duodenum, with a pH of 5 to 6, their is a probability of passive and pore diffusion, whilst in the ileum, where the pH approaches 8 pore diffusion of Pb^{2+} predominates; equilibria of the type

$$Pb(OH_2)^{2+} \underset{-OH^-}{\overset{+OH^-}{\rightleftharpoons}} Pb(OH_2)(OH)^+ \underset{-OH^-}{\overset{+OH^-}{\rightleftharpoons}} Pb(OH)_2$$

can be envisaged in this case.

The lead traversing the intestinal epithelium by either passive or pore diffusion will be removed, primarily, by blood. The rate of removal will be dependent on the chemical form of the metal.

Winne and Ochsenfahrt[712] developed an equation for the rate of absorption of a drug in a three compartment model involving lumen, intestitial space and streamline blood flow. The relationship derived was

$$\text{Rate of absorption} = \frac{C_{GL} - C_{AP}}{\frac{1}{P.A} + \frac{1}{f_B.Q_B.\rho}}$$

Applying this to the lead absorption model proposed, the absorption rate is then equivalent to the rate of appearance of the metal in the intestinal venous blood. The factors in the numerator C_{GL} and C_{AP} are the respective concentrations of the diffusing species in the gut lumen and arterial plasma. Resistance to absorption is represented by the terms in the denominator. P is the permeability coefficient of the epithelium to the lead and A is the mucosal surface area. f_B, Q_B and ρ represent resistance to drainage by blood. f_B is the fraction of total intestinal blood flow (Q_B) perfusing through the capillaries and ρ is the ratio of the concentration distribution of the metal between blood and plasma. From this it can be seen that absorption of the pore-diffusible Pb^{2+} species which will have a high permeability coefficient (P) will be perfusion limited. Whilst, conversely, the neutral $PbCl_2$ and PbS, which have a low

permeability coefficient, will have an absorption rate independent of blood flow. In other words pore-diffusion is limited solely by the rate at which the blood can remove the diffused lead, whilst passive diffusion will be limited by the rate of transit across the membrane, which, perforce, will be much slower than the blood flow clearance rate. The overall mechanism for absorption of lead should thus be dependent on the extent of dissociation into ionic species and the resulting equilibria. Whilst, in principle, the diffusion process could be reversible, the continual passage of splanchnic blood into the hepatic portal vein will ensure uni-directional transfer.

7.4.3 Particle Size Effects and the Model

A further consequence of the proposed partial dissolution of the lead into ions following reaction to form the chloride, will be a reduction in the particle size of the ingested Surma material. This, in turn, will give rise to an overall increase in surface area of the unionized molecular lead sulphide particles. Consider a modified application of the Noyes-Whitney dissolution rate law[713], whereby:

$$\frac{dC}{dt} = \frac{kDS}{Vh}(C_S - C)$$

C being the concentration of the metal in the bulk solution in which dissolution is occurring; C_S, the solubility in the medium;

D, the diffusion coefficient of the metal in the medium; V, the volume of solution; h, the thickness of the diffusion layer around the particle and S the surface area of undissolved solid. K is the constant of proportionality. If it is assumed that for the undissociated lead sulphide (or lead chloride) D will remain constant and, providing the same area of the gastrointestinal tract is considered, V and h will remain unchanged then

$$\frac{dC}{dt} = K'S\ (C_S - C)$$

It follows therefore that the overall increase in surface area of the unionized PbS or PbCl particles which results from loss of Pb^{2+} will give rise to an increase in the dissolution rate, and hence diffusion capability.

The recent work of Baltrop and Meek[714] has shown a five-fold enhancement in lead absorption in rats when the particle size is reduced from 196μ to 6μ. Photomicrograph examination, using a scanning electron microscope, of a number of Surmas has shown particle sizes ranging from slightly in excess of 100μ to less than 4μ (Figure 7.6). The reduction in particle size due to the process described above would, therefore, bring the majority of ingested Surma particles within the range where lead absorption in the gut has been shown to be most facile.

In order to obtain some measure of the rate of uptake of the Surma particles in gastric juice the following experiment was

Figure 7.6 Photomicrographs at different magnifications of a typical Surma material.

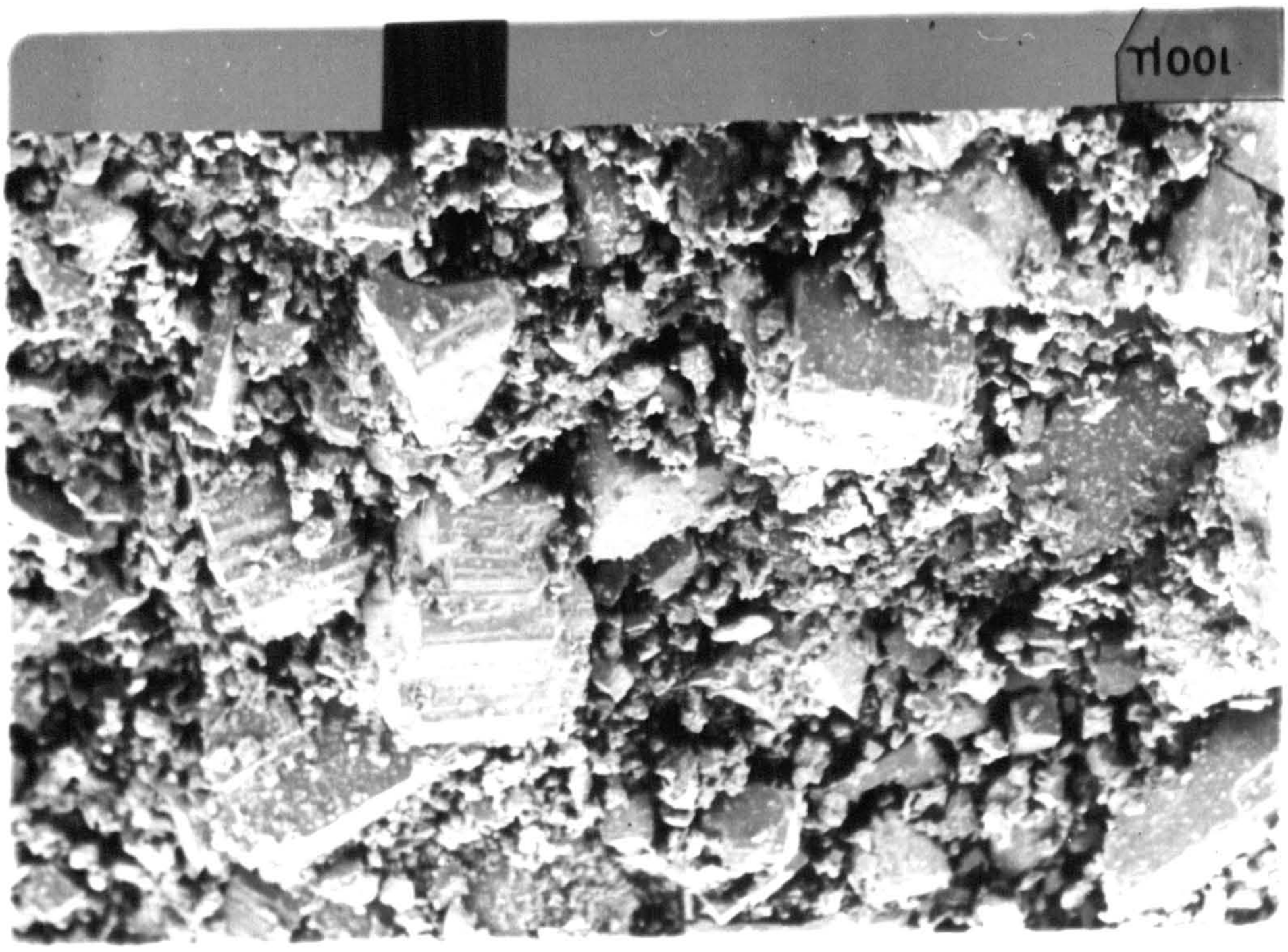
T1001

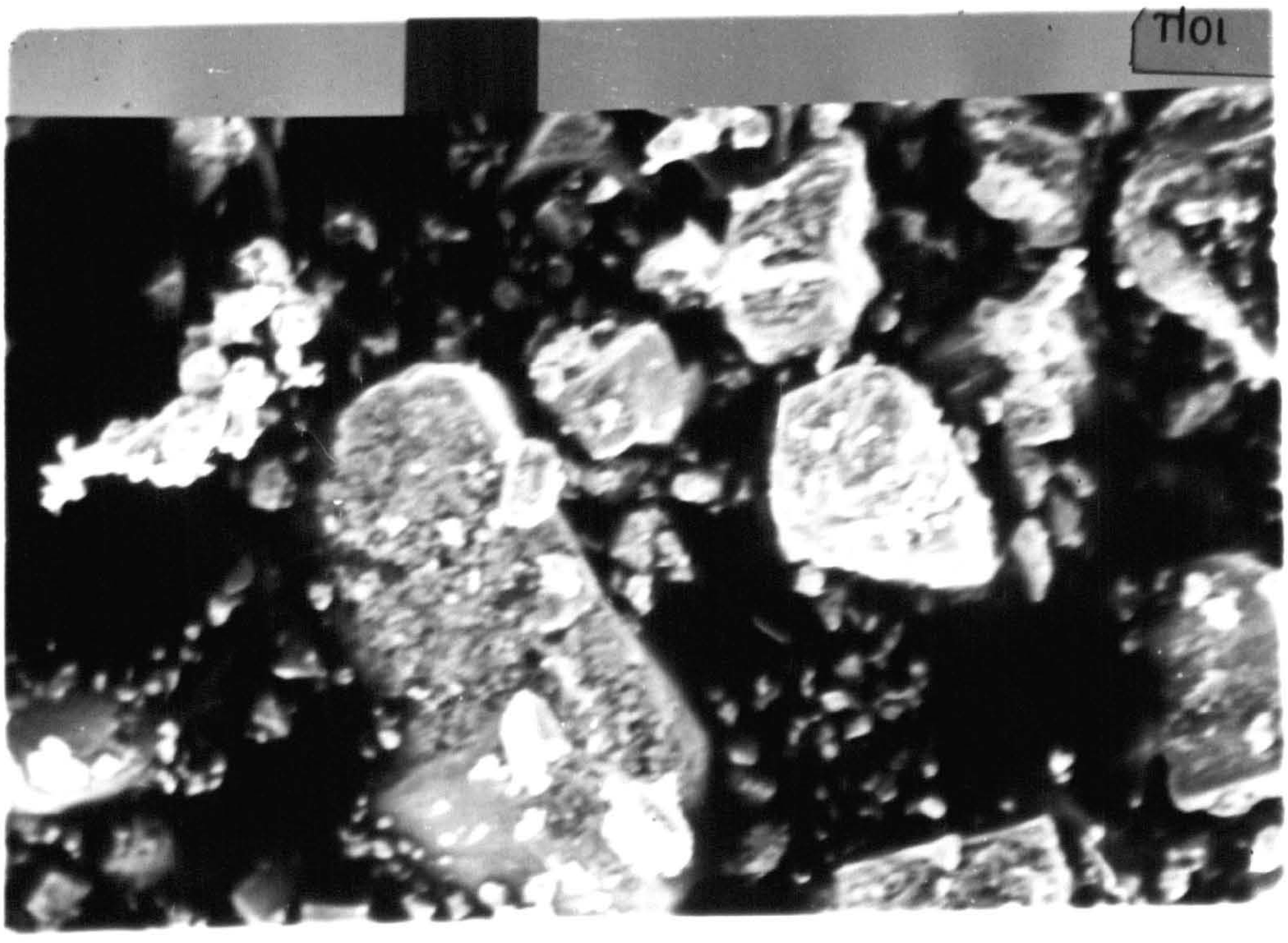
T101

performed.

Two lead sulphide Surma samples were selected which, according to electron microscopy measurements, had respective mean particle sizes of $90 \pm 20\mu$ and $30 \pm 20\mu$. Excess of each sample was added to separate, stirred portions of gastric fluid, obtained <u>in vivo</u> (as opposed to the simulated material), and maintained at a constant 36°. Aliquots of liquid were removed from each at fixed time intervals and after centrifuging and filtering made into solutions in which the lead content could be measured by atomic absorption spectroscopy. The results obtained (Table 7.5) show a marked increase in dissolution rate of the lead in the smaller particle size Surma when compared with the larger particle size material.

It can be seen that a plateau of about 480 mg/1000 cm^3 for the solubility of the lead in gastric fluid is reached in both samples. However, the time period is almost half in Surma B to Surma A. With the larger particles it would be possible for much of the material to pass away from a given absorption site before it could be rendered in a form suitable for absorption by either of the processes described.

It is notable that the value obtained for the solubility in real gastric juice is substantially lower than the measured solubilities of the Surma particles in the simulated gastric fluid. These disparities can readily be accounted for when the differing components, e.g. rennin, pepsin, and dissimilar viscosities between the two media are taken into consideration.

TABLE 7.5 Dependence on Particle Size of Solubility Rates of Lead Sulphide in Gastric Fluid

Time (minutes)	SOLUBILITY (mg/1000 cm^3) (Real Gastric Juice) SURMA A (particle size, 90μ)	SURMA B (particle size, 30μ)
10	60	311
20	121	346
30	170	376
40	230	408
50	245	430
60	260	441
90	365	460
120	422	473
180	474	478
270	473	481
420	-	480

A plot of these results is shown in Figure 7.7.

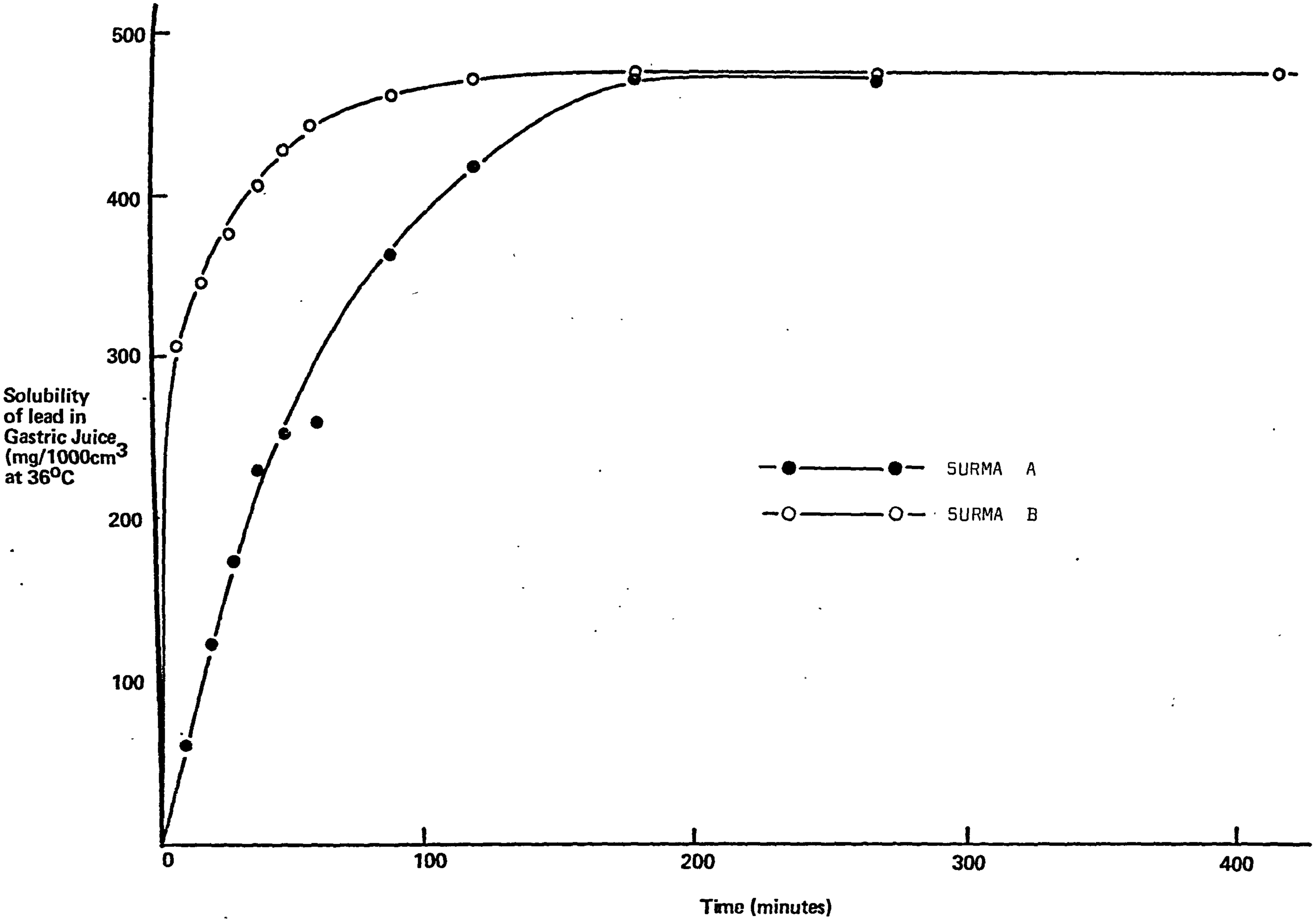

Figure 7.7 Dependence on Particle Size of Solubility Rates of Lead Sulphide in Gastric Fluid

Whilst the difference is a salutary comment on the value of physical data obtained from such simulated systems, nevertheless, the general increase in solubility observed with gastric fluid is still very considerable and therefore does not detract from the arguments made. The primary feature this experiment demonstrates is the fact that particle size is likely to affect absorption rate more through a limiting of the rate of release of lead into an available form in solution during the time the material remains within a given site, than through any change in absorption mode.

7.4.4 Factors Affecting the Absorption Process

In vivo other species than those ingested may have a role to play in absorption. For example, in this specific case, it is well known that the traditional Asian diet is generally high in phosphate. It is possible, therefore, that one of the species which may modify lead absorption after ingestion of Surma material may be a phosphate. Aub and Reznikoff[715] have proposed such a combination of lead with inorganic phosphate on the red cell membrane:

$$3PbCl_2 + 2\,Na_2HPO_4 \longrightarrow Pb_3(PO_4)_2 + 4NaCl + 2HCl$$

A concomitant reduction in lead absorption may, then, occur ($Pb_3(PO_4)_2$, solubility 1.34×10^{-4} g l^{-1} at $20^{o}C$). Although, as data discussed in the following Chapter shows, the interaction of lead with body-phosphate systems is not described by a single simple equation.

It is likely that food, especially as protein will increase the intestinal blood flow[716]. On the basis of the model proposed this would cause an enhancement in the pore-diffusion rate of Pb^{2+} which is perfusion controlled. However, a counterbalancing effect of food which may reduce any enhancement is the slowing in gastric emptying which will result. Other dietary factors, such as calcium intake levels have been mentioned (Section 7.4.2). A reduction in the amount of calcium and phosphate in the diet has been shown to increase the concentration of lead in the soft tissues[717,718].

Another possible modifying factor on absorption processes is the effect of stress. It is known that stress causes a reduction in splanchnic blood flow[719]. From observations we have made, it is clear that application of Surma induces a stressful state in the child. This may be sufficient to delay absorption, particularly with the larger particles ingested, and allow more lead to pass through the system than may otherwise have occurred.

Whilst the absorption of any heavy metal is unlikely to be a simple process, the model proposed appears to provide a rationale for explaining the clear relationship which has been demonstrated between ingestion of lead sulphide following the application of Surma, and an increased level of lead in the blood. In addition, it is not unreasonable to propose that other lead species will undergo similar reaction processes with the gastric juice and the same model, involving pore- and passive diffusion, could be applied

more generally. The data relating to rate of dissolution with particle size must also be relevant to other cases of lead exposure; the contaminated blackberry fruit (Chapter Six) being one example. It is known that the majority of aerosol lead emitted from vehicle exhausts is between 10μ and 0.2μ in diameter with a median about 2μ [720]. On this basis ingested lead from dust deposited on the blackberry fruit would be very rapidly absorbed. Sub-clinical levels of lead poisoning are, therefore, more likely to be attained.

REFERENCES

701 M. Aslam, Ph.D. Thesis, University of Nottingham (1979).

702 F.A. Alexander and H.T. Delves, Arch. Disease Childhood, (1972) 47 446.

703 A.R. Ali, O.R.C. Smales and M. Aslam, Brit. Med. J., (1978) 11 915.

704 S.D.R. Green, G.T.Lealman , M. Aslam and S.S. Davis, Publ. Health, London, (1979) 93 371.

705 P.S.I. Barry, Int. Symp. Envir. Hlth. Aspects of Lead (1972) Amsterdam.

706 R. Allcroft, J. Comp. Pathol and Therapeut., (1950) 60 190.

707 W.A. Ritschel, 'Laboratory Manual in Biopharmaceutics and Pharmacokinetics' (1974), Drug Intel. Publication, Illinois.

708 G.C. Harrold, J. Ind. Hyg. (1949) 31 327.

709 L.R. Karhausen, Int. Symp. Envir. Hlth, Aspects of Lead, (1972) Amsterdam.

710 M.R. Moore, Proc. Nutr. Soc., (1979) 38 243.

711 P.A. Meredith, M.R. Moore and A. Goldberg, Biochem, J., (1977) 166 531.

712 D. Winne and H. Ochsenfahrt, J. Theoret. Biol., (1967) 14 293.

713 R.E. Notari, 'Biopharmaceutics and Pharmacokinetics' 2nd Ed. (1974).

714 D. Baltrop and F. Meek, Arch. Envir. Hlth., (1979) 280.

715 J.C. Aub and P. Reznikoff, J. Exptl. Med., (1924) 40 189.

716 J.L. Brandt, L. Castleman, H.D. Ruskin, J. Greenwald and J.J. Kelly, J. Clin. Invest., (1955) 34 1017.

717 J.B. Shields and H.H. Mitchell, J. Nutrition, (1941) 21 541.

718 K.M. Six and R.A. Goyer, J. Lab. Clin. Med., (1970) 76 933.

719 M. Kampp and O. Lundgren, Acta Physiol. Scand., (1968) 72 282.

720 H.A. Waldron and D. Stöfen 'Sub-clinical Lead Poisoning' (1974) Academic, LONDON.

CHAPTER EIGHT

THE INTERACTION OF LEAD WITH BODY-PHOSPHATE SYSTEMS

8.1 INTRODUCTION

The pore-diffusion mechanism of ionic lead transport discussed in Chapter Seven can be visualised in terms of known chemical analogues in a number of absorption mechanisms, for example, molecular sieve systems. The passive diffusion process is less obvious, however, and requires a more detailed examination of the interaction between lead and biological components. In addition, it is reasonable to propose that if lead is capable of interacting with phosphorus systems involved in membrane structure, it is equally likely to affect other phosphorus systems within the body.

A number of texts have detailed the construction of biological membranes[801-803]. Whilst a comprehensive review of this subject is outside the mandate of this work, a brief outline of membrane structure is given in order to establish the nature and possible importance of any disruptive influence lead may have in this area. Similarly a survey of other major phosphorus-oxygen systems which may be involved in lead interaction is also included.

8.2 BIOLOGICAL MEMBRANES

8.2.1 Membrane Structure

There are two main components of any biological membrane : a protein and a lipid. The structural arrangement of these components varies widely between the various organisms and tissues depending on function. Several diagrammatic representations of the unit membrane structure have been proposed. One of the earliest was the Davson-Danielli model[804] (Figure 8.1a) which encompassed a lipid bilayer with polar groups exposed at the surface and the hydrocarbon fatty acid occupying the interior. A fixed globular protein layer forms the outer covering of the membrane. Robertson[805] modified this basic arrangement with the benefit of electron microscopy data and, whilst leaving the arrangement of the lipid bimolecular leaflet intact, replaced the globular protein layer by a more realistic polypeptide or polysaccharide chain (Figure 8.1b). Singer and Nicolson[806] subsequently re-examined this problem and proposed what appears to be a more satisfactory model with respect to experimental data. In principle they again envisage a mosaic structure with a lipid bilayer, but this is interspersed with integral globular proteins extending into, and passing through the system (Figure 8.2). The peripheral proteins associated with the exposed polar faces of the bilayer and occupying the spaces between the globular proteins are not depicted in this model. The basis for this being that

Figure 8.1 Diagrammatic representation of the unit membrane structure

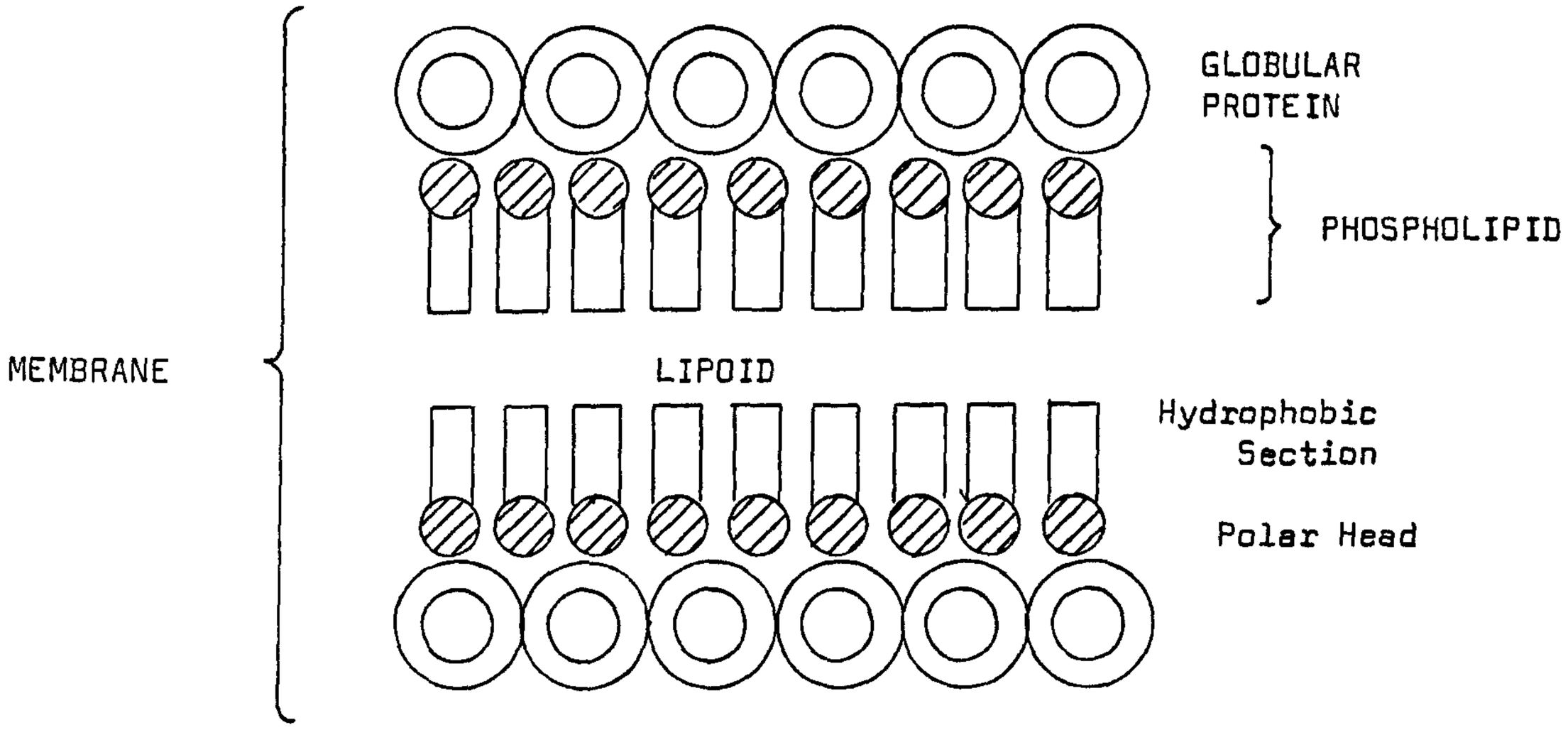

8.1a Davson-Danielli Model

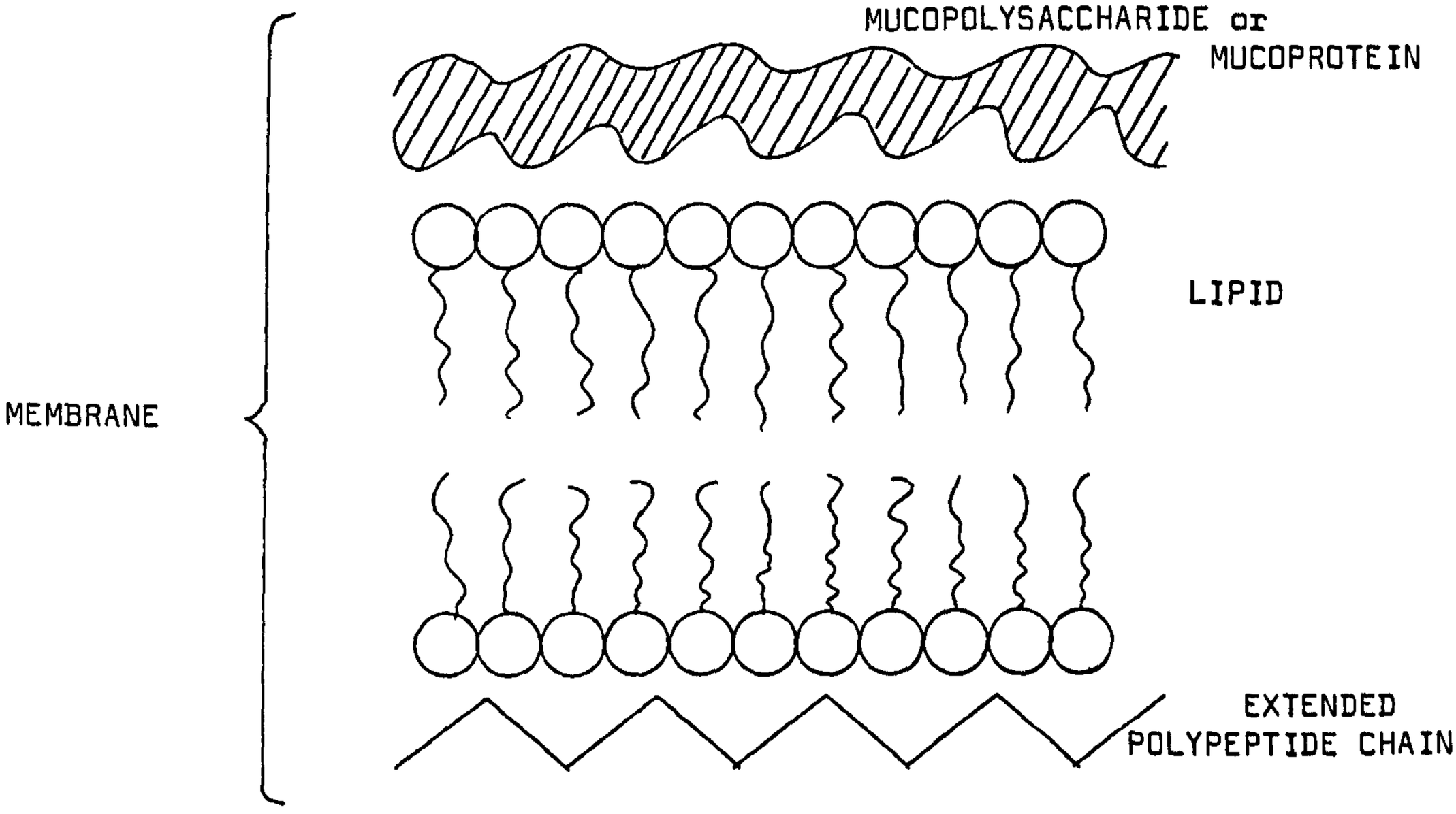

8.1b Robertson Modification

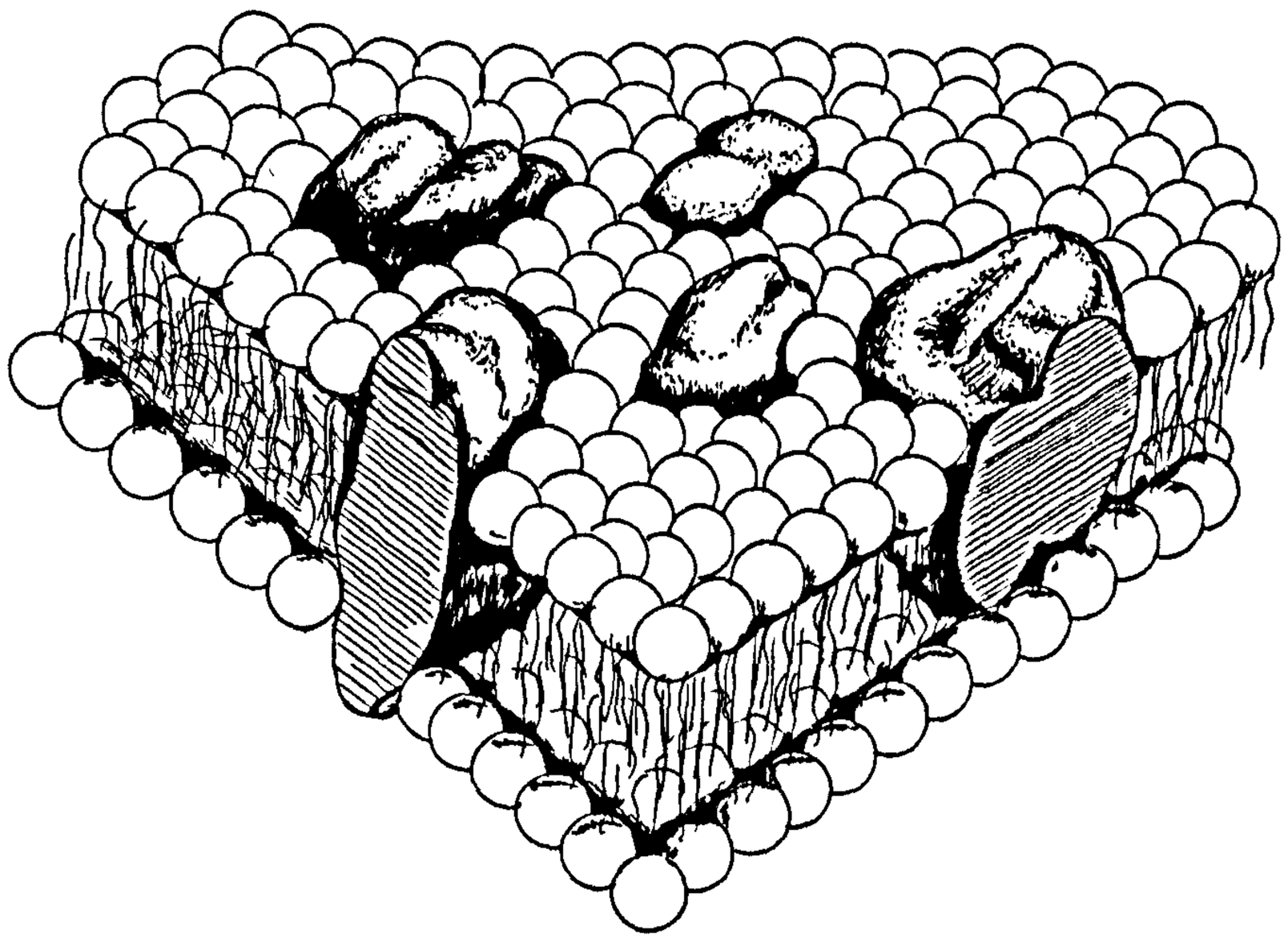

Figure 8.2 The Singer-Nicolson model of membrane structure.

Some of the globular proteins extend into the phospholipid bilayer and others extend through.

these proteins have mobility across the plane of the membrane and are not associated with a specific site.

A convenient cross-sectional 'picture' of a membrane structure which appears to satisfy experimental data, and is of assistance for the understanding of the basis for our model of absorption, involves considering the lipids to be associated in small globular micelles (Figure 8.3).

Figure 8.3 Membrane Components (Not to scale)

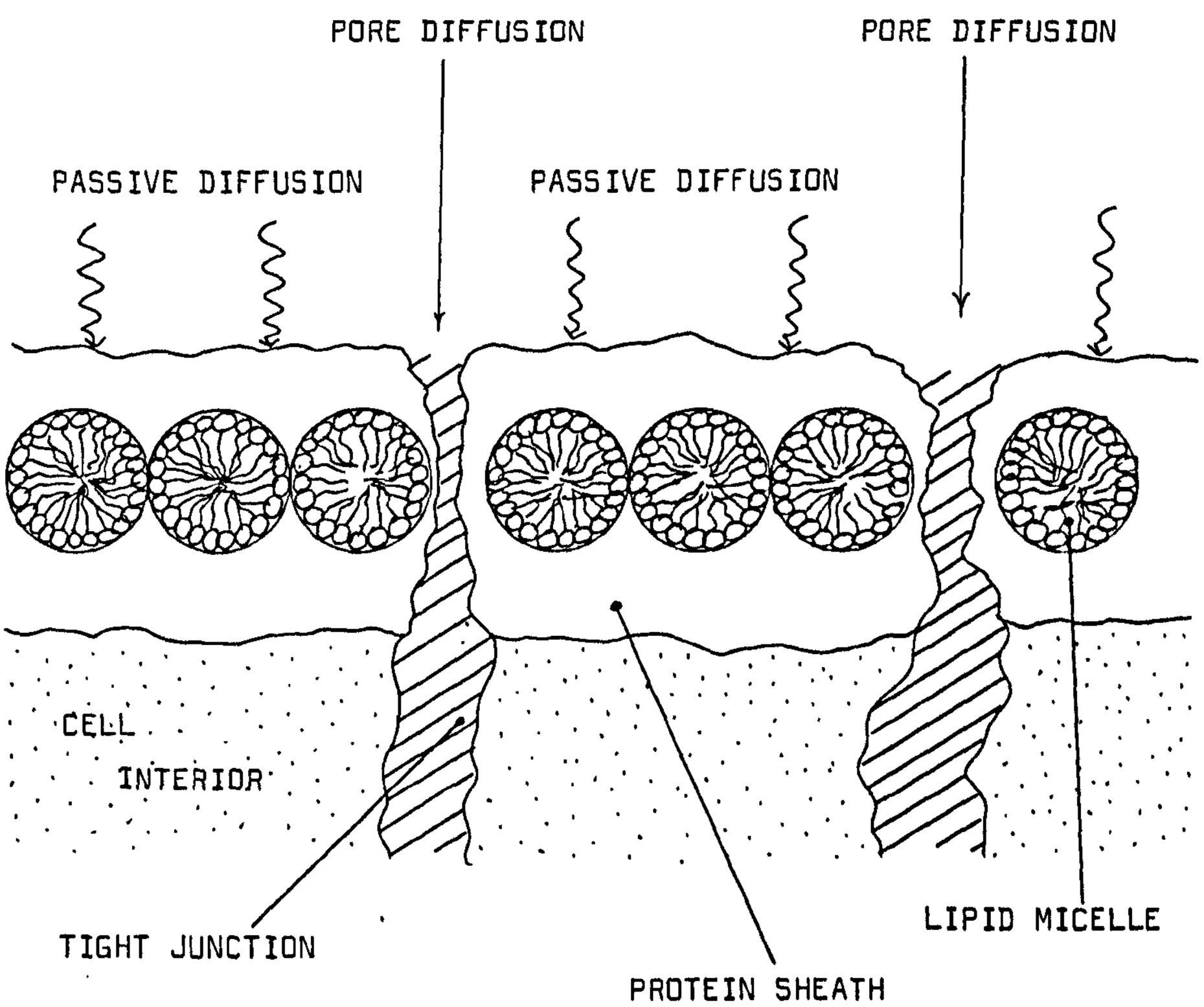

Figure 8.4 The relationship of the surface membrane to the whole cell structure of intestinal mucosal cells.

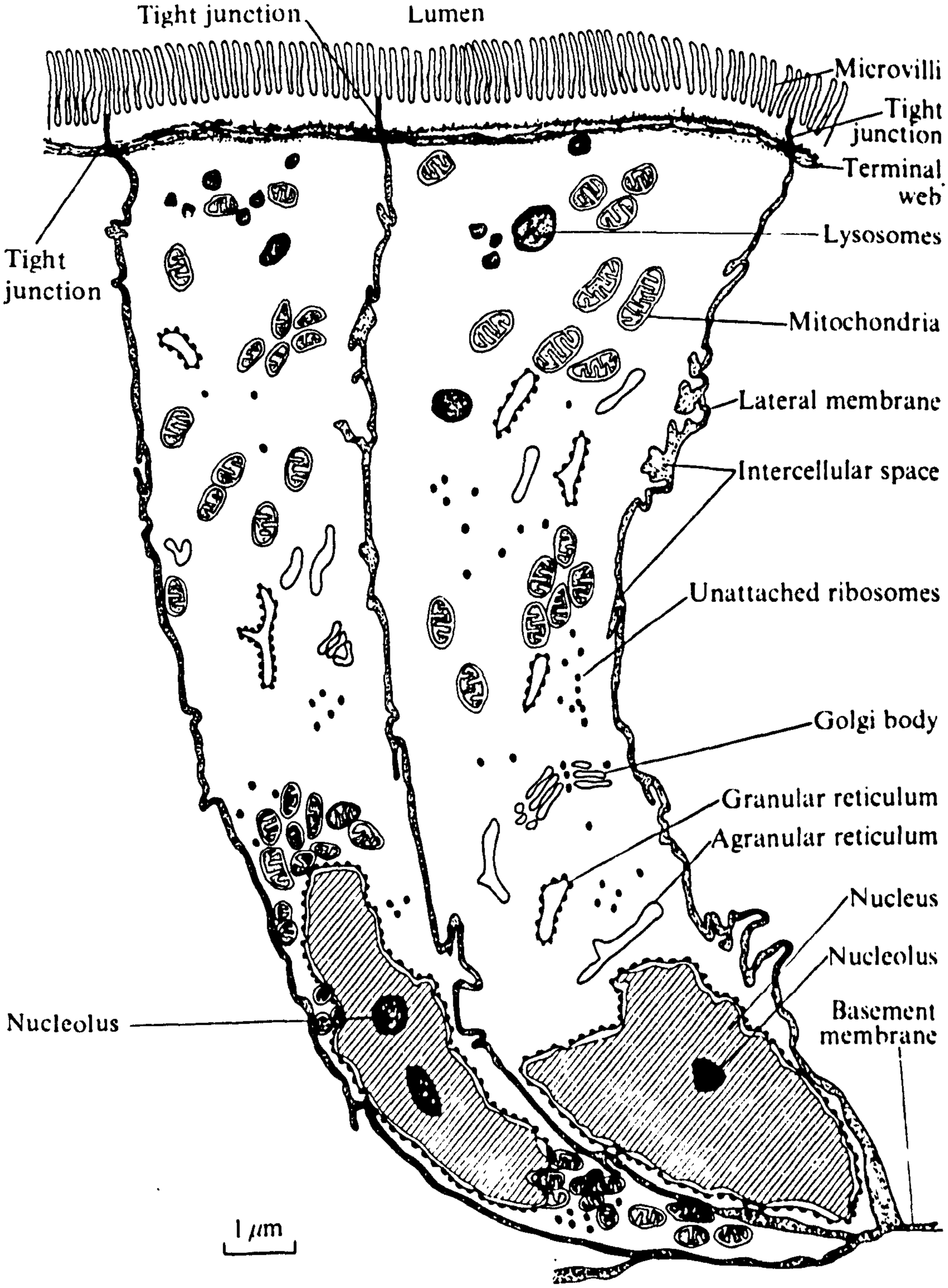
Tight junction
Lumen
Microvilli
Tight junction
Terminal web
Lysosomes
Tight junction
Mitochondria
Lateral membrane
Intercellular space
Unattached ribosomes
Golgi body
Granular reticulum
Agranular reticulum
Nucleus
Nucleolus
Basement membrane
Nucleolus
1 μm

These micelles are arranged in a plane and are encased on each side by a protein layer. Adjacent cells in the epithelial sheet are bound together at 'tight junctions' through which pore diffusion can occur. The relationship of this surface membrane to the whole cell system is illustrated by Figure 8.4 which is a diagram taken from an electron microscope picture of two adjacent intestinal mucosal cells[801].

8.2.2 Membrane Components

The lipid moiety of the membrane is held together by hydrophobic bonds. These are, of course, a direct consequence of the amphipathic nature of the lipids, which in the case of biological membranes are, specifically, phosphoglycerides (also called glycerol phosphatides).

The initial compound of the series is the phosphoric ester of glycerol, (I),

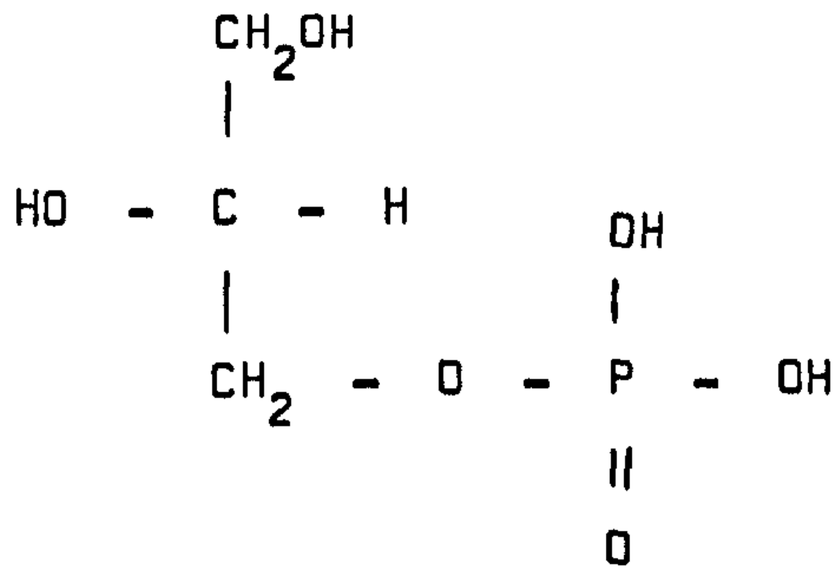

(I)

L - Glycerol - 3 - phosphoric acid.

In nature the remaining hydroxyl groups of the glycerol are esterified by fatty acids (linoleic, linolenic, oleic etc), giving the parent compound, phosphatidic acid, (II).

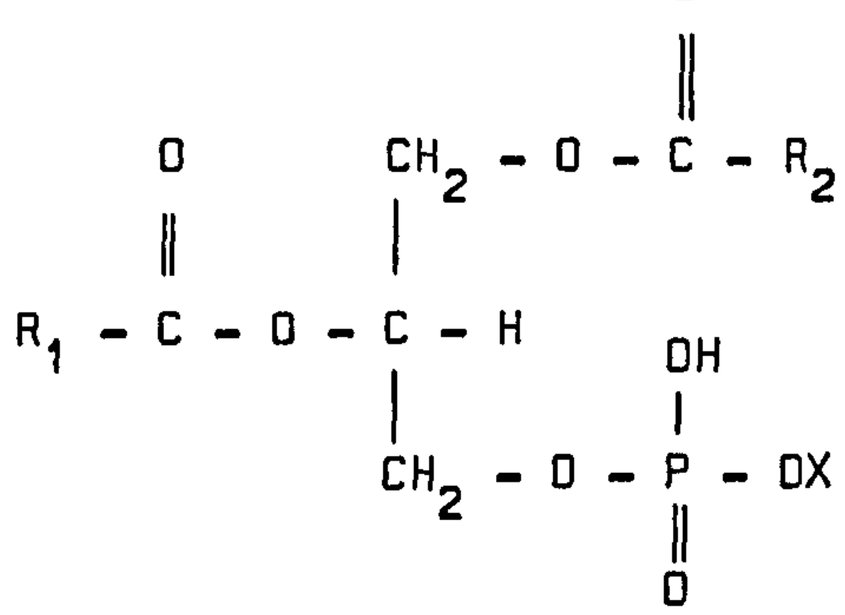

(II)

X = H = phosphatidic acid

Phosphatidic acid is found in only small quantities in nature, but insertion into X of the aminoalcohols, ethanolamine and choline produces, respectively, phosphatidylethanolamine and phosphatidylcholine (Table 8.1). Together these provide the main constituents of animal cell membrane (Table 8.2).

One other important group of phosphate compounds in animal membrane structure is the sphingomyelins. These consist of a sphingolipid with a phosphorylcholine or phosphorylethanolamine polar head group esterified to the 1-hydroxyl group of ceramide, (III),

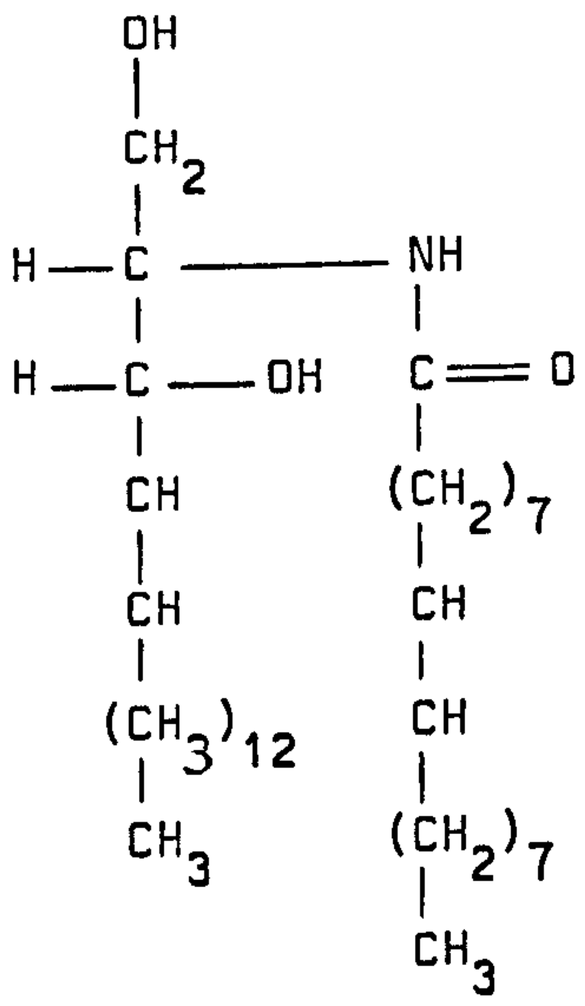

III Ceramide

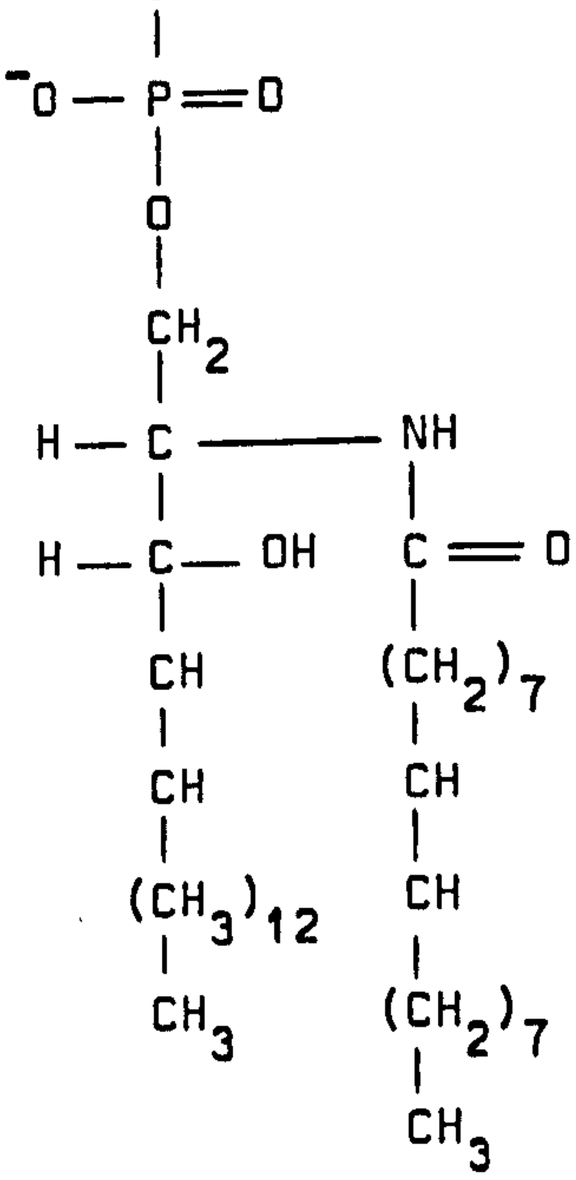

IV Sphingomyelin

Table 8.1 Polar Head Groups of the Principle Phosphoglycerides found in Human Tissue

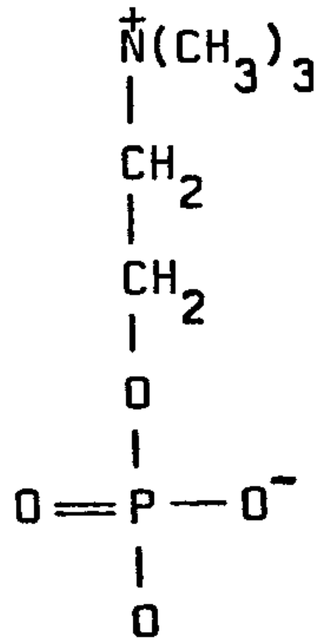

Phosphatidylcholine
(Lecithin)

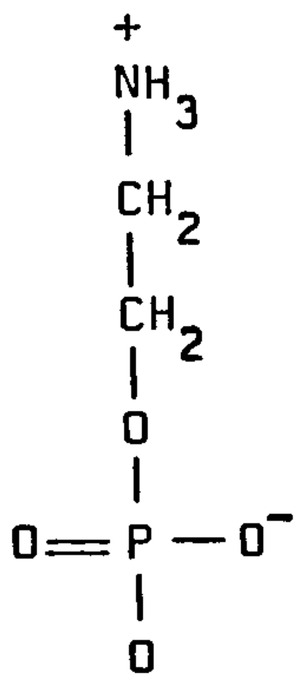

Phosphatidylethanolamine

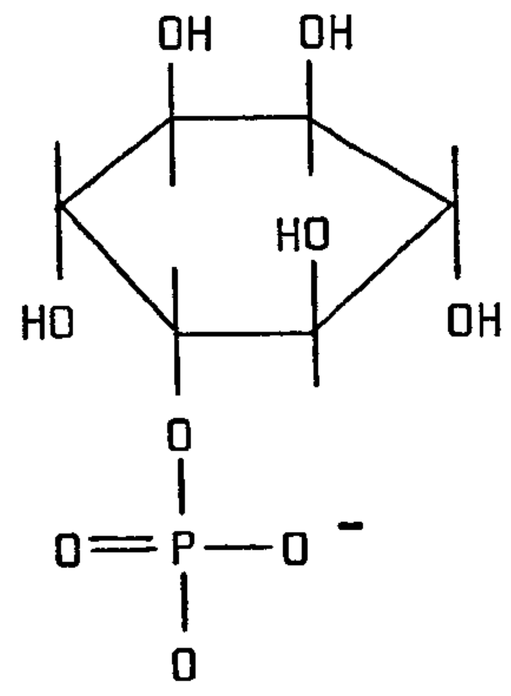

Phosphatidylinositol

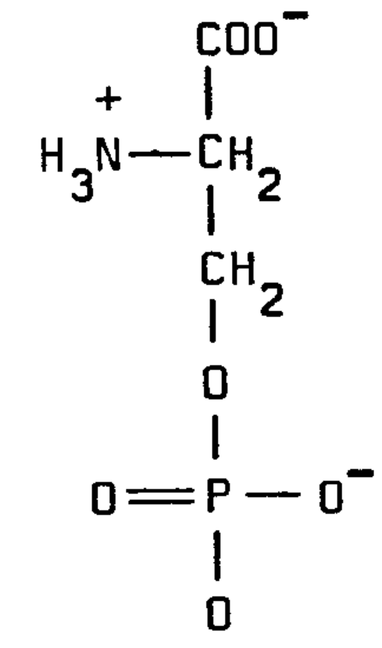

Phosphatidylserine

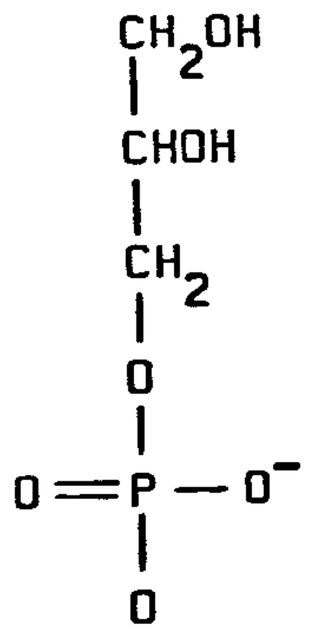

Phosphatidylglycerol

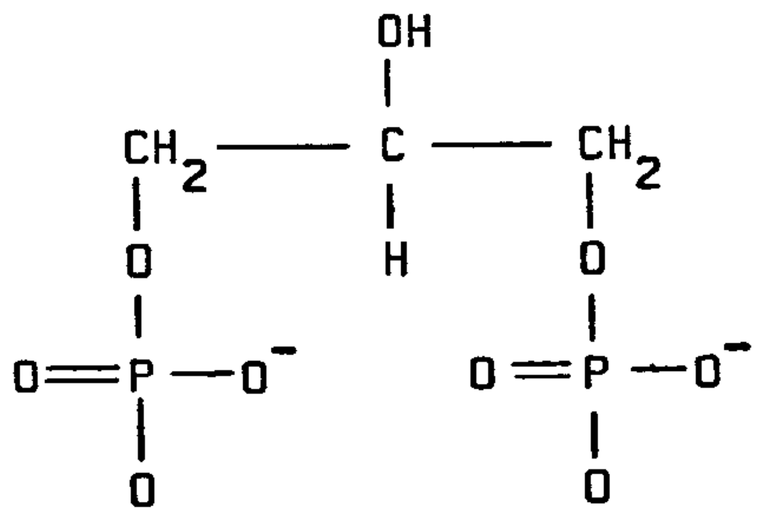

Diphosphatidylglycerol
(Cardiolipin)

Table 8.2 The principle phospholipid components of some human tissues[807]

TISSUE	INTESTINE	HEART	LUNG	KIDNEY	SPLEEN	LIVER	SKELETAL MUSCLE
	Percentage by weight						
Phosphatidyl-choline	53.5	40.0	47.5	33.1	41.2	43.6	55.7
Phosphatidyl-ethanolamine	25.4	26.3	17.5	27.4	24.5	27.9	21.9
Phosphatidyl-inositol	4.1	6.1	3.2	5.5	4.4	8.6	6.0
Phosphatidyl-serine	5.2	2.7	7.0	6.4	8.3	3.1	4.2
Phosphatidyl-glycerol	-	0.6	2.5	0.6	0.3	-	-
Diphosphatidyl-glycerol	2.8	9.0	1.0	4.2	1.0	3.7	4.7
Phosphatidic acid	3.2	0.2	0.5	0.4	0.2	0.7	0.3
Sphingomyelin	5.8	4.9	11.1	12.0	12.8	4.6	5.6

Sphingomyelin, phosphatidylcholine and phosphatidylethanolamine are zwitterions at pH 7 and thus have no net electric charge. Phosphatidylserine (Table 8.1), on the other hand, has a polar head group containing an α-amino and a carboxyl group which are both negatively charged at pH 7, giving a net negative charge to the molecule. This variation in the polarity of the head group and the size and shape of the molecule itself, modifies the mode of action and role played in membrane structure of the lipid. Similarly, the primary structure of the polypeptide and protein sheathing of the lipid bilayer and globular protein insertions is variable, depending upon the function of the particular epithelial system involved. The chemical nature of these surface coatings is, at present, not well understood. The outer layer of the membrane has a mucoprotein covering giving the characteristic jelly-like surface, which may be either slippery or sticky depending on function.

The mucoproteins consist of acid mucopolysaccharides complexed through the acid carboxyl or sulphuryl group to a specific protein. The most abundant mucopolysaccharide being hyaluronic acid (V).

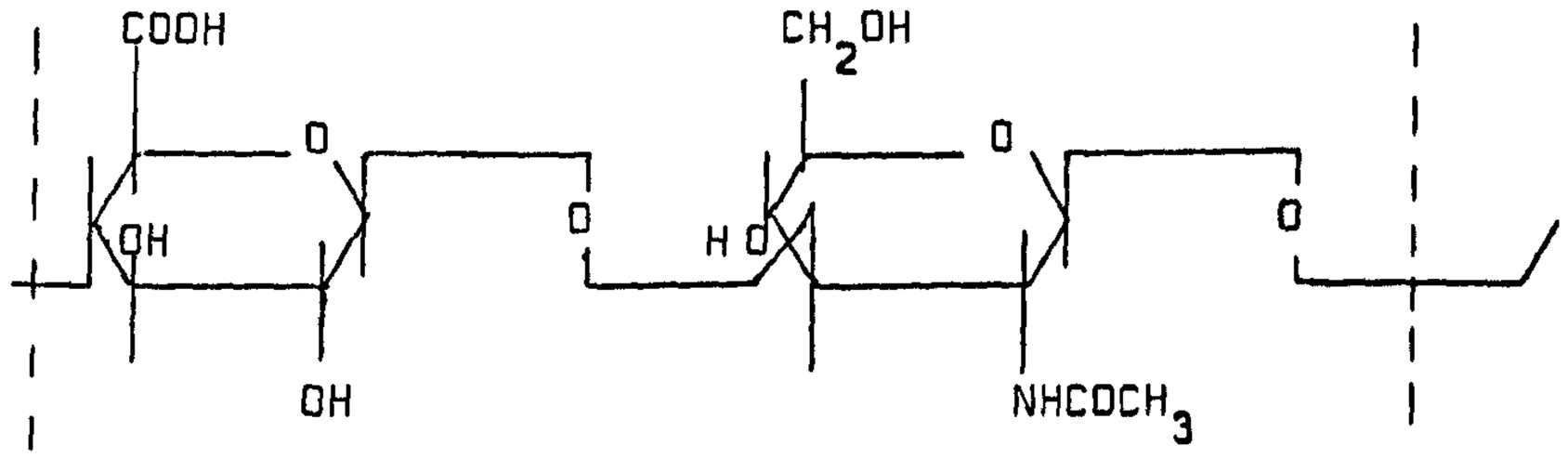

(V)

D-Glucuronic Acid N-Acetyl-D-glucosamine

Repeating unit of hyaluronic acid.

Whilst binding of lead to such protein systems is of considerable interest, and future work is proposed in this field, the main emphasis in this study is towards the interaction of the metal with body-phosphate systems. Therefore, the nature of the protein involvement is discussed no further.

8.3 NUCLEOTIDES AND NUCLEIC ACIDS

There are a number of phosphate systems of equal importance and ubiquity to the phospholipids of cell membranes. If interaction occurs between lead and phosphoglycerides, it is of equal probability that reaction will also proceed with these other body-phosphate systems.

Calcium phosphate in the hydroxyapatite form, $Ca_5(PO_4)_3OH$, is, of course, the primary inorganic structural component of bone and teeth (Section 8.5) and the storage and distribution of lead within bone has been extensively studied (Chapter Five). A similar contribution is made by sugar-phosphates which provide the skeletal backbone of nucleic acids. However, additional to these framework roles of phosphate so far discussed, is its use as a universal currency of energy in living organisms. From primary biosynthesis, through ion transport across membranes, to muscle contraction, the driving force is phosphoryl (PO_3) group transfer from high to low energy acceptors using, primarily, nucleotide systems.

Nucleotides are constructed from three main units : a

heterocyclic base, the ribose sugar unit, and a mono-, di- or triphosphate group. The heterocyclic base is either a purine (e.g. adenine or guanine), or a pyrimidine (e.g. Uracil, thymine or cytosine) derivative (Table 8.3). The general formula is thus:

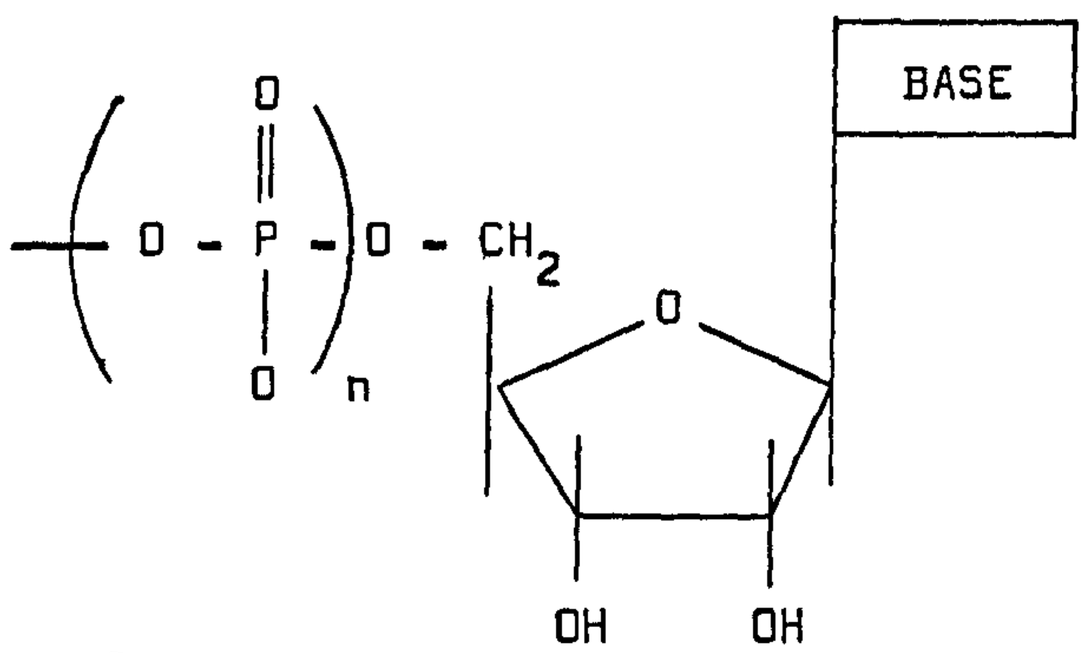

where n = 1, 2 or 3.

With the nucleic acids RNA and DNA, adenine, guanine, cytosine and uracil are the bases forming the most common ribonucleotides in RNA, and three of the above, together with oxygen loss at the 2' position on ribose gives the principle deoxyribonucleotides in DNA. Uracil is, however, replaced by thymine in DNA.

Of primary interest with respect to the energy processes mentioned are the adenosine-5'-mono-, di-, and triphosphates (AMP, ADP and ATP). The phosphodiester bond has considerable free energy of hydrolysis.

Table 8.3 Principle Purine and Pyrimidine Bases

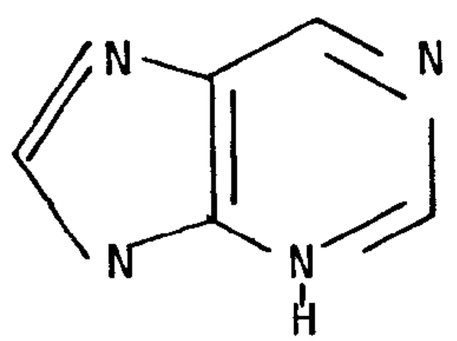

Purine : Parent Compound

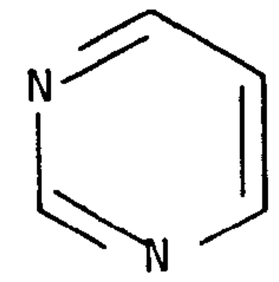

Pyrimidine : Parent Compound

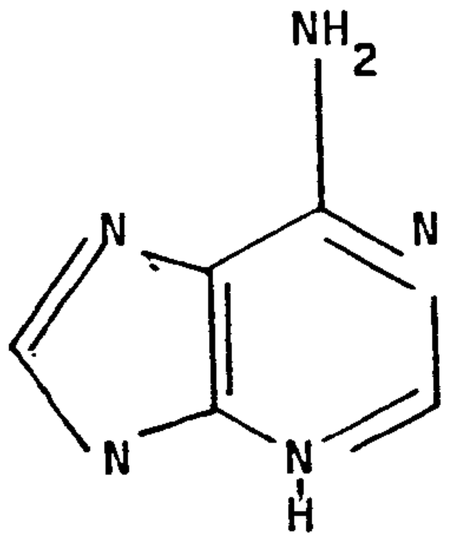

Adenine (6-amino purine)

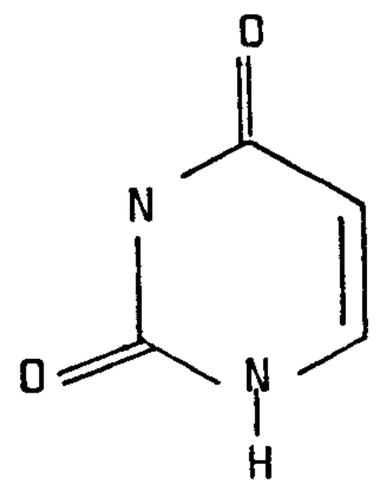

Uracil (2,4-dioxopyrimidine)

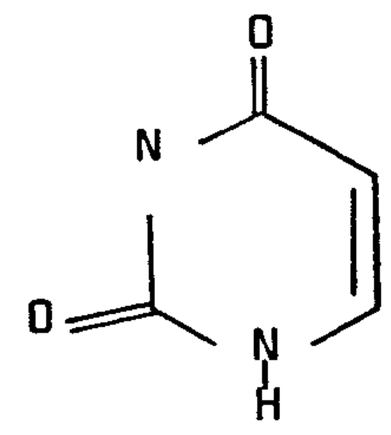

Thymine (5-methyl-2,4-dioxopyrimidine)

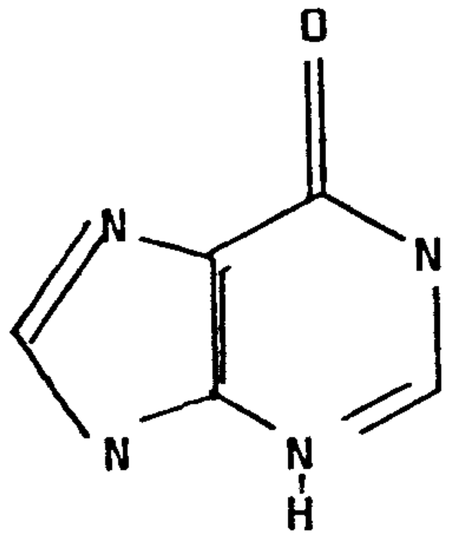

Guanine (2-amino-6-oxopurine)

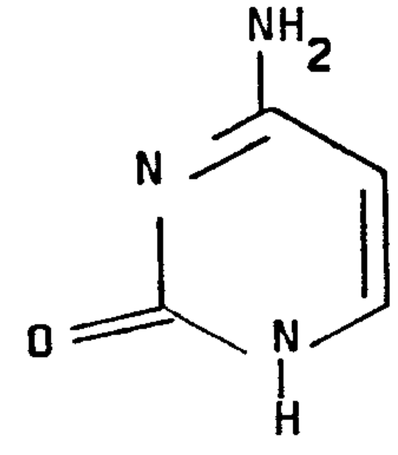

Cytosine (4-amino-2-oxopyrimidine)

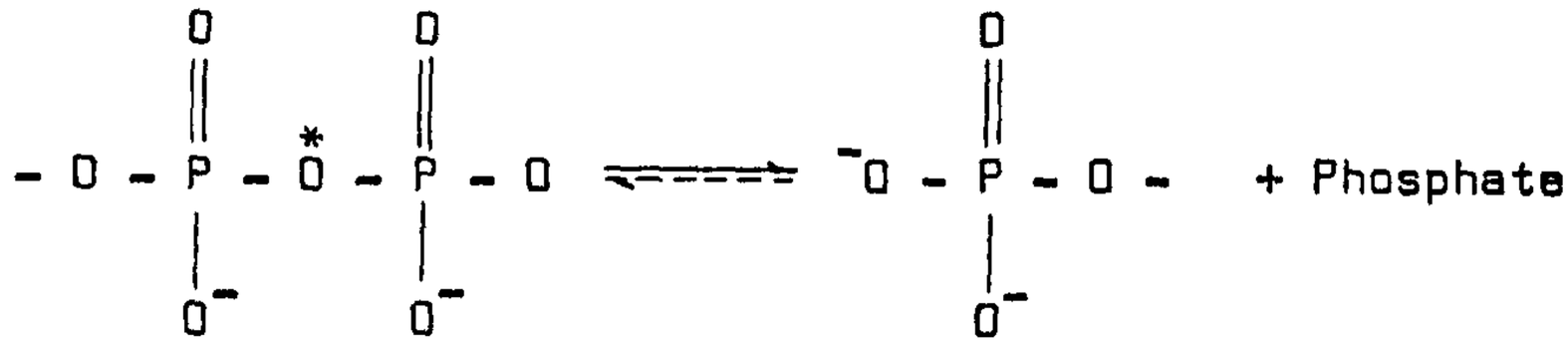

$$\Delta G^{O} = -7000 \text{ cal/mole}$$

* phosphodiester bond.

and for the specific reactions

$$ATP \rightleftharpoons ADP + Phosphate$$

or $$ATP \rightleftharpoons AMP + Pyrophosphate$$

ΔG^{O} = -7400 and -7600 cal/mole respectively. The effectiveness of these types of reaction in energy transfer is, perhaps, best illustrated by an example. Consider the reaction

$$\text{ribulose - 5 - phosphate} + \text{phosphate} \rightleftharpoons \text{ribulose - 1,5 - diphosphate}$$

The product is used in the biosynthesis of, *inter alia*, carbohydrates. However, ΔG^{O} for the reaction is + 3200 cal/mole. Bearing in mind

$$\Delta G^{O} = -RT \log_{e} k$$

$$\text{i.e.} \qquad \Delta G^{o} = -1364 \log_{10} k,$$

then for the above reaction

$$k = \text{antilog} - \frac{3200}{1364}$$

$$= 4.6 \times 10^{-3}$$

<u>against</u> formation of the product. However, if the above reaction is modified to:

ribulose - 5 - phosphate + ATP

$\rightleftharpoons$ ribulose - 1,5 - diphosphate + ADP

then $\Delta G^{o} = +3200 - 7400$ cal/mole

$= -4200$ cal/mole

and $k = \text{antilog}_{+} \frac{4200}{1364}$

$= 1.2 \times 10^{3}$

in favour of the product.

There are a number of similar systems to the adenosine phosphates which also take part in coupling reactions. A few of these materials, such as nicotinamide adenine dinucleotide phosphate, (NADP), and coenzyme A (Table 8.4) act as cofactors or prosthetic groups in enzyme systems. As many hundreds of such reactions occur within the body, any interruption in these processes would have drastic effects. Do heavy metal interactions occur within

Table 8.4 Phosphate enzyme cofactors and prosthetic groups

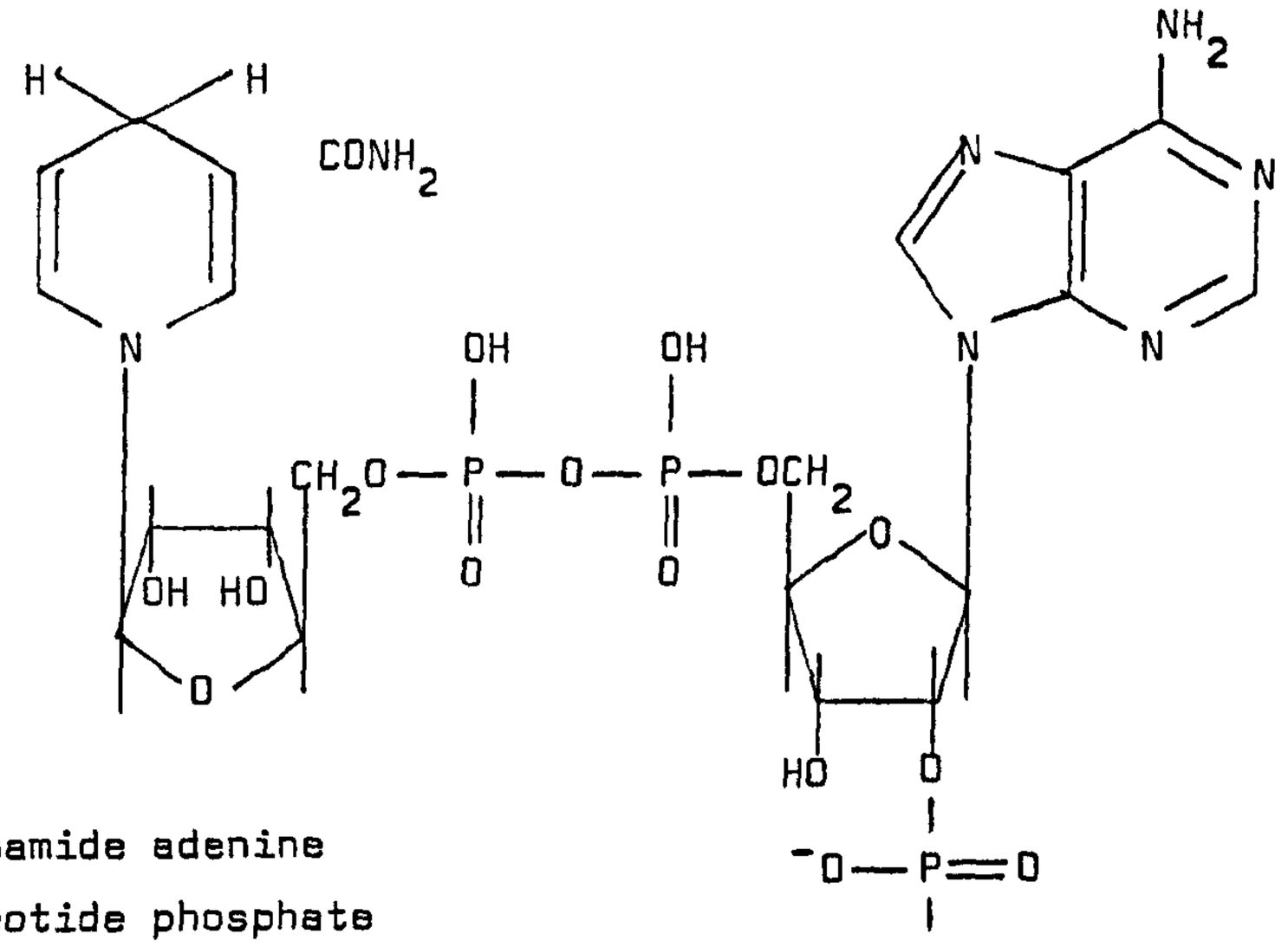

Nicotinamide adenine dinucleotide phosphate ($NADPH_2$)

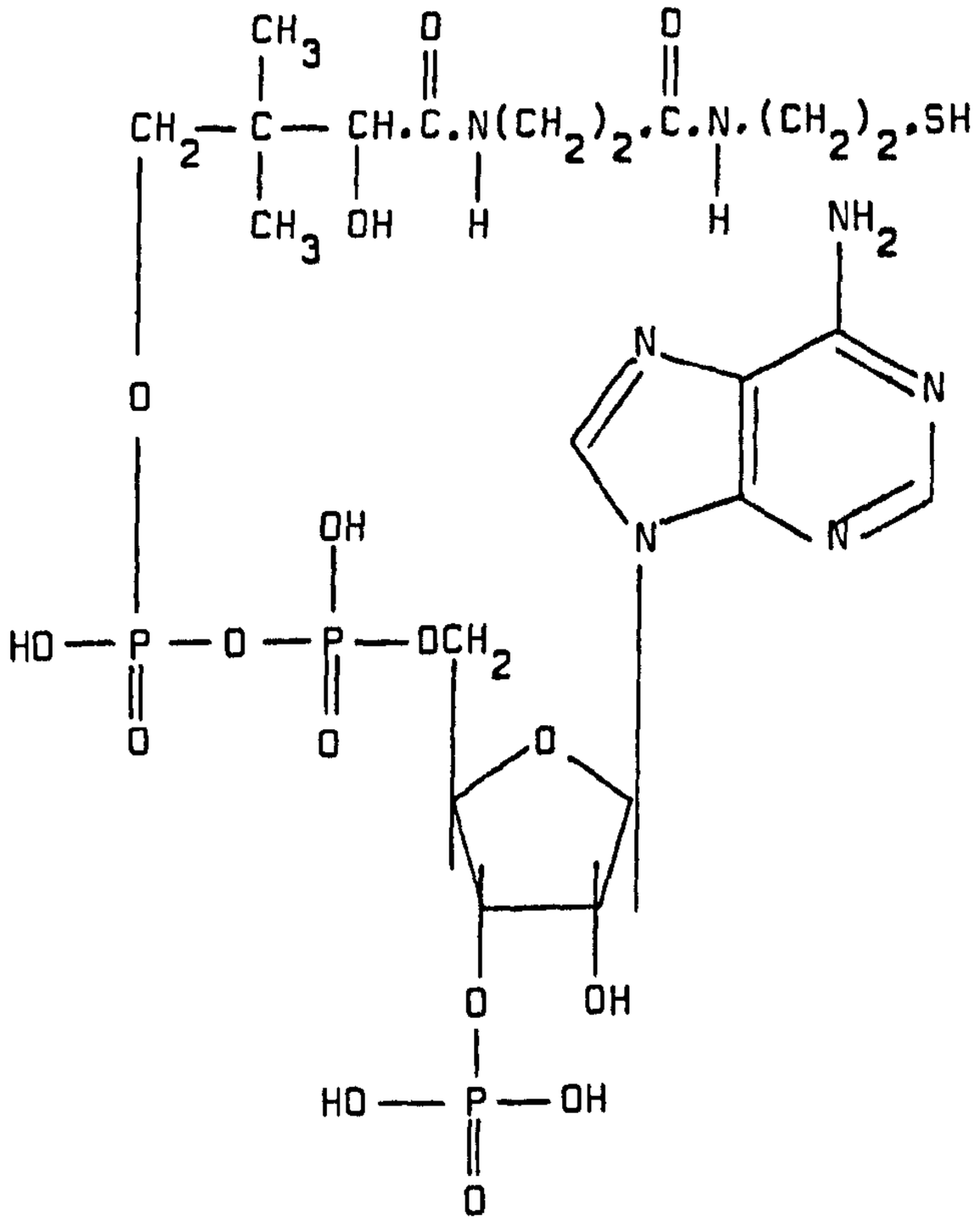

Coenzyme A (CoASH)

these systems and are they significant at low concentrations such as those associated with sub-clinical lead poisoning? It is in an attempt to answer questions such as these that our studies have been addressed.

8.4 A CHEMICAL MODEL FOR LEAD INTERACTIONS WITH BODY-PHOSPHATE SYSTEMS

8.4.1 Choice of Model

As the foregoing has illustrated, the substituted methoxyl-phosphoryl bond system is ubiquitous throughout the body. However, in vivo it is generally present as a moiety of a complex macromolecular unit. Therefore, in order to establish possible modes of interaction with lead it is more sensible to first examine a representative, but simpler, model. For this study dimethylphosphite (DMP) (VI) was chosen:

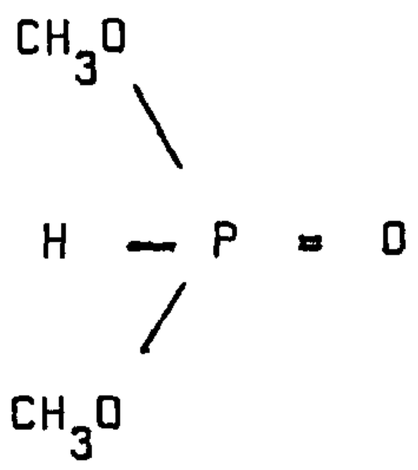

(VI)

Dimethylphosphite is a colourless, neutral liquid with a boiling point of 170°C and a molecular weight of 110.05. It is soluble in organic solvents and water, and is readily characterised by

spectroscopic techniques, particularly n.m.r., where the splitting produced by the single proton enables each site around the phosphorus atom; the individual methoxyl groups and the P-H bond itself, to be monitored independently. Additionally the ν(P-H) in the infrared spectrum is in a region clear of other interfering absorptions and is therefore also diagnostic. For these reasons it was chosen in preference to trimethylphosphate (VII)

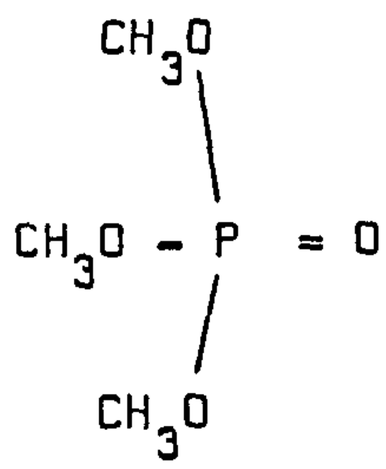

(VII)

which, although arguably more akin to the <u>in vivo</u> systems, has indistinguishable methoxyl groups and is, therefore, a less sensitive probe for interactions.

Choice of the lead system for use in this study is inhibited by the, generally, poor solubility of its compounds. However, lead(II) acetate, trihydrate, $Pb(OCOCH_3)_2.3H_2O$, is ideal, in that it has a satisfactory aqueous solubility (44.3g/100cm^3 at 20^o) and dissolves in both water and organic solvents such as methanol, thus allowing both neutral and ionic media to be investigated.

8.4.2 <u>Reactions of Dimethylphosphite with Lead(II) Acetate, Trihydrate</u>

The reactants used were commercial samples and were checked

for purity by spectroscopic measurements and by boiling point determination of the organic liquid. The initial reaction performed was as follows.

To 100 cm^3 of dried, freshly distilled methanol contained in a two-necked flask was added 404 mg (10.6 mM) of $Pb(OCOCH_3)_2.3H_2O$. After dissolution of the lead salt, 119 mg (10.8 mM) of dimethylphosphite (DMP) was injected dropwise to the stirred solution. After about 30 seconds the solution became cloudy and within five minutes reaction appeared to be complete. A small quantity of a white precipitate resulting. The supernatent liquid was decanted and aliquots centrifuged to remove suspended solid. The solid, combined, was then washed several times in methanol, followed by 3 x 50 ml of sodium dried diethyl ether. The resulting product was dried to a fine powder on a vacuum frame. A yield of 459 mg was achieved (87.8% for a 1 : 1 adduct). This dried material was then stored overnight in a sealed flask under argon. However, after 16 hours storage, subsequent examination revealed the formation of a small quantity of liquid and the product was no longer in a fine powder form, but had partially congealed. After further washing of the product an elemental microanalysis was made which gave the results C, 13.50; H, 3.17%. A 1 : 1 product requires C, 14.7 and H, 3.8%. The above reaction was, therefore, repeated in the same proportions but with a more concentrated (50 mM) medium. An identical preparative procedure was followed but immediately after washing and drying an elemental microanalysis was made. This gave the results C, 14.36;

H, 3.62; Pb, 40.8%. The 1 : 1 product $C_6H_{19}O_{10}PPb$ requires C, 14.7; H, 3.8 and Pb, 42.3%. Lead analyses were made by atomic absorption spectroscopy in the usual way. The material therefore analysed as the 1 : 1 adduct of dimethylphosphite and lead(II) diacetate, trihydrate (VIII).

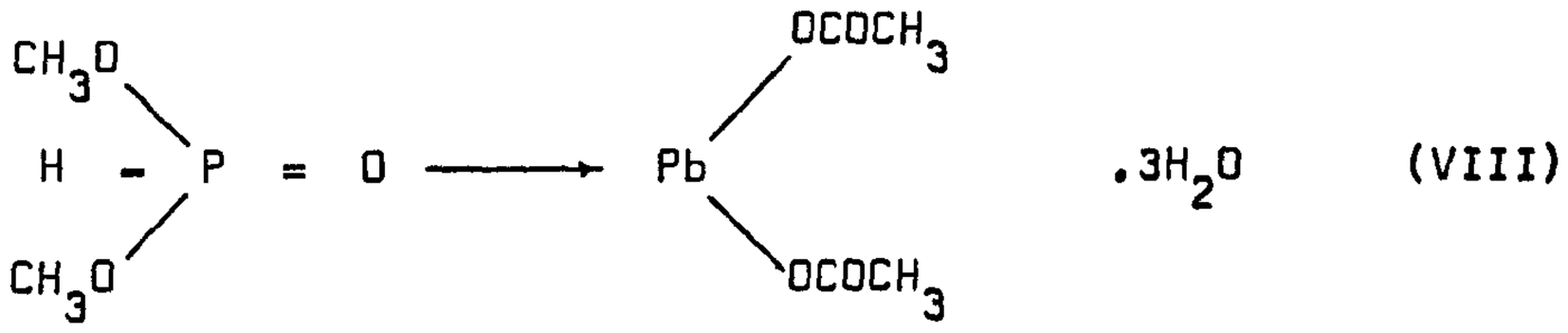

(VIII)

Further support for this proposal was found in the infrared data for the product. The spectrum (Table 8.5, Figure 8.5) was obtained as a KBr disc and shows bands characteristic of both the component systems. The ν(P-H) at 2430 cm^{-1} in DMP shows no change in frequency but the line width is markedly reduced in the product. Of much greater significance is the effect on the ν(P=O). In the free ligand this is found as a strong line at 1250 cm^{-1}, but in the adduct is absent at this frequency. Instead a new, strong band, not observed in the ligand occurs at 1140 cm^{-1}. This, therefore, is assigned to the ν(P=O). The shift of 110 cm^{-1} is a clear indication of strong phosporyl ⟶ lead coordination. A small change in the ν(P-O) from 973 to 997 cm^{-1} is also observed, possibly reflecting a weakening in the bond strength of that

Table 8.5 Infrared spectroscopic data for DMP, $Pb(OCOCH_3)_2.3H_2O$ and the 1 : 1 adduct

$Pb(OCOCH_3)_2.3H_2O$ [1]		DMP [2]		1 : 1 Adduct [1]	
Frequency (cm^{-1})	Assignment	Frequency (cm^{-1})	Assignment	Frequency (cm^{-1})	Assignment
		3520	combination		
3420 b.s.	ν_{as}(O-H)	3475		3430 b.s.	ν_{as}(O-H)
3280 b.s.	ν_{s}(O-H)			3280 b.s.	ν_{s}(O-H)
2995 w.	ν (C-H)	2995 m.	ν (C-H)	2995 m.	ν (C-H)
2960 w.		2950 m.		2970 m.	
2918 w.		2905 m.		2940 m.	
		2847 m.		2840 m.	
		2430 b.m.	ν (P-H)	2430 sh.m.	ν (P-H)
1540 b.s.	ν_{as}(COO)			1535 b.s.	ν_{as}(COO)
		1457 m.	δ_{as}(C-H)		
1405 b.s.	ν_{s}(COO)			1412 b.s.	ν_{s}(COO)
1335 s.	δ_{as}(C-H)			1337 m.	$\delta_{as}(CH_3)$
		1250 s.	ν (P=O)		
		1180 m.	ν_{as}(P-(O-C))	1180 m.	ν_{as}(P-(O-C))
				1140 s.	ν (P=O)
		1072 m.			

1043 m.	δ_s(C-H)			1047 m.	$\delta_s(CH_3)$
1015 m.		1037 s.	} ν (P-O)	1028 s.	} ν (P-O)
		973 s.		997 s.	
932 m.	ν (C-C)			932 m.	ν (C-C)
		820 w.			
		778 s.	ν_s((P-O)-C))	774 s.	ν_s((P-O)-C)
		760 w.			
660 s.	δ_s(OCO)			660 s.	δ (OCO)
612 m.	(COO) o.o.p.			613 m.	(COO) o.o.p.
		545 w.	δ_{as}(OCO)	545 s.	δ_{as}(OCO)
		502 w.			
467 w	δ_{as}(OCO)			460 w.	
		453 w.			
		403 w.	δ_s(OCO)	408 w.	δ_s(OCO)

1. KBr disc
2. Liquid film on AgBr

b, broad; sh, sharp; w, weak; m, medium; s, strong.

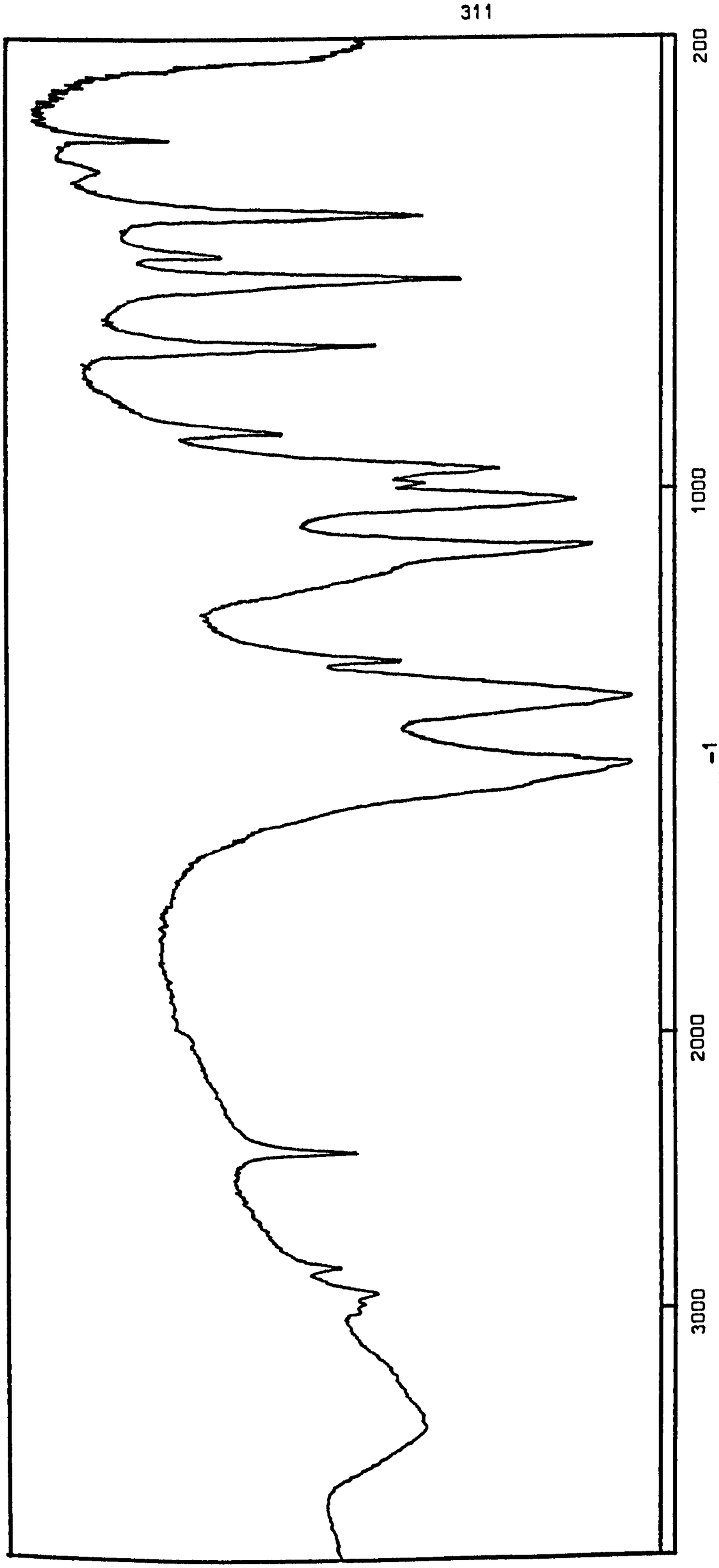

Figure 8.5 Infrared spectrum of the 1 ; 1 adduct of DMP with $Pb(OCOCH_3)_2 \cdot 3H_2O$.

moiety on coordination of DMP to lead.

Analysis of the liquid exuded on decomposition was also made. From the spectroscopic evidence obtained it was clear this was not simply dissolved 1 : 1 adduct. The infrared spectrum of a liquid film of this material (Table 8.6, Figure 8.6) shows a strong absorption due to the O-H vibrations in the appropriate regions and this resulted in partial masking of these areas to other bands. Details which were clear showed that the ν(P-H) region now contained three broad bands in place of the sharp, single line in the original product. The band at 1140 cm^{-1} previously assigned to coordinated P=O had disappeared and a strong broad signal between 1220 - 1170 cm^{-1} had developed, possibly indicating a weakening in the phosphoryl-lead coordination or a mixture of free and bound systems. Indeed, two small bands at 990 and 970 cm^{-1} are coincidant with the ν(P-O) values in the bound and free DMP. The presence of organic moieties could be discerned from the bands centred about 2905, 2830, 1447 and 1370 cm^{-1}, although the asymmetric carboxylate stretching mode occurring at 1540 cm^{-1} in $Pb(OCOCH_3)_2$ could not be resolved due to the broad O-H absorption in this region. In order to further elucidate the solution chemistry of the decomposition products investigations were made by n.m.r.

Table 8.7 lists the n.m.r. parameters obtained from the reactants DMP and $Pb(OCOCH_3)_2.3H_2O$ observing the nuclei ^{1}H, ^{13}C, ^{31}P and ^{207}Pb. The reactions and subsequent measurements were made

Table 8.6 Infrared spectroscopic data for liquid decomposition product from 1 : 1 adduct of DMP, $Pb(OCOCH_3)_2.3H_2O$. (liquid film on AgBr windows).

Frequency (cm^{-1})		Assignment
3400 - 3200	b.s.	ν (O-H)
2905	b.w.	ν (C-H)
2830	b.w	
2480	sh.m.	ν (P-H)
2420	b.m.	
2350	b.m.	
1700-1550	b.s.	δ (O-H) + ν_{as}(COO)
1447	m.	δ_{as}(C-H)
1370	m.	ν_s(COO)
1220 - 1170	b.s.	ν(P=O)
1050	s.	δ (C-H)
990	s.	ν(P-O)
970	s.	
930	m.	ν(C-C)
912	m.	
837	m.	
778	m.	ν ((P-O)-C)
690	sh.m.	
547	s.	δ_{as}(OPO)
510	s.	
415	s.	δ_s(OPO)

b, broad; sh, sharp; w, weak; m, medium; s, strong.

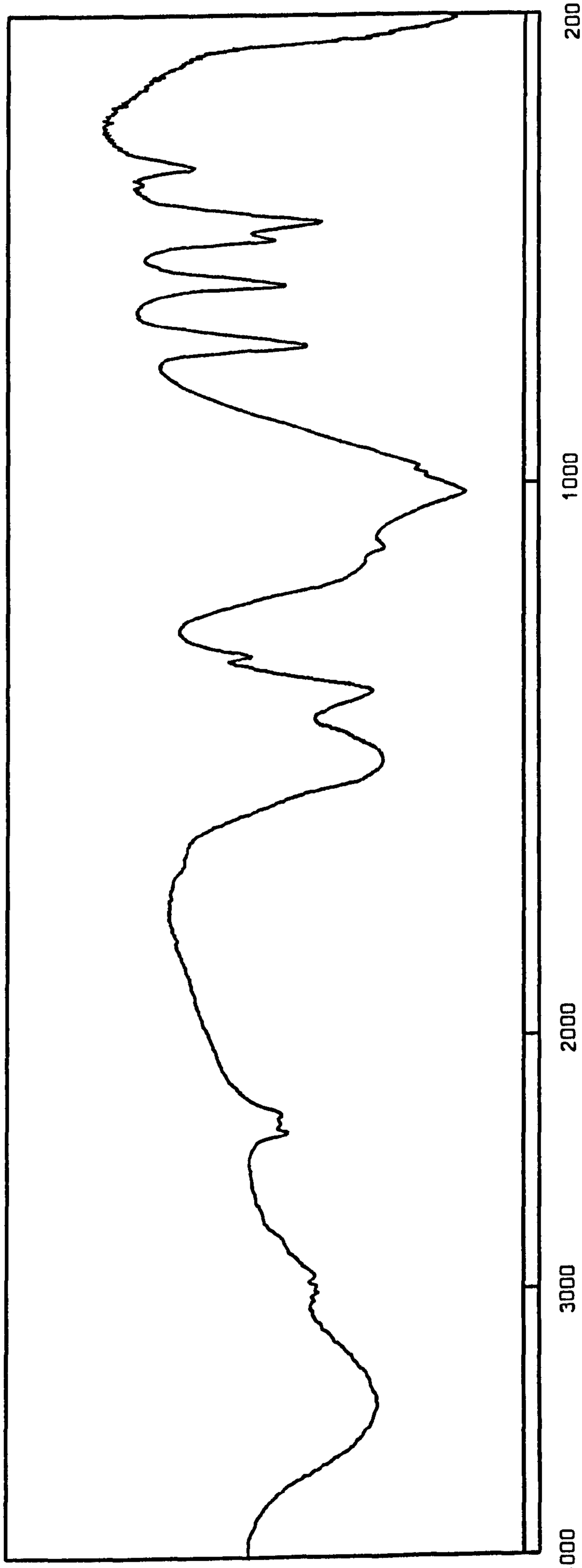
200
1000
2000
3000
4000
cm-1
Liquid decomposition product from DMP Pb(OCOCH3)2·3H2O. (Liquid film)

Figure 8.6

Table 8.7(a) N.m.r. parameters for dimethylphosphite in methanol

Nucleus	Chemical Shift (ppm)	Signal Multiplicity	Coupling Constant (Hz)	Assignment
^{1}H [a]	3.725	d	$^{3}J(P-H)$,12.20	P-O-C<u>H</u>$_3$
	6.789	d	$^{1}J(P-H)$,706.78	P-<u>H</u>
^{13}C [a]	52.08	d	$^{2}J(P-C)$,5.55	P-O-<u>C</u>H$_3$
^{31}P [b]	-123.02	d/sp	As above	<u>P</u>

[a] relative to Me_4Si = 0

[b] relative to 85% H_3PO_4 = 0

d, doublet; sp, septet.

Table 8.7(b) N.m.r. parameters for lead(II) diacetate, trihydrate in methanol (and water)

Nucleus	Chemical Shift (ppm)	Signal Multiplicity	Assignment
^{1}H [a]	2.09 (1.85)	s	$O_2CC\underline{H}_3$
	4.96 (4.75)	s	H_2O
^{13}C [a]	24.97	s	$O_2C\underline{C}H_3$
	179.65	s	$O_2\underline{C}CH_3$
^{207}Pb [b]	-1324 (-1343) [c]	s	Pb(II)

[a] relative to Me_4Si = 0

[b] relative to Me_4Pb = 0

s, singlet

[c] concentration dependent, values extrapolated to infinite dilution.

in CD_4OD using a Bruker WM 250 Fourier transform spectrometer with a superconducting magnet. ^1H spectra were measured either on a Jeol MH 100, 100 MHz instrument, or a Perkin-Elmer R32 operating at 90 MHz. 5 mm diameter sample tubes were used for proton studies, 10 mm for all others. The reference standards are those detailed in Table 8.7 and, as stated in Chapter Four, throughout this thesis the convention of highfield, low frequency shifts having negative values is used.

The methoxyl protons in DMP give rise to a septet in the ^{31}P spectrum which is then split into a characteristic doublet of septets by the directly bonded single proton. The converse magnetic interaction is observed in the ^1H spectrum where phosphorus coupling results in doublets for the two different proton environments. Typical coupling constants for such systems of $^2J(P-H)$ = 706.78 Hz and $^3J(P-H)$ = 12.20 Hz are observed. In the ^{13}C spectrum, the proton decoupled methoxyl carbon is again split by phosphorus into a doublet with $^2J(P-C)$ = 5.55 Hz.

The hydrated lead(II) acetate has two singlets due to the methyl, and waters of crystallization, in the ^1H spectrum and a slight solvent effect on going from methanol to water is observed. The undecoupled (^1H) ^{13}C spectrum has a quartet for the CH_3 and a singlet at much lower field for the carboxyl carbon. ^{207}Pb data gives a singlet in methanol at -1364.16 ppm to high field of Me_4Pb, whilst in water this resonance has moved to -1385.0 ppm.

For a 1 : 1 reaction between DMP and lead(II) acetate in methanol the initial ^1H solution spectrum taken 30 seconds after

addition of DMP has the characteristics of both components and gave resonances with chemical shifts identical to those above. However, within three minutes the DMP resonances had markedly reduced in intensity, whilst the methyl group resonance of the acetate had virtually disappeared. It is noteworthy that the O-H resonance due, initially, to the waters of crystallization did not significantly alter, vide infra. The sample contained a considerable quantity of precipitate and the resolution was adversely affected. No other marked changes were observed over a period of about 90 minutes, although further slight reductions in signal intensities were noted.

The reaction was also monitored using ^{207}Pb n.m.r. The resonance of unreacted lead acetate in methanol occurring at -1364.16 ppm to high field of Me_4Pb has a Lorentz line shape with a half-height line width of 2196 Hz. Addition of DMP resulted in gross asymmetry to this line with a shift in frequency of the maximum to -1450 ppm. This spectrum (Figure 8.7) was the result of 8000 accumulations over 719 seconds, commencing 90 seconds after addition of the DMP. A further 8000 accumulations were made, beginning 15 minutes after addition of DMP. The resulting signal was less asymmetric, sharper, with a half-height width of 1243 Hz, and had shifted to -1479.8 ppm. The results for subsequent runs under similar conditions are given in Table 8.7. For the first 60 minutes, a progressive decrease in line width occurs together with a steady shift in resonance position to high field. After 90 minutes this settles to about -1542 ppm but the solubility of

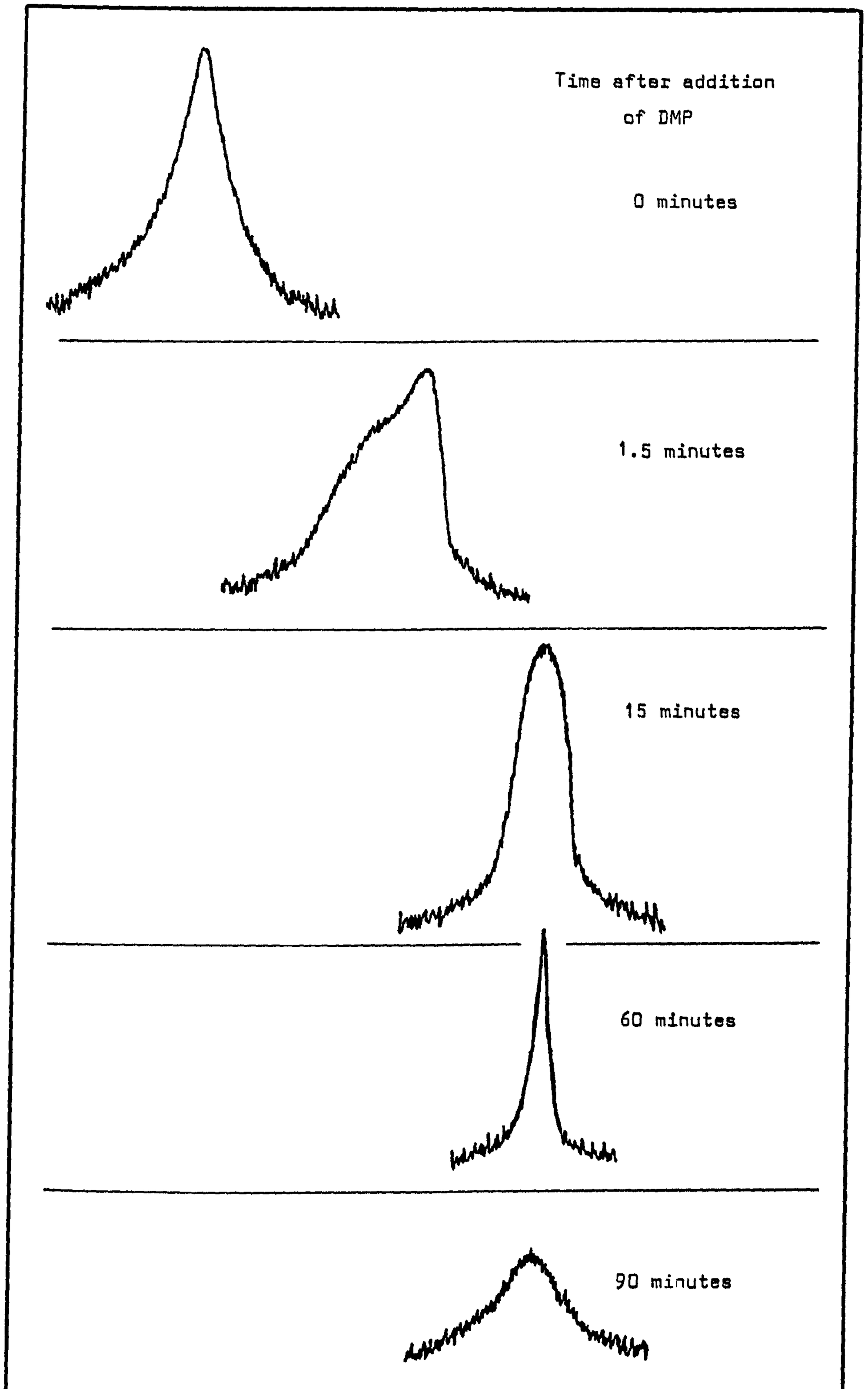

Figure 8.7 ^{207}Pb n.m.r. spectrum of $Pb(OCOCH_3)_2.3H_2O$ after addition of DMP.

Table 8.8 Effect on ^{207}Pb resonance of reaction between DMP and $Pb(OCOCH_3)_2.3H_2O$

Time Accumulation Commenced from addition of DMP (minutes)	Chemical Shift[a] (ppm)	Half-height line width (Hz)
0	-1364.16	2196
1.5	-1450.0	2984
15.0	-1479.8	1243
30.0	-1505.4	829
45.0	-1519.7	787
60.0	-1529.2	785
75.0	-1540.6	853
90.0	-1541.9	1036

[a] relative to Me_4Pb

the species produced is now a limiting factor and the line width also increases because of the quantity of solid now present in the sample tube. These results indicate an increased shielding of the lead atom and provision of an alternative relaxation mechanism allowing line sharpening. Both features which are consistent with the formation of a phosphoryl-lead coordinate bond occurring in solution as well as with the solid. The marked asymmetry in the line shape noted in the first run commenced 1.5 minutes after addition of DMP can be rationalized in terms of two signals, alternately increasing and decreasing, but which, because of the nature of the Fourier transform n.m.r. experiment 'blurr' into the line shape observed. Indeed on a subsequent run it was found possible to partially resolve the two resonances. The low field signal can be assigned to uncoordinated lead acetate, which is decreasing, whilst the high field resonance which actually increases in intensity is attributable to the coordinated lead acetate. As the solubility limit of the system is reached and continued precipitation occurs the signal decays.

If the sample is filtered and the resulting liquid allowed to stand for several days it is found that the resonance at -1542 ppm has disappeared. In its place, however, is a signal with a much greater high field shift at -2616 ppm. By analogy to the chemical shifts for the lead ion in aqueous solutions of $Pb(NO_3)_2$ (-2961.2 ppm) and $Pb(ClO_4)_2$ (-2950 ppm) it may be proposed that this signal corresponds to a hydrated lead ion of the type $Pb(OH_2)_n^{2+}$. Furthermore, it is most likely that the resonance

occurring in the region -1350 to -1550 ppm with lead acetate, which is mid-way between the ionic species and the organolead resonances (Me_4Pb = 0, Et_4Pb=+ 73.3, Me_3PbPh = -38.5 ppm), is infact the median position for a nucleus exchanging, at the limit, between the two environments. The conclusions drawn from the lead *n.m.r.* data support a mechanism suggested by ^{31}P studies.

The initial precipitation occurring in the first few minutes of reaction reduce the signal-to-noise ratio from 130 : 1 to 27 : 1 for the ^{31}P multiplets of DMP, although the splitting is still well defined. On standing for several hours additional signals are observed. These consist, in the first place, of a doublet of quartets and a single doublet to high field of the centroid of the DMP septets (Table 8.9). On leaving the solution a total of 12 hours and after filtration the doublet of quartets dominate the spectrum whilst the single doublet has not markedly changed in intensity. The doublet of septets has by this time moved -4.3 ppm to high field (Figure 8.8). A similar change had taken place in the ^{13}C spectrum (Figure 8.9). Signals due to the acetate had completely disappeared and the doublet from the methoxyl group on DMP had markedly reduced in intensity. A new doublet to high field (51.82 ppm, with a coupling constant of 5.55 Hz) of this signal as well as a strong singlet at 49.63 ppm had appeared. Concomitant alterations occurred in the ^{1}H spectrum (Table 8.10).

The original DMP doublets remained in the ^{1}H spectrum although

Table 8.9 Effect on ^{31}P resonances of reaction between DMP and $Pb(OCOCH_3)_2.3H_2O$

Time of Reaction (minutes)	Chemical Shift[a] (ppm)	Multiplicity of signals[b]	Coupling Constants (Hz)	Relative Intensities	Signal to Noise Ratio
0	-123.0	d/sp	706.78	1	130:1
120	-123.0	d/sp	699.4	3	
	-131.3	d/q	684.5	5	27:1
	-134.3	d/s	641.6	1	
720	-127.3	d/sp	717.2	3	
(sample	-131.3	d/q	682.9	9	115:1
filtered)	-134.3	d/s	641.6	1	

[a] Relative to 85% H_3PO_4

[b] Notation: d = doublet, s = singlet, q = quartet, sp = septet

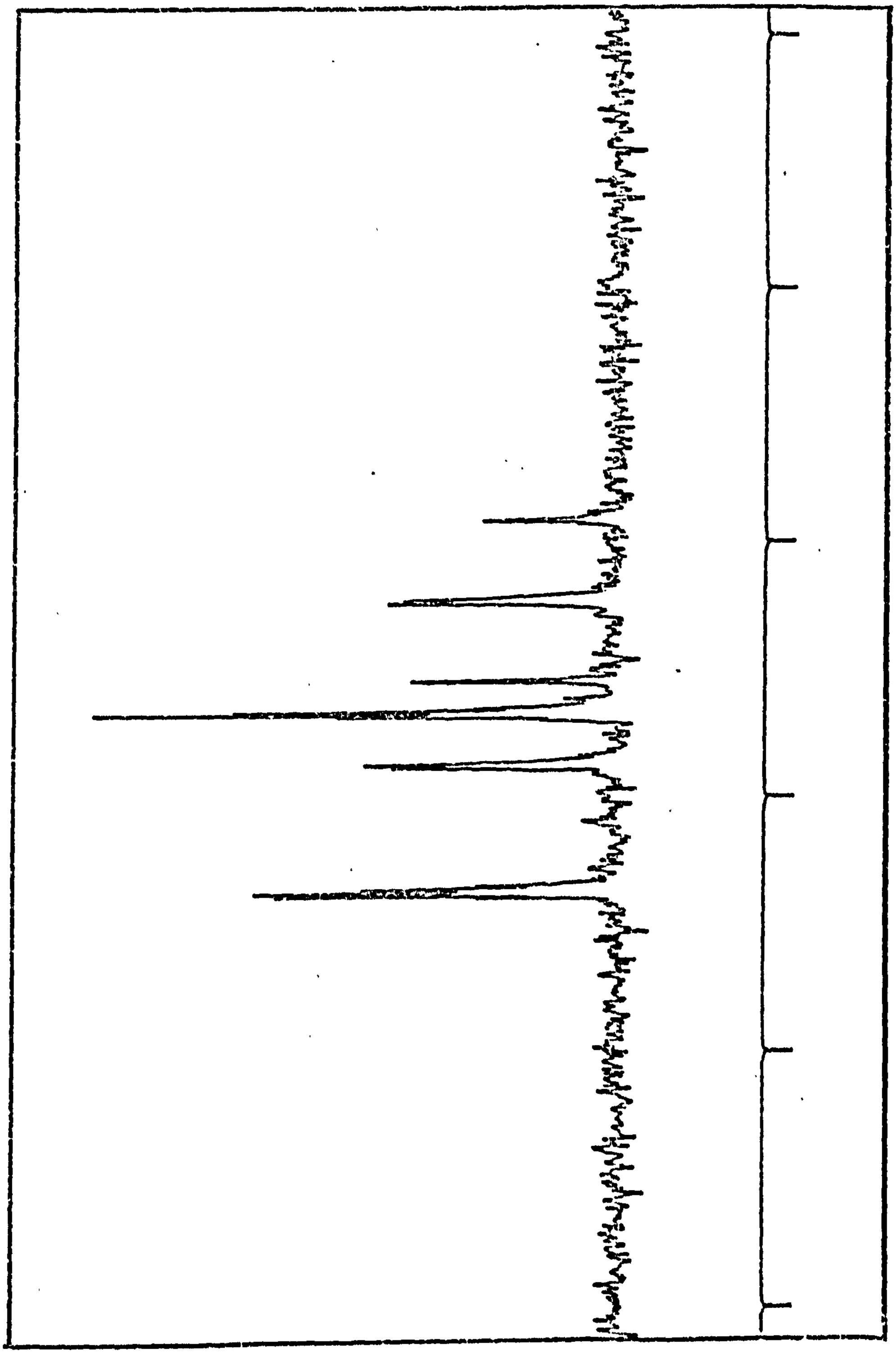

Figure 8.8a ^{31}P n.m.r. spectrum from reaction liquid of DMP and $Pb(OCOCH_3)_2 \cdot 3H_2O$ two hours after initiation.

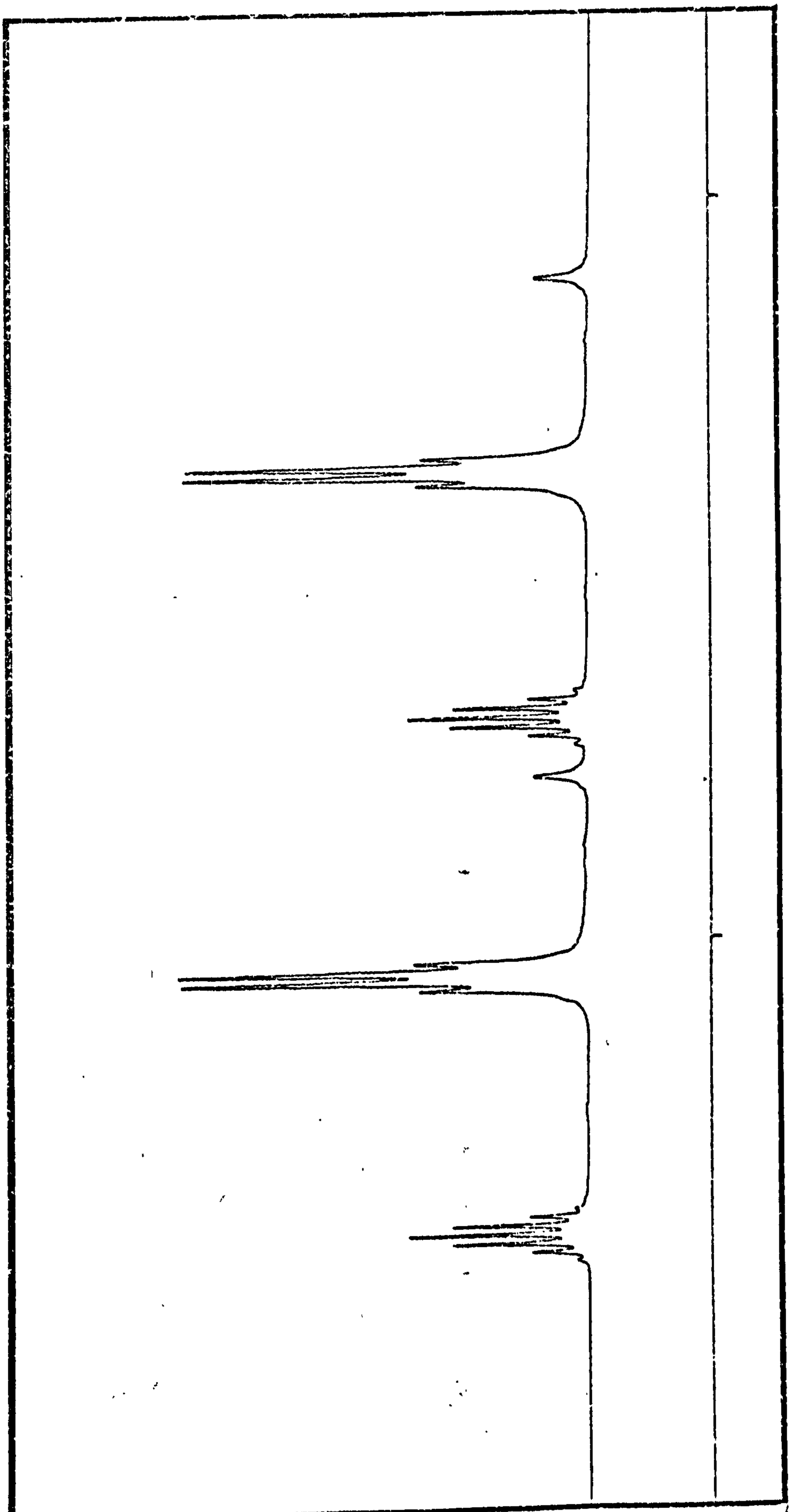

Figure 8.6b ^{31}P n.m.r. spectrum from reaction liquid of DMP and $Pb(OCOCH_3)_2 \cdot 3H_2O$

• Solution filtered.

12 hours after initiation. Note change in signal position and relative intensities from 8.8a.

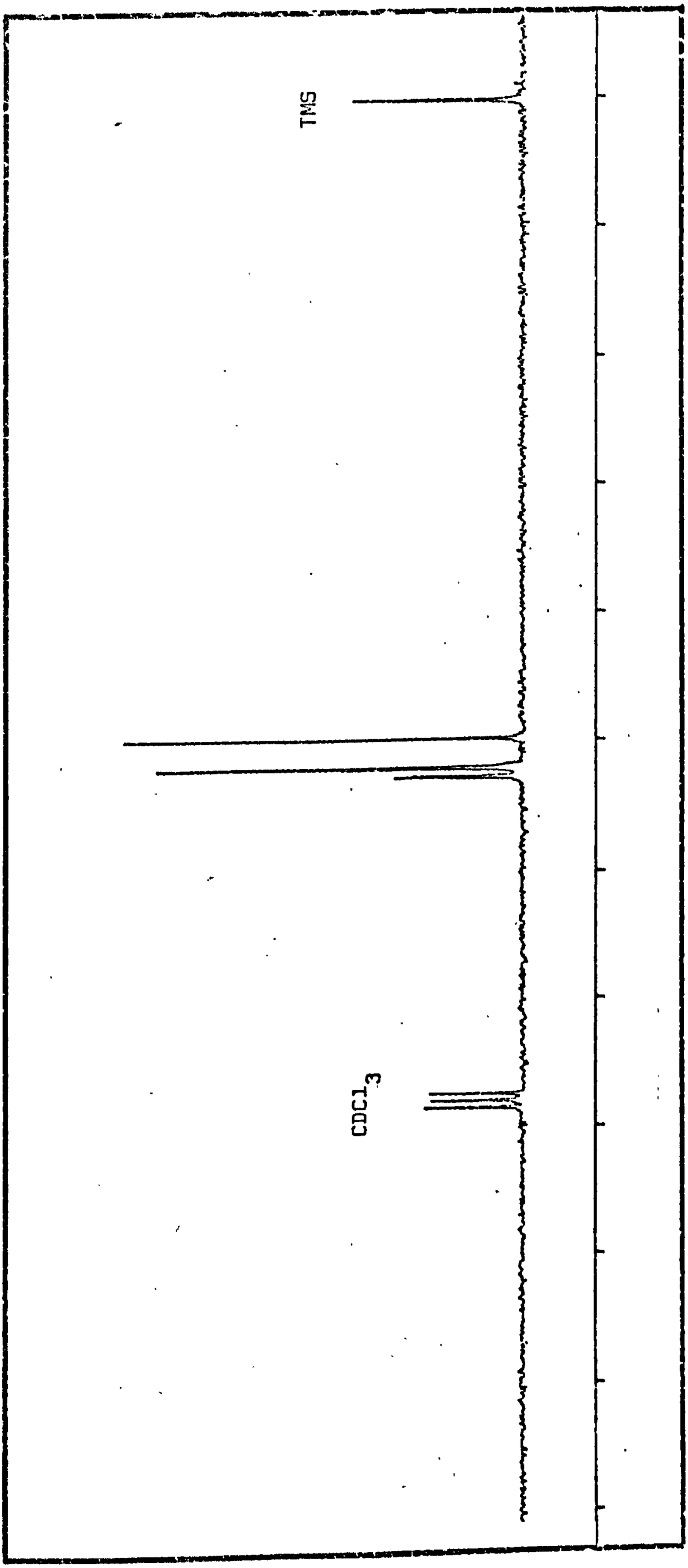

^{13}C n.m.r.spectrum of reaction liquid from DMP and $Pb(OCOCH_3)_2.3H_2O$ twelve hours after initiation.

Figure 8.9

Table 8.10 Effect on ^1H resonances of reaction between DMP and $Pb(OCOCH_3)_2.3H_2O$

Associated Resonances	Chemical Shift[1] (ppm)		Coupling Constant (Hz)
A	6.76	d	644
B	3.58	d	12.20
	6.69	d	683.0
C	3.49	d	12.20
	6.63	d	718.0
D	2.04	s	
	3.14	s	

[1] relative to Me_4Si = 0

d = doublet

s = singlet

moved in frequency. By comparison of coupling constants with those from ^{31}P data it was possible to assign the doublet centred at 3.49 ppm to the methoxyl protons and the associated P-H signal to resonances centred at 7.63 ppm; infact a slight high field shift in both resonances. In addition, two new sets of doublets centred at 3.58 and 6.69 ppm was observed. From the respective coupling constant values of 12.20 and 683 Hz it was clear these resulted from the doublet of quartets observed in the ^{31}P spectrum. A single doublet centred at 6.76 ppm with a coupling constant of 644 Hz was similarly related to the equivalent doublet noted in the ^{31}P data.

When water was used as solvent reaction was considerably slower (the solution became cloudy after about 14 minutes and slight precipitation was observed after 2 hours), although very similar spectra were obtained to those described above. However, the resulting solid collected after several days did not appear to contain carbon and a much lower yield ($\sim$ 14%) of solid product was obtained. As the evidence will show, the implication of this is that the liquid decomposition products from the reaction in methanol were, infact, the principle products when water was used as the reaction medium.

8.4.3 The reaction pathway

The initial step in the reaction in methanol is the formation of the 1 : 1 product (VIII). This then slowly, spontaneously

decomposes giving the liquid product analysed. The slight low field shift in the CH_3 group in the ^{13}C spectrum of DMP (from 52.08 to 52.52 ppm) indicates a weakening in the O-C bond, whilst the high field shift in the methoxyl protons indicates a strengthening of the C-H bond. The ν(P-O) frequency change from 973 to 990 cm^{-1} in the infrared spectrum previously discussed also indicates a weakening in the P-O bond. These data, together with the gradual increase in field of the phosphorus and lead resonances as reaction proceeds is consistent with an electron drift towards the phosphoryl bond and the presence of some coordinated lead — DMP species in solution. A much reduced signal intensity due to the acetate resonance in the ^{13}C and ^{1}H spectrum of the initial reaction medium indicates that, where lead is present as unionized lead acetate, it is precipitated. The higher yield of solid product in the methanolic solution where the proportion of unionized species would be higher (and Le Chateliers principle would operate), compared with the aqueous system, supports this. The unchanged nature of the O-H, apart from a slight upfield shift from 4.96 to 4.70 ppm in the ^{1}H spectrum, suggests the lead in solution may be of the form $Pb(OH_2)_n(OH)_2$; the resonance being at an equilibrium position. Further evidence for such a species is provided by the infrared spectrum of the liquid decomposition product (Table 8.6) which exhibits a very strong, broad OH absorption.

The weakening of the C-O bond and subsequent bond fission

is a feature of all the spectra. The process appears to be stepwise, however. Initial loss of one methyl group giving the characteristic doublet of quartets in the ^{31}P spectrum, followed by loss of the second methyl group giving the single doublet due to the remaining P-H moiety, loss of methoxyl groups would, of course, result in similar spectra. However, chemical evidence against this occurring will be provided below.

The sequence of reactions in methanol thus appear to be as shown in Table 8.11 whilst in water the route is similar but the proportion of products differs (Table 8.12). If these conclusions are correct then in both cases the final product in the solid and the liquid remaining at completion of the reaction sequence would be lead phosphite. From the n.m.r. data it would appear that a small quantity of hydrated lead phosphite remains in solution. This was tested for qualitatively.

Addition of silver nitrate to the liquid product produced a white precipitate which on heating became black. This is characteristic of a reaction with a phosphite;

$$PbHPO_3 + 2AgNO_3 \longrightarrow Ag_2HPO_3\downarrow + Pb(NO_3)_2$$

white precipitate

$$Ag_2HPO_3 + H_2O \longrightarrow 2Ag\downarrow + H_3PO_4$$

black precipitate

The final solution had a pH of 1.

Table 8.11 Reaction sequence between DMP and $Pb(OCOCH_3)_2.3H_2O$ in methanol

Table 8.12 Reaction sequence between DMP and $Pb(OCOCH_3)_2.3H_2O$ in water

DMP + $Pb(OCOCH_3)_2.3H_2O$

↓ Water

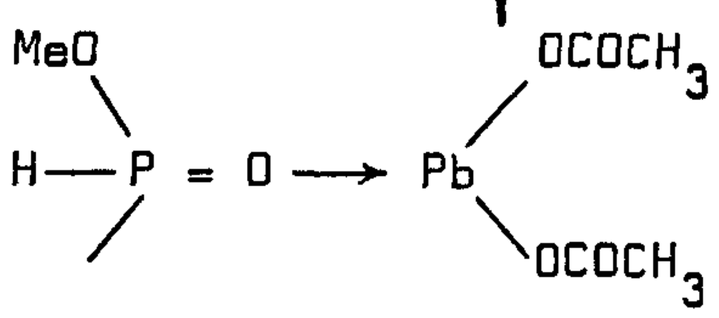

↓ Minor product (liquid)

SPONTANEOUS

RAPID PROCESS

↓

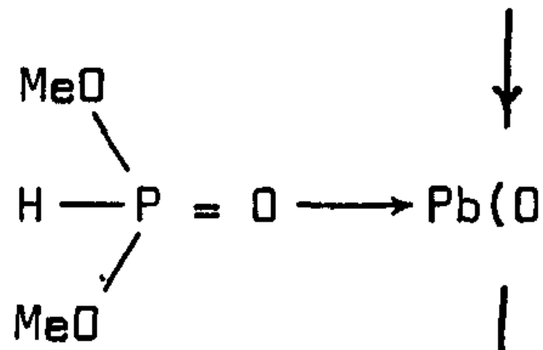

↓ Major product (liquid)

$X = CH_3COO^-$ or OH^-

STEPWISE DEMETHYLATION (AS TABLE 8.11)

↓

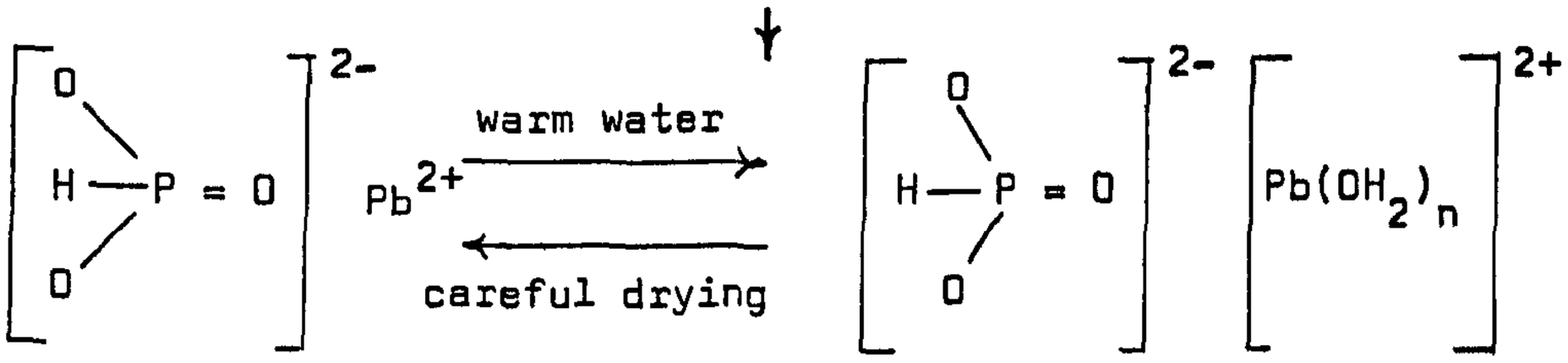

Solid — Main Product

Liquid — Minor Product

Additionally, reaction with copper(II) nitrate solution produced a pale blue precipitate, again confirmatory of an ionic phosphite:

$$PbHPO_3 + Cu(NO_3)_2 \longrightarrow \underset{\text{pale-blue precipitate}}{CuHPO_3} + Pb(NO_3)_2$$

Further supportive evidence is obtained from the action of heat on the final solid when the evolution of phosphine can be detected.

$$8\,PbHPO_3 \longrightarrow 2PH_3 + 2Pb_3(PO_4)_2 + Pb_2P_2O_7 + H_2O$$

Whilst warming this solid for five minutes in hot water ($\sim 85^oC$) produces a solution which gives these same reactions as the liquid. The ultimate proof of the phosphite product is obtained by comparison of the infrared spectrum of this product with that from a sample of $PbHPO_3$ (Table 8.13, Figure 8.10) prepared by a metathetical reaction between $Pb(OCOCH_3)_2.3H_2O$ and Na_2HPO_3. In addition, if the 1 : 1 solid is gently heated (110^oC, 8 minutes) the resulting solid has an infrared spectrum indistinguishable from $PbHPO_3$. The proposed sequence, therefore, appears to be validated.

The question which remains, however, is the mechanism of these reactions. One possible pathway involves the following

Table 8.13 Infrared data[b] for the lead salts; phosphite, nitrate and prepared phosphite and double-salt, phosphite-nitrate.

$PbHPO_3$ cm^{-1}	$PbHPO_3$[a] cm^{-1}	$Pb(NO_3)_2$ cm^{-1}	$Pb_2(HPO_3)(NO_3)_2$[a] cm^{-1}	Assignment
2470 b.m.	2480 sh.m.		2436 sh.m.	ν(P-H)
2360 m.	2360 m.		2360 m.	
2320 b.m.	2320 b.m.		2380 b.m.	
		1763 m.	1762 sh.m.	ν_{as}(N-O)
			1747 sh.m.	
		1383 s.	1383 s.	ν_s(N-O)
		1351 s.	1351 s.	
1050 s.	1050 s.			ν_{as}(P-O)
		1007 w.	1020 s.	
980 s.	983 s.		982 m.	δ (P-H)
960 s.	958 s.		965 s.	ν_s(P-O)
		825 w.	825 w.	NO_3 o.o.p.
		804 m.	809 m.	
		720 m.	720 m.	δ (ONO)
			706 w.	
583 s.	580 s.			δ_{as}(OPO)
565 m.	557 m.			
550 m.				
490 w.	496 w.			
467 s.	462 s.		467 s.	δ_s(OPO)
400 w.	400 w.		400 w.	

[a] material assigned this formula (see Section 8.4.4).

[b] spectra recorded as KBr discs

b, broad; sh, sharp.

w, weak; m, medium; s, strong.

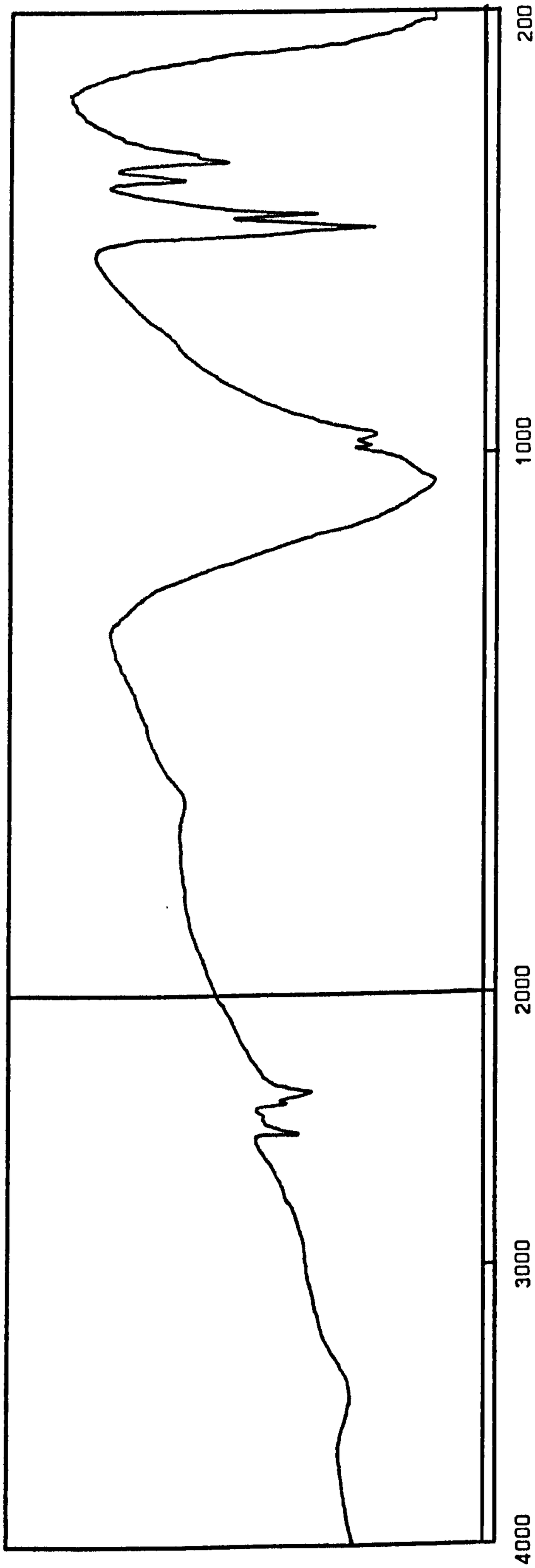

Figure 8.10a End product from reaction between DMP and $Pb(OCOCH_3)_2 \cdot 3H_2O$ as described formula $PbHPO_3 \cdot$. (KBr disc)

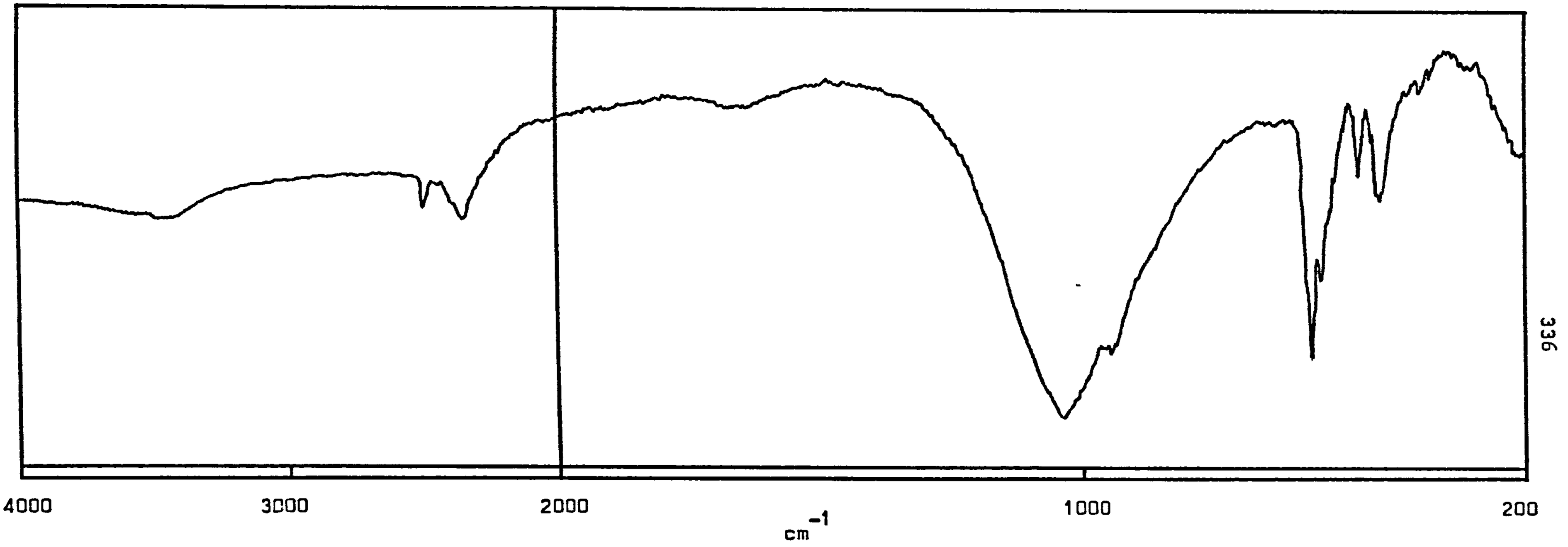

Figure 8.10b $PbHPO_3$ (KBr disc)

concerted reaction sequence:

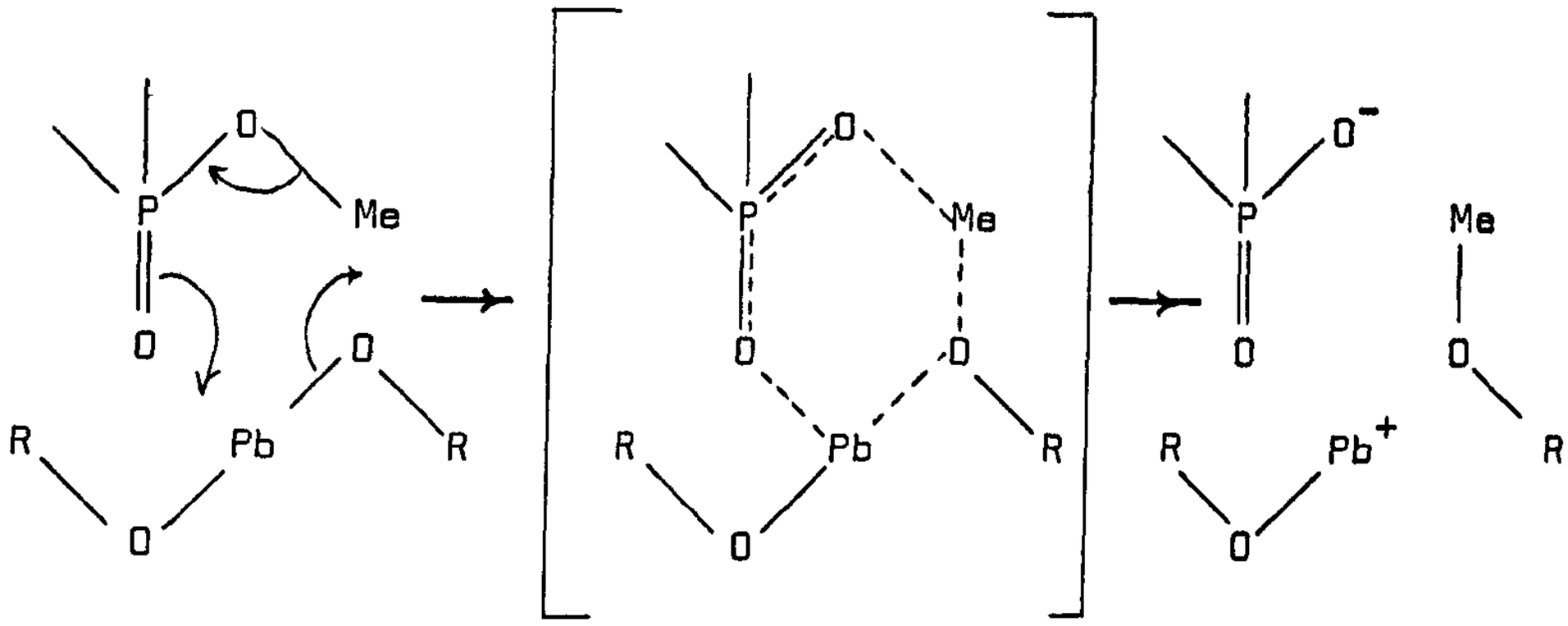

Transition State

where R = H or $COCH_3$

This would then repeat for the other methyl group giving the product

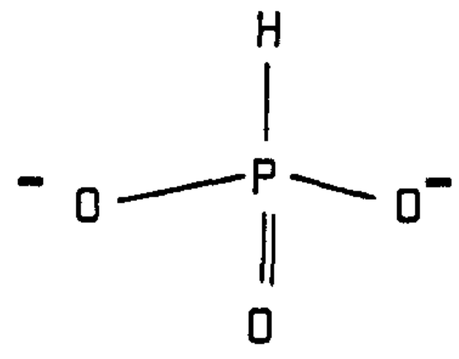

Pb^{2+}

The production of either methyl acetate or methanol is implicit in this mechanism. The ^{13}C n.m.r. spectrum of the liquid from the decomposition has a strong singlet at 49.63 ppm whilst the ^{1}H spectrum has two single lines at 2.04 and 3.14 ppm.

The ^{13}C resonance is exactly coincident with methanol and almost the same as the methoxyl group in an acetate. However, the carboxylate resonance in the 180 ppm region was not observed. The resonance at 3.15 ppm in the ^{1}H spectrum is also correct for the methoxyl protons in methanol. The absence of a signal due to free H^{+} around 11 ppm in a solution which is acidic, and of an OH^{-} signal at the other end of the spectral range, associated with the lead ion, together with the lack of a resonance between 4 and 5 ppm for the methanolic OH may all have the same explanation. The hydroxyl proton is well known for the extent to which its chemical shift can vary due to exchange processes. It is likely that this is precisely what is occurring in the above case, and the signal at 2.04 ppm is the result of a mixture of the three sites for the hydrogen nucleus.

The initial step in the spontaneous decomposition;

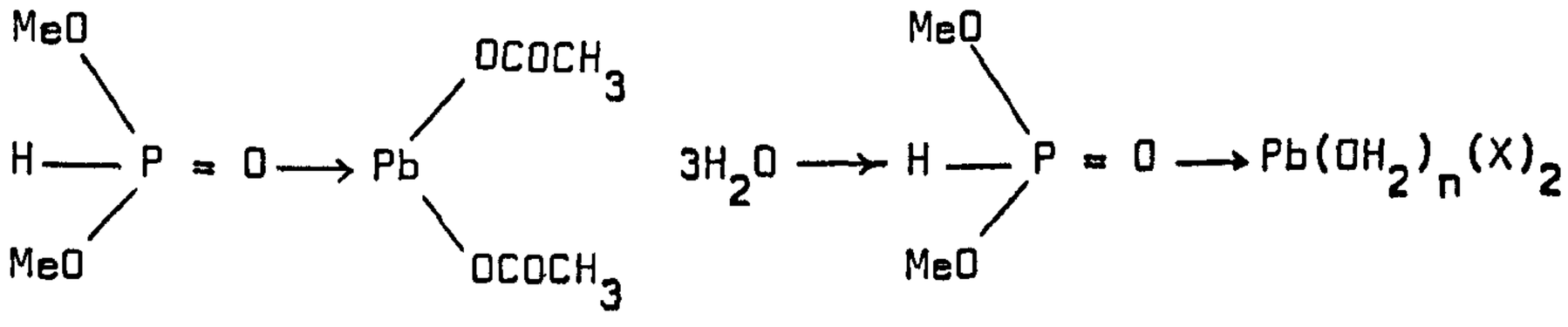

where $X = OCOCH_3^{-}$ or OH^{-}

implies the formation of acetic acid when X = OH.

$$HOH + OCOCH_3^{-} \rightleftharpoons {}'CH_3COOH' + OH^{-}$$

The pH of the decomposition liquid is 3 and a strong smell of acetic acid was noted. However, the small quantity of acetic acid which may be generated probably absorbs directly onto the remaining solid. Because of the acetate bands already present in the infrared, and the complex nature of the spectrum in this area rendering quantitative measurements of little value, it was not possible to distinguish the presence of any free acid, and the absence of the low field H^+ in the n.m.r. spectrum has already been discussed.

The acidic nature of the resulting decomposition liquid may well arise from the phosphite system itself. For example,

$$PbHPO_3 + 2H_2O \longrightarrow 'Pb(OH)_2' + H_3PO_3$$

resulting in phosphorous acid is a most likely possibility.

It is worthy of note here that where formulae such as $Pb(OH_2)_n(OH)_2$ or $Pb(OH)_2$ have been written it is not intended to imply the absolute stoichiometry. As discussed in Chapter Five, hydrated lead systems are often of complex composition. However, the above notations are convenient for illustrating the processes involved and knowledge of the precise species would not, in itself, alter the arguments propounded.

Experiments carried out with 1 : 2 and 2 : 1, respectively, of DMP and lead(II) acetate, in all cases resulted in an excess of the appropriate reactant remaining and the 1 : 1 compound being

formed.

The evidence for the reaction sequence and mechanism proposed is substantial, however, a fundamental question remains : how good is the model at representing lead-phosphorus-oxygen interactions? Indeed, what happens with other lead systems?

8.4.4 Reactions between DMP and Lead(II) Nitrate

In an attempt to answer the above questions similar reactions to those already described were performed between DMP and lead nitrate.

Because of the negligible solubility of lead nitrate in methanol the reactions were performed exclusively in an aqueous medium, and for convenience with the n.m.r. studies 99.8% D_2O was used throughout. The experimental procedure adopted was as previously described, using 0.05 M solutions. However, precipitation did not occur. Instead, over a period of 18 hours white crystals were produced. These analysed as the mixed salt $Pb_2(HPO_3)(NO_3)_2$ and the infrared spectrum of this material (Figure 8.11) taken as a KBr disc, is listed together with $Pb(NO_3)_2$ and $Pb(HPO_3)$ in Table 8.13. As can be seen, this contains all the bands of the component systems. The nitrate vibrations remain unchanged, however, the ν_{as}(P-O) shows sign of perturbation with a fall in frequency from 1050 cm^{-1} in the 'free' phosphite to 1020 cm^{-1} in this double salt. A slight change in the ν_s(P-O) is also observed in the 965 cm^{-1} region. The liquid remaining again gave

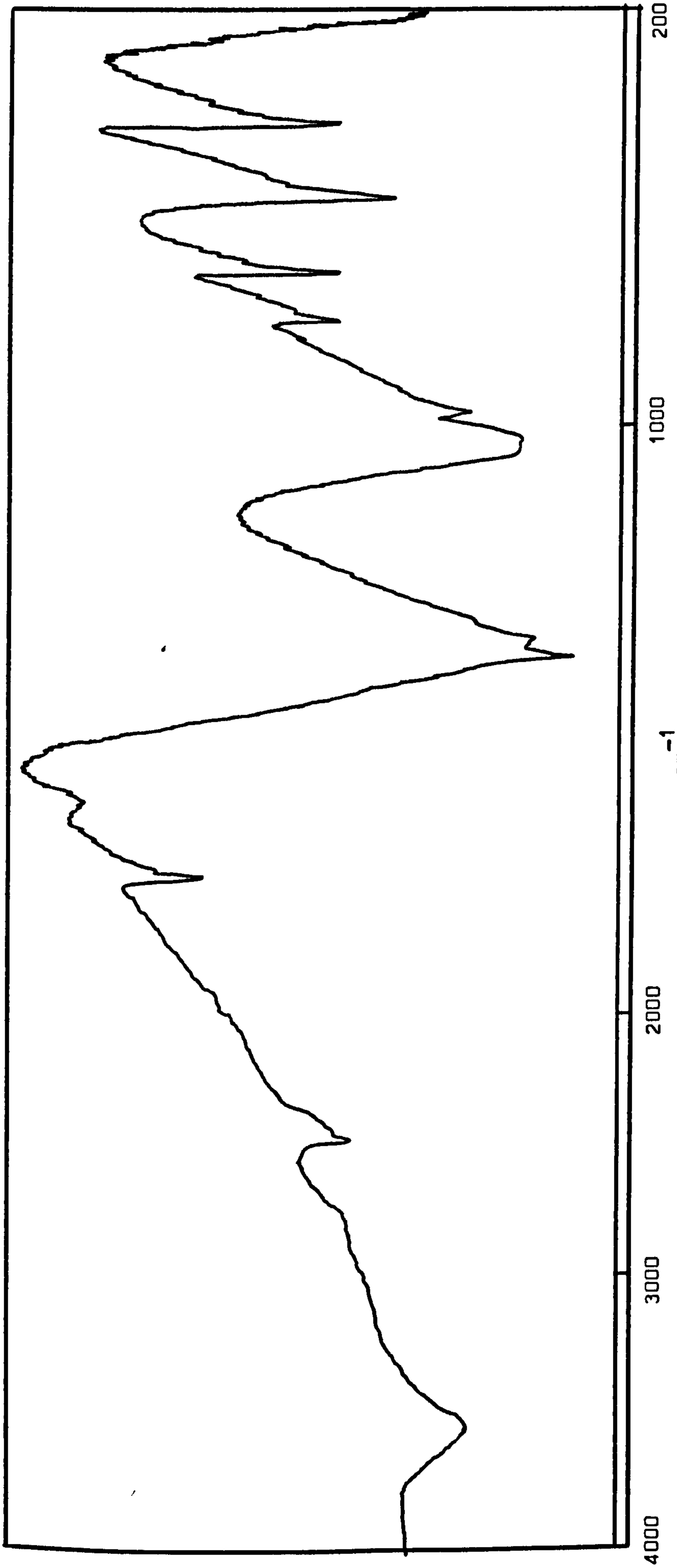

Figure 8.11 Reaction product from DMP and $Pb(NO_3)_2$, ascribed the formula $Pb_2(HPO_3)(NO_3)_2$. (KBr disc).

characteristic phosphite reactions with silver nitrate and copper(II) nitrate and the solid product on heating evolved PH_3. The n.m.r. signals corresponded to the chemical shifts found for DMP with the lead acetate reactions although no similar change in shielding, indicating coordinate species, was observed. The lack of a precipitate adds further support to the mechanistic sequence proposed as unionized $Pb(NO_3)_2$ can make no contribution.

Thus, the above reactions provide confirmation of the mode of action of lead compounds with DMP. It now remains to test whether these reactions are specific to DMP or if, as proposed, DMP is a good model system for interaction with heavy metals.

8.4.5 Reactions of Trimethylphosphate with lead(II) acetate, trihydrate

As mentioned previously, trimethylphosphate (TMP) is, arguably, a more representative system of body phosphates than DMP, although for the reasons detailed it is a considerably less facile spectroscopic probe of interactions. It does, however, provide a convenient check on the validity of the proposals already outlined for DMP and has, therefore, value as a check to the reaction sequence between DMP and lead acetate.

TMP is a clear, colourless, neutral liquid with a boiling point of 197^{o}C and a molecular weight of 140.08. As with DMP, it readily dissolves in water and organic solvents. For the

purposes of the reactions performed methanol was used as solvent. The experimental procedure previously described was again used in a 1 : 1 reaction between TMP and lead acetate. Again reaction is seen to occur with the lead salt, although precipitation was not quite as facile as for the DMP. The solution became cloudy after about six minutes and a deposit was noted within 20 minutes. The precipitate was crystalline and had a feather-like morphology. Elemental microanalysis gave C, 14.17; H, 2.86 and Pb, 41.29%. This corresponds to the stoichiometry having the structure (IX).

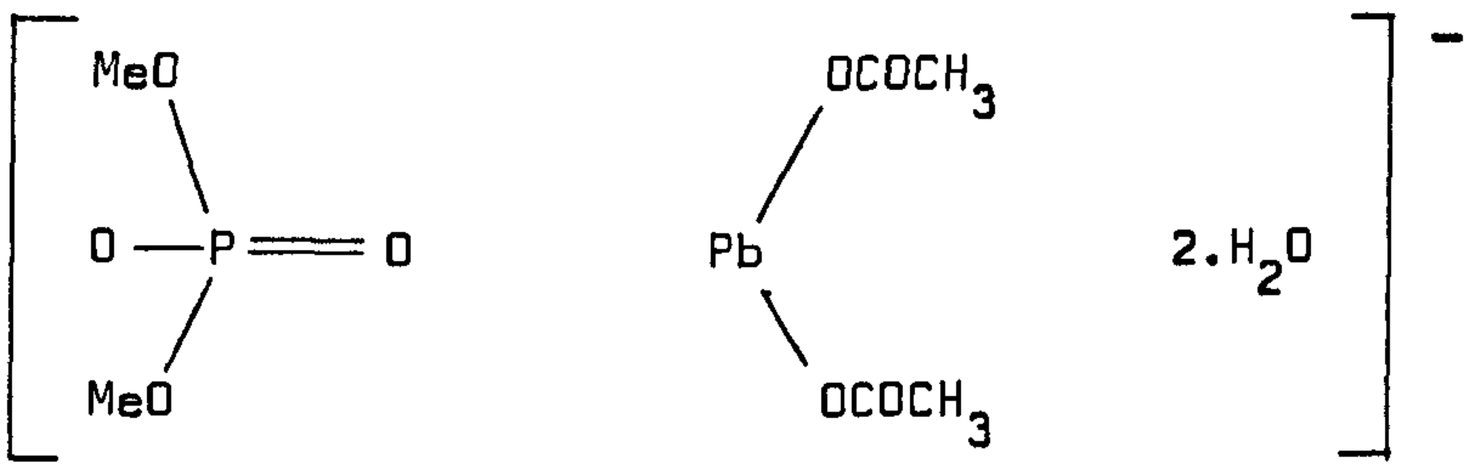

(IX)

The infrared spectrum of this material (Figure 8.12, Table 8.14) exhibited bands corresponding to those of the component reactants but there was no clear indication of any shifts in band positions confirming coordination of the phosphate to lead. The lack of any distinguishing features equivalent to the ν(P-H) of DMP does not allow firm assignment of interaction sites.

The ^{1}H n.m.r. spectrum of TMP consists of a doublet centred at 3.96 ppm with a coupling constant of $^{3}J(P-H) = 10.8$ Hz. On addition of a solution of $Pb(OCOCH_3)_2.3H_2O$ in CD_4OD to the TMP, the methoxyl resonances moved to slightly lower field and are centred at 4.07 ppm. The acetate resonance is at 2.17 ppm and is

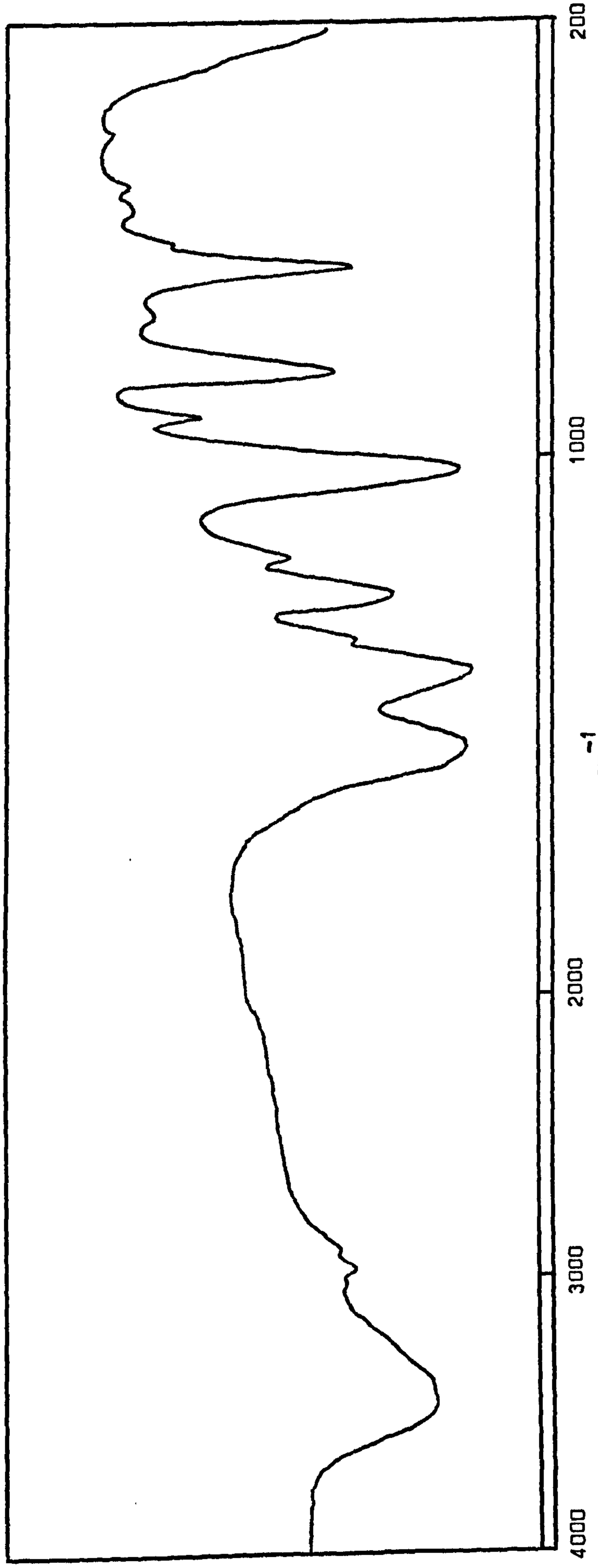

Figure 8.12 Product precipitated from the reaction between TMP and $Pb(OCOCH_3)_2 \cdot 3H_2O$. (KBr disc).

relatively broad; the half-height line width being 3.4 Hz. The OH resonance at 4.73 ppm is extremely broad, the half-height width being 14 Hz, and appeared to have a high-field component. After seven minutes the position and line shape of the methoxyl and acetate protons was unchanged. However, the O-H resonance had divided into two signals of equal intensity at 4.73 ppm and 4.62 ppm. The overall line width at half-height remained 14 Hz. After 14 minutes the acetate and methoxyl signals had markedly reduced in intensity and broadened, presumably due to the effect on the field homogeneity of the solid within the tube. A slight increase in shielding was indicated by a shift to 2.20 ppm and 3.94 ppm, respectively, for each of these groups. Interestingly, the hydroxyl resonance had not reduced in overall intensity, instead the high field signal at 4.62 ppm now predominated. Both methoxyl signals appeared to have high-field shoulders. The reaction was allowed to proceed to completion (24 hours) and the solid, after washing and drying was found to have an infrared spectrum identical to that of the solid produced in the first reaction.

It was found that this solid readily dissolved in water, and the subsequent ^{1}H n.m.r. spectrum recorded in D_2O solvent exhibited peaks at 2.37, 4.22, 4.31 and 5.18 ppm, indicative of a slight decrease in shielding in the acetate and methoxyl resonances and a marked change in position of the hydroxyl signal. Clearly, the broad resonance previously associated with this moiety was due to an exchange process between several different chemical

environments, as witness the signal width and multiplicity in the line. The resonance in the redissolved solid was sharp (half-height width = 1.4 Hz) and, almost certainly, arose from a single O-H environment.

What interpretation can be placed on these data? The evidence for any single species produced from TMP is not as conclusive as for the DMP. A firm conclusion, however, is that lead salts interact with TMP; which is, of course, supportive of a main tenet of this thesis; that lead interferes with body phosphate systems.

The decay of all but the OH resonance in the ^{1}H n.m.r. spectrum in methanol proves that it is the TMP and the acetate form of lead which are being precipitated, and this is supported by the infrared data. However, the product appears to be considerably more stable than the DMP complex. Elemental microanalysis suggests the mechanism of interaction again involves C-O bond cleavage and the loss of a methyl group. The formation of a more ionic phosphate system combined with lead which would result from this is supported by the precipitation of the product which occurs in methanol and the ability to redissolve in water. Indeed, when this reaction was run in water virtually no precipitation occurred and the n.m.r. data concurred with the values given above. From the changes which result in the OH signal line-shape and position in the ^{1}H n.m.r. spectrum it is likely that this again plays a role as both a free and bound

moiety and may be the agent for nucleophilic cleavage of the methoxyl;

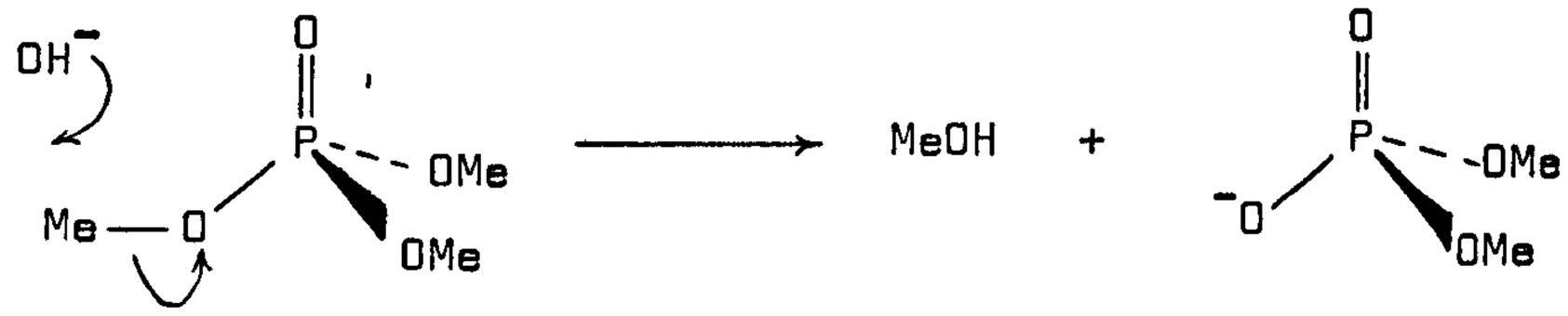

or possibly via an S_N2 process:

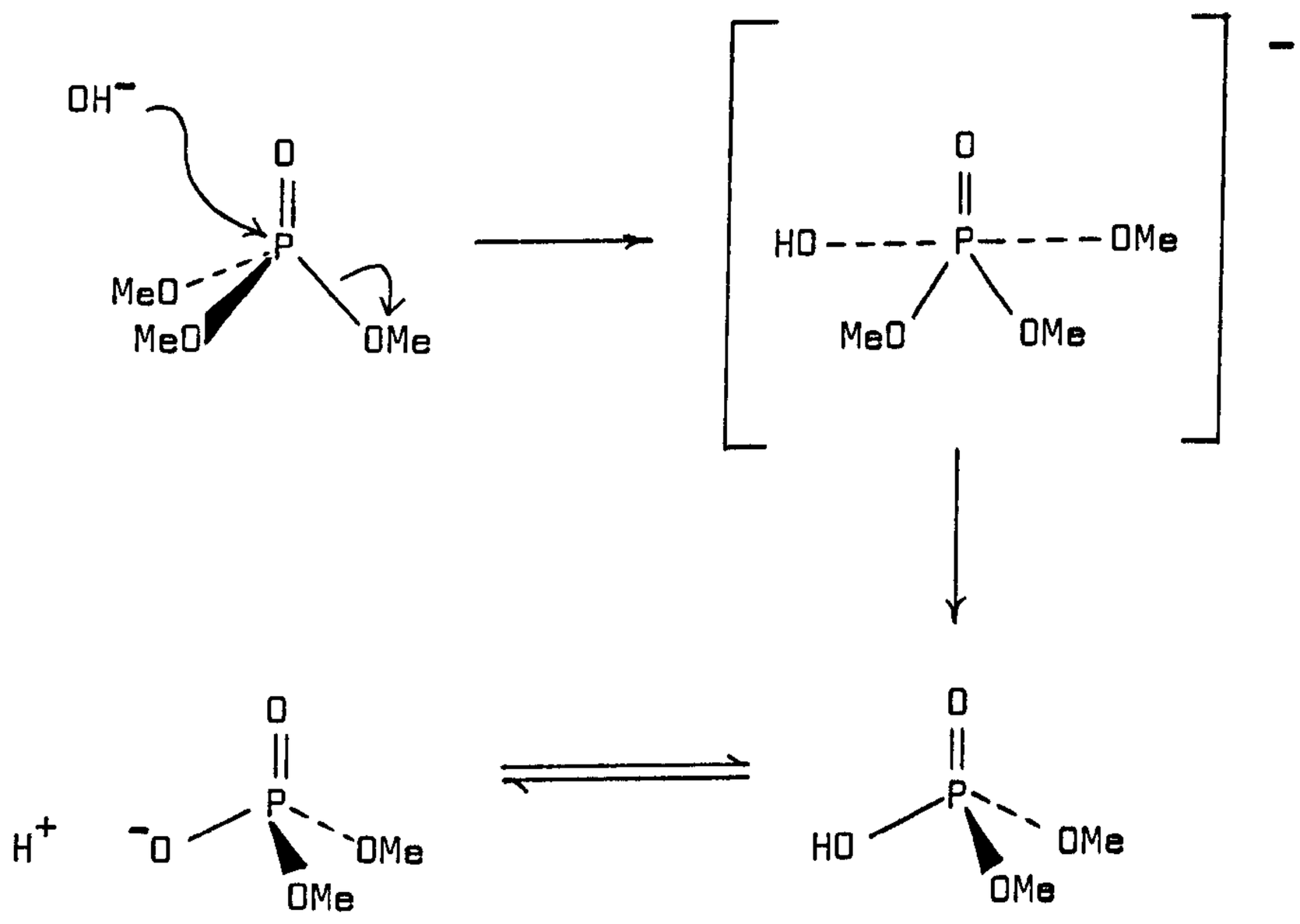

However, the role of either OH^- or H^+ is clearly less significant than for DMP. The solution does not become acidic, the reaction does not appear to proceed as far, and the resonance

position of the OH does not undergo the same magnitude of change.

The above sequence of reactions with DMP, TMP, lead acetate and lead nitrate clearly demonstrate that lead compounds have the ability to interact with organophosphorus systems modelling those found within the body, and have suggested a mechanism for such interactions. The next stage in this study was to check that these interactions did occur with typical body-phosphate systems.

8.4.6 Interactions of Lead(II) salts with Adenosine Phosphates

Adenosine triphosphate (ATP) and adenosine diphosphate (ADP) are, perforce, considerably more complex chemical structures than the model compound, DMP, chosen for these studies. A detailed examination of lead interaction with such systems remains to be done. However, some preliminary work is reported here which substantiates the main postulate of this thesis by demonstrating, beyond question, that at least one of the modes of interaction of lead in the body involves inhibition of phosphate systems.

The ATP and ADP used in the reactions described below were commercial samples obtained from Aldrich Chemical Co. Ltd. and were checked for purity by elemental analysis. The lead(II) acetate, trihydrate was, as previously used, Analar grade reagent obtained from BDH Chemicals Ltd. Aqueous solutions employed triply-distilled deionized water which was lead free to atomic absorption tests. The experiments performed are described below.

To an aqueous solution of ATP (510 mg in 10 cm^3; 0.1 M) was

slowly added 380 mg of lead(II) acetate, trihydrate dissolved in 10 cm^3 of water. A white precipitate formed immediately on contact between the two solutions. The solid obtained was removed by filtration and was then washed with several aliquots of water, followed by 3 x 20 cm^3 of diethyl ether. The product was dried on a vacuum frame for several hours. Elemental microanalysis gave the values, C, 10.91; H, 2.43; N, 6.73 and Pb, 40.22%. This corresponds to the formula $Pb_2ATP.6H_2O$, which requires C, 11.65; H, 2.62; N, 6.80; Pb, 40.02%. Whilst the carbon value was somewhat low, this may well have been due to instrumental difficulties which were being experienced at the time of this analysis, and the H, N and Pb are in excellent agreement with the theoretical values. Further drying of this material on a vacuum frame whilst gently warming with a water bath produced a solid which on re-analysis gave the results C, 12.83; H, 1.48; N, 7.23; Pb, 42.98% which indicates loss of four molecules of water. $Pb_2ATP.2H_2O$ requires C, 12.53; H, 1.88; N, 7.31 and Pb, 43.25%. A yield of 427 mg was achieved for this reaction which corresponds to 67.2% of the theoretical maximum for the above stoichiometry. Additional drying did not produce any further reduction in the water content.

The infrared spectrum of the product (Figure 8.13) is listed in Table 8.15. Notable differences between the free adenosine system and the lead complex are, firstly, a change in the NH_2 vibrations of the adenine moiety. The ν(N-H) modes (the separate

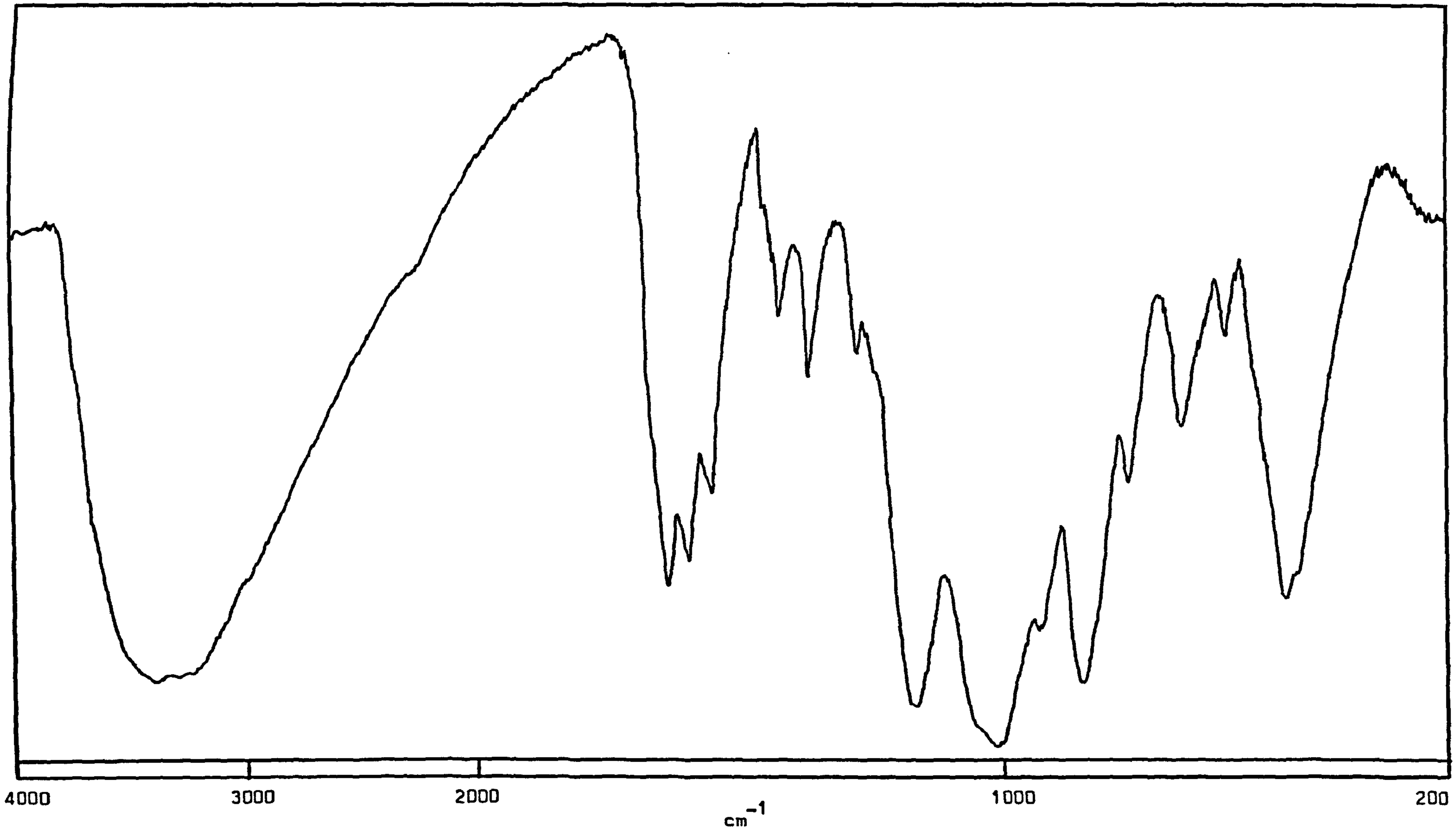

Figure 8.13 Infrared spectrum of reaction product from ATP and $Pb(OCOCH_3)_2.3H_2O$, ascribed the formula $Pb_2ATP.2H_2O$. (KBr disc).

peak positions are indistinguishable because the peak widths cause coalescence with the O-H vibrations) are shifted from 3500 cm^{-1} to 3400 cm^{-1} whilst the δ (N-H) is lowered by 21 cm^{-1} from 1708 cm^{-1} to 1687 cm^{-1}. The intramolecular hydrogen bonding of the P=O in the free molecule is confirmed by the characteristic band frequency at 1252 cm^{-1} for the stretching mode. In the lead compound this band is broadened and the centre moves to 1222 cm^{-1} with, possibly, an inflection remaining at 1252 cm^{-1}. This effect is clearly indicative of much stronger coordination to at least one of the P=O moieties with possibly one unchanged. Unlike the free triphosphate ion (X) the P=O and P-O units are distinguishable.

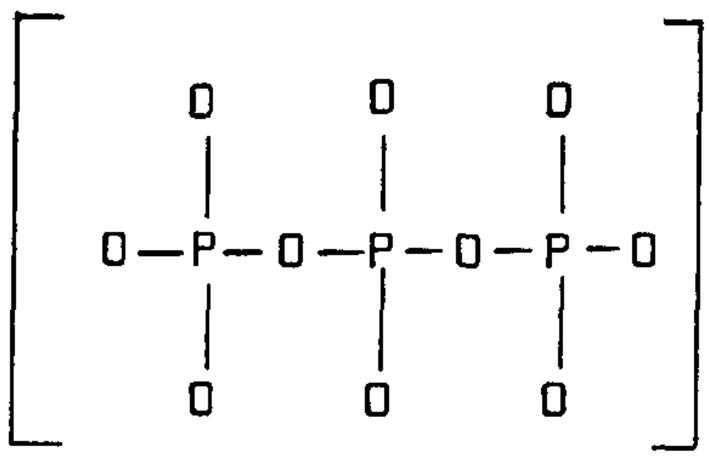

(X)

The ν(P-O) at 963 cm^{-1} in the free system has moved to 978 cm^{-1} in the lead complex : an effect observed in the DMP model on lead coordination. Here, again, presumably associated with an electron drift towards the P=O on coordination and away from the P-O. This is further supported by a change in the ν(P-(O-C)) from 1100 cm^{-1} to 1108 cm^{-1} in the complex and an increase in the O-P-O asymmetric and symmetric deformations from 511 cm^{-1} to 528 cm^{-1} and 472 to 500 cm^{-1} respectively. Other alterations in the infrared spectrum include an increase in intensity of the

Table 8.15 Infrared data [a] for ATP and the reaction products with $Pb(OCOCH_3)_2.3H_2O$

ATP		$Pb_2ATP.2H_2O$		Product, 3 days in water
Frequency (cm^{-1})	Assignment	Frequency (cm^{-1})	Assignment	(cm^{-1})
3500 b.s. 3340 b.s. 3142 b.s.	ν (N-H) and ν(O-H)	3400 b.s. 3340 b.s. 3142 b.s.	ν (N-H) and ν (O-H)	3360 - 3100 b.s.
2950 b.m.	ν(C-H)	2950 b.m.	ν (C-H)	
2700 w.	ν(P-OH)	2700 v.w.	ν (P-OH)	
1708 s.	δ (N-H)	1687 s.	δ (N-H)	
1646 s.	δ (O-H)	1642 s.	δ (O-H)	
1600 m.	ν(C=C)	1600 m.	ν (C=C)	1600 s.
1547 w.		1500 w.		1547 s.
1491 w.	ν (C=N)	1478 w.	ν (C=N)	
1409 w.	δ (C-H)	1417 w.	δ (C-H)	1403 m.
		1330 w.	δ (C-H)	
1252 s.	ν (P=O)	1250 w.	ν (P=O)	1245 w.
1225 s.	ν(C-N)	1222 s.	ν (P=O)Pb	1210 w.
1118 s.				

1100 s.	ν(P-(O-C))	1108 s.	ν (P-(O-C))	
1041 s.	ν_{as}(P-O)	1064 s.	ν_{as}(P-O)	1060 s.
1016 s.	δ (C-H)$_{ring}$			1016 w.
996 s.				
963 s.	ν_{s}(P-O)	978 s.	ν_{s}(P-O)	967 w.
910 m.				920 w.
897 s.	ν (C-C)	900 s.	ν (C-C)	
807 m.	δ (C-H)$_{ring}$	812 m.	δ (C-H)$_{ring}$	795 w.
718 m.	δ (C-H)$_{ring}$	718 m.	δ (C-H)$_{ring}$	
694 w.				656 m.
638 w.		638 w.		
626 w.				
560 w.				
511 s.	δ_{as}(O-P-O)	528 s.	δ_{as}(O-P-O)	534 m.
493 m.				
472 s.	δ_{s}(O-P-O)	500 s.	δ_{s}(O-P-O)	

[a] Obtained from KBr discs.

b, broad; w, weak; m, medium; s, strong.

mode due to O-H deformation at 1642 cm^{-1}, associated with the added water molecules.

It is found that if the product is allowed to stand in water for three days and the solid collected and dried, the infrared spectrum produced (Figure 8.14, Table 8.15) shows considerable differences from the above. The absorptions are generaly much broader and the ν(P=O) has all but disappeared. The ν (P-O) at 1060 cm^{-1} now dominates this region masking out other absorptions. A notable reduction in any bands associated with carbon is also observed.

Because of the very low solubility of the product n.m.r. data could not be obtained. However, after 70,000 scans of the ^{207}Pb spectrum there were indications of bands in the -1400 ppm and -2600 ppm regions, although the quality of the data was not sufficiently good to allow assignment with any degree of certainty. The only information provided by ^{13}C, ^{1}H and ^{31}P n.m.r. was to show that all the ATP was removed from solution on precipitation, whilst some of the acetate from the lead remained; presumably indicative of preferrential association of the lead to the ATP and away from the acetate. With the data available one may postulate as to the processes involved in lead interaction.

Lowering of the ν(P=O) frequency implies a coordination to lead in a manner similar to that shown for the model, DMP, with an associated electron drift in this direction. Divalent cations such as Mg^{2+}, are known to become 'caged' between the phosphate and adenine moieties of the molecule[802]. It is possible, therefore,

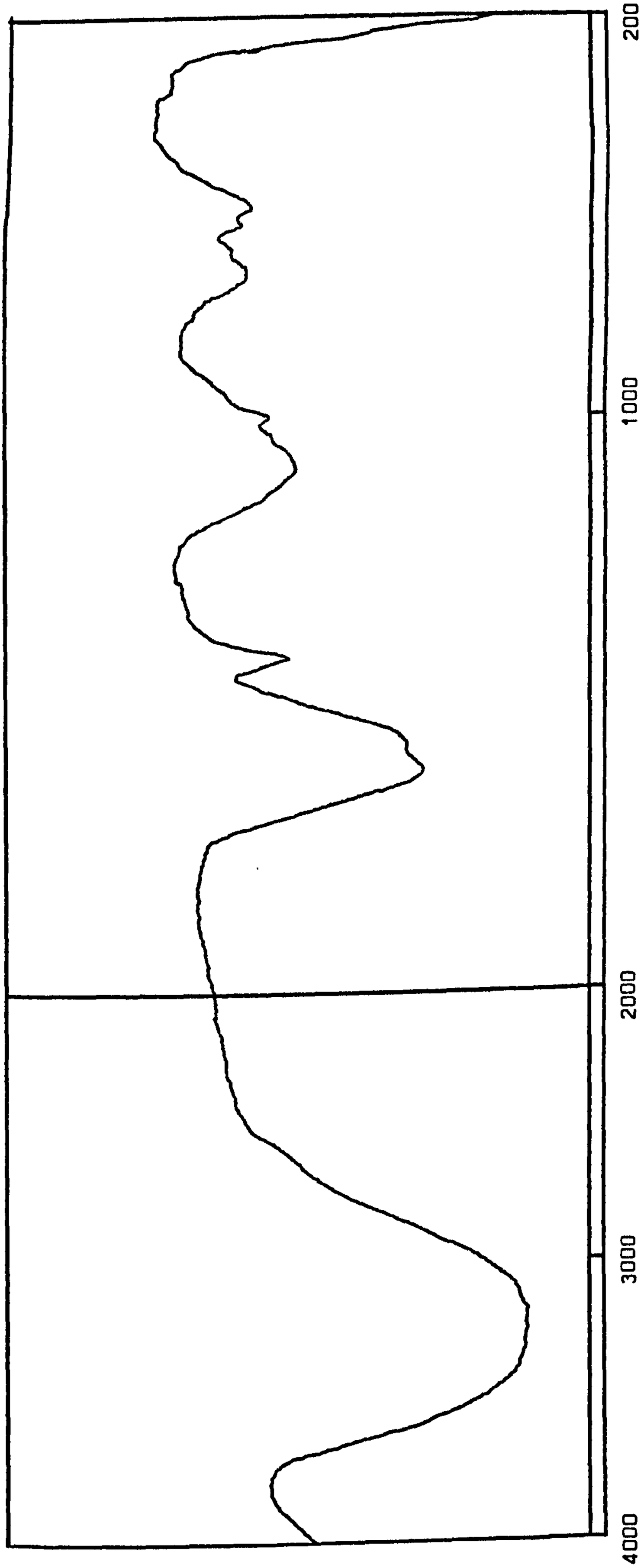

Figure 8.14 The infrared spectrum from the reaction product from ATP and $Pb(OCOCH_3)_2 \cdot 3H_2O$ after standing in water for 3 days. (KBr disc).

that in this instance the lead atoms are present, one as a coordinated lead, and the other as ionic Pb^{2+}. The data so far obtained does not allow a clear distinction to be drawn between the two possible stoichiometries $Pb_2ATP(OH)_2.H_2O$ and $Pb_2ATP.2H_2O$. The difference in elemental percentage compositions of these two systems is within the limits of experimental error for the measuring techniques and infrared data does not aid their identification. A possible structure (XI) which does satisfy the available information is shown in Figure 8.15 The change which occurs to the solid on standing in water can then be explained by analogy to the model. Whereby, cleavage of the CH_2-O bond of the ribose-phosphate linkage results leading to a lead(II) triphosphate type of system; as is indicated by comparison of the resulting infrared spectrum with that for known triphosphate systems[808].

In keeping with the work on the model systems the above experiments were repeated using lead nitrate, to eliminate the possibility of influence of a specific lead salt on the course of the reaction. Following exactly the procedure described above, except for the replacement of $Pb(OCOCH_3)_2.3H_2O$ by $Pb(NO_3)_2$, spontaneous precipitation again occurred immediately on addition of the lead solution. The solid was washed and dried and an infrared spectrum obtained as a KBr disc. The data resulting (Table 8.16), with the exception of a few minor peaks, are identical to the product obtained using lead(II) acetate.

A preliminary reaction was also run using adenosine diphosphate (ADP) in place of ATP. This again gave immediate precipitation

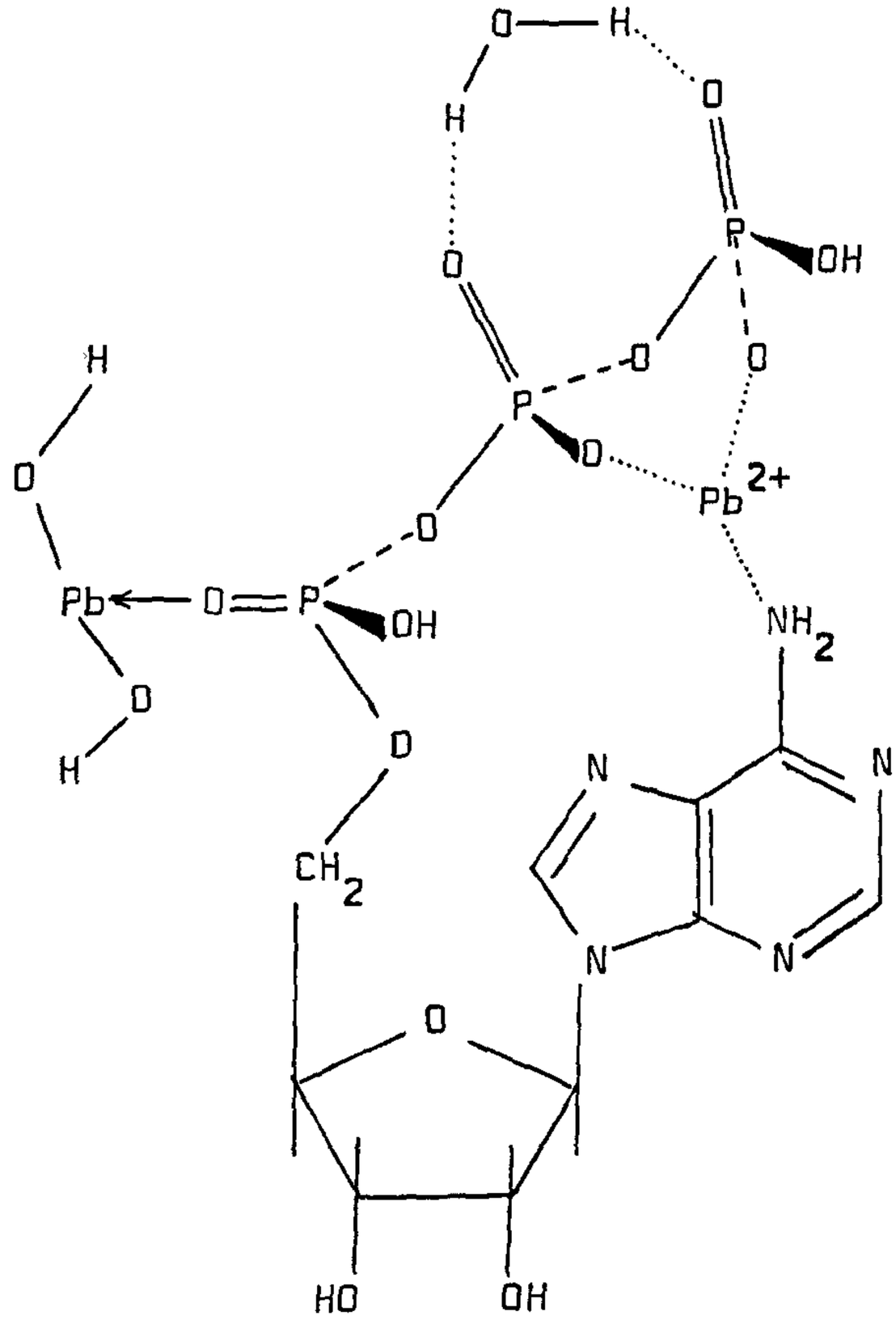

(XI)

Figure 8.15 Proposed structure of the lead-ATP complex

Table 8.16 Infrared data for the reaction product from ATP and $Pb(NO_3)_2$ [a]

Frequency (cm^{-1})		Assignment
3400	b.s.	ν(N-H) and ν(O-H)
3340	b.s.	
3180	b.s.	
3120	b.s.	
2950	b.m.	ν(C-H)
1687	m.	δ(N-H)
1642	s.	δ(O-H)
1604	m.	ν(C=C)
1575	m.	
1478	w.	ν(C=N)
1417	m.	δ_{as}(C-H)
1332	m.	δ_{s}(C-H)
1298	w.	
1230	b.s.	ν(P=O)
1108	b.s.	ν(P-O-C)
1064	s.	ν_{as}(P-O)
978	s.	ν_{s}(P-O)
900	s.	ν(C-C)
818	w.	δ(C-H)$_{ring}$
795	w.	δ(C-H)$_{ring}$
638	w.	
528	s.	δ_{as}(O-P-O)
499	s.	δ_{s}(O-P-O)

b, broad; w, weak; m, medium; s, strong.

[a] Recorded as a KBr disc.

on addition of aqueous solutions of lead(II) acetate and lead(II) nitrate. The solid from the acetate preparation was analysed for elemental composition and gave the results C, 10.86; H, 4.59; N, 4.74 and Pb, 36.3%. This equates to an approximate stoichiometry of $Pb_2ADP.15H_2O$, which requires C, 10.80; H, 4.14; N, 6.30 and Pb 37.26%. The nitrogen value was not satisfactory and the drying process appears to have been less efficient than for ATP. The drying process was repeated and an infrared spectrum recorded (Figure 8.16). This showed some interesting differences from the free ADP (Table 8.17).

Not unexpectedly the assignment is very similar to ATP. However, the δ (N-H) shows a low frequency shift of only 3 cm^{-1} on addition of lead instead of the 21 cm^{-1} seen for ATP. The (P=O) vibration moves to a value of 1064 cm^{-1}, as found for ATP. Similar shifts to those seen in ATP on lead complexation are also observed in the modes associated with P-O and it seems likely, therefore, that a structure similar to that proposed for the lead-ATP is formed. Although stereochemical constraints probably inhibit involvement of the NH_2 group on adenine to any marked extent, as is reflected in the infrared absorption frequency for that moiety.

By using light scattering from an Ar^+ laser it was possible to demonstrate that μM quantities of lead interact with 0.1 M solutions of ATP and ADP. It is clear, therefore, that sub-clinical levels of lead in the body will inhibit the action of ATP and ADP.

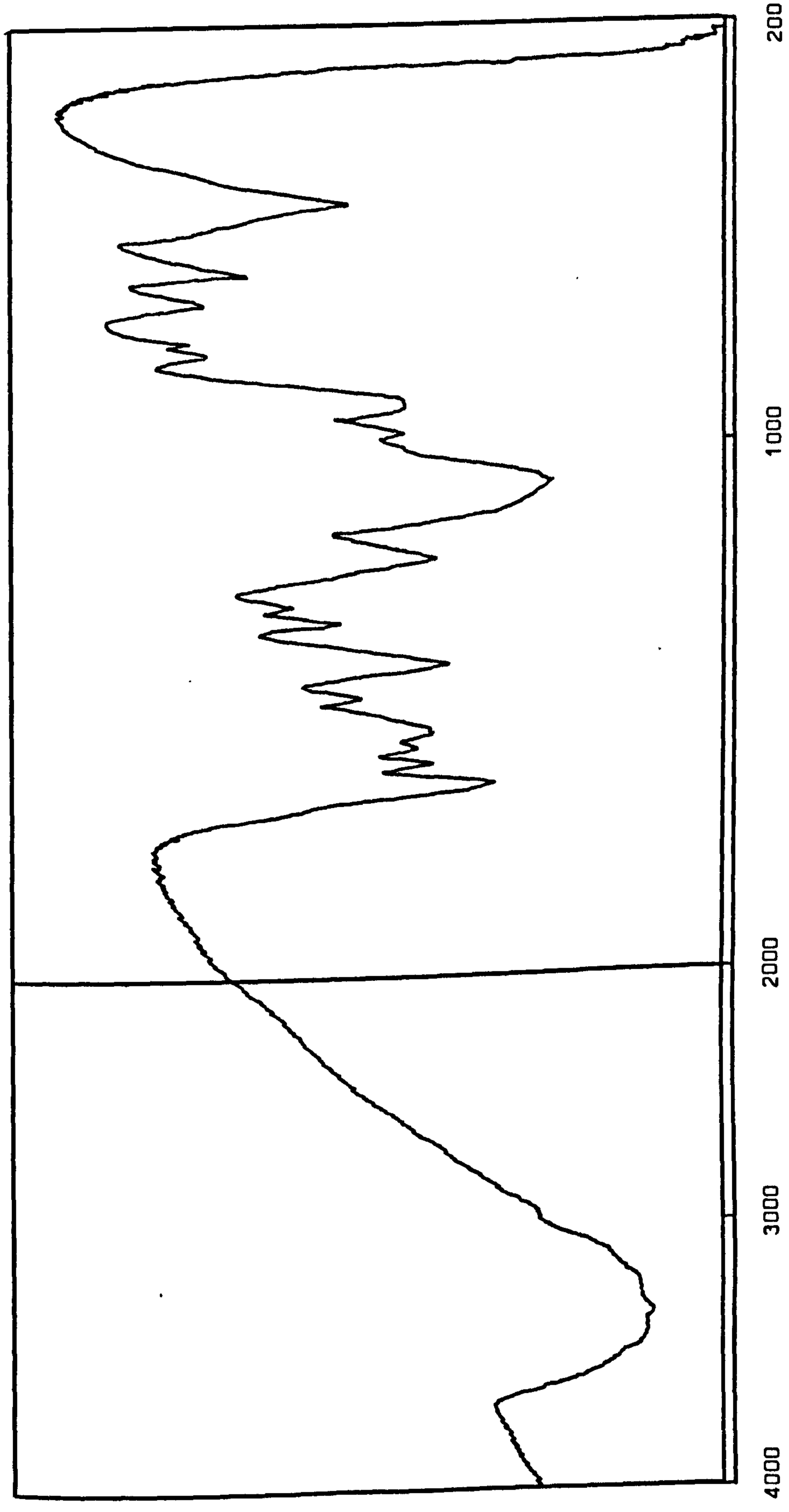

Figure 8.16 Infrared spectrum of the reaction product from ADP and $Pb(OCOCH_3)_2 \cdot 3H_2O$.
(KBr disc).

Table 8.17 Infrared data [a] for ADP hydrate and the reaction product with $Pb(OCOCH_3)_2.3H_2O$.

ADP Hydrate		ADP - Pb Product	
Frequency (cm^{-1})	Assignment	Frequency (cm^{-1})	Assignment
3350 b.s.	ν(N-H) and ν(O-H)	3350 b.s.	ν(N-H) and ν(O-H)
3160 b.s.		3170 b.s.	
2940 b.m.	ν(C-H)	2930 b.m.	ν(C-H)
2880 b.m.			
1690 s.	δ(N-H)	1687 m.	δ(N-H)
1650 s.	δ(O-H)	1650 vs.	δ(O-H)
1609 m.	ν(C=C)	1600 m.	ν(C=C)
1578 w.		1578 w.	
		1530 m.	
1478 m.	ν(C=N)	1478 w.	ν(C=N)
1417 m.	δ_{as}(C-H)	1417 s.	δ_{as}(C-H)
1336 m.	δ_{s}(C-H)	1333 w.	δ_{s}(C-H)
1222 s.	ν(P=O)	1202 s.	ν(P=O)
1108 s.	ν(P-(O-C))	1112 m.	ν(P-(O-C))
1077 s.	ν_{as}(P-O)	1064 b.s.	ν_{as}(P-O)
962 m.	ν_{s}(P-O)	978 m.	ν_{s}(P-O)
920 s.	ν(C-C)	920 s.	ν(C-C)
818 m.	δ(C-H)$_{ring}$	818 m.	δ(C-H)$_{ring}$
795 w.	δ(C-H)$_{ring}$	795 w.	δ(C-H)$_{ring}$
718 m.		718 m.	
638 m.		650 m.	
518 b.s.	δ(O-P-O)	526 s.	δ_{as}(O-P-O)
		486 s.	δ_{s}(O-P-O)

[a] Obtained using KBr Discs.

b, broad; s, strong; m, medium; w, weak.

8.5 CONCLUSIONS

The overwhelming tendency in previous work on lead poisoning has been to concentrate on three main areas of research:

i) *the source of contamination*,

ii) the pathological effects,

iii) analytical methods for the diagnosis of lead poisoning.

Surprisingly, very little attention has been given to the precise chemical processes involved in plumbism. Chemically, much effort has been expended in drawing up detailed lists of relative toxicities of lead compounds; MLD and LD_{50} as well as TLV values have been determined for a wide range of lead salts. Balance studies have been carried out, largely in immitation of the excellent work of Kehoe (see Chapter Five). Sites of toxic effects have been thoroughly mapped and the associated pathological consequences recorded in detail. Yet examination of Waldron and Stöfens monograph[809] which provides a comprehensive review of work on lead in the body to 1974, whilst detailing many studies in the three catagories mentioned, spares but several paragraphs for the chemical modes of lead interaction, and then mainly concerning the breakdcwn of lead tetraethyl. Current work continues the trend. For example, a recent study was made into neonatal lead toxicity and <u>in vitro</u> lipid peroxidation of rat brain[810]. In this work, neonatal rats were given intragastric doses of aqueous lead(II) acetate for 2 - 20 days of life. Blood lead levels and growth aberrations were monitored. Subsequently

the *in vitro* rate of lipid peroxidation of brain tissue as a function of lead dosage was established. The aim of the work being to study inhibition of enzymic oxidation by lead. However, whilst this study adds to the knowledge on the effects of lead, typically, it says nothing of the chemical involvement of lead. Even work on inhibition of haem synthesis by the metal has largely centred on which porphyrins or their precursors are affected and to what extent. The absence of a biochemical or medical background has forced us to examine the problem with the eye of an inorganic chemist. Hopefully, the results of this new approach reported herein, may contribute to a more fundamental understanding in the three areas typically studied.

The environmental analysis of roadside lead distribution has illustrated the fact that sub-clinical levels of lead are now a feature of such locations and that a) produce grown within the vicinity of such a road system is contaminated and b) people are consuming such produce and exposing themselves to sub-clinical levels of lead poisoning, particularly where fruit is gathered and made into preserves. Whilst the lead levels resulting from this route of ingestion are small the work on low levels of lead with ATP and ADP (Section 8.2.6) has shown interactions at these concentrations can occur. By definition, the very fact that a foreign agent is interrupting the normal body functioning means that lead at these levels is acting as a poison.

More seriously, clinical lead poisoning is an almost certain

consequence of use of some of the Asian medicines and cosmetics described in Chapter Seven. This source of poisoning had not previously been considered in treatment of maladies within that ethnic community in Western Society. In addition, a clear relationship between particle size ingested and degree of available lead has been shown. Most importantly, a specific site of interaction of absorbed lead within the body has been established, namely, the phosphorus-oxygen system.

It is clear that lead disrupts the connection of phosphate and phosphite analogues to the macromolecular units within the body. The main process appears to be binding of the metal to the phosphoryl group which, in turn, results in an electron drift which first weakens then finally cleaves the C-O bond linking the organic and phosphate units. Precipitation of an insoluble lead salt of the phosphorus moiety results and the macromolecule is deactivated towards its biological function. This effect can be linked to a number of known pathological consequences of plumbism.

Firstly, it supports the model for gastrointestinal absorption proposed in Chapter Seven in that binding of lead to the phosphoryl group will allow the metal to pass through the cell membrane. Because the gastrointestinal area is a dynamic system the lead is unlikely to reside a sufficient length of time to cause C-O cleavage, and hence direct passage of the lead through the cell interior and into the blood system will result. However, in a more static situation, for example, with nerve cells,

where lead will remain bound to the cell epithelium for a longer period, cleavage may occur and rupture of the cell membrane may result. Damage to the cell body of a neuron which may result in this way can lead to a prevention of the nerve functions. One of the symptoms of lead poisoning is peripheral neuropathy which could well arise from the process described. In adults the presenting symptoms of the early neurological effects of lead include a tingling sensation in the fingers and toes, whilst in children the possible long term consequences may be mental retardation. The extent of these effects is lead-concentration dependent, the tingling sensation may progress to muscle incapacity, 'wrist-drop' etc. This would fit a pattern of membrane interruption : the higher the lead content, the greater the phosphate interaction and the subsequent extent of membrane malfunction and hence paraesthesia and ataxia result. This would also fit into an aetiology of such a disease as multiple sclerosis, to which connections have been suggested with sub-clinical lead poisoning[811,812]. It may also be that the animal illness, swayback, which results from a demyelination process, previously associated with a copper deficient diet, may infact be another example of the above mechanism. The incidence of this disease is known to be high in Derbyshire, an area where soil lead levels are generally above the average.

Other well documented effects of lead poisoning can also be explained in terms of a lead-phosphorus-oxygen interaction.

This work has demonstrated the interaction of lead with ADP and ATP which are, as shown earlier, primary energy transfer agents within the body. Loss of these molecules would result in many essential metabolic processes being unable to function with resulting asthenia.

Because the phosphoryl system is so essential to the body processes it is possible to extend the examples to many other connections between presenting symptoms and areas where interruption of the phosphate action would give such consequences. In addition, in bone, for example, hydroxyapatite, $Ca_5(PO_4)_3OH$, contributes 23% of the crystalline material and almost 90% of tooth enamel, which, incidently, is, of course the reason for adding fluoride to water and toothpaste; the slow replacement of hydroxyl groups in hydroxyapatite giving fluoroapatite, $Ca_5(PO_4)_3F$, which is, infact, the least soluble of all the calcium phosphates. Bone and teeth are both sites for lead concentration and storage and a number of complex reactions may well be occurring. As discussed in Chapter Five, lead(II) hypophosphite has been shown to result from a metathetical reaction between calcium hypophosphite and lead(II) nitrate. Similar systems may be involved with the skeletal phosphate. Much further work is obviously needed in this field. However, it is hoped this study may have provided the first clues to at least one mechanism of chemical interaction of lead within the body, and in so doing may have opened a rich, new field for research.

REFERENCES

801. D.S. Parsons (Ed.), (Biological Membranes', (1975) Clarendon Press, Oxford.

802. A.L. Lehninger, 'Biochemistry', 2nd Ed. (1975) Worth Pub. Inc. New York.

803. M.S. Bretscher, Science (1973) 181 622.

804. H. Davson and J. Danielli, J. Cellular Comp. Physiol., (1935) 5 498.

805. J.D. Robertson 'Cellular Membranes in Development (1964) Ed. Locke, Academic Press, New York.

806. S.J. Singer and G.L. Nicolson, Science (1972) 175 720.

807. G.B. Ansell, J.N. Hawthorne and R.M.C. Watson, (Eds.) 'Form and Function of Phospholipids' Vol. 3. (1973), Elsevier, Amsterdam.

808. S. Greenfield and M. Clift 'Analytical Chemistry of the Condensed Phosphates (1975), Pergamon Press, London.

809. H.A. Waldron and D. Stöfen 'Sub-clinical Lead Poisoning' (1974) Academic Press, London and New York.

810. B.B. Grelman, I.A. Michaelson and R.L. Bornschein. J. Toxicol. Envir. Health, (1979) 5 683.

811. A.M.G. Campbell, F. Herdan, W.F.T. Tatlow and E.G. Whittle, Brain (1950) 73 52.

812. H.V. Warren, R.E. Delavault and C.H. Cross. Annals of the New York Acad. Sci., (1967) 136 657.

SURMA AND BLOOD LEAD IN CHILDREN

Departments of Chemistry and Pharmacy
University of Nottingham
Nottingham NG7 2RD

M. ASLAM
M.A. HEALY
S.S. DAVIS
A.R. ALI

Reprinted from THE LANCET
22 March 1980, pp. 658-9

* For part XXII see ref. 12.
** IOTG = *iso*-octythioglycollate, βMeOct = $SCH_2CH_2CCOC_7H_{15}$.

Reprinted from THE LANCET *March 22, 1980, pp.658-9*

SURMA AND BLOOD LEAD IN CHILDREN

SIR,—Dr Attenburrow and colleagues from Glasgow (Feb. 9, p. 323) studied the relation between the use of surma (the fine powder applied to the conjunctival margins of Asian infants and children) and blood lead levels, and conclude that "Surma remains a theoretical rather than a practical health hazard". They found mean blood lead concentrations of 0·799±0·285 μmol/l in surma users and 0·760±0·302 μmol/l in controls. The mean lead concentration for seven surma samples analysed was 21% (w/w), the highest value being 30%. Our studies[1] suggest that such values are considerably lower than the mean lead concentration of preparations generally used by Asians in Britain. The lead concentration in some proprietary surmas analysed by atomic absorption spectrometry (Perkin-Elmer 603) were:

Description	*Colour*	*%lead (w/w)*
Nargasi Surma (Hamdard, Pakistan)	Grey	77·3
Binger Surma (Hamdard, Pakistan)	Black	26·3
Surma Moqawi (Basar Taj Co., Lahore)	Grey	53·7
Bal Jyoti (Murrari Brothers, Delhi)	Grey-black	38·4
Nag Jyoti (Murrari Brothers, Delhi)	White	<0·5
M. D. Hashim Surma (Bunder Road, Karachi)	Grey	82·9
Multani (Ayurvedic, 36-H Connaught Circus, Delhi)	Grey	<0·5
Hashmi Surma (Jowahar Chaharam, Karachi)	Grey	80·2

The mean lead concentration for these surmas is 59·8% (w/w). We have also analysed a further 72 home-made surma samples obtained in Nottingham, Bradford, Manchester, Birmingham, and London. 46 contained lead (20–86% w/w, mean 54%).

Our experiments on rabbits eliminate the possibility of transcorneal transport of the lead, but passage down the nasolachrymal duct and, primarily, transference via the fingers to the mouth does occur. Some 20 mg of surma is deposited on the conjunctiyæ at each application. One can estimate from the amount transferred to the fingers on wiping the eyes and then sucking the fingers that about 0·2% of the applied surma is being ingested. If the surma with an average lead content of 50% were applied once daily this could produce a weekly ingestion of lead of the order of 140 μg. In children 25–50% of ingested lead may be absorbed in the gut,[2] so surma could contribute 35–70 μg of lead per week to the total body burden of the metal in a child. When we examined blood lead levels of 62 Asian children in Nottingham[3] we found that the surma users had a mean blood lead of 1·65±0·68 μmol/l, whilst the non-surma users had 0·98±0·42 μmol/l ($p<0·001$). In Bradford[4] 117 Asian children, 45 of whom had been surma users, and 49 White controls had their blood lead levels and similar results were obtained. 14% of the 117 Asian children had lead levels above 1·45 μmol/l and 5% had values greater than 1·7 μmol/l.

We also monitored the progress of an Asian child admitted to hospital in 1976 with plumbism believed to be attributable to surma since no other source of lead could be found. The child was receiving regular applications of a surma containing

---

* For part XXII see ref. 12.

** IOTG = *Iso-octylthioglycollate*, $SMeOct = SCH_2CH_2COOC_7H_{15}$.

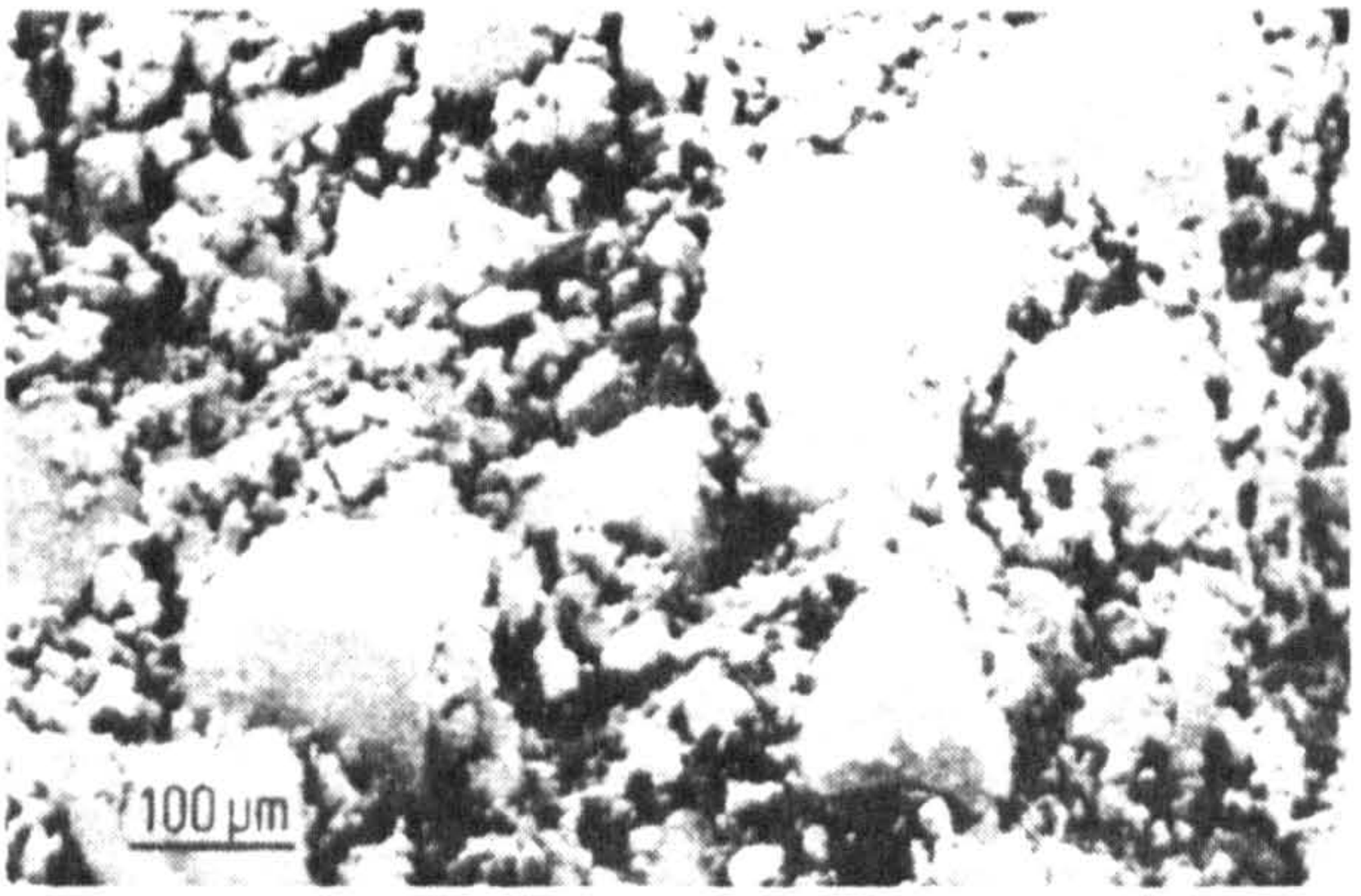

Photomicrograph of lead-containing surma particles.

86% lead. Despite warnings the mother continued to apply the material. In 1976 the child's blood lead was 2·4 µmol/l; in 1977 this had risen to 3·0 µmol/l; and on readmission to hospital with lead poisoning in 1978 he had 3·4 µmol/l of lead in his blood.

Baltrop and Meek[5] have reported a five-fold enhancement in absorption of lead in the gut when the particle size was reduced from 196 µm to 6 µm. Photomicrographs (see figure) show that most particles in the lead surmas fall at the lower end of this range, where absorption would be greatest.

Whilst it is encouraging to find that surma is not associated with lead poisoning in Glasgow and that the material is not widely used there, the possible health hazards and sequelæ[9] of surma use should not be disregarded. We recommend that the use of surma should be discouraged.

M. ASLAM
M. A. HEALY
S. S. DAVIS
A. R. ALI

Departments of Chemistry
and Pharmacy,
University of Nottingham,
Nottingham NG7 2RD

1. Aslam M, Davis SS, Healy MA. Heavy metals in some Asian medicines and cosmetics. *Publ Hlth Lond* 1979; **93:** 274–84.
2. Waldron HA, Stöfen D. Subclinical lead poisoning. London: Academic Press, 1974: 44.
3. Ali AR, Smales ORC, Aslam M. Surma and lead poisoning. *Br Med J* 1978; ii: 915–16.
4. Green SDR, Lealman GT, Aslam M, Davis SS. Surma and blood lead concentrations. *Publ Hlth London* 1979; **93:** 371–76.
5. Baltrop D, Meek F. Effect of particle size on lead absorption from the gut. *Arch Envir Hlth* 1979; **34:** 280–85.
6. Warley MA, Blackledge P, O'Gorman P. Lead poisoning in eye cosmetic. *Br Med J* 1968; i: 117.
7. Betts PR, Astley R, Raine DN. Lead intoxication in children in Birmingham. *Br Med J* 1973; i: 402–06.
8. Snodgrass GJAI, Ziderman DA, Gulati V, Richards J. Cosmetic plumbism. *Br Med J* 1973; iv: 230.
9. Aslam M, Davis SS, Healy MA, Rack PH. The presence of heavy metals in Asian medicines and cosmetics and the implication for mental health. *Bull Ment Hlth WHO* 1980 (in press).

Printed in
Great Britain

Journal of Organometallic Chemistry, 182 (1979) 17—36

STRUCTURAL STUDIES IN MAIN GROUP CHEMISTRY

XXIII *. ESTERTIN DERIVATIVES. STRUCTURAL AND SPECTROSCOPIC STUDIES

PHILIP G. HARRISON *, T.J. KING and M.A. HEALY

Department of Chemistry, University of Nottingham, University Park, Nottingham NG7 2RD (Great Britain)

(Received May 18th, 1979)

Summary

The crystal and molecular structures of three 'estertin' derivatives, $Cl_3SnCH_2CH_2CO_2Me$, $Cl_2Sn[CH_2CH_2CO_2Me]_2$ and $Cl_2Sn[CH_2CH_2CONH_2]_2$, are reported. Crystals of $Cl_3SnCH_2CH_2CO_2Me$ are orthorhombic, space group $P2_12_12_1$, with a 9.2981, b 10.5389, and c 10.0885 Å; those of $Cl_2Sn[CH_2CH_2CO_2Me]_2$ are monoclinic, space group $P2_{1/c}$, with a 8.0107, b 15.9104, c 13.4109 Å, and β 131.0044°; and those of $Cl_2Sn[CH_2CH_2CONH_2]_2$ are also monoclinic, space group C_c, with a 9.1314, b 12.8672, c 13.0317 Å, and β 126.6032°. Crystals of $Cl_3Sn(CH_2CH_2CO_2Me)$ and $Cl_2Sn[CH_2CH_2CO_2Me]_2$ both consist of discrete molecules, but extensive intermolecular hydrogen-bonding occurs in crystals of $Cl_2Sn[CH_2CH_2CONH_2]_2$. Intramolecular carbonyl oxygen-to-tin coordination occurs in all three compounds.

Vibrational and mass spectra are also reported, and are assigned in accordance with the determined structures.

Tin-119 Mössbauer studies demonstrate that it is possible to investigate the nature of organotin additives to PVC by this method. Preliminary investigations show that $Bu_2Sn(IOTG)_2$ ** added to PVC undergoes only partial IOTG for chlorine exchange at the milling stage, but is completely converted to Bu_2SnCl_2 after thermal degradation. Both $BuAcSn(IOTG)_3$ and $BuAcSn(\beta MeOct)_3$** undergo complete sulphur ligand for Cl exchange during the milling process giving $BuAcSnCl_3$ as the species detected. Degradation to some unidentified organotin species occurs on heating.

---

* For part XXII see ref. 12.

** IOTG = *iso*-octylthioglycollate, βMeOct = $SCH_2CH_2OCOC_7H_{15}$.

Introduction

The formation of β-carbonyl-substituted ethyltin compounds by the reactions of tin metal or tin (II) halides with a carbonyl-substituted alkene in the presence of hydrogen halide, a method devised by Burley, Hutton and Oakes [1], has facilitated the preparation of a new series of 'Estertin' stabilisers for PVC plastics. The syntheses, which appear to take place in a wide variety of solvents and over a large temperature range, may be summarised by the equations:

$$Sn + 2\,HX + 2\,R_2C{=}CR_2 \rightarrow X_2Sn(CR_2{-}CR_2H)_2 \quad (1)$$

$$SnX_2 + HX + R_2C{=}CR_2 \rightarrow X_3SnCR_2{-}CR_2H \quad (2)$$

X = Cl, Br, I.

where at least one of the groups R must be a carbonyl function (ester, ketone, amide, etc.). The mechanisms of the reactions were initially proposed to involve the intermediate formation of the halogenostannanes, X_3SnH and X_2SnH_2, but more recent investigations by Bulten [2] have indicated the intermediacy of $H_2SnCl_4 \cdot nEt_2O$ in both.

In this paper we report the structures of three estertin derivatives, as well as vibrational, mass spectral, and tin-119 Mössbauer data. Preliminary results of a Mössbauer study of estertin thiolate compounds in PVC are also presented.

Experimental

1. Syntheses

(i) Bis(β-carbomethoxyethyl)tin dichloride

The procedure used was essentially similar to that outlined by Hutton and Oakes [1]. To a stirred suspension of tin powder (3.5 g, 0.03 mol) in dry THF (15 cm^3) was added methyl acrylate (5.5 cm^3, 0.06 mol). Anhydrous hydrogen chloride gas was then passed through the mixture for ca. 2 h maintaining the temperature at ca. 20°C using a water bath. The white precipitate formed was washed with dry THF (3 × 10 cm^3) to remove any organotin trichloride. Extraction of the residue with hot chloroform (30 cm^3), and subsequent slow crystallisation yielded a highly crystalline sample of bis(β-carbomethoxyethyl)tin dichloride, mp. 132—133°C (lit. [1] 132°C). Found: C, 26.42; H, 4.14; Cl, 18.62%. $C_8H_{14}Cl_2O_4Sn$ calcd.: C, 26.37; H, 3.84; Cl, 19.30%.

(ii) β-Carbomethoxyethyltin trichloride

A similar procedure was adopted for the preparation of this compound using anhydrous tin(II) chloride (4.7 g, 0.025 mol) and methyl acrylate (2.25 cm^3, 0.025 mol) in dry toluene (20 cm^3). Anhydrous hydrogen chloride was passed through the solution for 1 h, when the solvent was removed under vacuum. Extraction and re-crystallisation from hot toluene yielded white crystalline β-carbomethoxyethyltin trichloride, mp. 71—72°C (lit. [1] 70°C). Found: C, 12.54; H, 1.90; Cl, 28.14%. $C_4H_7Cl_3O_2Sn$ calcd.: C, 12.55; H, 1.83; Cl, 27.85%.

(iii) Other compounds

All other compounds were provided by Dr. J.W. Burley of AKZO Chemie (UK) Ltd, and recrystallised where necessary.

2. *X-ray diffraction studies*

(i) β-Carbomethoxyethyltin trichloride

A crystal of approximate dimensions 0.3 × 0.3 × 0.5 mm was loaded into a Lindemann capillary and used for the initial photography and subsequent intensity data.

Crystal data: $C_4H_7Cl_3O_2Sn$, M = 312.29, Orthorhombic, a 9.2981, b 10.5389, c 10.0885 Å, V 988.59 Å^3, Z = 4, $F(000)$ = 592, μ(Mo-K_α) = 33.45 cm^{-1}, space group $P2_12_12_1$ by systematic absences ($h00$ for $h = 2n + 1$, $0k0$ for $k = 2n + 1$, and $00l$ for $l = 2n + 1$).

Cell measurements and data collection: The space group and initial cell parameters were determined from oscillation and zero- and first-layer Weissenberg photographs using a Nonius-Weissenberg Camera. Relative intensities up to θ = 27.5° were collected using Mo-K_α radiation (λ 0.71069 Å) on a Hilger and Watts Y290 four-circle automatic diffractometer. Accurate cell parameters were obtained by least squares refinement using ca. 23 reflections. Systematically absent reflections and reflections with $I < 3\sigma(I)$ were discarded reducing the total number of reflections from 1365 to 1198. Intensity corrections were made for Lorentz and polarization effects, but none were made for absorption due to the low value of μ.

Structure determination and refinement: The positional parameters of the tin atom were determined using a three dimensional Patterson synthesis. These coordinates were then used to phase the initial structure factor calculations. Subsequent alternate Fourier syntheses and least-squares isotropic refinement yielded the positions of the remaining light atoms. The final stages of the refinement were carried out with the atoms varying anisotropically, and when the R value reached convergence of 0.042, a weighting scheme based on the Chebychev series to five terms

$$w = \frac{1}{A(0)\,T(0)\,(X) + A(1)\,T(1)\,(X) + \ldots + A(n-1)\,T(n-1)\,(X)}$$

where $A(n)$ is the coefficient of the nth term and $X = F_0/F_{0(max)}$, was employed to minimise $\Sigma(F_0 - F_c)$ [4] over all reflections. The coefficients used were 791.49, 1350.07, 854.89, 379.59 and 94.37. After a further four cycles of full matrix, anisotropic least-squares refinement, a final R value of 0.0332 was obtained. Calculations were performed using the CRYSTALS [3] suite of programmes The scattering factors used were those neutral atoms. [4] Final fractional atomic coordinates and anisotropic thermal parameters are listed in Tables 1 and 2, respectively. Intramolecular bond lengths and angles are given in Table 3, and least-squares planes data are collected in Table 4. Fig. 1 shows the molecular geometry and atomic labelling, and a projection of the unit cell onto the bc plane is illustrated in Fig. 2.

(ii) Bis(β-carbomethoxyethyl)tin dichloride

A very similar procedure to that above was adopted using a crystal of approximate dimensions 0.3 × 0.3 × 0.4 mm mounted in a Lindemann capillary.

Crystal data: $C_8H_{14}O_4Cl_2Sn$, M = 363.81, Monoclinic, a 8.0107, b 15.9104, c 13.4109 Å, β 131.0044°, V 1289.13 Å^3, Z = 4, $F(000)$ = 712, μ(Mo-K_α) =

TABLE 1

FINAL FRACTIONAL ATOMIC COORDINATES IN β-CARBOMETHOXYETHYLTIN (IV) TRICHLORIDE $Cl_3SnCH_2CH_2CO_2CH_3$

Atom	x/a	y/b	z/c
Sn(1)	0.18463(4)	0.02702(5)	0.22049(4)
Cl(1)	0.4036(2)	0.1007(3)	0.2639(3)
Cl(2)	0.2227(3)	−0.2165(2)	0.2038(3)
Cl(3)	0.1036(2)	0.0558(3)	0.4246(2)
O(1)	−0.0351(5)	−0.0340(6)	0.1707(5)
O(2)	−0.1966(6)	0.0346(7)	0.0435(6)
C(1)	0.1335(7)	0.1821(8)	0.0788(7)
C(2)	0.0038(9)	0.1560(1)	0.0202(8)
C(3)	−0.768(9)	0.0440(1)	0.0855(9)
C(4)	−0.2840(9)	−0.0660(1)	0.1060(1)

Estimated standard deviations in parentheses

23.96 cm^{-1}. Space group $P2_{1/c}$ by systematic absences ($0k0$) for $k = 2n + 1$ and $h0l$ for $l = 2n + 1$).

Cell measurements and data collection: These were carried out as above collecting data up to $\theta = 25°$. Of 3109 reflections measured, those with $I < 3\sigma(I)$ were discarded leaving 2388 for the structure determination. Again corrections were made for Lorentz and polarization effects, but not for absorption.

Structure Determination and Refinement: This structure was also determined using an initial three-dimensional synthesis to locate the tin atom, followed by successive Fourier syntheses to locate the light atoms. Full-matrix, least-squares anisotropic refinement was carried out to an R value of 0.048, when a weighting scheme based on the Chebychev series in $T(n)(X)$ to give terms was used. The coefficients $A(0)$—$A(4)$, calculated to minimise $\Sigma(F_o - F_c)$ [4] over all reflections used were 162.91, 246.44, 118.66, 42.08 and 14.33. A final R value of 0.046 was obtained after a further three cycles of full-matrix, least-squares anisotropic refinement. All calculations were performed as above. Final fractional

TABLE 2

FINAL ANISOTROPIC THERMAL PARAMETERS FOR β-CARBOMETHOXYETHYL TIN (IV) TRICHLORIDE

Atom	U(11)	U(22)	U(33)	U(23)	U(13)	U(12)
Sn(1)	5.150(20)	5.580(20)	5.730(20)	1.350(20)	0.090(20)	0.00(20)
Cl(1)	5.120(9)	9.90(2)	10.20(2)	0.90(1)	−0.40(1)	−0.50(1)
Cl(2)	9.50(1)	5.80(1)	8.70(1)	1.10(1)	1.30(1)	1.40(1)
Cl(3)	7.10(1)	9.30(1)	5.90(1)	−0.30(1)	3.60(9)	−0.50(1)
O(1)	5.70(2)	6.10(3)	7.60(3)	1.90(3)	−1.60(2)	−0.40(3)
O(2)	6 90(3)	7.50(3)	9.60(4)	−0.60(3)	−3.20(3)	1.70(3)
C(1)	6.70(4)	7.10(4)	8.10(4)	3.20(3)	0.20(3)	0.00(3)
C(2)	8.20(5)	7.30(5)	6.50(4)	1.90(4)	−0.30(4)	1.10(5)
C(3)	5.90(4)	5.60(5)	6.10(5)	−1.10(4)	−0.30(4)	1.40(5)
C(4)	5.70(4)	8.20(6)	14.00(1)	0.40(6)	2.10(5)	0.50(4)

$U(ij)$ are of the form $10^2 \exp[-2\pi^2(h^2U(11)a^{*2} + k^2U(22)b^{*2} + l^2U(33)c^{*2} + 2hkU(12)a^*b^* + 2klU(23)b^*c^* + 2hlU(13)a^*c^*)]$. Standard deviations in parentheses.

TABLE 3

INTRAMOLECULAR BOND LENGTHS (Å) AND ANGLES (b) OF β-CARBOMETHOXYETHYLTIN-(IV) TRICHLORIDE

Bond lengths	
Sn(1)—Cl(1)	2.357(2)
Sn(1)—Cl(2)	2.303(2)
Sn(1)—Cl(3)	2.317(2)
Sn(1)—O(1)	2.347(5)
Sn(1)—C(1)	2.139(8)
C(1)—C(2)	1.47(1)
C(2)—C(3)	1.50(1)
C(3)—O(1)	1.23(1)
C(3)—O(2)	1.29(1)
C(4)—O(2)	1.45(2)
Angles	
Cl(1)—Sn(1)—Cl(2)	98.3(1)
Cl(1)—Sn(1)—Cl(3)	96.7(1)
Cl(2)—Sn(1)—Cl(3)	104.1(1)
Cl(1)—Sn(1)—O(1)	176.7(2)
Cl(1)—Sn(1)—C(1)	99.5(2)
Cl(2)—Sn(1)—O(1)	84.4(2)
Cl(2)—Sn(1)—C(1)	130.5(2)
Cl(3)—Sn(1)—O(1)	84.4(2)
Cl(3)—Sn(1)—C(1)	119.0(2)
O(1)—Sn(1)—C(1)	77.2(3)
Sn(1)—C(1)—C(2)	113.6(6)
C(1)—C(2)—C(3)	113.9(7)
C(2)—C(3)—O(1)	124.3(8)
C(2)—C(3)—O(2)	113.4(7)
O(1)—C(3)—O(2)	122.3(8)
Sn(1)—O(1)—C(3)	110.2(5)
C(3)—O(2)—C(4)	117.1(7)

Estimated standard deviations in parentheses.

TABLE 4

EQUATIONS OF THE MEAN PLANES THROUGH GROUPS OF ATOMS IN β-CARBOMETHOXYETHYLTIN (IV) TRICHLORIDE AND DEVIATIONS OF ATOMS FROM THE PLANES (Å)

PLANE 1. Sn(1), Cl(1), C(1), C(2), C(3), O(1), O(2), C(4).

Equation of the plane:

$8.22384x - 6.20538y - 7.0889z = -1.167$

Sn(1), 0.032; Cl(1), −0.027; C(1), −0.091; C(2), 0.066; C(3), 0.043; O(1), 0.055; O(2), 0.010; C(4), −0.088.

PLANE 2. Sn(1), Cl(2), Cl(3), C(1).

Equation of the plane:

$8.49338x + 2.67305y + 1.88094z = 1.998$

Sn(1), 0.242; Cl(2), −0.079; Cl(3), −0.067; C(1), −0.096.

Angle between plane 1 and plane 2 = 90.64°.

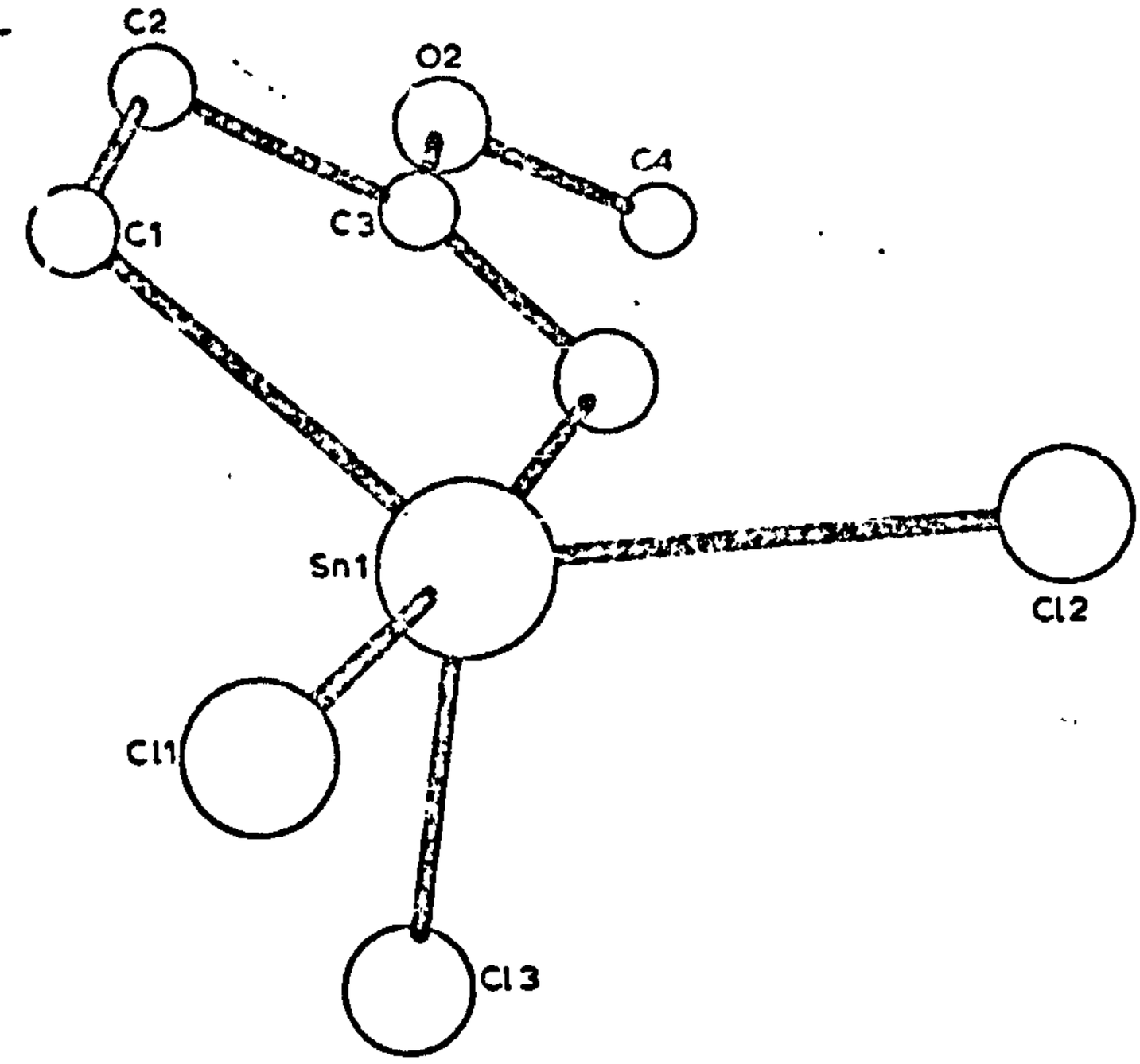

Fig. 1. The molecular structure and atomic labelling in $Cl_3SnCH_2CH_2CO_2Me$.

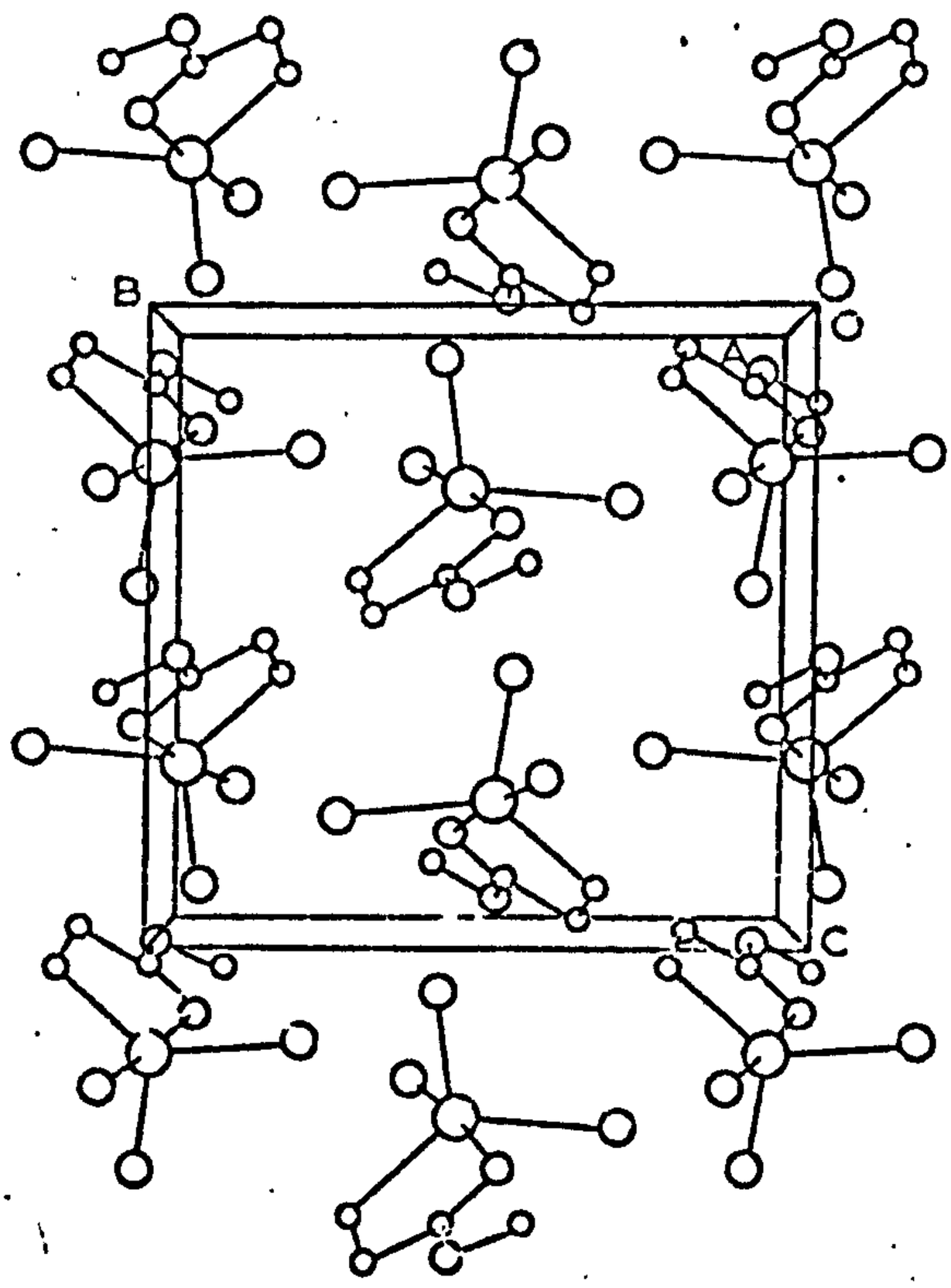

Fig. 2. Projection of the structure of $Cl_3SnCH_2CH_2CO_2Me$ onto the *bc* plane.

TABLE 5

FINAL FRACTIONAL ATOMIC COORDINATES IN BIS-(β-CARBOMETHOXYETHYL) TIN(IV) DICHLORIDE, $Cl_2Sn(CH_2CH_2CO_2CH_3)_2$.

Atom	x/a	y/b	z/c
Sn(1)	0.17179(6)	0.17907(2)	0.18179(3)
Cl(1)	0.4307(3)	0.0089(1)	0.1864(2)
Cl(2)	0.0891(4)	0.2811(1)	0.0220(2)
O(1)	−0.0814(8)	0.2603(3)	0.1900(5)
O(2)	−0.0664(7)	0.3725(3)	0.2985(4)
O(3)	0.229(10)	0.0744(4)	0.3432(7)
O(4)	0.0147(9)	−0.0033(3)	0.3579(6)
C(1)	0.3810(7)	0.2525(3)	0.3566(4)
C(2)	0.2633(7)	0.3302(3)	0.3502(4)
C(3)	0.024(1)	0.3162(4)	0.2760(6)
C(4)	−0.303(10)	0.3636(4)	0.2259(7)
C(5)	−0.108(10)	0.0978(5)	0.0714(7)
C(6)	−0.158(10)	0.0651(4)	0.1567(7)
C(7)	0.0478(9)	0.0462(3)	0.2945(6)
C(8)	0.208(10)	−0.0240(5)	0.4937(8)

Estimated standard deviations in parentheses.

atomic coordinates and anisotropic thermal parameters are listed in Tables 5 and 6, respectively. Intramolecular bond distances and angles are listed in Table 7. The molecular geometry and atomic numbering is shown in Fig. 3, and a projection of the unit cell onto the *bc* plane illustrated in Fig. 4. Planes data are given in Table 8.

(iii) Bis(β-amidoethyl)tin dichloride

The sample of bis(β-amidoethyl)tin dichloride, supplied by Dr. J.W. Burley,

TABLE 6

FINAL ANISOTROPIC THERMAL PARAMETERS FOR BIS-(β-CARBOMETHOXYETHYL) TIN (IV) DICHLORIDE

Atom	U(11)	U(22)	U(33)	U(23)	U(13)	U(12)
Sn(1)	4.90(20)	4.60(20)	4.85(20)	0.14(20)	3.45(20)	0.23(20)
Cl(1)	6.85(9)	8.30(1)	7.80(1)	1.50(9)	5.78(9)	2.42(8)
Cl(2)	10.10(1)	5.12(8)	7.20(1)	1.48(7)	6.30(1)	0.87(8)
O(1)	5.80(2)	6.00(2)	5.90(3)	−1.50(2)	3.90(2)	−0.60(2)
O(2)	7.70(2)	5.60(2)	7.00(2)	−1.20(2)	5.50(2)	−0.50(2)
O(3)	4.90(3)	6.70(4)	5.80(4)	0.70(3)	3.40(3)	−0.60(3)
O(4)	6.10(3)	6.20(3)	6.40(3)	0.60(2)	4.60(3)	−0.40(2)
C(1)	5.70(2)	6.10(2)	5.60(2)	−1.20(2)	2.30(2)	−0.30(2)
C(2)	5.70(2)	6.20(2)	6.60(2)	−2.00(2)	3.90(2)	−1.10(2)
C(3)	6.40(3)	4.80(3)	5.00(3)	−0.10(2)	4.10(3)	0.10(3)
C(4)	6.20(3)	8.80(3)	7.40(4)	−0.20(3)	4.90(3)	0.90(2)
C(5)	5.10(4)	4.50(4)	5.60(4)	−0.30(3)	3.30(3)	−0.30(3)
C(6)	5.20(3)	5.20(4)	7.20(3)	1.00(3)	4.20(3)	0.40(3)
C(7)	5.70(3)	4.00(3)	6.30(3)	0.10(2)	4.50(3)	0.40(3)
C(8)	6.40(4)	7.80(5)	6.30(4)	1.70(4)	4.20(3)	0.70(4)

(U) are of the form: $10^2 \exp[-2\pi^2(h^2U(11)a^{*2} + k^2U(22)b^{*2} + l^2U(33)c^{*2} + 2hkU(12)a^*b^* + klU(23)b^*c^* + 2hlU(13)a^*b^*)]$. Estimated standard deviations in parentheses.

TABLE 7

INTRAMOLECULAR BOND LENGTHS (Å) AND ANGLES (°) OF BIS-(β-CARBOMETHOXYETHYL) TIN (IV) DICHLORIDE

Distances			
Sn(1)—Cl(1)	2.401(2)		
Sn(1)—Cl(2)	2.409(2)		
Sn(1)—C(1)	2.124(6)		
Sn(1)—C(5)	2.127(5)		
Sn(1)—O(1)	2.520(4)		
Sn(1)—O(3)	2.524(4)		
Cl(1)—C(2)	1.523(9)	C(5)—C(6)	1.531(8)
C(2)—C(3)	1.487(9)	C(6)—C(7)	1.491(9)
C(3)—O(1)	1.205(7)	C(7)—O(3)	1.220(7)
C(3)—O(2)	1.306(7)	C(7)—O(4)	1.307(7)
C(4)—O(2)	1.463(8)	C(8)—O(4)	1.457(8)

Angles	
Cl(1)—Sn(1)—O(1)	175.5(1)
Cl(1)—Sn(1)—Cl(2)	96.3(1)
Cl(1)—Sn(1)—C(5)	101.0(2)
Cl(1)—Sn(1)—O(3)	87.7(1)
Cl(1)—Sn(1)—C(1)	102.8(2)
Cl(2)—Sn(1)—C(1)	99.7(2)
Cl(2)—Sn(1)—C(5)	103.9(2)
Cl(2)—Sn(1)—O(3)	175.5(1)
Cl(2)—Sn(1)—O(1)	87.4(1)
O(1)—Sn(1)—C(1)	74.0(2)
O(1)—Sn(1)—C(5)	80.5(2)
O(1)—Sn(1)—O(3)	88.7(2)
O(3)—Sn(1)—C(1)	81.3(2)
O(3)—Sn(1)—C(5)	73.3(2)
C(1)—S(1)—C(5)	144.1(3)
Sn(1)—C(1)—C(2)	111.9(4)
C(1)—C(2)—C(3)	113.3(5)
C(2)—C(3)—O(1)	123.2(5)
C(2)—C(3)—O(2)	114.2(5)
O(1)—C(3)—O(2)	122.5(6)
C(3)—O(2)—C(4)	116.9(5)
Sn(1)—O(1)—C(3)	108.4(4)
Sn(1)—C(5)—C(6)	111.0(4)
C(5)—C(6)—C(7)	112.2(5)
C(6)—C(7)—O(3)	123.2(6)
C(6)—C(7)—O(4)	113.4(4)
O(3)—C(7)—O(4)	123.4(6)
C(7)—O(4)—C(8)	116.5(5)
Sn(1)—O(3)—C(7)	107.5(4)

Estimated Standard deviations in parentheses.

was air-stable (decomp. >260°C. Found: C, 21.49; H, 4.16; N, 8.36; Cl, 21.11% $C_6H_{12}Cl_2N_2O_2Sn$ calcd.: C, 21.56; H, 3.59; Cl, 21.26%; N, 8.38.), and a suitable crystal (approximate dimensions 0.3 × 0.3 × 0.2 mm) was mounted in a Lindemann capillary.

TABLE 8

EQUATIONS OF THE MEAN PLANES THROUGH GROUPS OF ATOMS IN BIS-(β-CARBOMETHOXY-ETHYL) TIN (IV) DICHLORIDE, AND DEVIATION OF ATOMS FROM THE PLANES (Å)

PLANE 1. Sn(1), Cl(1), C(1), O(3), C(5).
equation of the plane:
$-1.12287x' + 11.87909y' - 5.34819z' = 0.203$
Sn(1), 0.759; Cl(1), −0.508; C(1), 0.461; O(3), −1.411; C(5), 0.698.
PLANE 2. Sn(1), Cl(1), Cl(2), O(3), O(1).
equation of the plane:
$2.87599x' + 8.83637y' + 4.43250z' = 2.887$
Sn(1), −0.005; Cl(1), 0.051; Cl(2), 0.049; O(3), −0.050; O(1), 0.052.
PLANE 3. Sn(1), Cl(2), C(5), O(1), C(1).
equation of the plane:
$4.95338x' - 11.04934y' - 1.71743z' = -2.203$
Sn(1), 0.763; Cl(2), −0.500; C(5), 0.467; O(1), −1.419; C(1), 0.689.
Angle between plane 1 and plane 2 = 97.09°
Angle between plane 1 and plane 3 = 147.61°
Angle between plane 2 and plane 3 = 83.55°

Equations are of the form $px' + qy' + rz' = s$ where x', y' and z' are orthogonal coordinates related to the monoclinic coordinates by: $x' = x + z\cos\beta$, $y' = y$ and $z' = z\sin\beta$ (7)

Crystal data: $C_6H_{12}Cl_2N_2O_2Sn$, M = 333.89, Monoclinic, a 9.1314, b 12.8672, c 13.0317 Å, β 126.6032°, V 1229.196 Å^3, Z = 4, $F(000)$ = 648, μ(Mo-K_α) 24.94 cm^{-1}. Space group C_c by systematic absences (hkl for $h + k = 2n + 1$, $h0l$ for $l = 2n + 1$ ($h = 2n + 1$), $0k0$ for $k = 2n + 1$).

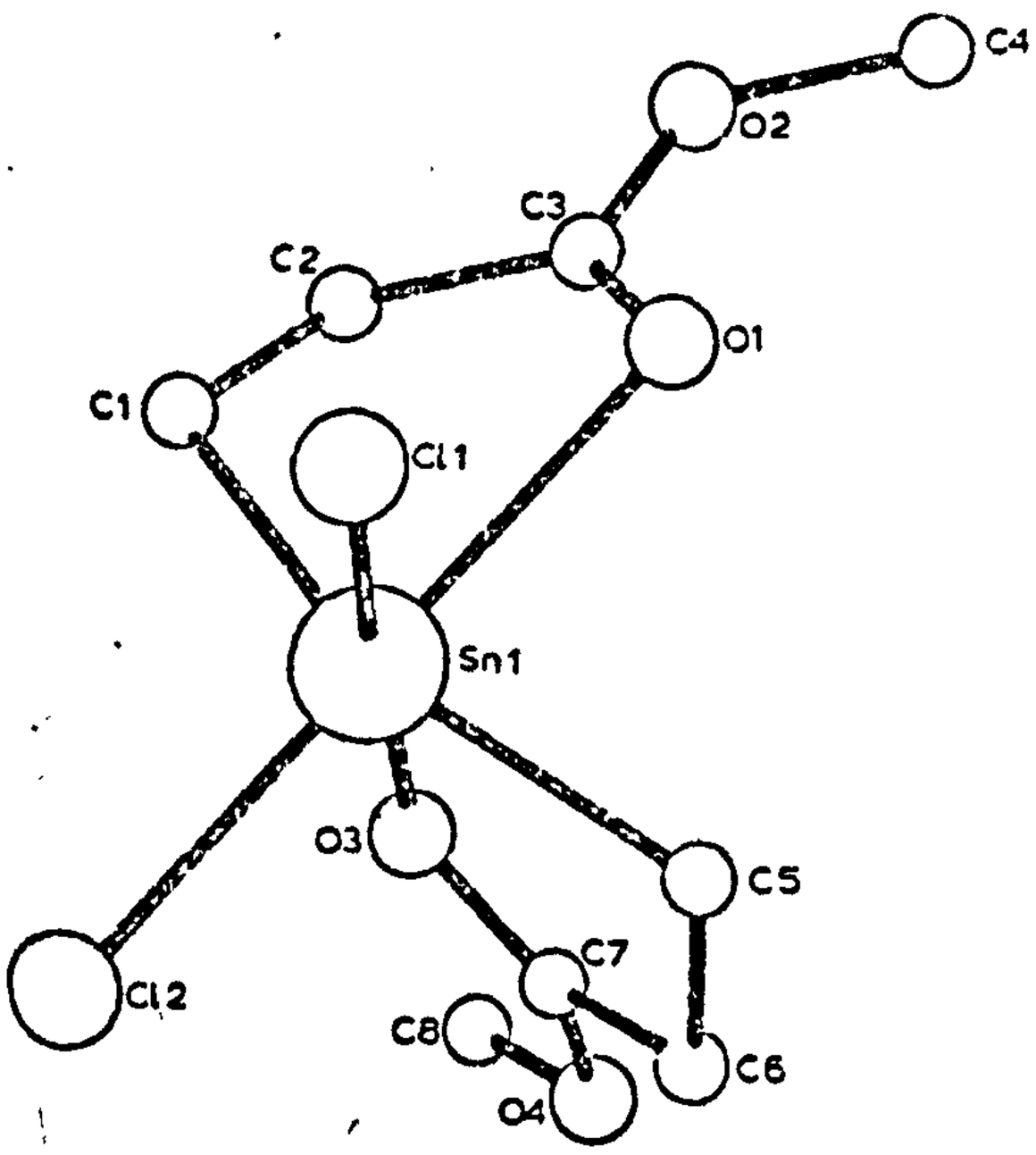

Fig. 3. The molecular structure and atomic labelling in $Cl_2Sn(CH_2CH_2CO_2Me)_2$.

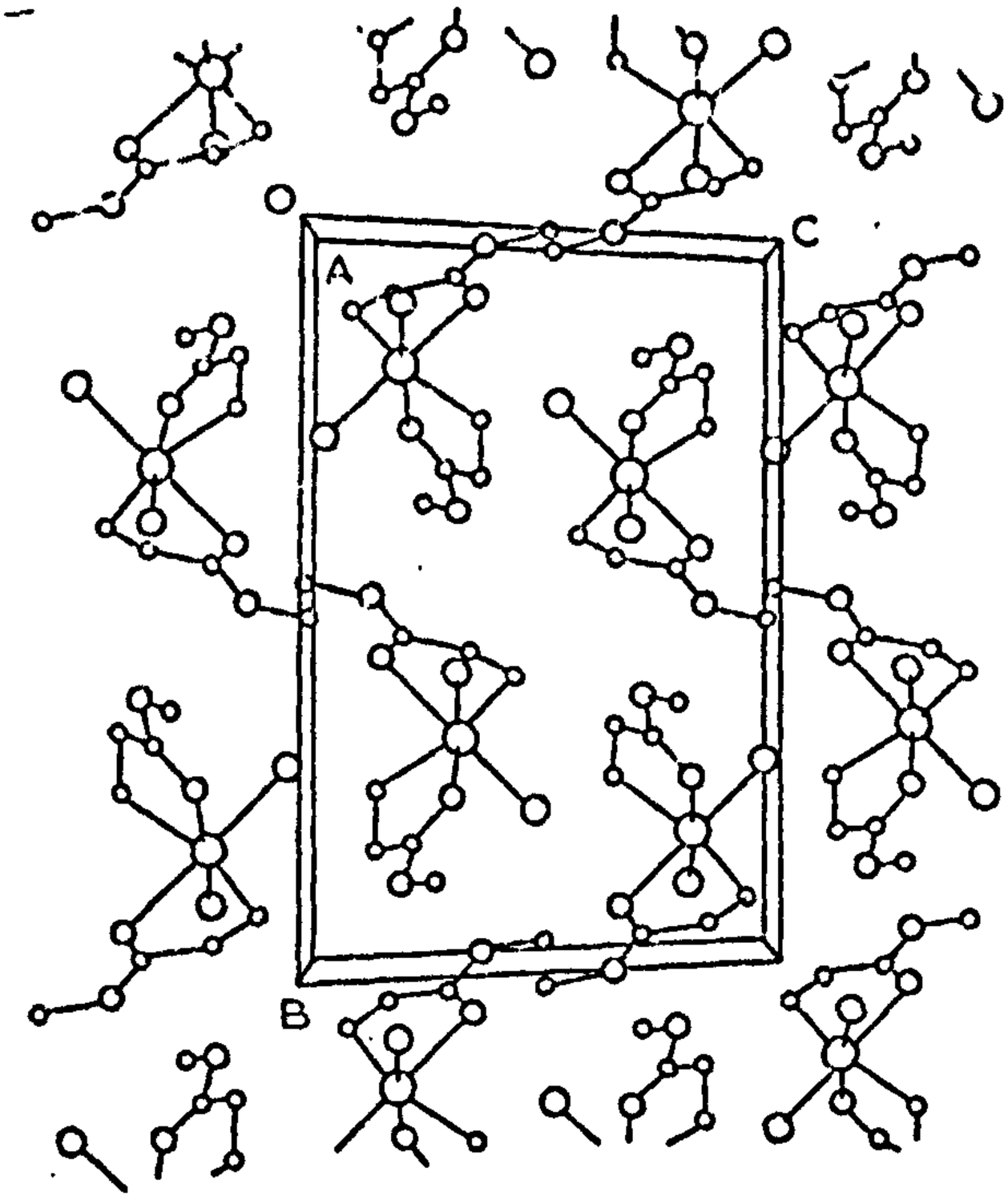

Fig. 4. Projection of the structure of $Cl_2Sn(CH_2CH_2CO_2Me)_2$ onto the *bc* plane.

Cell measurements and data collection: These were performed as before, relative intensities of 1472 independent reflections being collected up to $\theta = 25°$. Those with $I < 3\sigma(I)$ were discarded leaving 1024 for use in the structure determination.

Structure determination and refinement: Again a three dimensional Patterson synthesis was employed to locate the tin atom, and the remaining light atoms were located by successive Fourier syntheses. After full-matrix, least-squares anisotropic refinement, convergence was achieved at an R value of 0.029. The same type of Chebychev series weighting scheme as before (with coefficients 144.84, 219.39, 99.79, 22.75 and 1.86) was then employed, and further full-matrix, least-squares anisotropic refinement resulted in a final R value of 0.0268. Calculations were performed as before. Final fractional atomic coordinates, anisotropic thermal parameters, intramolecular bond distances and angle data, and least-squares planes data are listed in Tables 9—12, respectively. The molecular geometry and atomic numbering is shown in Fig. 5, and the projection of the unit cell onto the *ac* plane illustrated in Fig. 6.

3. *Spectroscopic Measurements*

Tin-119 Mössbauer spectra were collected at 77 K using a Harwell spectrometer calibrated with iron and β-tin foils. Data reduction to Lorentzian line shapes was achieved by usual least-squares methods.

Infrared spectra were recorded using a Perkin—Elmer 577 spectrophotometer. Raman spectra were obtained on a Cary 81 instrument using a He-Ne laser.

Mass spectra were obtained using a MS-902 instrument.

TABLE 9

FINAL FRACTIONAL ATOMIC COORDINATES IN BIS-(β-AMIDOETHYL) TIN (IV) DICHLORIDE, $Cl_2Sn(CH_2CH_2CONH_2)_2$

Atom	x/a	y/b	z/c
Sn(1)	0.0000	0.00672(3)	0.2500
Cl(1)	0.3844(8)	−0.1254(6)	0.4156(7)
Cl(2)	−0.1908(9)	−0.1184(6)	0.0756(8)
N(1)	0.397(2)	0.253(1)	0.436(1)
N(2)	−0.373(3)	0.265(1)	0.065(2)
O(1)	0.171(2)	0.141(1)	0.392(1)
O(2)	−0.170(2)	0.146(2)	0.117(2)
C(1)	0.279(2)	0.1732(9)	0.375(1)
C(2)	0.324(3)	0.123(2)	0.281(2)
C(3)	0.187(2)	0.036(1)	0.214(2)
C(4)	−0.191(3)	0.032(2)	0.297(2)
C(5)	−0.315(3)	0.122(2)	0.212(2)
C(6)	−0.297(3)	0.161(2)	0.127(2)

Standard deviations in parentheses.

TABLE 10

FINAL ANISOTOPIC THERMAL PARAMETERS FOR BIS-(β-AMIDOETHYL) TIN (IV) DICHLORIDE

Atom	U(11)	U(22)	U(33)	U(23)	U(13)	U(12)
Sn(1)	4.60(30)	4.09(30)	5.34(30)	−0.13(90)	3.34(20)	−0.16(80)
Cl(1)	5.7(3)	6.2(3)	9.4(4)	3.7(3)	4.8(3)	2.2(2)
Cl(2)	5.5(3)	8.1(4)	7.1(3)	−2.6(3)	3.2(2)	−0.1(2)
N(1)	5.6(7)	7.7(9)	7.9(8)	−3.8(7)	4.3(7)	−2.0(7)
N(2)	7.0(1)	5.6(8)	1.1(1)	1.0(8)	6.0(1)	2.7(7)
O(1)	4.5(6)	5.3(8)	6.5(7)	−1.5(6)	4.1(6)	−1.5(5)
O(2)	9.0(1)	6.3(9)	9.0(10)	2.1(7)	7.1(9)	2.9(8)
C(1)	5.4(8)	3.1(5)	5.1(7)	−2.0(5)	3.9(7)	−1.9(5)
C(2)	14.0(2)	10.0(1)	9.0(1)	−3.0(1)	8.0(1)	−2.0(1)
C(3)	4.8(7)	5.3(7)	4.5(7)	0.3(5)	2.9(6)	1.8(6)
C(4)	8.0(1)	5.8(9)	10.0(1)	2.5(7)	8.0(1)	3.1(7)
C(6)	3.9(7)	10.0(2)	8.0(1)	−4.0(1)	3.9(8)	−0.3(8)

$U(ij)$ are of the form $10^2 \exp[-2\pi^2(h^2U(11)a^{*2} + k^2U(22)b^{*2} + l^2U(33)c^{*2} + 2hkU(12)a^*b^* + 2klU(23)b^*c^* + 2hlU(13)a^*c^*)]$. Standard deviations in parentheses.

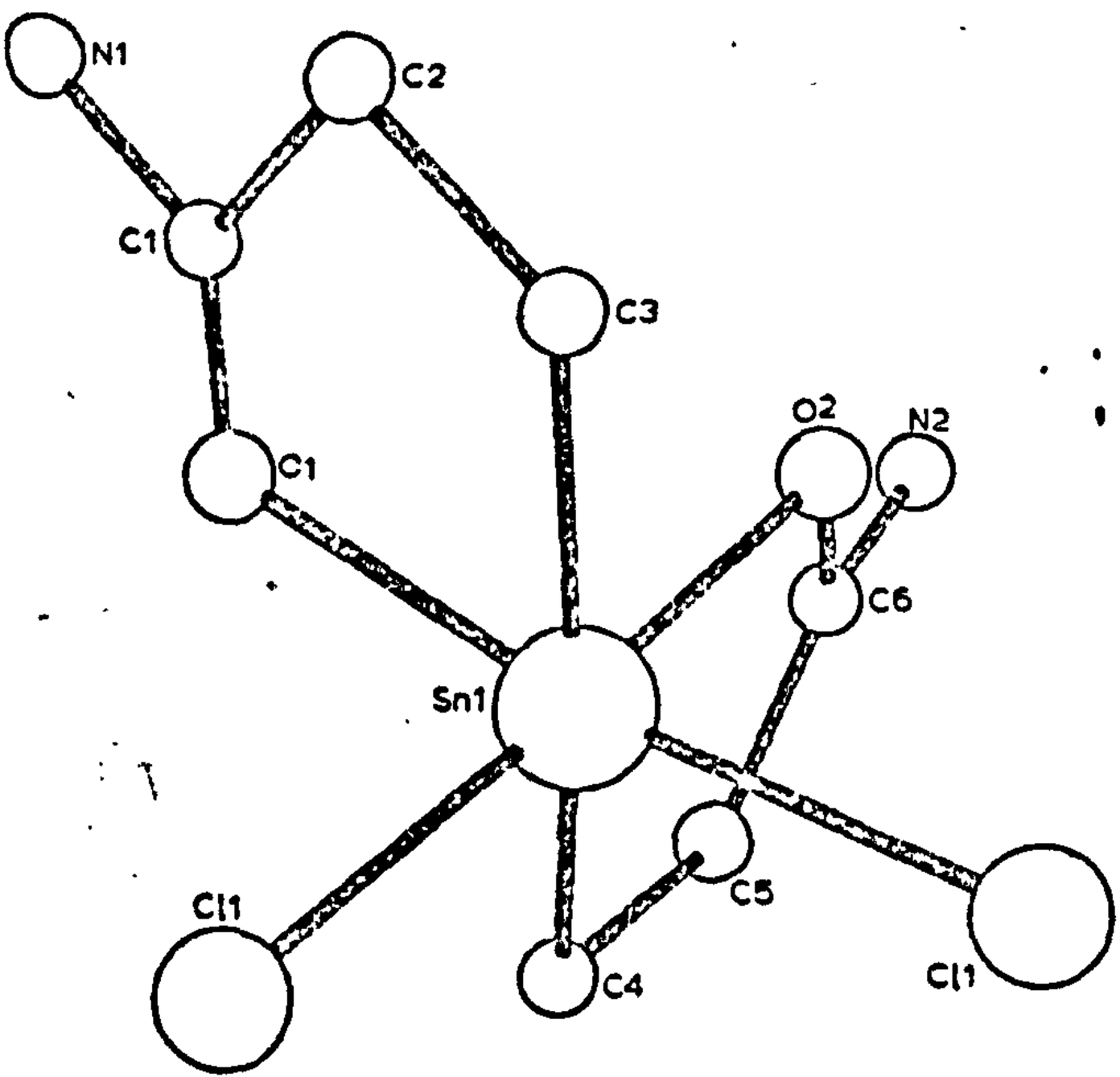

TABLE 11

INTRAMOLECULAR BOND DISTANCES (Å) AND ANGLES (DEG.) OF BIS-(β-AMIDOETHYL) TIN (IV) DICHLORIDE

Bond lengths			
Sn(1)—Cl(1)	2.460(7)	N(1)—O(2′) = 3.04(3)	
Sn(1)—Cl(2)	2.464(7)		
Sn(1)—O(1)	2.327(16)		
Sn(1)—O(2)	2.321(18)	N(2′)—O(1) = 2.83(3)	
Sn(1)—C(3)	2.059(17)		
Sn(1)—C(4)	2.190(16)		
C(3)—C(2)	1.52(3)	C(4)—C(5)	1.52(3)
C(2)—C(1)	1.64(3)	C(3)—C(6)	1.43(3)
C(1)—N(1)	1.36(2)	C(6)—N(2)	1.28(3)
C(1)—O(1)	1.21(2)	C(6)—O(2)	1.32(3)
Bond Angles			
Cl(1)—Sn(1)—Cl(2)	95.5(1)		
Cl(1)—Sn(1)—C(3)	95.6(5)	Cl(2)—Sn(1)—C(3)	97.7(6)
Cl(1)—Sn(1)—O(1)	91.8(5)	Cl(2)—Sn(1)—O(1)	171.9(5)
Cl(1)—Sn(1)—O(2)	171.6(5)	Cl(2)—Sn(1)—O(2)	91.4(5)
Cl(1)—Sn(1)—C(4)	95.7(5)	Cl(2)—Sn(1)—C(4)	96.4(6)
C(3)—Sn(1)—O(1)	78.0(6)	C(4)—Sn(1)—O(2)	78.7(6)
C(3)—Sn(1)—O(2)	88.2(6)	C(4)—Sn(1)—O(1)	86.3(6)
Sn(1)—C(3)—C(2)	121(1)	Sn(1)—C(4)—C(5)	106(1)
C(3)—C(2)—C(1)	103(1)	C(4)—C(5)—C(6)	126(1)
C(2)—C(1)—N(1)	106(1)	C(5)—C(6)—N(2)	132(2)
C(2)—C(1)—O(1)	127(1)	C(5)—C(6)—O(2)	114(2)
N(1)—C(1)—O(1)	128(1)	N(2)—C(6)—O(2)	114(2)
C(1)—O(1)—Sn(1)	110(1)	C(6)—O(2)—Sn(1)	115(2)
C(4)—Sn(1)—O(1)	75.6(6)	O(1)—Sn(1)—O(2)	79.8(6)
C(4)—Sn(1)—C(3)	191(1)		

Standard deviations in parentheses.

TABLE 12

EQUATIONS OF THE MEAN PLANES THROUGH GROUPS OF ATOMS IN BIS-(β-AMIDOETHYL) TIN (IV) DICHLORIDE AND DEVIATIONS OF ATOMS FROM THE PLANES (Å)

PLANE 1. Sn(1), Cl(1), O(2), C(6), N(2), C(5), C(4), C(3).

equation of the plane:

$-1.59410x - 8.25039y - 6.46102z = -1.359$

Sn(1), 0.188; Cl(1), −0.085; O(2), 0.171; C(6), 0.022; N(2), −0.155; C(5), −0.013; C(4), −0.018; C(3), −0.114.

PLANE 2. Sn(1), Cl(1), Cl(2), O(1), O(2).

equation of the plane:

$3.81727x + 0.22689y - 10.21725z = -2.563$

Sn(1), 0.010; Cl(1), −0.086; Cl(2), 0.031; O(1), 0.098; O(2), −0.103.

PLANE 3. Sn(1), Cl(2), O(1), C(1), N(1), C(2), C(3), C(4).

equation of the plane:

$-1.83290x + 8.66639y - 5.88257z = -1.230$

Sn(1), −0.183; Cl(2), 0.103; O(1), −0.170; C(1), 0.015; N(1), 0.133; C(2), 0.051; C(3), −0.063; C(4), 0.108.

Angle between Plane 1 and Plane 2 = 89.20°
Angle between Plane 1 and Plane 3 = 82.25°
Angle between Plane 2 and Plane 3 = 89.85°

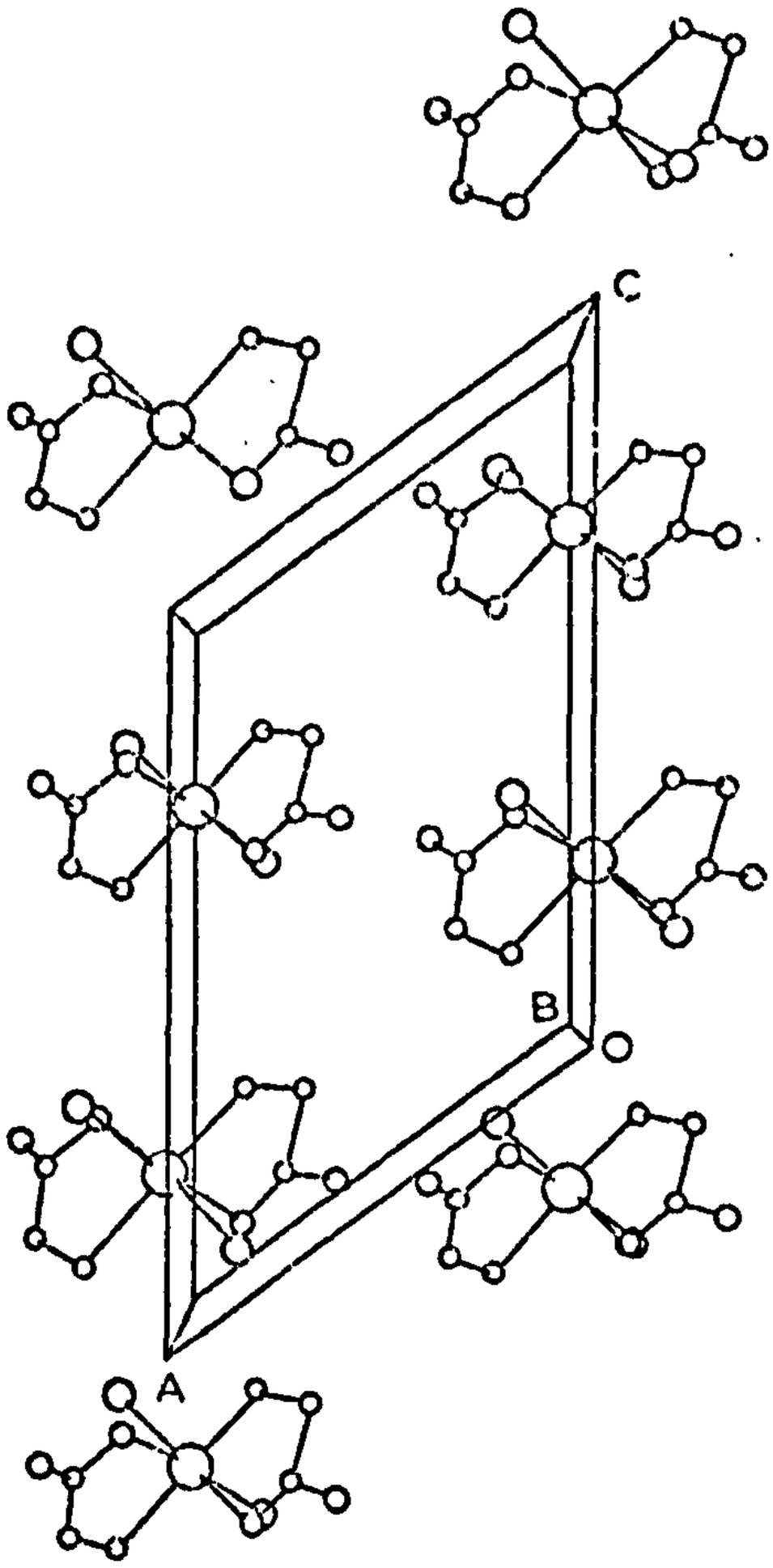

Fig. 6. Projection of the structure of $Cl_2Sn(CH_2CH_2CONH_2)_2$ onto the *ac* plane.

Results and discussion

Structural studies

No crystal structure of an organotin trichloride has yet been reported. β-Carbomethoxyethyltin trichloride, a somewhat less hygroscopic compound than an unsubstituted alkyl or aryltin analogue, contains five-coordinated tin via intramolecular coordination of the carbonyl group (Fig. 1). The geometry at tin is thus distorted trigonal bipyrimidal with the carbonyl oxygen and one chlorine atom occupying the axial positions, whilst the organic residue and the two remaining chlorine atoms are bonded at equatorial sites. Not unexpectedly, the $Sn—Cl_{ax}$ bond distance (2.357(2) Å) is somewhat longer than the $Sn—Cl_{eq}$ distances (2.303(2), 2.317(2) Å). The Sn—C distance is normal (2.129(8) Å), and the coordinate Sn—O bond distance (2.347(5) Å) is quite short, when compared with values of 2.332(6) Å for $Me_3SnCl \cdot (Ph_3PCHCOMe)$ [5] and 2.308(4) Å for $Ph_3Sn \cdot ONPh \cdot CO \cdot Ph$ [6].

Both bis(β-carbomethoxyethyl)tin dichloride and bis(β-amidoethyl)tin dichloride possess distorted octahedral geometries, with both substituted-ethyl

ligands functioning as chelating groups (Figs. 3 and 5). In both compounds, the two chlorine atoms occupy *cis* positions, whilst the two carbon atoms are mutually *trans*. The oxygen atoms are therefore in *cis* positions. It is noteworthy that, in the β-amidoethyltin derivatives, of the two possible donor atoms, carbonyl oxygen and amido nitrogen, the oxygen atom is preferred for coordination to tin. Although very similar within each compound, the Sn—Cl bond distances of the amidoethyl derivatives are longer (2.462(7) Å) than those in the carbomethoxyethyl derivative (2.405(2) Å). Both are shorter than those of Ph_2SnCl_2·bipy (2.520(2) Å), [7] but longer than in Et_2SnCl_2 (2.385(3) Å) [8]. In $Cl_2Sn(CH_2CH_2CONH_2)_2$, the Sn—O bond distances are similar (2.324(18) Å) to that in $Cl_3SnCH_2CH_2CO_2Me$ (2.347(5) Å) and $Me_2Sn(ONMeCOMe)_2$ (2.377(5) Å) [9] but longer than in $Me_2Sn(ONHCOMe)_2$ (2.228(4) Å), in which intermolecular hydrogen-bonding occurs [10]. The Sn—O distances in $Cl_2Sn(CH_2CH_2CO_2Me)_2$ are significantly longer (2.522(4) Å) reflecting a considerably weaker coordinate bond. The Sn—C bond distances in $Cl_2Sn(CH_2CH_2CO_2Me)_2$ are slightly shorter (2.126(6) Å) than in Et_2SnCl_2 (2.132(13), 2.167(15) Å) [8], but those in the amidoethyl analogues are quite dissimilar (2.059(17) and 2.190(16) Å).

The bond distances within the carbomethoxyethyl residue of $Cl_3SnCH_2CH_2COMe$ and $Cl_2Sn(CH_2CH_2CO_2Me)_2$ are quite similar, with the C=O distances falling in the range 1.205(7)—1.227(10) Å. The Me—O distances are much longer (1.448(15)—1.463(8) Å) than the C(10)—O distances (1.290(10)—1.307(7) Å).

The distances within the two amidoethyl residues in $Cl_2Sn(CH_2CH_2CONH_2)_2$ are quite dissimilar. In one, the carbonyl distance is short (1.205(20) Å), and the C—N and C(:O)—C distances relatively long (1.355(20) and 1.638(26) Å, respectively). In the other the carbonyl distance is very long (1.321(25) Å), whereas the corresponding C—N and C(:O)—C distances are short (1.277(29) Å and 1.427(30) Å, respectively). The dissimilarity is most probably due to the presence of hydrogen-bonding involving the amide and carbonyl groups, the longer carbonyl and C—N distances being associated with a short (2.827 Å) C : O···H—N hydrogen bond, and the shorter carbonyl and C—N distances with the longer (3.043 Å) C : O···H—N hydrogen bond.

Vibrational spectra

The vibrational spectra of the two β-carbomethoxytin chlorides, $Cl_nSn(CH_2CH_2CO_2Me)_{4-n}$ (n = 2, 3), together with that of methyl acrylate, are listed in Table 13. As expected, the ν(C=C) vibration of the alkene at 1637 cm^{-1} is absent in the two tin derivatives. In addition, the carbonyl stretching band, at 1740 cm^{-1} in methyl acrylate, moves to 1650 cm^{-1} in $Cl_3SnCH_2CH_2CO_2Me$ and 1674 cm^{-1} in $Cl_2Sn(CH_2CH_2CO_2Me)_2$, indicative of carbonyl → tin coordination as shown by the crystallographic studies. The dissimilarity of the strength of these coordinate interactions, shown by the different Sn—O bond distances, is also reflected in the vibrational spectra: the carbonyl band being at much lower energy in the tin trichloride than the dichloride. In $Cl_2Sn(CH_2CH_2CONH_2)_2$, the carbonyl stretching mode occurs at 1651 cm^{-1} (Table 14). Tin—carbon and tin—chlorine stretching modes for all three compounds are also assigned.

TABLE 13

INFRARED AND RAMAN DATA FOR $Cl_3SnCH_2CH_2CO_2CH_3$ AND $Cl_2Sn[CH_2CH_2CO_2CH_3]_2$ (cm^{-1})

$CH_2{=}CHCO_2CH$ Infrared Liquid film	$Cl_3SnCH_2CO_2CH_3$			$Cl_2Sn[CH_2CH_2CO_2CH_3]_2$			Assignment
	Infrared		Raman	Infrared		Raman	
	KBr disc	Nujol mull	Solid	KBr disc	Nujol mull	Solid	
3033 (sh)							
3004m	3010w		3012m	3010w		3010m	
2962s	2962m		2966s	2950m		2963s	ν(C—H)
2918w	2930w		2932w	2930w		2930s	
2863w	2872w		2872s	2858w		2870w	
1740s	1650vvs	1650vvs	1652m	1674vs	1674vs	1683m	ν(C=O)
1650 (sh)							
1637m							ν(C=C)
1625 (sh)							
1444s	1448s	1460s	1451m	1442s	1442s	1464m	
1408s	1401m	1401m	1404m	1404m	1404m	1406m	
	1370s	1374s	1376w	1363s	1366s		
1280s	1272s	1272s		1270s	1270s		
1213s	1250 (sh)	1250 (sh)		1228vs	1228vs	1235m	ν(C—O)
1187 (sh)	1188w	1188w		1186m	1186m		
	1134w	1134w	1144m	1155vw	1155vw		
			1126m	1140 (sh)	1140 (sh)	1140w	
			1103m	1132m	1132m	1129m	
1073s	1047w	1047w		1031m	1031m		
992s							
975 (sh)	956m	956m	952w	957m	957m	952w	
				922w	922w		
858m	900w	902w	900m	892w	892w	890m	
817s	746 (sh)	730sh		757m	757m	750w	
668w	700m	704m		694m	694m		
	580vw	578vw	573m	592w	592w	584m	
		546vw	548m	553vw	553vw		ν(Sn—C)
				526vw	526vw		
	468w	470w	468m	467vw	467vw	463m	
	422 (sh)	422vw					
	404s	404s	398m				
	365s	376s		382m	382m	373m	
	350s	350s	345vs				ν(Sn—Cl)
	322s	324s	313vs	310s	310s		
				297vs	297vs	300vvs	
				288 (sh)	288s		
		254m	267w			267w	
			248w	240w	240w	246w	skeletal
						185m (br)	deformation
			138vs			133vs	modes.
			116m			117vs	
			105m				
			75w			77w	

Mass spectra

Mass spectral data for all three compounds are listed in Table 15. Both β-carbomethoxyethyltin derivatives exhibit weak parent ions, and in addition $Cl_3SnCH_2CH_2CO_2Me$ exhibited an unidentified low intensity fragment at m/e = $(P + 8)^+$. The fragmentation patterns of both compounds were similar, the major processes involving tin—carbon and tin—chlorine bond fission, although loss of a

TABLE 14

INFRARED AND RAMAN DATA FOR $Cl_2Sn(CH_2CH_2CONH_2)_2$ (cm^{-1})

CH_2=CHCONH$_2$ Infrared KBr disc	$Cl_2Sn(CH_2CH_2CONH_2)_2$		Assignment
	Infrared KBr disc	Raman Solid	
	3420s		
3340vs (br)	3340s	3360m (br)	ν(N—H)
3160vs (br)	3280w	3194w (br)	
	2985s	2935	
	2930m (sh)	2958s	ν(C—H)
		2919s	
2800w	2871m		
1660vs (br)	1651vvs	1672w	ν(C=O)
1605vs (br)	1625m		
	1547m		
		1474w	
1425vs	1450m	1438w	
		1428w	
		1409w	
1350s			
1280s	1282m	1297w	
	1266m	1256w	
	1169w		
1137m		1134w	
	1110s	1120s	
1051mw	1067m		
990m	979w		
962m	932w	906vw	
	884w		
841m		852w	
819s	820 (sh)		
	805m		
	775 (sh)		
700m (vbr)	724m	700w (br)	
	683s		
630m (vbr)	650m		
570m	579w	568s	ν(Sn—C)
	537w		
		478s	
	371s	344w	
315m	318vs	312m	ν(Sn—Cl)
		269vvs	
		229w	
		169w (sh)	
		150s	
		112s	
		56vs	

(CO_2Me) fragment from the organic ligand leading to $[Cl_nSnCH_2CH_2]^+$ ions, particularly for $Cl_3SnCH_2CH_2CO_2Me$, is observed. Loss of a (MeO) fragment from one organic group in $Cl_2Sn(CH_2CH_2CO_2Me)_2$ also occurs. In both compounds, the most abundant ion is $[Cl_2SnCH_2CH_2COMe]^+$.

The fragmentation pattern of the β-amido-ethyltin derivative, $Cl_2Sn(CH_2CH_2CONH_2)_2$, again involved both tin—chlorine and tin—carbon bond

TABLE 15

MAJOR FRAGMENTS [a] IN THE MASS SPECTRUM OF $Cl_3SnCH_2CH_2CO_2CH_3$, $Cl_2Sn(CH_2CH_2CO_2CH_3)_2$ and $Cl_2Sn(CH_2CH_2CONH_2)_2$

m/e	Relative Intensity [b]	Assignment
$Cl_3SnCH_2CH_2CO_2CH_3$ [c]		
319	4.7	
311	1.4	$Cl_3SnCH_2CH_2CO_2CH_3^+$
276	100.00	$Cl_2SnCH_2CH_2CO_2CH_3$
252	29.5	$Cl_3SnCH_2CH_2^+$
224	38.6	$SnCl_3^+$
217	14.0	$Cl_2SnCH_2CH_2^+$
189	26.6	$SnCl_2^+$
154	97.0	$SnCl^+$
147	24.2	$SnCH_2CH_2^+$
119	35.1	Sn^+
$Cl_2Sn(CH_2CH_2CO_2CH_3)_2$ [d]		
363	1.5	$Cl_2Sn(CH_2CH_2CO_2CH_3)_2^+$
328	23.3	$ClSn(CH_2CH_2CO_2CH_3)_2^+$
297	1.4	$ClSn(CH_2CH_2CO_2CH_3)CH_2CH_2CO^+$
276	100.00	$Cl_2SnCH_2CH_2CO_2CH_3$
241	8.2	$ClSnCH_2CH_2CO_2CH_3^+$
219	4.1	
206	16.4	$SnCH_2CH_2CO_2CH_3^+$
186	8.2	$ClSnCH_2CH_2$
154	27.4	$SnCl^+$
119	10.9	Sn^+
$Cl_2Sn(CH_2CH_2CONH_2)_2$ [e]		
333	0.37	$Cl_2Sn(CH_2CH_2CONH_2)_2^+$
299	29.63	$ClSn(CH_2CH_2CONH_2)(CH_2CH_2CONH_3)^+$
280	92.50	$ClSn(CH_2CH_2CONH_2)CH_2CH_2CN^+$
261	48.10	$Cl_2Sn(CH_2CH_2CONH_2)^+$
243	5.53	$Cl_2Sn(CH_2CH_2CN)$
226	20.46	$ClSn(CH_2CH_2CONH_2)^+$
208	7.48	$ClSn(CH_2CH_2CN)^+$
191	46.30	$Sn(CH_2CH_2CONH_2)^+$
154	100.00	$ClSn^+$
135	33.34	SnO^+
119	20.37	Sn^+

[a] Based on ^{119}Sn and ^{35}Cl. [b] Relative to the most intense tin containing fragment. [c] Spectrum obtained by direct injection at 130°C. [d] Spectrum obtained by direct injection at 190°C. [e] Spectrum obtained by direct injection at 190°C.

fission as major processes, although dehydration of the amidoethyl group to afford cyanoethyltin ions was also important.

Tin-119m Mössbauer Data

Tin-119*m* Mössbauer data for the three compounds under study as well as for several β-carbobutoxytin derivatives are listed in Table 16. All the spectra consisted of quadrupole split doublets. The I.S. and Q.S. for $BuAcSnCl_3$ and $(BuAc)_2SnCl_2$ are, not unexpectedly, similar to those of $Cl_3SnCH_2CH_2CO_2Me$ and $Cl_2Sn(CH_2CH_2CO_2Me)_2$ respectively, indicating a general structural similarity. The amidoethyltin compound, $Cl_2Sn(CH_2CH_2CONH_2)_2$, exhibits a lower I.S. and

TABLE 16

TIN-119*m* MOSSBAUER DATA FOR CARBONYL-SUBSTITUTED-ETHYLTIN COMPOUNDS

Compound [a]	I.S. [bc]	Q.S. [c]	Γ_1 [cd]	Γ_2 [c]	I_1/I_2
$MeAcSnCl_3$	1.00	2.18	1.01	1.01	1.01
$BuAcSnCl_3$	1.11	2.06	1.12	1.07	1.05
$BuAcSnCl_2(IOTG)$	1.26	2.68	0.95	1.02	1.02
$BuAcSnCl(IOTG)_2$	1.33	2.45	1.03	0.98	1.01
$BuAcSn(IOTG)_3$	1.39	1.64	0.89	0.89	1.00
$BuAcSnCl_2(\beta MeOct)$	1.26	2.32	1.00	1.12	1.01
$BuAcSnCl(\beta MeOct)_2$	1.30	2.15	1.08	1.02	0.99
$BuAcSn(\beta MeOct)_3$	1.33	1.48	0.98	0.87	0.98
$MeAc_2SnCl_2$	1.50	3.45	0.94	0.94	1.00
$BuAc_2SnCl_2$	1.45	3.44	1.06	1.01	1.02
$BuAc_2Sn(IOTG)_2$	1.48	2.16	0.87	0.87	0.99
$Bu_2Sn(IOTG)_2$	1.46	2.31	0.91	0.91	1.01
$AmAc_2SnCl_2$	1.39	3.71	0.90	0.90	0.98

[a] MeAc = $MeO{\cdot}C(:O){\cdot}CH_2CH_2$—; BuAc = $BuO{\cdot}C(:O){\cdot}CH_2CH_2$—; AmAc = $H_2N{\cdot}C(:O){\cdot}CH_2CH_2$—; IOTG = *iso*-octylthioglycollate; βMeOct = $SCH_2CH_2OCOC_7H_{15}$. [b] Relative to $CaSnO_3$ = 0. [c] Mm s^{-1}. [d] The subscripts 1 and 2 refer to the lower and higher velocity lines, respectively.

a higher Q.S. than $Cl_2Sn(CH_2CH_2CO_2Me)_2$ as a consequence of both the significantly shorter Sn—O bond distances and lower distortion from linearity of the C—Sn—C unit in the former.

As chlorine atoms are successively replaced by sulphur (IOTG and βMeOct) ligands, the isomer shift progressively increases. However, the quadrupole splitting at first increases and then decreases, the final low value of the quadrupole splitting for $BuAcSn(IOTG)_3$ (1.64 mm^{-1}) and $BuAcSn(\beta MeOct)_3$ (1.48 mm^{-1}) suggesting a four-coordinated structure for both. The isomer shifts of $BuAc_2SnCl_2$, $BuAc_2Sn(IOTG)_2$ and $Bu_2Sn(IOTG)_2$ are very similar, but the quadrupole splittings of the two latter compounds are much lower than of $BuAc_2SnCl_2$ (3.44 mm^{-1}). The close similarity of the data for the two IOTG derivatives strongly suggests that both possess similar structures, most probably tetrahedral.

The different isomer shift and quadrupole splitting value for the compounds demonstrates that each should be identifiable when present in a PVC matrix. In order to test this hypothesis, we have attempted to record spectra from PVC samples containing 1—2 per cent of various thiolatotin additives as stabilisers. PVC samples with three different organotin additives were investigated: $Bu_2Sn(IOTG)_2$, $BuAcSn(IOTG)_3$, and $BuAcSn(\beta MeOct)_3$. Thermally degraded as well as freshly milled samples were studied. Although doublet spectra could be detected for all samples, several could not be quantified due to the weakness of the Mössbauer source. Several of the samples did, nevertheless, yield useful results, and a typical such spectrum is illustrated in Fig. 7. Although the signal-to-noise ratio in this spectrum is not particularly satisfactory, it does demonstrate that useful spectra can be recorded from PVC samples and the structure of the tin species present investigated, thus providing an insight into the mechanism of stabilisation. The useful data obtained are listed in Table 17, together with comparative data.

The isomer shift of freshly-milled $BuSn(IOTG)_2$-PVC was uncharged from that

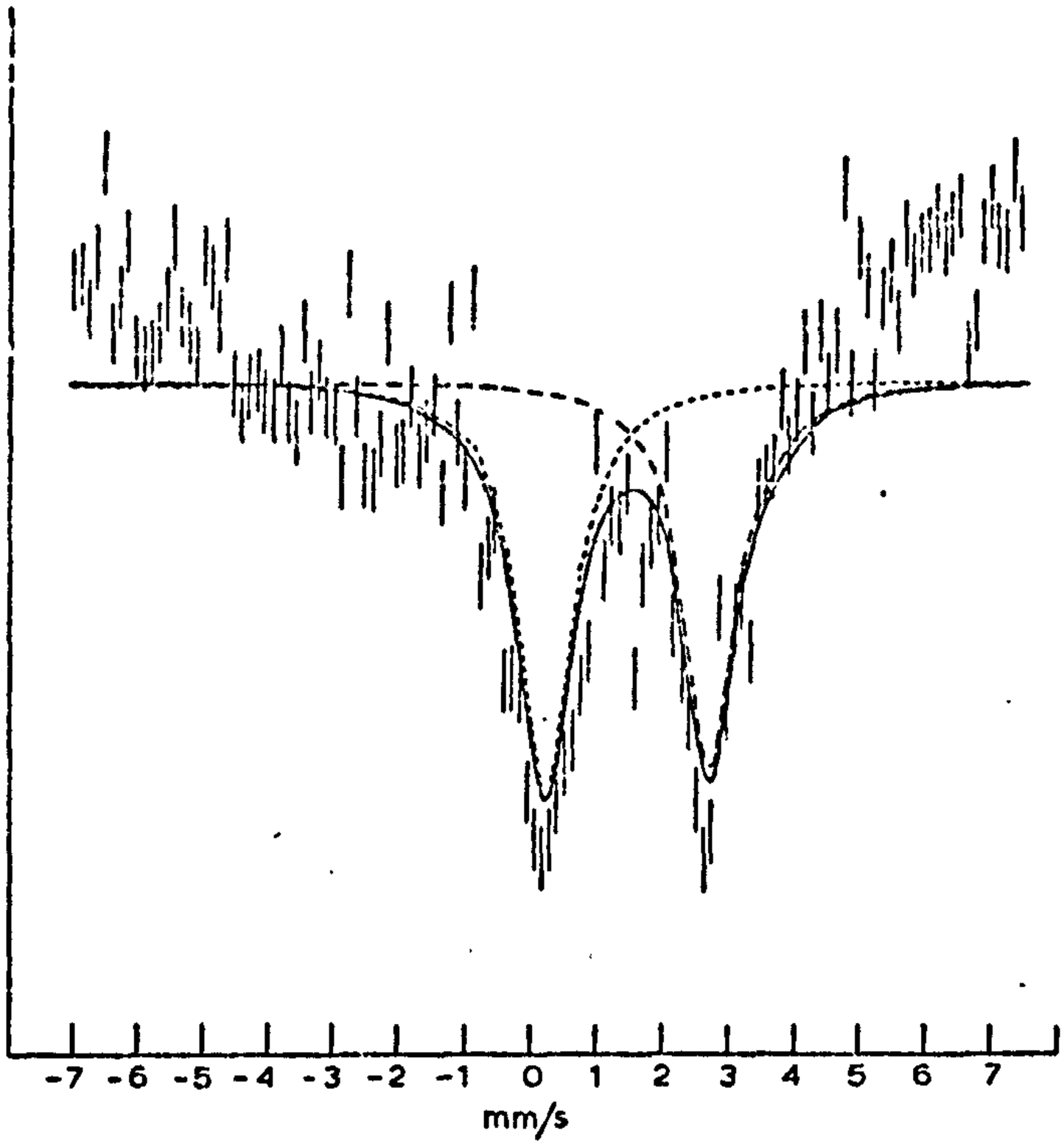

Fig. 7. Tin-119 Mössbauer spectrum of $Bu_2Sn(IOTG)_2$ in PVC.

of neat $Bu_2Sn(IOTG)_2$, although the quadrupole splitting increased somewhat (from 2.31 to 2.48 mm^{-1}). This would suggest that, in the freshly-milled PVC, only part of the available IOTG groups have been exchanged for chlorine, and the organotin species present is most probably $Bu_2SnCl(IOTG)$. Thermal degradation, however, substantially increases both the I.S. and the Q.S. to values which are close to those of Bu_2SnCl_2. At this stage, therefore, complete IOTG-for-chlorine exchange has taken place. Both the freshly-milled samples of BuAcSn-

TABLE 17

TIN-119*m* MOSSBAUER DATA FOR ORGANOTIN-STABILISED PVC SAMPLES TOGETHER WITH COMPARATIVE DATA

Sample	I.S. [ab]	Q.S. [a]
PVC — $Bu_2Sn(IOTG)_2$		
— Freshly milled	1.48	2.48
— Thermally degraded	1.58	3.14
PVC — $BuAcSn(IOTG)_3$		
— Freshly milled	1.1	2.0
PVC — $BuAcSn(\beta MeOct)_3$		
— Freshly milled	1.09	1.98
— Thermally degraded	1.0	1.0
Bu_2SnCl_2 [c]	1.60	3.25

[a] Mm s^{-1}. [b] Relative to $CaSnO_3$ = 0. [c] ref. 11.

-(IOTG)$_3$-PVC and BuAcSn(βMeOct)$_3$-PVC exhibited spectra identical to that of $BuAcSnCl_3$, showing that, in these cases, complete sulphur for chlorine ligand exchange takes place in the milling process. The spectra from the thermally degraded samples were generally of lower quality, but no tin(II) species could be detected. The Q.S. values for the degraded samples was much lower ($\simeq$1.0 min^{-1}) than that of the freshly-milled samples suggesting further degradation, possibly to mono-alkyltin oxides or sulphides.

References

1 J.W. Burley, R.E. Hutton and V. Oakes, J. Chem. Soc. Chem. Commun. (1976) 803; R.E. Hutton and V. Oakes, Adv. Chem. Ser. 157 (1976) 123.
2 E.J. Bulten and J.W.G. Hurk, J. Organometal. Chem., 162 (1978) 161.
3 CRYSTALS suite of programmes, Oxford University.
4 International Tables for X-ray Crystallography, vol. III, Kynoch Press, Birmingham (1963).
5 J. Buckle, P.G. Harrison, T.J. King and J.A. Richards, J. Chem. Soc. Dalton (1975) 1552.
6 P.G. Harrison and T.J. King, J. Chem. Soc. Dalton (1974) 2298.
7 P.G. Harrison, T.J. King and J.A. Richards, J. Chem. Soc. Dalton (1974) 1723.
8 N.W. Alcock and J.F. Sawyer, J. Chem. Soc. Dalton (1977) 1090.
9 P.G. Harrison, T.J. King and J.A. Richards, J. Chem. Soc. Dalton (1975) 826.
10 P.G. Harrison, T.J. King and R.C. Phillips, J. Chem. Soc. Dalton (1976) 2317.
11 A.Yu. Aleksandrov, Ya. G. Dofman, O.L. Lependina, K.P. Mitofanov, M.V. Plotnikov, L.S. Polak, A.Y. Jemkin and V.S. Shpinel, Russ. J. Phys. Chem. 38 (1964) 1185.
12 P.G. Harrison, K. Molloy, R.C. Phillips, P.J. Smith and A.J. Crowe, J. Organometal. Chem., 160 (1978) 421.

Publ. Hlth, Lond (1980) 94, 78–88

The Distribution of Lead in a Roadside Environment and Its Consequences for Health

M. A. Healy
B. Sc., C. Chem., M. R. I. C.
Department of Chemistry
and M. Aslam
Ph. D., M. P. S.
Department of Pharmacy, University of Nottingham, University Park, Nottingham. NG7 2RD

The distribution of deposited and absorbed lead originating from vehicle exhaust emissions along a section of the A52 trunk road is examined. Significant quantities of the metal are found. Roadside dust contains up to 210 ppm with both dilution and concentration occurring at different locations after rainfall. The level of contamination in soil is shown to relate to the distance from the roadway and the depth of sampling. Grasses growing on the verges retain airborne lead-containing particles which then concentrate into the upper levels of the soil. Blackberry plants absorb 1·6 ppm of lead in their shoots whilst the fruit is contaminated with up to 6·36 ppm, mainly as a surface deposit, at sites adjacent to lay-bys where gathering is most facile.

The pattern of distribution observed suggests that fruit and vegetables grown in gardens in close proximity to a major roadway may present a potential health hazard. Where possible new houses should not be built with gardens extending to within 15 m of such a road.

Wild blackberry fruit collected from the hedgerows in areas of high traffic density could significantly add to the lead body burden; particularly when used to make preserves where up to 4 ppm could be present. Steps should be taken to warn the public of the inherent dangers in such wild fruit and Local Councils should remove readily accessible plants.

Introduction

Much interest has arisen in recent years over the role of lead in the environment. Industrial consumption of the metal in the United Kingdom in 1977[1] was of the order of 290 x 10^3 metric tons, of which 55 x 10^3 tons were used in the manufacture of lead alkyls: primarily tetramethyl lead and tetraethyl lead for use as petroleum additive anti-knock agents to improve combustion characteristics. Although approximately three-quarters of the lead alkyl production is exported, it is this form of the metal which has given rise to greatest concern because of the widespread distribution its use in petrol causes.

In anti-knock fluids 1,2-dihaloethanes are used as scavengers of decomposition products from the lead alkyls. The oxides resulting from combustion of the lead alkyls are thus able to react to form mixed halides. The principal chemical forms of the metal emitted from car exhausts[2] are, therefore, lead bromochloride (PbBr.Cl) and the alpha and beta forms of ammonium chloride lead bromochloride (NH_4 Cl.2Pb Br. Cl and $2NH_4$ Cl.Pb Br.Cl) together with trace amounts of mixed oxide (Pb0.PbBr.Cl$H_2$0) and sulphate ($PbSO_4$). Degradation

0038–3506/80/020078+11 $01.00/0

of these particles leading to halogen loss and conversion to oxide and/or carbonate[3] produces a reduction in particle size with a concomitant increase in solubility. Dissipation and precipitation of the emitted aerosol lead is dependent on particle size and meteorologic factors, but about half the lead containing particulate matter is removed from the air by gravity within a few hundred feet of a roadway.[4]

A number of studies have been made of the lead content of tree leaves and grasses adjacent to major road systems[5] as well as in roadside fruit and berries.[6] In the work we report here the overall distribution deposited and absorbed lead is examined in detail at the boundaries of a typical trunk road system. The aim being to establish the pattern of the lead environment and its significance as a health hazard.

Location of Study

Sites along a dual carriageway section of the A52 trunk road between the M1 Motorway, Junction 25, at Sandiacre, Derbyshire and the five-road intersecting island at Bramcote, Nottinghamshire were chosen for this study. The road runs in an east/west direction at this section and as well as providing the main link between Nottingham and Derby, acts as a feed road from both cities to the M1 Motorway. The traffic density is of the order of 24,000 vehicles in a 24 hour period.[7]

The selected section of this road is bordered by various areas of fields and rose gardens, a school and playingfields, an industrial estate and houses with gardens in places extending to within 4 metres of the roadway. The terrain is undulating with several sections of the A52 elevated over a road and railway system. There is thus a complete cross section of the population from babies in prams in gardens to school children, and adults at home and at work represented within the confines selected. Where possible, sites on both sides of the carriageway adjacent to each of the areas described were chosen for the collection of samples of road dust, soil, grasses, blackberry plants and fruits for examination of lead content.

Experimental Procedure

Dust deposits were collected at sites from each direction along the roadway. Sampling was first made during a period of dry weather (in excess of 7 days) and again from the same locations after heavy rainfall (0·78 ins). Material was collected randomly and no attempt was made to select particle size which was found to vary between approximately 0·2mm and about 3mm for the samples taken. This material was weighed and the lead extracted by digestion in 5M.A.R. nitric acid. The resulting solutions were filtered under reduced pressure and the filtrate made up to known volumes using triply-distilled, de-ionized water.

Samples of soil were collected at various intervals between 1 and 9m from the roadway. They were obtained by making borings 2·5cm in diameter to a depth of 60cm. Sections at known depths were removed from each drill, dried, weighed and the lead extracted into solutions as the nitrate.

The grasses removed from each site were firstly trimmed to remove any root system. The samples were then divided. One portion was dried to constant weights at 110°C, and 20g amounts digested by simmering in A.R. nitric acid for 15 minutes. After filtering, 100ml aqueous solutions were prepared for analysis. The second portion of grasses collected was thoroughly washed by immersion and agitation for one hour in a pneumatic trough fed by continuously running cold water. Samples were then dried to constant weight and treated as for the unwashed grasses.

Blackberry plant canes, each approximately 2 m in length were selected. All fruit was removed but the leaves were retained. The shoots were then sectioned to lengths of about 5cm

and thoroughly washed for one hour in a manner similar to that used for the grass samples. Because of the greater difficulty in digestion of the plant stems it was necessary to simmer known weights of the blackberry plants for 35 minutes in nitric acid. After which solutions for analysis were prepared as previously described.

Samples of blackberry fruit were collected during mid-September and mid-October. Care was taken to achieve a uniformity of development of fruit chosen, so that the samples did not contain very young undeveloped fruit or old overripe berries but were representative of the type which was most likely to be picked for use. The fruit from each site was divided. One portion was subjected for one hour to the washing procedure described. The fruit was then allowed to drain on absorbent tissue under warm air. Samples from both portions were then weighed as undried fruit and treated with nitric acid to extract the lead content. Resulting solutions were filtered under reduced pressure and made up to known volumes with the triply distilled, de-ionized water used throughout these measurements.

In all cases during the extraction process the vessel containing the material was partially covered to prevent loss of any material by evaporation.

Lead analyzes were made by atomic absorption spectrophotometery using a Perkin-Elmer Model 603. Background correction was used for all measurements and final results were obtained as an average of at least five readings over a ten second integration time. Standard solutions were prepared from B.D.H. atomic absorption reagents and results obtained, via the microprocessor of the instrument, in direct concentration units.

Results and Discussion

Roadside dust

The results obtained show significant concentrations of lead in the dust collected, the highest being 210 ppm. However, the range of values is wide, reflecting the variability in sample composition. No distinct pattern emerges as to distribution of the lead between east and west traffic directions although, in general, a higher level was found in the offside section of roadway. This is probably due to lead deposition occurring from traffic travelling in both directions. The central reservation being approximately 3 m in width.

The overall lead content is lower than might have been expected from earlier data. For example, Giubileo[8] found between 1360–2360 ppm in the street dust of central Milan with a decrease to 800 ppm in peripheral streets. Hogger[9] found a maximum level of 2040 ppm in Zurich. However, in these locations wind distribution of the aerosol lead is confined by the surrounding buildings whereas in the sites of the present study the area is open and in places elevated which would enable a much wider spread of the material to be achieved

Whilst at a number of sites the effect of rain was to reduce the lead content by between 20 and 30%, it is notable that in others an increase was observed. The efficiency of rainwater in fractionating the lead is, clearly, dependent on a number of factors. Rameau[10] has shown that there is an increase in lead content in sub-fractions of different particle sizes of street dust. However, we believe that in the case of roadside dust the most significant factor in lead distribution after rainfall must be mobility and direction of flow of the resulting ground water. The primary process will then be one of simple transport of dust and lead combined rather than dependent on lead solubility and hence particle size. It is this factor which the results in Table 1 illustrate. Where samples were collected at sites on inclined sections of roadway where the ground water is free-flowing a reduction of overall lead content was observed. At sites on level sections of roadway where pools of water could collect the lead level had decreased by a smaller amount or, in fact, increased after rainfall.

The primary health hazard which can be associated with the roadside dust arises because the

TABLE 1. Lead content of dust collected from a section of the A52 trunk road

Sample	Location on road and gradient	Traffic direction	Lead content (ppm) Before rain	After rain
G1	Nearside/inclined	East	180	160
G2	Offside/inclined	East	210	156
G3	Nearside/level	West	132	147
G4	Offside/level	West	146	132
G5	Nearside/inclined	East	117	112
G6	Offside/inclined	East	92	76
G7	Nearside/level	West	121	118
G8	Offside/level	West	137	142
G9	Lay-By/level	East	180	191
G10	Lay-By/inclined	West	142	107

lead coated particles are of a size which would readily adhere to clothing and thereby be transported. This was clearly evident on examination of the authors shoes and clothing after collection of samples. Thus the dust provides a vehicle for distribution of the lead to areas which would normally be relatively uncontaminated.

Soil

Table 2 and Figures 1 and 2 show the distribution of lead in the soil bordering the A52 roadway.

TABLE 2. Lead distribution with depth of soil and distance from roadway

Distance from road (m)	Depth (cm)	Lead content (ppm) East	West
1	5	134	126
1	15	61	67
1	30	43	45
1	60	36	29
3	5	114	102
3	15	67	69
3	30	45	39
3	60	27	34
6	5	87	95
6	15	73	68
6	30	42	31
6	60	31	32
9	5	82	89
9	15	56	52
9	30	34	34
9	60	23	30

A significant concentration is built up in the top few centimetres of the soil, the amount showing a clear relationship to proximity to the roadway. At greater depths the lead concentrations do not vary as widely with distance from the traffic, indicating some retention

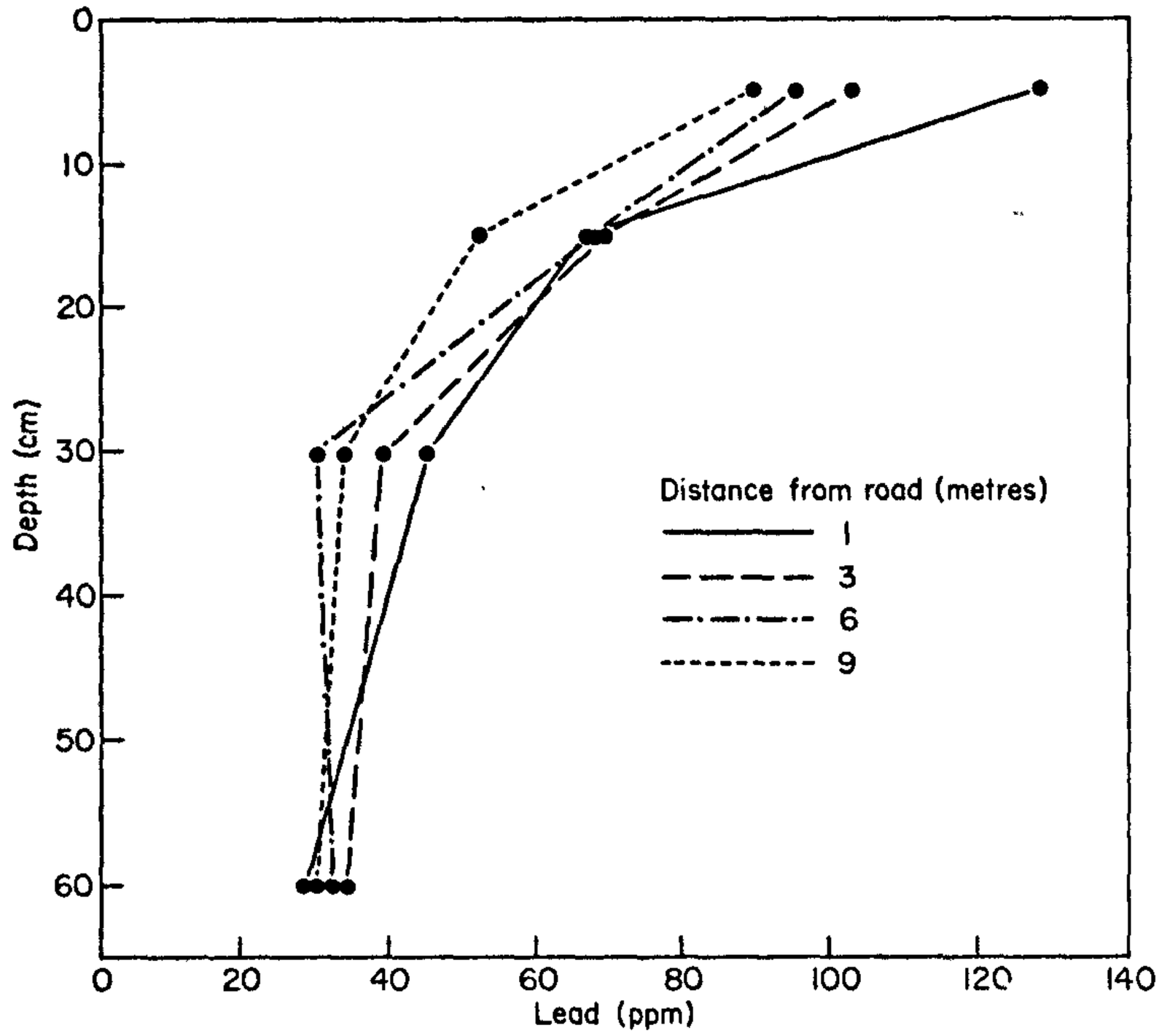

Figure 1. Distribution of lead in soil with depth and distance from roadway – traffic direction west.

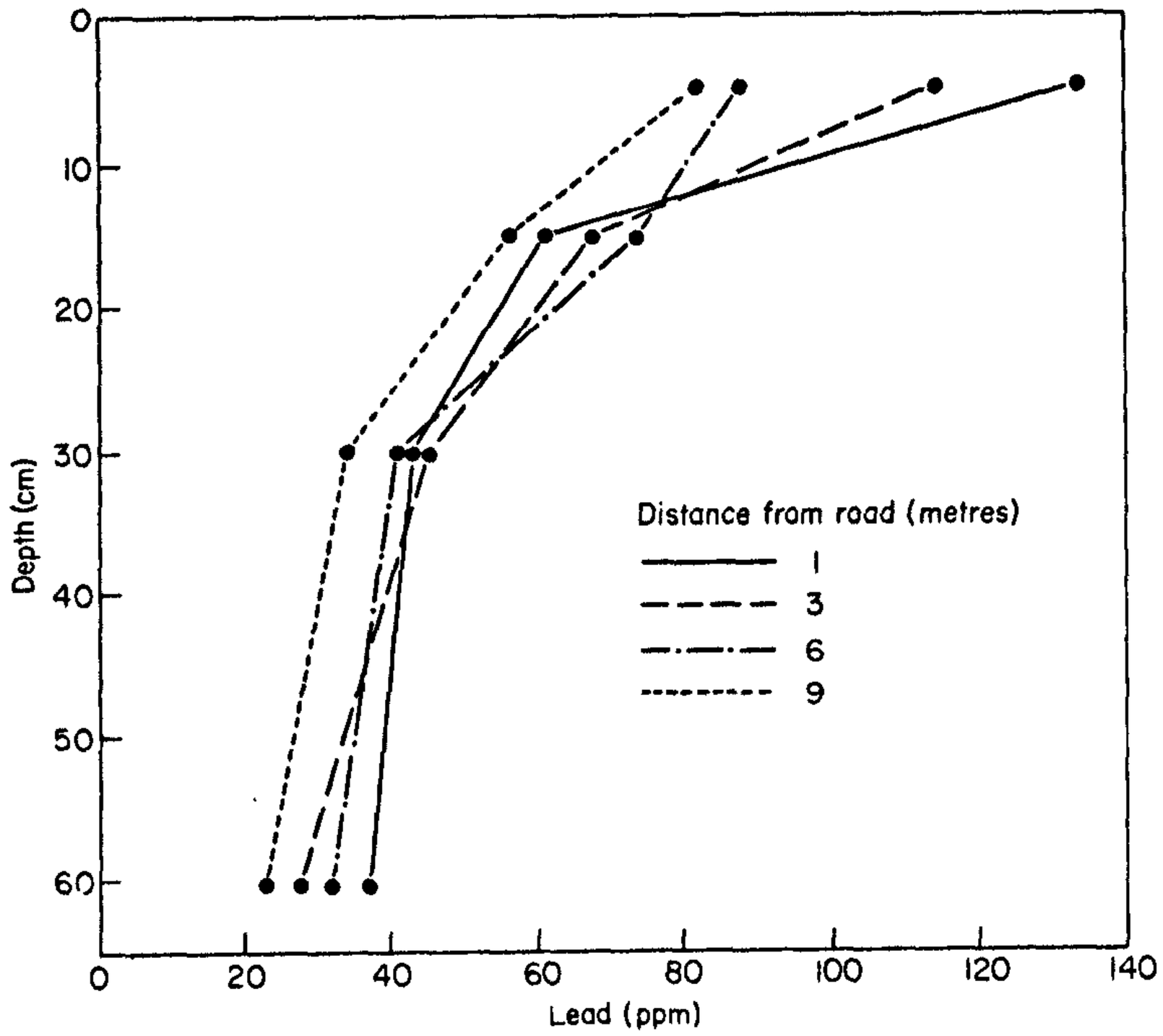

Figure 2. Distribution of lead in soil with depth and distance from roadway – traffic direction east.

in the upper levels possibly caused by a cycling of the lead between the soil and plant root systems.

Bearing in mind the mean concentration of lead in soil is of the order of 16 ppm the lead levels found at the lower depths are not markedly elevated.

No significant variations were observed between the lead content of soil from the verges of the east bound carriageway to those from the west.

Grasses

The lead content on the blades of grasses again showed a decrease with distance from the roadway. The highest lead concentrations were much lower then those found in the sub-surface soils, indicating that the lead levels in the soil reflect an accumulation of the metal. The grasses, thus, provide a physical trap for the collection and retention of lead in a given site.

TABLE 3. Absorbed lead content of grasses

Distance from roadway (m)	Mean lead content	
	Unwashed	Washed
1	45	32
3	38	31
6	34	26
9	28	23

Figure 3. Absorbed lead content of grasses. Variation with distance from roadway.

Washing the grasses did not produce a marked change in the lead level. Because of the smooth surface of the grass blades it was anticipated that the surface deposited lead would be only weakly absorbed and therefore readily removed. This did not prove to be the case. Whilst the work of, for example, Motto *et al.*[11] showed an increased lead content in plants growing adjacent to a highway, it would be unwise to draw the conclusion that the high lead yield obtained in the present work after washing was as a result of absorbed lead within the grass

structure. Further work would be required to determine if such results arose from an inefficiency of the washing process and whether this could be improved by the use of surfactants.

Blackberry plants

Care was taken to ensure that as much of the surface deposited lead as possible was removed from the canes used in the experiment by thoroughly washing and wiping with absorbent tissue. The results obtained gave a mean lead content within the shoots of 1·6 ppm. This did not vary outside experimental error for any of the samples analyzed. The inference being, that above a certain level the amount of lead absorbed is largely independent of the concentration of the element in the surrounding soil. The significance of the metal in the blackberry plant arises from the annual habit of the growth of the shoots. This yearly replacement process enables a measure of the ability of the plant to absorb lead in a single growth cycle to be established.

The level of 1·6 ppm in the canes gives an indication of the maximum probable lead content within the fruit. Because of the relatively short period of development and growth of the fruit it is unlikely to concentrate the lead to a higher value.

Blackberry fruit

Because of the duplet structure it is virtually impossible to ensure complete removal of surface deposites from the fruit, and hence obtain an accurate measure of the lead contained within. The extrapolated value from the plant canes, as measured above, gives the best fit to the maximum absolute value of lead within the fruit. Table 4 lists the level of lead found in wild blackberry fruit.

TABLE 4. Lead contamination of wild blackberry fruit

Site reference	Mean distance from roadway (m)	Lead content (ppm) – undried fruit			
		Mid-September		Mid-October	
		Unwashed	Washed	Unwashed	Washed
A1	7	0·46	0·31	0·45	0·33
A2	7	0·44	0·28	0·49	0·37
A3	6	0·87	0·71	0·87	0·64
A4	7	0·86	0·67	0·91	0·68
B5	3	2·74	2·05	2·66	1·89
B6	3	2·77	1·89	2·83	1·74
B7	2·5	2·81	1·97	3·12	2·22
B8	3	2·76	2·07	2·67	1·89
C9	3·5	2·62	1·73	2·65	1·94
C10	3·5	2·73	2·10	2·83	1·93
C11	2·5	2·71	1·82	2·59	1·77
C12	3	2·68	1·86	2·76	1·93
D13	1	3·96	2·56	4·07	2·87
D14	1	3·59	2·31	3·32	2·56
D15	1	5·77	4·60	5·98	4·77
D16	1	6·12	4·97	6·36	5·04

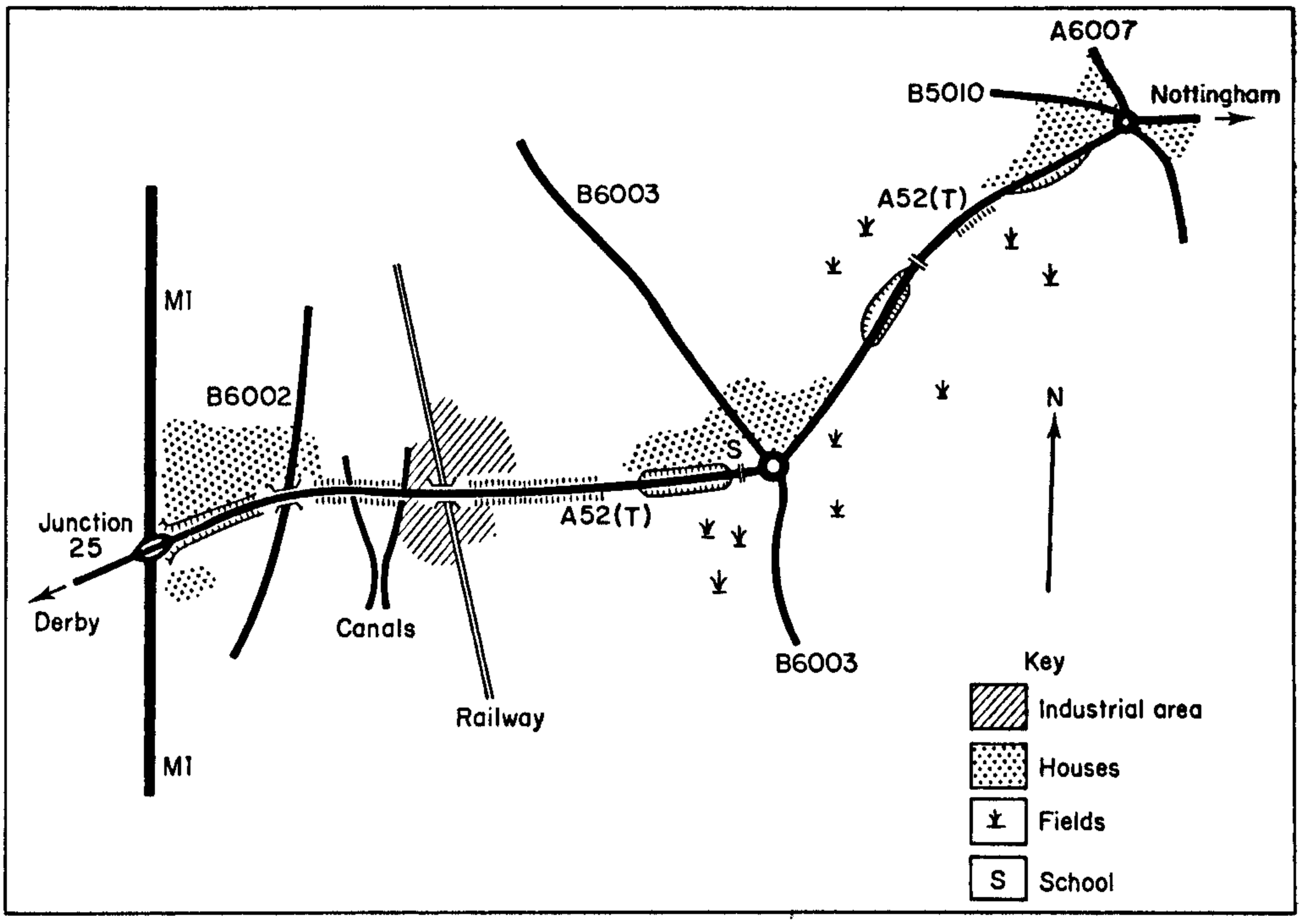

Figure 4. Section of A52 trunk road used in this study and the surrounding area.

Site references A1 and A2 were to the rear of an embankment and show the lowest levels of lead on the blackberry fruit. Fruit taken from plants at the same distance but facing the roadway show almost twice the level of lead (A3 and A4). The bank therefore, appears to act as a partial barrier to the lead.

The highest lead contents were found in fruit from plants directly adjacent to lay-bys (D15 and D16). These had levels of lead much higher than from plants at the same distance but adjacent to moving traffic (D13 and D14). Sites B5 and C9 were elevated 4–5 metres above road level. Fruit collected in these locations did show a slightly lower lead content than fruit from plants at sites similar distances but not elevated (B6 and C10). Fruit samples from B7 and B8, and C11 and C12 were to the front and rear, respectively, of the same plants. Over such small distances no meaningful differences in the lead content of the fruit was observed. The sharp increase in lead content which occurs between 7 m and 3 m from the roadside was unexpected. This may well relate to the efficient design of the blackberrry fruit for entrapment of airborne dust particles which will be carried in the following vortices of passing traffic. These will have sufficient energy to effect the distribution of additional lead laden dust (*vide supra*) to the shorter distances from the roadway.

Washing of the fruit reduced the lead content by approximately 20–35%. However, it is reasonable to assume that the overwhelming contribution to the lead contamination arises from surface deposited lead and not absorbed lead.

The values show slight increase in most cases between fruit collected in mid-September and that gathered in mid-October. This probably arises because the mean age of the fruit in the latter case was higher and therefore the samples had experienced a longer exposure to the leaded atmosphere. The lead contamination we observed is higher than that reported by Fowles[6] for

blackberry fruit. However, his highest values were obtained from samples collected from sites which probably had a lower traffic density. Taking this into account the value he obtained of 0·57 ppm at a distance of 6 m from the roadway is in good agreement with our value of 0·87 ppm at site A3. The highest value of 6·36 ppm is less than the highest values reported for elderberries (6·77 ppm) and hawthorn berries (23·8 ppm) collected from similar roadsystems.[6]

Whilst atmospheric lead has been estimated to contribute about 13 μg a day to the body burden in urban areas of Britain,[12] it is the diet, especially plants, which provides the major source of metal in man. Table 5 shows the average estimated daily intake of lead in food.[13]

TABLE 5. The estimated average daily intake of lead from food[13]

Food type	Mean lead Content (mg/kg)	Weight of food eaten (kg)	Lead intake per person (ug/day)
Cereals	0·12	0·27	32
Meat and Fish	0·16	0·18	29
Fruits and Preserves	0·11	0·25	28
Green Vegetables	0·19	0·11	21
Root Vegetables	0·09	0·21	19
Milk	0·02	0·40	8
Fats	0·08	0·08	6
TOTALS	0·09*	1·50	143

*Weighted according to proportion of food type eaten.

From this it can be seen that fruits and preserves make a significant contribution. In 1961 the Lead in Food Regulations set a maximum content for lead in undried fruit and vegetables of 2 ppm. Clearly the levels of lead detected in wild blackberries are unacceptable and give rise to particular concern in the case of children where the absorption of lead is considerably more facile than in adults. All the sites we chose showed clear signs of being regularly used for gathering fruit and in many instances actual collection was observed before and after our sampling.

The fruit growing on plants adjacent to lay-bys is particularly accessible for collection, yet it is in precisely these locations that the fruit is most contaminated. The simple action of gathering the fruit ensures that lead is transferred to the hands as one clambers up a bank holding to the grass for support or brushing against the dust covered plants. In children this lead could readily be transferred to the mouth and hence to the digestive tract.

Whilst eating the fruit directly presents an unnecessary health hazard, because of the relatively short season for the crop the risk is limited. Of perhaps greater concern is the use of the blackberries in preserves. From the results we obtained it would be quite possible, using fruit collected at sites similar to ours, to prepare jams containing between 2 and 4 ppm of lead. These would then be consumed over a much longer period than the fresh fruit and hence, particularly if fed to young children and babies, could present a distinct accumulative hazard. A similar danger has been shown to exist when wild fruit is collected from the banks of busy roadways and used in wine making. Wine from elderberries was found to contain 1·23 ppm of lead.[6]

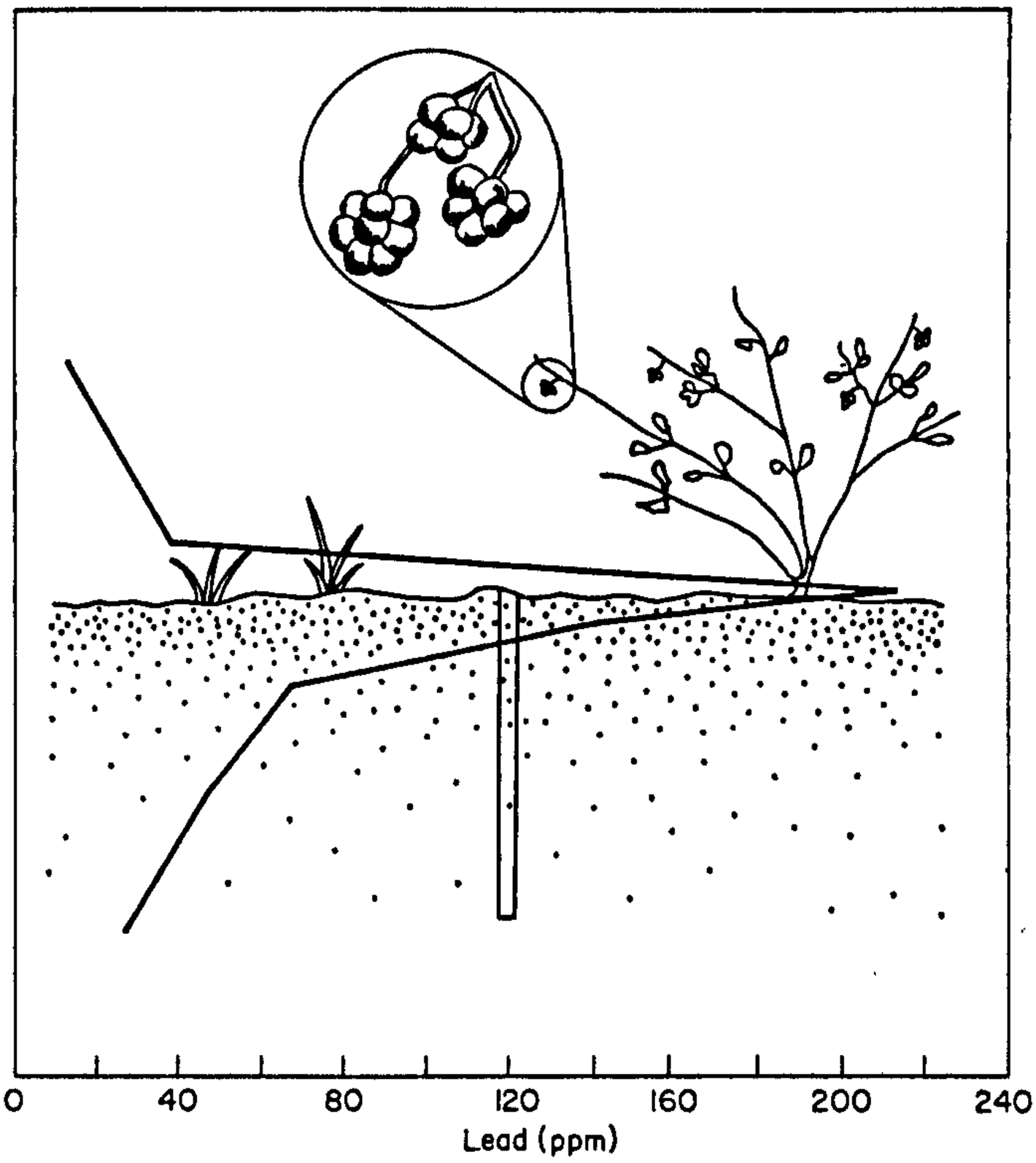

Figure 5. Diagrammatic representation of the distribution of deposited lead in the roadside environment of the A52 (T).

Conclusions

The results obtained clearly allow a number of important conclusions to be drawn which are directly relevant to public health.

(1) New houses should not be built with gardens which extend to within 15 m of a major roadway.

(2) In the many houses which are already built with gardens much nearer to the roadway than 15 m (4m was the boundary between road and garden for some houses in this study) it may be unwise to grow fruit and vegetables for consumption other than in a greenhouse or cloches. The evidence tends to support the belief that whilst plants grown in close proximity to a major roadway have a higher lead content, the main hazard arises from airborne lead depositions rather than absorbed lead within the plants. In all cases the produce should be washed with particular care.

(3) Wild blackberries should not be gathered from the hedgerows of major roadways.

(4) Where possible Local Authorities should act to remove wild blackberry plants from areas similar to those used in this study which are readily accessible to both lead and the public.

It is important that a programme is set in motion to educate the public to the inherent dangers to health which exist from consumption of wild fruit. This could be achieved by use of

the press and television services. There must be many people who may now be eating preserves produces from fruit collected at sites similar to those employed in this study. Whilst it is clearly essential not to give rise to undue alarm, a timely warning would be apposite.

Acknowledgement

The authors wish to express their thanks to Mr I. R. Marshall for his experimental assistance. M. Aslam wishes to thank the D.H.S.S. (London) for financial support.

References

1. *World Metal Statistics*, 1961–1978.
2. Waldron, H. A. & Stöfen, D. (1974). *Sub-Clinical Lead Poisoning.* London: Academic Press.
3. Ter Haar, G. & Bayard, M. (1971). *Nature* 232, 553.
4. Daines, R., Motto, H. & Chilko, D. (1970). *Environmental Science Technology* 4, 318.
5. Davies, B. E. & Holmes, P. C. (1972). *Cambridge Journal of Agricultural Science* 79, 479.
6. Fowles, G. W. A. (1976). *Food Chemistry* 1, 33.
7. *Personal Communication*, (1979). Data Collection Department, Nottinghamshire County Council.
8. Giubileo, M. (1957). *Medicina del Lavoro* 48, 165.
9. Högger, D. (1971). *Bulletin des Eidgenössichen Gesundheitsamtes B3.*
10. Rameau, J . Th. L. B., (1972). *International Symposium on Environmental Health Aspects of Lead.* Amsterdam.
11. Motto, H. L., Daines, R. H., Chilko, D. M. & Motto, C. K., (1970). *Environmental Science Technology* 4, 231.
12. Report, (1974). *Inter-Department. Working Group in Heavy Metals.* H.M.S.O.
13. *Survey of Lead in Food*, (1970). Ministry of Agriculture, Food and Fisheries. H.M.S.O.

Reprinted from *Publ. Hlth, Lond.* (1979) **93**, 274–284

Heavy Metals in Some Asian Medicines and Cosmetics

M. Aslam
Ph.D. M.P.S.
S. S. Davis
Ph.D. M.P.S.
Department of Pharmacy
and
M. A. Healy
B.Sc. C.chem. M.R.I.C.
Department of Chemistry, University of Nottingham, University Park, Nottingham NG7 2RD

Significant concentrations of heavy metals have been found in a number of Asian medicines and cosmetics. The herbal baby tonic, Bal Jivan Chamcho contained lead leached from the coating of the spoon with which it was supplied. Some samples of Surma were found to have a lead content as high as 86%. Amongst other metals, mercury, lead and arsenic were found in the aphrodisiac and tonic Kushtay. A Warak which purported to be gold was a copper/zinc alloy.

No mercury was found in the cosmetic Sandurs and Kum-Kum pastes we examined, but unacceptably high concentrations of lead and antimony were found in some pills, and of lead and arsenic in a powder intended for medicinal use.

The use of traditional Asian remedies involves a substantial risk of heavy metal poisoning to which the medical profession should be alerted.

Control by legislation alone would not be effective as many of the preparations are sent by relatives in Asia.

Introduction

Since 1950 there has been a marked increase in the number of Asian immigrants to the United Kingdom, a high proportion coming from the Indo-Pakistan sub-continent. With this influx has come not only the religious and dietary practices of these peoples, but also their own system of medicine. We report here some results from our research into the effects of this.

Bal Jivan Chamcho

One of the first Asian preparations we investigated was Bal Jivan Chamcho, which was being imported and sold through the Grocery trade as a baby tonic. In October 1976, a child admitted to hospital in Luton with clinical lead poisoning was found to have been administered regular doses of this baby tonic.

Medicines, such as Bal Jivan Chamcho, have been available on the Indian market for many years and in principle appear innocuous. They are compounded preparations from a

0038-3506/79/050274+11 $01.00/0

variety of botanical substances; the extracts and remainders of which are made into a paste and spread on a spatula-shaped spoon and allowed to dry. The dried preparations, with the spoon as a carrier, are then packaged into a small carton for sale. The label on the container of the Bal Jivan Chamcho is printed in English, Gujerati and Hindi with the directions:

"Children Diseases viz Varadha Capilliary, Bronchitis, Greenish Diarrhoea, Rickets, Croup, Convulsions etc. Rubbing the medicine with water or milk until it gets colour. To be taken twice a day."

The herbal preparation is, thus, allowed to soak in about 5 cm^3 of milk or water for several minutes after which the milk is then administered to the child. The preparation itself is not taken but is reused in a similar manner for a period of up to several months.

Our investigations revealed that when the recommended procedure for administering the medicine was followed, an average dose of 12 ppm of lead was inadvertently given every time the material was used. In addition, the quantity of lead ingested increased in proportion to the reuse of the herbal preparation. The plating on the spoon in all the samples we examined was found to show considerable corrosion before the material had been used (Fig. 1). This increased with each period of use. By using atomic absorption spectroscopy to analyze the compound and the spoon, the results we obtained (Table 1) clearly showed the spoon to be the primary source of contamination from lead. The leaching action into the herbal preparation was enhanced by addition of moisture which, thus, caused further corrosion and increased solubility of the lead from the spoon.

As the high lead content of these herbal medicines was a toxic hazard, particularly in infants, for whose treatment it was recommended, it was proposed that an emergency order prohibiting the import, sale and supply of these preparations should be implemented. Such an order was made effective from February 1977 to May 1977 and a permanent order for Bal Jivan Chamcho was introduced in May of that year.

Surma

During the course of our studies into the role of the Hakim (healer) in Asian communities within this country, we became interested in the Surma (Fig. 2) which he manufactured for patients. This Surma is applied to the eye, apparently for medicinal purposes, and has the appearance of mascara. However, application is not to the outside of the eyelid but to the conjunctival surface (Fig. 3). Its use by Asian families can be traced back many centuries. They believe it strengthens and protects the eyes against disease and improves appearance. The Surmas used in our study ranged in colour from black, through various shades of grey to white. From X-ray powder diffraction analysis of an initial batch from 13 different manufacturers, 11 were found to contain lead whilst carbon was indicated as the main constituent of the remaining two. More detailed analyses for metals, again using atomic absorption spectroscopy, revealed lead concentrations as high as 86% in the grey surmas which were found to be composed, almost exclusively, of lead sulphide. Indeed, this material formed the base for the majority of Surmas we have analyzed. Carbon is added in varying amounts in some compounds, the proportion used modifying the characteristic dark colouration. Various herbs, pearls and menthol were also detected, whilst elements present in trace quantities (<0·5%) included iron, copper, zinc, silver, antimony and strontium.

In 1976 we became interested in a 4 year old Asian child who was suffering from lead poisoning. This appeared to be attributable to the use of a Surma which was found to contain 86% lead as lead sulphide. The medical staff at the hospital of admittance had warned the parents against continuous use of the eye cosmetic but because the child was

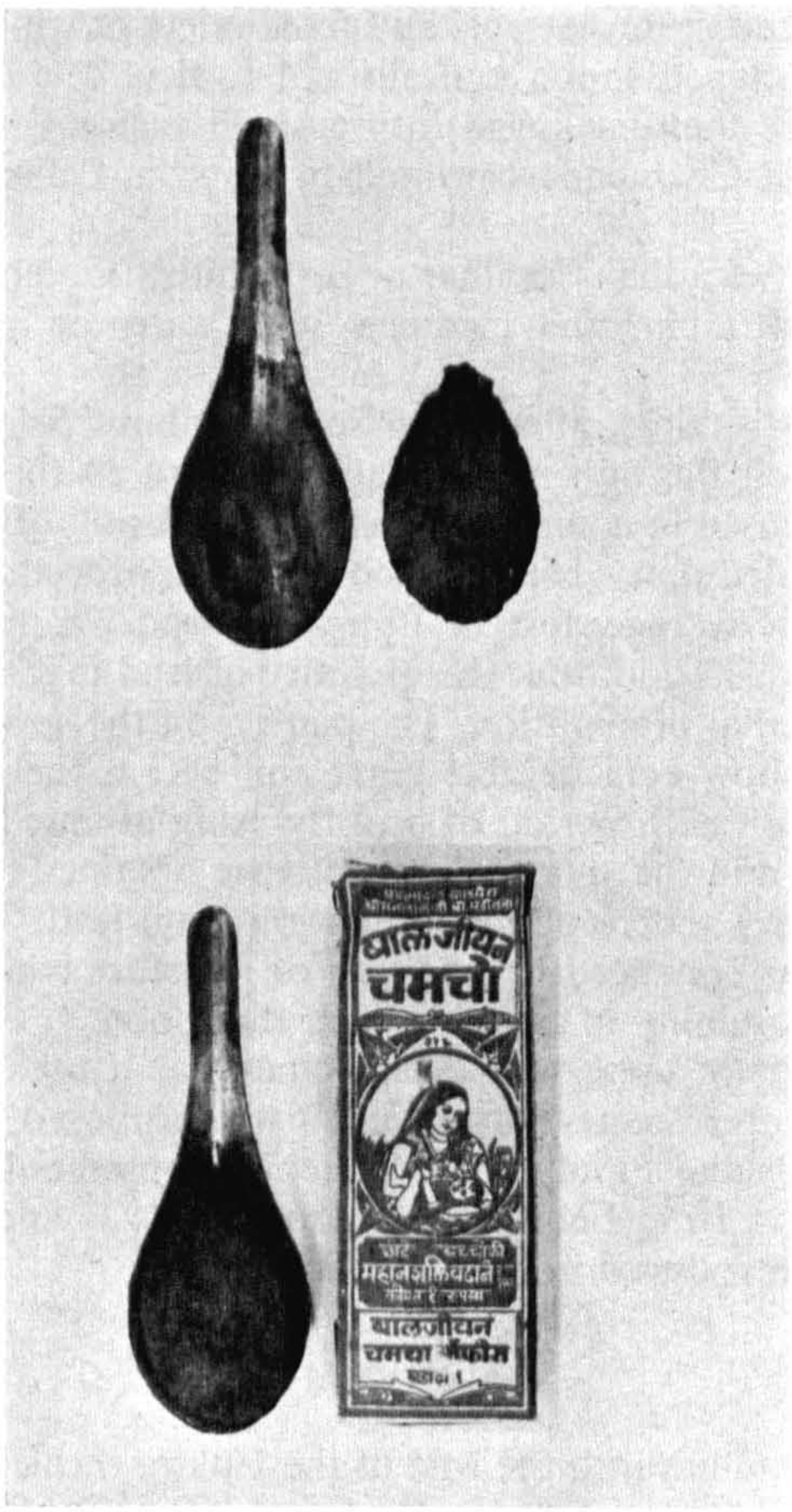

Figure 1. Bal Jivan Chamcho showing corroded spoon.

TABLE 1. Analysis of Bal Jivan Chamcho for lead content

Sample	Lead content of spoon (percentage)	Lead content of herbal preparation (ppm)
1	26·5	310
2	83·3	1,040
3	32·7	225
4	30·1	265

a boy he was the subject of preferential treatment by his parents. On visiting the home of this child it became obvious that each time the sample of Surma was collected from the parents by the Health Authorities a further sample was immediately forthcoming from anxious grandparents in Pakistan.

In addition to the usual application of Surma, it is the custom with a Moslem child to place a small dot of the material on the forehead to ward off the "evil-eye". Because of the

Figure 2. A sample of proprietary Surmas.

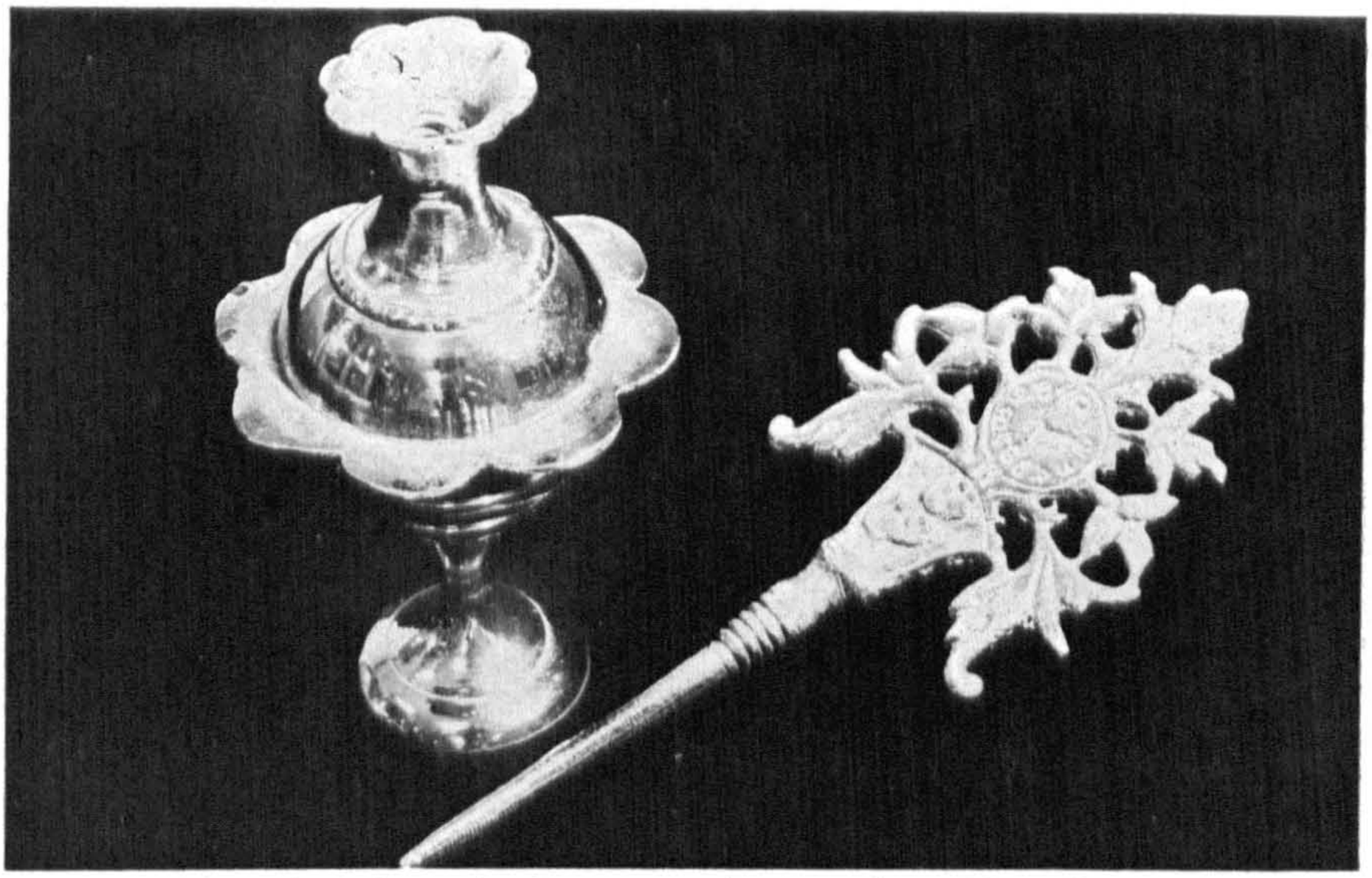

Figure 3. A decorative Surma container complete with applicator.

superstitious nature of this child's parents they had also tied lengths of blackened string around his wrists for the same purpose. Their belief was that as a black mark is considered a blemish, the combination of the black dot and string would outwit the "evil-eyed one" and cause him to think the child unattractive.

In 1978 we collected further samples of Surma from this child's parents which on analysis were all found to be of the type containing around 86% lead as lead sulphide. The mother of the child admitted that she had continued to administer Surma on a regular daily basis after the child's release from hospital, but asked that this information be withheld from her doctor "as he would not understand". The mean blood-lead levels measured in this child were

1976 2·4 μmol/l
1977 3·0 μmol/l
1978 3·4 μmol/l

He has now been readmitted to hospital with diagnosed plumbism.

In a further study, carried out at the Childrens' Hospital, Nottingham, measurements were made of the blood-lead levels in a group of Asian children[1] who were known to have used Surma and a control group who had not. The values obtained gave a mean blood-lead level of 1·6 μmol/l for those children using Surma and 1·0 μmol/l for those Asian children who had not had the cosmetic regularly applied. In his recent paper Joseph[2] comments that 5 of the 82 (6%) Asian children for which he measured blood-lead levels had levels in excess of 1·8 μmol/l. Of the Surma users at Nottingham, 10 of the 26 (38%) had greater than 1·8 μmol/l of lead in their blood. It is also interesting to note that Dr Joseph obtained a value of 1·0 μmol/l for his controls on non-Asian children, the same value as in the Nottingham controls. It is apparent that these investigations at Nottingham have shown a clear association between blood-lead levels and the use of Surma. Indeed, recently, it was considered that Surma had contributed to the death due to lead encephalopathy of a 4-year-old Asian boy in Oldham.

Our most recent analyses of proprietary Surmas sold or imported in the United Kingdom, but manufactured in India or Pakistan are shown in Table 2. Thirty-six per cent of these had lead concentrations in excess of 50%. One sample contained zinc. The use of menthol in Surmas could well exacerbate the risk of poisoning as it causes excessive lachrymation.

TABLE 2. Chemical analysis of proprietary Surmas sold or brought into the United Kingdom but manufactured in India or Pakistan

Description	Powder colour	Percentage lead
Hashmi Surma Jowahar Chaharam, Karachi.	Grey	80·2
Surma Moqawi Basar Taj Company, Lahore.	Grey	53·7
Multani, Ayurvedic 36-H Connaught Circus, Delhi.	Grey	Trace
Nag Jyoti, Murrari Brothers, Delhi.	White	Trace (Zinc 4·5% + Menthol)
MD Hashim Surma, Bunder Road, Karachi.	Grey	82·9
Bal Jyoti, Murrari Brothers, Delhi.	Grey-Black	38·4
Indian Surma.	Cream	Trace
Bhimsaini Kajal With Aela, Murrari Brothers, Delhi.	Black Paste	Trace
Nargasi Surma, Hamdard, Pakistan.	Grey	77·3
Binger Surma, Hamdard, Pakistan.	Black	26·3
*(Bhimsaini Kajal With Aela.	Black Paste	Trace)

Trace = <0·5%.
*Carbon in soft paraffin base.

Many of the infants we observed responded to the administration of this type of Surma with profuse tear formation at which they invariably rubbed their eyes. Inevitably many then sucked their fingers, and hence swallowed the Surma suspended in tears. Of particular

concern are the claims made on the containers of these Surmas: "Makes eyes beautiful and protects eyesight", or "Use to prevent eye disease and vision defects". Despite the evidence against Surmas it is clear their use in immigrant Asian communities remains widespread. Somewhat to our surprise, on a recent random sampling of 20 homes of Asian families in Bradford we were able to collect 20 samples of Surmas.

After our report on the analysis of Surma samples bought in Bradford and Nottingham a new safety code was announced by the then Prices Minister, Mr John Fraser in August 1978. Under these new regulations it will be a criminal offence for cosmetic manufacturers, importers or retailers to market any product which is liable to damage health. Our fear, however, is that legislation preventing the sale of Surmas will prove ineffective as our investigations indicate that the majority are obtained directly from abroad by the user, his friends or relatives or the hakim.

Kushtay and Waraks

A further group of medicines which we have recently examined also give rise to concern. These are the Kushtay (Fig. 4). The word Kushta is derived from the Persian and means "killed" or "conquered". It is applied to these preparations because of their supposed efficacy at "killing" or "conquering" the affliction for which they are prescribed. Their composition is mainly oxidized heavy metals including lead, mercury, arsenic, gold, silver and zinc ground together with various herbs. They are prescribed by the hakim as a tonic or as an aphrodisiac. Our study centred in Bradford which is believed to have a high incidence of nephropathy amongst its Asian population. We wished, therefore, to examine any possible connections this may have with Kushtay.

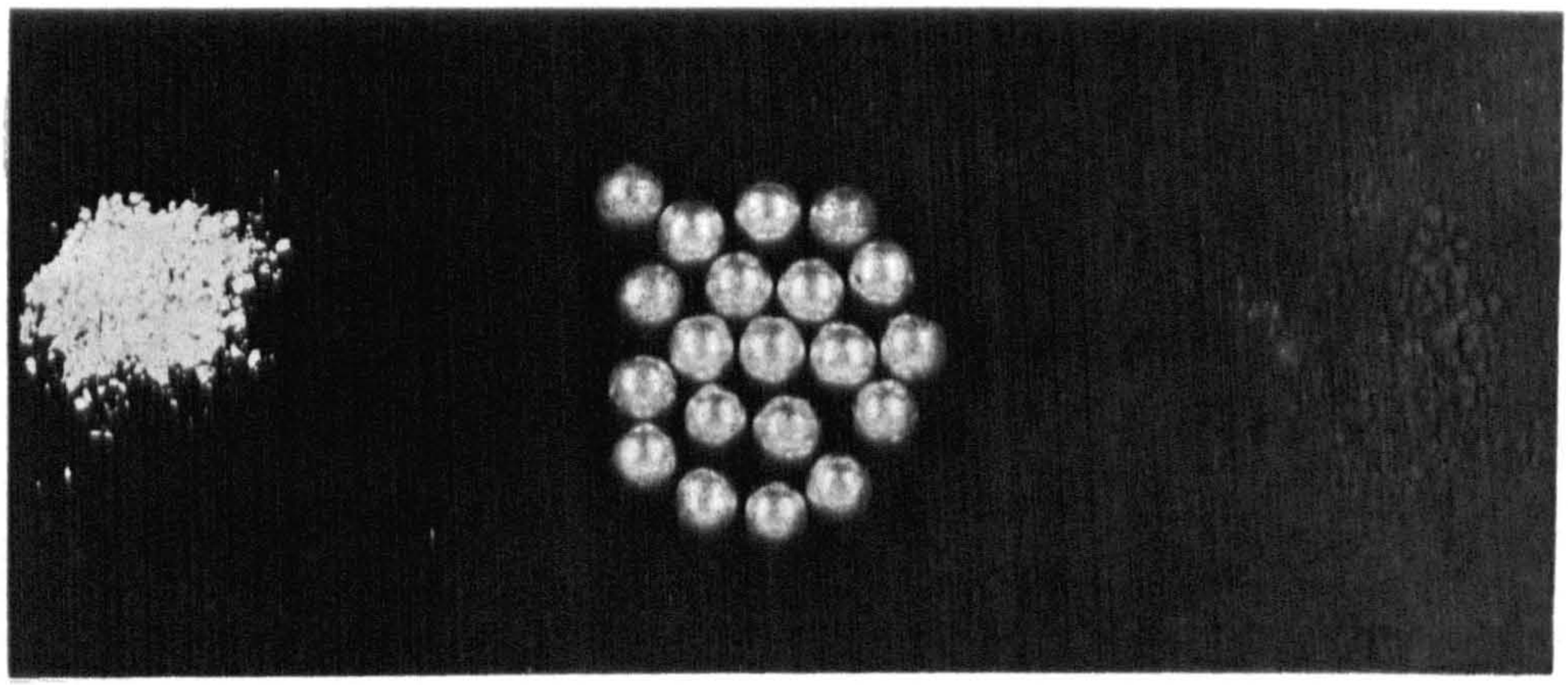

Figure 4. Some sample Kushtay powders and pills.

The preparations of Kushtay are set out in the Hamdard Pharmacopoeia but our study revealed numerous other formulations listed in texts on Unani and Ayurvedic medical systems. In addition, many of the Hakims in Bradford devised their own Kushtay, and others were produced by individual members of the community who purchased the ingredients to prepare Kushtay in their homes.

Because Kushtay are often used as aphrodisiacs and hence are treated in a secretive manner, we recognized that difficulties would be experienced in obtaining a true assessment

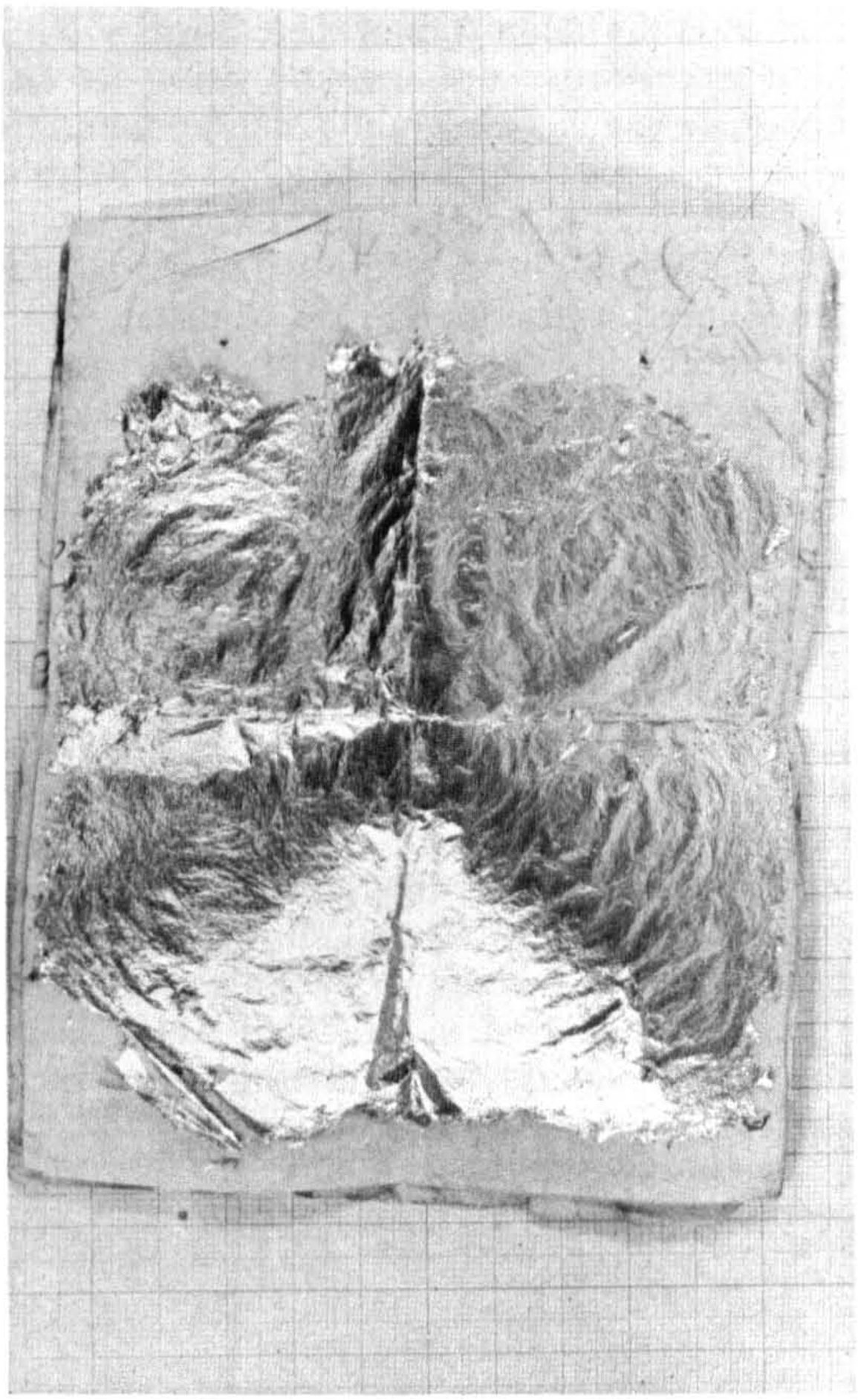

Figure 5. A silver Warak.

of the scale of usage and, hence, the magnitude of the problem. However, during a 10 month period we investigated a series of patients consulting a Hakim and/or attending hospital in Bradford for treatment of various psychiatric disorders. Eighty per cent of the 360 patients we interviewed were male adults and 18% were female adults, the remainder of the group were children. From 37 of the 82 who admitted using Kushtay we were able to collect a sample. All 37 samples were subjected to analysis by X-ray fluorescence and diffraction techniques. In addition to these samples we obtained several Waraks (Fig. 5). Waraks are metal foils, supposedly elemental gold or silver, which are used to adorn sweet meats. They are prescribed for the same purposes as the Kushtay and we have therefore included these in our study.

The analytical data we obtained enabled classification of the samples into four main categories. Eleven samples contained mercury, lead or arsenic as the major constituents with silver, zinc, iron, tin, copper barium and antimony present as trace elements. Six Kushtay had major components of iron, copper and zinc with trace quantities of tin, manganese and silver, although in two of these samples the metals were contained only in the coatings of the pills, the pills themselves being compounded from herbs. One additional sample which fits into this group was a Warak which purported to be gold but on analysis the colouration was found to be provided by a copper/zinc alloy. One sample of a silver

TABLE 3. Proprietary names of the Kushtay analyzed and their source of origin

Sample names	Dominant element	Manufacturer/Origin
Akseri		Birmingham
Gold Warak	Cu, Zn	Pakistan (note absence of gold)
Jawarish Jalinoos	no heavy metals	Bradford
Kushta faulad	Fe	Hakim, Bradford
Kushta faulad mada		Bradford
Kushta gaodanti	As	Sheffield, Hakim
Kushta jaist	Zn	Hakim, Bradford
Kushta Kali	As	Hakim, Bradford
Kushta Khubsul-Hadeed	Fe	Hamdard
Kushta mirgand		
Kushta nuqra	Ag	Bradford
Kushta para	Fe, Hg	Home-made, Bradford
Kushta qalai	Sn	Hakim, Bradford
Kushta sankhia	As (?)	Home-made, Bradford
Kushta shangrof	As	
Kushta surb	Pb	Hakim, Bradford
Kushta tamba safaid	Cu	Hakim, Bradford
Kushta tamesar	Cu	Hakim, Bradford
Kushta tamesar	Fe, Cu	Hamdard
Kushta tila kalan		Hamdard
Kushta tila marwaraidi	Hg	Bradford, Hakim
Kushta zamarrud	Calcite and Quartz	
Kushta indet	As	Home-made, Bradford
Kushta indet	Hg	Home-made, Bradford
Kushta indet	Sn, Pb, Hg	Home-made, Bradford
Maha sudarshan churna		
Nugra	Ag	Bradford
Kushta (Pill)	Ag (coating on pill only)	Zandu, Bombay
Shafi	Ag, Fe	Hamdard
Silver Warak	Zn, Cu	Bradford
Kushta	no heavy metals (trace Pb)	
Kushta	no heavy metals (trace Pb)	Bradford

Warak was found to be pure silver. Of the remaining samples, two were composed of calcite ($CaCO_3$) and quartz (SiO_2) whilst the rest were prepared from organic substances alone. In two of the Kushtay containing arsenic, the element was found to be present as As_2O_3. Table 3 lists the proprietary names of some of the Kushtay analyzed together with their source of origin. Typical formulae are given in Table 4. The cowdung is included not as a drug but as a fuel providing heat for the oxidation of the metals.

Because Kushtay are directly ingested they are potentially far more hazardous than Surma. However, it may be that the herbs and, indeed, the other metals present in these preparations, may affect the rate of absorption in the body. It is common practice when Kushtay are prescribed to advise that they are taken together with an animal oil such as butter (ghee) which may also affect the passage of the metal in the alimentary canal. Irrespective of these possibilities, it is clear that the use of Kushtay should be discouraged and that much additional work is required in the field of metal-metal and metal-organic matter interaction.

Of particular concern is the presence of As(111) in several samples. From 100–300 mg of As_2O_3 may be lethal if absorption is rapid. It is most likely that insufficient heating and time for oxidation was allowed in their preparation; a likely occurrence, particularly with home-made preparations.

TABLE 4. Some typical formulae for Kushtay

Kushta Mirgang	
Purified mercury (para musaffa)	60 g.
Purified tin (qal'ai musaffa)	60 g.
Processed sulphur (gandhak amia sar)	60 g.
Ammonium chloride (naushadar desi)	60 g.
Saltpetre (shora qalmi)	6 g.
Mica 2 sq. in. (abrak)	1
Soft clay	

Kushta Para	
Purified mercury (para mussafa)	60 g.
Purified lead (qal'ai mussafa)	60 g.
Litsea chinesis, finely ground (meda lakri sayida)	180 g.
Symplocos racemosus finely ground (lodh pathani sayida)	10 kg.
Cow-dung pieces (uplay)	10 kg.
Large cow-dung pieces (baray uplay do-do kelo kay)	4

Kushta Musallas	
Tin (qal'ai)	250 g.
Zinc (jast)	250 g.
Lead (sisa)	250 g.
Saltpetre (shora qalmi)	750 g.
Aloe barbadensis juice (ab ghaikwar)	500 g.
Bamboo pole, 2 yards long (bans)	1
Cow-dung pieces (uplay)	40 kg.

Kushta Sam-Ul-Far (*Sankhia*)	
White Arsenic oxide (sam-ul-far) (sankhai safaid)	60 g.
Achyranthes aspera ash (rakh chirchitta)	+500 kg.
Cow-dung pieces (uplay)	5 kg.

TABLE 5. Sandurs and Kum-Kum powders and pastes analyzed

Material	Colour
Ambar Kajal	Orange
Shinagar Kumkum	Orange
Ambar Kumkum tube	Blue
Joina 13 Colour Kumkum	Blue
Ambar Kumkum	Red
Shrinagar Blue-Green	Green

Sandurs and Kum-Kum Pastes

Suggestions have been made of the possible inclusion of mercury in some Asian cosmetics.[3] These were Sandurs and Kum-Kum powders and pastes. Sandurs are used by Bengali, Bihari or North Indian women to colour the parting of the hair whilst the husband is alive. Kum-Kum powders and pastes are used as a spot on the forehead of married women, also only whilst their husband is living.

After discussing these materials further with the Environmental Health officials in

TABLE 6. Heavy metal impurities in some Asian medicines

Product name	Impurities: Major component	Impurities: Minor component	Impurities: Trace component	Remarks
Khamira gaozaban			Zn 130 ppm contained with 41% dextrose and silver particles.	Maximum acceptable 50 ppm. This could cause minor irritation in sensitive individuals.
Female fertility stimulant—silver coated			Silver	No evidence of the presence of hormones, steroids or aloes.
Male fertility stimulant, orange brown, pliable mass			Zn. 168 ppm contained in 15% sucrose together with vegetable matter.	No evidence of hormones or steroids.
Maha sudarshan. Churna powder		Iron	Titanium, manganese, zinc, rubidium, strontium	Essentially soil components presumably derived from the large number of components in the formulation.
Cogoni oil			Iron, zinc.	
Bajar, used by men and women	(Nicotine)		Manganese, iron, zinc, lead, copper.	Powder of tobacco-like substance which is rubbed on gums and swallowed.
Queen's balm			Zinc	Topical application. Zinc trace *not* important.
Bala guti pills (useful for Children's diseases)			Lead 58 ppm, antimony 750 ppm, arsenic 2 ppm	Lead and antimony too high for infant use. (It is used as a cure for calcium deficiency).
Hari taki tablets			Iron, zinc, rubidium.	
chandraprapha pills	Iron	Titanium, chromium, manganese, nickel, zinc, arsenic, strontium.		
Terminalia chebula powder	Zinc, rubidium	Iron		
Pushyanug churna powder		Iron	Titanium, manganese, nickel, zinc, arsenic, strontium, lead.	Lead and arsenic levels unacceptably high in view of the recommended dose (1–4 daily)—maximum intake thus becomes As 4 g, Pb 160 g.
Khadiradi pills		Iron	Titanium, manganese, copper, zinc, rubidium, strontium.	
Withania somnifera		Iron	Titanium, manganese, zinc, arsenic (2 ppm), strontium.	
Marayan churna			Manganese, zinc, strontium.	

Birmingham, we conducted our own series of analyses on the substances listed in Table 5 using atomic absorption spectrophotometry and X-ray diffraction methods. However, our results did not show the presence of any mercury in the samples we analyzed.

Other Asian Preparations

In addition to the materials discussed we analyzed a further range of Asian medicines which, according to the Pharmacopoeia should have been free from heavy metals, the only exception to this being the Chandraprapha pills which contain iron.

As Table 6 illustrates, the materials contained a wide range of heavy metal impurities. Of particular concern are the Bala Guti Pills, which are prescribed (as a children's tonic) in a similar manner to the Bal Jivan Chamchos. In the pills we analyzed we found 58 ppm of lead and 750 ppm of antimony as well as 2 ppm of arsenic.

Conclusion

Our study is the first to examine the role of Asian medicines in a Western community. The results we report here give rise to much concern. At the present time there is considerable public interest centred on the role of lead in petrol and the possible environmental and health hazards which may occur because of this. However, if the lead levels in petrol are compared with the quantity of heavy metals which are regularly being ingested by consumption of some of the substances we have examined, the need for action becomes obvious. It is our firm belief, however, that legislation is only a partial solution and may, indeed, only serve to drive the problem underground. The prime requirement is for effective communication and education to bring about a change in attitude towards the use of these materials within the Asian community. Data we are still collecting indicates that the results we report here are but a small part of a much wider problem. The need for centralization and collation of this information is, we feel, paramount in order to assist in the treatment of Asian patients and bring about an awareness of the special risk to which they may be open.

References

1. Ali, A. R., Smales, O. R. C. & Aslam, M. (1978). *British Medical Journal ii*, 915.
2. Josephs, D. S. (1977). *Public Health* (*London*) **91**, 133.
3. Rao, V. R. (1979). *Personal Communication*. Sandwell Area Health Authority.

Printed in Great Britain by Henry Ling Ltd., at the Dorset Press, Dorchester, Dorset

Sealing Valve for Nuclear Magnetic Resonance Sample Tubes

M. A. Healy

Department of Chemistry, Nottingham University, University Park, Nottingham NG7 2RD, England

In nuclear magnetic resonance experiments involving the use of highly volatile materials, difficulties are often experienced in the filling and subsequent sealing of the glass sample tube. Permanent sealing of the tube can be extremely hazardous because of the presence of condensed oxygen if the sample is initially cooled in liquid nitrogen. Standard moulded polyethylene caps are also unsatisfactory.

Emsley, Feeney, and Sutcliffe (*1*) have described a polytetrafluoroethylene screw cap for temporary sealing of sample tubes which has advantages over the previously described methods. However, the device described below in addition to satisfactorily sealing the sample tube allows direct connection to a vacuum-line system, thus greatly simplifying sample manipulation.

The design of the valve is specifically to suit a Varian HA 100 spectrometer using 5-mm o.d. sample tubes but may easily be modified to suit other experimental arrangements. The valve is in three main sections, the filling port and tap, the valve body, and the sample tube clamp and spinner turbine (Figure 1).

The tap is surmounted by a B 10 size cone to enable connection to a vacuum system. Below the cone is a knurled ring which assists tightening of the "V" cross-sectioned base onto an "O" ring in the valve body. A double "O" ring seal is used around the sides of the tap to prevent escape of liquid through the threaded section. The tap is hollow with two holes drilled immediately above the base to meet the orifice so formed.

The internal construction of the valve body has a thread to accept the tap, a narrow section which acts as a guide to the sample tube, and a further threaded section for the tube clamp. A good seal onto the sample tube is obtained by sloping the seat of the sealing ring which is thus forced in toward the tube on tightening the clamp.

The tube clamp is shaped to form the spinner turbine and, with careful manufacture, the resulting assembly gives perfect spinning.

Material is introduced to the sample tube by connection of the B 10 cone to a vacuum system. The tap is raised off the "O" ring seat in the valve body and the sample distilled into the sample tube via the small holes in the base of the tap.

Involatile solids may be loaded into the sample tube in a dry-box before the tube is connected to the sealing valve. Solvent can then be distilled onto the solute using the above procedure.

On completion of sample preparation the tap is tightened onto the "O" ring seat and the system is ready for use.

The choice of material for construction of the valve depends to some extent upon the substances under investigation. P.T.F.E. and Nylon have both proved satisfactory. The "O" ring seals used were Edwards High Vacuum Limited Viton type VIT 2A for the tap base and tube and two type VIT 0009 on the side seal of the tap.

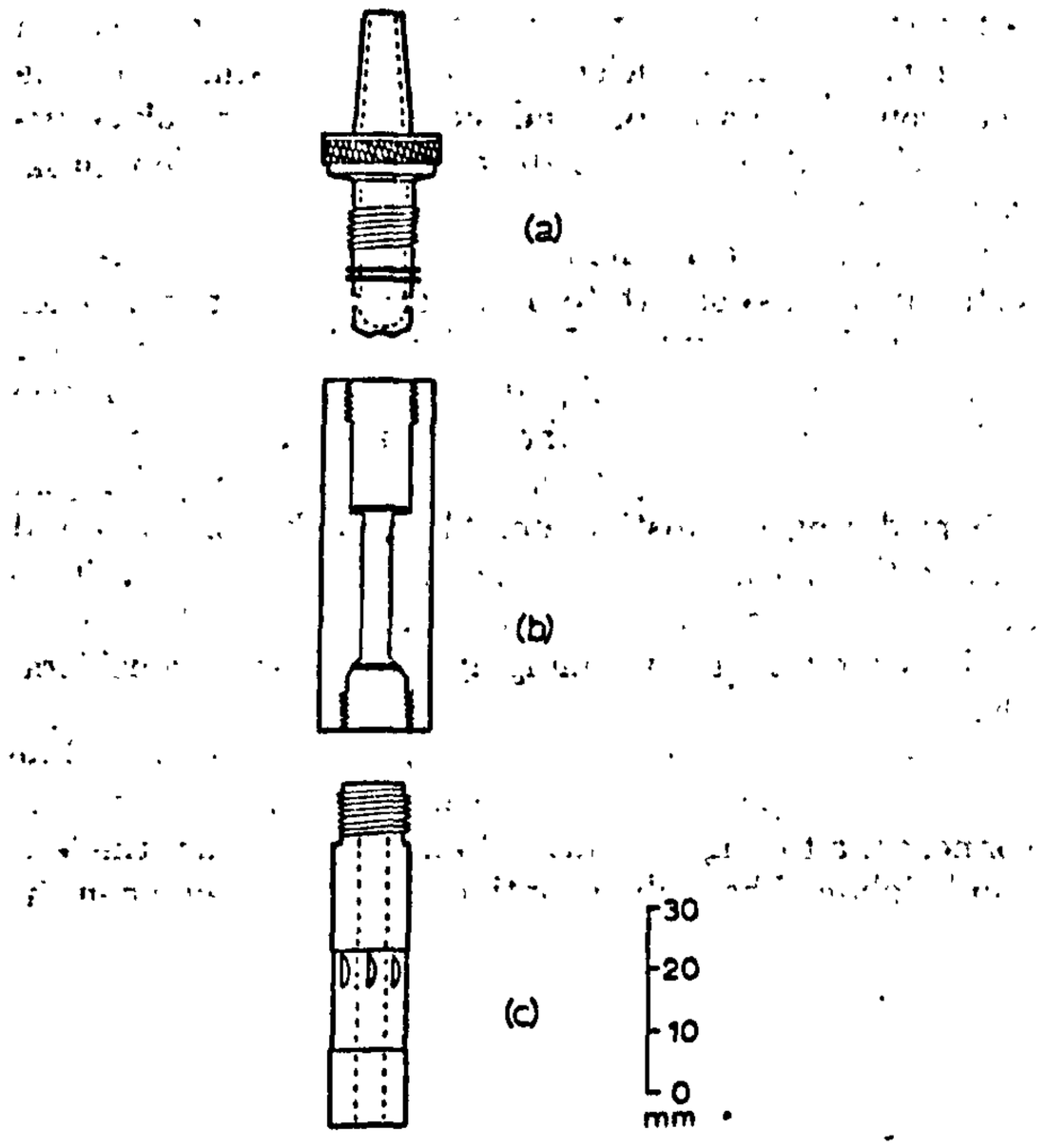

Figure 1. Internal construction of sealing valve showing (*a*) tap, (*b*) valve body, and (*c*) tube clamp with spinner turbine

RECEIVED for review September 6, 1974. Accepted November 11, 1974.

LITERATURE CITED

(1) J. W. Emsley, J. Feeney, and L. H. Sutcliffe, "High Resolution Nuclear Magnetic Resonance Spectroscopy," Pergamon Press, London, 1965, p 272.